THE
PHYSICAL REVIEW

A journal of experimental and theoretical physics established by E. L. Nichols in 1893

SECOND SERIES, VOL. 78, NO. 3 MAY 1, 1950

Neutron Deficient Isotopes of Iodine*

LUIS MARQUEZ AND I. PERLMAN
Radiation Laboratory and Department of Chemistry, University of California, Berkeley, California
(Received January 13, 1950)

The iodine isotopes I^{123}, I^{122}, I^{121}, and I^{120}(?) have been made by bombarding antimony with α-particles. Their characteristics are summarized and evidence for mass assignments presented.

DURING the course of some investigations of abnormal change in nuclear charge following irradiation with high energy particles, some of the nuclides encountered proved to be light isotopes of iodine which had not been reported previously. The main study will be reported at a later date while the present communication describes some work done to characterize and identify the iodine isotopes. The mass number region of interest is that below I^{124} as higher isotopes are well known.[1]

Four new isotopes of iodine have been identified with mass assignments and decay characteristics as indicated in Table I. The method of making mass assignments for some of these was to compare shapes of excitation curves of (α,xn) reactions on antimony in which known iodine activities were produced from Sb^{123} and the new ones to be assigned from Sb^{121}. The excitation functions as shown in Fig. 1 are fairly crude as the only objective was to compare shapes in order to assign mass numbers. The experimental procedure was to irradiate antimony (57 percent Sb^{121}, 43 percent Sb^{123}) with helium ions of different energies, to isolate the iodine by a method in which the chemical yield could be measured, and then to resolve the iodine decay curves into the several components making use of distinctive radioactive properties.

13-HR. I^{123}

A 13-hr. component was assigned to I^{123} since its excitation function paralleled that for 56-day I^{125}, both curves being of the shape that would be expected for $(\alpha,2n)$ reactions; in this case, on Sb^{121} and Sb^{123}, respectively. The yields as shown include corrections for natural abundances of Sb^{121} and Sb^{123}, and are based on the assumption that both the 13-hr. I^{123} and 56-day I^{125} have one K x-ray per disintegration, and assuming one percent counting efficiency in the argon-filled Geiger tubes. The 13-hr. I^{123} has conversion electrons of 150 ± 15 kev energy as determined with a low resolution beta-ray spectrometer and by absorption in beryllium. Gamma-rays corresponding to this energy were also observed. This activity with similar half-life and radiation characteristics has been reported recently by Mitchell, Mei, Maienschein, and Peacock.[2]

4.5-DAY I^{124} AND 13-DAY I^{126}

The curves for both of these isotopes using normal antimony as a target are shown as appropriately labeled solid curves in Fig. 1. The curve for I^{126} is characteristic of an (α,n) reaction as is the low energy part of that for I^{124}. The upswing beyond 30 Mev in the I^{124} curve is due to the $(\alpha,3n)$ reaction on Sb^{123}. The points shown for the broken-line projection of the I^{124} curve were obtained from the irradiation of separated† Sb^{121} from which I^{124} can be formed only by the (α,n) reaction.

TABLE I. Radioactivity of the isotopes of iodine.

Mass No.	Half-life	Radiation	Energy
124	4.5 days	K, β^+	$\beta^+=2.1\pm0.1$ Mev
123	13 hr.	K, γ, e^-	$e^-=150\pm15$ kev
122	4 min.	$\beta^+(K,\gamma?)$	$\beta^+=2.9\pm0.1$ Mev
121	1.8 hr.	K, β^+, γ, e^-	$e^-=185\pm10$ kev $\beta^+=1.2\pm0.1$ Mev
120?	~30 min.	$\beta^+, \gamma(K?)$	$\beta^+=4.0\pm0.2$ Mev

* This work was performed under the auspices of the AEC.

[1] For summary of data see G. T. Seaborg and I. Perlman, Rev. Mod. Phys. 20, 585 (1948).

[2] Mitchell, Mei, Maienschein, and Peacock, Phys. Rev. 76, 1450 (1949).

† The sample of separated antimony consisting of 99.3 percent Sb^{121}, 0.7 percent Sb^{123} was obtained from the Isotopes Division of the U.S. AEC.

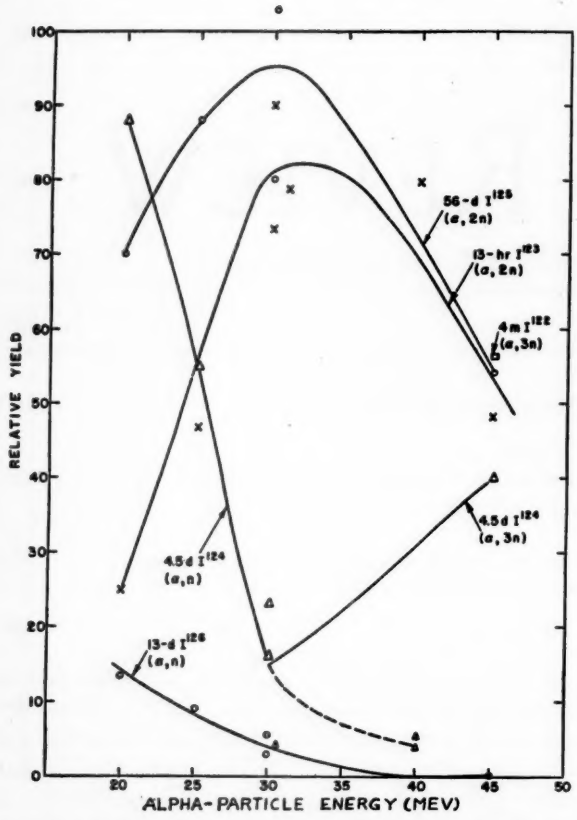

FIG. 1. Excitation functions for (α,xn) reactions on antimony.

The discrepancy in yields at 20 Mev between I^{126} and I^{124} is not explained; but it may be remarked that in other cases such as the fission of bismuth[3] and the (γ,n) reaction on iodine,[4] the measured yield of I^{126} has been much lower than expected, making it appear that not all of the decay events take place through the 1-Mev beta-particle upon which the yields are based.

The half-life of I^{124} was measured as 4.5 days and the β^+-energy as 2.1 ± 0.1 Mev. It is estimated from the yield of K x-rays that this isotope decays only about 30 percent by positron-emission and 70 percent by electron-capture.

[3] R. H. Goeckermann and I. Perlman, Phys. Rev. **76**, 628 (1949).
[4] M. L. Perlman, Phys. Rev. **75**, 988 (1949).

4-MIN. I^{122}

In experiments in which an hour was consumed in chemical separation, no activity appeared which followed the excitation function of that part of the 4.5-day I^{124} curve produced by the $(\alpha,3n)$ reaction. It was therefore assumed that I^{122}, which would be formed by the $Sb^{121}(\alpha,3n)I^{122}$ reaction, is short-lived. More rapid chemistry showed a 4-min. iodine activity, and a single yield determination at 45 Mev showed it to be in the expected range as indicated in Fig. 1. The positron has an energy of 2.9 ± 0.1 Mev, and it is estimated that there is some electron-capture branching.

The assignment of this activity to I^{122} is also based on the fact that it was the only new activity beyond I^{123}, I^{124}, I^{125}, and I^{126} to appear at 45 Mev. A 1.8-hr. activity assigned to I^{121} (from $\alpha,4n$ reaction) did not appear at this energy.

1.8-HR. I^{121}

An activity with 1.8-hr. half-life with a 1.2-Mev positron and conversion electrons of 185 kev appeared in irradiation of antimony with 60-, 100-, and 360-Mev helium ions. Its decay is followed by the appearance of 17-day Te^{121} in approximately the proper yield for a parent-daughter relationship.

30-MIN. I^{120}(?)

In the higher energy irradiations (100 and 360 Mev) a 30-min. activity appeared, having a hard positron of 4.0 Mev. The decay of the iodine containing this activity was followed by the appearance of a tellurium activity which could not be resolved uniquely but which does have a half-life of several days. It is possible that this activity is 4.5-day Te^{119}. This would indicate that I^{119} was present. However, the observed positron energy of the 30-min. period is in better agreement with the prediction for I^{120} which may mean that I^{119} was also present but unobserved.

We wish to thank Dr. J. G. Hamilton and the staff of the Crocker Laboratory cyclotron and Mr. James Vale and the group operating the 184-inch cyclotron for the irradiations used in these studies. We also wish to acknowledge the contribution to some of the early phases of this work by Dr. M. Lindner now at the State College of Washington, Pullman, Washington.

Isotopic Assignments of Bismuth Isotopes Produced with High Energy Particles*

H. M. NEUMANN AND I. PERLMAN
Radiation Laboratory and Department of Chemistry, University of California, Berkeley, California
(Received December 29, 1949)

A number of isotopes of bismuth have been identified from the bombardment of lead with high energy deuterons and protons. Evidence for these assignments is based chiefly on the daughter lead and thallium activities resulting from electron-capture decay.

Isotope	Half-life	Mode of decay	Electron-capture decay products
Bi^{203}	12 hr.	E.C.	52-hr. Pb
Bi^{201}	110 min.	E.C.	8-hr. Pb
Bi^{201}	62 min.	α, E.C.	72-hr. Tl
Bi^{200}	35 min.	E.C.	18-hr. Pb 27-hr. Tl
Bi^{199}	25 min.	α, E.C.	80-min. Pb 7-hr. Tl
Bi^{198}	7 min.	α, E.C.	25-min. Pb 1.8-hr. Tl
$Bi^{<198}$	1.7 min.	α, E.C.(?)	

Those isotopes exhibiting alpha-decay have been investigated as to energy and half-life for this mode of decay. A discussion is given of the relationship between half-life and energy for all known alpha-active bismuth isotopes.

I. INTRODUCTION

SOME time ago it was found in this laboratory that the irradiation of lead with high energy deuterons resulted in the production of highly neutron-deficient bismuth isotopes, some 10-mass units below stable bismuth, and that several of these emit alpha-particles in competition with predominant electron-capture decay.[1] It has long been known that the heavy isotopes of bismuth which are members of the natural radioactive decay series are measurably alpha-unstable, and that alpha-emission effectively disappears in the mass number range below Bi^{211}. This disappearance of alpha-activity with reappearance at around mass number 200 has recently been interpreted in terms of nuclear stability in the region of 126 neutrons and 82 protons superimposed on the general alpha-decay systematics as deduced from nuclei outside of this region.[2] The present communication is concerned with further progress on the isotopic assignments and alpha-energies of these light bismuth isotopes, giving experimental justification for some of the values already summarized in a review article.[3] Further discussion is also given for the alpha-decay half-life and energy relationship for bismuth isotopes.

II. METHODS

When lead is irradiated with deuterons or protons in the 100-Mev range, the mixture of bismuth isotopes produced is far too complex to allow accurate resolution of the decay curves; and in any case it would be difficult to make isotopic assignments by excitation functions because of the mass number range of the target lead isotopes and the difficulty of separating such reactions as $(d,8n)$ and $(d,9n)$. Furthermore, the short half-lives of most of these bismuth isotopes make it most difficult to attempt to determine distinctive radiation characteristics of the different species and thereby obtain additional aid in the resolution. The alpha-particles are somewhat easier to resolve because of their distinctive energies, but this alone is not of much help in making definite mass assignments. The alpha-branching is too minute to permit isolation of the alpha-decay daughters free of a preponderant amount of thallium and lead activities from the electron-capture decay processes.

The method used for making isotopic assignments of the bismuth isotopes began by purifying the bismuth fraction from the irradiated lead, followed by the removal from this fraction, at short equal intervals, of the lead isotopes which grew from the electron-capture decay. In those cases in which the mixture was fairly simple the lead activities could be resolved, and the rate of decrease of each component in the successive separations indicated the half-life of its bismuth parent. With the genetic relationship between bismuth parent and lead daughter established, it remained to assign mass numbers to the lead isotopes. These were either known or could be determined by observing the known thallium daughters[4] of the lead isotopes.

In most cases the lead fractions removed from the initially purified bismuth fraction were themselves too complex for resolution, and the rate of decrease in growth of each lead component was determined by allowing the lead fraction to stand for definite intervals after which the thallium daughters that had grown in were removed. The amount of a particular thallium component in successive fractions will decrease at a

* This work was done under the auspices of the U. S. AEC.
[1] D. H. Templeton and I. Perlman, Phys. Rev. **73**, 1211 (1948).
[2] Perlman, Ghiorso, and Seaborg, Phys. Rev. **77**, 26 (1950); **74**, 1730 (1948); **75**, 1096 (1949).
[3] G. T. Seaborg and I. Perlman, Rev. Mod. Phys. **20**, 585 (1948).
[4] Orth, Heiman, Marquez, and Templeton, Phys. Rev. **75**, 1100 (1949).

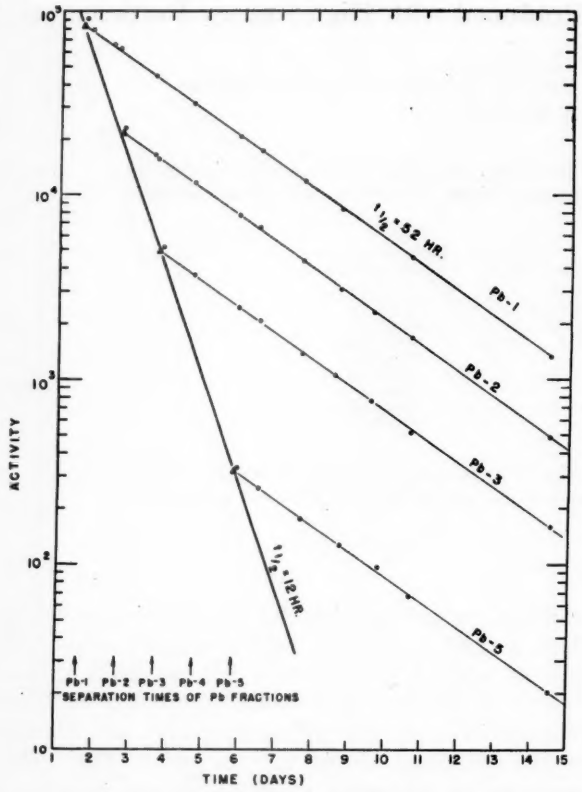

FIG. 1. Data showing the genetic relationship between 52-hr. Pb^{203} and its 12-hr. bismuth parent.

rate corresponding to the half-life of the bismuth grandparent when plotted against the time of lead-bismuth separation. The lead-thallium genetic relationships were determined by removing thallium at periodic intervals from a pure lead fraction. These methods will appear clearer when actual examples are discussed.

The initial bismuth separation from irradiated lead was made in one of two ways. For rapid purification (20 min.–1 hr., depending on degree of purity demanded) the lead was dissolved in $6M$ HNO_3; and, after bringing almost to neutrality with sodium hydroxide, the bismuth was plated on a nickel foil upon immersion for several minutes in the warm solution. The nickel foil with bismuth was dissolved in nitric acid, bismuth hydroxide precipitated with ammonia after adding bismuth carrier, and then dissolved in hydrochloric acid. Upon dilution and warming, BiOCl precipitated and this step was repeated several times. The yield of bismuth in the plating step is only about 10 percent for 5-min. exposure and increases for longer periods. A slower procedure, which removed bismuth from the irradiated lead more nearly quantitatively, began with the dissolution of the target with $6M$ HNO_3, after which most of the lead was crystallized as $Pb(NO_3)_2$ by the successive evaporation of most of the dilute nitric acid and addition of fuming nitric acid. The bismuth carrier which had been previously added was then precipitated from the nitric acid supernatant solution upon neutralization with ammonia. The bismuth hydroxide was dissolved in hydrochloric acid and the oxychloride precipitated as described. Since, at the irradiation energies employed, spallation products including thallium, mercury, and gold might be formed in good yield, carriers for these elements were added in all cases before bismuth precipitation as the oxychloride.

In removing lead activities periodically from the purified bismuth fractions the same chemistry was employed; that is, bismuth oxychloride was precipitated leaving lead in solution. When thallium activities were to be removed from a lead fraction, the solution was adjusted to $6M$ HCl and the thallium extracted as thallic chloride into ether.

In those experiments in which the bismuth alpha-activity was to be measured, the bismuth was plated on nickel foils and these constituted the samples for measurement. For measurement of the short-lived alpha-emitters, the chemistry could be done in ten minutes or less, as no effort was made to remove gold and mercury activities, which also plate on the nickel.

In order to simplify as much as possible the mixtures of activities produced, different proton and deuteron energies were used to confine the reactions to a relatively small mass number region. For example, at 40-Mev proton energy, of the alpha-ϵ mitters only 62-min. Bi^{201} was produced. The electron-capture decay processes were followed with mica end-window Geiger tubes using absorbers to accentuate particular activities. The alpha-particles were measured in standard parallel plate chambers, and the energies were determined with an alpha-particle pulse analyzer.[5]

III. RESULTS

In Table I are summarized the half-lives and genetic relationships of the bismuth, lead, and thallium nuclides pertinent to this study. As no positrons could be measured for any of the species shown, it is assumed

TABLE I. Genetic relationships and half-lives of the bismuth, lead, and thallium nuclides.

Z \ A	198	199	200	201	202	203
Bi	7±1 min.	25±5 min.	35±5 min.	62±8 min. 110±10 min.		12±1 hr.
Pb	~25 min.	~80 min.	18±3 hr.	8±2 hr.	(very long)	(52 hr.)
Tl	(1.8 hr.)	(7 hr.)	(27 hr.)	72±3 hr.	(12 day)	stable

[5] Ghiorso, Jaffey, Robinson, and Weissbourd, National Nuclear Energy Series, Plutonium Project Record Vol. 14B, *The Transuranium Elements: Research Papers* (McGraw-Hill Book Company, Inc., New York, 1949), Paper No. 16.8.

that all decay by electron-capture, with the exception of the minor alpha-branching of some of the bismuth isotopes which will be discussed. Half-life values shown in parentheses in Table I had been known previously.

12-Hr. Bi^{203}

No attempt was made to resolve this period directly out of the bismuth fraction nor to determine radiation characteristics, since it has the same half-life as Bi^{204} which was always present. However, the half-life was readily discerned by periodically removing the lead fraction; and upon resolution of 52-hr. Pb^{203}, it was found that its yield decreased with a half-life of 12 ± 1 hr. The radiation characteristics of the 52-hr. lead agreed well with those previously published, and a discussion of the assignment of this 52-hr. period to Pb^{203} is given in an earlier paper.[6]

The results of one of the experiments which proved the genetic relationship between 52-hr. Pb^{203} and a 12-hr. bismuth activity is shown in Fig. 1. Lead was irradiated for about 1 hr. with 60-Mev protons and a bismuth fraction was purified 4 hours later. At exact intervals of 25.5 hours (arbitrary choice) lead activities which grew from the bismuth were removed and their decay curves followed in order to resolve the 52-hr. period. These decay curves are shown in Fig. 1 with each vertical arrow indicating the time of separation for the particular lead sample. The 52-hr. components extrapolated to time of separation (points indicated by triangles) define a line which is the decay curve of the parent, shown in Fig. 1 by the heavy line with half-life of about 12 hr. The small amount of a shorter-lived component noted in the lead decay curves before tailing into 52 hr. is principally due to 68-min. Pb^{204m}.

A bismuth activity of 12-hr. half-life had previously[6] been reported as Bi^{204}, but it is fairly certain that the two 12-hr. activities are different isotopes. In the assignment of the 12-hr. bismuth to Bi^{204}, Tl was irradiated with 38-Mev helium ions, the bismuth fraction was separated, and the 68-min. lead was found to grow from a 12-hr. bismuth parent.[6] Recently Karraker and Templeton[7] have prepared a 4-hr. polonium activity assigned to Po^{204} which, in its electron-capture branching, decays successively through a 12-hr. bismuth and 68-min. lead in agreement with the mass assignment already cited.[6] In addition they found the 12-hr. bismuth with the 52-hr. Pb^{203} daughter, and this pair grew from a polonium isotope of about 48-min. half-life making a consistent picture if this is assigned to Po^{203}.

Bi^{202}

This isotope of bismuth could not be identified by the techniques used in these studies because its decay product, Pb^{202}, has never been seen and is undoubtedly very long-lived. A minimum half-life of 500 yr. was set on the basis of the estimated yield from a thallium irradiation.[6] From work of Karraker and Templeton[7] Bi^{202} is a 1.5-hr. activity decaying by electron-capture. In the present experiments the combined lead decay products from several bismuth fractions were examined for the growth of 12-day Tl^{202} from electron-capture decay of Pb^{202}. No activity was found, and from the estimated amount of Bi^{202} which should have been formed, a lower limit for the half-life of Pb^{202} may be set which is about the same as that mentioned.

Bi^{201} Isomers

The assignment of a pair of isomers to Bi^{201} came about through an apparent discrepancy in the assignment of an alpha-decay period and electron-capture decay period to the same isotope. In a previous study[1] a weak alpha-activity of 1–2-hr. half life was reported in the bismuth fraction from the irradiation of lead with

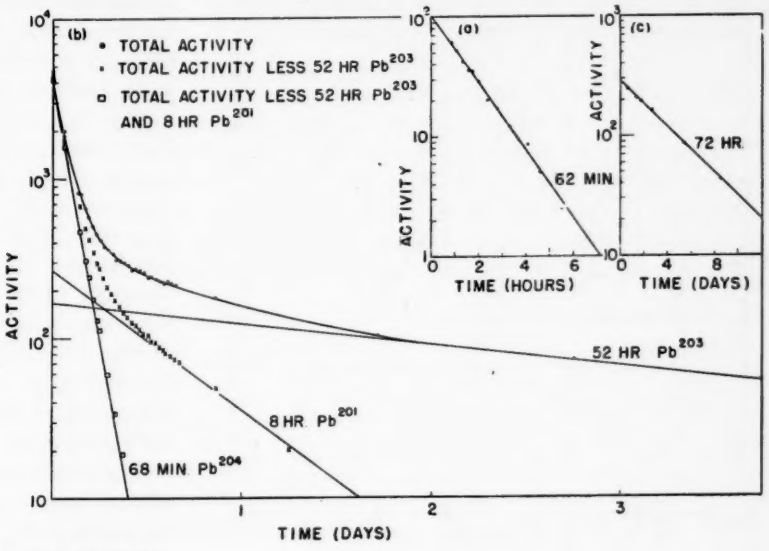

FIG. 2. Activities resulting from irradiation of lead with 40-Mev protons. (a) Bismuth alpha-activity decay curve. (b) Electron-capture activities of lead formed by decay of bismuth. (c) Electron-capture activity of thallium formed by decay of lead activities shown in (b).

[6] Templeton, Howland, and Perlman, Phys. Rev. **72**, 766 (1947).
[7] D. G. Karraker and D. H. Templeton (private communication).

100-Mev deuterons. In the present studies the half-life has been more accurately determined as 62 min., and excitation functions showed it to be the heaviest of the several bismuth alpha-emitters. Through knowledge of the characteristics of Bi^{202}, Bi^{203}, and Bi^{204}, it was deduced that this activity belongs to rare alpha-branching in the decay of Bi^{201}. It should therefore be possible to identify the lead and thallium daughters; and by the methods already described for identifying the bismuth parent, their yields should decrease with the half-life of the parent. When this experiment was done, a new decay chain consisting of an 8-hr. lead and 72-hr. thallium was indeed found. The thallium in particular was best assigned to Tl^{201}, because Tl^{198}, Tl^{199}, and Tl^{200} have been assigned[4] to other activities, while Tl^{202} is not only assigned to a different activity, but would be blocked by long-lived Pb^{202}. However, the half-life for the Bi^{201} parent in the first experiments turned out to be about 90 min. rather than 62 min., the half-life of the alpha-activity thought to be Bi^{201}. The most promising solution at present is to assume that there are independently decaying isomers, one of about 1-hr. half-life which has measurable alpha-branching, and another of about 2-hr. half-life which only exhibits electron-capture decay. It would not be easy to resolve accurately two such components even if they alone were present, but in this case the bismuth fraction itself is hopelessly complex, and one must resort to periodic removal of lead, and from this, thallium, to obtain the progressive decrease in yield of 72-hr. Tl^{201}. The inaccuracies inherent in such a procedure make it possible to fit the data equally well to a single component for Bi^{201} of 90-min. half-life, or two components of 1- and 2-hr. half-lives.

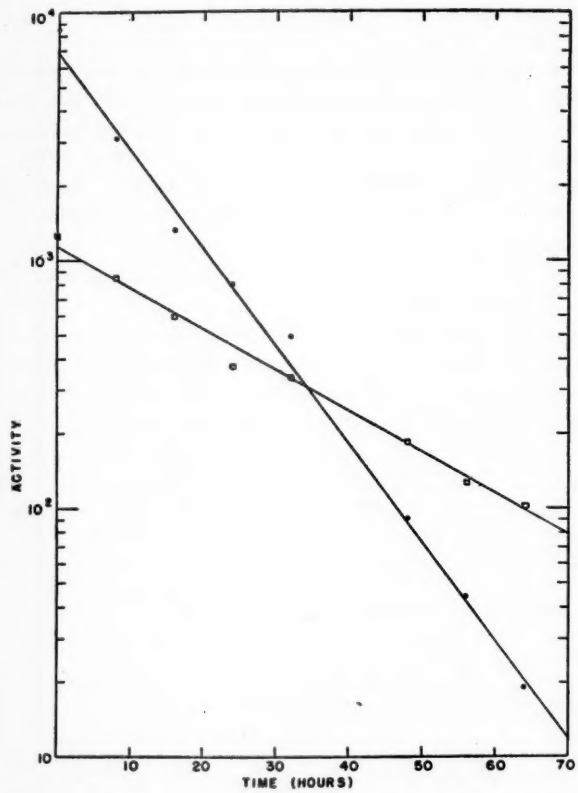

FIG. 3. Half-lives of lead parents of 72-hr. Tl (○) and of 27-hr. Tl (□). Data obtained from yields of respective Tl daughters.

One experiment yielded results which give somewhat more substance to the postulate of isomers for Bi^{201}. A sample of lead irradiated with 100-Mev protons had its bismuth fraction removed some 5 hr. after irradiation, and from this a lead fraction was removed at 155-min. intervals for the next 13 hr. Each lead fraction was allowed to decay a definite period of time (36 hr.) and thallium was removed, its decay followed, and the 72-hr. component resolved. When the yields of 72-hr. Tl^{201} were extrapolated back to the respective times of separation, the half-life for Bi^{201} defined by these points turned out to be 110 min. rather than 90 min. No other experiments were carried out in which the bismuth decay was followed for such a long period of time, and presumably in this experiment the 1-hr. component had largely decayed allowing the detection of the 2-hr. component. While the assumption of isomers for Bi^{201} explains the discrepancies between the decay rates of the alpha-particles and the other radiation, and fits the decay data obtained through the 72-hr. Tl^{201} as well as any other assumption, this assignment cannot be considered as definitely proved.

The association of 72-hr. thallium with the 62-min. bismuth alpha-emitter comes about also from excitation function measurements. Here too, the assignments are not unique, but the observations are in accord with the most likely assignments made according to the previous discussion. When lead was irradiated with 40-Mev protons, the only bismuth alpha-emitter found was the 1-hr. period shown in Fig. 2(a). Purification of the bismuth had taken place less than 1 hr. after irradiation so that the 25-min. period would have been noted had it been produced. The thallium fraction which was removed from lead, which in turn came from the bismuth fraction, showed only the 72-hr. period as seen in Fig. 2(c), showing again that the 27-hr. thallium and 7-hr. thallium lie at lower mass numbers. Finally, as shown in Fig. 2(b), the lead fraction removed from the bismuth fraction could be resolved into three components: 52-hr. Pb^{203} in good yield, an 8-hr. period attributable to Pb^{201}, and a 68-min. period which is probably Pb^{204m}. The 72-hr. thallium growing from the 8-hr. lead would not affect appreciably the decay curve of the 52-hr. Pb^{203}. The curves of Fig. 2(a), (b), (c) are therefore consistent with the assignment of the 1-hr. alpha-emitter to Bi^{201} and the 72-hr. thallium to Tl^{201} coming via 8-hr. Pb^{201}.

The establishment of the half-life for the Pb^{201} parent of the 72-hr. Tl^{201} resulted from a separate experiment in which the genetically related pair 18-hr. Pb^{200} and 27-hr. Tl^{200} was also observed. Following the irradiation of lead with 180-Mev deuterons, the bismuth fraction

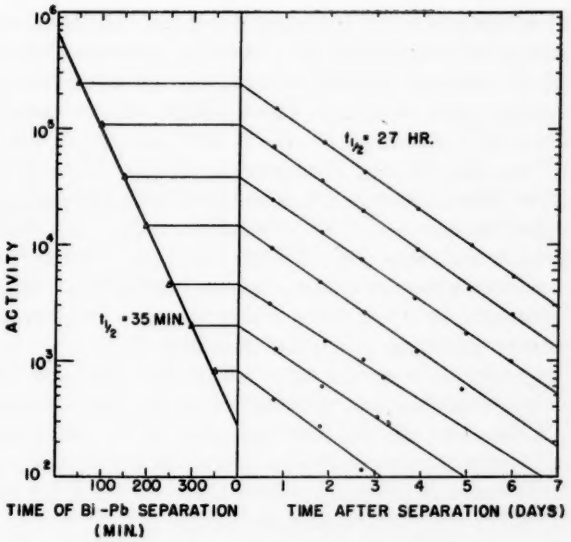

FIG. 4. Data showing genetic relationship between 27-hr. Tl^{200} and a 35-min. bismuth.

was purified and allowed to stand for an hour to grow lead daughters. The lead fraction from this was then purified and after 8 hours the thallium was removed, with further thallium separations at succeeding 8-hr. intervals. These thallium fractions were followed, resolved into 72- and 27-hr. components, and the yields of each plotted according to the successive times of separation from the parent lead fraction. Aside from the first thallium sample which contained in addition some 7-hr. Tl^{199} from Pb^{199} still present, the thallium decay curves be resolved into only the two components. These data are shown in Fig. 3 from which it may be seen that the lead parent of 72-hr. Tl^{201} has a half-life of about 8 hr., while that of the 27-hr. Tl^{200} is about 18 hr.

Some of the radiation characteristics of 72-hr. Tl^{201} were determined by absorption methods and by means of a crude beta-ray spectrometer. In a sample of purified thallium in which the decay showed an essentially straight 72-hr. decay period, the beta-ray spectrometer showed a strong conversion line at 130 kev and a weaker one at 190 kev which correspond to the *K*- and *L*-lines of an approximately 210-kev γ-ray. Absorption curves taken with lead could be resolved into a component of 710 mg/cm² and 200 mg/cm² which are taken to be the 210-kev γ-ray and 70-kev *K* x-ray. Within the accuracy limits, the resolution is not unique but can be made consistent with the observed electron lines. The degree of conversion of the 210-kev γ-ray cannot be known better than the counting yield of the 210-kev γ-rays in the argon-filled counters, and this is poorly known. Assuming 0.3 percent for the counting yield after correcting for geometry loss, the indicated internal conversion is 60 percent. Both *K* and *L* x-rays have been resolved roughly in conformity with the decay scheme of *K*-capture to a 210-kev state whose γ-ray is largely converted in the *K*-shell. Because of uncertainties in counting efficiencies of electromagnetic radiation, it is not possible to say whether or not all of the *K*-capture processes go to the 210-kev state nor to give an accurate conversion coefficient for the γ-ray.

35-Min. Bi^{200}

The assignment of this isotope is based upon the assignment[4] of the 27-hr. thallium to Tl^{200}. The decay sequence starts with 35-min. Bi^{200}, the daughter of which is an 18-hr. lead activity. The distinguishing property of 27-hr. Tl^{200} is hard gamma-radiation which is totally absent from the 72-hr. Tl^{201}, making it possible to measure the 27-hr. period in the presence of large amounts of the 72-hr. period. Following the irradiation of lead with 150-Mev protons, bismuth was removed, and the daughter lead separated from the bismuth parent after a 1-hr. growth period. The lead fraction was then allowed to decay for 35 hours, following which thallium was removed. The decay of the thallium was followed, both without absorbers and through 11.5 g/cm² lead with 234 mg/cm² beryllium to absorb secondary electrons created in the lead absorbers. The decay curve taken without absorbers could be resolved into 27- and 72-hr. periods, while that taken through lead showed only the 27-hr. half-life. Lead absorption curves showed the presence of a γ-ray of 1.6 Mev, and a softer one of about 300–400 kev in about equal abundance. Gold when irradiated with 38-Mev alpha-particles should produce the 27-hr. period by the (α,n) reaction according to earlier work;[4] and when this experiment was tried, the 27-hr. period did show up. Furthermore, its lead absorption curve was identical with that of the 27-hr. period obtained from bismuth decay. A group of electrons of ~350 kev in low abundance is also found associated with Tl^{200}.

The genetic relationship between the 27-hr. thallium and a lead parent of 18-hr. half-life was shown in the same experiment that the 8-hr. lead was linked with the 72-hr. thallium (see Fig. 3 and its explanation in the previous discussion). The establishment of a 35-min. bismuth as the parent of the 18-hr. Pb^{200} and 27-hr. Tl^{200} was accomplished in a manner somewhat analogous to that already described in relation to Fig. 1 for the 12-hr. Bi^{203}–52-hr. Pb^{203} pair. In the present case lead was irradiated with 150-Mev deuterons for 45 min., the bismuth fraction purified 70 min. after the bombardment, and the lead fraction removed at 50-

TABLE II. Alpha-decay properties of neutron deficient bismuth isotopes.

Mass number	Half-life	α-particle energy (Mev)	"Threshold" (protons on natural lead)	Ratio EC/α	α-decay half-life
Bi^{201}	62 min.	5.15	<40	3×10^4	2.6 yr.
Bi^{199}	25 min.	5.47	50–60	8×10^3	140 days
Bi^{198}	7 min.	5.83	60–80	2×10^3	10 days
$Bi^{<198}$	1.7 min.	6.2	<180		

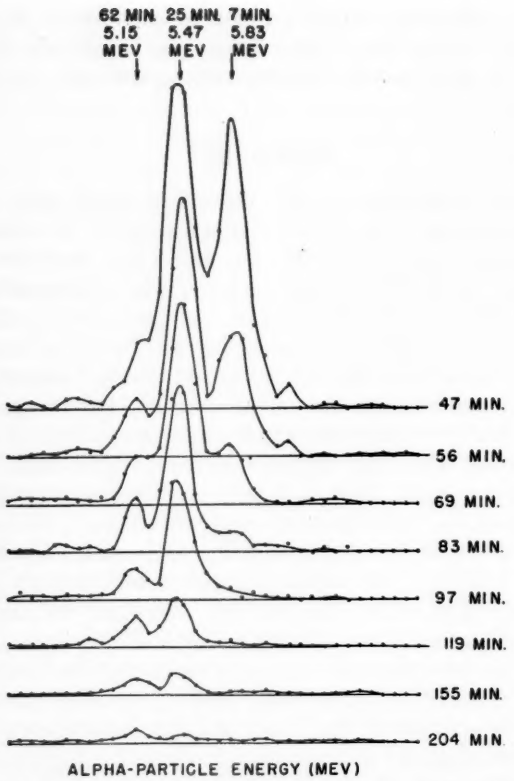

FIG. 5. Successive alpha-energy analyses of bismuth activities produced by irradiation of lead with 180-Mev deuterons. The time to the right of each curve indicates interval between end of irradiation and mid-time of analysis. Original data normalized to equal counting time.

min. intervals thereafter. After allowing each lead sample so obtained to decay for 25 hours, thallium fractions were removed and their decay periods followed. By taking the decay curves through lead absorbers (4 g/cm^2), only the 27-hr. thallium appeared so that there was no problem of resolution. The yields of 27-hr. components, extrapolated back to times of separation, define the decay curve of the bismuth parent. This is shown in Fig. 4 in which the abscissa has a split time scale in order to accommodate the 35-min. period and 27-hr. period on the same graph.

No alpha-activity accompanying the 35-min. Bi^{200} could be identified. As will be shown, there is alpha-activity of 25-min. half-life which has been associated with Bi^{199}, and the apparent absence of a separate group for Bi^{200} may only mean that the alpha-half-life of Bi^{200} is 10 times greater than that of Bi^{199}.

25-Min. Bi^{199}

A bismuth of this period was first noted through its alpha-emission,[1] and has now been assigned to Bi^{199} through its genetic relationship to 7-hr. Tl^{199} by way of electron-capture decay. The method of determining these assignments is similar to others already discussed. In this case the best data were obtained from the irradiation of lead with 180-Mev deuterons for 15 min., after which bismuth was purified (time—1 hr.) and the lead fraction removed from it at 20-min. intervals. These lead fractions were allowed to decay for 4 hours and thallium then removed. The thallium decay curves contained the 72-hr. Tl^{201}, 27-hr. Tl^{200}, as well as 7-hr. Tl^{199} so that it was necessary to resolve the decay curves. When this was done the 7-hr. Tl^{199} yields, extrapolated to points of lead separation, defined a rather good 25-min. curve for the Bi^{199}. The probable error of the determination in this experiment was only a couple of minutes, but the agreement between a number of separate experiments was not this close.

In order to determine the half-life for Pb^{199}, one of the lead fractions was subjected to successive removals of thallium at 60-min. intervals, and the yields of the 7-hr. component were used to define the half-life of the Pb^{199} parent. A value of ~80 min. was obtained for the half-life of Pb^{199} in this manner.

7-Min. $Bi^{198(?)}$

It had been previously reported[4] that a 1.8-hr. thallium results from the irradiation of gold with 38-Mev alpha-particles, and that the most likely assignment for this activity is Tl^{198}. An attempt has been made to see if this thallium activity can be linked through electron-capture processes to one of the light bismuth alpha-emitters, in particular that previously reported[1] with a 9-min. period. A short irradiation (10 min.) of lead with 120-Mev protons was followed by rapid bismuth isolation (25 min.), and lead removal from the bismuth fraction at 10-min. intervals. Each of these lead fractions was allowed to stand 53 min. after which thallium was isolated. The decay of these fractions was followed in an attempt to resolve any 1.8-hr. component present. About all that can be said is that the thallium fractions contained a small amount of activity shorter than 7 hr. and entirely consistent with being 1.8 hr., and this short-lived activity disappeared rapidly in successive fractions. When the short-lived thallium was resolved from the complex decay curve with 1.8-hr. half-life, the yields of this component indicated a half-life for the bismuth ancestor of 7 min.

One of the early lead fractions itself was followed and showed a component of about 25-min. half-life which is probably Pb^{198}, since a similar activity was prepared by Karraker and Templeton[7] from protons on thallium and this was shown to decay to 1.8-hr. Tl^{198}.

IV. ALPHA-DECAY PROPERTIES

The earlier work[1] on these alpha-emitting bismuth isotopes showed four periods: 2 min., 9 min., 27 min., and 1–2 hr. of which the shortest was not proved to be bismuth. It was recognized that the half-lives were those of the electron-capture decay and the alpha-particles arose from rare alpha-branching. In addition the energies could be but poorly determined, and the particles from the three longer periods were thought to lie in the range 5.2–5.8 Mev. Better energy values and

decay periods have now been obtained with some excitation function data identifying these alpha-periods with some of the electron-capture activities already discussed. Table II summarizes the information that has thus far been obtained.

The 1-hr. alpha-emitter can be prepared free of shorter periods by choice of irradiation energy. When deuterons of 60 Mev only are used, a 62-min. alpha-emitter was in evidence and this was found in low yield. The alpha-particle energy determined by an ionization chamber with pulse-height analyzer was 5.15±0.06 Mev. The activity also appeared with 40-, 50-, and 60-Mev protons, and with 60-Mev protons just a trace of the 25-min. alpha-emitter began to appear. These facts place the 62-min. alpha-emitter at a higher mass number than the others. By eliminating bismuth isotopes of mass number 202 or greater it would seem reasonable to assign this period to Bi^{200} or Bi^{201}. Bi^{200} decay has already been shown rather definitely to be governed by a 35-min. half-life (see previous discussion), and the most consistent picture would be to assign the 62-min. activity to an isomeric state of Bi^{201} as already discussed.

It has already been mentioned that no alpha-activity has been found which could be attributed to Bi^{200}. In the experiment just mentioned with the 60-Mev deuterons on lead in which only the 62-min. alpha-emitter was seen, it was found that thallium fractions from bismuth decay showed comparable amounts of 72-hr. Tl^{201} and 27-hr. Tl^{200}. This means that Bi^{200} was present in good yield but has no detectable alpha-particles, for any present would have gone down with a half-life of 35 min.

The best half-life for the period previously reported[1] as 27 min. was obtained by following the alpha-group on the alpha-particle pulse analyzer. This turned out to be 25 min. which is within the range of values found for the electron-capture half-life for Bi^{199}. This assignment also conforms with the appearance of these alpha-particles at a proton threshold energy of 60 Mev, some 20 Mev higher than the threshold for the activity assigned to Bi^{201}. The alpha-particle energy was found to be 5.47±0.06 Mev.

At higher bombardment energies (100 Mev for good yield) the shorter period appeared which was called 9 min. in the earlier report.[1] The best half-life obtained by following the alpha-group on the alpha-pulse analyzer was 7 min., which agrees with the half-life ascribed to Bi^{198} through its electron-capture relationship with 1.8-hr. Tl^{198}. Since its order of appearance in the excitation function also is in harmony with the assignment of such a low mass number, it is probable that these alpha-particles of 5.83±0.06 Mev should be assigned to Bi^{198}.

Finally, the 1.7-min. alpha-activity has been shown to be bismuth, insofar as chemical plating on nickel foil is a criterion, and the alpha-particle energy was determined as 6.2±0.1 Mev. It is probable that the mass number is still lower than Bi^{198} and has been so indicated in Table II. No attempt has been made to measure the electron-capture decay sequence of this nuclide, because

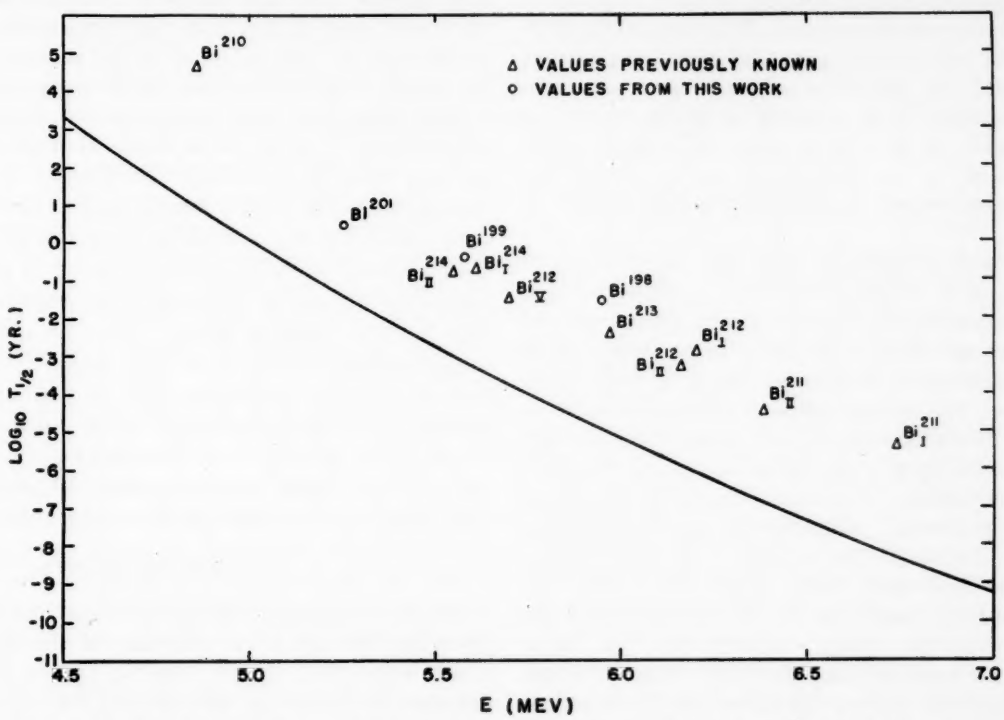

FIG. 6. Partial alpha-half-life *vs.* alpha-decay energy. The curve gives values calculated for transitions unprohibited by nuclear type and assuming the nuclear radius equals $1.48A^{\frac{1}{3}}\times10^{-13}$ cm.

the short half-life would make it most difficult to perform the necessary chemical separations.

In Fig. 5 is shown a series of alpha-particle pulse analyzer curves taken on the bismuth fraction from the irradiation of lead with 180-Mev deuterons. The abscissa gives the alpha-energy or, as the data is taken, the channels of the pulse-height discriminator, while the ordinates indicate the number of counts registered in each channel normalized to the same counting period. The time indicated for each curve is that from the end of irradiation to the time that the alpha-particle energy analysis was made. It is seen, first of all, why in the previous study[1] it was not possible to obtain a good half-life for the 5.15-Mev group by following the gross decay. It is only when the bombardment energy is lowered to the point at which this is the only alpha-group formed that it is possible to obtain the 62-min. period. It can be seen that the decay periods for the 5.47- and 5.83-Mev groups may readily be determined by following each peak separately, and it was by data of the type shown in Fig. 5 that the 25- and 7-min. periods were obtained. From Fig. 5 it may be seen in a qualitative fashion that the 5.83-Mev group disappears first so that in the interval 1–2 hr. after bombardment, the 5.47-Mev group is the principal one present, and that the 5.15-Mev group only begins to appear distinctly after about half of the 5.47-Mev group has decayed.

Half-Life and Energy Relationship

One of the major points of interest in these artificially produced bismuth alpha-emitters is their relation in the systematics of alpha-decay. Reference is made to the paper[2] in which the trends in alpha-decay properties are discussed. In particular, alpha-emission in these bismuth isotopes is interpreted as a resumption of alpha-emission of the heavy bismuth isotopes, which is interrupted by the unfavorable energetics toward alpha-emission caused by crossing the region of 126 neutrons.

One of the generalizations that came from the study of alpha-decay systematics[2] was that the half-life decay energy relationships for the even-even nuclei were in quantitative agreement with alpha-decay theory, while other types deviated in the direction of prohibition in alpha-decay. The general cause for the prohibition is attributed to the existence of odd nucleons and is only slightly affected by spin change in the particle emission. One of the parameters in alpha-decay theory which cannot be evaluated independently to the precision required is the nuclear radius, and a significant point is that the even-even nuclei (and presumably the others) in a broad region can be described by the same function for nuclear radius, $r=1.48A^{\frac{1}{3}}\cdot 10^{-13}$ cm. However, there are even-even nuclides which show forbidden alpha-decay if the radius is described by this function, and the obvious explanation is that the nuclear radius is smaller than would be calculated in this manner. Such nuclides are those which have 126 neutrons and less or those which decay into or through the region of 82 protons. The position of the bismuth alpha-emitters is somewhat difficult to assess since the quantitative treatment is complicated by the necessity of estimating the degree of prohibition due to odd nucleons. However, the degree of prohibition for the bismuth nuclides Bi^{214} to Bi^{210} is such that one must attribute part of the effect to abnormally low nuclear radius. This would be explainable by nuclear radius change for decaying through lead (82 protons) and in some cases through 126 neutrons.

It would be of interest to compare the new light bismuth isotopes with the heavier ones to see if any trend in nuclear radius can be inferred. Unfortunately, one can have little confidence in the estimation of the alpha-decay half-lives for these new light bismuth isotopes, since they must be calculated from extremely rare alpha-branching of electron-capture processes. The number of electron-capture events for each alpha-emission must be calculated from the yield of the thallium decay product (from two electron-capture events), since it is not possible to resolve the decay curves of the bismuth fraction itself. Furthermore, one is faced with the general unsatisfactory situation of estimating numbers of electron-capture events. For present purposes we have attempted to resolve the K x-rays as the common denominator in all of the electron-capture processes and to assume one K x-ray per disintegration. This assumption could give low values if there is L-capture, and high values if there are K internal-conversion events. The counting yield for mercury K x-rays (70 kev) was taken to be 0.3 percent in argon-filled Geiger tubes, corrected to 100 percent geometry.

The alpha-decay branching ratios estimated for Bi^{198}, Bi^{199}, and Bi^{201} are shown in Table II. Figure 6 shows a plot of the half-lives of bismuth isotopes with reference to a calculated line which would apply to these isotopes if their decay were not prohibited by the nuclear type (odd nucleons), and if the nuclear radius in this region could be described by the above-mentioned expression. The highly forbidden nature of all of these alpha-emitters makes it seem likely that all have low nuclear radii. Since the prohibition due to odd nucleons is known to vary considerably,[2] it is only possible to guess at the effect of nuclear radius. About all that can be said is that values lower by about 10 percent from those given by $r=1.48A^{\frac{1}{3}}\cdot 10^{-13}$ cm seem to be required.

V. ACKNOWLEDGMENTS

We are indebted to Mr. James Vale, and the group operating the 184-inch cyclotron for the irradiations which made these studies possible, and to Mr. Albert Ghiorso for his aid in determining the alpha-particle energies.

Inelastic Scattering of Protons by Aluminum and Carbon*

C. LEVINTHAL, E. A. MARTINELLI, AND A. SILVERMAN
Radiation Laboratory, Department of Physics, University of California, Berkeley, California
(Received December 28, 1949)

The energy distributions of inelastically scattered protons from carbon and aluminum were found by range measurements with the detection taking place in photographic plates. The carbon distribution shows two levels in C^{12}, one at 4.8 and one at 10.1 Mev. There is also a third peak whose energy and intensity lead us to assign it to deuterons in which the C^{11} from the reaction $C^{12}(p,d)C^{11}$ is left in its ground state. The aluminum results show a continuum. An attempt is made to fit the distribution using a nuclear level density of from $W(E)=C\exp(AE^{\frac{1}{2}})$ as suggested by Weisskopf. The results fit fairly well at excitations above 15 Mev and not at all at excitations below that.

I. INTRODUCTION

WHEN a nuclear reaction is induced by monoenergetic incident particles the energy distribution of the emitted particles yields information about the excited states of the residual nucleus. When the separation of these states is larger than both their natural width and the minimum energy spread that the experiment can resolve, the emitted particles fall into discrete energy groups; see, for example, Fulbright and Bush.[1] When the level density is larger, the energy distribution appears continuous, but the shape of this continuum can yield information about the level density of the residual nucleus, as discussed by Feld[2] and Weisskopf.[3] Using photographic plates to detect the charged particles we have investigated the energy spectra of protons emitted from carbon and aluminum when bombarded by protons of 32 and 16 Mev from the Berkeley linear accelerator.

II. EXPERIMENTAL METHOD

A camera was constructed (Fig. 1) which allows eight plates to be exposed simultaneously each with its center at an angle of 96° with the beam axis and each plate set so that particles from the target enter it within 20° of grazing incidence. To cover the energy range desired, an absorber of either copper or aluminum was placed between the target and each plate. The absorbers were increased by steps of seven mils (48 mg/sq. cm) equivalent of aluminum which corresponds to 160μ of emulsion. Track lengths in the region from 15–200μ were read on each plate (tracks less than 15 μ were considered unreliable) and so there was an overlap region of 25μ from plate to plate. This method requires that about 24 plates be read to cover the region 0–32 Mev. Reading track lengths of 200μ or less has two advantages: (a) It makes corrections for tracks scattering out of the emulsion negligible, and (b) it makes counting the tracks quite simple since they all fall well within one field of view of the microscope with a convenient magnification of 440. The tracks are measured by means of an eyepiece reticule calibrated against a Bausch and Lomb stage micrometer.

The absorbers were placed on an approximately spherical surface of radius 6.3 cm centered on the target. This insured that the effective thickness of the absorber for the scattered protons varied by less than 0.2 percent. All tracks read were at a polar angle of 96±4°.

Ilford E-1, 100μ, plates were used. These plates are sufficiently insensitive to distinguish alpha-particles but not deuterons from protons. In order to minimize the number of tracks arising from recoil protons struck by neutrons incident on the plates, only those tracks coming from the direction of the target and starting at the top surface of the emulsion were read.

The background tracks were determined in two separate ways, with no target present and by using an absorber thick enough to cut out all scattered protons. In the high energy tail of the aluminum curve (Fig. 5) the background amounted to about 20 percent. In other regions of interest, it was much less than that.

III. RESULTS AND CONCLUSIONS

Carbon

A one-mil polystyrene target was used in two sets of runs, one at 16.3 Mev and one at 31.5 Mev. The experiment at the lower energy is essentially a duplication of work done by Fulbright and Bush[1] and provided a check on our method. The results are shown in Figs. 2–4. Figure 2 shows the distribution *vs.* range in the 31.5-Mev run as an example of the raw data taken from the plates. Each run shows two levels in C^{12}, the 16.3-Mev run at 4.8 and 10.2 Mev; the 31.6-Mev run at 4.7 and 10.1 Mev. Fulbright and Bush find three levels, at 9.7, 5.5, and 4.4 Mev, but their results were obtained at 162° and some of these levels probably have strong angular variations. Gibson[4] found levels at 4.47, 9.72, and, less certainly, at 7.7 Mev. The half-width at half-maximum is about 0.4 Mev for the 32-Mev run and about 0.5 Mev for the 16-Mev run. The half-width calculated from straggling, spread in polar angle, and target thickness is 0.3 Mev. The half-width in the

* This work was sponsored by the AEC.
[1] H. W. Fulbright and R. R. Bush, Phys. Rev. 74, 1323 (1948).
[2] B. T. Feld, Phys. Rev. 75, 1115 (1949).
[3] V. Weisskopf, Phys. Rev. 52, 295 (1937).
[4] W. M. Gibson, Proc. Phys. Soc. A62, 586 (1949).

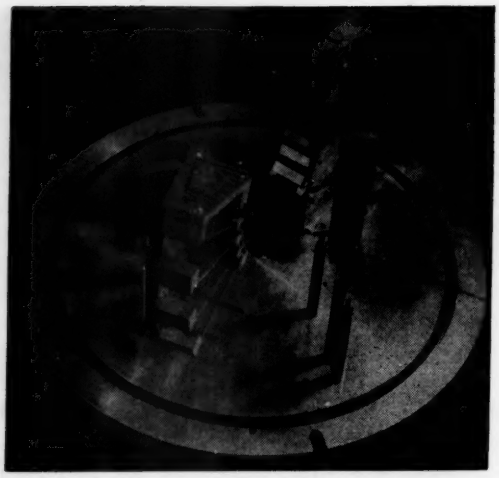

FIG. 1. General view of the construction of the camera.

16-Mev run is larger because of the energy spread introduced by stopping down the beam.

The third level shown in the 31.6-Mev run has two possible interpretations. It may be either deuterons or protons. Considered as deuterons going to the ground state of C^{11} it leads to a threshold of 16.7 Mev for the $C^{12}(p,d)C^{11}$ reactions. The threshold for the reaction calculated from the masses is 16.5 Mev. Considered as protons it leads to a level at 21.2 Mev in C^{12}. The low energy tracks could be associated with levels in C^{12} at excitations between 20–28 Mev or could be associated with protons arising from $C^{12}(p,np)C^{11}$ or $C^{12}(p,\alpha p)Be^{8}$ reactions.

The energy and the relative intensity of the third level in the 32-Mev run seem to indicate that it is composed of deuterons. From the threshold of the $C^{12}(p,pn)C^{11}$ reactions, Panofsky and Phillips[5] showed that deuterons are emitted at threshold and the intensity of the supposed deuterons in this experiment suggests that a substantial fraction of the C^{11} is due to deuteron emission even at 32 Mev. This is not surprising in view of the sparsity of levels in C^{12} and the high binding energy of a neutron to N^{13}, both of which mean that the processes competing with the deuteron emission are very much reduced.

The relative intensities of the excited states are of some interest. From the volume available in phase space, neglecting selection rules and statistical weights of the states of the excited nucleus, the ratio of the intensities should be simply the ratio of the energies of the emitted protons. The calculated and observed intensities are shown in Table I. The agreements between the calculated and observed results indicate that all of the reactions are equally allowed.

Aluminum

The target was one-mil aluminum foil and the bombarding energy 30.4 Mev. The distribution in Fig. 5 shows no levels except the elastic peak. Dicke and Marshall[6] have shown that there are levels in aluminum at 0.87, 2.03, 2.70, and 3.5 Mev. These could not be seen as separated levels, probably because the levels are too close to be resolved with the statistics available in this region. The elastic scattering is assumed to be due primarily to diffraction scattering since it is much more intense than the low lying excited levels. The experimental cross section for the elastic scattering is $\sigma(96°)=4.1\times10^{-27}$ sq. cm/sterad. The theoretical cross section, assuming only diffraction scattering, is given by[7]

$$\sigma(\theta)d\Omega=(\lambda\!\!\!^{-2}/4)\left|\sum_l(2l+1)(\beta_l-1)P_l(\theta)\right|^2d\Omega. \quad (1)$$

Here $1-|\beta_l|^2$ is the sticking probability of protons of angular momentum l. If one assumes a completely absorbing nucleus, $\beta_l=0$. If the sum is taken to $l_{max}=R/\lambda\!\!\!^{-}$, approximately 5 in this case, where R=radius of aluminum nucleus, one finds $\sigma(\pi/2)=5.53\times10^{-27}$ sq. cm/sterad. This agreement is probably better than one should expect from the crude model used. However, it indicates that this explanation is not unreasonable.

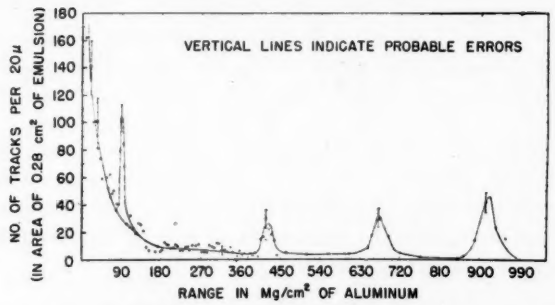

FIG. 2. Range distribution of charged particles from carbon bombarded with 31.5-Mev protons.

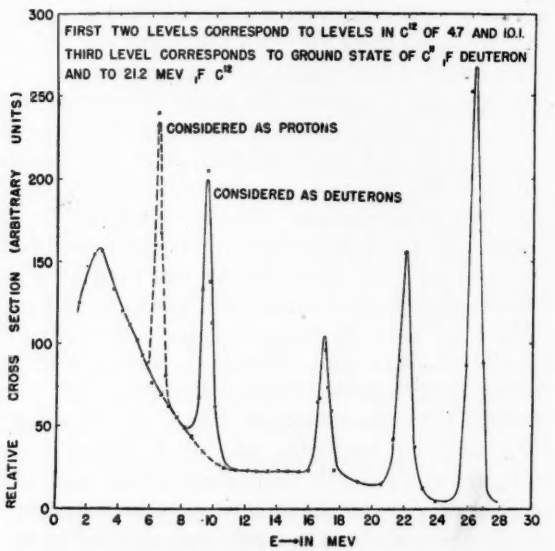
FIRST TWO LEVELS CORRESPOND TO LEVELS IN C¹² OF 4.7 AND 10.1.
THIRD LEVEL CORRESPONDS TO GROUND STATE OF C¹³ ,F DEUTERON
AND TO 21.2 MEV ,F C¹²
CONSIDERED AS PROTONS
CONSIDERED AS DEUTERONS
RELATIVE CROSS SECTION (ARBITRARY UNITS)
0
50
100
150
200
250
300
0 2 4 6 8 10 12 14 16 18 20 22 24 26 28 30
E⟶IN MEV

FIG. 3. Energy distribution of protons from carbon bombarded with 31.5-Mev protons.

[5] W. K. H. Panofsky and R. Phillips, Phys. Rev. **74**, 1732 (1948).

[6] R. H. Dicke and J. Marshall, Jr., Phys. Rev. **63**, 86 (1943).

[7] H. A. Bethe, Phys. Rev. **57**, 1125 (1940).

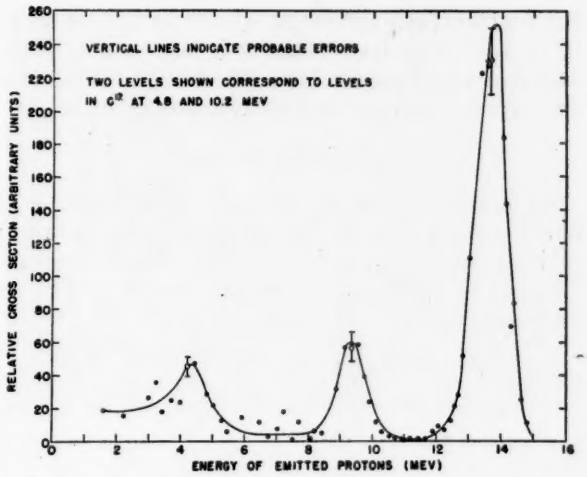
VERTICAL LINES INDICATE PROBABLE ERRORS
TWO LEVELS SHOWN CORRESPOND TO LEVELS IN C12 AT 4.8 AND 10.2 MEV
RELATIVE CROSS SECTION (ARBITRARY UNITS)
ENERGY OF EMITTED PROTONS (MEV)

FIG. 4. Energy distribution of protons from C^{12} bombarded with 16.3-Mev protons.

By assuming a statistical model for the nucleus, one can use the data to calculate the variation of level density with energy. At excitations of about 30 Mev it seems likely that even as light an element as aluminum can be treated by these methods. The energy distribution of the emitted protons can be shown to be given by[3]

$$I(\epsilon)d\epsilon = K\epsilon\omega_R(E)\sigma_c(\epsilon)d\epsilon, \qquad (2)$$

where $I(\epsilon)$ is the number of protons of energy ϵ emitted per unit time; $\omega_R(E)$ is the density of levels of the residual nucleus at excitation E; $\sigma_c(\epsilon)$ is the capture cross section for protons of energy ϵ; and K is the constant independent of energy. In all calculations $\sigma_c(\epsilon)$ was taken as $\pi R^2 P(\epsilon)$. Here $P(\epsilon)$ is probability of a proton of energy ϵ penetrating the Coulomb barrier.

Weisskopf[3] gives $W_R(E) = B\exp(AE^{\frac{1}{2}})$. Here $E = 29.4 - \epsilon$, where 29.4 is energy of the protons in the center-of-mass system. Thus, by plotting $\ln[I(\epsilon)/\epsilon]$ *vs.* $(29.4-\epsilon)^{\frac{1}{2}}$, one gets the constant A as the slope of the curve. However, this neglects the fact that not all the protons measured come from the $Al^{27}(p,p)Al^{27*}$ reaction. They may also come from multiple reactions such as $Al^{27}(p,np)Al^{26*}$ or $Al^{27}(p,2p)Mg^{26*}$. From an analysis of the binding energies involved one can estimate that about half of all the protons arise from multiple reactions and that the energy distribution of the second proton would be about the same whether it follows a neutron or a proton. One can find the energy distribution of these protons as follows.[8] Let the distribution of second protons be given by

$$I(\epsilon')d\epsilon' = K\epsilon'\exp[A(E'-\epsilon')^{\frac{1}{2}}]\sigma_c(\epsilon')d\epsilon'.$$

$E' = 29.4 - E_b - \epsilon$, where E_b = binding energy of proton to Al^{27}. $E' - \epsilon'$ is the excitation of Mg^{26} after emission of second proton. This must now be multiplied by the probability of the first proton being emitted with energy ϵ and integrated over all ϵ for which ϵ' is possible.

Thus:

$$I(\epsilon')d\epsilon' = K\epsilon'\sigma_c(\epsilon')\int_0^{29.4-E_b-\epsilon'} \epsilon\sigma_c(\epsilon) \times \exp A[(29.3-E_b-\epsilon'-\epsilon)^{\frac{1}{2}}+(29.3-\epsilon)^{\frac{1}{2}}]d\epsilon.$$

This integral was evaluated numerically as a function of ϵ' for $A = 3.0(\text{Mev})^{-\frac{1}{2}}$ and $A = 3.6(\text{Mev})^{-\frac{1}{2}}$ and the resulting distribution normalized so that it contained half the total number of protons. This was then added to the distribution expected for the first proton assuming the same value of A. The smooth curve (Fig. 5) is calculated for $A = 3.6$ and the dashed curve for $A = 3.0$.[9] There seems to be a qualitative agreement between the experimental and calculated distributions for energies below 12 Mev. This corresponds to an excitation of the aluminum of about 15 Mev. Thus, the evidence seems to be that at excitations above 15 Mev the density of levels increases quite rapidly and possibly exponentially. The much slower decrease of the experi-

TABLE I. Ratio of intensities.

	16-Mev run		32-Mev run	
	Observed	Calculated	Observed	Calculated
Ratio of intensity of first excited state to second excited state	2.2	2.1 Assuming deuteron	1.6	1.2 Assuming proton
	Observed	Calculated[a] A	B	Calculated
Ratio of intensity of first excited state to third level in 32-Mev run	1.4	1.25	0.8	4.2

[a] Case "A" neglects the statistical weight of the deuteron. Case "B" ascribes a statistical weight of 3/2 relative to that of proton. One cannot decide which is correct without knowing the angular momentum of the original excited state of C^{12}. It is likely that many states with different angular momenta are excited.

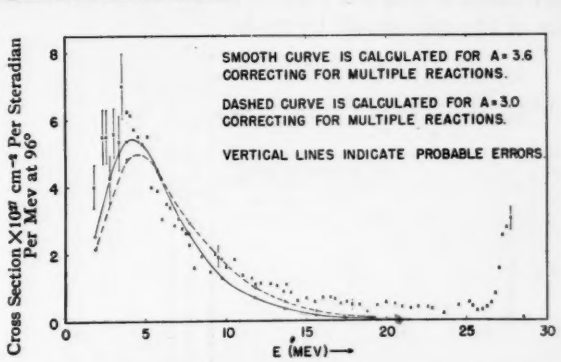
SMOOTH CURVE IS CALCULATED FOR A = 3.6 CORRECTING FOR MULTIPLE REACTIONS.
DASHED CURVE IS CALCULATED FOR A = 3.0 CORRECTING FOR MULTIPLE REACTIONS.
VERTICAL LINES INDICATE PROBABLE ERRORS.
Cross Section X10²⁷ cm⁻² Per Steradian Per Mev at 90°
E (MEV)

FIG. 5. Energy distribution of protons from aluminum bombarded with 30.4-Mev protons.

[8] The calculation is done for the $Al^{27}(p,2p)Mg^{26*}$ reaction. As stated in text, there would be no substantial difference if it were done for the $Al^{27}(p,np)Al^{26*}$ reaction.

[9] The value of A calculated directly from the raw data is 3.8 $\text{Mev}^{-\frac{1}{2}}$. It is seen that the correction for the protons from multiple reactions does not change the value of A very much. This is because the distribution of these protons is not greatly different from the distribution of the first protons.

mental curve than the calculated one above 12 Mev indicates that for excitations less than 15 Mev the level density changes much more slowly than the exponential form chosen in the calculations. Weisskopf[3] estimates $A=3.1$ for light nuclei. Bethe[10] gives $A\cong(M/2.2)^{\frac{1}{2}}$, or $A=3.5$ Mev^{-1} for Al, where $M=$mass number.

One can estimate the absolute level density at any excitation from Eq. (2), by using relative values of $I(\epsilon)$ and assuming a value of $\omega(E)$ at some energy. Using the known levels[6] to get the average density for the first few Mev, one arrives at a level distance of 10 kv at 20 Mev. This level distance is considerably larger than one would obtain from the statistical models of the nucleus which are used by Weisskopf and Bethe.

[10] H. A. Bethe, Phys. Rev. **50**, 332 (1936).

ACKNOWLEDGMENTS

We wish to express our gratitude to Professors A. C. Helmholz and W. K. H. Panofsky for continual guidance and encouragement. Our thanks are also extended to the linear accelerator crew for their complete cooperation at all times.

PHYSICAL REVIEW VOLUME 78, NUMBER 3 MAY 1, 1950

On the Nuclear Spin of B^{10} *

M. T. Weiss M. W. P. Strandberg, R. B. Lawrance, and C. C. Loomis
Research Laboratory of Electronics Massachusetts Institute of Technology, Cambridge, Massachusetts

(Received January 3, 1950)

From measurements on the fine structure of the $J=0\rightarrow1$ rotational transition of $H_3B^{10}CO$ near 17,960 Mc/sec. we are able to establish that the spin of B^{10} is 3 as had previously been reported by Gordy, Ring, and Burg. A quadrupole coupling constant of 3.44 ± 0.1 has also been determined for this molecule. A brief description of our spectroscope is included.

INTRODUCTION

IT has been reported by Gordy, Ring, and Burg[1] that the spin of B^{10} is 3 and is not 1 as had been assumed for theoretical reasons. They deduced this spin value from observation of quadrupole fine structure in the $J=1\rightarrow2$ microwave transition of borine carbonyl, $H_3B^{10}CO$. This spectrum is complicated because of the K splitting of both the $J=1$ and the $J=2$ levels. The calculated spectrum consists of 20 lines in a region extending over 3 Mc/sec. Because of the great theoretical importance[2] of the certain knowledge of the B^{10} spin value, it was felt that an independent determination of the spin should be made.

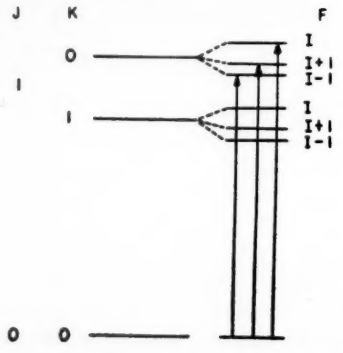

FIG. 1. Energy level diagram for $J=0$ and $J=1$ of $H_3B^{10}CO$ (not to scale).

* This work has been supported in part by the Signal Corps, the Air Materiel Command and ONR.

[1] Gordy, Ring, and Burg, Phys. Rev. **74**, 1191 (1948).

[2] M. Goldhaber, Phys. Rev. **74**, 1194 (1948).

THEORY

For our experiment we have taken advantage of the simplicity of the borine carbonyl $J=0\rightarrow1$ transition near 17,960 Mc/sec. This rotational transition would produce a single absorption line were it not for the interaction of the nuclear electric quadrupole moment with the molecular electric fields. For a symmetric top molecule this energy of interaction is related to the molecular and nuclear parameters by[3]

$$E=-eqQ\left[1-\frac{3K^2}{J(J+1)}\right]\frac{\left[\frac{3}{4}C(C+1)-I(I+1)J(J+1)\right]}{2I(2I-1)(2J-1)(2J+3)}$$

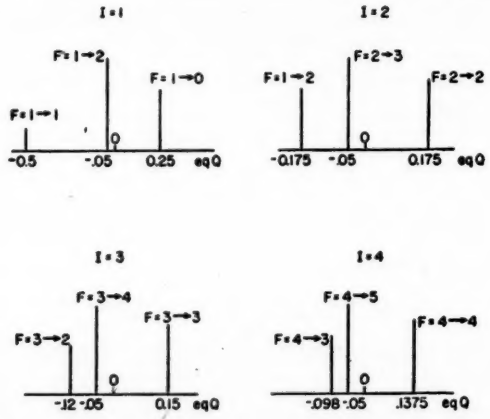

FIG. 2. Fine structure for $J=0\rightarrow1$ transition for several values of I.

[3] J. Bardeen and C. H. Townes, Phys. Rev. **73**, 97 (1948).

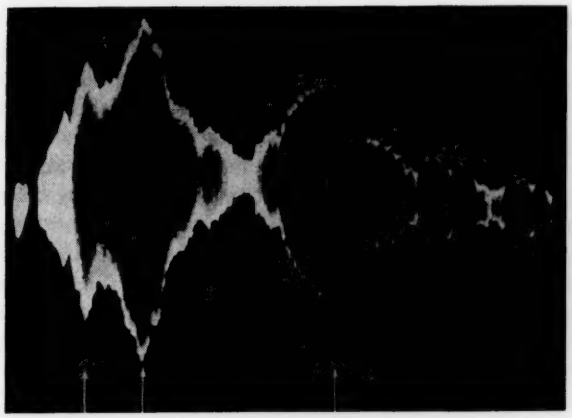

FIG. 3. Observed $J=0\rightarrow1$ transition.

where $C=F(F+1)-I(I+1)-J(J+1)$; F is the vectorial sum of I and J; and the other symbols have their usual meanings.[3]

The simplicity of the $J=0\rightarrow1$ pattern is due in part to the fact that for $J=0$ this quadrupole interaction is identically zero. Furthermore, although the $J=1$ level is split into six sub-levels, as shown in Fig. 1, the only observable transitions at our frequency are those terminating on the three levels with $K=0$.

Figure 2, drawn for positive eqQ, shows the resulting patterns for several possible values of I. If eqQ were negative, the frequency scale would be transposed. The relative intensities have been calculated from atomic multiplet intensities[4] by the customary association of quantum numbers: $L\rightarrow J$, $S\rightarrow I$, $J\rightarrow F$.

Even though the sign of eqQ is initially unknown, the ratio of the frequencies by which the two outer components are respectively separated from the inner component is a sensitive and unambiguous test for the spin I. For $I=1$, 2, 3, and 4 this ratio has the values 1.50 (0.667), 0.556, 0.350, and 0.257 respectively. In general this ratio is as follows:

$$\frac{2I+1}{(2I+1)I-1} \xrightarrow[I\rightarrow\infty]{} \frac{1}{I}.$$

Thus it is a decreasing function and therefore uniquely determines I.

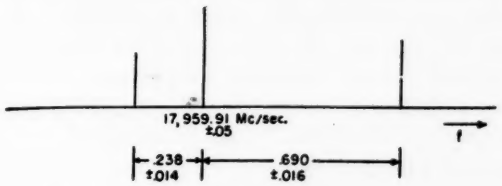

FIG. 4. Observed data.

EXPERIMENT

A previous attempt at this laboratory[5] to resolve the fine structure of the $J=0\rightarrow1$ transition of $H_3B^{10}CO$ failed because of sample decomposition at low pressures. In the present investigation, the wave guide absorption cell was kept at dry ice temperature, and by increased sensitivity in the detection system it was possible to resolve the three components with the sample at a pressure of about three microns. The power incident on the gas was also kept down to the order of two microwatts so as to prevent saturation. B^{10} occurred in natural abundance.

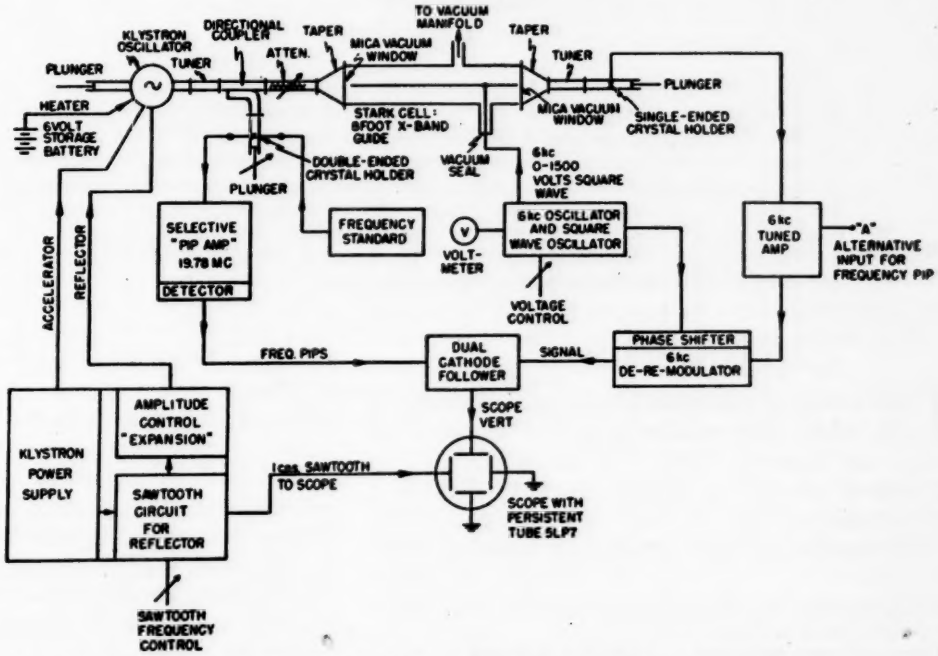

FIG. 5. Microwave spectroscope.

[4] H. E. White, *Introduction to Atomic Spectra* (McGraw-Hill Book Company, Inc., New York, 1934), p. 206.

[5] Strandberg, Pearsall, and Weiss, J. Chem. Phys. 17, 429 (1949). (The frequency stated in this reference is in error by about 1 Mc/sec. due to the particular absorption detection technique used in that experiment, but since discarded.)

Figure 3 shows a photograph of the observed lines with a compressed oscilloscope sweep so that all three lines are shown. In this photograph the oscilloscope sweep is somewhat non-linear. Accurate frequency measurements were made by the method described by Strandberg, Wentink, and Kyhl[6] wherein a precisely known frequency pip is superimposed on the absorption line. These measurements were made with a technique whereby differences in frequency are accurately determined, while the absolute values, not being of primary concern, were less precisely measured.

RESULTS

The observed data are shown in Fig. 4 and give a ratio of frequency differences of 0.345 ± 0.015. Comparison with the theoretical value of 0.350 proves that the B^{10} spin is 3. The quadrupole coupling, eqQ, for this molecule is determined to be $+3.44\pm0.1$ Mc/sec., as compared to the 3.30 ± 0.1 Mc/sec. reported in reference 1.

APPARATUS

The spectroscope used in this experiment is shown in Fig. 5 and is in many respects similar to the Stark modulation systems in common use elsewhere. Its distinguishing features include the use of an X-band wave guide gas cell and an adjustable zero-based 6-kc/sec. square wave modulating voltage. As is well known, the use of oversize wave guide affords higher resolution because of greater mean free path and reduced energy density. The comparatively low Stark modulation frequency simplifies instrumentation problems and apparently entails very little loss in sensitivity. The detecting system involves a high gain selective amplifier, a homodyne detector, resistance capacity filtering, and remodulation for convenience in oscilloscope viewing. The use of a persistent phosphor (P-7) tube improves the effective integrating time while retaining the many advantages of oscilloscopic observation. A recording milliammeter circuit is also provided, but was not used in the present experiment.

[6] Strandberg, Wentink, and Kyhl, Phys. Rev. **75**, 270 (1949).

ACKNOWLEDGMENT

We should like to acknowledge the use of a sample of diborane kindly supplied by Dr. L. B. McCarty of the General Electric Company, and to thank Miss Mary T. Westergaard for her assistance in the chemical preparation of the borine carbonyl.

PHYSICAL REVIEW VOLUME 78, NUMBER 3 MAY 1, 1950

Relative Nuclear Moments of H^1 and H^2.*

E. C. LEVINTHAL†
Stanford University, Stanford, California‡
(Received January 9, 1950)

An accurate determination of the relative moments of proton and deuteron has been carried out, using the techniques of nuclear induction, together with a measurement of the spin and the sign of the deuteron moment. The different line shapes of the proton and deuteron signals have been explained in terms of relaxation times and spins. Symmetrical signals have been obtained by a systematic way of introducing a homodyning signal of the correct phase. The symmetry of the separate and superimposed signals, and hence the occurrence of resonance at a common value of the d.c. magnetic field were determined by photographic analysis. The ratio of the moments of proton and deuteron has been found to be $\mu_P/\mu_D=3.257204\pm0.000015$ or $\mu_D/\mu_P=0.3070117\pm0.0000015$. The facts that the spin of the deuteron is $j=1$ and that the sign of its magnetic moment is positive have been verified.

I. INTRODUCTION

THE subject of this paper is a series of experiments in which the relative magnetic moments of proton and deuteron have been measured with an accuracy of one part in 150,000. A report of the first observations has been published.[1] Previously, the most accurate results had been obtained by molecular beam methods.[2] These determinations gave a precision of 1:3000.

One of the motives in obtaining a result of high accuracy was its bearing on the interpretation of the ground state of the deuteron, in connection with a measurement of the neutron moment in terms of that of the proton which has been carried out simultaneously in this laboratory.[3] A comparison of the results gives the difference between the deuteron moment and the algebraic sum of the moments of the proton and the

* This has been submitted in partial fulfillment of the requirements for a Ph.D. at Stanford University.
† Now at Varian Associates, San Carlos, California.
‡ Supported by grants from the Research Corporation and from the Joint Program of the ONR and AEC.
[1] Bloch, Levinthal, and Packard, Phys. Rev. **72**, 1125 (1947).
[2] Kellogg, Rabi, Ramsey, and Zacharias, Phys. Rev. **56**, 728 (1939).
[3] Bloch, Nicodemus, and Staub, Phys. Rev. **74**, 1025 (1948).

neutron. This deviation from additivity can appear for two independent reasons. First, there is the fact that the ground state of the deuteron is not a pure S-state, but rather a mixture of an S-state and a D-state. The deviation arising from this effect has been calculated by Rarita and Schwinger[4] and Bethe,[5] and is approximately equal to 0.02 nuclear magnetons. Second, there is a relativistic correction to the magnetic moment of the deuteron arising from the large velocities of the proton and the neutron in the deuteron.[6,7] This correction is not well known, since it depends strongly on the nature of the nuclear fields. Widely different estimates of the magnitude of the effect and even different signs of the effect have been obtained for different assumed interactions. According to Breit[7] the effect will presumably not exceed 0.01 nuclear magnetons. Even though the present knowledge of nuclear forces is insufficient to give a reliable answer, it seemed well worth while to determine the effect experimentally with considerable accuracy.

Another reason for carrying out the measurements with even greater precision is to permit an accurate comparison of the measured values of the hyperfine structure separation ν_D of deuterium, and the ratio of this separation to ν_H, that of hydrogen, with those values calculated from the measured magnetic moments. Both ν_D and ν_D/ν_H have been measured to a precision of $1:10^5$.[8] The discrepancy between the measured and calculated values of ν_D amounts to 0.26 percent and can be explained largely by a small additional electron spin magnetic moment.[9] With a comparable accuracy for the ratio of the magnetic moments of the proton and the deuteron as obtained from our measurements another discrepancy, of 0.017 percent, appears in the value of ν_H/ν_D. This has been explained by Bohr[10] as being due to the essential asymmetry in the interaction of the electron with the nucleons composing the deuteron. His results lead to a correction of 0.018 percent in the ratio ν_H/ν_D, agreeing very closely with the observed value.

The fact that nuclear moments can be measured with accuracies of the order of 1:100,000 has arisen from the discovery of the electromagnetic effects accompanying magnetic resonance.[11–13] The electromagnetic method is based on the observation by induction of the forced precession impressed upon nuclei, in a constant magnetic field, by an applied r-f field, and therefore has been termed nuclear induction. It is this method which has been used in the experiments discussed in this paper, to determine with high precision the ratio μ_D/μ_P of the magnetic moments μ_D and μ_P of deuteron and proton, respectively. Similar experiments yielding a somewhat lower accuracy have been performed by other investigators.[14–16]

If a substance containing nuclei with a magnetic moment is placed in a constant magnetic field it will have a resultant macroscopic moment proportional to the field. This is the result of the equilibrium distribution of the magnetic moments of the individual nuclei in the polarizing field. There is a characteristic time T_1, called the longitudinal relaxation time, which is a measure of how long one must wait after the application of the constant field for the establishment of this thermal equilibrium.

The resultant macroscopic magnetic moment of the nuclei will precess about the constant magnetic field H_0 at a frequency ω, called the Larmor precession frequency, where $\omega=\gamma H_0$ and γ, the gyromagnetic ratio, is the ratio of the nuclear moment to the angular momentum characteristic of the nuclei under consideration. A radiofrequency field at right angles to the constant field causes a forced precession of the total polarization vector around the constant field with decreasing latitude as the Larmor frequency approaches adiabatically the frequency of the radiofrequency field. Thus there results a component of the nuclear polarization at right angles to both the constant and the radiofrequency fields, and it can be shown that under normal laboratory conditions this component can induce observable voltages. Quantum-mechanically this is the result of transitions among the energy levels of the spin system, spaced in frequency by an amount $\omega=\gamma H_0$. The interaction between the moments of different nuclei, inhomogeneities in the external field and other causes lead to a finite width of the line. If this width, in terms of the magnetic field, is expressed by ΔH, one can relate it to a second time $T_2'=1/\gamma\Delta H$ which has been termed the transverse relaxation time.

According to the principle of nuclear induction outlined above, the experimental procedure requires a constant magnetic field H_0 to polarize the nuclear magnetic moments, a radiofrequency field to cause a change in orientation of the nuclear moments at resonance, and a method of detecting the consequent induced electromotive force in a coil surrounding the sample. The term "resonance" refers to the condition that the frequency of the radiofrequency field is equal to the Larmor precession frequency in the constant field.

The radiofrequency field is produced by a transmitter coil which contains the sample and which is at right angles to the receiver coil across which the voltage is induced by the precessing resultant nuclear magnetic moment. In order to know that this induced voltage is

[4] W. Rarita and J. Schwinger, Phys. Rev. **59**, 436 (1941).
[5] H. A. Bethe, Phys. Rev. **57**, 390 (1940).
[6] H. Margenau, Phys. Rev. **57**, 3031 (1940); P. Caldirola, Phys. Rev. **69**, 608 (1946); R. G. Sachs, Phys. Rev. **72**, 91 (1947); H. Primakoff, Phys. Rev. **72**, 118 (1947).
[7] G. Breit and I. Bloch, Phys. Rev. **72**, 135 (1947).
[8] J. E. Nafe and E. B. Nelson, Phys. Rev. **73**, 718 (1948).
[9] J. Schwinger, Phys. Rev. **73**, 416 (1948).
[10] A. Bohr, Phys. Rev. **73**, 1109 (1948).
[11] Purcell, Torrey, and Pound, Phys. Rev. **69**, 37 (1946).
[12] Bloch, Hansen, and Packard, Phys. Rev. **69**, 127 (1946); **70**, 474 (1946).
[13] F. Bloch, Phys. Rev. **70**, 460 (1946).
[14] W. R. Arnold and A. Roberts, Phys. Rev. **70**, 320 (1946); **71**, 878 (1947); *ibid.* **72**, 979 (1947).
[15] Bitter, Alpert, Nagle, and Poss, Phys. Rev. **72**, 1271 (1947).
[16] K. Siegbahn and G. Lindstrom, Nature **163**, 211 (1948).

caused by the nuclear moments it is essential that the signal due to the nuclei be varied, or modulated. This is accomplished by a small audiofrequency field in the direction of the field H_0 which then varies about its resonance value $H_0=\omega/\gamma$. Even though the transmitter and receiver coils are at right angles, they are not completely decoupled so that normally the transmitter field still produces a voltage across the receiver coil several orders of magnitude larger than the signal. A large part of this leakage voltage is canceled out by methods described in Sections II and III. Since it is desirable to heterodyne to some frequency lower than the resonant frequency, the leakage is not reduced to zero and is used as a source of local oscillator voltage. Hence we have a system of detection where the local oscillator and the signal to be observed are at the same frequency; this is sometimes referred to as homodyning in contrast to the more familiar heterodyne principle of detection. As a result of the audiofrequency modulation of the field, after detection we have an audio signal which can be amplified and presented on a cathode-ray tube whose horizontal plates give a deflection proportional to the variation in H_0.

In our method for measuring relative moments the observation of fine details is essential. This requires a better noise figure than that used in the original rather crude observation of proton signals and a somewhat more refined technique of observation which is described in the following sections.

II. METHOD

The principle used in these experiments is the same as that employed in the measurement of the relative moment of the proton and triton.[17] Highly accurate values for the relative moments are obtained by using a liquid sample containing a mixture of the two isotopes so that they are observed under identical conditions. A paramagnetic salt was dissolved in the sample to shorten the relaxation time. This sample is placed in a transmitter coil which produces two superimposed radiofrequency fields of different frequencies. The receiver is made to respond to the two frequencies simultaneously and designed so that the instantaneous sum of the two signals, received from both isotopes, is presented on an oscilloscope screen with a horizontal sweep, synchronous to the modulating field of the magnet. One of the two frequencies is then adjusted until resonance is observed for both nuclei at the same horizontal position on the screen and therefore at the same value of the magnetic field. For known spins the relative moments of the two isotopes are then determined directly from the ratio of the two frequencies.

In the case of the proton and triton the application of this method is greatly facilitated by the fact that their gyromagnetic ratios and their relaxation times in the same sample are nearly equal. One then obtains similar signals from the two isotopes and it is relatively easy to ascertain a common value of their resonance fields. This problem is considerably more difficult in the case of the deuteron since its gyromagnetic ratio γ_D is very different from γ_H, the gyromagnetic ratio of the proton, so that the signals from these two isotopes have very different shapes, and their sum has a complicated form. In order to obtain high precision, in such a case, one must carefully establish criteria which can be used to ascertain simultaneous resonance.

Such criteria are furnished by certain symmetry properties of the equations given by Bloch to describe the dynamics of a collection of nuclei in a homogeneous magnetic field.[18] Their solutions can generally be written as a sum of two terms known as the v and u components of the signal and characterized by their phase relationship with the rotating field H_1, the v component of the magnetic moment being in-phase and the u component ninety degrees out-of-phase with this field. Whether or not one observes the v or the u component of the signal or some linear combination of these depends on whether the phase of the leakage, or homodyning, signal used for detection is respectively in-phase, at ninety degrees, or at some other phase angle with respect to the r-f field. Under conditions of slow passage, the v component corresponding to absorption, gives a signal symmetrical with respect to resonance, while the u component corresponds to dispersion and gives an antisymmetrical signal.

In the case of the proton and the deuteron it is not feasible to work under conditions which result in slow passage observation for both isotopes, so that the above mentioned symmetry criterion for ascertaining resonance is not applicable. The solution of Bloch's equations and their more general symmetry properties are discussed in a paper by Jacobsohn and Wangsness.[18] They show that the two traces of the signal will appear symmetrical about the resonance point for the v component and antisymmetrical for the u component if the signal is observed on the screen of an oscilloscope, the horizontal sweep of which is synchronized with the field modulation and if this modulation is equal on either side of resonance. This property is independent of the magnitude of the r-f field H_1, the relaxation times T_1 and T_2, and the rate of change or the phase of the field modulation.

It is this symmetry of the v component which we have used as a criterion for ascertaining simultaneous resonance for protons and deuterons. The phase of the homodyning signal at the proton and deuteron frequencies is adjusted so that one observes only the v component of both signals. The proton resonance is then varied until, with both signals present, the pattern on the oscilloscope screen is symmetrical about a point at the center of the sweep, thus indicating that the two resonances occur at the same value of the field H_0.

[17] Bloch, Graves, Packard, and Spence, Phys. Rev. 71, 551 (1947).

[18] B. A. Jacobsohn and R. K. Wangsness, Phys. Rev. 73, 942 (1948).

There then remains only the problem of measuring the frequency difference and the deuteron resonance frequency to determine the relative magnetic moments. The details of this procedure and the determination of symmetry are discussed in Section IV.

The procedure outlined above is only directly applicable if the inhomogeneities in the magnetic field do do not affect the symmetry of the signals. The effect of these inhomogeneities can be determined by a careful photographic study of the shapes of the separate signals when these are due to the v component alone. Any asymmetry in these signals would be due to the field inhomogeneities. The magnitude of these inhomogeneities or the field gradient across the sample can be determined by a measurement of the relaxation time T_2 as a function of the concentration of the paramagnetic salt added to the sample. This allows one to separate the broadening of the line due to the field inhomogeneity from that due to the paramagnetic salt (see Section IV A).

It was found in this manner, that the variation of the magnetic field over the sample region amounted to about 1 part in 10^5. With this value, and using the asymptotic expression of Jacobsohn and Wangsness[18] for the v component, an estimate was made of the asymmetry of the signal for the case in which field distribution over the sample region has rotational symmetry about the center of the sample. It showed that the asymmetry due to field inhomogeneities would not increase the error in the final results by more than 2 percent so that it could be safely neglected. The absence of any noticeable asymmetry was also experimentally verified (see Section IV). The fact that inhomogeneities did not affect our precision was finally tested by ascertaining that the results were not changed when the sample was moved to a region of the magnet with significantly different inhomogeneities (see Section IV).

III. APPARATUS

The apparatus in principle is similar to that first described by Bloch, Hansen, and Packard.[12] The physical arrangement of the receiver and transmitter coils in the radiofrequency "head" closely resembles that shown in an article by Packard.[19] In these measurements of the relative magnetic moments of the proton and deuteron, as distinct from the proton and triton measurements, the gyromagnetic ratios of the two isotopes are quite different. Thus there will be a large difference in the magnitude of the signal and the resonant frequency of

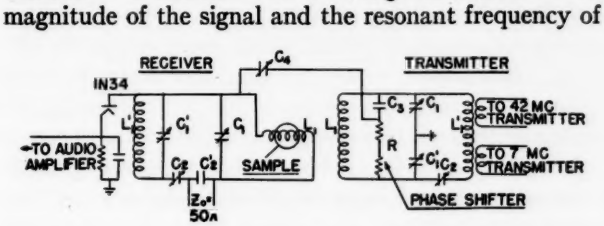

FIG. 1. Circuit of r-f head.

[19] M. E. Packard, Rev. Sci. Inst. 19, 435 (1948).

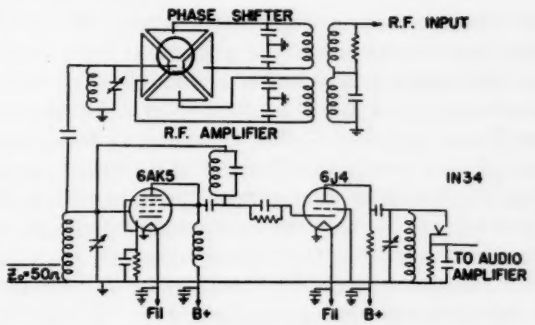

FIG. 2. R-F amplifier for deuteron signal.

the two isotopes. This difference required the use of a radiofrequency amplifier to make the signal-to-noise ratio due to the deuterons comparable to that due to the protons, and it necessitated two phase shifters to adjust the phase of the homodyning signal at both the proton and deuteron frequencies.

At the fields used, which were in the neighborhood of 10,000 gauss, the technique for the measurement of the relative moments of proton and deuteron required that the circuits respond simultaneously to frequencies of approximately 7 mc and 42 mc. This is accomplished by means of the doubly tuned circuits used in the r-f head and shown schematically in Fig. 1. The capacitors C_1, C_1', C_2, and C_2' are chosen such that both the receiver and the transmitter circuits resonate at 42 and 7 mc. The wide separation of these two frequencies allows almost independent tuning since the impedances of the coils L_1, and L_1', for the high frequency are large compared to that of C_2, and C_2' and for the low frequency small compared to that of C_1, and C_1'.

In order to locate the r-f amplifier conveniently outside the magnetic field, the 7-mc signal is fed through a 50-ohm cable to the amplifier. The function of the capacitor C_2' is to terminate this cable by its characteristic impedance Z_0. To accomplish this, C_2 and C_2' in the receiver circuit are related by the equation $Z_0/R_{sh}=[C_2/(C_2+C_2')]^2$, where R_{sh} is the shunt impedance of the receiver circuit at 7 mc. The 42-mc signal was directly rectified in a 1N34 crystal diode. The deuteron signal appeared here also but without r-f amplification so that it was small compared to the proton signal.

As pointed out in Section II, the method used here for the measurement of the relative moments of the proton and deuteron depends on the ability to observe only the v component of the proton and deuteron signal. This requires that any resistive component of the homodyning signal, which is ninety degrees out of phase with the r-f field, must be made sufficiently small so that the observed u component of the nuclear induction signal is negligible, and that the in-phase or reactive leakage is large compared to the signal. The magnitude of the reactive leakage is adjusted by means of a paddle originally described in the paper of Bloch, Hansen, and Packard.[12] The paddle is slightly rotated from its posi-

tion of minimum leakage to introduce the in-phase component of the homodyning signal at both frequencies. The resistive component of the 42-mc r-f leakage is cancelled by means of a phase sifter consisting of C_3 and R shown in Fig. 1. The capacitor C_3 consists of a turn of wire around the lead of the transmitter coil, while C_4 adjusts the amplitude of the leakage-cancelling signal fed into the receiver and consists merely of a wire whose distance from the receiver coil lead is variable. With the above-described phase shifter so adjusted as to cancel the resistive component at 42 mc, there remains the independent corresponding cancellation at 7 mc. This is achieved by means of the phase shifter,[20] external to the r-f head, shown in Fig. 2. The output voltage of this phase shifter is capacitively coupled to the r-f amplifier input.

The r-f amplifier, shown in Fig. 2 and used to improve the signal-to-noise ratio of the deuteron signal, is

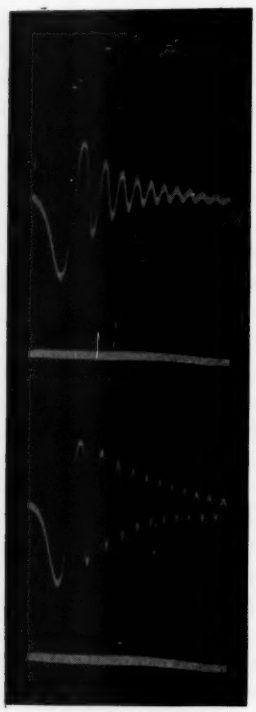

FIG. 3. Photographs for measurements of relaxation times of deuterons in 0.6-M and 0.2-M solutions of $MnSO_4$. (A) Time marker, (B) 0.6-M solution, (C) off resonance, (D) 0.2-M solution, (E) off resonance.

described in detail in an article by Wallman, Macnee, and Gadsden.[21]

Both the proton and deuteron signals are fed into a differential audio amplifier consisting of four push-pull stages of 6SL7. The audio amplifier has a low frequency half-power point at 20 cycles per sec. The half-power point at the high frequency end of the response can be adjusted to either 1000 c.p.s., 6000 c.p.s., or 25,000 c.p.s. The output of the audio amplifier is displayed in the usual manner on an oscilloscope with the horizontal sweep synchronous with the modulating field. In order to facilitate precise measurements of the form of the signals, photographs were taken with a camera fitted to the oscilloscope and using a Sonnar f1.5 lens with a 5-cm focal length.

The 7-mc transmitter uses a 6SJ7 as a 3.5-mc electron-coupled oscillator followed by a 6AG7 buffer stage which drives the output stage, an 815 used as a doubler. This supplies the r-f field for the transmitter coil as well as the signal for the external phase shifter. The 42-mc transmitter starts with a 6SJ7 electron-coupled oscillator operating at about 7-mc followed by a 6AG7 buffer and a 6L6 tripler. This drives the final doubler stage which uses an 815 tube.

Signals from the output of the 7-mc transmitter and from the electron-coupled oscillator of the 42-mc transmitter are introduced into a General Radio combined heterodyne frequency meter and crystal-controlled calibrator, model LR-1. The audio output of the heterodyne frequency meter is connected to the horizontal plates of an oscilloscope whose vertical plates are coupled to a Hewlett-Packard audio oscillator, model 200D. Combined with the setting on the herodyne frequency meter the resulting Lissajous pattern gives to within a few cycles the frequencies $\Delta=\frac{1}{6}\nu_P-\nu_D$ and ν_D, where ν_P is the proton and ν_D the deuteron resonance frequency. The audio oscillator was calibrated against the 440 audio modulation on the 10-mc WWV carrier.

IV. MEASUREMENTS

To achieve high precision the method, described in Section II for determining the relative moments of the proton and the deuteron, requires the observation of a common value of the resonance field for the two isotopes well within the region of field values over which the signals are extended. It was felt that such an observation, involving rather fine details in the shape of the signals, could not be completely trusted unless it was tested that the appearance of the signals was understood quantitatively.

One of the most striking features was the fact that the two isotopes, although contained in the same mixture and in the same modulated magnetic field, exhibited very different signal shapes. With a concentration of the paramagnetic salt $MnSO_4$, such that the v component of the proton signal appeared as a simple absorption curve, characteristic for relatively short relaxation time and consequently slow passage, the deuteron signal showed a great number of oscillations, following the passage through resonance. According to the theory of Jacobsohn and Wangsness,[18] this indicates that the relaxation time for deuterons is considerably longer than that of the protons, a fact which, in turn, can be understood in view of the different gyromagnetic ratios γ_D and γ_P and leads to the expectation that the relaxation time

[20] F. E. Terman, Radio Eng. Handbook, p. 949.
[21] Wallman, Macnee and Gadsden, Proc. I.R.E. 36, 700 (1948).

for the deuteron is $(\gamma_P/\gamma_D)^2$ times larger than that of the proton.[22]

The first set of the measurements was concerned with the verification of this fact and served at the same time as a test that the observed signals were correctly interpreted. A second related set, to verify that the spin of the deuteron is unity and that its magnetic moment is positive, served a similar purpose and was also undertaken to demonstrate the reliability of nuclear induction as a method for the determination of spin values. The third set of measurements dealt with the central purpose of this investigation, the determination of the relative magnetic moments of deuteron and proton.

A. Measurements of Relaxation Time

Our measurements refer to the transverse relaxation time T_2, although it can be safely assumed in this case to be equal to the longitudinal relaxation time, usually denoted as T_1.[22] In view of the very different characteristics of the proton and the deuteron signal, entirely different criteria had to be used for the determination of the respective relaxation times T_{2P} and T_{2D}. In the case of the proton, a 0.1-molar concentration of $MnSO_4$, was sufficient to give completely slow passage so that the relation $T_2=1/\Delta\omega$ between relaxation time T_2, and line width $\Delta\omega$ in circular frequency scale, could be used. The latter, which could be directly measured on the oscilloscope screen to an accuracy of ten percent, was observed as a function of the molar concentration of $MnSO_4$.

For the deuteron, on the other hand, the signals exhibited rapid passage characteristics even for saturated $MnSO_4$ solutions and particularly a series of pronounced oscillations after passage through resonance. Based on the theory of Jacobsohn and Wangsness,[18] it was here the damping rate of these oscillations which could be used as a convenient measure for T_{2D}.

Figure 3 illustrates the actual technique for measurement. The field modulation was a 60-c.p.s. sine function, but the oscilloscope sweep was a linear function of the time. Figures 3B and 3D are signals from 0.6-molar and 0.2-molar solutions of $MnSO_4$ in D_2O. Figures 3C and 3E are photographs of the signals with the field off the resonance value. The purpose of these photographs was to allow one to correct for any spurious 60 c.p.s. voltage. In taking these photographs the lens was stopped down to f4 and a 10-second exposure used. The width of the trace was approximately doubled by the introduction of a 100-kc voltage on the vertical plates. This, together with the 10-second exposure, gives considerable improvement in the effective signal-to-noise ratio.[23] By intensity-modulating the oscilloscope with 600 c.p.s. a set of time markers was recorded as illustrated in Fig. 3A.

The measurement of the exponential decrement of the maxima and minima of the oscillations about the slow passage value, shown in Figs. 3B and 3D gives the value of $1/T_2$ directly. This measurement was carried out for solutions of 0.2-, 0.6-, 1.0- and 1.8-molar $MnSO_4$ in D_2O, with the r-f head in a fixed position in the magnetic field. A plot of the corresponding experimental values of $1/T_2$ is given in Fig. 4.

A source of error in the above measurements can be the response of the audio amplifier. Care was taken to have the high frequency cut-off considerably larger than the largest value of $1/T_2$ to be measured. It was verified that this was indeed sufficient to avoid this error.

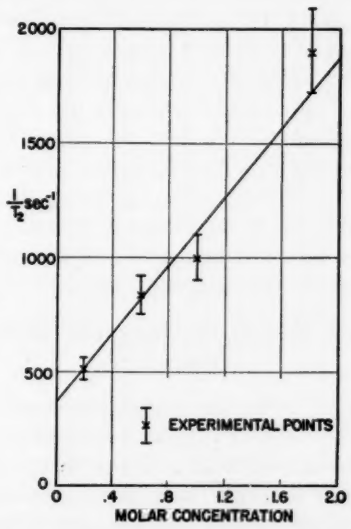

FIG. 4. Variation of $1/T_2$ as a function of $MnSO_4$ concentration in D_2O.

It also has to be kept in mind that the experimentally determined value of T_2 depends in general on the external magnetic field and in particular on the magnitude of the r-f field and the inhomogeneity of the d.c. field. By choosing a sufficiently small amplitude for the r-f field its influence on T_2 could be made negligible. In order to separate the influence of field inhomogeneities on T_2 from its "natural" value, mainly determined by the presence of $MnSO_4$, we made use of the fact that one has approximately

$$1/T_2=1/T_2'+1/T_2'', \tag{1}$$

where T_2 is the experimental value, T_2' the contribution caused by inhomogeneities in H_0, and T_2'' the "natural" value. Furthermore, using the fact that $1/T_2''$ can be expected to be proportional to the molar concentration, a plot of $1/T_2$ *versus* the latter should give a straight line whose intercept with the axis of the ordinate indicates $1/T_2'$ and whose elevation above this intercept gives $1/T_2''$.

The best fitting straight line is drawn in Fig. 4. It gives $1/T_2'=350$ sec.$^{-1}$ and a corresponding effective variation $\Delta H=1/\gamma T_2'=0.08$ gauss. It is this value corresponding to about 1 part in 10^5 of the total field $H_0=10{,}000$ gauss, which has been used in Section II

[22] Bloembergen, Purcell, and Pound, Phys. Rev. **73**, 679 (1948).
[23] F. Bloch and D. Garber (to be published).

TABLE I. Comparison of observed and calculated ratio of amplitudes.

Observed ratio of amplitudes	Calculated ratio of amplitudes	
0.67±0.06	$j=1/2$	0.23
	$j=1$	0.62
	$j=3/2$	1.15
	$j=2$	1.85

with the conclusion that this variation is sufficiently small not to affect the symmetry of the signals within the accuracy of our measurements.

The 1.0-molar concentration gives a value $1/T_2''=750\pm38$ sec.$^{-1}$. By comparison with the proton line width, equal to 2.5±0.25 gauss for the same molar concentration of $MnSO_4$, corrected also for $1/T_2'$ one obtains $T_{2D}''/T_{2P}''=43.2\pm6.5$. On the other hand, one has $(\gamma_P/\gamma_D)^2=42.3$. The fact that these two numbers agree within the experimental error can be considered both as a test of the underlying theory and as a proof that the difference in the shapes of proton and deuteron signals is a natural consequence of the corresponding difference in the gyromagnetic ratios.

B. Spin and Sign of the Magnetic Moment of the Deuteron

Observation of nuclear induction signals yields not only the gyromagnetic ratio of a nucleus in terms of the values of resonance field and frequency, but through the magnitude and sign of the signal gives also information concerning its spin and the sign of the magnetic moment.[13] While an absolute determination of the signal magnitude would be possible in principle, it is easier and more reliable to determine it relative to the signal of a nucleus with known spin. Similarly it is convenient in practice to determine the sign relative to the sign of a known moment. In our case protons were used as the standard of comparisons. For slow passage and for small r-f fields we have for the maximum value of the v component of the signal, $v=|\gamma|H_1T_2M_0$, where $2H_1$ is the amplitude of the r-f oscillating field and M_0 is the resultant nuclear magnetic moment per unit volume. Therefore if H_1 and ω are the same for both measurements one obtains for the ratio of the signals:

$$v_{\text{Deuteron}}/v_{\text{Proton}}=\gamma_DT_{2D}M_{0D}/\gamma_PT_{2P}M_{0P}$$
$$=j_D(j_D+1)\gamma_D^2T_{2D}N_D/j_P(j_P+1)\gamma_P^2T_{2P}N_P, \quad (2)$$

where $j_{P,D}$ refers to the spin and $N_{P,D}$ to the number of protons and deuterons, respectively. Thus with a sample with known concentrations of protons and deuterons and measured relaxation times, the spin can be determined. In such an experiment the sign of the moment would be indicated by the sign of the deuteron signal voltage relative to that of the proton.

Even with concentrations of $MnSO_4$ as large as 1.8 molar it was not possible in the case of the deuteron to achieve the slow passage condition with the 60-c.p.s. modulation field used. It was therefore necessary to apply corrections for the deviations from slow passage. The dependence of the amplitude of the v component on the parameter $a=\gamma dH_0/dt$, is given in the paper of Jacobsohn and Wangsness.[18] Using a 1.8-molar solution of $MnSO_4$ in a 1:3 mixture of D_2O and H_2O, the theoretical curves were checked against experimental values. The ratio of the first maximum to the first minimum was compared for the cases $a^{\frac{1}{2}}T_2=1$ and $a^{\frac{1}{2}}T_2=2$. The agreement was within 10 percent. With the frequency held constant and the r-f field fixed in the linear region for deuterium, thus changing merely the magnetic field, photographs were taken of the proton and deuteron signal. The modulation amplitude was adjusted so that $a^{\frac{1}{2}}T_2=1$ for the deuterons and $a^{\frac{1}{2}}T_2=0.1$ for the protons. The ratio of the amplitude was, after correcting for the deviation of the deuteron signal from slow passage conditions, 0.67 ±0.06.

Table I shows clearly that this ratio of amplitudes confirms the earlier determinations of the deuteron spin, being compatible only with the value unity. Although a half-integer spin cannot occur for the deuteron, the values $j=\frac{1}{2}$ and $j=\frac{3}{2}$ are included to show the uniqueness of the result.

Since the sign of the deuteron signal voltage was the same as that of the protons, the sign of the magnetic moment of the deuterons is determined to be positive. Although the spin and sign of the deuteron were known previously,[24,25] this independent verification serves as a good test that nuclear induction is reliable for such measurements, and as a quantitative check on the proper interpretation of the signal form.

C. Relative Moments of H^1 and H^2

As pointed out in Section II, in the discussion of the symmetry properties, the first step in determining the relative nuclear moments of H^1 and H^2 is to make certain that both the proton and deuteron signal are due to the v component alone. If, by means of the two phase shifters and the paddle, described in Section III, the leakage is made so small that no signal can be observed, and then the paddle is rotated, only an in-phase homodyning signal is introduced and one observes the in-phase or symmetrical v component alone of the two signals. With the phase shifters and the paddle, the homodyning signal was first adjusted so that the signal for both the proton and deuteron was no more than the noise. After rotating the paddle photographs were taken of the proton and deuteron signals. It was observed that the signals showed almost complete symmetry (see Section V). This demonstrates that the observations were carried out under the proper conditions. Such photographs of the separate signals were taken also at the middle and end of each run.

The next step in the procedure was to set the field

[24] G. M. Murphy and H. Johnston, Phys. Rev. **45**, 761 (1934).
[25] Kellogg, Rabi, and Zacharias, Phys. Rev. **50**, 472 (1936).

so that the center of symmetry of the deuteron signal was at the center of the trace on the oscilloscope screen and to measure for this field ν_D, the deuteron resonance frequency. The horizontal sweep of the oscilloscope and the field modulation were sixty-c.p.s. sine functions. The proton frequency ν_P, was adjusted to different values grouped around the frequency setting which was visually observed to make the superposition of the proton and deuteron signals approximately symmetrical (see Section II). For each of these values of the proton frequency a photograph was taken, and the frequency $\Delta=\frac{1}{6}\nu_P-\nu_D$ was measured. Off-resonance pictures alternating with the above photographs, were made to correct for distortions due to spurious voltages. The visual observations were made on an oscilloscope whose horizontal sweep was a sinusoidal function of the time. The horizontal sweep on the oscilloscope to which the camera was attached was a linear function of the time. The linear sweep was used to simplify the corrections due to the spurious voltages.

The frequency measurements were carried out as indicated in the discussion of the apparatus in Section III. The photographic technique was the same as that used for the measurements of the relaxation times. A photograph was made of a network of time markers on the oscilloscope. This permitted one to ascertain the absence of any noticeable distortions occurring because of photographic or enlarging processes. All photographs were enlarged by a factor of five and corrected for spurious signal voltages.

Figures 5B and 5D are photographs of the separate proton and deuteron signals, respectively. Figure 5F

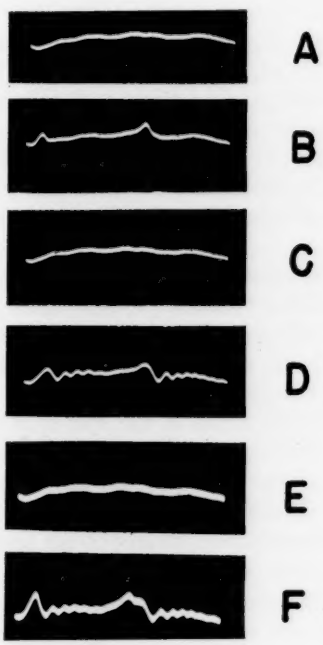

FIG. 5. Photograph of proton, deuteron, and superimposed signals. (A) Off resonance, (B) proton, (C) off resonance, (D) deuteron, (E) off resonance, (F) superimposed signals.

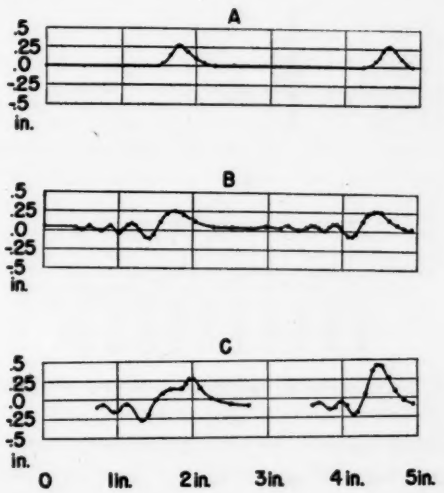

FIG. 6. Enlarged and corrected plots of proton, deuteron and superimposed signals of Fig. 5. (A) Proton, (B) deuteron, (C) superimposed signal.

shows the superimposed signals with $\nu_D=7.220160$ mc and $\Delta=0.619264$ mc. It is apparent from the asymmetry that resonance for the proton and the deuteron does not in this case occur at a common field. Figure 6 shows the proton, deuteron, and super-imposed signals of Fig. 5 after being enlarged and corrected.

In Section II it was stated that common resonance is indicated by the symmetry of the pattern if a sinusoidal sweep is used on the oscilloscope. The same criterion, using a linear sweep, is exhibited by the fact that the two separate signals appearing on the trace are identical. A quantitative method of comparison is to choose a criterion such as the difference in maximum amplitude of the two signals. This difference was measured for each value of Δ at which signals were observed. At the value $\Delta=\Delta^*$, for which this difference vanishes, resonance occurs at a common value of the field.

Figure 7 is a plot of this difference in maximum amplitude as a function of Δ for one of the sets of measurements with $\nu_D=7.220040$ mc. For two sets of measurements the difference in half-width of the two signals was used as another independent criterion in addition to the difference in maximum amplitude. The two differences both were zero, and thus indicated symmetry, for the same value of Δ.

From the enlarged curves of the separate signals a series of signals was calculated by adding these curves together for different values of Δ. Figure 8 illustrates some of these calculated curves. Each curve is the central portion of one of the calculated superimposed signals of the trace. The adjacent curves differ from each other by 52 cycles in Δ. These curves were then compared with the actual observed superimposed signals to show that these really represented the addition of two superimposed signals. Such a comparison is shown by the crosses, representing the observed superimposed signal, on curve 0 of Fig. 8. The *same* experimental points are

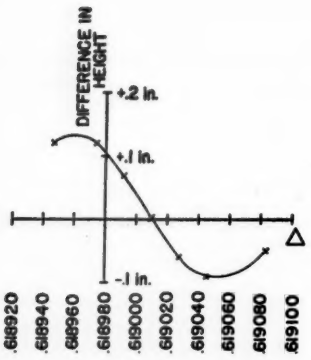

FIG. 7. Difference in height *versus* Δ for $\nu_D = 7.220040$.

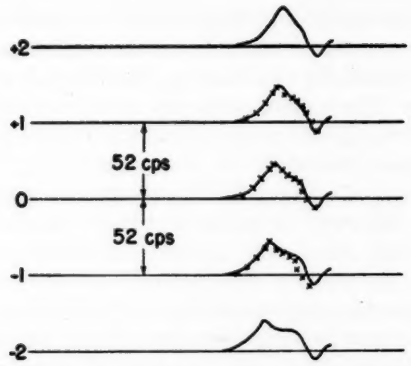

FIG. 8. Calculated superimposed signals.

indicated in curves +1 and −1 to demonstrate, in these cases, the lack of agreement or, in other words, the sensitiveness of the comparison as a function of Δ.

Three such sets of data were taken with the deuteron resonance frequency in the neighborhood of 7.22 mc. In one case the sample was purposely moved to a different part of the field sufficiently less homogeneous than that previously used so that the total relaxation time, T_2, of the deuteron signal was reduced by a factor of two. The agreement of the results shows that the calculations mentioned in Section II were correct in indicating that for the part of the signal used in determining μ_P/μ_D the contribution of the field inhomogeneities to the signal asymmetry could be neglected. A fourth set of data was taken with the deuteron resonance frequency at 6.3 mc. This was to determine, as well as the present apparatus permitted, whether or not μ_P/μ_D was dependent on the magnitude of the field H_0 in which it was measured.

All of these measurements were carried out with 1.5 cc of 0.1-molar solution of $MnSO_4$ in water, consisting of equal amounts of H_2O and D_2O. This concentration of paramagnetic salt was used since it gave the shortest relaxation time for the deuteron compatible with the absence of appreciable broadening of the proton signal.

V. PRECISION OF THE RESULTS

There are two aspects of the measurements that determine fundamentally the precision of the results. In the first place, there is the accuracy of the frequency measurements. Secondly, there is the limitation in determining the symmetry of the signals and thereby the common occurrence of resonance.

Any particular measurement of the deuteron resonance frequency ν_D could be made with an error of ±5 c.p.s. Taking into account the observed drift of this frequency throughout the course of a run, we find find that the error in ν_D equals ±50 c.p.s. This leads to an error in μ_P/μ_D of approximately $1:10^6$. The frequency difference Δ, which was measured simultaneously with each photograph of a superimposed signal, was measured with an accuracy of ±5 c.p.s., likewise giving an error in μ_P/μ_D of approximately $1:10^6$.

The error due to asymmetry enters in two ways: through asymmetry of the separate signals and, even in its absence, in the exact ascertainment of symmetry in the superimposed signal. The asymmetry of the separate signals can be caused by either a mixture of the u and v components of the signal or inhomogeneities of the field. It was estimated (see Section II) that the latter contribution to the asymmetry is negligible over the part of the signal used in the measurements. A ten percent mixture of the asymmetrical u component was calculated to give a shift corresponding to an error in Δ of ±15 c.p.s. One gets an experimental determination of this error due to both effects by measuring the asymmetry of the separate signals. We find that asymmetries of the proton and deuteron signal each contribute an error in μ_P/μ_D equal to $3:10^6$. This includes the error due to the finite limit of the precision with which the absence of asymmetry could be ascertained. From the enlarged photographs one is able to make measurements of the symmetry criteria, for example, the difference in maxima between the left- and right-hand trace of the signal, to a precision of 0.05 inch out of a value of approximately 1.5 inches for the magnitude of the signal amplitudes. From Fig. 8 one finds that this leads to an error in Δ equal to approximately ±15 c.p.s. Thus the three significant contributions to the error in μ_P/μ_D are all approximately the same, and equal to $3:10^6$.

It should be pointed out that it has been assumed that resonances for the two isotopes in a mixed sample occur in the same effective field. While this is true for the external field one may wonder whether, in analogy to the molecular beam magnetic resonance of the deuteron in HD, quadratic terms in the spin-spin interaction of neighboring hydrogen nuclei may not involve falsifying corrections. It has been pointed out to the author by Professor F. Bloch that the conditions of observation in a liquid are radically different from those in a highly rarefied gas used in the molecular beam. Whereas one deals in the molecular beam with well-defined rotational states of a single molecule during the time of observation, one may assume that, due to collision and exchange of deuterons by protons, and *vice versa*, the interactions between two neighboring hydrogen nuclei in a liquid

TABLE II. Results of four sets of measurements.

ν_D	Δ^*	$\mu_P/\mu_D=3(1+\Delta^*/\nu_D)$
7.220130 mc	0.619010±0.000025 mc	3.257202±0.000015
7.220160 mc	0.619030±0.000025 mc	3.257208±0.000015
7.220040 mc	0.619010±0.000025 mc	3.257205±0.000015
6.300130 mc	0.540134±0.000025 mc	3.257201±0.000015

undergo random interruptions at the rate of approximately 10^{12} per second. Consequently the interaction terms which are present in a given state of the HD molecule are largely cancelled out by the many interruptions which take place during a Larmor period τ_L. A qualitative estimate of the remaining effect is obtained by considering the effect of a weak disturbing field whose average value vanishes and which undergoes appreciable changes during a time of the order of τ. The resulting quadratic line shift is found, for $\tau \ll \tau_L$, to be reduced by a factor of the order $(\tau/\tau_L)^2$ from its "static" value, which would be obtained in the opposite limit $\tau \gg \tau_L$, i.e., if there were practically no interruptions during a Larmor period. Using the data for the second-order perturbations of the lines of D in D_2 and D in HD,[26] we get the "static" value as approximately 10 gauss. With $\tau \cong 10^{-12}$ sec. and $\tau_L=1.4\times10^{-7}$ sec., we come to the conclusion that for deuterons the relative shift, due to this effect, is of the order of 5×10^{-10}. Similarly, from the second-order perturbations of H in HD[26] and H_2[27] we get a correction of the order of 2×10^{-9}. It seems safe thus to neglect this effect even with our present high accuracy. Taking into account the errors of a particular set of measurements and the results at the two values of the field used, we can conclude experimentally that any such effect must be less than 1:30,000. It is noteworthy that Siegbahn[5] has made a larger variation in the fields used for his measurements. The agreement between his measurements at 3530 and 5700 gauss shows that any field dependence of the measured value of μ_P/μ_D is less than $4:10^6$.

VI. RESULTS

To obtain the ratio of the magnetic moments from the measured frequencies Δ^* and ν_D, one must remember that the spins of the protons and deuterons are $\frac{1}{2}$ and 1, respectively. One then has

$$\mu_P/\mu_D=\gamma_P/2\gamma_D=\nu_P/2\nu_D.$$

Or, with $\Delta^*=\frac{1}{6}\nu_P-\nu_D$,

$$\mu_P/\mu_D=3(1+\Delta^*/\nu_D). \quad (3)$$

Table II gives the results of the four sets of measurements. The third set of data was taken with the sample moved to a less homogeneous portion of the field.

The relative error of approximately $5:10^6$ has been estimated on the basis of considerations given in Section V. It is seen that the measurements are actually consistent to about $2:10^6$. Although this must be considered somewhat fortuitous, it indicates that the estimates of the error do not overstate the precision.

We find thus that the ratio of the moments of proton and deuteron is given by

$$\mu_P/\mu_D=3.257204\pm0.000015$$

or

$$\mu_D/\mu_P=0.3070117\pm0.0000015. \quad (4)$$

Although not all the detailed precautions reported in this paper were taken at that time, this result agrees with the value previously obtained and published.[1] The determination by Roberts[14] gave for μ_P/μ_D a value 3.25731 ± 0.00015, which within its large error agrees with the above value. The results of Bitter *et al.*[15] give $\mu_D/\mu_P=0.307021+0.000005$. The value obtained by Siegbahn[16] and Lindstrom is

$$\mu_D/\mu_P=0.3070183\pm0.0000015.$$

Our result with its given error lies outside the error limits given by both Bitter *et al.* and Siegbahn and Lindstrom. It is not possible on the basis of the present information available to explain this discrepancy. It should be pointed out, however, that in the experiments of Bitter *et al.* and of Siegbahn and Lindstrom separate samples were used for the protons and deuterons while in our experiments a mixed sample was used, with the advantage that both isotopes are certainly under the same external conditions, both with respect to the external field and its modification due to the paramagnetic salt.[28]

Using the absolute value of the magnetic moment of the proton,

$$\mu_P=(1.4100\pm0.0003)\times10^{-23} \text{ gauss cm}^3, \quad (5)$$

as recently measured by Thomas, Driscoll, and Hipple,[29] one finds

$$\mu_D=(0.43289\pm0.00009)\times10^{-23} \text{ gauss cm}^3. \quad (6)$$

From the recent work of Taub and Kusch[30] we have

$$\mu_P=(15.2106\pm0.0008)\times10^{-4} \text{ Bohr magnetons.} \quad (7)$$

This gives

$$\mu_D=(4.6698\pm0.0002)\times10^{-4} \text{ Bohr magnetons.} \quad (8)$$

In conclusion, I would like to thank Professor F. Bloch for suggesting these measurements and for his aid and encouragement during their performance.

[26] Kellogg, Rabi, Ramsey, and Zacharias, Phys. Rev. 57, 677 (1940).
[27] Kellogg, Rabi, and Ramsey, Phys. Rev. 56, 728 (1939).
[28] While this paper was in preparation Dr. Aage Bohr drew our attention to recent work of Bitter's group (M.I.T. Quarterly Progress Report (July 15, 1949), p. 29). The preliminary measurements with a mixed sample indicate results in agreement with ours.
[29] Thomas, Driscoll, and Hipple, Phys. Rev. 75, 902 (1949).
[30] H. Taub and P. Kusch, Phys. Rev. 75, 1481 (1949).

Nuclear Specific Heats in Paramagnetic Salts*

B. BLEANEY
Harvard University and Massachusetts Institute of Technology, Cambridge, Massachusetts†
(Received January 17, 1950)

This paper considers theoretically the contribution to the specific heat arising from the hyperfine structure, i.e., from the interaction of the magnetic moment and electric quadrupole moment of the nucleus with its surroundings. This contribution is important only at low temperatures, where it is approximately of the form A/T^2. The coefficient A is calculated for a number of copper, manganese, and cobalt salts. Agreement with the limited amount of experimental data available is reasonably good. The influence of the hyperfine structure on the magnetic susceptibility is negligible unless the temperature is exceedingly low, for even in single crystals it begins only with terms of the third order in a series development in $1/T$. In manganese ammonium sulphate, the electronic Stark splitting deduced from paramagnetic resonance at 20° and 90°K does not agree with that obtained from the paramagnetic anisotropy between 90° and 300°K.

IN paramagnetic salts where the nucleus of the paramagnetic ion possesses a spin, a hyperfine structure is observed in the paramagnetic resonance spectrum caused by interaction between the nucleus and the electron shell of the ion. This interaction consists of two parts; a magnetic interaction between the nuclear magnetic moment and the magnetic field due to the spin and the unquenched residual orbital momentum of the electron, and an electric interaction between the nuclear quadrupole moment and the gradient of the electric field produced by the electronic charge. Exact evaluation of these effects is difficult owing to the enormous crystalline electric field, but when the latter has axial symmetry it has been found that the Hamiltonian

$$AS_zI_z+B(S_xI_x+S_yI_y)+Q\{I_z^2-\tfrac{1}{3}I(1+1)\} \quad (1)$$

accounts for the observed hyperfine structure. (Here S and I refer to the electronic and nuclear spins, respectively.) The constants A, B, and Q can then be determined directly by microwave measurements.

The nuclear interaction gives rise to a hyperfine structure of the energy levels which affects the thermal properties of the salt at very low temperatures. An anomalous specific heat maximum should be observed below 1°K, the tail of which can be detected, for example, by paramagnetic relaxation measurements in the helium region (Benzie and Cooke[1]). This tail can be evaluated as a power series in $(1/T)$, of which the first term is

$$C/R=(1/T^2N^2)\{N\textstyle\sum_i W_i^2-(\sum_i W_i)^2\}(hc/k)^2,$$

where the W_i are the energy levels (in cm^{-1}) in zero magnetic field, and N is the total number of such levels $=(2S+1)(2I+1)$. The two terms $\sum_i W_i$ and $\sum_i W_i^2$ are simply the traces of the matrices for the energy and the square of the energy, and their evaluation yields the result

$$(CT^2/R)=(hc/k)^2\{(1/9)(A^2+2B^2)S(S+1)I(I+1)+(1/45)Q^2I(I+1)(2I-1)(2I+3)\}, \quad (2)$$

where A, B, and Q are in cm^{-1}.

This result may be applied to a number of salts where the constants A, B, and Q have been determined.

For the copper Tutton salts, measurements of Ingram[2] give

	A	B	Q	CT^2/R (calc.)
Copper ammonium sulphate	0.0133	0.0020	0.0009	1.2×10^{-4}
Copper rubidium sulphate	0.0119	0.0009	0.0011	1.0×10^{-4}.

The values of CT^2/R are in good agreement with the direct measurements of Benzie and Cooke,[1] which give 1.1×10^{-4}.

In cobalt salts, paramagnetic measurements by Bleaney and Ingram[3] and their interpretation by Pryce[4] show that the ground electronic state is a Kramers' doublet, which may be treated as a case of $S=\frac{1}{2}$. The value of I is 7/2. Two salts have been examined:

	A	B	CT^2/R (calc.)
Cobalt ammonium sulphate	0.024	0.0028	16×10^{-4}
Cobalt fluosilicate	0.020	0.0052	12×10^{-4}.

The magnitude of Q has not yet been determined, but appears to be small. Preliminary measurements of Benzie and Cooke give $CT^2/R=17\times10^{-4}$ for the cobalt ammonium sulphate.

In the case of manganese, the nuclear spin is 5/2, and the electronic spin is also 5/2. The electronic levels are split, and in the first approximation can be fitted by an additional term, suggested by Pryce,

$$D\{S_z^2-\tfrac{1}{3}S(S+1)\} \quad (3)$$

in the Hamiltonian. This will give a contribution to the specific heat similar to that due to the term in Q.

* This work was assisted by the ONR.
† Present address: Clarendon Laboratory, Oxford, England.
[1] R. J. Benzie and A. H. Cooke, Nature **164**, 837 (1949).
[2] D. J. E. Ingram, Proc. Phys. Soc. London **62A**, 664 (1949).
[3] B. Bleaney and D. J. E. Ingram, Nature **164**, 116 (1949).
[4] M. H. L. Pryce, Nature **164**, 117 (1949).

Preliminary analysis of two salts gives the values

	A	B	D	CT^2/R (calc.)
Manganese ammonium sulphate	0.009	0.009	-0.028	1.4×10^{-2}
Manganese fluosilicate	0.009	0.009	$+0.014$	0.7×10^{-2}.

The sign of D is determined from second-order effects in the paramagnetic resonance spectrum.

In manganese ammonium sulphate there appears to be a small departure from tetragonal symmetry, which would give an additional specific heat increasing the total by about 5 percent. This would bring it into agreement with preliminary measurements of Benzie and Cooke. No quadrupole term has been detected, and its contribution to the specific heat is probably negligible.

In general the signs of A, B, and Q have not yet been determined, but this does not affect the values of CT^2/R since only the squares are involved. Interpretation of adiabatic demagnetization measurements on these salts requires a knowledge of the energy level system in zero magnetic field, which cannot be given exactly without determination of these signs. Nevertheless it may be of interest to give the levels for copper ammonium sulphate, assuming A positive, for the alternative cases of Q having positive and negative signs. These levels are independent of the sign of B, but should be inverted on reversing all the signs.

	$Q=+0.0009$ cm^{-1}	$Q=-0.0009$ cm^{-1}
Doublet	0.0109 cm^{-1}	0.0091 cm^{-1}
Doublet	0.0027	0.0044
Singlet	-0.0022	-0.0004
Singlet	-0.0062	-0.0044
Doublet	-0.0093	-0.0110.

The over-all separation is 0.020 cm^{-1} in each case, and it seems that curves of entropy etc. will be almost independent of the signs of A, B, and Q until temperatures of the order of 0.01°K are reached.

For cobalt the level system consists of seven doublets and two singlets; for cobalt ammonium sulphate the relatively small value of B means that these may be approximately taken as eight equally spaced doublets with an over-all splitting of 0.084 cm^{-1}.

For manganese the system will contain 15 doublets and six singlets, the over-all splitting being about 0.3 cm^{-1} and 0.2 cm^{-1} for the ammonium sulphate and fluosilicate respectively.

SUSCEPTIBILITY

The diagonal sum method may be applied to the calculation of the susceptibility as a power series in $1/T$. It turns out that the hyperfine structure leaves the term in $1/T$ unaltered, and introduces no term in $(1/T)^2$ even for a single crystal. Thus the hyperfine structure cannot be detected by the presence of an effective "Weiss constant" in the susceptibility.

This behavior contrasts with that due to an electronic splitting, which gives rise to terms in $(1/T)^2$ in the principal susceptibilities. With the Hamiltonian (3) above one finds

$$\chi_{\parallel}=\frac{Ng_{\parallel}^2\beta^2S(S+1)}{3kT}\left\{1-\frac{D(2S-1)(2S+3)}{15kT}\right\}$$
$$\chi_{\perp}=\frac{Ng_{\perp}^2\beta^2S(S+1)}{3kT}\left\{1+\frac{D(2S-1)(2S+3)}{30kT}\right\}. \quad (4)$$

The second-order terms average to zero for a powder, as pointed out by Van Vleck and Penney.[5]

These formulas may be used to obtain an independent estimate of D for manganese. The best measurements of anisotropy in manganese ammonium sulphate are those of Krishnan, Mookherji, and Bose[6] between room temperature and 90°K. With two ions in unit cell, two interpretations are possible, giving $D=-0.057$ cm^{-1} or $+0.059$ cm^{-1}. These are clearly too large, as the specific heat due to the electronic splitting alone would then be greater than that observed in the undiluted salt.[7,8] Moreover the paramagnetic measurements resolve the ambiguity of interpretation, and show that the measured anisotropy corresponds to $D=+0.059$ cm^{-1}, i.e., that the sign is wrong. As however the maximum anisotropy observed was about 1 in 400, the discrepancy is not surprising.

This work was carried out during a visit to Harvard and to Massachusetts Institute of Technology made possible by the generosity of these universities, for which the author wishes to record his gratitude.

---

[5] J. H. Van Vleck and W. G. Penney, Phil. Mag. 17, 961 (1934).
[6] Krishnan, Mookherji, and Bose, Phil. Trans. A238, 125 (1939).
[7] A. H. Cooke, Proc. Phys. Soc. London 62A, 269 (1949).
[8] R. J. Benzie and A. H. Cooke, Proc. Phys. Soc. London (to be published).

Neutron-Deuteron Scattering at High Energies*

FREDERIC DE HOFFMANN†
Lyman Laboratory of Physics, Harvard University, Cambridge, Massachusetts
(Received August 23, 1949)

Stationary-state perturbation theory is applied to the problem of *n-d* scattering at high neutron energies. The Born approximation is used and exchange, but not tensor, forces are considered. It is shown that the *n-d* cross section, even in the case of general exchange forces, is made up of three distinct contributions: the cross sections for the scattering of the incoming neutron from the bound proton or neutron, respectively, averaged over the momentum distribution of the particle in the deuteron; and the cross-terms due to interference and the Pauli principle.

THIS paper is an attempt to establish a general formulation for the *n-d* cross section at high energies, assuming an exchange but not a tensor type of nuclear interaction and using the Born approximation. The usual time-dependent perturbation theory leads to some difficulties when applied to this problem. Hence our emphasis shall be to show that a stationary-state perturbation theory, using a symbolic expansion for certain operators, can be used to derive the desired formulas.

It will be shown that one can always split the *n-d* cross section into three parts: (1) the cross section for the scattering of the incoming neutron from the bound proton, averaged over the momentum distribution of the proton in the deuteron; (2) the cross section for the scattering of the incoming neutron from the bound neutron, averaged over the momentum distribution of the neutron in the deuteron; (3) cross-terms due to interference because of the presence of two scattering centers and due to the operation of the Pauli principle.

We shall illustrate our method by treating the problem with Wigner forces alone, i.e., we assume no exchange forces of any kind.

I. WIGNER FORCES

In order to effect the separation of the scattering from the proton and the neutron, we shall retain the laboratory system of coordinates, although we occasionally make use of the relative coordinates between any two of the particles.

Let particles 1, 2, and 3 denote the bound proton, bound neutron, and incoming neutron, respectively, each of mass M. Then the coordinates are designated $\mathbf{r}_1$, $\mathbf{r}_2$, and $\mathbf{r}_3$, respectively.[1] We shall further introduce relative coordinates between particles 1 and 2, i.e.,

$$\mathbf{r}=\mathbf{r}_1-\mathbf{r}_2. \tag{1}$$

Introduce the following momenta in the laboratory system.

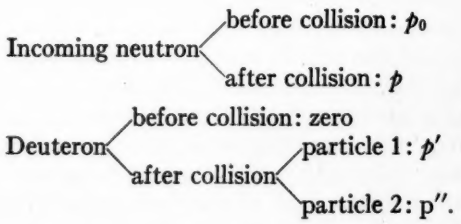

We define $\psi_i(\mathbf{r}, t)$ and $\psi_f(\mathbf{r}, t)$, respectively, as the initial and final wave function of the three-particle system. Further, E_f and E_i are total final and total initial energies of the system. We shall have occasion to use the quantity E_f^0, the final energy of binding between particles 1 and 2. Thus we have

$$E_f^0=(1/2M)(p^2+p'^2+p''^2), \tag{2}$$

$$E_i=(p_0^2/2M)-\epsilon, \tag{3}$$

where M is the average mass of the nucleons and ϵ is the binding energy of the deuteron.

It turns out that, if we wish to find an expression for σ_{nd} by means of the usual time-dependent perturbation theory, this procedure leads to difficulties when the Pauli principle is considered. These arise from the fact that, in such a treatment, the small magnitude of the potential between the particles in the deuteron, compared to the Hamiltonian of the entire system, is considered at a very late stage of the treatment. We shall here use a stationary-state perturbation theory that makes use of this fact as early as possible.

Denote the nuclear potential between neutron and proton by $V_{np}(\mathbf{r}_1-\mathbf{r}_2)$, and set

$$V_{nd}=V_{np}(\mathbf{r}_1-\mathbf{r}_3)+V_{nn}(\mathbf{r}_2-\mathbf{r}_3). \tag{4}$$

Also introduce the notation

$$H=H_0+V_{12}, \tag{5}$$

where

$$H_0=(-\hbar^2/2M)(\nabla_1^2+\nabla_2^2+\nabla_3^2) \tag{6}$$

and

$$V_{12}=V_{np}(\mathbf{r}_1-\mathbf{r}_2). \tag{7}$$

The wave function ψ of the entire system will be understood to contain a spin-dependent part, but the

* This paper is based on a portion of a thesis presented in partial fulfillment of the requirements for the Degree of Doctor of Philosophy in the Department of Physics at Harvard University.

† Now at Los Alamos Scientific Laboratory, Los Alamos, New Mexico.

[1] We shall omit making a distinction between the writing of vectorial and scalar quantities, since the meaning should be clear from the context.

potentials are spin-independent. Thus, let

$$\psi=\exp[-(i/\hbar)(E_i+i\eta)t]\phi, \tag{8}$$

i.e., ϕ describes the wave function with the time suppressed. Here η denotes a small imaginary contribution to the energy E_i, and eventually we shall let η go to zero. In essence then, η will serve as a convergence factor in our integrations. Thus,

$$(E_i+i\eta)\phi=(H+V_{nd})\phi. \tag{9}$$

Thus, if we write ϕ_i for the solution of the homogeneous equation corresponding to Eq. (9), we may write symbolically

$$\phi=\phi_i+\frac{1}{E_i-H+i\eta}V_{nd}\phi. \tag{10}$$

If we set

$$\phi=\phi_i+\phi_{sc} \tag{11}$$

and recall Eq. (8), we get, in the Born approximation,

$$\phi_{sc}=\frac{1}{E_i-H_0+i\eta-V_{12}}V_{nd}\phi_i. \tag{12}$$

Expanding, because V_{12} is so small, we find

$$\phi_{sc}=\left[\frac{1}{E_i-H_0+i\eta}+\frac{1}{E_i-H_0+i\eta}V_{12}\frac{1}{E_i-H_0+i\eta}\right]V_{nd}\phi_i. \tag{13}$$

Thus, we find that ϕ_{sc} gets broken up into a main term and a correction term to it.

Now we examine the commutability of H_0 and V_{12}. We know that

$$(H_0V_{12}-V_{12}H_0)_{EE'}=(E-E')(V_{12})_{EE'}, \tag{14}$$

where E and E' are eigenvalues of H_0. Now if we choose any model for V_{12} (say a Yukawa potential, for instance), we see at once that $(V_{12})_{EE'}$ is significant[2] only when $E-E'<\langle p_d^2\rangle_{Av}/M$. Thus $[H_0, V_{12}]$ is almost but not quite zero. Consider now, however, that V_{12} occurs only in the correction term of (13). Thus the noncommutability of V_{12} with H_0 is only a correction to the correction and we shall ignore this in the approximation to which we are working.

Recall now that, for the purpose of this section, we have assumed only Wigner potentials so that V_{12} and V_{nd} commute. Further, V_{nd} and H_0 commute, so far as the second term of (13) is concerned, by an argument analogous to that presented above for V_{12} and H_0. Thus ϕ_{sc} becomes

$$\phi_{sc}=\frac{1}{E_i-H_0+i\eta}V_{nd}\left\{1+\frac{1}{E_i-H_0-i\eta}V_{12}\right\}\phi_i. \tag{15}$$

[2] Here we have set $p''=p_d$ to indicate more clearly that we are dealing with the relative energy in the deuteron.

Now we may set

$$V_{12}\phi_i=(-\epsilon-T_{12})\phi_i, \tag{16}$$

where T_{12} is the kinetic-energy operator corresponding to the potential operator V_{12}. Now re-express ϕ_i as a superposition of plane waves:

$$\phi_i=\frac{1}{W^2}\exp\left(\frac{i}{\hbar}p_0\cdot r_3\right)\chi(r_1-r_2), \tag{17}$$

where we recognize $\chi(r_1-r_2)$ to be the wave function of the deuteron and W denotes a large volume to which we normalize. Thus if we denote the momentum transform of $\chi(r)$ by $\Phi(p'')$, we may write

$$\phi_i=\frac{1}{W^2}\frac{\exp\left[\frac{i}{\hbar}p_0\cdot r_3\right]}{\hbar^3}\times\int\exp\left[\frac{i}{\hbar}p_d\cdot(r_1-r_2)\right]\Phi(p_d)dp_d. \tag{18}$$

Hence,

$$T_{12}\phi_i=T_{12}(p_d)\phi_i, \tag{19}$$

where

$$T_{12}(p_d)=p_d^2/M. \tag{20}$$

Symbolically we may write

$$\phi_i=\sum_m a_m\exp\left[\frac{i}{\hbar}p_{dm}(r_1-r_2)\right]=\sum_m\phi_{im}, \tag{21}$$

so that

$$\phi_{sc}=\sum_m\frac{1}{E_i-H_0+i\eta}V_{nd}\left\{1-\frac{T_{12}(p_{dm})+\epsilon}{E_i-H_0+i\eta}\right\}. \tag{22}$$

If now we write $E_i=E_i^0-\epsilon$ and recall that T_{12} is small, we may say that

$$\phi_{sc}=\sum_m\frac{1}{E_i^0+T_{12}(p_{dm})-H_0+i\eta}V_{nd}\phi_{im}, \tag{23}$$

where we have permuted V_{nd} in analogy with our previous argument.

We must now meet the condition laid down by the Pauli principle and antisymmetrize the wave function ϕ in particles 2 and 3. Let us call the antisymmetrized wave function $\phi=\phi_i+\phi_{sc}$. Then denoting the particles in the deuteron by a bar, we have

$$\phi_i=\frac{1}{\sqrt{2}}[\phi_i(3,\overline{12})-\phi_i(2,\overline{13})], \tag{24}$$

$$\phi_{sc}=\frac{1}{\sqrt{2}}[\phi_{sc}(3,\overline{12})-\phi_{sc}(2,\overline{13})]. \tag{25}$$

The fact that the normalization constant of ϕ is indeed $1/\sqrt{2}$ to an approximation consistent with the solution of our problem is proved in Appendix B.

The derivation of the cross section now proceeds as follows: the probability of finding the system in a certain final state "f," where the deuteron is disrupted and all three particles have certain definite momenta, is given by

$$|b_f|^2=|(\psi_f^0, \psi_{sc})|^2 \tag{26}$$

or

$$|b_f|^2=\exp(2\eta t/\hbar)|(\phi_f^0, \phi_{sc})|^2. \tag{27}$$

Thus the total transition probability is given by

$$\omega=\frac{\partial}{\partial t}\int|(\phi_f^0, \phi_{sc})|^2\rho_{Ef}\exp(2\eta t/\hbar)dE_f, \tag{28}$$

where ρ_{Ef} is the density of states with energy E_f, i.e.,

$$\rho_{Ef}dE_f=W^3dpdp'dp''/h^9. \tag{29}$$

Hence,

$$\sigma_{nd}=\tfrac{1}{6}\textstyle\sum_i(W/p_0/M)(\partial\omega/\partial t), \tag{30}$$

where the factor $\frac{1}{6}\sum_i$ merely expresses the fact that we must average over the six equally likely initial spin states of a three-nucleon system.

Our next task, therefore, is the evaluation of the quantity $|(\phi_f^0, \phi_{sc})|^2$. For this purpose, we shall recall that, by Eq. (23), ϕ_{sc} involves V_{nd} and, further, that V_{nd} is made up of V_{np} and V_{nn} [see Eq. (4)]. Thus there will be contributions to ϕ_{sc} from V_{np} and V_{nn} which we shall denote by ϕ_{sc}^A and ϕ_{sc}^B, respectively. These will give rise to contributions to σ_{nd} which will be denoted by σ_A and σ_B, respectively. In addition, σ_{nd} will have a cross-term σ_C arising from the mixing of ϕ_{sc}^A and ϕ_{sc}^B. We shall first consider σ_A.

1. Evaluation of σ_A

Here we need to examine

$$(\phi_f^0, \phi_{sc}^A)=\left(\phi_f^0, \frac{1}{\sqrt{2}}\sum_m\frac{1}{E_i^0+T_{12}(p_{dm})-H_0+i\eta}V_{np}\phi_{im}\right)$$

$$-\left(\phi_f^0, \frac{I_{23}}{\sqrt{2}}\sum_k\frac{1}{E_i^0+T_{12}(p_{dk})-H_0+i\eta}V_{np}\phi_{ik}\right). \tag{31}$$

Now examine the first matrix element in (31). This involves the wave function

$$\phi_f^0\sim\exp\left[\frac{i}{\hbar}(p'\cdot r_1+p''\cdot r_2+p\cdot r_3)\right], \tag{32}$$

$$\phi_{im}^{0*}\sim\exp\left[\frac{i}{\hbar}p_{dm}(r_2-r_1)\right]. \tag{33}$$

We see that the momentum of coordinate r_2 is unchanged, and thus

$$p_{dm}=p''. \tag{34}$$

Further, the second matrix element of (34) involves ϕ_f^0 and $I_{23}\phi_{ik}$, and again the momentum of coordinate r_2 is unchanged, yielding

$$p_{dk}=p''. \tag{35}$$

We may therefore rewrite (34) as

$$(\phi_f^0, \phi_{sc}^A)=\left|\left(\phi_f^0, \frac{(1-I_{23})}{\sqrt{2}}V_{np}\phi_i\right)\right|^2$$

$$\times\left|\frac{1}{E_i^0+T_{12}(p'')-E_f^0+i\eta}\right|^2. \tag{36}$$

Now let us permit η to approach zero. Use the relation

$$\lim_{\eta\to 0}\frac{\eta}{x^2+\eta^2}=\pi\delta(x). \tag{37}$$

Then

$$\sigma_A=\frac{1}{6}\sum_i\left(\frac{W}{p_0/M}\right)\frac{2\pi}{\hbar}\int\frac{|(\phi_f^0, (1-I_{23})V_{np}\phi_i)|^2}{2}$$

$$\times\delta\left(\frac{p^2+p'^2-p''^2-p_0^2}{2M}\right)\rho_{Ef}dE_f. \tag{38}$$

Now note that $(1-I_{23})$ may be applied to ϕ_f^0 by virtue of the commutability of $(1-I_{23})$ with H_0. Further, we have the operator

$$(1-I_{23})^2=2(1-I_{23}), \tag{39}$$

so that

$$\frac{|(\phi_f^0, (1-I_{23})V_{np}\phi_i)|^2}{2}=|(\phi_f^0, V_{np}\phi_i)|^2$$

$$-(\phi_f^0, V_{np}\phi_i)(\phi_i, V_{np}I_{23}\phi_f^0). \tag{40}$$

In analogy with Eq. (40), we shall break up σ_A into σ_{A1} and σ_{A2}.

First examine σ_{A1}. Since it is our aim to reduce this cross section to one equivalent to the collision of two particles, we must reduce out the extraneous space coordinate r_2 referring to the neutron not concerned in $V_{np}(r_1-r_3)$. For this purpose, let

$$\phi=\phi'\nu, \tag{41}$$

where ν denotes the spin function of the three-particle system.

Using Eq. (1), the momentum transform for $\chi(r)$, writing the δ-function in terms of its integral representation, and finally replacing $-p''$ by p_d, we get

$$\sigma_{A1}=\frac{1}{6}\sum_i\sum_f\frac{M}{\hbar h^6p_0W}\int\left|\int\Gamma_f\nu_fV_{np}(r_1-r_3)\Gamma_i\nu_idr_1dr_3\right|^2$$

$$\times|\Phi(p_d)|^2\exp[(i\lambda/2M)(p^2+p'^2-p_d^2-p_0^2)]$$

$$\times d\lambda dpdp'dp_d, \tag{42}$$

where

$$\Gamma_f=\exp[-(i/\hbar)(p\cdot r_3+p'\cdot r_1)], \tag{43}$$

$$\Gamma_i=\exp[+(i/\hbar)(p_0\cdot r_3+p_d\cdot r_1)]. \tag{44}$$

On the other hand, consider now the collision of a neutron of momentum p_0 with a proton of momentum p_d. It is easily verified that, in the Born approximation, the cross section for this two-particle collision is given by

$$\sigma_{nd}(p_0-p_d)=\frac{1}{4}\sum_i\sum_f\frac{M}{\hbar h^6|p_0-p_d|W}\times\int\left|\int\Gamma_f\xi_f V_{np}(r_1-r_3)\Gamma_i\xi_i dr_1dr_3\right|^2\times\exp[(i\lambda/2M)(p^2+p'^2-p_0^2-p_d^2)]d\lambda dpdp', \quad (45)$$

where ξ is the spin wave function of this two-particle system, each particle having spin $\frac{1}{2}$.

In case V_{np} is spin-independent, it is evident that[3]

$$\tfrac{1}{6}\sum_i\sum_f|(\nu_f|V_{np}|\nu_i)|^2=\tfrac{1}{4}\sum_i\sum_f|(\xi_f|V_{np}|\xi_i)|^2. \quad (46)$$

Thus we see that

$$\sigma_{A1}=\int\frac{|p_0-p_d|}{p_0}\sigma_{np}(p_0-p_d)|\Phi(p_d)|^2dp_d, \quad (47)$$

i.e., $\sigma_{A1}=\langle\sigma_{np}\rangle_{Av}$, where $\langle\sigma_{np}\rangle_{Av}$ expresses the cross section for the collision between the incoming neutron of momentum p_0 with the proton of momentum p_d averaged over the momentum distribution of the proton.

It may be worth noting in passing that $\langle\sigma_{np}\rangle_{Av}$ can be expanded for the case of high p_0, to yield

$$\langle\sigma_{np}\rangle_{Av}=\sigma_{np}(p_0)+\tfrac{1}{6}(\langle p_d^2\rangle_{Av}/p_0^2)(d^2/dp_0^2)\{p_0^2\sigma_{np}(p_0)\}. \quad (48)$$

An examination of σ_{A2} shows that it is a correction term arising in the Pauli principle treatment only by virtue of the finite binding between particles 1 and 2. We can easily verify that σ_{A2} vanishes for the case of no binding between particles 1 and 2. This is a result we must require physically, since the mere presence of the extra neutron number 2 should not influence the *n-p* scattering in the case where we have three free particles.

2. Evaluation of σ_B

By an analogous but slightly more involved treatment than that for σ_A, we can show that

$$\sigma_B=\int\frac{|p_0-p_d|}{p_0}\sigma_{nn}(p_0-p_d)|\Phi(p_d)|^2dp_d, \quad (49)$$

where $\sigma_{nn}(p_0-p_d)$ represents the Born cross section for the collision of a neutron of momentum p_0 with a neutron of momentum p_d, taking due account of the Pauli principle operating between the two neutrons. Thus $\sigma_B=\langle\sigma_{nn}\rangle_{Av}$.

[3] Actually, it can be proved that relation (46) holds for any potential where the spin-dependent part is of the form $(\gamma_1+\gamma_2\sigma_1\cdot\sigma_3)$.

3. Cross-Term

The cross-term with which we are left is given by an expression that involves the product of two matrix elements of type (31), with the first one containing V_{np} and the second one V_{nn}. Thus the first matrix element yields $P_{dm}=p''$ and the second one $p_{dn}=p'$, which seems to present complications. Recall now, however, that the cross-term is of the order of a correction term to σ_{nd}. In first approximation, therefore, we may set $p_{dn}=p_{dm}$ and obtain

$$\sigma_C=\frac{1}{6}\sum_i\left(\frac{W}{p_0/M}\right)\frac{2\pi}{\hbar}Re\int(\phi_f^0,(1-I_{23})V_{np}\phi_i)\times(\phi_f^0,(1-I_{23})V_{nn}\phi_i)^*\times\delta\left(\frac{p^2+p'^2-p''^2-p_0^2}{2M}\right)\rho_{Ef}dE_f. \quad (50)$$

Professor Hans A. Bethe has recently shown[4] that this cross-term can be evaluated in good approximation using elementary interference theory. The method used in this evaluation corresponds to neglecting the second term in Eq. (48) and the corresponding term in the expression for the *n-n* portion. In particular, Professor Bethe finds that the interference term depends strongly on the spin dependence of the forces. For the case of spin independence, the cross-term is of the order of σ_{nn}. Assuming a reasonable spin dependence, he finds that the cross-term is probably smaller than σ_{nn}.

II. SPIN AND SPACE EXCHANGE FORCES

Let us consider the potentials to be given by

$$V_{np}(r_1-r_3)=(a_1+b_1\sigma_1\cdot\sigma_3)(c_1+d_1P_{13})A_{np}(r_1-r_3), \quad (51)$$

$$V_{nn}(r_2-r_3)=(a_2+b_2\sigma_2\cdot\sigma_3)(c_2+d_2P_{23})B_{nn}(r_2-r_3), \quad (52)$$

where P stands for space exchange. In this case, ϕ_{sc} is more complicated and may be written as

$$\phi_{sc}=\phi_{sc,0}+\phi_{sc,\lambda}, \quad (53)$$

with

$$\phi_{sc,0}=\frac{1}{\sqrt{2}}\sum_m\frac{1}{E_i^0+T_{12}(p_{dm})-H_0+i\eta}V_{nd}\phi_{im}-\frac{1}{\sqrt{2}}I_{23}\sum_k\frac{1}{E_i^0+T_{12}(p_{dk})-H_0+i\eta}V_{nd}\phi_{ik} \quad (54)$$

and

$$\phi_{sc,\lambda}=\frac{(1-I_{23})}{\sqrt{2}}\left(\frac{1}{E_i^0-H_0+i\eta}\right)^2[V_{12},V_{nd}]\phi_i. \quad (55)$$

Thus the cross section is proportional to

$$|(\phi_f^0,\phi_{sc})|^2=|(\phi_f^0,\phi_{sc,0})|^2+|(\phi_f^0,\phi_{sc,\lambda})|^2+2Re(\phi_f^0,\phi_{sc,0})(\phi_{sc,\lambda},\phi_f^0), \quad (56)$$

[4] H. A. Bethe (private communication).

and we may introduce an equivalent notation for the cross section,

$$\sigma=\sigma_0+\sigma_\lambda+\sigma_{0,\lambda}. \tag{57}$$

The σ_0 part yields the usual terms corresponding to $\sigma_{0,A1}$, $\sigma_{0,A2}$, $\sigma_{0,B}$, and $\sigma_{0,C}$. The term $\sigma_{0,A1}$ can be identified as $\langle\sigma_{np}\rangle_{Av}$; $\sigma_{0,B}$ as $\langle\sigma_{nn}\rangle_{Av}$; σ_C is given by Eq. (50) and $\sigma_{0,A2}$ is given by

$$\sigma_{0,A2}=\frac{-1}{6}\sum_i\sum_f\left(\frac{MW^4}{\hbar h^9 p_0}\right)$$

$$\times\int(\phi_i|V_{np}I_{23}|\phi_f{}^0)(\phi_f{}^0|V_{np}|\phi_i)$$

$$\times\exp[(i\lambda/2M)(p^2+p'^2-p''^2-p_0)]d\lambda dpdp'dp''. \tag{58}$$

Again, this term is due solely to the introduction of the Pauli principle and vanishes for the case of no binding between particles 1 and 2.

Upon examining $\phi_{sc,\lambda}$ as given by (55), we note that, on squaring this term, it is of order V^4. Now the chief terms of σ_{nd} are of the order V^2; the correction terms in which we are interested are of one order higher, namely V^3; thus we may drop terms of order V^4. Hence we shall neglect σ_λ.

Lastly, we examine the $\sigma_{0,\lambda}$ term. It does have a contribution of order V^3 and we must retain this portion, namely,

$$\sigma_{0,\lambda}=\frac{-1}{6}\sum_i\left(\frac{W}{p_0/M}\right)\frac{2\pi}{\hbar}Re\int\frac{\partial}{\partial E_f{}^0}\Big\{(\phi_f{}^0,V_{nd}\phi_i)$$

$$\times(\phi_f{}^0,[V_{12},V_{nd}]\phi_i)\Big\}\rho_{Ef}\delta(E_f{}^0-E_i)dE_f{}^0. \tag{59}$$

Summarizing, we note that we are again successful in separating out $\langle\sigma_{np}\rangle_{Av}$ and $\langle\sigma_{nn}\rangle_{Av}$, representing the cross sections averaged over the appropriate momentum distribution. The term $\sigma_{0,A2}$ is, as before, due to the Pauli principle. The main cross-term $\sigma_{0,C}$ is unchanged and a term $\sigma_{0,\lambda}$ is added due to the added complexity of ϕ_{sc}.

ACKNOWLEDGMENT

The author wishes to thank Professor Julian Schwinger for suggesting this problem, as well as for his guidance of the work and many helpful suggestions during the course of it. Thanks are also due Dr. K. M. Case for discussions concerning this problem as well as Professor Hans Bethe for discussions and permission to quote before publication his results concerning the cross-term.

The work was carried out while the author was the holder of a National Research Council Predoctoral Fellowship. This financial assistance is gratefully acknowledged.

APPENDIX A

Theorem:

If $B<A$, then in first approximation

$$(e^{A+B})_{aa'}=(e^A)_{aa'}+(B)_{aa'}\left(\frac{e^a-e^{a'}}{a-a'}\right). \tag{A1}$$

Proof:

We know that

$$e^x=\sum_{n=0}^{\infty}\frac{x^n}{n!}. \tag{A2}$$

Using (A2), expand (A1), keeping first powers of B. Then

$$(e^{A+B})_{aa'}=\sum_{n=0}^{\infty}\frac{1}{n!}\Big[(A^n)_{aa'}+\sum_{m=0}^{n-1}\sum_{a''a'''}(A^{n-1-m})_{aa''}\times(B)_{a''a'''}(A^m)_{a'''a'}\Big], \tag{A3}$$

$$\sum_{a''a'''}(A^{n-1-m})_{aa'}(B)_{a''a'''}(A^m)_{a'''a'}=a^{n-1-m}(B)_{aa'}a'^m. \tag{A4}$$

Thus

$$(e^{A+B})_{aa'}=(e^A)+(B)_{aa'}\sum_{n=0}^{\infty}\sum_{m=0}^{n-1}\frac{a^{n-1-m}a'^m}{n!}. \tag{A5}$$

Now consider

$$L=(e^a-e^{a'})/(a-a'). \tag{A6}$$

Suppose first that $a'<a$; then

$$L=\sum_{n=0}^{\infty}\frac{a^n-a'^n}{(a-a')n!}, \tag{A7}$$

or

$$L=\sum_{n=0}^{\infty}\frac{a^n[1-(a'/a)^n]}{n!a[1-(a'/a)]}=\sum_{n=0}^{\infty}\sum_{m=0}^{n-1}\frac{a^{n-1}}{n!}\left(\frac{a'}{a}\right)^m \tag{A8}$$

The condition clearly holds also for $a'>a$ by reversing the grouping, i.e., considering (a/a') as a unit. When $a'=a$, the condition is self-evident since then $L=1$.

APPENDIX B

In this Appendix we shall prove the normalization constant of ϕ. By assumption, most of the wave function ϕ is due to ϕ_1. Thus it will be sufficient to determine the normalization of ϕ_i. We have

$$\phi_i=c(1-I_{23})\phi_i, \tag{B1}$$

where c is the normalization constant to be determined. Making use of Eq. (39), we may write

$$2c^2(\phi_i,\phi_i)-2c^2(\phi_i,I_{23}\phi_i)=1. \tag{B2}$$

We shall now prove that $(\phi_i,I_{23}\phi_i)$ is zero to the approximation in which we are interested. In particular, this means we must prove that terms arising from $(\phi_i,I_{23}\phi_i)$ are not of order $(1/p_0)^2$ or lower. Consider now that

$$(\phi_i,I_{23}\phi_i)=(1/W^2)\Sigma_s\int\exp[-(i/\hbar)p_0\cdot r_3]\chi^*(r_1-r_2)$$

$$\times\exp[+(i/\hbar)p_0\cdot r_2]\chi(r_1-r_3)\nu_i(s)\nu_i(I_{23}s)dr_1dr_2dr_3. \tag{B3}$$

Now let

$$\chi(r_1-r_2)=(1/\hbar^3)\int\exp[+(i/\hbar)p_d(r_i-r_2)]\Phi(p_d)dp_d. \tag{B4}$$

Substitute in (B3), carrying out integrations, which yields

$$(\phi_i,I_{23}\phi_i)=\Phi(p_0)\Phi^*(p_0)\Sigma_s\,\nu_i(s)\nu_i(I_{23}s). \tag{B5}$$

We know that $\int|\Phi(p_0)|^2dp_0$ must be finite, since in a deuteron there must be finite total chance of finding the given momentum state. Thus $|\Phi(p_0)|^2$ must go at least as $(1/p_0)^4$ to have the integral converge. Hence, to our approximation, $(\phi_i,I_{23}\phi_i)=0$ and $c=1/\sqrt{2}$.

Quadrupole Moment of the Electron Distribution in Hydrogen Molecules*

NORMAN F. RAMSEY
Lyman Laboratory of Physics, Harvard University, Cambridge, Massachusetts
(Received January 16, 1950)

In molecular beam experiments on hydrogen molecules, measurements have been made in the past both of the rotational magnetic moment and of the dependence of the diamagnetic susceptibility on the orientation of the molecules' rotational angular momentum. It is shown in this paper that these two experimental results can be combined to give an experimental determination of the quadrupole moment of the electron distribution in hydrogen molecules. The results of this analysis are that the mean value of $\Sigma_j(3z_j^2-r_j^2)$ with z taken along the internuclear axis of the molecule is $(0.38\pm0.15)\times10^{-16}$ cm^2. Alternatively, if the z axis is the axis of quantization, the mean value of $\Sigma_j(3z_j^2-r^2)$ in the rotational state $M_J=J=1$ is $(0.076\pm0.030)\times10^{-16}$ cm^2. The first figure can be compared to the value 0.31×10^{-16} cm^2 calculated from the hydrogen molecular wave function by James and Coolidge. Although the precision of the past measurements is small, a gain of a factor of about a hundred in the precision of this measurement should be possible with some experiments now in progress.

1. INTRODUCTION

IN studying the rotational magnetic moments of hydrogen molecules by the molecular beam magnetic resonance method, Ramsey[1] also measured the dependence of the diamagnetic susceptibility of the hydrogen molecule on the orientation of its rotational angular momentum. Thus if ξ_M represents the diamagnetic susceptibility of a molecule with rotational quantum number $J=1$ and with the rotational magnetic quantum number equal to M, a result of his experiment was that

$$\xi_{\pm1}-\xi_0=-(4.5\pm2.0)\times10^{-31}. \tag{1}$$

At the time of the experiments no special interpretation was given to this result. However, this quantity is directly related to the quadrupole moment of the electron distribution in the hydrogen molecule.

The detailed derivation of the relationship is somewhat complicated by the occurrence of high frequency matrix elements in the theory of the diamagnetic susceptibility of molecules as discussed by Van Vleck.[2] As is shown in the next section, the contribution of the high frequency elements can be directly evaluated from the experimentally measured molecular rotational magnetic moment. It is also shown in this way that the contribution of the high frequency matrix elements is only about 10 percent. Once the contribution of the high frequency terms has been evaluated, it can be seen that (1) provides a measure of the departure of the molecular electron distribution from spherical symmetry since, for a magnetic field along the z axis, the ordinary diamagnetic susceptibility is proportional to the mean value of $\sum_j(x_j^2+y_j^2)$. That (1) directly yields the quadrupole moment of the electron distribution in the hydrogen molecule is shown in the next section.

* This work was partially supported by the joint program of the ONR and the AEC.
[1] N. F. Ramsey, Phys. Rev. **58**, 226 (1940).
[2] J. H. Van Vleck, *Electric and Magnetic Susceptibilities* (Oxford University Press, New York, 1932), pp. 145 and 275 ff.

2. DERIVATION

Ordinarily the quadrupole moment of the electron distribution of a molecule is referred to the internuclear axis of the molecule so a transformation will be made to such axes. Let ξ_a be the diamagnetic susceptibility of the molecule for a field applied perpendicular to the nuclear axis and ξ_c be the susceptibility for a field along the internuclear axis. Then if θ is the angle between the axis of quantization and the internuclear axis and if the brackets indicate that the enclosed quantity is averaged over the state concerned.

$$\xi_M=\xi_a\langle\sin^2\theta\rangle_M+\xi_c\langle\cos^2\theta\rangle_M \tag{2}$$

$\langle\sin^2\theta\rangle_M$ and $\langle\cos^2\theta\rangle_M$ may be evaluated from

$$\begin{aligned}\psi_{\pm1}&=\mp\tfrac{1}{2}(3/[2\pi])^{\frac{1}{2}}\sin\theta\exp(\pm i\phi)\\ \psi_0&=\tfrac{1}{2}(3/\pi)^{\frac{1}{2}}\cos\theta\end{aligned} \tag{3}$$

with the result that

$$\begin{aligned}\langle\sin^2\theta\rangle_{\pm1}&=\tfrac{4}{5} \quad \langle\sin^2\theta\rangle_0=\tfrac{2}{5}\\ \langle\cos^2\theta\rangle_{\pm1}&=\tfrac{1}{5} \quad \langle\cos^2\theta\rangle_0=\tfrac{3}{5}.\end{aligned} \tag{4}$$

Therefore

$$\begin{aligned}\xi_{\pm1}&=\tfrac{4}{5}\xi_a+\tfrac{1}{5}\xi_c\\ \xi_0&=\tfrac{2}{5}\xi_a+\tfrac{3}{5}\xi_c\end{aligned} \tag{5}$$

and

$$\xi_{\pm1}-\xi_0=\tfrac{2}{5}(\xi_a-\xi_c). \tag{6}$$

As is shown by Van Vleck[2] if α_j, β_j, γ_j, are coordinates of the jth electron relative to axes fixed in the molecule with the γ_j-axis being parallel to the internuclear axis,

$$\xi_a=\xi_{a,D}+\xi_{a,HF}, \tag{7}$$

where

$$\xi_{a,D}=[e^2/(4mc^2)]\sum_j\langle\beta_j^2+\gamma_j^2\rangle \tag{8}$$

and

$$\xi_{a,HF}=2\sum_n{}'|(0|m_a{}^0|n)|^2/(E_n-E_0) \tag{9}$$

with

$$m_a{}^0=-\frac{e\hbar}{2mci}\sum_j\left(\beta_j\frac{\partial}{\partial\gamma_j}-\gamma_j\frac{\partial}{\partial\beta_j}\right). \tag{10}$$

On the other hand

$$\xi_e=\xi_{e,D}=[e^2/(4mc^2)]\sum_j\langle\alpha_j^2+\beta_j^2\rangle, \quad (11)$$

since $\xi_{e,HF}$ is zero because of the symmetry of the Hamiltonian of the electrons about the internuclear axis of the molecule as a result of which there are no non-diagonal matrix elements of the angular momentum about this axis between electronic states of different energy.

From the above

$$\begin{aligned}\xi_{\pm1}-\xi_0&=\tfrac{2}{5}(\xi_{a,D}-\xi_{c,D})+\tfrac{2}{5}\xi_{a,HF}\\&=[e^2/(10mc^2)]\sum_j\langle\gamma_j^2-\alpha_j^2\rangle+\tfrac{2}{5}\xi_{a,HF}\\&=[e^2/(20mc^2)]\sum_j\langle 3\gamma_j^2-r_j^2\rangle+\tfrac{2}{5}\xi_{a,HF}, \quad (12)\end{aligned}$$

since $\langle\alpha_j^2\rangle$ equals $\frac{1}{2}\langle r_j^2-\gamma_j^2\rangle$ as a result of $\langle\alpha_j^2\rangle$ and $\langle\beta_j^2\rangle$ being equal by symmetry. If ξ_{HF} is the average contribution of the high frequency matrix elements averaged over all molecular orientations

$$\xi_{HF}=\tfrac{1}{3}(\xi_{a,HF}+\xi_{b,HF}+\xi_{c,HF})=\tfrac{2}{3}\xi_{a,HF}. \quad (13)$$

Therefore, Q_e, the quadrupole moment of the electron distribution is

$$Q_e=\sum_j\langle 3\gamma_j^2-r_j^2\rangle=(20mc^2/e^2)[(\xi_{\pm1}-\xi_0)-\tfrac{3}{5}\xi_{HF}]. \quad (14)$$

This is the quadrupole moment relative to the internuclear axis of the molecule, which is the form in which electronic quadrupole moments of molecules are usually expressed. However, one can also express this in the form which is characteristic of the definition of nuclear quadrupole moments, i.e., in terms of

$$Q_e'=\int\rho_{M=J}(3z^2-r^2)d\tau, \quad (15)$$

where $\rho_{M=J}$ is the probability density of the electrons in the state with magnetic quantum number M equal to J. In this case, as shown by Nordsieck,[3]

$$Q_e'=-[J/(2J+3)]Q_e \quad (16)$$

and if J is 1

$$Q_e'=\tfrac{1}{5}Q_e. \quad (17)$$

3. NUMERICAL RESULTS

From the experimental measurements of the rotational magnetic moment, Ramsey[1] has determined the value of the contribution of the high frequency terms to the molar susceptibility of H_2 to be $(0.093\pm0.007)\times10^{-6}$ per mole. Therefore, per molecule

$$\xi_{HF}=1.54\times10^{-31}. \quad (18)$$

From (1), (14), and (18)

$$Q_e=(0.38\pm0.15)\times10^{-16}\text{ cm}^2. \quad (19)$$

Hence from (17)

$$Q_e'=(0.076\pm0.030)\times10^{-16}\text{ cm}^2. \quad (20)$$

The above result may be compared with the quadrupole moment of the ground state of H_2 calculated by James and Coolidge[4] where, with a being the internuclear distance, they define the quadrupole moment of the molecule as

$$\begin{aligned}N=2e\langle\tfrac{1}{4}a^2+\alpha_1^2-\gamma_1^2\rangle&=e\langle\tfrac{1}{2}a^2-(3\gamma_1^2-r_1^2)\rangle\\&=\tfrac{1}{2}e(a^2-Qe). \quad (21)\end{aligned}$$

With the James-Coolidge computed value of N and with 0.74A for a, the theoretical value of Q_e is

$$Q_e=0.31\times10^{-16}\text{ cm}^2, \quad (22)$$

which agrees with the above experimental results within the experimental error.

4. DISCUSSION

Although the experimental results for the quadrupole moment of the electron distribution by the above method at present are of relatively low precision, the precision can be markedly improved in future experiments. The chief source of error is in the experimental value of $\xi_{\pm1}-\xi_0$. Since the diamagnetic interaction energy is proportional to H^2 the precision of the experimental results can be increased by about a factor of ten by making the measurements at 10,000 gauss instead of at the 3000 gauss used in the past experiments. A further increase in precision should be obtainable by lengthening the time the molecules are in the homogeneous magnetic field and by using the new molecular beam resonance technique recently suggested by Ramsey.[5] Experiments incorporating all of these improvements are now being prepared at Harvard as a result of which the precision in the above experimental determination of the quadrupole moment of the of the electron distribution in an H_2 molecule should be increased by a factor of about one hundred.

[3] A. Nordsieck, Phys. Rev. 58, 310 (1940).

[4] H. M. James and J. S. Coolidge, Astrophys. J. 87, 447 (1938).

[5] N. F. Ramsey, Phys. Rev. 76, 996 (1940).

On Scattering Induced Curvature for Fast Charged Particles*

W. T. Scott
Smith College, Northampton, Massachusetts

AND

H. S. Snyder
Brookhaven National Laboratory, Upton, New York

(Received January 6, 1950)

The exact solution recently obtained for the small-angle plural and multiple scattering of fast charged particles is used to derive several theorems of interest concerning scattering-produced curvatures, and calculations are reported of the probability distribution of such curvatures. Formulas are provided for obtaining the probability of occurrence of curvatures greater than any given amount, for any scattering material and energy, as long as the scattering is not too large. The types of curvature measurement dealt with are: (a) three-point observation, (b) mean curvature using the tangents to the track at each end, and (c) difference between the two curvatures obtained in (b). Asymptotic formulas allow the calculations to be extended for unusually rare events.

It is shown, first, that knowledge of the probability of a lateral displacement x, after a track length z, is sufficient to find the distribution of scattering-produced curvatures c obtained by observing the ends of the track and any one interior point. The appropriate relationship is $x=z^2c/2$.

It is further shown that by introducing a lateral displacement angle $\phi=x/z$ the probability of observing ϕ in length z may be obtained by a "duplication formula" from the distribution in ϕ_1 at any $z_1<z$ and the distribution in $\phi-\phi_1$ in a track of length $z-z_1$.

From the basic correlated distribution formula, we have obtained distributions for the curvatures of the two circles tangent to either end of the track and passing through the other end. The mean $\bar{c}$ of these two curvatures (a special "four-point" curvature) follows the same distribution law as the directional distribution of the previous paper, with $\eta=z\bar{c}$. The difference of these curvatures, D, follows the same law as the three-point curvature c, above.

Finally, we have shown that the distribution in x and η, or in c and $\bar{c}$, are nearly the same if we write $\eta=\sqrt{3}(x/z)$ or $\bar{c}=\sqrt{3}c/2$, although the exact solution yields different expressions for the appropriate Fourier transforms.

Calculations are here reported and summarized in graphs of the differential and integral distributions in $\phi=x/z$, in terms of dimensionless units z/λ and ϕ/η_0 as in the previous work. Integral distributions in angular displacement, η, derived from the previous calculations, are included for completeness.

1. INTRODUCTION

THE multiple scattering of charged particles gives rise to curvature of a particle track which interferes with the determination of the momentum of the particle as determined by curvature measurements in a magnetic field. The quantitative treatments[1] of the scattering-induced curvature have to this date been based on the Gaussian approximation[2] to the distribution function for the correlated angular and lateral displacements of the scattered particles. In this paper we solve the problem of the curvature distributions without the introduction of the Fokker-Planck approximation to the Boltzmann diffusion equation. Specifically, we calculate the probability distribution for the curvature as measured by using three points on the track. As Scott[3] has shown, the use of more than three points for the Gaussian approximation case does not greatly sharpen the curvature probability distribution. Bothe[4] has shown, using the Gaussian approximation, that other methods of measuring curvature lead to essentially the same results. He has, in addition, dealt with the case in which the track bends through a large fraction of a circle under the influence of the magnetic field; for which our results are not applicable. One would expect that the qualitative aspects of these conclusions would not be upset by the use of more accurate distribution functions. Further remarks on this matter will be made in Section 4 of this paper.

2. THE CORRELATED DISTRIBUTION FUNCTION

The paper on the multiple scattering of fast charged particles by Snyder and Scott,[5] which paper we shall call **A**, contains an explicit expression, (A-7), for the correlated probabilities of angular and lateral displacements. Since all the pertinent information concerning the distribution function is contained in **A**, we will simply reproduce here those portions of **A** which are applicable to the curvature problem without including any unnecessary developments or proofs. Thus, from (A-7, 8, 11–16), we have

$$w(\eta, x|z)=\frac{1}{4\pi^2}\int_{-\infty}^{\infty}ds\int_{-\infty}^{\infty}dt \times\exp\left\{i(\eta s+xt)-\frac{h(s+tz)-h(s)}{\lambda t}\right\} \quad (1)$$

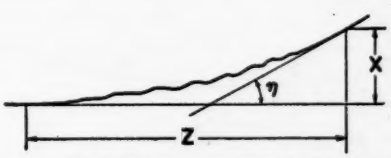

FIG. 1. A scattered particle track referred to the initial direction, illustrating the basic distribution (1).

* Work performed at the Brookhaven National Laboratory, under the auspices of the AEC.

[1] H. A. Bethe, Phys. Rev. **70**, 821 (1946).

[2] B. Rossi and K. Greisen, Rev. Mod. Phys. **13**, 240 (1941).

[3] W. T. Scott, Phys. Rev. **76**, 212 (1949).

[4] W. Bothe, S. B. Heidelberg Akad. Wiss., Math.-Naturwiss. Klg. 107 (1948).

[5] H. S. Snyder and W. T. Scott, Phys. Rev. **76**, 220 (1949). This is referred to as paper **A** in the text.

with

$$h(s)=\int_0^s [1-q(s)]ds, \quad q(s)=\int_{-\infty}^{\infty} e^{i\eta u}p(\eta)d\eta, \quad (2)$$

$$p(\eta)=\frac{\eta_0^2}{2(\eta^2+\eta_0^2)^{\frac{3}{2}}}, \quad (3)$$

$$\eta_0=\frac{Z'm}{137\mu(E^2-1)^{\frac{1}{2}}}, \quad (4)$$

$$1/\lambda=4\pi Z^{4/3}Z'^2N(137r_0)^2E^2/(E^2-1). \quad (5)$$

From (2) and (3) one obtains

$$q(s)-1=\frac{(s\eta_0)^2}{2}\left\{\ln\left(\frac{s\eta_0}{2}\right)+0.0772157\cdots\right\}+\frac{(s\eta_0)^4}{16}\left\{\ln\left(\frac{s\eta_0}{2}\right)-0.6727843\cdots\right\}+\frac{(s\eta_0)^6}{384}\left\{\ln\left(\frac{s\eta_0}{2}\right)-1.089451\cdots\right\}+\cdots. \quad (6)$$

In the above equations, z is the distance the particle has traveled through the scattering material, x is the lateral component of displacement of the particle in a fixed direction perpendicular to the original direction of the particle, and η is the angle between the projection of the particle track on the xz plane and the z axis. $W(\eta, x|z)$ is the probability per unit of η and per unit of x of obtaining a given angular displacement η and lateral displacement x for a particle which has traveled a distance z if it started out parallel to the z axis (see Fig. 1). $p(\eta)$ is the probability per unit of η of scattering the particle through the angle η in a single scattering. The constants in these equations are: μ the mass of the scattered particle, c the velocity of light, E the total energy of the scattered particle in units of its rest energy, r_0 the classical electron-radius e^2/mc^2, Z' the atomic number of the scattered particle and Z the atomic number of the scattering atoms, m the mass of the electron, N the number of scattering atoms per unit volume, and λ the mean free path for scattering. We assume here that changes in the energy of the particle may be neglected, so that λ and η_0 are constants. The above relations are valid only if $|\eta|\ll 1$ and $|x|\ll Z$ which conditions were used in the derivation of (1).

3. DISTRIBUTION IN CURVATURES

The main point of this paper is that a knowledge of the distribution in lateral displacement x at a track length z is sufficient to yield the distribution in curvatures observed if a track of the same length is measured at three points, equally or unequally spaced. This result may be expressed in a theorem which we will now prove.

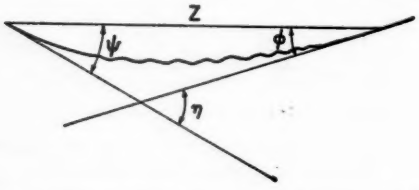

FIG. 2. A scattered particle track, referred to its chord, illustrating the distribution (9).

Theorem

The probability of finding a curvature between c and $c+dc$ is given by

$$p(c|z)dc=W(\tfrac{1}{2}z^2c|z)\tfrac{1}{2}z^2dc=\tfrac{1}{2}zw(\psi|z)dc; \quad \psi=\tfrac{1}{2}zc=x/z \quad (7)$$

with

$$W(x|z)=\int_{-\infty}^{\infty}W(\eta, x|z)d\eta=\frac{1}{2\pi z}\int_{-\infty}^{\infty}ds\exp\left\{i\frac{xs}{z}-\frac{zh(s)}{\lambda s}\right\}=\frac{1}{2\pi}\int_{-\infty}^{\infty}dt\exp\left\{ixt-\frac{h(tz)}{\lambda t}\right\}. \quad (8)$$

$W(x|z)$ is the probability of a lateral displacement x at z, obtained by integrating (1) over η (see Fig. 1).

Proof

Let us express the fundamental distribution (1) in terms of the initial and final angles between track and chord, ψ and ϕ (see Fig. 2). (z may equally well be taken as chord or track projection in our approximation of small angles.)[6] In Eq. (1) we set $x/z=\psi$, $\eta-\psi=\phi$, and also $s+tz=u$. Then if

$$W(\eta, x|z)d\eta dx=U(\psi, \phi|z)d\psi d\phi,$$

we have

$$U(\psi, \phi|z)=\frac{1}{4\pi^2}\int_{-\infty}^{\infty}du\int_{-\infty}^{\infty}ds\times\exp\left\{i(\psi u+\phi s)-\frac{z}{\lambda}\frac{h(u)-h(s)}{u-s}\right\}. \quad (9)$$

Since the probability distributions are independent of whether we specify a specific direction z or a chord on the actual track, of length z, we see that (9) gives indeed the correlated distribution of the angles ψ and ϕ when the track is known to pass through the end points of the chord z.

Now let us observe a track at three points, and ask for the resulting distribution in scattering-produced curvature. Let us apply (9) to two successive segments of track, as in Fig. 3. The two chords are z_1 and z_2, and the angle between them $\alpha=\phi_1+\psi_2$. Then we have the

[6] To take care of large magnetic curvatures, while maintaining small scattering angles, one would require an additional term in the diffusion equation. See reference 4 for a different treatment.

curvature of a circle through the three points

$$c=2\alpha/(z_1+z_2).$$

The distribution in α is obtained by integrating

$$w(\alpha|z)d\alpha=d\alpha\int_{-\infty}^{\infty}d\psi_1\int_{-\infty}^{\infty}d\phi_1\int_{-\infty}^{\infty}d\phi_2$$

$$\times\frac{1}{(2\pi)^4}\int_{-\infty}^{\infty}du_1\int_{-\infty}^{\infty}ds_1\int_{-\infty}^{\infty}du_2\int_{-\infty}^{\infty}ds_2$$

$$\times\exp\left\{i(\psi_1u_1+\phi_1s_1-\phi_1u_2+\phi_2s_2+\alpha u_2)\right.$$

$$\left.-\frac{z_1}{\lambda}\frac{h(u_1)-h(s_1)}{u_1-s_1}-\frac{z_2}{\lambda}\frac{h(u_2)-h(s_2)}{u_2-s_2}\right\}$$

$$=\frac{d\alpha}{2\pi}\int_{-\infty}^{\infty}du_2\exp\left\{i\alpha u_2-\frac{z_1+z_2}{\lambda}\frac{h(u_2)}{u_2}\right\}.$$

Hence, setting $z=z_1+z_2$, the curvature distribution is

$$p(c|z)=\frac{z}{4\pi}\int_{-\infty}^{\infty}du\exp\left\{i\tfrac{1}{2}zcu-\frac{zh(u)}{\lambda u}\right\},$$

which agrees with (7) and (8). Thus, all that is required for a three-point curvature distribution is a two-point lateral-displacement calculation, which we have carried out in a similar way to the calculations of A. This remarkable result holds for any type of elementary scattering law and depends only on the small-angle approximation.

Another remarkable theorem, which was necessary for the calculations, is a similar duplication formula to Eq. (23) of A. We have with

$$w(\psi|z)=\int_{-\infty}^{\infty}U(\psi,\phi|z)d\phi=\int_{-\infty}^{\infty}U(\phi,\psi|z)d\phi$$

$$w(\psi|z)=\int_{-\infty}^{\infty}d\psi_1w(\psi_1|z_1)w(\psi-\psi_1|z-z_1). \qquad (10)$$

For any z, this theorem is, in fact, a simple consequence of the exponential character in z of the Fourier transform of w. The right side of (10) is just a faltungsintegral, corresponding to a product of the two corresponding Fourier transforms.

4. A SPECIAL FOUR-POINT CURVATURE DISTRIBUTION

In the paper by Scott,[3] it was shown that in the Gaussian approximation the curvature distribution function obtained by utilizing the directions of the tangents to the particle track at the ends was the sharpest curvature distribution function that could be obtained. For the Gaussian case, this distribution function is narrower than the three-point distribution function by a factor of $\sqrt{3}/2$. Although we shall not prove it, it would not be surprising if the same situation were essentially true for the distribution functions used in this paper. In any event, we have the information available for the calculation of the mean curvature as determined from the directions of the tangent to the particle track at the two ends of the track. This information is contained in the distribution function $U(\psi, \phi|z)$ as it is given in (9). From Fig. 2 one can see that the curvature of the circle which is tangent to

FIG. 3. A scattered particle track of two segments, with tangents and chords, illustrating the curvature theorem of Section 3.

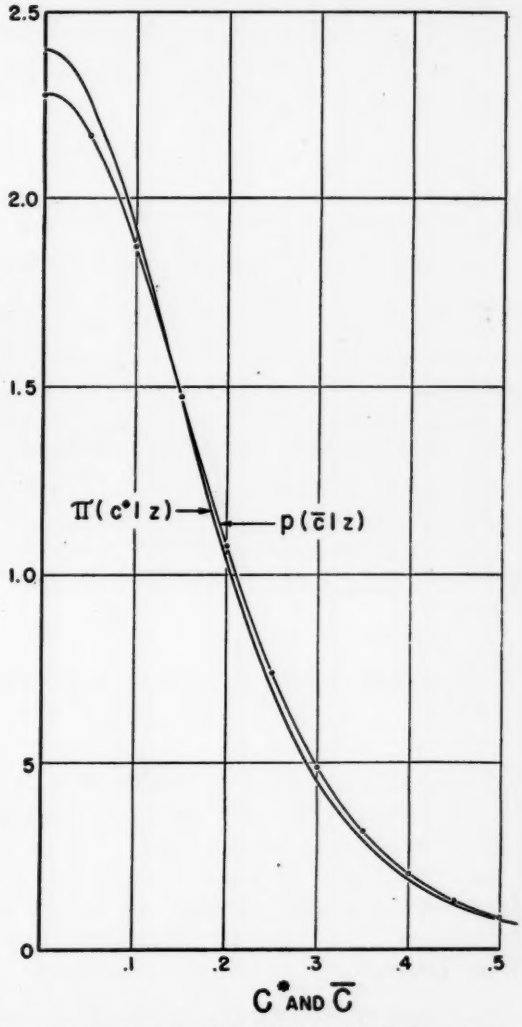

FIG. 4. A comparison of $\mathfrak{P}(\bar{c}|z)$, the distribution of the mean of curvatures determined by the tangents of the two ends of a track, with $\pi(c^*|z)$ the distribution of $\sqrt{3}/2$ times the curvature c determined by three points on the track. These curves also compare the lateral and angular distributions derived from Eq. (1). (See Section 4.)

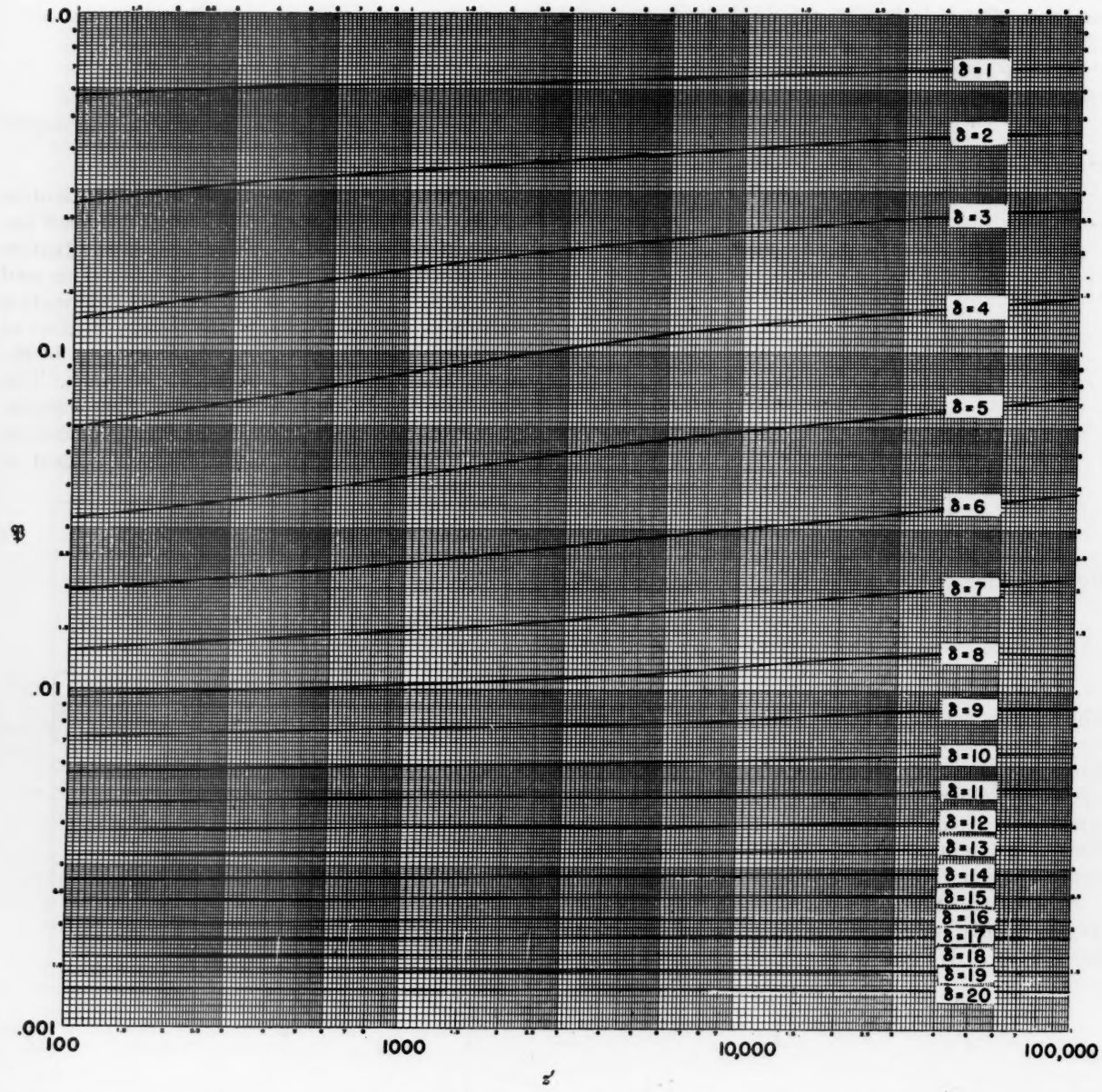

FIG. 5. $P(\phi'|z')$, the probability of exceeding a lateral displacement angle $\phi'=x'/z'=x/z\eta_0$, plotted as a function of the track length $z'=z/\lambda$, for values of $\epsilon=\phi'/(z')^{\frac{1}{2}}$ from 0.25 to 10.0.

the particle track at point 0 and passes through P is $c_\phi=(2\phi/z)$. Similarly, the curvature of a circle tangent at point P and passing through point 0 is $c_\psi=(2\psi/z)$. The mean curvature of these two circles is $\bar{c}=\frac{1}{2}(c_\phi+c_\psi)=(1/z)(\phi+\psi)$ and the difference of curvature is $D=(2/z)(\phi-\psi)$. The probability distribution function for $\bar{c}$ and D satisfies

$$\mathfrak{P}(\bar{c}, D|z)d\bar{c}dD=U(\phi, \psi|z)d\phi d\psi$$

from which we get

$$\mathfrak{P}(\bar{c}, D|z)=\tfrac{1}{4}z^2U(\tfrac{1}{2}z[\bar{c}+\tfrac{1}{2}D], \tfrac{1}{2}z[\bar{c}-\tfrac{1}{2}D]|z). \quad (11)$$

From (9) and (11) one can immediately verify that

$$\mathfrak{P}(\bar{c}|z)=\int_{-\infty}^{\infty}\mathfrak{P}(\bar{c}, D|z)dD=zW(\eta|z); \quad \eta=z\bar{c} \quad (12)$$

in which $W(\eta|z)$ is the angular distribution function for the angle between the initial particle direction and the particle direction at the end of the track. It is this function $W(\eta|z)$ which was tabulated in **A**. We now wish to compare the curvature distribution function $\mathfrak{P}(\bar{c}|z)$ with the curvature distribution function $p(c|z)$. Integrating Eq. (1) with respect to x and using (6) we

get

$$\mathfrak{P}(\bar{c}|z)=\frac{z}{2\pi}\int_{-\infty}^{\infty}ds\,\exp\left\{iz\bar{c}s+\frac{z}{\lambda}\left[\frac{(s\eta_0)^2}{2}\left\{\ln\left(\frac{s\eta_0}{2}\right)+0.0772\cdots\right\}+\cdots\right]\right\}. \quad (13)$$

Now, one can write (8) in the form

$$p(c|z)=\frac{z}{2\pi}\int_{-\infty}^{\infty}ds\,\exp\left\{izcs-\frac{z}{\lambda}\frac{h(2s)}{2s}\right\}. \quad (14)$$

From the value of $h(s)$ as determined by (2) and the values of $q(s)-1$ as given by (6) we get

$$-\frac{h(s)}{s}=\frac{(s\eta_0)^2}{6}\left\{\ln\left(\frac{s\eta_0}{2}\right)+0.0772\cdots-\tfrac{1}{3}\right\}+\frac{(s\eta_0)^4}{80}\left\{\ln\left(\frac{s\eta_0}{2}\right)-0.76278\cdots-\tfrac{1}{5}\right\}+\cdots. \quad (15)$$

If we now introduce a new variable $c^*=\sqrt{3}c/2$ into (14), together with its corresponding distribution function

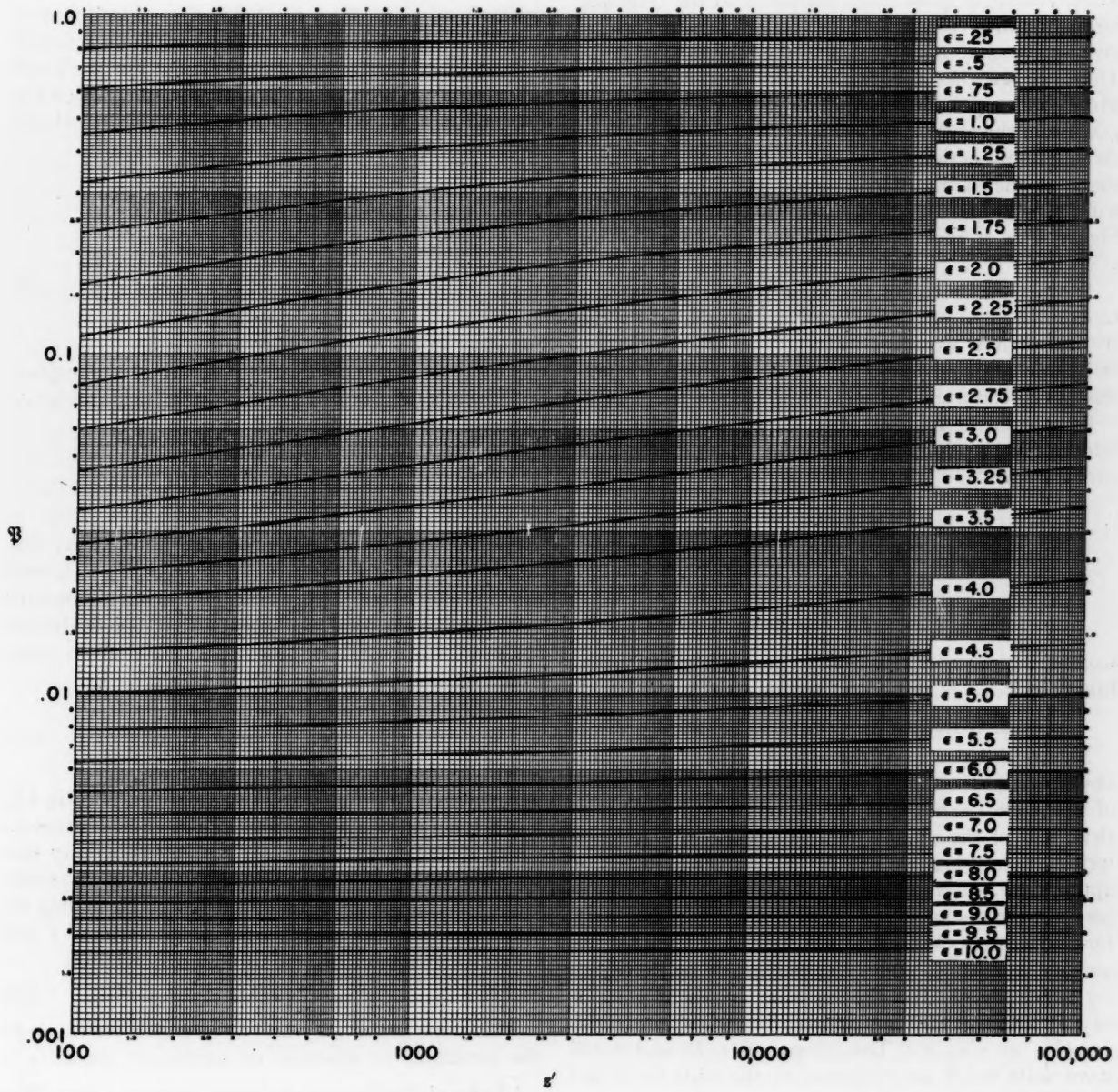

FIG. 6. $\mathfrak{P}(\eta'|z')$, the probability of exceeding an angular displacement $\eta'=\eta/\eta_0$, plotted as a function of the track length $z'=z/\lambda$, for values of $\delta=\eta'/(z')^{\frac{1}{2}}$ from 1 to 20.

$\pi(c^*|z)dc^*=p(c|z)dc$ we find using (15) that

$$\pi(c^*|z)=\frac{z}{2\pi}\int_{-\infty}^{\infty}ds\exp\left\{isc^*s+\frac{z}{\lambda}\left[\frac{(s\eta_0)^2}{2}\right.\right.$$
$$\left.\left.\times\left\{\ln\left(\frac{s\eta_0}{2}\right)+0.0772\cdots+\tfrac{1}{2}\ln 3-\tfrac{1}{3}\right\}+\cdots\right]\right\}. \quad (16)$$

If we now compare the expressions for $p(c|z)$ and $\pi(c^*|z)$ as given by (13) and by (16) we see that they are quite similar. In fact, the only difference in the coefficient of z/λ is that the constant which is added to the logarithm is different for these two expressions. We now note that the major contributions to these integrals come from very small values of $s\eta$ if z/λ is very large. Thus, $|\ln s\eta_0|$ is quite large compared to the constant terms in either (13) or (16) for those values of s which give appreciable contributions to the integrals for $z\gg\lambda$. Thus, we see that the two distributions $\pi(c^*|z)$ and $\mathfrak{P}(\bar{c}|z)$ will approach one another in the limit of large z/λ. From the above argument we thus expect that the distribution function $\mathfrak{P}(\bar{c}|z)$ will have roughly the same shape as the distribution function $p(c|z)$, and that it will be narrower than the latter by a factor of $\sqrt{3}/2$.[7] Figure 4 is a plot of both $p(\bar{c}|z)$ and $\pi(c^*|z)$ for $z/\lambda=100$.

Another statement of the same relation is that the function $W(x|z)$ of (8) is closely approximated by the $W(\eta|z)$ of A if we set $\eta=\sqrt{3}x/z$. This transformation leads to exact equivalence in the Gaussian approximation, as is seen from Eqs. (11a) and (13) of reference 3.

By integrating Eq. (11) with respect to $\bar{c}$, additional information is obtained concerning the difference of curvature, D.

$$\mathfrak{P}_0(D|z)=\int_{-\infty}^{\infty}\mathfrak{P}(\bar{c},D|z)d\bar{c}$$
$$=\frac{z}{2}w\left(\frac{zD}{2}\middle|z\right)=\frac{z^2}{2}W\left(\frac{z^2c}{2}\middle|z\right). \quad (17)$$

Comparing (7) and (17) we see that the distribution functions $\mathfrak{P}_0(D|z)$ and $p(c|z)$ are identical.

5. NUMERICAL COMPUTATIONS

As was the case in A, the results of our calculations are expressible in a universal form which is independent of the mass, charge, and energy of the scattered particle, and of the atomic number and density of scattering atoms when we express the results in terms of appropriate variables. This is readily done by expressing the distance z in units of the mean free path for scattering λ. We have thus used as a variable the average number of times the particle is scattered, z', for which $z=z'\lambda$. We also measure angles in units of η_0 and thus use for angular variables ϕ', η', etc., with $\phi=\phi'\eta_0$, $\eta=\eta'\eta_0$, etc. The curvatures c, D, and $\bar{c}$ will have units which are reciprocal to the units for λ and can be expressed in terms of ϕ', $\phi'-\psi'$ and η' as $c=2\phi'\eta_0/z'\lambda$, $D=2\eta_0(\phi'-\psi')/z'\lambda$, and $\bar{c}=\eta_0\eta'/z'\lambda$. We also note that $x=\eta_0\lambda x'$ in order to have $x'=\phi'z'$, and $c=\eta_0c'/\lambda$ in order to have $c'=2\phi'/z'$. It is in terms of these universal variables x', ϕ', z', η', etc., that all our calculations were made. One must convert from the system of primed variables to the unprimed variables by computing the value of η_0 and λ for any particular problem by using Eqs. (4) and (5) and the above connections between the two systems of units. The equations of the distribution functions in primed variables are simply obtained by setting η_0 and λ equal to unity in all of the preceding equations and placing a prime on all the variables entering into these expressions.

In the numerical calculations we computed $w'(\phi'|z')$ for small values of ϕ' for $z'=100$ and $z'=3200$ by using Eqs. (7), (8), and (15). The values of these integrals were obtained by numerical integration. For the larger values of ϕ' we used an asymptotic formula, which was obtained in a manner identical to that used to obtain (A-21), giving

$$w'(\phi'|z')=\frac{z'}{6(\phi')^3}\left[1+\frac{2z'}{(\phi')^2}\{\ln\phi'-0.44691+\cdots\}\right.$$
$$\left.\frac{5(z')^2}{(\phi')^4}\{\ln^2\phi'-1.95317\ln\phi'+.16715\}+\cdots\right]. \quad (18)$$

For other values of z' the distribution function $w'(\phi'|z')$ was computed by numerically integrating† the duplication formula (10) for small ϕ' and using (18) for large ϕ'. Formula (18) is useful only if

$$\frac{2z'}{(\phi')^2}\{\ln\phi'-0.44691\}<0.2.$$

For the purpose of presenting the information contained in the distribution function $w'(\phi'|z')$ in a form which is most useful for applications, we have computed numerically the total probability that the scattering angle ϕ' will exceed in absolute value a given value which we also call ϕ'. We thus calculated

$$P(\phi'|z)=2\int_{\phi'}^{\infty}w(\phi'|z')d\phi'. \quad (19)$$

The values of this function $P(\phi'|z')$ are graphed in Fig. 5 as a function of z' for various values of an argument ϵ which is defined to be $\epsilon=\phi'/(z')^{\frac{1}{2}}$. The probability that the absolute value of the curvature will exceed a certain value c may then be found on this graph by finding the value of P corresponding to the given value of z' and ϵ where c is connected to ϵ through the relation

$$c=2\eta_0\epsilon/\lambda(z')^{\frac{1}{2}}. \quad (20)$$

This same graph may also be useful in checking for the presence, or absence, of significant amounts of

[7] W. Bothe, reference 4, p. 12, gives the same result for small magnetic deflections.

† Tables of these functions for eleven values of z' from 100 to 102,400 are available from the Information and Publications Division of Brookhaven National Laboratory, upon request.

turbulence in cloud chambers and distortion in emulsions. As was remarked at the end of Section 3, the difference of curvature, D, between the two ends of the track has the same distribution function as the curvature measured by using three points. Thus, if we connect D to ϵ through the relation

$$D=2\eta_0\epsilon/\lambda(z')^{\frac{1}{2}}, \tag{21}$$

then the probability that the absolute value of D will exceed the value of D given in (21) will be given by the value of P corresponding to the values of ϵ and z' as given in Fig. 5, provided scattering alone is responsible for the induced distortion D. Improbably large measured values of D may reasonably be interpreted as due to the presence of turbulence in a cloud chamber, or distortion in an emulsion.

We have also included in this paper a graph, Fig. 6, of the function

$$\mathfrak{P}(\eta'|z')=2\int_{\eta'}^{\infty} W(\eta'|z')d\eta', \tag{22}$$

which is the probability that the absolute value of η' will exceed the value η'. The curves on this graph are the values of $\mathfrak{P}(\eta'|z')$ as a function of z' for constant values of $\delta=\eta'/(z')^{\frac{1}{2}}$. This graph may be used in the same manner as one uses Fig. 5 to determine the probability that the absolute value of the mean curvature, $\bar{c}$, will exceed the value $\bar{c}$ determined by δ through

$$\bar{c}=\eta_0\delta/\lambda(z')^{\frac{1}{2}}. \tag{23}$$

6. MISCELLANEOUS FACTS AND FORMULAS

Although the graphs of Figs. 5 and 6 should be extensive enough to cover most of the needs of experimental physicists, it may be useful to give simple formulas by means of which the type of information contained in these graphs could be extended to the rare events. To do this, we integrate $w'(\phi'|z')$ with respect to ϕ' using the asymptotic form for $w'(\phi'|z')$ given in Eq. (18) and obtain

$$\begin{aligned}P(\phi'|z')&=2\int_{\phi'}^{\infty} w'(\phi'(z')d\phi'\\&=\frac{z'}{6(\phi')^2}\Big[1+\frac{z'}{(\phi')^2}\{\ln\phi'-0.19695\}\\&\quad+\frac{5}{3}\frac{(z')^2}{(\phi')^4}\{\ln^2\phi'-1.61984\ln\phi'\\&\qquad-0.10282\}+\cdots\Big]\\&=\frac{1}{6\epsilon^2}\Big[1+\frac{1}{\epsilon^2}\{\ln\epsilon(z')^{\frac{1}{2}}-0.19695\}\\&\quad+\frac{5}{3\epsilon^4}\{\ln^2\phi'(z')^{\frac{1}{2}}-1.6984\ln\phi'(z')^{\frac{1}{2}}\\&\qquad-0.10282\}+\cdots\Big]\end{aligned} \tag{24}$$

with, of course, $\epsilon=\phi'/(z')^{\frac{1}{2}}$. One now sees by inspection of (24) the reason for the curves of $P(\phi'|z')$ for fixed ϵ being so nearly constant as a function of z' for large ϵ. We also note here that in the Gaussian approximation, the corresponding curves would have been straight horizontal lines. The distribution as a function of ϵ would, however, have been very different for large values of ϵ being determined by an error function of ϵ instead of an essentially inverse square power of ϵ.

We also give here the asymptotic form

$$\begin{aligned}\mathfrak{P}(\eta'|z')&=\frac{z'}{2(\eta')^2}\Big[1+\frac{3z'}{4(\eta')^2}\{\ln\eta'-0.6340\}\\&\quad+\frac{15}{4}\frac{(z')^2}{(\eta')^4}\{\ln^2\eta'-2.28667\ln\eta'\\&\qquad+0.95952\}+\cdots\Big]\\&=\frac{1}{2\delta^2}\Big[1+\frac{3}{4\delta^2}\{\ln\delta(z')^{\frac{1}{2}}-0.6340\}\\&\quad+\frac{15}{4\delta^4}\{\ln^2\delta(z')^{\frac{1}{2}}-2.28667\ln\delta(z')^{\frac{1}{2}}\\&\qquad+0.95952\}+\cdots\Big].\end{aligned} \tag{25}$$

The same comments hold for $\mathfrak{P}(\eta'|z')$ as for $P(\phi'|z')$.

In the paper of Scott[3] it was shown using the Gaussian approximation, that the selection of tracks according to a criterion of symmetry does not change the distribution of scattering induced curvature. This conclusion no longer holds true for the exact distribution given here. To see this, we return to (9) and (11) and find for the joint distribution functions for $\bar{c}$ and D the explicit expression

$$\begin{aligned}\mathfrak{P}(\bar{c},D|z)&=\frac{1}{4\pi^2}\int_{-\infty}^{\infty}ds\int_{-\infty}^{\infty}dt\exp\Big\{i(\bar{c}s+Dt)\\&\quad+\frac{z^2}{4\lambda t}\Big[h\Big(\frac{s-2t}{z}\Big)-h\Big(\frac{s+2t}{z}\Big)\Big]\Big\}\\&=\frac{1}{4\pi^2}\int_{-\infty}^{\infty}ds\int_{-\infty}^{\infty}dt\exp\Big\{i(\bar{c}s+Dt)\\&\quad+\frac{z^2}{24\lambda\eta_0 t}\Big[\Big(\frac{(s+2t)\eta_0}{z}\Big)^3\\&\quad\times\Big(\ln\frac{(s+2t)\eta_0}{2z}-0.25612\Big)\\&\quad-\Big(\frac{(s-2t)\eta_0}{z}\Big)^3\Big(\ln\frac{(s-2t)\eta_0}{2z}\\&\qquad-0.25612\Big)\Big]+\cdots\Big\}.\end{aligned} \tag{26}$$

The logarithm in the integrals (25) prevents the factorization of $\mathfrak{P}(\bar{c}, D|z)$ into the product of the distribution function of $\bar{c}$ by the distribution function of D which was the origin of the theorem in the Gaussian case. In fact, the Gaussian approximation is obtained from (25) by replacing the logarithm by an appropriate negative constant and neglecting all higher terms in the expansion of $h(s)$. Since we have not carried out the numerical evaluation of joint distributions $\mathfrak{P}(\bar{c}, D|z)$ we cannot say how much a selection of tracks, according to the requirement that D should be less than a certain predetermined value, would sharpen the corresponding distribution function in $\bar{c}$. Even a preliminary examination of this question for one value of z' would require about ten times the amount of numerical calculation we have carried out at this time. For the relatively meager amount of information which would thereby be acquired, it is not worth while to carry out such a program. Also, from the fact that in the Gaussian approximations no improvement is to be expected, one would expect that very little improvement would be obtained for the exact distributions.

In most practical cases the scattering atoms are not composed only of a single atomic species, but there is usually a mixture of different elements. The results of our calculations may, however, be applied to the case of mixtures provided the constants η_0 and λ are properly evaluated. To do this we note that the function

$$\frac{\eta_0^2}{\lambda(\eta^2+\eta_0^2)^{\frac{1}{2}}}, \tag{27}$$

which appears in the diffusion Eq. (A-5) is, in the case of mixtures, replaced

$$\sum_i \frac{\eta_i^2}{\lambda_i(\eta^2+\eta_i^2)^{\frac{1}{2}}}, \tag{28}$$

in which λ_i is the mean free path for scattering by the ith type of atom having a charge Z_i and density N_i, and η_i is calculated by (4) using the value Z_i instead of Z. It is, of course, not possible for any function with single values of λ and η_0 to fit exactly the more complicated function involving a sum of such terms. However, if the distribution function $W(\eta, x|z)$ is to approach the correct values for large η when we approximate (28) by (27), then these expressions must become the same for large values of η, from which we obtain the condition

$$\eta_0^2/\lambda=\sum_i(\eta_i^2/\lambda_i). \tag{29}$$

Another condition which we may reasonably use is that the mean free path shall be correctly given by both expressions which gives us

$$1/\lambda=\sum_i(1/\lambda_i). \tag{30}$$

Actually, condition (29) is far more important than (30) and a small departure of λ from its value as given by (3) makes very little difference in e.g., the probability distribution function $p(c|z)$ when this is expressed in terms of the actual curvature c and physical length z rather than in terms of c' and z'. The reason for this lies in the fact that the functions $P(\phi'|z')$ for fixed ϵ are nearly independent of z'. A way of seeing the importance of (29) is through the connection between ϵ and the curvature c in terms of the physically measured track length z:

$$c=(2\epsilon/z^{\frac{1}{2}})(\eta_0/\lambda^{\frac{1}{2}}). \tag{31}$$

In this form of the connection between c and ϵ the importance of the correct ratio for η_0^2/λ is evident.

We wish to thank Miss Theresa Danielson and Miss Jean Snover who are primarily responsible for the numerical work and preparation of the graphs.

Preparation of Rhenium Emitters and Measurements of Their Thermionic Properties*

ROBERTO LEVI AND GEORGE A. ESPERSEN
Philips Laboratories, Inc., Irvington-on-Hudson, New York
(Received December 6, 1949)

A method is described for electroplating stable rhenium on a tungsten wire. The thermionic emission properties of rhenium were investigated and values of the work function, $\phi = 4.74$ ev and of the emissivity $A = 720$ amp./cm²/deg.² were obtained. An increase of temperature produces no change of activation in a rhenium cathode. Emission results were reproducible.

1. INTRODUCTION

IT is noted that emitters of the high temperature type, such as tungsten, tantalum, molybdenum, etc., have been thermionically investigated to a far greater extent than has rhenium. Although this metal possesses the good quality of a high melting point of 3170°C ±60°C, which is just below that of tungsten, its emission behavior has only once been reported upon in the literature.[1] This may be accounted for partially by the unavailability of rhenium in a form which is readily applicable to such experimental procedures. However, rhenium has been recognized as a possible substitute for, or an addition to, tungsten for use as filaments in incandescent lamps and in thermionic emission tubes.[2] It has been stated[2] that the volatilization of rhenium is less than that of tungsten. This would make it desirable for use in x-ray tubes which now utilize tungsten filament cathodes. Any tendency to decrease unwanted tungsten contamination lines from x-ray records would certainly warrant the further investigation of rhenium.

2. NATURE OF MATERIAL

a. Preparation of Rhenium

In connection with our studies of electron emission from rhenium metal, several attempts were made to obtain rhenium in wire or strip form. It appeared, however, that no metallic rhenium was available in this country other than in powder form and we therefore decided to make our own emitters by electro-depositing rhenium onto filaments of a high melting metal such as tungsten.

For this purpose we used a plating bath of the sulfate type having the following composition:

Potassium perrhenate ($KReO_4$), 11 grams per liter of solution. Concentrated sulfuric acid (H_2SO_4) sp. gr. 1.84, to bring the bath's pH to 0.9. Such a bath, which had previously been described by Colin G. Fink and P. Deren,[3] was operated at 25 to 45°C and at a current density of 10 to 14 amp./dm² as recommended by these authors.

The rhenium deposits we obtained were hard and bright but also extremely unstable upon exposure to the atmosphere at room temperature. After a few days exposure, the rhenium plating disappeared entirely leaving only a few drops of perrhenic acid on the filament base. These results confirmed the findings of Lundell and Knowles[4] and the unstable character of such an electro-deposit was very undesirable for our purposes.

However, as massive rhenium has the same resistance to air and water vapor as massive tungsten,[5] we attempted to find a method of improving the stability of electro-deposited rhenium so as to prevent it from oxidizing to perrhenic acid upon exposure to the atmosphere at ordinary temperatures, and we have found that this result can be obtained simply by firing the rhenium plated filament immediately after the plating operation in a hydrogen atmosphere at a temperature of about 1000°C.

If relatively thick rhenium deposits are desired, such as 0.001 in. or over, the rhenium has a tendency to crack and flake off during the firing operation. However, this may be avoided by first interrupting the plating process after the filament is barely covered with an extremely thin rhenium layer and then firing the filament as mentioned above. Subsequently, a rhenium layer having a thickness of about 0.0001 in.—0.0002 in. should be electro-deposited and again fired. By alternating the plating and firing process every time a 0.0001 in. —0.0002 in. rhenium layer has been deposited, it is possible to build up relatively thick deposits which have no tendency to crack or flake off and are stable for indefinite periods at ordinary temperatures under exposure to moist air.

It should be noted that the method we have described above can also be used in making foil, seamless hollow cylinders, etc., of solid rhenium. This may be done by suitably electroplating rhenium onto a base which can subsequently be dissolved without damaging the electrodeposit. We have found that a base conforming with the above requirements may consist of nickel which in turn can be dissolved with hydrochloric acid.

* This work was carried out as a partial fulfillment of ONR contract N6onr-261, Task Order I.

[1] Agte, Alterthum, Becker, Heyne, and Moers, Zeits. f. anorg. allgem. Chemie 196, 137 (1931).

[2] U. S. Patent 1,829,756 (November 3, 1931).

[3] C. G. Fink and P. Deren, Trans. Am. Electrochem. Soc. 66, 471 (1934).

[4] G. E. F. Lundell and H. B. Knowles, J. Research Nat. Bur. Stand. 18, 629 (1937).

[5] B. S. Hopkins, *Chapters in the Chemistry of the Less Familiar Elements* (Stipes Publishing Company, Champaign, Illinois), Chapter 20.

b. X-Ray Analysis

X-ray diffraction powder photographs were taken of the fired and unfired rhenium samples and are shown in Fig. 1. All photographs were taken with the new Philips camera[6] 114.6-mm diameter, using CuK, 45KVP, 25Ma, 0.0006-in. nickel foil filter, two hours' exposure. Figure 1A shows the uncoated tungsten wire, 0.010-in. diameter. Figure 1B shows a sample of pure rhenium powder coated on a 0.005-in. diameter Pyrex fiber. Figure 1C shows the rhenium plated onto tungsten wire and fired. The pattern is identical with the pure rhenium sample. None of the tungsten lines appear on this photograph because of the high absorption and complete coating of the tungsten by the rhenium. The lines in the back-reflection region are too broad to allow precision measurement of the lattice constants and hence it cannot be determined from this photograph whether the rhenium and tungsten formed a solid solution in the firing process. The last picture, Fig. 1D shows an unfired sample of rhenium plated onto tungsten wire. Only two pairs of broad lines appear, which is typical of an amorphous or poorly crystallized sample. This shows that the firing is required to produce crystalline rhenium and that the freshly plated unfired rhenium is non-crystalline. The innermost pair of lines of Fig. 1D has a d spacing of approximately 2.18A and lies between the strongest tungsten line, $d=2.22$A and the strongest rhenium line, $d=2.09$A. The second pair of lines has a much smaller spacing but is too diffuse for visual measurement. An additional sample of rhenium-plated tungsten wire was prepared. It was not fired but was placed immediately in a thin-walled Lindemann glass capillary with the ends sealed off (but not evacuated). The x-ray powder pattern of this sample showed the same broad rings as the other unfired sample exposed to air. The x-ray measurements are summarized in Table I.

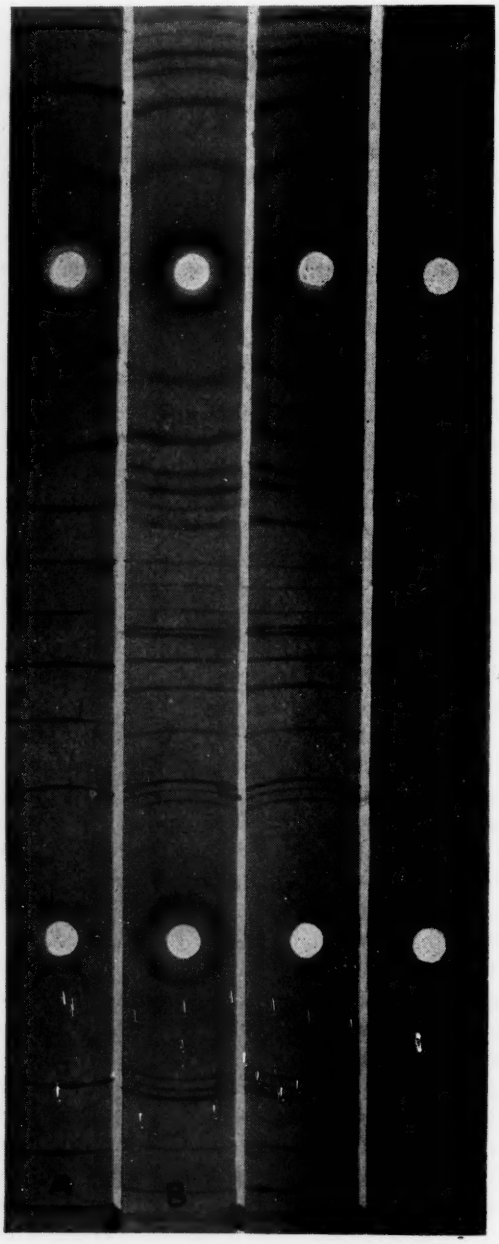

FIG. 1. X-ray diffraction powder photographs of hydrogen fired and unfired rhenium-plated tungsten samples, as compared with pure rhenium. A—uncoated tungsten wire; B—pure rhenium powder coated on a 0.005-in. diameter Pyrex filter; C—rhenium plated on a tungsten wire and fired; D—unfired sample of rhenium plated on tungsten wire.

[6] W. Parrish and E. Cisney, Philips Tech. Rev. **10**, 157 (1948).

TABLE I. X-ray powder data for rhenium.

$hk\cdot l$	θ corrected[I]	d measured	d calculated[II]	I relative[III]
10·0	18.91°	2.379A	2.3909A	4
00·2	20.35	2.217	2.2291	3
10·1	21.56	2.098	2.1070	10
10·2*	28.35	1.623	1.6304	3
11·0	34.04	1.377	1.3804	5
10·3	37.69	1.261	1.2621	4
20·0	40.19	1.1945	1.1955	1
11·2	41.12	1.172	1.1736	5
20·1	42.00	1.152	1.1547	4
00·4	43.92	1.1115	1.1146	1
20·2	47.18	1.051	1.0535	2
10·4	50.02	1.006	1.0101	2
20·3	56.10	0.9303	0.9315	3
21·0	58.64	0.9027	0.9037	2
21·1	60.61	0.8847	0.8857	6
11·4	62.87	0.8662	0.8672	4
10·5	67.30	0.8357	0.8354	5
30·0	75.35	0.7967	0.7970	1

[I] Cu$K\alpha$, $\lambda=1.5418$A.
[II] Based on $a=2.760$A, $c=4.4582$A from K. Moeller, Naturwiss. **19**, 575 (1931), who gives $a=2.755kX$, $c=4.450kX$.
[III] Visual comparisons based on 10·1 = 10.
* The lines begin to broaden at about 30° θ and become broader and more diffuse with increasing θ and $K\alpha_1-K\alpha_2$ resolution not seen.

3. EXPERIMENTAL PROCEDURE AND RESULTS

Diodes for the measurement of emission constants consisted of a conventional guard-ring type with guard rings having the same diameter as the middle measuring anode. These guard-ring anodes were 0.75 in. long and

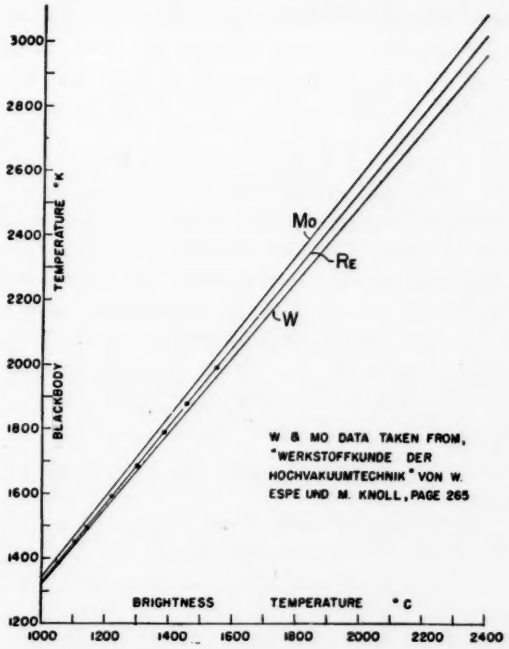

FIG. 2. Blackbody temperature plotted against brightness temperature for molybdenum, rhenium, and tungsten.

the center anode was 0.375 in. long with an inside diameter of 0.375 in. and having a separation of 0.031 in. between the guard-ring anodes and the center anode.

The cathodes consisted of the rhenium-plated tungsten wire previously described. The anodes were formed from 0.007-in. thick tantalum ribbon. A zirconium getter[7] of the coiled-coil type of construction which can be heated by electrical conduction is included in each diode. This type of getter is recommended since it does not deposit thermionically active materials within the diode envelope. Before the mounted stem assembly is sealed into a glass bulb it is inserted into a vacuum bell jar where it is baked at 425°C for two hours. The zirconium getter is then glowed at[8] 1700°C until the vacuum reaches a pressure less than 1.0×10^{-6} mm Hg. The anodes are then outgassed by radiofrequency bombardment at 1600°C for approximately 15 minutes after which the filaments are glowed at 2500°C for 30 minutes. The anodes are then thoroughly outgassed by electronic bombardment for 30 minutes at a temperature of 1500°C until the vacuum pressure is less than 1.0×10^{-6} mm Hg. The getter is again flashed at 1700°C for 3 minutes prior to flushing with dry hydrogen after which the diode assembly is removed from the vacuum bell jar position. The diode assembly is then sealed immediately into a glass envelope, passing a flush of dry nitrogen through the envelope during the sealing, until the seal cools to room temperature.

[7] (a) G. A. Espersen, Proc. I.R.E. 34, No. 3, (1946); W. G. Guldner and L. A. Wooten, Trans. Am. Electrochem. Soc. 93, 223 (1948).

[8] All temperature readings in this section are brightness temperatures.

The sealed-in diode assembly is then attached to a high vacuum position and the diode is again processed according to the procedure indicated in the above paragraph. The tube is sealed off at a pressure of 5.0×10^{-7} mm Hg.

It is noted that in the evacuation process in the determination of the emission characteristics of rhenium, every precaution was taken to insure adequate outgassing of the filaments at a temperature at least several hundred degrees higher than the highest operating temperature. This is done to insure ion-free emission current readings.

Before any data were taken on any tube, the filaments were aged for 250 hours at 1500°C and for 50 hours at 1800°C with no potential applied to the anodes. This practice should assist in stabilizing the surface of the filaments prior to test. In the measurement of their emission characteristics, the filaments were heated by an alternating conduction current which was stabilized by means of a Sorensen-type voltage regulator, model 1750. Variations of voltage which might have occurred during operation were insufficient to cause appreciable change in any temperature readings which were being taken as was well, within the experimental error of observation. The primary anode supply was a 1000-volt electronically regulated supply which could be varied over the entire range. Weston meters were used for voltage and current readings which were calibrated to within ½ percent. All temperature measurements were made with a Leeds and Northrup optical pyrometer 8622-C in conjunction with an objective lens as-

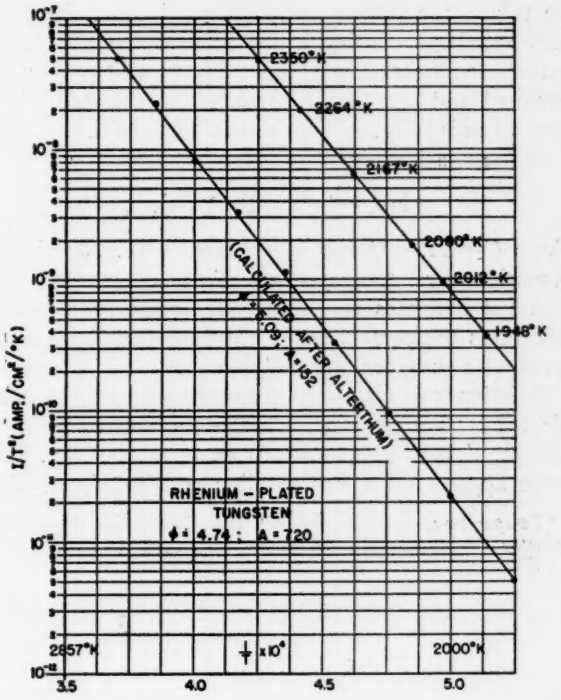

FIG. 3. A Richardson plot of d.c. emission data taken from an average of eleven diodes having rhenium-plated tungsten emitters.

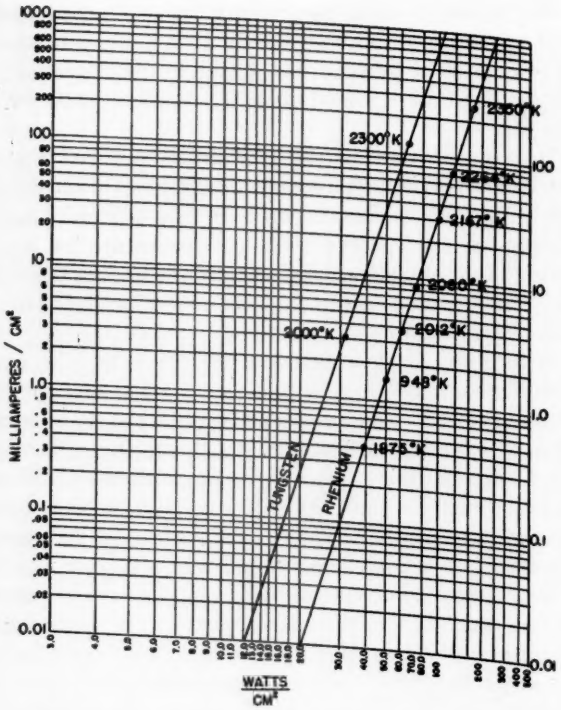

FIG. 4. A power emission plot taken on tungsten and rhenium-plated tungsten emitters.

sembly, Std. 3301–5. Such a micropyrometer arrangement was necessary for measuring filaments which were less than $\frac{1}{32}$ in. in diameter.

During the vigorous outgassing of the metal parts of the tube some metals are evaporated upon the glass bulb forming a coating which reduces the amount of transmitted light. The amount of absorption was determined and the proper corrections were made. The spectral emissivity, ϵ_λ, was calculated to be 0.366 based upon the relationship[9]

$$\ln\epsilon_\lambda = C_2/\lambda(1/T - 1/S_\lambda),$$

where $C_2 = 14,362$ micron-degrees, $\lambda = 0.650$ micron, S_λ = brightness temperature, T = true temperature. Figure 2 indicates the blackbody temperature *versus* brightness temperature of a rhenium surface as compared with tungsten and molybdenum.

Emission currents were corrected for the Schottky effect by plotting the logarithm of current at any voltage, V, *versus* the square root of the voltage. This curve approaches a straight line relationship at high voltages, i.e., from 100 to 500 volts and higher. By extrapolation the intercept of this line at the ordinate gives the current value when the field at the cathode surface is zero. Figures 3 and 4 give the Richardson plot and power emission plot, respectively.

After all emission measurements had been taken, the deposit which had evaporated on the inner surface of the tube was analyzed spectroscopically and showed no trace of tungsten. This total absence of tungsten proves that not only was the electroplated rhenium covering the whole tungsten surface, as has already been indicated by x-ray diffraction analysis, but that during operation tungsten did not diffuse through the rhenium layer to the surface. There is no doubt that the emission results as obtained are from rhenium.

4. DISCUSSION AND CONCLUSIONS

The emission constants derived from these experimental determinations are found from Fig. 3. It will be noted that in comparison with tungsten itself, rhenium has a work function of 4.74 (based on determinations obtained from eleven different samples) in comparison with 4.52 for tungsten. Alterthum[1] gives a value of 5.1 for the work function of rhenium. It is quite possible that because of no Schottky correction and the large crystals he obtained from his vapor phase decomposition of a rhenium salt, his value of 5.1 may actually be lower. Our value of A was found to be 720, while the published value due to Alterthum is 200.

The value of 4.74 is given to two decimal places but the experimental error involved is such that the last place figure should not be taken too seriously. Temperature measurement errors are within $\frac{1}{2}$ percent at 2000°K true temperature, after corrections are taken into account; however, the true surface area of the emitting area is in doubt. It was assumed to be smooth even though there is a slight surface roughness. Such an area could be determined if one used the Brunauer, Emmett, and Teller adsorption theory[10] in conjunction with a graphical method for determining areas,[11] as used at Oak Ridge.

ACKNOWLEDGMENT

The writers wish to express their indebtedness to William Parrish, in whose section the x-ray measurements were made, and to Miriam Gabin who performed these measurements.

[9] *Temperature, Its Measurement and Control in Science and Industry* (Reinhold Publishing Corporation, New York, 1941), p. 1171.

[10] Brunauer, Emmett, and Teller, J. Am. Chem. Soc. **60**, 309 (1938).

[11] F. Miles and W. McMillan, MDDC—1086, Tech. Information Div., Oak Ridge, Tennessee.

On the Compressibility of Metallic Cesium*

R. STERNHEIMER**
*University of Chicago, Chicago, Illinois and Yale University,*** *New Haven, Connecticut*
(Received November 1, 1949)

The volume discontinuity of cesium at 45,000 kg/cm² is attributed to a shift of the valence electrons from the 6*s* zone to the empty 5*d* zones. A Wigner-Seitz calculation for the 6*s* and 5*d* bands supports this explanation. The potential used is described and tabulated. The possible existence of similar transitions for potassium and rubidium is discussed.

I. INTRODUCTION

IN investigating the compressibility of cesium, Bridgman[1] found a volume discontinuity of 11 percent at 45,000 kg/cm². Above the transition the compressibility is unexpectedly small in comparison with the other alkalies and decreases abnormally rapidly with increasing pressure. Figure 1 shows the volume as a function of the pressure.

In order to explain the phase transition, Fermi proposed that the valence electron is forced into a vacant internal orbit. This hypothesis is suggested by the large volume change and the proximity of cesium to the rare earths. The two available orbits are 4*f* and 5*d*. The possibility that the 4*f* orbit becomes occupied can be ruled out on the following basis. If this hypothesis is to be accepted, the energy of the 4*f* state must be close to that of the 6*s* band in the compressed metal (about $-0.3\,Ry$). This can be true only if the effective potential for 4*f* has an attractive trough[2] in the neighborhood of $r=0.5\,a_H$ (r=distance from nucleus, a_H=Bohr radius for hydrogen), as is the case for the rare earths and for the heavier elements. Integration of the Schroedinger equation shows that the trough must be at least 7 to 8 *Ry* deep for the existence of a stationary state. The first element for which the 4*f* function is internal is cerium, $Z=58$. A change of nuclear charge by one unit changes the potential at $r=0.5\,a_H$ by about 1 *Ry*, as is shown by an estimate based on the Thomas-Fermi potential. Hence for cesium, $Z=55$, the potential valley is insufficient by a few Rydberg units to give an internal 4*f* function. This conclusion remains valid throughout the pressure range studied by Bridgman, because in this range the compression has a negligible effect on the potential near the nucleus.

A shift of the valence electron to 5*d* is made plausible by spectroscopic evidence. Table I gives the energy of configurations[3] involving *d* and *s* states of the K, Rb and Cs atoms and of the corresponding alkaline earth ions. The difference in energy between the *d* state and the *s* state decreases with increasing Z and with increasing ionization. In both cases, the potential acting on the valence electron becomes more attractive. In the compression of a metal, the valence electrons are brought closer to the nucleus inside each lattice cell, hence the distance between the 6*s* band and the 5*d* band of cesium is expected to decrease with decreasing volume. As is shown by the calculations (see Section II), an overlapping of the two bands occurs at the smaller volumes and affords an explanation of the phase transition.

II. THE ENERGY OF THE 6*s* AND 5*d* BANDS

The pressure is given by $-\partial E/\partial V$, where E is the energy and V is the volume per atom of the lattice. In order to obtain E, the positions of the 6*s* and 5*d* bands were determined by the method of Wigner and Seitz.[4] In this method the cellular polyhedron surrounding each nucleus is replaced by a sphere of volume V which will be called the *s* sphere. The lowest level of a band is obtained by solving the Schroedinger equation inside the *s* sphere, subject to the condition $\partial\psi/\partial r=0$ at $r=r_0$, where r_0 is the radius of the sphere. Somewhat

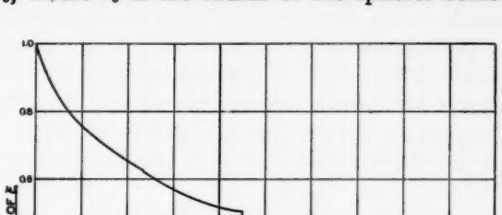

FIG. 1. Volume of cesium as a function of the pressure. The ordinate ξ is the ratio of the volume to the volume at normal pressure. (From Bridgman, reference 1.)

* This paper was written as a Ph.D. thesis in the Department of Physics, University of Chicago, Chicago, Illinois.

** Now at Los Alamos Scientific Laboratory, Los Alamos, New Mexico.

*** Assisted by the ONR and the AEC.

[1] P. W. Bridgman, Phys. Rev. **72**, 533 (1947); Proc. Am. Acad. Arts Sci. **76**, 55 (1948). I am very much indebted to Professor Bridgman for sending me a table of the volume compression of the alkalies before publication.

[2] M. G. Mayer, Phys. Rev. **60**, 184 (1941).

[3] From R. F. Bacher and S. Goudsmit, *Atomic Energy States* (McGraw-Hill Book Company, Inc., New York, 1932).

[4] E. Wigner and F. Seitz, Phys. Rev. **43**, 804 (1933); **46**, 509 (1934).

TABLE I. Energy in *Ry* units of *s* and *d* states for K, Rb, and Cs and the corresponding alkaline earth ions. The zero of energy corresponds to ionization of the valence electron. (From Bacher and Goudsmit, reference 3.)

K	4*s*	−0.3190	Ca II	4*s*	−0.8725
	3*d*	−0.1227		3*d*	−0.7478
Rb	5*s*	−0.3070	Sr II	5*s*	−0.8106
	4*d*	−0.1306		4*d*	−0.6764
Cs	6*s*	−0.2862	Ba II	6*s*	−0.7350
	5*d*	−0.1535		5*d*	−0.6862

different potentials, V_{6s}' and V_{5d}', were used for 6*s* and 5*d*. The determination of these potentials is described in Section III. They are based on the Hartree-Fock equations and are adjusted to give agreement with the respective atomic levels, $E_{6s}=-0.2862\ Ry$ and $E_{5d}=-0.1535\ Ry$. In Table II the energies $E_{6s}{}^B$ and $E_{5d}{}^B$ of the bottom of the 6*s* and of the 5*d* band are given as a function of r_0. These energies are also shown in Fig. 2. Below each r_0, we have listed the corresponding ratio V/V_{th} where V_{th} is the volume at normal pressure obtained from the present calculations. As shown below, V_{th} corresponds to $r_0=5.92\ a_H$; the experimental value is $5.59\ a_H$. We note that in an accurate calculation, the atomic 5*d* level would split into two levels for zero wave-number, one twofold and one threefold degenerate. This splitting is not obtained in the *s* sphere approximation. However, it is believed that it would not affect the essential results of the present work.

The width of the bands will now be determined. For each band we let p_0 be the momentum for the highest filled level and E_F the width of the occupied region, on the assumption that all valence electrons occupy levels in the band considered. For the 6*s* band,

$$p_0=(9\pi/4)^{\frac{1}{3}}(\hbar/r_0). \tag{1}$$

For the 5*d* band, there are five zones which correspond in the present method to the values of the magnetic quantum number *M*. On the assumption that levels having the same wave number vector but different *M* are degenerate, the density of states is five times the density for the 6*s* band, and p_0 is smaller than (1) by a factor $5^{\frac{1}{3}}$.

The width E_F would be $p_0^2/(2m)$ if the electrons could be considered as perfectly free. Wigner and Seitz[5] have treated the effect of the ion cores on the band width by perturbation theory. They found that the energy E_κ of the wave with wave number vector κ is given by

$$E_\kappa=E_0+\frac{\hbar^2\kappa^2}{2m}\left[1-\frac{2\hbar^2}{m\kappa^2}\sum_\lambda\frac{|\int(\kappa\cdot\mathrm{grad}\psi_0)\psi^{\lambda*}d\tau|^2}{E^\lambda-E_0}\right], \tag{2}$$

where E_0 and ψ_0 are the energy and the wave function for the bottom of the band, respectively; the sum extends over all eigenfunctions ψ^λ of the Schroedinger equation,

$$-(\hbar^2/2m)\Delta\psi^\lambda+V_0\psi^\lambda=E^\lambda\psi^\lambda, \tag{3}$$

which is to be solved inside the *s* sphere, subject to the condition $\psi^\lambda=0$ at $r=r_0$; E^λ is the eigenvalue and V_0 is the potential representing the interaction with the core. In Eq. (2) the integral extends over the *s* sphere. If E_0 and E^λ are expressed in *Ry* and lengths are in units a_H, one obtains

$$E_F=\frac{p_0^2}{2m}\left[1-\sum_\lambda\frac{4|\alpha_\lambda|^2}{E^\lambda-E_0}\right], \tag{4}$$

with

$$\alpha_\lambda=2\pi\int_0^\pi\int_0^{r_0}(\partial\psi_0/\partial r)\cos\theta\psi^{\lambda*}r^2dr\sin\theta d\theta. \tag{5}$$

Here θ is the angle between the radius vector in the integrand and the axis of quantization of the spherical harmonics of ψ_0 and ψ^λ. For the 6*s* band the *p* states[6] give,

$$\alpha_\lambda=(1/\sqrt{3})\int_0^{r_0}(dR_{6s}/dr)R_\lambda{}^{(p)}r^2dr, \tag{5a}$$

where R_{6s} is the wave function for the bottom of the 6*s* band, $R_\lambda{}^{(p)}$ is the radial part of the *p* function ψ^λ; the normalization is

$$\int_0^{r_0}R_{6s}{}^2r^2dr=\int_0^{r_0}(R_\lambda{}^{(p)})^2r^2dr=1.$$

TABLE II. Position of the bottom of the 6*s* and of the 5*d* band for various r_0. Energies are in *Ry* units, r_0 is in units a_H.

r_0	$-E_{6s}{}^B$	$-E_{5d}{}^B$
6.0	0.4151	
5.8	0.4217	
5.6	0.4267	0.2371
5.4	0.4303	0.2419
5.2	0.4322	0.2473
5.0	0.4308	0.2533
4.8	0.4263	0.2598
4.6	0.4140	0.2673
4.4	0.3948	0.2764
4.2	0.3617	0.2855
4.0	0.3108	0.2972

Table III gives the values of α_λ and the corresponding energy denominators for several r_0. The sign of α_λ pertains to the choice in which all functions have the same sign near $r=0$. In calculating the 6*p*, 7*p* and 8*p* functions the potential V_0 in Eq. (4) was taken as V_{6s}'. For 4*p* the Hartree[6] function for Cs^+ was used, and the 5*p* functions were determined by means of the potential V_{5p} described below. Including a correction for the *p* states not listed in the table, one obtains the values of the square bracket in Eq. (4) which are tabulated as $m/m_{6s}{}^*$; $m_{6s}{}^*$ is the effective mass for the 6*s* band.

[5] See, for example, F. Seitz, *The Modern Theory of Solids* (McGraw-Hill Book, Company, Inc., New York, 1940), Chapters IX and X.

[6] D. R. Hartree, Proc. Roy. Soc. 143, 506 (1934).

As a check on the reliability of Eq. (4), the fourth-order perturbation term was calculated. This term gives the following contribution to the average energy,[7]

$$(3p_0^2/10m)(1.315\lambda_2/r_0^2), \tag{6}$$

where

$$\lambda_2=\lambda_1\sum_\lambda \frac{8|\alpha_\lambda|^2}{(E^\lambda-E_0)^2}, \tag{6a}$$

and

$$\lambda_1=1-m/m_{6s}{}^*=\sum_\lambda \frac{4|\alpha_\lambda|^2}{E^\lambda-E_0}. \tag{6b}$$

The factor $1.315\ \lambda_2/r_0^2$ is shown as Δ in Table III. It is seen that the fourth-order correction is small, except in the region of small r_0. It was not included in the compressibility calculations.

For the $5d$ zone with magnetic quantum number M, α_λ is given by

$$\alpha_{\lambda M}=\int_0^\pi\int_0^{r_0}(dR_{5d}/dr)\Theta_2{}^M\cos\theta\Theta_l{}^{M*}R_\lambda r^2dr\sin\theta d\theta d\theta, \tag{7}$$

where R_{5d} is the radial function for the bottom of the $5d$ band, $\Theta_L{}^M$ is the spherical harmonic pertaining to quantum numbers L and M, R_λ is the radial part of ψ^λ, l is the azimuthal quantum number of ψ^λ; the normalization is

$$\int_0^{r_0}R_{5d}{}^2r^2dr=\int_0^{r_0}R_\lambda{}^2r^2dr=1;\quad \int_0^\pi|\Theta_L{}^M|^2\sin\theta d\theta d\theta=1.$$

$\alpha_{\lambda M}$ vanishes unless $l=1$ or $l=3$; hence only p and f states contribute. Because of the dependence of $\alpha_{\lambda M}$ on M, the degeneracy of the levels for the same wave vector κ is removed. By determining κ for the highest occupied state in each zone, it is found, for

$$|\alpha_{\lambda M}|^2/(E^\lambda-E_0)\ll 1,$$

that E_F is given by Eq. (4), if one takes

$$|\alpha_\lambda|^2=(1/5)\sum_{M=-2}^{2}|\alpha_{\lambda M}|^2, \tag{8}$$

and

$$p_0=(9\pi/20)^{\frac{1}{3}}\hbar/r_0. \tag{1a}$$

We thus obtain

$$\alpha_\lambda=\begin{cases}(2/15)^{\frac{1}{2}}\int_0^{r_0}(dR_{5d}/dr)R_\lambda r^2dr, & (l=1)\\ (1/5)^{\frac{1}{2}}\int_0^{r_0}(dR_{5d}/dr)R_\lambda r^2dr. & (l=3).\end{cases} \tag{8a}$$

Table IV gives the values of α_λ and the corresponding energy denominators. Including a correction for the p and f states not listed, one obtains the values of the square bracket in Eq. (4) which are tabulated as $m/m_{5d}{}^*$. The contribution of the f states to the sum in Eq. (4) is shown as S_f. The fourth-order perturbation term is negligible for the $5d$ band.

When the appropriate width is added to $E_{6s}{}^B$ and to $E_{5d}{}^B$, one obtains the energy of the highest occupied level on the assumption that all valence electrons are in $6s$ or in $5d$ states, respectively; these energies are given as $E_{6s}{}^T$ and $E_{5d}{}^T$ in Fig. 2. This figure shows that at $r_0=5.22\ a_H$, the curve for the bottom of $5d$ intersects the curve for the top of $6s$. As the metal is further compressed electrons from the top of $6s$ move into $5d$. The fraction g of the electrons which occupies $5d$ can be obtained from the following equation for the energy E^T of the highest occupied level,

$$E^T=E_{6s}{}^B+(E_{6s}{}^T-E_{6s}{}^B)(1-g)^{\frac{1}{3}}=E_{5d}{}^B+(E_{5d}{}^T-E_{5d}{}^B)g^{\frac{1}{3}}. \tag{9}$$

The shift to the $5d$ zones is rapid. The reasons are that $E_{5d}{}^B$ decreases, while $E_{6s}{}^B$ increases with decreasing volume and that the $5d$ band has a greater density of levels than the $6s$ band. The different behavior of the $6s$ and $5d$ curves for the lowest states is due to the smaller number of radial nodes of the $5d$ function (see Fig. 3). The minimum of the energy curve arises from the combined effect of the kinetic and the potential energy. The former increases with decreasing volume because of the decreasing effective wave-length of the electrons, while the potential energy is lowered in a compression. The volume at which the first effect predominates is smaller for $5d$ than for $6s$, because of the relative position of the outermost nodes.

The average energy E^A of the valence electrons is obtained by adding the mean translational energy to the energy of the lowest level of each band. We have,

$$E^A=(1-g)[E_{6s}{}^B+3/5(E^T-E_{6s}{}^B)]+g[E_{5d}{}^B+3/5(E^T-E_{5d}{}^B)]. \tag{10}$$

The curve of E^A is shown in Fig. 2. The minimum at $r_0=5.86\ a_H$ corresponds to normal pressure. With decreasing r_0, presumably between $4\ a_H$ and $5\ a_H$, E^A ceases to be a good approximation to the total energy, because of the repulsion of the $5s$ and $5p$ shells. Hence

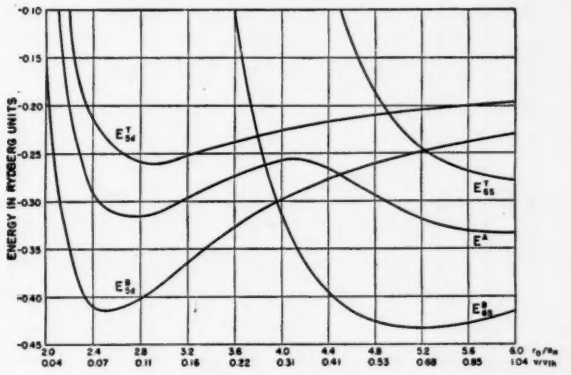

FIG. 2. Position of the $6s$ and $5d$ bands and average energy E^A, as a function of r_0 or of V/V_{th}.

[7] F. Seitz, Phys. Rev. 47, 400 (1935).

TABLE III. Values of α_λ and of $E^\lambda - E_0$ for obtaining m/m_{6s}^* and values of m/m_{6s}^* for various radii r_0. Energies are in Ry units, r_0 is in units a_H.

	r_0	5.8	5.2	4.6	4.0
$4p$	α_λ	0.214	0.216	0.274	0.466
	$E^\lambda - E_0$	−11.3	−11.3	−11.3	−11.4
$5p$	α_λ	0.276	0.281	0.357	0.601
	$E^\lambda - E_0$	−0.84	−0.83	−0.83	−0.89
$6p$	α_λ	−0.011	−0.028	−0.081	−0.199
	$E^\lambda - E_0$	0.79	1.08	1.52	2.211
$7p$	α_λ	−0.087	−0.095	−0.128	−0.258
	$E^\lambda - E_0$	2.62	3.45	4.70	6.58
$8p$	α_λ	−0.092	−0.096	−0.138	−0.250
	$E^\lambda - E_0$	5.24	6.74	8.96	12.68
	m/m_{6s}^*	1.349	1.372	1.592	2.555
	Δ	−0.012	−0.017	−0.056	−0.479

the second minimum at $r_0 = 2.79\, a_H$ has no direct significance.

In order to obtain some information on the effects due to $5s$ and $5p$ electrons, the energies for the bottom and the top of the $5s$ and $5p$ bands were calculated by integrating the Schroedinger equation subject to the conditions $\partial\psi/\partial r = 0$ (bottom) and $\psi = 0$ (top[8]) at $r = r_0$. The potentials V_{5s} and V_{5p} used in these integrations are obtained in Section III. Table V gives the energies $E_{5s}{}^B$ and $E_{5s}{}^T$ for the bottom and the top of $5s$ and the energies $E_{5p}{}^B$ and $E_{5p}{}^T$ for the bottom and the top of $5p$.

The contribution E_{int} of $5s$ and $5p$ to the total energy E is given by

$$E_{\text{int}}(r_0) = 2E_{5s}{}^A(r_0) + 6E_{5p}{}^A(r_0) - 2E_{5s} - 6E_{5p}. \quad (11)$$

TABLE IV. Values of α_λ and of $E^\lambda - E_0$ for obtaining m/m_{5d}^* and values of S_f and m/m_{5d}^* for various radii r_0. Energies are in Ry units, r_0 is in units a_H.

	r_0	5.2	4.6	4.0
$4p$	α_λ	0.159	0.181	0.212
	$E^\lambda - E_0$	−11.5	−11.4	−11.4
$5p$	α_λ	−0.034	−0.044	−0.060
	$E^\lambda - E_0$	−1.01	−0.98	−0.91
$6p$	α_λ	−0.044	−0.049	−0.055
	$E^\lambda - E_0$	0.89	1.37	2.19
$7p$	α_λ	−0.030	−0.033	−0.038
	$E^\lambda - E_0$	3.27	4.55	6.57
$8p$	α_λ	−0.025	−0.027	−0.028
	$E^\lambda - E_0$	6.56	8.82	12.67
$4f$	α_λ	0.085	0.106	0.136
	$E^\lambda - E_0$	0.57	0.61	0.67
$5f$	α_λ	0.079	0.077	0.068
	$E^\lambda - E_0$	1.41	1.80	2.37
$6f$	α_λ	0.017	−0.004	−0.041
	$E^\lambda - E_0$	3.23	4.10	5.47
	S_f	0.077	0.095	0.128
	m/m_{5d}^*	0.913	0.897	0.865

[8] J. C. Slater, Phys. Rev. 45, 794 (1934).

Here $E_{5s}{}^A$ and $E_{5p}{}^A$ are the average energies of the electrons in the $5s$ and the $5p$ band; E_{5s} and E_{5p} are the atomic levels for the potentials V_{5s} and V_{5p}, respectively. A theoretical determination of E_{int}, which would require a calculation of the distribution of levels in the two bands, was not carried out. E_{int} is expected to increase rapidly with decreasing r_0 at the smaller volumes, since it includes the exchange repulsion. This effect will be discussed below. Here we note that the second estimate given in this discussion, which leads to a repulsion energy of 0.024 Ry at $r_0 = 4.0\, a_H$, can be correlated with the calculation of the bands, if one assumes that the average energy in each band is related to the energies for the lowest and highest levels by the following equations.

$$\begin{aligned} E_{5s}{}^A &= \alpha E_{5s}{}^B + (1-\alpha) E_{5s}{}^T, \\ E_{5p}{}^A &= \alpha E_{5p}{}^B + (1-\alpha) E_{5p}{}^T, \end{aligned} \quad (12)$$

where α is a constant parameter independent of r_0. One finds that for $\alpha = 0.39$, $E_{\text{int}}(r_0)$ (see Eq. (11)) agrees with the estimate of the repulsion energy throughout the range of r_0.

For the energy of interaction between the free electrons we used the following expression, taken from the treatment of Wigner and Seitz,[5]

$$E_f = \frac{0.6e^2}{r_0} - \frac{0.458e^2}{r_0} - \frac{0.288e^2}{r_0 + 5.1\, a_H}. \quad (13)$$

The terms in (13) represent, respectively, the Coulomb repulsion, the exchange interaction and the electrostatic correlation.

The cohesive energy and the radius r_0 at normal pressure will now be compared with experiment. The curve of $E^A + E_f$ has a minimum of -0.3374 Ry which lies at $5.92\, a_H$. One thus finds a theoretical cohesive energy of 16.1 kg cal./mole. The heat of sublimation[9] is 18.8 kg cal./mole. Upon making the appropriate temperature correction ($300 \times (6-3) = 900$ cal./mole), one obtains 19.7 kg cal./mole for the experimental cohesive energy. The experimental value of r_0 is $5.59\, a_H$. Thus the agreement with experiment is comparable to that obtained in similar calculations[5] for lithium, sodium and potassium.

Table VI gives the energy E_{th}, defined by

$$E_{th} = E^A + E_f$$

and the increase of energy ΔE_{th},

$$\Delta E_{th}(r_0) = E_{th}(r_0) - E_{th}(5.92\, a_H).$$

We note that E_{th} and ΔE_{th} do not include the exchange repulsion, which will be discussed below. The experimental increase of energy, to be denoted by ΔE_{exp}, will now be obtained from Bridgman's measurements. In first approximation the increase of internal energy in a compression through dV is PdV (P=pressure).

[9] F. Seitz, reference 5, p. 3.

The heat released by the sample in this compression is

$$-T(\partial S/\partial V)_T dV = T(\partial P/\partial V)_T(\partial V/\partial T)_P dV,$$

where T is the temperature which will be taken as 0°C, and S is the entropy per atom. In order to evaluate this term, $(\partial P/\partial V)_T$ can be obtained from the observed compression. The dependence of $(\partial V/\partial T)_P$ on the pressure is not known for cesium. $(\partial V/\partial T)_P$ was therefore estimated on the basis of Bridgman's measurements[10] of the expansion coefficient for lithium, sodium and potassium up to 20,000 kg/cm². It was found that the heat given up in the compression to 100,000 kg/cm² is only 0.002 Ry per atom. We now define,

$$\Delta E_{\exp}(r_0) = \int_{V_{\exp}(r_0/5.92\,a_H)^3}^{V_{\exp}} [P - T(\partial S/\partial V)_T] dV, \quad (14)$$

where $V_{\exp} = (4\pi/3)(5.59\,a_H)^3$ is the experimental volume per atom at normal pressure and absolute zero. Equation (14) implies that we compare points on the experimental and the theoretical curves of energy *vs.* volume which correspond to equal ratios of the volume to the volume for the minimum of the curve. Because of the thermal expansion, $V_{\exp}$ is a fraction $(1+273\beta)^{-3}$ of the volume at normal pressure and 0°C, where β is the linear expansion coefficient; upon taking[11] $\beta = 97\times10^{-6}$ one finds a value of 0.925. Hence if ξ denotes the observed ratio of volume to volume at normal pressure (see Fig. 1), Eq. (11) becomes

$$\Delta E_{\exp}(r_0) = \frac{V_{\exp}}{0.925}\int_{0.925(r_0/5.92\,a_H)^3}^{0.925} [P - T(\partial S/\partial V)_T] d\xi. \quad (14a)$$

$\Delta E_{\exp}$ is given in Table VI. This table also lists the average pressure $P_a(r_0)$ for the region between r_0 and $r_0+\delta$ (δ = interval for which r_0 is tabulated), calculated as follows,

$$P_a(r_0) = \frac{\Delta E_{th}(r_0) - \Delta E_{th}(r_0+\delta)}{4\pi(r_0+\tfrac{1}{2}\delta)^2\delta}.$$

The value which P_a would have if the electrons were restricted to the 6s zone is given as P_{6s}. In the last column $P_{\exp}(r_0)$ is the observed pressure, extrapolated to absolute zero, for the volume

$$V_{\exp}[(r_0+\tfrac{1}{2}\delta)/5.92\,a_H]^3.$$

Since P_a does not include the exchange repulsion, it cannot be compared directly with $P_{\exp}$ at the smaller volumes. However $P_{6s}-P_a$ depends only on the position of the bands and shows the effect of the 5d states.

The volume discontinuity and the exchange repulsion will now be discussed. The observed limits of the discontinuity correspond to

$$V/V_{\exp} = 0.506/0.925 = 0.547,$$
$$V/V_{\exp} = 0.449/0.925 = 0.485.$$

Here 0.506 and 0.449 are the values of ξ at the limits of the transition; the factor 1/0.925 takes into account the thermal expansion at normal pressure. For the existence of a volume discontinuity it is necessary that the curve of total energy E *vs.* V have a region of downward curvature; the volume changes discontinuously between the two points with common tangent. Figure 4 shows the energies $\Delta E_{\exp}$ and ΔE_{th}. The curve of ΔE_{th} is approximately a straight line in the region from $V/V_{th}=0.55$ to 0.4. In order to obtain the curvature of E, the ionic repulsion energy must be added to ΔE_{th}. For an estimate of the repulsion term we use the expression due to Born and Mayer[12] for the interaction between two neighboring ions, to be denoted

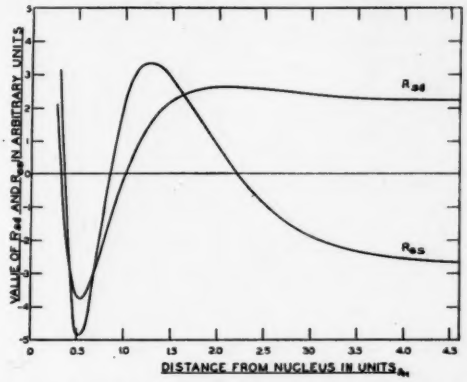

FIG. 3. Wave functions R_{ss} and R_{sd} for the radius $r_0=4.6\,a_H$ of the s sphere.

TABLE V. Position of the 5s and of the 5p band for various r_0. Energies are in Ry units, r_0 is in units a_H.

r_0	$-E_{5s}{}^B$	$-E_{5s}{}^T$	$-E_{5p}{}^B$	$-E_{5p}{}^T$
5.8	2.491	2.491	1.271	1.265
5.2	2.492	2.490	1.278	1.261
4.6	2.497	2.487	1.299	1.247
4.0	2.518	2.473	1.357	1.205

TABLE VI. Energy terms and values of the pressure. Energies are in Ry units, pressures are in units 1000 kg/cm², r_0 is in units a_H.

r_0	$-E_{th}$	ΔE_{th}	$\Delta E_{\exp}$	P_a	$P_{\exp}$	P_{6s}
5.8	0.3369	0.05×10^{-2}	0.05×10^{-2}			
5.6	0.3342	0.32	0.28	5.0	4.9	
5.4	0.3292	0.82	0.73	9.9	11	
5.2	0.3213	1.61	1.48	17	19	
5.0	0.3073	3.01	2.48	32	27	38
4.8	0.2920	4.54	3.74	38	39	55
4.6	0.2757	6.17	5.20	44	45	95
4.4	0.2604	7.70	6.96	45	60	182

[10] P. W. Bridgman, Proc. Am. Acad. **70**, 71 (1934).

[11] *International Critical Tables* (McGraw-Hill Book Company, Inc., New York, 1926), first edition, Volume I, p. 104.

[12] M. Born and J. E. Mayer, Zeits. f. Physik **75**, 1 (1932).

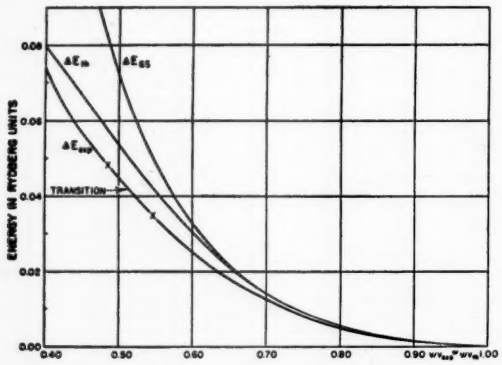

FIG. 4. Increase of energy ΔE_{exp} as a function of V/V_{exp}; the theoretical results ΔE_{th} and ΔE_{6s} are plotted *versus* V/V_{th}. The repulsion energy must be added to ΔE_{th} in order to obtain the theoretical total energy.

by E_{ion},

$$E_{\text{ion}}=A\exp[(2r_i-D)/a]. \tag{15}$$

Here D is the distance between the nuclei, r_i is the ionic radius, A and a are constants whose values will be taken first from the work of Bardeen[13] $A=1.25\times10^{-12}$ erg, $r_i=1.75$A, $a=0.21$A. It will be assumed that the lattice is close-packed, in accordance with Bardeen's explanation[13] of the transition at 23,000 kg/cm² as due to the change from the body-centered to a close-packed structure. One finds that the repulsion energy per atom, $6E_{\text{ion}}$, increases from 0.0047 Ry at $r_0=4.6\,a_{\text{H}}$ to 0.072 Ry at $r_0=4.0\,a_{\text{H}}$. The increase of E_{ion} is sensitive to the constants in the exponent. The constants obtained by Huggins and Mayer,[14] $r_i=1.455$A, $a=0.345$A, $A=1.25\times10^{-12}$ erg, would lead to an increase of $6E_{\text{ion}}$ from 0.0046 Ry at $r_0=4.6\,a_{\text{H}}$ to 0.024 Ry at $r_0=4.0\,a_{\text{H}}$. These estimates are compatible with the assumption that the repulsion energy does not become important until the metal is compressed to about $r_0=4.5\,a_{\text{H}}$ ($V/V_{th}=0.44$). On this basis there is a region between $V/V_{th}\sim0.55$ and $V/V_{th}\sim0.44$ in which the curve of E, as obtained here, is approximately a straight line. This result may be taken as an indication of the observed phase transition. It should be emphasized that an exact agreement with the details of the compressibility curve cannot be expected, on account of the approximations made in the calculation of the energy.

According to the present picture, the repulsion energy effectively determines the lower limit of the transition, which otherwise would extend to a smaller volume, as is shown by the curve of E^A in Fig. 2. A comparison with the increase of ΔE_{exp} indicates that the repulsion energy probably is sufficiently large to account for the low compressibility above the transition. We note that when the repulsion energy is added to ΔE_{th} for $V/V_{th}=0.40$, the resulting increase of the total energy is between 1.2 and 1.5 times the observed value ΔE_{exp}. It is believed that this disagreement lies within the uncertainty of the calculations.

In Fig. 4 we have also shown the increase of energy ΔE_{6s}, obtained by assuming that all valence electrons are in 6s,

$$\Delta E_{6s}(r_0)=E_{6s}{}^A(r_0)+E_f(r_0)-E_{th}(5.92\,a_{\text{H}}),$$

where $E_{6s}{}^A$ is the average energy for the states of the 6s band. ΔE_{th} is in much closer agreement with the experimental curve than ΔE_{6s}. The repulsion energy, which must be added to ΔE_{6s}, would further increase the departure of the 6s curve from the experimental results.

It is of interest to examine the behavior of E near the volume at which 5d begins to overlap the occupied region of 6s; this volume will be denoted by V_1. It will be shown that the term in E, associated with the occupation of 5d, varies as $(V_1-V)^{5/2}$. In first approximation, $E_{6s}{}^T-E_{5d}{}^B$ is linear in V_1-V, so that the number of 5d electrons is proportional to $(V_1-V)^{3/2}$. Since the energy of these electrons is lowered by an amount of the order of $E_{6s}{}^T-E_{5d}{}^B$, one finds a dependence $(V_1-V)^{5/2}$ for the change of the average energy. If the term in E is written as $-\eta(V_1-V)^{5/2}$ ($\eta>0$), we have

$$\left(\frac{d^2E}{dV^2}=\frac{d^2E}{dV^2}\right)_{V_1}-\frac{15}{4}\eta(V_1-V)^{\frac{1}{2}}+\cdots,\quad(V<V_1) \tag{16}$$

for small V_1-V. The term $d^2E/dV^2)_{V_1}$ is characteristic of 6s and is positive. Because of the second and higher terms in the expansion, d^2E/dV^2 becomes negative unless the exchange repulsion predominates. The limits of the discontinuity lie outside the region where $d^2E/dV^2<0$ and the upper limit is not expected to coincide with V_1. Thus for small η or strong ionic repulsion, the transition rends to occur after the bands have begun to overlap. We note that the 6s–5d overlapping occurs for $V_1/V_{th}=0.686$, while the transition starts at $V/V_{\text{exp}}=0.547$.

If the present explanation is correct, the phase transition is associated with a marked increase of the magnetic susceptibility. For perfectly free electrons, the susceptibility (per gram) χ_p due to spin paramagnetism[15] is

$$\chi_p=\frac{3N_0}{2AE_F}\left(\frac{e\hbar}{2mc}\right)^2, \tag{17}$$

(N_0=Avogadro's number, A=atomic weight). Upon taking $E_F=p_0^2/(2m^*)$ (see Eq. (4)), we find $\chi_p=0.090\times10^{-6}$ for the 6s band and 0.448×10^{-6} for the 5d band, at $r_0=4.40\,a_{\text{H}}$ (lower limit of transition). For the total susceptibility χ we obtain

$$\chi=\tfrac{2}{3}(0.45\times10^{-6})-0.29\times10^{-6}=0.01\times10^{-6}.$$

Here the factor $\frac{2}{3}$ accounts for the diamagnetism of the

[13] J. Bardeen, J. Chem. Phys. 6, 372 (1938).
[14] M. L. Huggins and J. E. Mayer, J. Chem. Phys. 1, 643 (1933).
[15] See, for example, F. Seitz, reference 5, p. 160.

free electrons and the second term is the contribution of the ion core.[16] A similar estimate for normal pressure[17] gives $\chi=-0.13\times10^{-6}$.

The absence of similar transitions for potassium and rubidium[1] in the range up to 100,000 kg/cm² will now be discussed. The separation of the atomic d and s levels (Table I) suggests that a greater increase of energy than for cesium is required to raise the s band above the lowest d level. The work done in the compression to 100,000 kg/cm², as obtained from Bridgman's data,[1] is 0.044 Ry for potassium and 0.059 Ry for rubidium. While these values exceed the work for cesium up to 45,000 kg/cm² (0.037 Ry), the increase of energy may be insufficient to produce the transition.

This possible explanation will be considered in greater detail. At 100,000 kg/cm² the energy E per atom is

$$E=-E_i-E_c+W, \tag{18}$$

where E_i is the ionization potential, E_c and W denote, respectively, the cohesive energy at normal pressure and the work done in the compression, both extrapolated to absolute zero. With E_i as given in Table I and E_c obtained from the heat of sublimation,[9] one finds $E=-0.343\,Ry$ for potassium and $-0.313\,Ry$ for rubidium at 100,000 kg/cm², while the energy for cesium is $-0.312\,Ry$ at the start of the transition (45,000 kg/cm²). In view of the results obtained for cesium, it seems reasonable to expect that the start of the transition will lie close to the volume at which the average energy of the states of the s band equals the energy of the lowest d level. On the assumption that the ionic repulsion is small and that most valence electrons occupy s levels at the pressure for which E has been calculated, E gives approximately the average energy of the s band. On this basis a comparison of the values of E shows that a phase transition below 100,000 kg/cm² is unlikely for potassium and rubidium, if the botton of the d band at 100,000 kg/cm² lies at a higher energy than the bottom of $5d$ for cesium at the start of the transition. From the observed compression, one obtains $r_0=3.92\,a_H$ for potassium and $r_0=4.14\,a_H$ for rubidium at 100,000 kg/cm², while the radius for cesium at 45,000 kg/cm² is $4.57\,a_H$. The energy of d levels is lowered in a compression; the fact that r_0 is smaller for potassium and rubidium tends to favor a lower energy than for cesium. On the other hand, the relative position of the d levels of the three alkalies for a given r_0 is not known. If the trend is the same as for the atomic levels, the energy increases in the order of decreasing Z. This effect would tend to compensate the effect of the smaller radius. A definite conclusion cannot be drawn from these considerations. If the present explanation is correct, a volume discontinuity should occur above 100,000 kg/cm², in the region in which the shift of the electrons from the s to the d states is most rapid, unless the ionic repulsion predominates at the corresponding volume.

[16] A. Sommerfeld and H. Bethe, *Handbuch der Physik* XXIV/2 (Julius Springer, Berlin, 1933), p. 473.

[17] N. F. Mott and H. Jones, *The Theory of the Properties of Metals and Alloys* (Clarendon Press, Oxford, 1936).

III. THE EFFECTIVE POTENTIALS

In this section the calculations leading to the poteintials V_{6s}' and V_{5d}' will be described. The main part of this work was concerned with the determination of the potential energy terms in the Hartree-Fock equations for the $6s$ and $5d$ wave functions.

The calculations were based on Hartree's field without exchange[6] for Cs^+. The wave functions for $1s$, $2s$, $\cdots$, $4d$ were taken from Hartree's work and the Hartree-Fock equations were solved to a sufficient approximation for $5s^25p^66s$ with boundary conditions appropriate to the metal for $r_0=4.6\,a_H$. In this calculation it was assumed that all free electrons occupy $6s$ states. For $5s$ and $5p$ two functions were considered at each stage of the calculation, namely, those for the lowest and the highest state of the band, satisfying the conditions $\partial\psi/\partial r=0$ and $\psi=0$ at $r=r_0$, respectively. It was assumed that the electrostatic potential due to $5s$ and $5p$ for the next stage of the calculation is the same as if half the electrons of each zone occupied the lowest and half the highest state. For $6s$ the effective charge distribution was obtained from a single wave function determined from the boundary condition,

$$(\partial\psi/\partial r)+1/2(\psi/r)=0$$

at $r=r_0$, which is intermediate between the boundary conditions for the lowest and the highest state of the zone. The preceding approximations do not significantly affect the potentials for $6s$ and $5d$, because the difference between the wave functions for the lowest and the highest occupied state of each zone is small for $r_0=4.6\,a_H$.

The potential due to the $1s$, $2s$, $\cdots$, $4d$ electrons was obtained from Hartree's charge distribution.[6] The exchange of $5s$, $5p$ and $6s$ with these electrons was represented by an added term in the potential,[18] obtained as follows. Consider two free electrons with wave functions $(1/\sqrt{\Omega})\exp(i\kappa_1\cdot\mathbf{r}_1)$, $(1/\sqrt{\Omega})\exp(i\kappa_2\cdot\mathbf{r}_2)$; here κ_1 and κ_2 are the wave-number vectors, $\mathbf{r}_1$ and $\mathbf{r}_2$ are the position vectors of the electrons, Ω is the volume of normalization. In the Hartree-Fock equation exchange appears as a term[19]

$$\left[-\frac{e^2}{\Omega}\int_\Omega\frac{\exp(-i(\kappa_1-\kappa_2)\cdot(\mathbf{r}_1-\mathbf{r}_2)}{|\mathbf{r}_1-\mathbf{r}_2|}d\mathbf{r}_2\right]\frac{\exp(i\kappa_1\cdot\mathbf{r}_1)}{\sqrt{\Omega}} \tag{19}$$

in the equation for electron 1. In the limit $\Omega\to\infty$ the integral is independent of $\mathbf{r}_1$ and its value, denoted by K, is

$$K=4\pi/|\kappa_1-\kappa_2|^2. \tag{19a}$$

Hence (19) is just a constant times the wave function.

[18] I am very much indebted to Dr. J. Steinberger and Professor E. Teller who developed this treatment of exchange.

[19] See, for example, F. Seitz, reference 5, p. 339.

This well-known result for free electrons suggests the following representation of exchange of an outer electron ($5s$, $5p$, $6s$) with one of the inner shells at $\mathbf{r}$. The electrons are considered as free with wave numbers corresponding to their classical kinetic energy. Thus we have,

$$\hbar^2\kappa_i^2/(2m)=\epsilon_i-V_i(r), \quad (i=1, 2)$$

where κ_1 and κ_2 are the wave-numbers, ϵ_1 and ϵ_2 are the Hartree eigenvalues, V_1 and V_2 are the Hartree self-consistent potentials for the outer and the inner shell, respectively. It is assumed that the motion of the inner electrons is isotropic and K is averaged over all orientations of κ_2. $1/\Omega$ is replaced by the density $(2l_2+1)\psi_2^2(r)$ or the electrons of parallel spin, ψ_2 being the normalized radial Hartree function for the inner shell and l_2 its azimuthal quantum number. The resulting value of the bracket in (19), to be denoted by V_{ex}, is

$$V_{ex}=-\frac{2\pi(2l_2+1)e^2\psi_2^2}{\kappa_1\kappa_2}\log\left|\frac{\kappa_1+\kappa_2}{\kappa_1-\kappa_2}\right|. \tag{20}$$

In the equations for $5s$, $5p$ and $6s$, one term V_{ex} was introduced for each inner shell. When V_{ex}, ϵ_i and V_i are in Ry units and ψ_2 is normalized according to

$$\int_0^\infty \psi_2^2 r^2 dr=1,$$

with r in units a_H, Eq. (20) becomes

$$V_{ex}=-\frac{(2l_2+1)\psi_2^2}{(\epsilon_1-V_1)^{\frac{1}{2}}(\epsilon_2-V_2)^{\frac{1}{2}}}\log\left|\frac{(\epsilon_1-V_1)^{\frac{1}{2}}+(\epsilon_2-V_2)^{\frac{1}{2}}}{(\epsilon_1-V_1)^{\frac{1}{2}}-(\epsilon_2-V_2)^{\frac{1}{2}}}\right|. \tag{20a}$$

In the region where $\epsilon_2-V_2<0$, the limit of (20a) for $\epsilon_2-V_2\to 0$ was taken, giving

$$V_{ex}=-\frac{2(2l_2+1)\psi_2^2}{\epsilon_1-V_1}. \tag{20b}$$

The potential for exchange based on Eq. (20) will be compared below with one obtained directly from the Hartree-Fock equation.

In obtaining the exchange between $5s$, $5p$ and $6s$ the following approximation was made. Let R^B and R^T be the normalized radial functions for the lowest and the highest state, respectively, of $5s$ or $5p$. At any stage when R^B and R^T were obtained, R^B+R^T was normalized and the resulting function, to be denoted by R^A, was used in evaluating the exchange terms involving this band. The expressions for the exchange terms were taken from the tables of Hartree and Hartree[20] for closed shells, except for the exchange of $6s$ in the equations for the $5s$ and $5p$ functions. For these terms half the tabulated value was taken, since there is a probability $\frac{1}{2}$ that the $6s$ in the atomic sphere has a given spin direction. We thus obtain the following equation for $5s$, in which u_{5s} is r times the $5s$ function,

$$\begin{aligned}-\frac{d^2u_{5s}}{dr^2}&+(V_c+V_{ex,5s}+\mathcal{U}_{5s}+6\mathcal{U}_{5p}+\mathcal{U}_{6s})u_{5s}\\ &=\epsilon_{5s}u_{5s}+\Big[\Big(\frac{2}{r^2}\int_0^r u_{5s}{}^A u_{5p}{}^A r'dr'\\ &\quad+2r\int_r^{r_0} u_{5s}{}^A u_{5p}{}^A\frac{1}{r'^2}dr'\Big)u_{5p}{}^A\\ &\quad+\Big(\frac{1}{r}\int_0^r u_{5s}{}^A u_{6s}dr'+\int_r^{r_0} u_{5s}{}^A u_{6s}\frac{1}{r'}dr'\Big)u_{6s}\Big]. \end{aligned}\tag{21}$$

Here $u_{5s}{}^A$ and $u_{5p}{}^A$ are r times the functions R^A for $5s$ and $5p$, respectively; u_{6s} is r times the $6s$ function;[21] V_c is the potential due to the nucleus and the inner electrons; $V_{ex,5s}$ is the potential for exchange with $1s$, $2s$, $\cdots$, $4d$; $\mathcal{U}_{5s}$, $\mathcal{U}_{5p}$, $\mathcal{U}_{6s}$ are the potentials due to $5s$, $5p$, $6s$, respectively, ϵ_{5s} is the eigenvalue. The potentials and ϵ_{5s} are in Ry units, lengths are in units a_H and the normalization is

$$\int_0^{r_0}(u_{5s}{}^A)^2dr=\int_0^{r_0}(u_{5p}{}^A)^2dr=\int_0^{r_0}u_{6s}{}^2dr=1.$$

At each stage of the calculation an equivalent potential V_{5s} was obtained by adding to the Coulomb terms on the left side of (21), $-1/u_{5s}{}^A$ times the exchange terms in the square bracket. The Schroedinger equation with V_{5s} was solved, instead of the inhomogeneous Eq. (21). The same procedure was used for $5p$ and $6s$, involving potentials denoted by V_{5p} and V_{6s}. After a reasonable V_{6s} was obtained, the $6s$ function was kept fixed, while the $5s$ and $5p$ functions were made more self-consistent. The final V_{5s} and V_{5p} of this calculation are the potentials mentioned in Section II. The $6s$ function was then redetermined. It is estimated that

TABLE VII. Values of $rV_{6s}'\cdot V_{6s}'$ is in Ry units, r is in units a_H.

r	rV_{6s}'	r	rV_{6s}'
0.00	110	0.8	17.47
0.01	104.41	0.9	14.19
0.02	99.83	1.0	12.45
0.03	95.32	1.2	9.79
0.04	90.68	1.4	8.03
0.06	84.08	1.6	6.70
0.08	78.49	1.8	5.78
0.10	73.91	2.0	5.35
0.15	61.65	2.4	3.13
0.20	53.05	2.8	2.95
0.25	47.02	3.2	2.69
0.30	42.26	3.6	2.51
0.35	37.47	4.0	2.41
0.4	32.61	5.0	2.25
0.5	27.30	6.0	2.15
0.6	23.05	7.0	2.10
0.7	19.58	8.0	2.05

[20] D. R. Hartree and W. Hartree, Proc. Roy. Soc. **156**, 45 (1936).

[21] The terms involving Lagrangian parameters were omitted. However, $u_{5s}{}^A$ and u_{6s} were nearly orthogonal in the final stages of the calculation; the integral over $u_{5s}{}^A u_{6s}$ had values ~ 0.03.

the resulting V_{6s} differs by less than 0.04 Ry at $r=1.0\ a_H$ and 0.01 Ry at $r=4.6\ a_H$ from that of a completely self-consistent calculation. Since this uncertainty is smaller than the correction applied to V_{6s} (see below), the approximation to self-consistency was sufficient.

The exchange part of V_{6s} was then improved by replacing the potential for exchange with $1s$, $2s$, $\cdots$, $4d$ (Eq. (20)) by $1/u_{6s}$ times the corresponding terms[20] in the Hartree-Fock equation for $6s$. In evaluating the exchange integrals, Hartree's $1s$, $2s$, $\cdots$, $4d$ functions[6] were used. For comparison we shall list some values (in Ry units) of the two exchange potentials; the Hartree-Fock exchange is given in parentheses: 22.7 (25.3) at $r=0.08\ a_H$; 3.06 (1.15) at $r=0.4\ a_H$; 3.15 (1.65) at $r=0.8\ a_H$; 0.884 (0.500) at $r=1.2\ a_H$; 0.175 (0.181) at $r=1.6\ a_H$. The values given by Eq. (20) are considerably too large between $r=0.4\ a_H$ and $1.2\ a_H$. We note that for the exchange of $5d$ with $1s$, $2s$, $\cdots$, $4d$, Eq. (20) gives a better approximation to the Hartree-Fock values; the agreement is within 20 percent for $r<0.8\ a_H$.

The atomic eigenvalue for the resulting potential V_{6s} lies 0.03 Ry above the observed level. It is reasonable to attribute a major part of the discrepancy to the electrostatic correlation of $6s$ with the core electrons. A small term of the proper magnitude to give agreement with the atomic level was added to V_{6s}. The dependence on r of this term was obtained from a classical model of the correlation. The potential V_{6s}' thus determined is given in Table VII.[22]

In determining V_{5d}' the Coulomb interaction with the core was taken from V_{6s}. The exchange contribution was obtained by evaluating the corresponding terms[20] in the Hartree-Fock equation for $5d$. As for $6s$, a small attractive term was added to the resulting potential, in order to obtain agreement with the observed atomic level.

IV. ACKNOWLEDGMENTS

I would like to thank Professor E. Fermi, who suggested the line of approach to this problem, and Professor E. Teller for many invaluable discussions. Sincere thanks are also due Professor G. Breit, Professor J. E. Mayer, Dr. J. Steinberger, Professor E. Wigner and Dr. C. N. Yang for very helpful discussions.

[22] The rapid decrease of $V_{6s}'r$ between $r=2.0\ a_H$ and $r=2.4\ a_H$ is not significant. The exchange potential changes from a large positive to a large negative value, because the $6s$ function has a node near $2.2\ a_H$. However, the contribution of this term to $V_{6s}'u_{6s}^2$ remains small.

PHYSICAL REVIEW VOLUME 78, NUMBER 3 MAY 1, 1950

The Magnetic Deviation of Cosmic-Ray Particles in the Atmosphere*

W. F. G. SWANN
Bartol Research Foundation of the Franklin Institute, Swarthmore, Pennsylvania
(Received January 23, 1950)

The paper concerns the possibility of the path of a cosmic-ray α-particle, proton, or mesotron being bent in the atmosphere by the earth's magnetic field in such a manner as to pass vertically upward through a counter telescope.

In order to pass vertically upward through the telescope, it is necessary for the ray to have been horizontal at some time during its path; and taking into account the minimum energies necessitated by absorption along the path, it appears that, for a telescope at an altitude comparable with 100,000 ft., neither an α-particle nor a proton would have "vertical room" between the telescope and the earth to describe the angle $(\pi/2)$ necessary to take it from the horizontal to the vertical upward direction. For a mesotron there would be room, but in this case the mesotron "mean life" operates to prevent the phenomenon happening in appreciable degree; it is shown that regardless of energy or the law of energy loss, only a fraction $e^{-11.6}$ of any assigned number of mesotrons can live long enough to travel through a right angle in the earth's magnetic field.

I. INTRODUCTION

THE importance of high altitude measurements with Geiger counter telescopes has occasionally raised the question as to whether such measurements may be influenced by effects of the earth's magnetic field in bending the orbits of protons, α-particles, or mesotrons to the extent of causing rays to enter the telescopes from the under side. It has been thought well to investigate this matter for the case of a vertically directed telescope, the illustration in mind being the recent observations of Pomerantz.[1] The calculations for an inclined telescope may be carried out in an analogous manner.

II. THE CASE OF PROTONS AND ALPHA-PARTICLES

It is easy to show that for a fixed magnetic field H, the situation is most favorable for resulting in upward rays through the telescope when H is horizontal. We shall consequently confine attention to this case.

* Assisted by the joint program of the ONR and AEC.

[1] M. A. Pomerantz and M. S. Vallarta, Phys. Rev. 76, 1889 (1949); also M. A. Pomerantz, Phys. Rev. 77, 830 (1950).

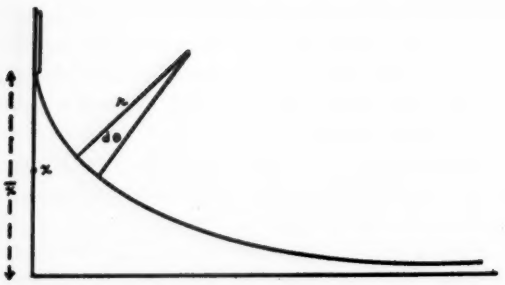

FIG. 1. Geometrical considerations on the particle trajectory.

Consider a particle of atomic number Z_1 entering the atmosphere and having momentum p in a region where the magnetic field is H. The radius of curvature r of its path will be given by

$$r=(pc)/(HeZ_1),$$

where Z_1e is its charge. Now if $d\theta$ is the bending in the path length ds

$$rd\theta=ds.$$

The loss of momentum per unit mass equivalent traversed is of the form $Z_1^2f(p/m_0c)$ where $f(p/m_0c)$ is a function only of p/m_0c for an assigned medium.[2] Thus the momentum change dp in the path length ds is

$$dp=-Z_1^2f(p/m_0c)\rho ds, \tag{1}$$

where ρ is the density of the medium. Thus

$$d\theta=-\frac{dp}{\rho rZ_1^2f(p/m_0c)}=-\frac{HeZ_1dp}{\rho cZ_1^2pf(p/m_0c)}. \tag{2}$$

Hence the change of angle during change of momentum from p_1 to p_2 is

$$\theta-\theta_2=\frac{He}{cZ_1}\int_{p_2}^{p_1}\frac{dp}{\rho pf(p/m_0c)}, \tag{3}$$

where θ_2 is the angle, measured from any arbitrary direction, when p has the value p_2.

Writing

$$P\equiv p/m_0c,$$

the expression for $Z_1^2f(p/m_0c)$ or $Z_1^2f(P)$ is[2]

$$Z_1^2f(P)=Z_1^2\left(\frac{2.4\times10^{-7}}{c}\right)\frac{(1+P^2)^{\frac{1}{2}}}{P^3}$$

$$\times\left[2\log P+13.84-\log 13.5Z-\frac{P^2}{1+P^2}\right], \tag{4}$$

where Z is the atomic number of the medium and where we have recognized, as is easily shown, that $v^2/c^2=P^2/(1+P^2)$, where v is the velocity of the particle.

[2] See B. Rossi and K. Greisen, Rev. Mod. Phys. 13, 240 (1941). See in particular, Eqs. (1.11a) and (1.13).

Thus (3) becomes

$$\theta-\theta_2=\frac{He}{cZ_1}\int_{P_2}^{P_1}\frac{dP}{\rho Pf(P)}, \tag{5}$$

where

$$P_1\equiv p_1/m_0c;\quad P_2\equiv p_2/m_0c.$$

It will be observed that (5) is independent of m_0 for assigned values of P_1 and P_2.

The angle θ is less that the value obtained by putting ρ equal to ρ_m, the least value of ρ over the portion of the path of the particle which interests us. Thus

$$\theta-\theta_2<\frac{He}{cZ_1\rho_m}\int_{P_2}^{P_1}\frac{dP}{Pf(P)}. \tag{6}$$

In general, H may be regarded as constant in the region concerned. However, even if we did not regard it as constant, the only change would be to keep it under the integral sign, and we could still say that (6) holds with H taken as the maximum value in the region, which naturally is the value in the vicinity of the apparatus as distinct from points farther away from the earth's center.

III. ADJUSTMENT OF THE THEORETICAL CONSIDERATIONS TO OUR PROBLEM

Equation (6) can only be evaluated by numerical integration. Moreover, it is desirable to choose the problem to be formulated as the one simplest of solution while giving the information necessary for our interests.

It is clear that any ray which passes vertically upward through the telescope must, at some point, have been horizontal in its complete journey from outer space. From the position of this horizontal part of the trajectory, a certain value P_M of P will be necessary in order that it shall be able to reach the telescope and arrive with the value of P necessary to penetrate the apparatus, and a certain vertical distance $\bar{x}$ of travel will be necessary in order that the ray will have "room" to describe the necessary trajectory. If this vertical distance is greater than the vertical distance of the apparatus above the earth, the ray will be unable to

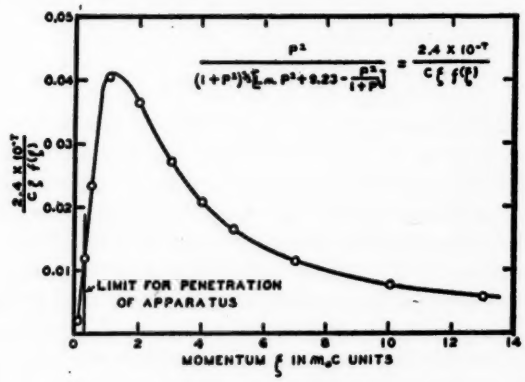

FIG. 2. Plot of $1/\zeta f(\zeta)$ vs. ζ.

exist and there will, in fact, be no vertical rays passing through the telescope from below.[3]

Let x be measured vertically downward from the telescope, $\bar{x}$ being, as stated, the vertical distance to the point 0, Fig. 1, where the ray is horizontal.

At any point on the trajectory

$$dx=(rd\theta)\cos\theta,$$

where θ is the angle between the direction of the ray (traced downward) and the vertical. Thus

$$\bar{x}=\int_0^{\pi/2} r\cos\theta d\theta.$$

Since

$$p/r=Z_1He/c,$$

we have

$$r=pc/HeZ_1=Pm_0c^2/HeZ_1,$$

so that

$$\bar{x}=\frac{m_0c^2}{HeZ_1}\int_0^{\pi/2} P\cos\theta d\theta. \tag{7}$$

It is convenient at this point to change the notation of Eq. (6) and write

$$\theta-\theta_2<\frac{He}{cZ_1\rho_m}\int_{P_2}^{P}\frac{d\zeta}{\zeta f(\zeta)}, \tag{8}$$

which expresses $\theta-\theta_2$ as a function of the lower limit P_2 and the variable upper limit P. It is important to notice that with this understanding (8) applies for any section of the trajectory. It is convenient, moreover, to think of the trajectory as being described in the direction of increasing P, i.e., reversed from its actual direction.

If in (8) we temporarily replace the $<$ sign by a sign of equality, we can calculate from Fig. 2, by a graphical procedure,[4] the angle $\theta-\theta_2$ as a function of P and the lower limit P_2. Thus we can get P as a function of $\theta-\theta_2$, the lower limit P_2 and, of course, of ρ_m. Let us suppose it is of the form $F[(\theta-\theta_2), P_2, \rho_m]$. Then, in view of the $<$ sign in (8), the true value of P for any assigned θ in the interval will be such that

$$P>F[(\theta-\theta_2), P_2, \rho_m]. \tag{9}$$

If in Eq. (8) we take ρ_m equal to the value ρ_0 of ρ applicable at the altitude of the apparatus, say 102,000 ft., where the density is 0.00129×10^{-2} g/cm^3, and if we apply the values of $F[(\theta-\theta_2), P_2, \rho_0]$ calculated on this basis for the whole range $\theta-\theta_2=0$ to $\theta-\theta_2=\pi/2$, using for P_2 the value $P_0=0.3$ necessary for penetration of the apparatus by a proton, we shall have, from (8), in view of the inequality of (9)

$$\bar{x}>\frac{m_0c^2}{HeZ_1}\int_0^{\pi/2} F[(\theta-\theta_2), P_0, \rho_m]\cos\theta d\theta, \tag{10}$$

where P_0 is the value of P necessary to penetrate the apparatus.

Taking the case of a proton,

$$m_0c^2/e=9\times10^8/300;\quad Z_1=1,$$

and if $H=0.75$, the graphical evaluation of the integral leads to $\bar{x}>2.3\times10^6$ cm. Since 102,000 ft. corresponds to about 3×10^6 cm, we cannot conclude from this test that the trajectory could not be described. However, the use of $\rho_0=1.29\times10^{-5}$ throughout the path of the trajectory from $\theta=0$ to $\theta=\pi/2$ has weakened considerably the potentialities of the test and we shall conserve those potentialities better if we divide the angular turn $\pi/2$ into four segments, each equal to $\pi/8$ and use in each of these segments the lowest value of ρ for the segment. This we shall presently do, but we shall first state that the test in its weak form, with $\rho=1.29\times10^{-5}$ throughout, is sufficient to show that an α-particle could not find room to describe the trajectory. This is seen at once by referring to (8) and observing that m_0/Z_1 for an α-particle is twice the value for a proton so that, since P_0 is the same for an α-particle as for a proton[5] we can conclude that, for an α-particle,

$$\bar{x}>2\times2.3\times10^6 \quad \text{i.e.}>4.6\times10^6 \text{ cm}$$

and this is greater than 102,000 ft.

Returning to the case of the proton, we shall proceed as follows: starting at the telescope and tracing the trajectory backward, we shall divide the $\pi/2$ turn into four steps each equal to $\pi/8$. With $P_0=0.3$, corresponding to penetration of the apparatus, we have, from (9), for the first step, recognizing that $\theta_2=0$

$$P>F[\theta, P_0, \rho_0],$$

where ρ_0 refers to the density at the telescope. This, the contribution of the range $\theta=0$ to $\pi/8$ to the complete integral in (10), yields, for the corresponding contri-

[3] A rough way of getting a preliminary picture of orders of magnitude in this matter is the following: The radius of curvature is always greater than the value r_0 corresponding to $P=P_0$, the value of P necessary for penetrating the apparatus. We have, for a proton,

$$P_0/r_0=He/m_0c^2=H\times300/9\times10^8.$$

For $P_0=0.3$, corresponding to 4.4 g/cm^2 of lead, and $H=0.75$, we find $r_0=1.2\times10^6$ cm. This is less than 102,000 ft., the altitude which we shall assign for the apparatus so that a circular orbit (reversed) with radius r_0, and starting vertically downward from the telescope, would reach the horizontal part of its trajectory above the earth. However, in practice r increases as we descend on account of energy loss in the actual orbit, and this circumstance operates, as we shall see, to the extent of causing an altitude of 102,000 ft. to be too little to provide room for the trajectory.

[4] The area of the curve in Fig. 2 between any values $\zeta=P_2$ and $\zeta=P$ when multiplied by $He/cZ_1\rho_m$ gives $(\theta-\theta_2)$ for the said value of P. The additional plotting of P against $(\theta-\theta_2)$ provides the curve representing the function $F[(\theta-\theta_2), P_2, \rho_m]$ from the value of P_2 onward over the interval concerned.

[5] Equation (1) shows that

$$ds=-dp/\rho Z_1^2 f(p/m_0c)=-m_0cdP/Z_1^2\rho f(P),$$

so that, since m_0/Z_1^2 is the same for an α-particle as for a proton, the range is the same for both kinds of particle for the same value of P.

bution $\bar{x}_1$ to $\bar{x}$,

$$\bar{x}_1 > \frac{m_0c^2}{HeZ_1}\int_0^{\pi/8} F[\theta, P_0, \rho_0]\cos\theta d\theta. \quad (11)$$

The contribution from $\theta=\pi/8$ to $\theta=2\pi/8$ yields

$$\bar{x}_2 > \frac{m_0c^2}{HeZ_1}\int_{\pi/8}^{2\pi/8} F\left[\left(\theta-\frac{\pi}{8}\right), P_1, \rho_1\right]\cos\theta d\theta, \quad (12)$$

where ρ_1 is the density at the depth $\bar{x}_1$, i.e., the least density over the range of $\bar{x}_2$ and P_1 is the value of P to which the ray has grown on tracing it back to the point corresponding to $\theta=\pi/8$. The value of P_1 is, of course, the value of ζ in Fig. 2 for which $He/cZ_1\rho_0$ times the area from $\zeta=P_0$ to $\zeta=P_1$ has the value $\pi/8$.

The contribution from $\theta=2\pi/8$ to $\theta=3\pi/8$ yields

$$\bar{x}_3 > \frac{m_0c^2}{HeZ_1}\int_{2\pi/8}^{3\pi/8} F\left[\left(\theta-\frac{2\pi}{8}\right), P_2, \rho_2\right]\cos\theta d\theta, \quad (13)$$

where ρ_2 is the density at the depth $\bar{x}_1+\bar{x}_2$, and $P_2=P_1+P_{12}$, where P_{12} is the value of ζ on Fig. 2 for which $He/cZ_1\rho_1$ times the area from $\zeta=P_1$ to $\zeta=P_1+P_{12}$ has the value $\pi/8$. Similarly,

$$\bar{x}_4 > \frac{m_0c^2}{HeZ_1}\int_{3\pi/8}^{4\pi/8} F\left[\left(\theta-\frac{3\pi}{8}\right), P_3, \rho_3\right]\cos\theta d\theta, \quad (14)$$

where ρ_3 is the density at depth $\bar{x}_1+\bar{x}_2+\bar{x}_3$ and $P_3=P_2+P_{23}$, where P_{23} is the value of ζ on Fig. 2 for which $He/cZ_1\rho_2$ times the area from $\zeta=P_2$ to $\zeta=P_2+P_{23}$ has the value $\pi/8$. Thus,

$$\bar{x} > (m_0c^2/HeZ_1)I,$$

where I is the sum of the integrals in relations (11)–(14) inclusive. Putting $Z_1=1$ for a proton and $m_0c^2/e=9\times10^8/300$ and putting $H=0.75$, we find as follows, where the relevant quantity is, of course, $\bar{x}$ but the intermediate steps and quantities involved in its calculation are given for general interest. To the list in Table I we have added P_4, the value of P for the lowest point of the trajectory. Since 102,000 ft. corresponds to only 3×10^6 cm, we see that there would be no room for the proton to describe the trajectory necessary to enable it to enter the telescope vertically from below. We have already seen that an α-particle is prohibited to an even greater degree from describing the necessary trajectory.

TABLE I. Calculated deflections for a proton. $m_0c^2/e=3\times10^8$.

ρ_0 $\times10^5$	ρ_1 $\times10^5$	ρ_2 $\times10^5$	ρ_3 $\times10^5$	P_0	P_1	P_2	P_3	P_4	$\bar{x}_1$ $\times10^{-5}$	$\bar{x}_2$ $\times10^{-5}$	$\bar{x}_3$ $\times10^{-5}$	$\bar{x}_4$ $\times10^{-5}$
1.29	3.38	13.5	60.5	0.3	0.48	0.79	1.68	12.4	6.5	8.75	10.7	12.4

$\bar{x}=\bar{x}_1+\bar{x}_2+\bar{x}_3+\bar{x}_4=3.8\times10^6$ cm

The story for the mesotron would be less favorable on these considerations, since, as may be seen from (10), $\bar{x}$ involves m_0 as a factor, and is otherwise independent of m_0 explicitly. For mesotrons, however, there is another very potent consideration, *viz.*, mean life, which operates to reduce to negligible importance the bending of mesotron paths through as much as a right angle. These considerations are as follows.

IV. THE CASE OF MESOTRONS

It has been shown by W. F. G. Swann[6] that, in the case of a mesotron, regardless of the energy of the mesotrons or of the law governing their loss of energy in passing through the atmosphere, the fraction of any group which can travel far enough to experience a deviation θ in the foregoing sense is R where

$$R=\exp[-m_0c^2\theta/\tau_0Hec]. \quad (15)$$

Here τ_0 is the rest mean life, and m_0 is the rest mass of the mesotron. Here m_0c^2/e is the rest energy in e.s.u. $=10^8/300$, $\tau_0=2\times10^{-6}$ sec., so that, putting $H=0.75$, we have, for $\theta=\pi/2$, for example,

$$R=e^{-\eta},$$

where

$$\eta=\frac{10^8\pi}{2\times2\times10^{-6}\times0.75\times3\times10^{10}\times300}=11.6.$$

Hence, less than $e^{-11.6}$ of any group of mesotrons can turn through a right angle in the earth's magnetic field.

I wish to acknowledge the services of S. H. Forbes and D. Seymour in carrying out the numerical computations and graphical integrations in this paper.

[6] W. F. G. Swann, Phys. Rev. **76**, 157 (1949).

Cosmic-Ray Induced Nuclear Disintegrations at 11,000 Meters*

H. H. FORSTER†
Department of Physics, University of California, Berkeley, California
(Received December 5, 1949)

The equivalent absorption depth in air of the star-producing radiation is determined as 125±8 g/cm² by means of the photographic emulsion technique. The energy spectrum of alpha-particles emitted in nuclear disintegrations is obtained. It is found that the fraction of the number of stars with given prong number to the total number of disintegrations is not strongly dependent upon altitude up to elevations of 11,000 m. The contribution of different cosmic-ray particles to star production is discussed. Electrons, photons, and light mesons are ruled out as the major agency for star production from consideration of their altitude dependence, π-mesons from consideration of lifetime and momentum. The results are shown to be consistent with the assumption of neutrons as the main star-producing agency. However, the fact that the penetrating showers also decrease exponentially with an absorption depth of 123 g/cm² suggests that the star-producing particle may be a by-product of penetrating showers, in which case the absorption depth of 125 g/cm² would be a measure of the creation rather than of the absorption of the star-producing radiation.

I. INTRODUCTION

MEASUREMENTS of the absorption of the radiation producing nuclear disintegrations in the atmosphere have been shown by various investigators to follow an exponential law of decrease with atmospheric depth. The first determination of the mean range of this radiation in air by Wambacher[1] gave a value of 80 g/cm² and based on these measurements Bagge[2] concluded that the electron-photon component was responsible for star production. Later investigations[3,4] showed Wambacher's value to be too low and yielded values in the neighborhood of 150 g/cm². In this paper measurements on the altitude variation of cosmic-ray induced nuclear disintegrations have been carried out by means of the photographic emulsion technique and an attempt has been made to draw from the results conclusions concerning the nature and origin of the star-producing radiation.

II. EXPERIMENTAL PROCEDURE

Kodak NTB plates and Ilford nuclear research plates of Type B1 and C2 wrapped in photographic black paper and packed in cardboard boxes were exposed to cosmic radiation on a series of B-29 flights from Inyokern, California, at altitudes ranging from 7000 m to 11,000 m. During the flight time, which was varied from one to ninety hours, the cabin of the plane was temperature-controlled. For each plate exposed at high altitude, control plates from the same batch were left at sea level on the roof of LeConte Hall at the University of California in Berkeley for the entire period of exposure. The control plates, wrapped and processed simultaneously with the high altitude plates, provided the basis for the calculation of the intensity of star production at sea level. Data for intermediate elevations were obtained from plates exposed on Mt. Evans, Colorado, at 4160 m. A 4-mm apochromatic objective and 10× compensated eyepieces (magnification 450) were used in scanning the developed plates.

A star was defined as a nuclear disintegration in which two or more ionizing particles were ejected; however, two particle events were counted as stars only if the interpretation as a large angle scattering of a single particle could be excluded with certainty. The total number of stars counted was about 10,000. An effective elevation of exposure was calculated for each plate by averaging the time spent at each altitude, taking into account the exponential increase shown by the star-producing radiation; the high altitude data were corrected for background as obtained from the control plates. Let r_0 and r_h be the rates of star production in number per hour per cc of emulsion at sea level and at an altitude h; then the relative rate of star production between the two elevations is defined as: $R=r_h/r_0$.

III. RESULTS AND DISCUSSION

While the emphasis of the experiment was on the altitude dependence of the star-producing radiation, a study was made of the charged particles emitted in nuclear disintegrations. To this end it was necessary to identify the star particles; since fast charged particles moving through the emulsion lose energy mainly by ionization, the identification of the particles can be based on their rate of energy change and multiple scattering. Once the particle was identified its energy was obtained from known range energy relations for the emulsion. Mesons, protons, deuterons, alpha-particles, and heavier fragments were identified as the particles which are emitted in star processes.

The energy spectrum of alpha-particles emitted from stars is reproduced in Fig. 1. It shows a pronounced maximum at about 6 Mev and the existence of a lower energy limit at 3 Mev, below which the particle cannot leave the nucleus except by leakage through the potential barrier.

* Assisted by the Joint Program of the ONR and the AEC.
† Now at the University of Southern California, Los Angeles, California.
[1] G. Stetter and H. Wambacher, Physik. Zeits. **40**, 702 (1939).
[2] E. Bagge, Ann. d. Physik **39**, 512 (1941).
[3] E. P. George, Nature **162**, 333 (1948).
[4] D. H. Perkins, Nature **160**, 707 (1947).

The composition of the charged particles emitted in stars remained essentially unaltered from sea level to 11,000 m. The ratio of the number of alpha-particles and heavier fragments to the number of protons and deuterons was found to be about unity throughout this altitude range for stars with a number of tracks less than five.

The relative number of disintegrations with a given prong number for plates exposed at different altitudes shows no significant variation with altitude for stars of three or more prongs. This can be seen from Fig. 2 where the number of stars with prong number $N>n$ is plotted logarithmically *versus* n. This number depends exponentially on n.

An inference from the relative composition of stars concerning the energy of the star-initiating radiation is not warranted since Gardner[5] has shown that the prong number is only weakly dependent on the energy of the star-initiating radiation. But the similarity of the star distribution at various altitudes is an indication that the relative energy distribution of the star-producing radiation does not vary essentially with altitude.

It is difficult to assign an absolute value to the number of disintegrations occurring per cc of emulsion per hour due to large fluctuations in the sensitivity of the photographic emulsion. It can only be said that the number of stars with two or more prongs lies at sea level between three and six per cc per hour, depending on the type of plate used. The rate of star production was found to increase rapidly with increasing elevation. The ratio (R) of the number of stars at various elevations to the corresponding number at sea level, computed as indicated previously, is plotted as a function of atmospheric depth in Fig. 3. It can be seen from the graph that the decrease of star production is an exponential function of atmospheric depth, with an absorption depth of 125 ± 8 g/cm^2.

The number of heavy particle tracks found in the emulsion showed an exponential decrease with atmospheric depth similar to that of stars; the equivalent absorption depth was determined at 133 ± 7 g/cm^2. It is slightly higher than the absorption depth for stars but its agreement with the latter within 10 percent suggests that the majority of the single tracks found in the photographic emulsion originate in nuclear disintegrations produced in the neighborhood of the photographic plate.

Experiments with the Berkeley cyclotron have shown that several different particles can produce nuclear disintegrations provided they have sufficient energy. However, as shown below, it will be possible to rule out certain components of the cosmic radiation from any major contribution to star production.

The electron-photon component of the cosmic radiation increases by a factor of 100 between sea level and

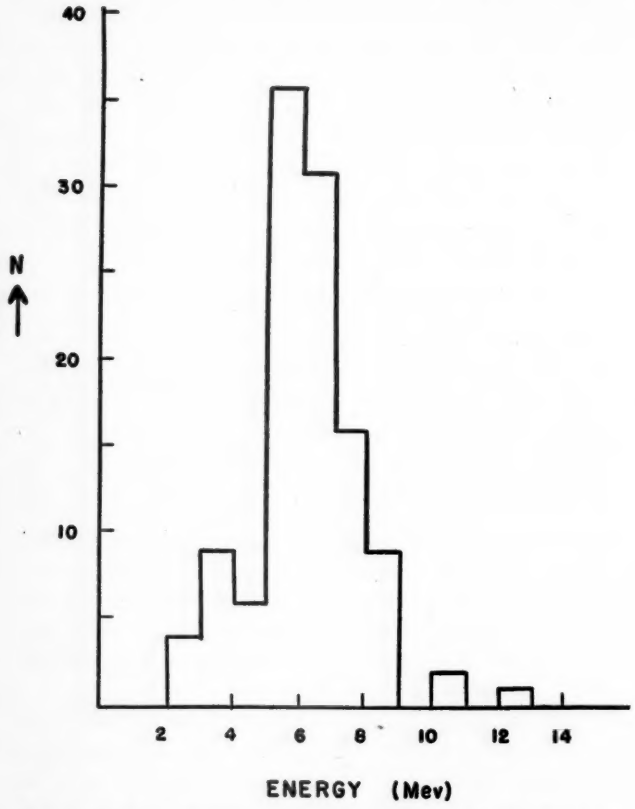

FIG. 1. The energy spectrum of alpha-particles emitted in nuclear disintegrations at sea level.

[5] E. Gardner and V. Peterson, Phys. Rev. 75, 364 (1949).

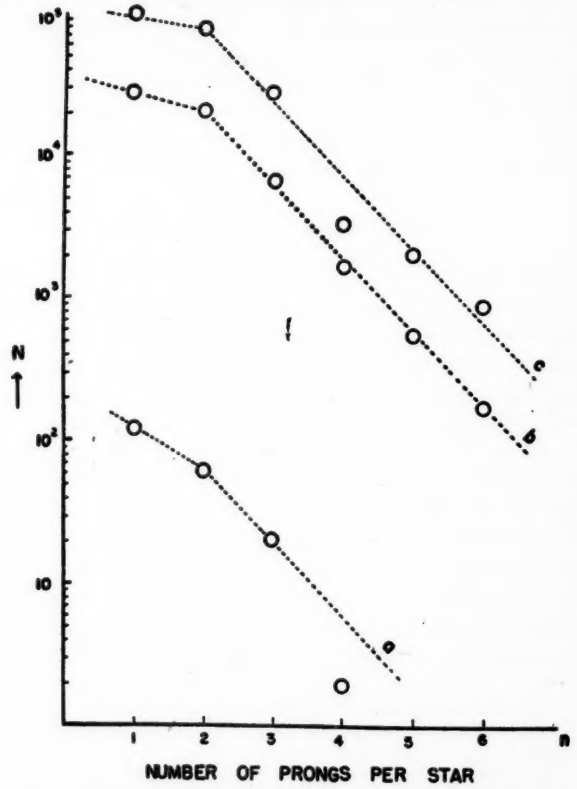

FIG. 2. Number of stars (N) per cc per day with prong number greater than n as a function of n. (a) sea level, (b) 7870 m, (c) 11,300 m.

11,000 m, while the star intensity increases by a factor of 790±237 between the same elevations. Moreover, experiments performed by George and Jason[6] under different thicknesses of lead failed to show any transition curve for the star-producing radiation comparable to that of electrons. The contribution of the electron-photon component to star production is therefore of minor importance.

The relative intensity of μ-mesons increases by a factor of 30 between sea level and 11,000 m. It appears therefore from this and other experiments[7] in which no star-initiating particle could be identified with μ-mesons that light negative mesons do not take part in star production.

Since π-mesons decay with a mean life of 10^{-8} sec., their mean free path before decay can be made comparable to the mean free path for star production of the order of 100 g/cm² only by assigning to the mesons a momentum of the order of 5×10^{10} ev/c. Such an assumption is not justified; π-mesons, therefore, unless locally produced, cannot be a major factor in star production.

Perkins[4] has suggested that neutral mesons may be responsible for star production. If this be the case, it is possible to obtain an estimate of the minimum mean lifetime of this particle from consideration of the absorption depth of the star-producing radiation. The absorption depth of 125 g/cm² in air corresponds to a range, L, of about 10^6 cm at sea level and increases with increasing elevation. If, for a first estimate, the absorption of neutral mesons by star production is considered small as compared with their attenuation by decay, then the range of 10^6 cm corresponds to the mean free path of the particle before decay. The mean lifetime is then $\tau=Lm/P$. It is reasonable to assume that the momentum spectrum of the neutral meson is comparable to that of the μ-meson; if its momentum is taken to be 10^3 Mev/c and its mass as 150 Mev/c, a lifetime of about 10^{-6} sec. is obtained. This, however, is contrary to preliminary experimental results[8] which are being obtained with the Berkeley cyclotron and which indicate a lieftime of the neutral meson of 10^{-12} sec. or less. The lieftime expected from theoretical considerations[9] is of the same order of magnitude. Thus a lifetime larger by a factor of 10^6 would have to be ascribed to the neutral meson in order to account for the attenuation of star production by meson decay. The order of magnitude of the lifetime remains unchanged if the diminution of neutral mesons by star production is taken into consideration. Bernadini, Cortini, and Manfredini[10] have measured the absorption depth of the star-producing radiation in aluminum as 166 g/cm².

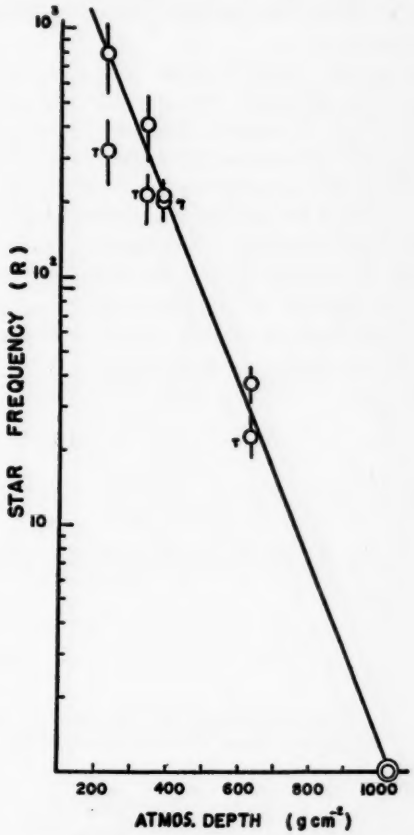

FIG. 3. Ratio (R) of the number of cosmic-ray events at various altitudes to the corresponding number of events at sea level. O stars, T single tracks.

From this value and the value of 125 g/cm² reported here, calculations carried out analogous to the determination of the decay time of μ-mesons by Rossi, Hilberry, and Hoag,[11] give a mean range of 6×10^5 cm for the neutral meson. This gives again a life time of the order of 10^{-6} sec. Both results seem sufficient to discard the assumption of neutral mesons as the star-producing agency.

Disregarding any radiation as yet unknown, the proton-neutron component remains as the only radiation that has not been discussed with regard to star production. If it is assumed that protons and neutrons are generated in equal numbers and have equal cross sections for star production, the majority of nuclear disruptions will be caused by neutrons since most protons will be stopped by ionization losses before they have a chance to produce a nuclear disintegration. This reasoning is borne out by the large number of nuclear disintegrations observed in cloud chambers where no ionizing particle initiating the disruption could be detected. The hypothesis that neutrons are the star-producing radiation is compatible with measurements by Hildebrand and Moyer[12] who found a value of 95

[6] E. P. George and A. C. Jason, Proc. Phys. Soc. London A62, 243 (1949).
[7] W. M. Powell, Phys. Rev. 69, 385 (1946).
[8] Private communication.
[9] R. J. Finkelstein, Phys. Rev. 72, 415 (1947).
[10] Bernadini, Cortini, and Manfredini, Phys. Rev. 74, 1878 (1948).
[11] Rossi, Hilberry, and Hoag, Phys. Rev. 57, 466 (1940).
[12] R. Hildebrand and B. J. Moyer, Phys. Rev. 72, 1258 (1947).

g/cm² for the mean free path for nuclear interactions of 90-Mev neutrons.

The foregoing considerations indicate that if the star-producing radiation comes from the top of the atmosphere then it consists largely of neutrons. If on the other hand, it is created throughout the atmosphere, then the measured absorption depth of 125 g/cm² is in reality a measure for the decrease of the creation of the star-producing radiation. In this connection the absorption depth of 123±10 g/cm² obtained by Fretter[13] for penetrating showers is significant and suggests that star and penetrating shower production are related phenomena. The fact that slow protons and neutrons are produced abundantly in penetrating showers is further evidence for this assumption. This would mean that the absorption depth of 125 g/cm² is not the mean free path for star production but rather measures the creation of star-producing radiation.

The author takes this opportunity to thank Professor R. B. Brode, who suggested the problem, for his constant interest and valuable advice in the progress of the work. It is a pleasure to thank Mr. C. L. D'Ooge and the maintenance crew of the B-29 of the Naval Ordnance Test Station at Inyokern, California, for the assistance rendered in exposing the photographic plates.

[13] W. B. Fretter, Phys. Rev. 76, 511 (1949).

PHYSICAL REVIEW VOLUME 78, NUMBER 3 MAY 1, 1950

Avalanche Transformation during Breakdown in Uniform Fields

G. M. PETROPOULOS
National Technical University, Athens, Greece
(Received October 28, 1949)

The transformation of the avalanche into an anode-directed streamer is considered in the case of uniform field gaps, submitted to minimum breakdown voltage.

I. INTRODUCTION

BREAKDOWN voltages or field strengths can be calculated with a satisfactory accuracy by means of Meek[1] or Raether[2] equations. Results in the case of uniform field are compiled in Table I. In accordance with Meek's mechanism, after crossing the gap the avalanche electrons are laid on the anode, the remaining positive ion charge causing an additional field

$$X_1 \sim 5.27\times10^{-7}\frac{\alpha e^{\alpha x}}{(x/p)^{\frac{1}{2}}}. \quad (1)$$

Breakdown occurs when, for $x=d$, field $X_1=KX_a$ (X_a the applied field, K a numerical factor between 0.1 and 1). Equation (1) is derived on the assumption of a positive ion density at the anode

$$N_+=(\alpha e^{\alpha d})/(\pi r^2), \quad (2)$$

where

$$r=[0.133(x/p)]^{\frac{1}{2}}, \quad (3)$$

the radius of the avalanche head. Raether computes the radial field at the avalanche head, from the total number of electrons

$$n_-=e^{\alpha x}, \quad (4)$$

concentrated in a sphere of radius r. Equating the radial tip field to the impressed field, Raether obtains

$$e^{\alpha x}=2\times10^8 x, \quad (5)$$

which equation for $x=d$ (or $x=0.8d$) constitutes the breakdown condition.

In spite of the fact that the above conditions can be considered equivalent, as leading to about the same values of breakdown voltages (see Table I), the mechanisms adopted by the authors mentioned above are substantially different. Raether assumes that the avalanche, after crossing at constant velocity ($\sim1.25\times10^7$ cm/sec.) a distance x_k at which $\alpha x_k\sim20$, is transformed into a streamer starting from the tip and progressing to the anode at a higher speed ($\sim8\times10^7$ cm/sec.). At the moment at which this streamer reaches the anode, a rectrograde streamer starts from the anode and crosses the gap at a speed of 1 to $2\cdot10^8$ cm/sec. Meek does not consider the existence of an anode directed streamer and assumes that the avalanche grows regularly until it reaches the anode, the resulting positive charge field causing the formation of the cathode directed streamer.

It is interesting to examine which of the above mechanisms represents more accurately the actual conditions, under minimum breakdown voltage in uniform field, since the transformation of the avalanche into an anode-directed streamer under overvoltages is an experimental fact.[3]

Raether[2] gives a considerable argument on behalf of

[1] J. M. Meek, Phys. Rev. 57, 722 (1940); L. B. Loeb and J. M. Meek, *The Mechanism of the Electric Spark* (Stanford University Press, Stanford, 1941).
[2] H. Raether, Zeits. f. Physik 117, 375 (1941).
[3] H. Raether, Zeits. f. Physik 112, 464 (1939).

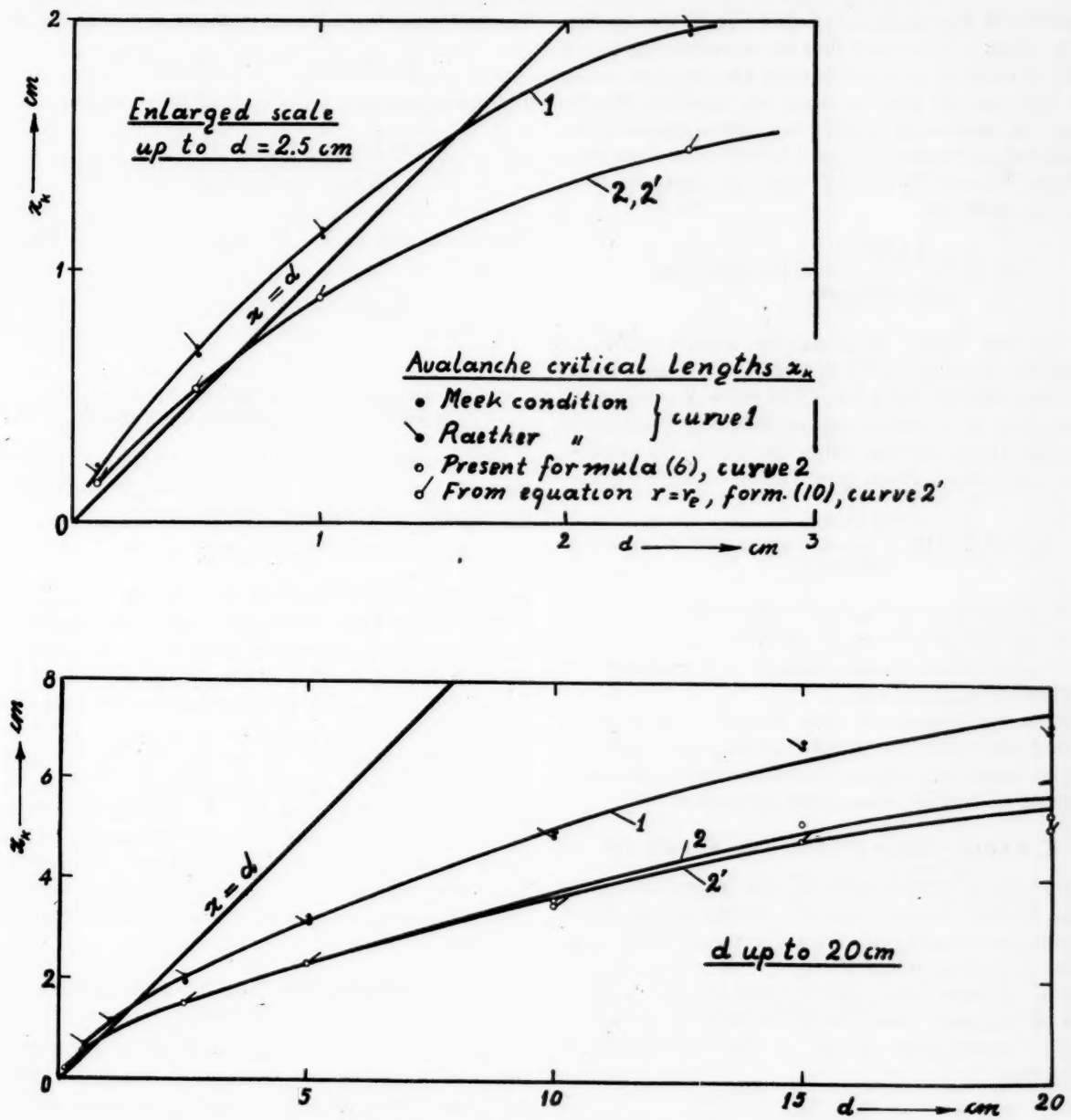

FIG. 1. Critical lengths of avalanches as computed from various conditions.

the transformation: The spaces x_k swept by the avalanches, as computed from Eq. (5) with α_0 values corresponding to observed breakdown fields (X_0 in Table I) in various gap lengths d, are essentially smaller than the gap lengths. Results are given by curve 1 of Fig. 1. The critical spaces x_k computed from Meek's condition with the experimental values of X_0, for $X_1 = X_0$, are given by same curve 1 of this figure, being very closely the same.

It may be concluded that both conditions do not represent the actual breakdown phenomena and that their unquestionable success in giving the breakdown field X_s (Table I) is very probably due to the presence of term $e^{\alpha x}$ in their expressions, and to the great de-

TABLE I. Results for breakdown in the case of uniform fields after Meek* and Raether.†

d (cm)	V_s (volts) Meek	V_s (volts) Raether	V_0 (volts) observed	X_0 (V/cm)	X_0/p (p = 760 mm)	α_0 Sanders
0.1	——	——	4500	45000	59.2	92
0.5	18250	——	17300	34600	45.5	27
1	32200	32400	31600	31600	41.5	16.5
2.5	70500	71300	73000	29300	38.5	10
5	132000	132000	138000	27600	36.4	6.5
10	249000	249000	265000	26500	34.9	4.25
15	363000	378000	386000	25700	33.8	3.15
20	474000	——	510000	25500	33.7	3.0

* See reference 1.
† See reference 2.

pendence of the ionization number from the applied field,[2] unless it is assumed that the experimental values of X_0 or those of α_0 are inaccurate. On the other hand, Eqs. (2) and (1) lead to other less plausible results. Thus, the positive ion density in a 10-cm gap after the avalanche has crossed the space between the electrodes, with $p=760$ mm Hg $\alpha_0=4.25$ and r as computed from Eq. (3), would be

$$N_+=\frac{4.25e^{42.5}}{\pi 0.133(10/760)}=2.2\times10^{21}/\text{cm}^3,$$

i.e. by two orders of magnitude greater than the Avogadro constant ($2.7\times10^{19}/\text{cm}^3$). The same calculation carried out for a 5-cm gap gives $N_+=0.3\times10^{18}/\text{cm}^3$, that is a density approaching the constant in question. If, on the other hand, the field X_1 is computed from Eq. (1) for a 10-cm gap, with $\alpha_0=4.25$, we obtain

$$X_1=5.27\times10^{-7}\frac{4.25e^{42.5}}{(10/760)^{\frac{1}{2}}}=0.56\times10^{14}V/\text{cm}.$$

Field strengths of such a high magnitude are unlikely, since very probably long before they reach this level, other phenomena would change the conditions of progress of the avalanche.

Under the assumption that X_0 and α_0 as given in Table I are correct, the transformation of the avalanche can be supported during breakdown under minimum sparking voltage by some other arguments.

II. RADIAL FIELD AT THE AVALANCHE TIP

In trying to obtain a more accurate expression for the radial tip field of the avalanche, charges of both polarities are considered: All avalanche electrons are supposed to be in a sphere of radius r; it is also assumed that in the same sphere are included as many positive ions as computed from the sphere volume, multiplied by their density given by Eq. (2). The total number of electrons is

$$n_-=e^{\alpha x}$$

while the number of positive ions,

$$n_+=(4/3)r\alpha e^{\alpha x}.$$

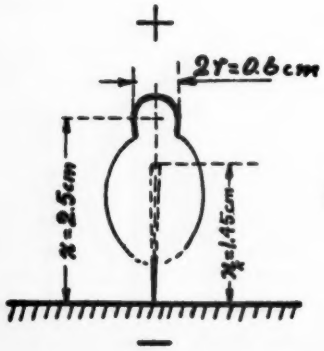

FIG. 2. Avalanche in Raether's cloud chamber.

Therefore, the total charge included in the sphere is

$$q=(n_+\epsilon-n_-\epsilon)=\epsilon e^{\alpha x}(4r\alpha/3-1),$$

and the radial field, with $\epsilon=1.6\times10^{-19}$ coulomb,

$$X_1=\frac{14.4\times10^{-7}(4r\alpha/3-1)e^{\alpha x}}{r^2}\ (\text{in } V/\text{cm}). \quad (6)$$

With r as given by Eq. (3) under $p=760$ mm Hg, we obtain

$$X_1=\frac{8.25\times10^{-7}(0.0177\alpha x^{\frac{1}{2}}-1)e^{\alpha x}}{x}\ (\text{in } V/\text{cm}). \quad (7)$$

III. AVALANCHE CRITICAL LENGTH AND TOWNSEND SPARKING CRITERION

The avalanche should start to transform itself as soon as the radial tip field becomes an appreciable percentage of the applied field X_0, say

$$X_1=X_0/20. \quad (8)$$

Introducing this value in Eq. (7) we find, with X_0 and α_0 from Table I for various gap lengths at atmospheric pressure, critical avalanche lengths x_k, as given by curve 2 of Fig. 1. This curve intersects straight line $x=d$ at a point with an abscissa $d\sim0.64$ cm, while curve 1 does this at a point with $d\sim1.6$ cm. These gap lengths determine limits of validity for the Townsend sparking criterion[2] under atmospheric pressure, i.e. $pd=0.64\cdot760\sim500$ and $pd=1.6\cdot760\sim1200$ respectively, for any pressure. It may be concluded that curve 2 and consequently Eqs. (6) and (7) approach more to actual conditions, as limit $pd\sim500$ is closer to that manifoldly computed by Loeb and Meek,[1] i.e. $pd\sim200$.

IV. TRANSFORMATION DUE TO ELECTROSTATIC REPULSION

The avalanche tip radius, as given by Eq. (3) has been computed by considering the thermal electron diffusion.[1,4] The avalanche may be widened by the electrostatic repulsion between the electrons. The dependence of the radius from the space x swept by the avalanche, may be found in this case, in the manner indicated by Raether.[4] The formula thus obtained is

$$r_e=0.756\times10^{-2}(e^{\alpha_0 x}/\alpha_0 X_0)^{\frac{1}{2}}, \quad (9)$$

where X_0 the applied field and α_0 the corresponding ionization factor.*

[4] H. Raether, Zeits. f. Physik **107**, 104 (1937).

* The avalanche having swept the critical length, the field strength at the tip front (X_0+X_1) becomes appreciably higher than X_0 and the corresponding ionization number increases rapidly $(\alpha>\alpha_0)$ so that Eq. (9) becomes inapplicable. However, accepting the formula for lengths slightly exceeding x_k we can estimate the tip radius of an avalanche photographed by Raether[3] in his cloud chamber, which is redrawn in Fig. 2. It was obtained under $p=273$ mm Hg, $X_0=3330V/\text{cm}$ and, as it can be deduced from Sanders' curves, under $\alpha_0=8.1$. First, the critical length will

Figure 3 shows the radius variations, in a 5-cm gap at atmospheric pressure, as computed from Eq. (3) and from Eq. (9). Corresponding curves intersect at about $x=2.4$ cm. Above this length, the avalanche enlargement due to electrostatic repulsion is more rapid than that due to the thermal electron diffusion. This variation is equivalent to an avalanche transformation.

Equating the expressions (3) and (9) for the radii we obtain

$$[0.133(x/p)]^{\frac{1}{2}}=0.756\times10^{-2}(\exp(\alpha_0 x)/\alpha_0 X_0)^{\frac{1}{2}},$$

and therefore, for $p=760$ mm Hg.

$$\exp(\alpha_0 x)=5.35\alpha_0 X_0 x^{1.5}. \qquad (10)$$

From this the critical lengths at which avalanche transformation occurs can be computed in gaps with various electrode distances. The results thus obtained are given by curve 2′ of Fig. 1 and, as it can be seen, they coincide very approximately with those deduced from Eq. (6) with $X_1=X_0/20$ (curve 2). This result is of interest as it shows that both calculations lead to same critical lengths x_k at which the avalanche starts swelling, i.e. transforming itself, and that this occurs when the tip field becomes an appreciable percentage of the applied field (about five percent).

It seems very difficult to follow quantitatively the avalanche evolution once it has reached the critical length. Until the new criterion suggested by Loeb[5] leads to a quantitative solution of the problem of streamer formation, the mechanism qualitatively described by Raether[2] and completed, as regards the renewal of the avalanche by Szpor,[6,7] seems to be a satisfactory description of the actual phenomena.

V. CONCLUSIONS

(1) Equation (6) seems to offer a higher degree of approximation for the tip field, as the critical lengths computed by its application determine a validity limit for Townsend criterion, closer to that otherwise obtained (Loeb and Meek[1]).

(2) The fact that the critical lengths, as calculated by two different methods, i.e. from Eq. (7) with $X_1=X_0/20$ on one hand, and from the condition giving the spaces at which the electrostatic repulsion starts predominating on the other hand, are quite close, may be considered as a further argument on behalf of an avalanche transformation in the case of uniform field gaps submitted to minimum breakdown voltage, as happens under overvoltages.

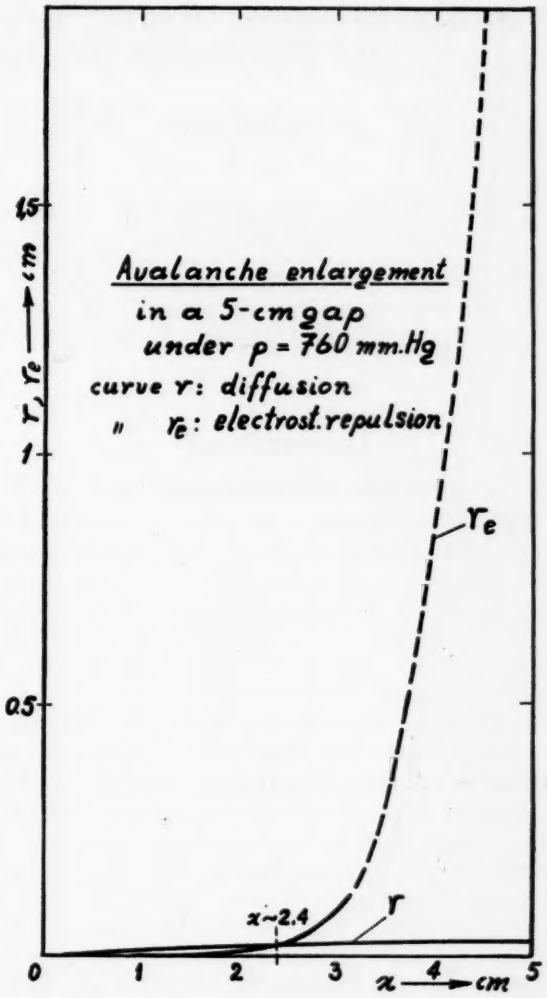

FIG. 3. Avalanche tip radius in a 5-cm gap at atmospheric pressure.

ACKNOWLEDGMENT

The author expresses his best thanks to Mr. Ph. Ventouratos, Electrical Engineer, for assistance during the preparation of this paper.

be estimated from Eqs. (3) and (6), with $X_1=X_0/20$. We have,

$$0.05\times3330=\frac{14.4\times10^{-7}[(4\times8.1/3)(0.133x_k/273)^{\frac{1}{2}}-1]}{0.133x_k/273}e^{8.1x_k}$$

from which we obtain $x_k\sim1.45$ cm. At this length the tip radius is, as computed from Eq. (3), $r\sim0.027$ cm.

Applying now Eq. (9), we find the radius corresponding to the electrostatic repulsion at $x=2.5$ cm:

$$r_e=0.756\times10^{-2}(e^{20.3}/8.1\times3330)^{\frac{1}{2}}=0.21 \text{ cm},$$

instead of an apparent radius of 0.3 cm, as shown in Fig. 2. The approximation may be considered satisfactory if one takes into account the diffusion of the condensation drops which has very probably occurred after the passage of the applied voltage impulse (see reference 3).

[5] L. B. Loeb, Phys. Rev. **74**, 210 (1948).
[6] S. Szpor, Bull. Ass. Suisse Elect. No. 1 (1942).
[7] S. Szpor, Requeil d. travaux d. Polonais int. en Suisse, **2** (1944).

Electrical Phenomena Occurring during the Freezing of Dilute Aqueous Solutions and Their Possible Relationship to Thunderstorm Electricity

E. J. WORKMAN AND S. E. REYNOLDS
Research and Development Division, New Mexico School of Mines, Socorro, New Mexico
(Received October 10, 1949)

The discovery of an electrical effect accompanying the orderly freezing of dilute aqueous solutions is reported. Potential differences as great as 230 volts are measured across the water-ice interface during the the freezing process. At a freeezing rate of about 1 cc per min., a current of 1 μamp. is measured. The character of the effect is a function of the nature and concentration of the solute. The dependence of the effect on the structure of the ions of the solute and the molecular structure of water is shown.

Possible application of this effect to chemical detection and to the formation of thunderstorm electricity is discussed.

INTRODUCTION

IN the fall of 1946, the authors undertook a series of laboratory tests with the hope of discovering a physical process which might be considered basic in the generation of thunderstorm electricity.[1] A careful consideration of the electrical properties of thunderstorms gave strong support to the notion that electrical charge separation in the cloud is related in an essential way to the formation of glaze ice or hail.[2]

Accordingly, the assumed environment of the charge generating process was simulated by having supercooled waterdrops fall through cold air to build up layers of glaze ice by impingement on an insulated cold metal plate. Charge detection was made by measuring the charge acquired by the insulated plate and the charge carried by the unfrozen droplets "splashing" from the growing ice surface. These early tests, although simple to perform, were difficult to interpret. It appeared, however, that the arrangement produced spectacular, but somewhat erratic electrical effects. Most noteworthy was the observation that a potential of 50 volts or more was measured on the cold plate when unfrozen water at the lower tip of the ice was connected to ground.

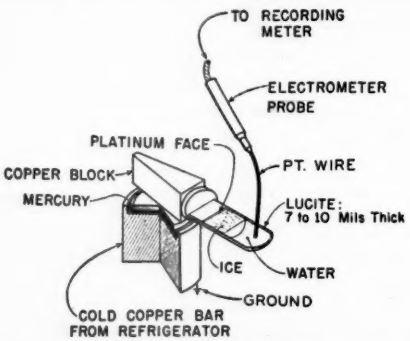

FIG. 1. Apparatus for measurement of potentials.

Subsequently, apparatus shown in Fig. 1 was found to give the best exhibition of this electrical effect. Here the cold copper block, maintained at −5 to −30°C, caused the water in the trough to freeze in an orderly fashion[3] from the cold platinum face outward. It was found that, when water contaminated with slight amounts (10^{-3} to 10^{-6} normal) of materials which ionize in aqueous solution were frozen in this manner, relatively large potential differences were developed between the water and the ice—as much as 230 volts with a weak solution of ammonium hydroxide. The phenomenon is more than electrostatic in nature, inasmuch as certain conditions of contamination permit the measurement of a considerable amount of charge transfer during the freezing process. These measurements may be made by placing a shunt of from 1 to 100 megohms from the electrometer to ground. (See Fig. 1.) A shunt of high resistance was chosen to maintain the potential drop large compared to thermal and contact potential differences.

The observed electrical effect results from freezing. It starts when freezing starts, and stops when freezing stops. The potential barrier is at the water-ice interface; it persists during mechanical stirring of the liquid phase. A reverse potential is not realized during melting because of prior neutralization through the semiconducting ice. The magnitude of the open circuit potential difference is independent of freezing rate over a wide range. In fact, it appears variable only to the extent that internal leakage currents reduce the observable potential for slow rates of freezing, and that crystal disorder reduces it at high rates of freezing. Also, when random crystal orientation results from spontaneous freezing because of a high degree of supercooling, little or no electrical effect is observed. *The sign and mag-*

[1] This work has been supported by the Signal Corps of the United States Army.

[2] See: E. J. Workman and R. E. Holzer, NACA Technical Note No. 850 (1942). Workman, Holzer, and Pelsor, NACA Technical Note No. 864 (1942). C. T. R. Wilson, J. Franklin Inst. **208**, 1 (1929). Horace R. Byers, Terr. Mag. Elec. **45**, 345 (1940). Lt. Robert C. Edwards, USNR, and Capt. George W. Brock, USAAF, J. Meteorology **2** (1945). E. J. Workman and S. E. Reynolds, Bull. Am. Meteorological Soc. **39** (1949).

[3] When a body of water freezes by losing heat through a refrigerating surface the *C* axes of the ice crystals are oriented perpendicular to the refrigerating surface if the transfer of heat is slow. If the rate of heat transfer is very rapid the orientation of the crystals becomes random. When spontaneous freezing occurs in water in a supercooled state, complete disorder of the crystal axes is favored.

nitude of the potential difference developed and the quantity of charge separated during freezing are functions of the kind and amount of contaminants in solution with the water.

EXPERIMENTS AND DISCUSSION

Aqueous solutions of more than 40 different substances have been tested. It is inappropriate to present here complete data on the behavior of these materials in their various concentrations, but approximate characteristics are given in Table I. A discussion of a few solutions will serve to illustrate the nature of the effect and to provide a basis for an attempt at interpretation.

Doubly distilled water (2.5 megohm cm resistivity) develops upon freezing a potential difference of about 60 volts, the water being negative with respect to the ice. As solidification of a given sample proceeds, the potential difference diminishes and frequently reverses in sign to a value of from 10 to 20 volts. Since ammonia is known to be a persistent contaminant of water, samples were prepared and handled in such a way as to eliminate ammonia as a contaminant. These samples yielded only a few volts potential difference during subsequent freezing. When prepared solutions of ammonium hydroxide (5×10^{-5} normal) were used, potentials as great as 230 volts were observed—the water being negative with respect to the ice.

When sodium chloride is used as a contaminant in ordinary distilled water, assumed to contain residual ammonia, the negative potential difference characteristic of ammonia decreases as the concentration of the sodium chloride is increased. The potential difference is reduced to zero at about 10^{-5} normal concentration of the salt. Further increase in concentration of the salt causes a reversal of the potential difference, which reaches a maximum of about 30 volts at 10^{-4} normal. At this concentration 90,000 e.s.u. of charge were separated for each cc of solution frozen. When the concentration is increased beyond about 5×10^{-4} normal the potential difference is again zero.

Tests of the 43 prepared solutions listed in Table I show that the behavior of ammonium and fluorine ions is outstanding. In a sense they may be considered representative of a special device. In general, it is the ion with large electronegativity that is incorporated into the ice structure. The remarkable behavior of the ammonium ion in exception to this generality is attributed to its isomorphism with the hydronium ion. Fluorine ions have a position of preference for two reasons: their high electronegativity and their similarity to hydroxyl ions in structure. These factors cause the selection of the anion in place of the cation when ammonium fluoride is used—an action which is not observed with any of the other eight ammonium compounds studied.

The compatability of the electrical structure, or the lack of it, is seen to be important in other exceptional cases where the electropositive ion enters the ice selectively. Nitrate ions and acetate ions in aqueous solutions, are rejected by the ice.

In the series sodium fluoride, chloride, bromide and iodide, the measured charge separation decreases in going from fluorine to iodine as does the electronegativity of the anion. (See Table I.)

The phenomenon apparently belongs to a class of phenomena which are encountered in solid state physics, and for which only speculative interpretations exist. Charge separation measurements indicate that the number of impurity centers per cc in the ice of dilute solutions approximates the number of impurity centers in semiconducting crystals used as rectifiers.

TABLE I. Electrical characteristics of various solutions.

Substance	Maximum P.D.* corresponding normality (N)** or specific conductance (C)		Maximum charge separation and corresponding normality		Notes
NaF	+21 volts	$20N\times10^{-4}$	530,000 e.s.u./cc	1.0×10^{-4}	
NaCl	+30	$100N$	92,000	1.0	
NaBr	+19	$50N$	88,000	1.0	
NaI	+2	$10N$	Negligible	All	
CsF	+34	$30N$	440,000	10.0	
CsCl	+14	$400N$	79,000	4.0	
KCl	+14	$200N$			
LiCl	+14	$150N$			
NH_4Cl	−105	$70N$	104,000	1.0	a
NH_4OH	−232	$30N$	260,000	0.2	a
NH_4NO_3	−185	$3N$	83,000	0.2	
NH_4I	−109	$6C$			b
NH_4Ac	−75	$80C$			b
NH_4Br	−84	$10C$			b
$(NH_4)_2CO_3$	−109	$8C$			b
$(NH_4)_2SO_4$	−61	$4C$			b
NH_4F	+9	$1000N$	82,000	10.0	
$BaCl_2$	+10	$8C$			
CaF_2	+13	$8C$	46,000	0.7	
$CaCl_2$	+14	$9C$			
$CdCl_2$	+16	$9C$			
$HgCl_2$	Negligible	All			
$MgCl_2$	+12	$9C$			
$MnCl_2$	+15	$7C$			
$NiCl_2$	+12	$7C$			
$ZnCl_2$	+17	$8C$			
$CuCl_2$	+5	$20C$			
$AlCl_3$		$8C$	Negligible	All	c
$NaNO_3$		$7C$	—	—	c
Na_3PO_4		$20C$	—	—	c
H_2O_2		$5C$	—	—	c
HCl		$4C$	—	—	c
HF		$2C$	—	—	c
CO_2		$2C$	—	—	c
H_2SO_4		$2C$	—	—	c
$AgNO_3$	−39	$2C$	Negligible	All	d
$Pb(Ac)_2$	−100	$3C$	14,000	0.9	
NaCN	+36	$6C$			
Na_2HPO_4	−63	$2C$	Negligible	All	e
NaOH	+11	$50N$			
$Ca(OH)_2$	+75	$60N$	12,500	0.6	f
$Ba(OH)_2$	+18	$3N$			f
$CaCO_3$	+20	$50N$	9000	0.8	f

* Potential of liquid with respect to ice.

** In the work with many of the substances listed, specific conductance (mho-cm) was used as a measure of contamination rather than normality to facilitate the experiments.

[a] Amount of charge separated using these two compounds not consistently reproducible. Concentration apparently critical factor.

[b] One test only on these compounds, therefore, values given do not necessarily represent maxima.

[c] Addition of these compounds merely decreases potential measurable using uncontaminated water. (10^{-6} specific conductivity approx.) Conductivity values shown are for concentration at which potential reached zero. Greater concentration did not cause reversal of potential.

[d] May belong in classification immediately above. However, substantial potentials (−15 volt) observed at 10^{-5}C.

[e] Zero potential at 1.5×10^{-5}C.

[f] Potential extremely sensitive to amount of CO_2 in solution.

In the largest transfer of ions observed, about one foreign ion in 3×10^7 water molecules was involved—approximately 10^{15} ion centers per cc of ice.

The conductivity of ice samples prepared in this way is extremely sensitive (according to preliminary tests) to the concentrations of the contaminant. For example, using ammonium hydroxide, the conductivity changed by a factor of 200 when the concentration was varied from 6.5×10^{-5} to 9.5×10^{-5}.

The following exploratory tests showed that ice samples prepared from dilute solutions possess significant rectification properties. With two platinum plates (approx. 2.5 cm²) in a vertical position about 1 cm apart in the ice and at right angles to the direction of freezing, an open circuit d.c. potential of from 0.2 to 0.4 of a volt, or a direct current of 0.7 μamp. was produced when an a.c. signal of 14 volts at 18 cycles was applied to the electrodes after the sample had reached temperature equilibrium. At 60 cycles values of about one-half these were produced, while at 200 cycles no rectifying properties were observable. The polarity of the d.c. potential produced was such that the probe most distant from what had been the refrigerating surface was positive. If the plates were frozen into the ice parallel to the direction of freezing, no rectifying effect was detectable.

When a "cat's whisker" of No. 36 platinum wire was used in place of one of the platinum plates, and the thickness of the sample reduced to about one-half cm, open circuit d.c. potentials of from 1.0 to 2.5 volts or d.c. currents of about 0.1 μamp. were measured at 14 volts and 18 cycles. Frequency sensitivity was similar to that found for plate electrodes. The effect was not sensitive to the orientation of the platinum plate, but the rectifying properties were changed by moving the "cat's whisker." These changes did not seem to be related to the freezing axis of the sample.

Considering the fact that we are dealing here with a phenomenon which characterizes solutions in concentrations of 10^{-5} normal and less, interest is aroused in just how characteristic the effect is of the material and its concentration. These points are related to the possible use of this effect for detection and analysis. Bearing in mind that, for the most part, only single known contaminants have been studied, the features which we list below are characteristic of the contaminant and its concentration:

1. The sign and magnitude of the potential measured.
2. The amount of charge separated under standardized conditions.
3. The rate of rise of the potential curve as the ice forms.

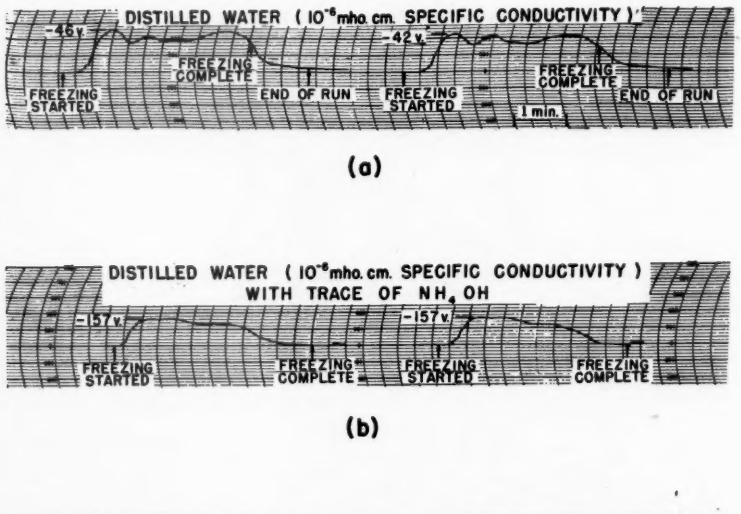

FIG. 2. Time variation of the potentials.

4. The type of the potential *vs.* time curve as freezing progresses.
   (a) Characteristic inflections.
   (b) Frequency of inflections.
   (c) Constancy of value during freezing.
5. Changes in the potential curve as freezing nears completion, particularly as this may be related to chemical changes caused by ion capture process.

The potential *vs.* time curves of Fig. 2 which were obtained by freezing solutions in a nickel-plated copper dish about $\frac{1}{4}$ in. deep and $1\frac{1}{4}$ in. in diameter, illustrate the aforementioned characteristics. The potential shown is that of the liquid with respect to the solid. The period of 10 to 15 seconds between the time that freezing begins at the bottom of the dish and the time that measurable potentials exist, is the period required for the grounded metal walls of the dish to become insulated from the water by a thin film of ice. The slight but sharp inflection at about 15 seconds after measurable potentials are observed and the inflection at about the time freezing is complete are noteworthy in the case of distilled water (Fig. 2a). The first of these is not readily explainable, but the latter is believed to be caused by the dissipation of the accumulated charge following the completion of the freezing process. In this connection, the rate of decay using distilled water should be compared to that observed when sodium fluoride is used. Measurements show that the resistivity of ice prepared from ordinary distilled water may be 1000 times as great as that prepared from a 10^{-4} normal solution of sodium fluoride.

The characteristically wavering manner in which the potential rises in the case of distilled water and in very dilute ammonium hydroxide solution (Figs. 2a and 2b) should be compared to the definite and sharp manner in which the potential rises in the case of the other two compounds (Fig. 2c and 2d). The effect of the changes in concentration on the potential *vs.* time curve is well illustrated by Figs. 2d. The manner in which the major inflections during the freezing process are reproduced when like samples are frozen is typified in each of the sets of curves. These inflections are believed to be the result of changes in the kind and number of ions in solution in the liquid phase during the freezing process. This is certainly true in the case of a substance like sodium chloride where the hydroxyl ion replaces some of the chlorine ions in the liquid phase, and where changes in the concentration of the contaminant in the liquid phase is brought about by the rejection of impurities by the ice in the ordinary sense.

The following tests leave little doubt as to the ionic character of the effect. Samples of dilute sodium chloride solution (7×10^{-5} normal) were partially frozen in the cup shown in Fig. 1. To avoid carbon dioxide complications, the tests were conducted entirely in an atmosphere of helium. The electrometer shunt (20 meghoms) was used during freezing in such a way as to permit the flow of the electrical current produced at a potential difference of several volts. The unfrozen portion was poured into one cleaned vessel, and the ice dropped into another and permitted to melt. When both portions were at room temperature *p*H measurements were made on each portion with a Beckman meter. Results of these tests were as follows: Sample before freezing, 6.3; frozen fraction, 6.2; unfrozen fraction 7.0. These results substantiate the view that the chlorine ions were trapped selectively in the ice while sodium ions discharged in the liquid phase, forming sodium hydroxide and thus decreasing the hydrogen ion concentration. Calculation indicates that this change in *p*H value represents an increase of 2.4×10^{14} hydroxyl ions or the discharge of this number of sodium ions per cc in the unfrozen portion. Discharge of these ions would liberate 102,000 e.s.u. of charge. Considering that some electrical leakage must go on during the freezing process, this value is an excellent agreement with the value of about 90,000 e.s.u./cc usually measured during the freezing of sodium chloride solution at concentrations of about 10^{-4} normal. Since the *p*H measurements at this dilution are difficult such excellent agreement is probably fortuitous, but the interpretation appears to be validated.

Consideration should be given to the energy involved in this ion selection. A potential difference of 200 volts or more indicates energy per ion of more than 3×10^{-10} ergs—approximately three thousand times the latent heat of fusion of each molecule of water, or perhaps more pertinently two or three hundred times the total energy of attraction per molecule in ice. Energy of this magnitude suggests collective action on the part of the crystal elements of the water at the interface.

Errera has found justification for the hypothesis that liquid substances having permanent dipoles (highly associated) pass through a "colloidal" transition stage in freezing. He reports: "Thus, associated structures would be formed in such a manner that their dimensions would cause them to come under the category of media in the state of colloidal division, that is to say of which the particles have a diameter between a few $\mu\mu$ and about $500\mu\mu$. Further, we must suppose that the arrangement of the molecular dipoles inside the colloidal structures is such that these last have a high electric moment, higher, indeed, than that of the molecular dipoles."[4]

It seems reasonable to suppose that these associated colloidal particles in the process of formation might avoid an increment of potential energy by incorporating ions of compatible form into their structure in such a way as to form a non-polar electrical domain. Questions of why ice does not exhibit polar properties have been the subject of much speculation by investigators.[5,6] It is not likely that one foreign ion in ten or a thousand million crystal units will, by its position alone, neutralize the polarization of a crystal viewed as a static system. Collective action at the growing crystal face

[4] Jacques Errera, Trans. Faraday Soc. **24**, 162 (1927).
[5] J. D. Bernal and R. H. Fowler, J. Chem. Phys. **1**, 523 (1933).
[6] John Mead Adams, Proc. Roy. Soc. **A128**, 588 (1930).

would produce adequate energy of attraction to maintain the observed potential barrier, and once there, the ion may facilitate the arrangement, or modify the resonance pattern of the crystal units.

On the assumption that the phenomena observed were related in a primary way to structural changes accompanying freezing (Pauling estimates that 15 percent of the hydrogen bonds must be broken upon change of state of water) similar effects were predicted for other compounds undergoing marked change in bond structure in the liquid to solid transition. Salol (phenyl salicylate) is such a compound. An electrical effect, believed to be similar to that found for water, was observed when salol solidified. The flow of current during freezing was detectable, but small (the electrical conductivity of solid salol is low). Potential differences of 45 volts, with the solid positive with respect to the liquid, were measured. The nature of the impurities in the material was not determined, and the effect of known impurities in solution in this substance has not been investigated. Confirmation of this prediction for salol gives at least circumstantial evidence as to the true nature of the effect.

APPLICATION TO THUNDERSTORMS

In considering mechanisms for charge separation in thunderstorms, it is well to recall properties of the storms on which there is general agreement. A thunderstorm is a vertical, or nearly vertical, development in thermodynamically unstable air. The depth of the cloud (for example, from the 8°C isotherm to the −40°C isotherm) indicates a large water content. The storm cloud in the "going" stage exhibits a diffuse positive charge center in the upper region, and a more integrated negative charge center near the 0°C isotherm. These centers are characteristically discharged by lightning strokes between them, or from the lower negative center to ground. These electrical effects are not evidenced until the cloud top rises high enough to initiate precipitation processes by glaciation, and until the resulting precipitation particles have become large and numerous. (At this stage they give detectable 3 cm radar returns.) The locale of the charge separation process appears to be between the 0°C and the −10°C isotherms.

This elementary thunderstorm model dictates the dependence of lightning discharges upon sizeable precipitation particles, and suggests the dependence of charge separation upon the change of state (freezing) of the particles.

Assuming such a model, the following hypothesis of interaction between ice and water can be made: suppose that an ice crystal formed by sublimation near the top of the cloud begins to fall. It will encounter supercooled waterdrops at sufficiently low temperature to form a rime ice pellet or graupel. Growth by this process, or by sublimation, will continue until a level of about −10°C or −15°C is reached, where glaze ice will form upon the pellet. It will grow by this process and its rate of fall will increase relative to the suspended, or perhaps ascending, supercooled waterdrops. In the region of about −10°C, if conditions are favorable, these drops should impinge upon the cold glazed pellet, and a portion of the water should freeze to its surface in a thin layer. The remaining portion of the water, because of splash effects and the velocity of the hail pellet with respect to the air, will become detached in small drops carrying positive charges which will be transported into the cloud above. The shape of the hail pellet along with the aerodynamic situation favors grazing impact of the drops. This process will not continue long because the pellet will reach such an electrical potential that the detaching drop will no longer separate positive charge. Moreover, the hailstone is traveling faster and faster into a warmer region of the cloud and its heat capacity is limited. The degree of supercooling of impinging waterdrops decreases to the extent that the hail will cease its growth and start melting. At this point of the hailstone's history, the waterdrops which impinge on it will share the electrical charge of the hailstone and eventually will reduce its charge toward zero.

A very important feature in this series of events is the action of the negative drops which arise from contact with the hail in the lower regions when they are carried upward and impinge again upon negatively charged hailstones. Their previously acquired negative charge makes it possible for the potential of the new pellets encountered to be increased. This cycle of events may (depending, of course, upon the potential attainable with the contaminants present and the size of the particles involved) be required in order to raise the potential of the hail pellet, and consequently the charge per unit volume of precipitation, to the value necessary to produce the observed amount of thunderstorm electricity.

An important consideration favoring this type of cycle is that, consistent with observation, it serves to maintain the negative charge center within a definite altitude zone in the cloud. No postulate for charge separation heretofore advanced provides for this crucial property of the lower charge center. Another critical feature of the storm which is satisfied by this postulate is that the cloud must include and extend some distance below the 0°C isotherm.

Laboratory tests with a simulated hailstone in a specially constructed cold chamber showed that potentials consistent in sign and magnitude with those achieved by freezing bulk water in cups could be attained by grazing collision of waterdrops and ice pellets. The results to be expected from repeated collisions were realized. After the hail pellet became warmed to 0°C by collision with waterdrops, subsequent collision resulted in the carrying away, by the waterdrop, of the pellet's accumulated charge.

Resistivity measurements on samples of water collected within active thunderstorms (collected mostly as

ice pellets 1 mm to 2 mm in diameter) showed a concentration of about 10^{-4} normal. The principal contaminants found in samples collected near Albuquerque, New Mexico, were calcite and sodium chloride.

It is interesting to note that one of the most abundant aerosol particles is the relatively insoluble calcium carbonate. This material provides an effective complex because of the relatively high solubility of carbon dioxide in water at temperatures near 0°C. The calcium bicarbonate thus formed is highly active in producing large potential differences during freezing. Since the amount of carbon dioxide available is reasonably constant, an abundance of calcium carbonate aerosols might provide for adequate concentrations of the bicarbonate and hence uniform electrical properties of storms.

A thunderstorm possibly could be made by 1 e.s.u. of electrical charge per cc of water, but more charge, perhaps 5 e.s.u., seems a more reasonable estimate. The electrical effects produced by the freezing of the collected samples, and samples synthesized in the laboratory, were of the correct sign and ample in charge production, with a factoral margin of at least 1000, provided, of course, that a process involving repeated collisions can be realized.

It should be mentioned that we have considered it essential to think of thunderstorm precipitation, in part at least, as melted hailstones or ice pellets, which have fallen through the clouds. This view of the matter may be an oversimplification. Some critics have suggested that the infrequency with which hail is encountered by aircraft in thunderstorms seems to deny the importance of hail in thunderstorm electrification. To refute this argument, the following statements can be made: (1) The falling ice particles need not necessarily conform to the usual definition of hail as reported by flying aircraft. (2) Information received from Dr. Roscoe R. Braham shows that hail was encountered in 21 of 38 thunderstorms studied in Ohio, but that hail was observed during only a few of the total of 812 aircraft traverses through these storms. Inasmuch as hail was observed in more than half of the storms, but during only a few traverses, one might infer that hail actually occurred in limited regions of all of the storms. Our current view is that the unit cell of convection, precipitation, and electrical activity may be only a few hundred feet in diameter, and that a single storm may be made up of many of these cells. The number of these cells that are at any one time in the "going" stage, electrically, may be small even in a large sto_m.

Dr. Vincent Schaefer recently has described to us, verbally, experiments which indicate that the electrification accompanying the freezing of water may be effective in separating charges during the growth of microscopic crystals by sublimation. Some incidental thunderstorm electrification may occur, therefore, when ice pellets of appreciable size are not present.

SPECULATION

The fact that the effects produced during freezing are characteristic of the particular ions in solution (see Fig. 2) and the ability of water to absorb certain gaseous materials, such as carbon dioxide, ammonia, and others, lead to considerable promise in detecting extremely minute quantities of these materials. The freezing tests may be performed with a drop of solution, and detection of 10^{-7} or 10^{-8} gram of contaminant is possible. Ammonium hydroxide, for example, produces a relatively large negative potential even when the amount added cannot be detected by resistivity measurements. With 10^{-4} normal calcium hydroxide solution, the potential achieved may be changed from 1 or 2 volts to as much as 75 volts by the addition of a trace of carbon dioxide. This results from the replacement of hydroxyl ions by bicarbonate ions.

Of further speculative interest is the amount of charge which might be separated by freezing large volumes of these weak solutions: 100,000 c.g.s. units of charge per cc amounts to 30 coulombs per cubic meter, or 3×10^{10} coulombs per cubic kilometer. It is conceivable that this effect might produce currents of geophysical significance in arctic regions. In other situations, induced electrolysis might be effective in influencing the distribution of terrestrial substances.

Assumption of the mechanism described for the production of thunderstorm electrification suggests possibilities for the control of lightning discharges. Inasmuch as the solution concentration required to produce the effects is small, the addition of certain chemicals to the atmosphere in the environment of a thunderstorm might either enhance or inhibit the electrical effects.

Laboratory tests were conducted which showed that 1000 pounds of ammonia, properly distributed, would be enough to stop electrical discharges in a large storm. Two field tests involving cloud contamination have been performed. Data collected have not yet been analyzed, but the immediately observable results gave encouragement for further experimentation. The very nature of this experiment requires a number of tests to produce conclusive results.

Magnetic Properties of a Rotating Superconductor*

AARON WEXLER AND W. S. CORAK
Research Laboratories, Westinghouse Electric Corporation, East Pittsburgh, Pennsylvania
(Received November 23, 1949)

The magnetic properties of a superconductive lead sphere have been studied through the measurement of the voltage induced between the axis and the periphery of the sphere rotated as a Faraday disk at constant speed in an axial magnetic field. Measurements were made in the range 0–10,800 r.p.m. The data are consistent in all details, including critical field and the amount of frozen flux, with the properties of the stationary sphere. In the course of this work, it was found that films of colloidal graphite serve as useful resistance thermometers in the liquid helium range.

I. INTRODUCTION

THE magnetic properties of superconductors are fundamental to the elucidation of the nature of superconductivity from both the macroscopic and microscopic points of view. Since its discovery by Meissner and Ochsenfeld[1] in 1933, the $B=0$ property of a superconductor has been assumed to be of general validity; it had clarified the reason for the success of the application of thermodynamics to the transition[2] and has also been used extensively to resolve apparent inconsistencies in the experimentally determined critical data for "non-ideal" superconductors.[3] The report by Houston and Squire[4] that the voltage induced in a Faraday disk of lead, in the form of a flattened spheroid, remained practically unchanged as the transition range was traversed demanded immediate verification since it implied that the $B=0$ property did not hold for a rotating superconductor. Our preliminary work[5] showed that for rotational speeds up to 300 r.p.m. the magnetic properties of a rotating superconductor are identical with those of a stationary one. The experiments have been extended to cover the range of speeds in which Houston and Squire worked. Recently, these workers[6] have reported that their findings were in error as a result of an experimental difficulty. Although the nature of the discrepancy between our respective results has been clarified, we are presenting our data because they show quantitatively the details of the isothermal changes in B as a function of H by a method not previously used. Further, these results bear directly upon the possibility[7] of affecting the amount of flux frozen in a superconductor.

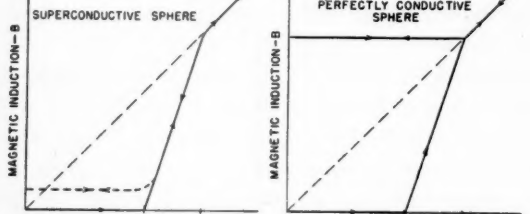

FIG. 1. Comparison of magnetic properties of a superconductive with a perfectly conductive sphere.

A spherical conductor of radius a rotated as a Faraday disk[8] with angular velocity ω in an axial magnetic field, which produces a uniform magnetic induction B within it, gives rise to a voltage

$$E=B\omega a^2/2 \tag{1}$$

between its axis and the periphery.

If Φ is the total flux threading the area bounded by the great circle of the disk normal to the axis, this relation may be written as

$$E=\Phi\omega/2\pi. \tag{2}$$

The Faraday disk machine, or homo-polar generator, becomes a uni-polar generator if the flux threading the sphere arises from its permanent magnetization. The time average† of the induced voltage under these conditions is independent of the distribution of the flux and is given by Eq. (2).

In connection with the results to be expected in experiments of the type to be described, it is desirable to review the B *vs.* H relation for a stationary sphere as shown in Fig. 1. From Maxwell's equation, $\dot{B}=-c\,\mathrm{curl}E$, it can be deduced that a perfectly conductive sphere, made to pass into this state in zero applied field, would retain the value $B=0$ with increasing H so long as the field acting on the sphere remains everywhere less than the critical field H_c. It is found, however, that the prediction of frozen flux, equal to that obtained at $H=H_c$, upon the reduction of the applied field below $H=H_c$, is not in accord with the experimental facts.

* This paper is based on material presented at the International Conference on the Physics of Very Low Temperatures, M.I.T., Cambridge, Massachusetts (September 8, 1949).

[1] W. Meissner and R. Ochsenfeld, Naturwiss. **21**, 787 (1933).
[2] C. J. Gorter and H. Casimir, Physica **1**, 305 (1934).
[3] D. Shoenberg, Proc. Camb. Phil. Soc. **36**, 84 (1939).
[4] W. V. Houston and C. F. Squire, Science **109**, 439 (1949).
[5] A. Wexler and W. S. Corak, Phys. Rev. **76**, 432 (1949).
[6] W. V. Houston and C. F. Squire, Phys. Rev. **76**, 685 (1949).
[7] Love, Blunt, and Alers, Phys. Rev. **76**, 305 (1949).
[8] See, for example, L. Page and N. I. Adams, Jr., *Principles of Electricity* (D. Van Nostrand Company, Inc., New York, 1949), pp. 314–318 and 332.

† This fact was pointed out to the authors by Dr. J. Slepian. It is perhaps important to note this as it might otherwise be tempting to use the data obtained for the case of a rotating superconductor with frozen flux as a basis for speculation concerning the spacial distribution of the flux.

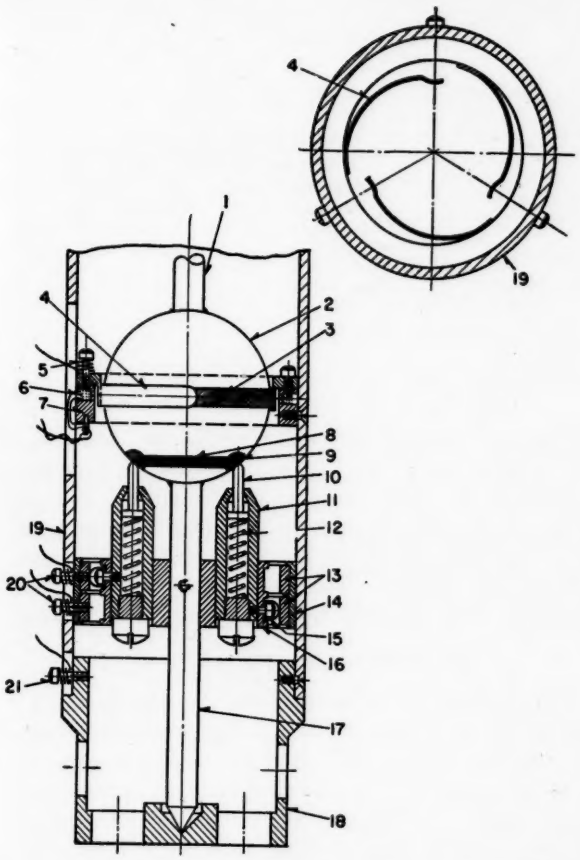

FIG. 2. Details of rotor assembly. 1. Copper rod-connecting sphere to drive shaft. 2. Lead sphere. 3. ½-mil thick gold-plated band. 4. Phosphor bronze leaf spring contact. 5. Spring-loaded contact screw. 6. Pick-up coil for B, H measurement. 108 turns of No. 42 enameled Cu wire, average diamater 1.080 in. 7. Plexiglas holder. 8. Graphite film thermometer. 9. Evaporated gold contacts. 10. Copper contact. 11. Spring retainer. 12. Phosphor bronze loading spring. 13. Stationary brass contact rings. 14. Plexiglas stationary contact holder. 15. Phosphor bronze leaf spring contact. 16. Plexiglas moving contact holder. 17. Copper rod electrode. 18. Brass bearing and contact block. 19. Main Plexiglas support tube. 20, 21. Spring-loaded contact screws.

For ideal conditions,[9] the property is independent of the history of the specimen. That is to say, it is necessary to distinguish between the results which Maxwell's equations predict, Fig. 1b, and those which experiment shows to be a new property, Fig. 1a; the curve for the latter case is not shown to be entirely reversible because in practice a small amount of frozen flux due to chemical or physical imperfections is always found. In particular, Shoenberg has studied the isothermal magnetization curve for lead spheres, and in the case of pure polycrystalline lead found a frozen flux equal to 3 percent of the flux within the sample at $H=H_c$. The penetration of the flux at $H=2H_c/3$ is due to the fact that the field acting on the sphere at the great circle perpendicular to the applied field is intensified to H_c by the demagnetizing properties of the diamagnetic sphere. Thus, since the voltage induced in a Faraday disk is proportional to the magnetic induction B within it, isothermal voltage measurements as a function of the applied field should be of the form of Fig. 1a if the $B=0$ characteristic holds for a rotating superconductor or of the form of Fig. 1b if it does not. It is instructive, moreover, to compare the B, H relation for the stationary sphere with the E, H curves at different rotational speeds.

[9] D. Shoenberg, Proc. Roy. Soc. London, **A155**, 712 (1936).

II. EXPERIMENTAL

A one-inch lead sphere (2) was machined to within 0.001 in. on any diameter from a sample of 99.998

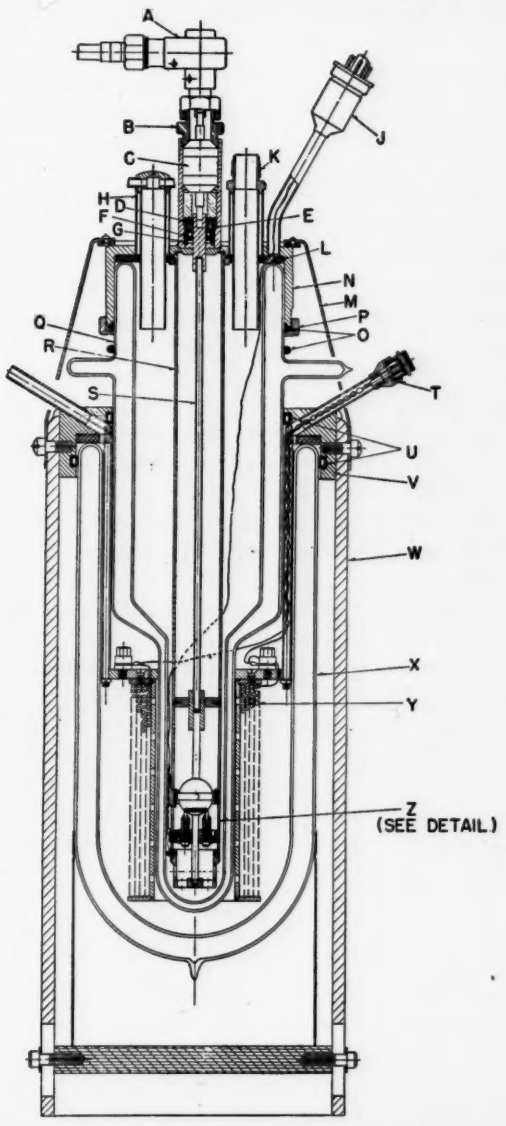

FIG. 3. Liquid helium cryostat. A. Right-angle gear. B. Gear box retaining nut. C. Interchangeable gear box. D. Packing retainer. E. Ball bearing. F. Garlock seal. G. "O" ring. H. Manometer and gas vent line. J. Wire seal. K. Filling and pumping line. L. Felt gasket pad. M. Brass support brace. N. Brass Dewar cap. O. "O" ring. P. Cap nut. Q. Helium Dewar. R. Main Plexiglas support tube. S. Thin-wall monel drive shaft. T. Gas-tight solenoid power plug. U. Rubber tube Dewar seals. V. Micarta nitrogen Dewar cap. W. Brass uprights. X. Nitrogen Dewar. Y. Liquid nitrogen cooled solenoid. Z. Rotor assembly (see Fig. 2).

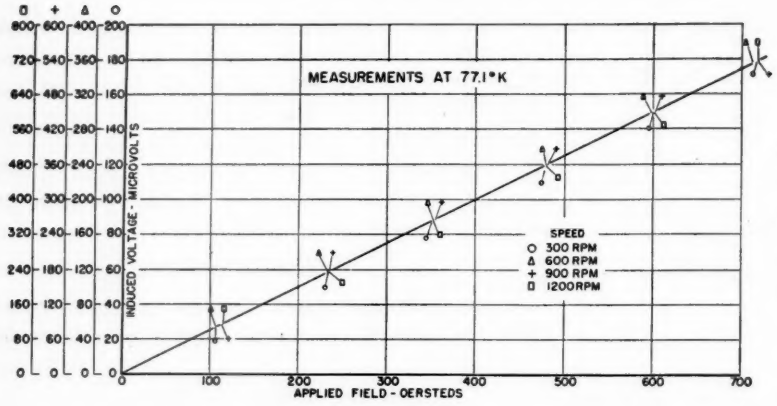

FIG. 4. Isothermal measurements at the nitrogen boiling point. (The experimental points are at the extremities of the indicating lines, opposite the identification symbols.)

percent lead kindly supplied by the National Lead Company of Pennsylvania. It was mounted in the manner shown in Fig. 2. The copper rod (17), acting as one of the leads, was soldered to one pole, and another short rod (1), connected the ball through a Micarta spacer to a thin-wall monel tube acting as a drive shaft. The other contact was made through a phosphor bronze leaf spring arrangement shown in detail in the insert. A resistance thermometer (8) was affixed to the ball by first painting the under region with insulating lacquer. Gold contacts (9) were deposited by evaporation, and a film of colloidal graphite‡ was painted and dry rubbed between the contacts. A spring contact arrangement, rotating with the ball, was used to make electrical connection to the fixed rings (13). The copper pick-up coil (6) was used to measure the B, H curve of the sphere. All friction contacts were gold plated.

The lead ball assembly is shown in place in the cryostat in Fig. 3. It is located at the center of a liquid nitrogen cooled solenoid Y giving a magnetic field, equal to 475 oersteds per ampere, uniform to ± 1 percent over the region occupied by the sphere. The sphere was bathed by the refrigerant which established the temperature, and the arrangement was such as to permit the adjustment of the temperature of the bath by the regulation of the vapor pressure of the liquid in Dewar, Q. The details of construction are indicated in the legends under the figures. The cap arrangement may be of special interest to experimenters. The "O" ring construction resulted in a helium leak detector[10] tight apparatus, and the re-entrant tube arrangement allowed the cap to remain practically at room temperature even when the inside Dewar was being filled.

III. MEASURING TECHNIQUES

It was desirable to arrange for the measurement of the isothermal induced voltage, E, *versus* applied field, H, relation over a wide range of rotational speeds so that the nature of any observed changes in the critical data could be evaluated. Since the calculated output of the rotating sphere acting as a generator is 8.45 microvolts per 100 gauss per 100 r.p.m. and because it was of interest to observe whether there occur transient effects in the magnetization,[11] arrangements were made to amplify the output of the generator and to present the amplified output on a 0–10 millivolts Speedomax recording potentiometer. The output of the generator was fed into the e.m.f. terminals of a Type K2 potentiometer whose galvanometer terminals were connected to the input of a Perkin-Elmer breaker type d.c. amplifier. The output of the amplifier was connected to the recording potentiometer through a suitable filter network. Normally, the Type K2 potentiometer was

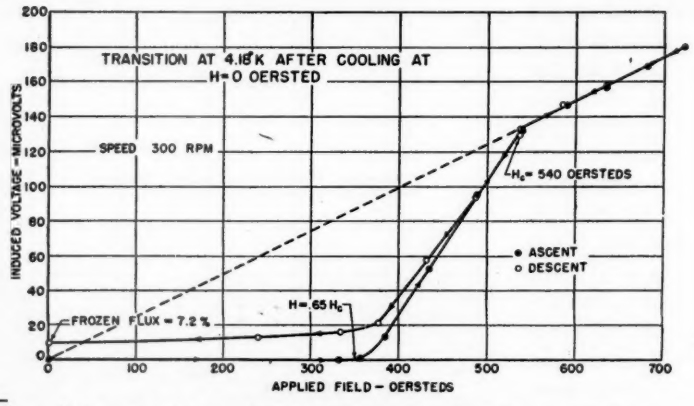

FIG. 5. Transition at 300 r.p.m.

‡ Dag 154 supplied by the Acheson Colloids Corporation, Port Huron, Michigan, was used for this purpose.

[10] Thomas, Williams, and Hipple, Rev. Sci. Inst. **17**, 368 (1946).

[11] J. G. Daunt and K. Mendelssohn, Proc. Roy. Soc. London **A160**, 127 (1937).

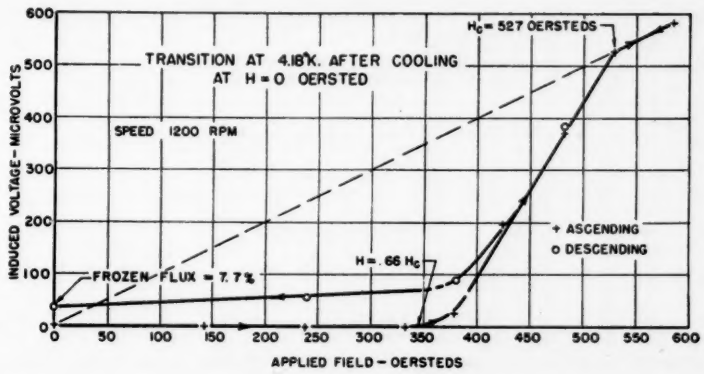
H_c = 527 OERSTEDS
TRANSITION AT 4.18°K. AFTER COOLING AT H = 0 OERSTED
SPEED 1200 RPM
+ ASCENDING
o DESCENDING
H = .66 H_c
FROZEN FLUX = 7.7%
INDUCED VOLTAGE - MICROVOLTS
APPLIED FIELD - OERSTEDS

FIG. 6. Transition at 1200 r.p.m.

set at zero when E, H data were being obtained. However, the connections were such that the potentiometer could be used to buck out the generator output; this was done in order to obtain an accurate calibration of the amplifier gain. Sufficient resistance was placed in the amplifier input circuit to make its gain practically independent of contact resistance fluctuations except for the highest speeds. The recorder's strip chart was run at 180″ per hour; transient effects of duration greater than 2 seconds could be detected. For the highest speeds, the output of the generator could be fed directly into the recording potentiometer.

The calibrated solenoid was powered by a constant current supply,¶ the current being determined from the voltage drop across a standard resistance in series with it, as read on a Type K2 potentiometer. Conventional B, H measurements were made with the aid of a test coil connected to a Grassot fluxmeter having a sensitivity of 14,000 maxwell-turns per division.

Resistance thermometer measurements were made in two ways. For precision measurements, the voltage drop across the thermometer and across a standard resistance in series with it could be determined with a Type K2 potentiometer. It was found that with a Perkin-Elmer d.c. amplifier connected across the galvanometer terminals it was possible to balance to ± 0.1 microvolt for resistances as high as 20,000 ohms. When the power dissipated in an experiment precluded time consuming balancing operations, the resistance was determined with the aid of a Speedomax recording potentiometer.

IV. EXPERIMENTAL RESULTS

A check on the operation of the apparatus is indicated in Fig. 4. Isothermal measurements were conveniently carried out with the sphere assembly immersed in boiling nitrogen at 77.1°K. For each rotational speed, the induced voltage was accurately a linear function of the applied field. The measured induced voltages were consistently lower by 1.7 percent than the values calculated from the drive speeds and the room temperature radius of the sphere. About one-third of this difference is to be ascribed to the thermal contraction of the sphere.

A typical isothermal transition at a bath temperature of 4.18°K is shown in Fig. 5. The procedure was to cool the lead sphere in the absence of field to the boiling point of helium by direct immersion and to observe the induced voltage as the field was varied while the sphere was rotated at constant speed. It is to be noted that the magnetic field began to penetrate at almost the theoretical fraction of the field at which penetration was complete. The frozen flux was manifested by the induced voltage in zero applied field at the conclusion of the field cycling. The sphere was thus permanently magnetized; stopping the rotation did not affect the induced voltage when the rotation was again resumed at $H=0$. The significance of the critical field, $H_c=540$ oersteds, will be discussed later.

Figure 6 shows a similar transition at a rotational speed of 1200 r.p.m. The lowered value of the critical field is particularly to be noted.

The highest speed at which an isothermal transition was observed was 10,800 r.p.m.; the data are given in Fig. 7. Here the uncertainty in the data, due to contact resistance fluctuations, was about 2 percent at $H=H_c$. The variation in frozen flux percentages is within the uncertainty of these values.

The magnetic properties of the stationary sphere were

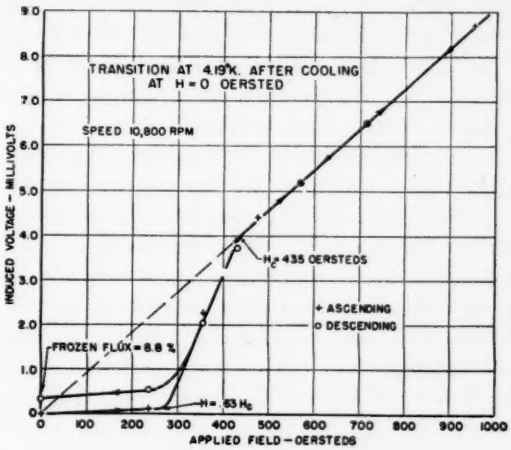
TRANSITION AT 4.19°K. AFTER COOLING AT H = 0 OERSTED
SPEED 10,800 RPM
H_c = 435 OERSTEDS
+ ASCENDING
o DESCENDING
FROZEN FLUX = 8.8 %
H = .63 H_c
INDUCED VOLTAGE - MILLIVOLTS
APPLIED FIELD - OERSTEDS

FIG. 7. Transition at 10,800 r.p.m.

¶ We are indebted to Mr. D. J. Grove of these Laboratories for the design and construction of the constant current source and to Mrs. Fay H. Hickman for the accurate calibration of the solenoid.

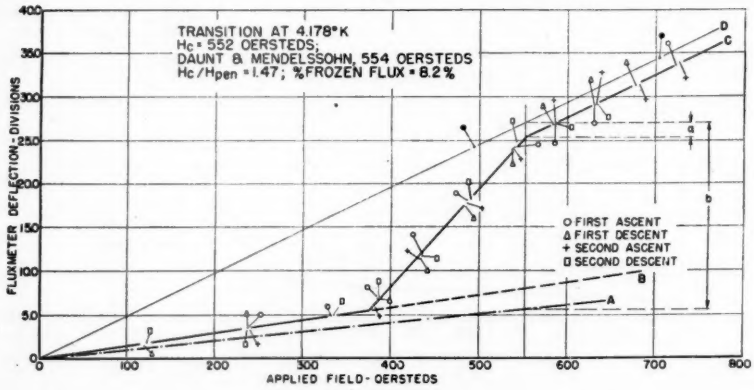

FIG. 8. Magnetic induction in the stationary sphere.

determined by the method used by Kelley and Mendelssohn.[12] The sphere was cooled in the absence of field to the helium boiling point. The magnetic field was then increased and decreased in steps; each point shown on Fig. 8 represents the average of a number of observations of the fluxmeter deflection corresponding to the establishment and the removal of the magnetic field. Curve B represents the fluxmeter deflections due to the flux between the sphere and the coil. Curve A gives the fluxmeter deflections which would have been observed if the superconductor had a zero demagnetizing factor. Curve D corresponds to the deflections which are obtained when the core of the coil has essentially unit permeability; it was obtained from readings at the nitrogen boiling point. The percentage of frozen flux, taken as 100 a/b, is subject to a maximum uncertainty of the order of 15 percent due to a possible relative error of $\frac{1}{2}$ percent in either D or C at $H=H_c$. The agreement with the previously reported data of Daunt and Mendelssohn[11] with respect to the critical field is seen to be quite good.

It appeared that the only difference between the magnetic behavior of the stationary ball and of the rotating ball was the progressively decreasing value of H_c with increasing rotational speed. It was thought that the regular decrease of H_c corresponded to the fact that the lead sphere, in virtue of the high power dissipation at the peripheral contact, was at a temperature higher than that of the bath by just such an amount as would account for the decrements, as indicated in Fig. 9. The H_c, T values were estimated from the data of Daunt and Mendelssohn. Temperature rises deduced from the carbon thermometer readings supported this view. Indeed, the original observations of Houston and Squire[6] are attributed to the circumstance that the frictional heat at the contacts prevented the rotor from reaching a temperature sufficiently low to permit the establishment of superconductivity. In this connection it is interesting to note that in our experiment involving the highest rotational speed, 10,800 r.p.m., helium was boiled out at the rate of 500 cc per minute which corresponds to 24 watts of heat generation.

Measurements were also made of the voltage induced in the rotating sphere when it was cooled below the transition temperature in a constant magnetic field. Although the data were subject to considerable fluctuations because of thermal voltages, they demonstrated clearly the expected drop in the induced voltage at the transition temperature corresponding to the applied field.

It is of interest to note that no time effects in the magnetization of duration greater than two seconds were observed. The experimental arrangement was particularly suited for studying such effects.

In the course of this work, it was found that colloidal graphite films function as useful resistance thermometers in the liquid helium range. They are especially useful because of the ease with which they can be placed in good thermal contact with the body whose temperature is to be measured. Figure 10 gives an example of the characteristics of such films. The helium boiling point resistance of this film was about 12,000 ohms. The three sets of readings correspond to data obtained on different days between which the thermometer was warmed to room temperature and exposed to the atmosphere. The details of the current and magnetic field dependence of the resistivity of these films, as well as data designed to resolve the apparent inconsistencies[13] in the low temperature resistivities of carbon

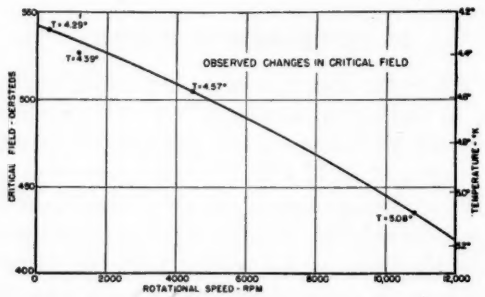

FIG. 9. Effect of rotational speed on the rotor temperature.

[12] T. C. Kelley and K. Mendelssohn, Proc. Roy. Soc. London **A154**, 378 (1936).

[13] W. J. deHaas and P. M. van Alphen, Leiden Comm. 212e (1931); Giauque, Stout, and Clark, J. Am. Chem. Soc. **60**, 1053

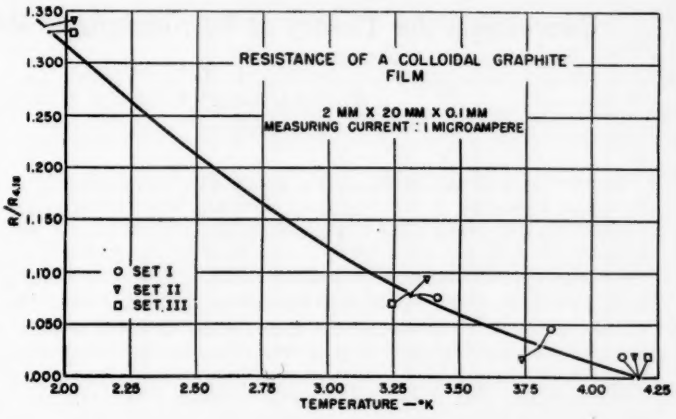

FIG. 10. Resistance, temperature relation for graphite film.

in its various physical states, will be presented in a subsequent communication.

V. CONCLUSIONS

The experiments described in this paper showed conclusively that the magnetic properties of a rotating superconductor are, in all details, identical with those of a stationary one. In particular, the critical field and the amount of frozen flux are the same. In this connection, the recent report[7] to the effect that the amount of frozen flux can be reduced to zero by rotating the superconductor while it passes through the intermediate state is inconsistent with our observations. If the axis of rotation and the applied field direction do not coincide, then due to the random orientation of frozen magnetic moments set up when the transition range is slowly traversed, there will be zero component of the *net* frozen moment perpendicular to the rotational axis. This, however, is clearly not a question of eliminating frozen flux.

(1938); A. Goetz and A. Holser, Trans. Am. Electrochem. Soc. **82**, 391 (1942); R. A. Buerschaper, J. App. Phys. **15**, 452 (1944).

VI. ACKNOWLEDGMENTS

It is a pleasure of acknowledge the interest and cooperation in this research of a large number of the members of the Westinghouse Research Laboratories. We wish particularly to express our appreciation to Dr. J. Slepian for calling our attention to this problem and for illuminating discussions concerning the questions it raised with regard to electromagnetic theory. Discussions involving questions in magnetism with J. E. Goldman have been very helpful. Finally, to G. T. Cunningham we are indebted for substantial contributions to the design of the apparatus, for the excellence of its construction, and for help in the measurements.

Concerning the Theory of Ferromagnetic Resonance Absorption

J. H. VAN VLECK
Harvard University, Cambridge, Massachusetts
(Received January 5, 1950)

The first part of this paper gives a simple quantum-mechanical derivation of Kittel's formula for the resonance frequency of ferromagnetic materials. The interactions between the elementary dipoles are handled directly, rather than through the *ad hoc* introduction of macroscopic demagnetization factors, as is usually done. In Section 3, Kittel's corrections for the effect of anisotropy on frequency are derived from the microscopic standpoint with a model having quadrupolar coupling between atoms. Section 4 discusses qualitatively the effect of exchange narrowing on the line-width. In Section 5 it is shown that Kittel's relation $g-2=2-g'$ connecting the spectroscopic splitting factor g and the gyromagnetic ratio g' is a general consequence of first-order perturbation theory. Throughout the paper it is stressed that ferromagnetic bodies may have important short-range forces of dipolar structure which arise from anisotropic exchange rather than from true magnetic coupling. It is shown that in the first approximation, inclusion of these anomalous forces does not modify Kittel's results.

1. INTRODUCTION

AN interesting development in microwave spectroscopy is the discovery of sharp resonance lines in ferromagnetic bodies in the presence of a constant magnetic field perpendicular to the oscillating or "measuring" field. At first thought, one would expect the resonance to occur at the Larmor frequency $geH/4\pi mc$, provided, of course, that one includes the Landé factor g in defining this frequency. Actually, the resonance frequency depends on the shape of the specimen and involves the demagnetizing corrections. Kittel[1] shows that if the constant field is applied along the z axis, and the measuring field along the x direction, as we suppose throughout the paper, then the resonance frequency is

$$\nu=\frac{ge}{4\pi mc}\{[H+(N_y-N_z)M][H+(N_x-N_z)M]\}^{\frac{1}{2}}, \quad (1)$$

where M is the z component of the intensity of magnetization, and where N_x, N_y, N_z are respectively the demagnetizing corrections for fields applied in the x, y, and z directions. The case most commonly investigated is that in which the specimen is much thinner in the x than in the y and z directions. Then (1) reduces to the simple and by now well-known formula

$$\nu=(ge/4\pi mc)(BH)^{\frac{1}{2}}.$$

In evaluating the shape of the specimen, allowance must be made for any diminution in the effective size which results from limitation of penetration by the skin effect. The direction perpendicular to the wall of a wave guide is thus usually to be classed as short even though the material may extend indefinitely in this direction.

Kittel derived his fundamental formula, our Eq. (1), by a very ingenious method based on classical theory. Although his type of argument is such that one expects it to hold also in quantum theory, nevertheless, it is desirable to have a quantum-mechanical derivation of (1). The quantum eigenvalues for the entire specimen regarded as a single unit have been obtained by Luttinger and Kittel,[2] and by Richardson.[3] Their resulting derivation of (1), however, still utilizes the classical macroscopic theory of demagnetizing corrections. Polder[4] has given a general formal proof of the equivalence of the classical and quantum-mechanical results, so that there is no loss of rigor in using classical demagnetizing fields. Any approach of this character is, however, a little devious. In Section 2 we shall give a simple quantum-mechanical proof of (1) in which the demagnetizing corrections follow as a direct consequence of the inclusion of the interaction between the elementary dipoles.

2. DERIVATION OF KITTEL'S FORMULA

For our purpose any terms can be dropped from the Hamiltonian function which do not depend on spin orientation. The Hamiltonian matrix can hence be taken to be

$$\mathcal{H}=Hg\beta\sum_j S_{zj}+\sum_{k>j} A_{jk}\mathbf{S}_j\cdot\mathbf{S}_k+\sum_{k>j} D_{jk}[\mathbf{S}_j\cdot\mathbf{S}_k-3r_{jk}^{-2}(\mathbf{r}_{jk}\cdot\mathbf{S}_j)(\mathbf{r}_{jk}\cdot\mathbf{S}_k)], \quad (2)$$

where β is the Bohr magneton $he/4\pi mc$, and $\mathbf{S}_j$ is the spin moment vector of atom j, measured in multiples of the quantum unit $h/2\pi$. The first right-hand member of (2) is the Zeeman energy associated with the constant magnetic field applied along the z axis. It is unnecessary for us to include explicitly the energy associated with the alternating magnetic field directed along the x axis, inasmuch as the method of moments which we use evaluates

[1] C. Kittel, Phys. Rev. **71**, 270 (1947); **73**, 155 (1948).
[2] J. M. Luttinger and C. Kittel, Helv. Phys. Acta **21**, 480 (1948).
[3] J. M. Richardson, Phys. Rev. **75**, 1630 (1949).
[4] D. Polder, Phil. Mag. **11**, 99 (1949).

the resonance frequencies directly without requiring examination of the work performed by the alternating field. The second member of (2) is the spin-dependent part of the exchange energy, and, except for a constant factor, the coefficient A_{jk} is identical with the exchange integral. The third member of (2) embodies the ordinary dipolar interaction, i.e., the mutual magnetic energy of the spins, and in addition any other coupling which has a dipole-like structure as regards dependence on spin alignment. With conventional dipolar coupling, the value of the coefficient D_{jk} is

$$D_{jk}=g^2\beta^2/r_{jk}^3. \tag{3}$$

Actually, however, the interplay between spin-orbit interaction and orbital valence may give an energy of dipolar type as regards dependence on spin alignment, an effect sometimes called anisotropic exchange coupling. In other words, in the language of nuclear physicists, there may be "tensor" forces not of purely magnetic origin. This non-magnetic, pseudo-dipolar coupling (which is closely related to what is called rho-type tripling in the spectra of diatomic molecules) was discussed in considerable detail in a paper[5] of the author on ferromagnetic anisotropy, and so will not be elaborated here. Suffice it to say that such coupling is of comparatively short range. Thus the deviations of D_{jk} from the value (3) may be expected to be important only when atoms j and k are adjacent, or nearly so. In a previous article,[6] henceforth referred to as *l.c.*, in which we treated the width of paramagnetic (not ferromagnetic) resonance lines, we assumed that the coefficient of the term of dipolar structure had the normal, purely magnetic value (3). This supposition was quite warranted in the case of nuclear paramagnetism, but may not be in that of electronic paramagnetism if the magnetic ions are closely spaced. In the latter event, the mean square line-breadth may be higher than that calculated on the basis of purely magnetic coupling, and correspondingly there will be an increase in the amount of "exchange narrowing" (a term explained in *l.c.*) which is needed to explain the sharpness of paramagnetic resonance lines.

The first part of the term of (2) involving D_{jk} merely introduces a coupling of the same structure, *viz.* a scalar product, as that involved in the exchange member of (2), and hence may be omitted if the coefficient A_{jk} is redefined. This we henceforth tacitly suppose done.

The equations of motion

$$d\mathbf{S}_j/dt=(2\pi i/h)[\mathfrak{H}\mathbf{S}_j-\mathbf{S}_j\mathfrak{H}] \tag{4}$$

along with the commutation relations

$$S_{xj}S_{yk}-S_{yk}S_{xj}=i\delta_k{}^jS_{zj} \quad \text{etc.} \tag{5}$$

give immediately

$$(h/2\pi)\dot{S}_x=-Hg\beta S_y+3\textstyle\sum_{k\neq j} D_{jk}(\alpha_{jk}S_{xj}+\beta_{jk}S_{yj}+\gamma_{jk}S_{zj})(-\beta_{jk}S_{zk}+\gamma_{jk}S_{yk}) \tag{6a}$$

$$(h/2\pi)\dot{S}_y=Hg\beta S_x+3\textstyle\sum_{k\neq j} D_{jk}(\alpha_{jk}S_{xj}+\beta_{jk}S_{yj}+\gamma_{jk}S_{zj})(\alpha_{jk}S_{zk}-\gamma_{jk}S_{xk}) \tag{6b}$$

$$(h/2\pi)\dot{S}_z=3\textstyle\sum_{k\neq j} D_{jk}(\alpha_{jk}S_{xj}+\beta_{jk}S_{yj}+\gamma_{jk}S_{zj})(-\alpha_{jk}S_{yk}+\beta_{jk}S_{xk}). \tag{6c}$$

Here $\mathbf{S}$ denotes the total spin vector $\sum_j \mathbf{S}_j$, and α_{jk}, β_{jk}, γ_{jk} are the direction cosines of r_{jk}. We throughout suppose the wave-length long compared to the effective extension of the sample in the direction of propagation, so that the important vector for the absorption is the sum $S_x=\sum_j S_{xj}$ of the x components of the individual atomic spins.

We now proceed to make certain approximations which are usually well warranted, and whose physical meaning is clarified to a considerable extent by the calculation itself. We omit from (6) all terms involving products $S_{xj}S_{xk}$, $S_{xj}S_{yk}$, $S_{yj}S_{yk}$. This omission can be justified in either of two counts. In the first place, in ferromagnetic media, the material will be magnetized practically to saturation in the z direction, and so the matrix elements of S_{xj} or S_{yj} will be small compared with those of S_{zj}. Also, quite irrespective of magnitude, the effect of the omitted terms is to introduce satellite lines falling in a different frequency region than that in which we are interested.[7] These satellites correspond to harmonics of the frequency (1), and will be faint compared with the fundamental.

In the remaining terms, involving $S_{xj}S_{zk}$ or $S_{yj}S_{zk}$, we replace S_{zk} (or S_{zj}) by its mean value[8] $-M/g\beta N$. Here M is the macroscopic intensity of magnetization, and N the number of atoms per unit volume. The effect of including a correction for the difference $[S_{zj}-(-M/g\beta N)]$ would be to introduce oscillations which are of importance for the width of the line, but not its central frequency.

With the approximations explained in the two preceding paragraphs, Eqs. (6) become

$$(h/2\pi)\dot{S}_x=-Hg\beta S_y-3(M/g\beta N)\textstyle\sum_{k\neq j} D_{jk}[-\alpha_{jk}\beta_{jk}S_{xj}+\beta_{jk}\gamma_{jk}(M/g\beta N)+(\gamma_{jk}{}^2-\beta_{jk}{}^2)S_{yj}], \tag{7a}$$

$$(h/2\pi)\dot{S}_y=Hg\beta S_x-3(M/g\beta N)\textstyle\sum_{k\neq j} D_{jk}[\alpha_{jk}\gamma_{jk}(-M/g\beta N)+\alpha_{jk}\beta_{jk}S_{yj}+(\alpha_{jk}{}^2-\gamma_{jk}{}^2)S_{zj}], \tag{7b}$$

$$(h/2\pi)\dot{S}_z=3(M/g\beta N)\textstyle\sum_{k\neq j} D_{jk}(\alpha_{jk}\gamma_{jk}S_{yj}-\beta_{jk}\gamma_{jk}S_{xj}). \tag{7c}$$

[5] J. H. Van Vleck, Phys. Rev. **52**, 1178 (1937).
[6] J. H. Van Vleck, Phys. Rev. **74**, 1168 (1948).
[7] For further details on the satellites see reference 6, p. 1170.
[8] The minus sign appears here because the ratio of magnetic moment to angular momentum is negative for electron spin. The state of lowest energy is consequently that in which the spin angular momentum is antiparallel to the field.

Now if there are planes of symmetry at each atom, sums involving products of different direction cosines will vanish. Thus we have

$$\sum_k \alpha_{jk}\beta_{jk}D_{jk}=0, \quad \text{etc.} \tag{8}$$

(If there are not such symmetry planes, sums such as (8) will alternate in sign as one goes from one lattice point to another, and when the summation over j is performed, the effect is substantially the same as though (8) were satisfied, at least as far as the short-range forces are concerned.)

The classical demagnetization factor N_x in the x direction has the value[9]

$$N_x=N^{-1}\sum_k [1-3\alpha_{jk}^2]r_{jk}^{-3}+(4\pi/3), \tag{9}$$

where N is the number of atoms per unit volume. This formula presupposes that the sum in (9) is independent of j, or in other words that the concept of a uniform demagnetization factor for the specimen is valid. A similar assumption is also necessary to make the long-range forces satisfy (8). Only an ellipsoidally cut body fulfills this criterion, and the Kittel formula (1) applies rigorously only for this shape.

If the coefficients D_{jk} have the "normal" or classical values (3), the non-vanishing sums in (7) can be evaluated by means of (9). Even if there are anomalous short-range forces which add a correction term to (3) for closely spaced atoms, nevertheless these corrections will disappear if the atoms are spaced with cubic symmetry, for then the anomalous contributions will cancel out of differences such as $\sum_k (\gamma_{jk}^2-\beta_{jk}^2)\ D_{jk}$ which are involved in (7). Fortunately, the common ferromagnetic materials, e.g., iron or nickel, have cubic lattices.[10] It is not necessary that the body be cut in a cube, and it is, in fact, the deviations from cubic or spherical symmetry which make sums of type in (9) different from zero, and the demagnetization factors different from $4\pi/3$. Boundary effects, which are evidenced by the usual demagnetizating fields, are not influenced by anomalous short-range forces of dipolar structure, since these forces fall off much more rapidly than those caused by true magnetic coupling, and so give rise only to sums which converge much more rapidly than the inverse cube type entering in (9).

If we use (3), (8), and (9), the double sums in (7) reduce to single ones over j which can immediately be simplified by using the relations $S_\nu=\sum_j S_{\nu j}$ etc. Thus Eqs. (7) become

$$(h/2\pi)\dot{S}_x=-g\beta HS_y+(N_z-N_y)g\beta MS_y, \tag{10a}$$
$$(h/2\pi)\dot{S}_y=g\beta HS_x-(N_z-N_x)g\beta MS_x, \quad \dot{S}_z=0. \tag{10b, c}$$

These are precisely Kittel's equations. To solve them, we set

$$S_x=S_{x0}\exp(2\pi i\nu t), \quad S_y=S_{y0}\exp(-2\pi i\nu t).$$

Then (10a) and (10b) yield a pair of simultaneous homogeneous linear equations in the amplitudes S_{x0}, S_{y0}. For a non-trivial solution, the determinant of the coefficients must vanish, and so one obtains the standard expression (1) for the resonance frequency.

3. EFFECT OF ANISOTROPY ON THE RESONANCE FREQUENCY

Kittel has considered how the resonance frequency is influenced by the addition of an anisotropy energy macroscopically of the form

$$E=K_1(\lambda_x^2\mu_x^2+\mu_x^2\nu_x^2+\lambda_x^2\nu_x^2), \tag{11}$$

where λ_x, μ_x, ν_x are the direction cosines of the magnetization relative to the principal cubic axes. Kittel handles this anisotropic term by showing that its effect can be included by proper alteration of the demagnetization factors to be used in (1).

We will derive Kittel's anisotropic corrections in a different fashion. He does not investigate the microscopic origin of the energy of anisotropy. We will instead start with an explicit microscopic potential. As our potential is somewhat special in character, our calculation is less general than Kittel's. Also it is more complicated. Nevertheless, despite the power and simplicity of the macroscopic method, it is perhaps worth while to give our microscopic derivation of Kittel's results since it starts more basically and since it reveals somewhat more clearly the approximations inherent in obtaining the final formulae.

The simplest model of anisotropy is that in which there is a coupling between spins of the quadrupolar type

$$\sum'_{k>j} K_{jk}r_{jk}^{-4}(\mathbf{S}_j\cdot\mathbf{r}_{jk})^2(\mathbf{S}_k\cdot\mathbf{r}_{jk})^2. \tag{12}$$

The addition of (12) to the Hamiltonian (2) adds the following member to the right side of Eq. (6a):

$$-\sum_{k\neq j} K_{jk}(\alpha_{jk}S_{xj}+\beta_{jk}S_{yj}+\gamma_{jk}S_{zj})^2[(\alpha_{jk}S_{xk}+\beta_{jk}S_{yk}+\gamma_{jk}S_{zk})(-\beta_{jk}S_{xk}+\gamma_{jk}S_{yk})$$
$$+(-\beta_{jk}S_{xk}+\gamma_{jk}S_{yk})(\alpha_{jk}S_{xk}+\beta_{jk}S_{yk}+\gamma_{jk}S_{zk})]. \tag{13a}$$

There are corresponding additional members (13b), (13c), which we shall not write down, for the remaining equations of motion (6b), (6c).

We now proceed to simplify the expressions (13) as follows. We replace each term which involves the square

[9] See, for instance, J. H. Van Vleck, J. Chem. Phys. **5**, 326 and 327 (1937).

[10] In non-cubic crystals such as cobalt, the effect of anomalous short-range forces does not drop out because of symmetry considerations. Then these forces presumably have an important influence on the resonance frequency. They also, however, give rise to anisotropy. Presumably their contribution to the frequency is indirectly included, at least approximately, in any macroscopic theory giving the correction to the resonance frequency caused by the phenomenological energy of anisotropy in the non-cubic case.

of a spin component by its average value, and assume that the averages can be taken over the different atoms independently. We suppose that the quantization is dominantly with respect to the direction of the applied magnetic field, and that any distortion caused by demagnetization corrections or anisotropy is subordinate. The averages are then symmetrical around the z axis and we have

$$\langle S_{xj}^2\rangle_{Av}=\langle S_{yj}^2\rangle_{Av}=\tfrac{1}{2}[S(S+1)-\langle S_{zj}^2\rangle_{Av}]. \tag{14}$$

We can take

$$S_{xj}S_{yj}+S_{yj}S_{xj}=0 \tag{15}$$

since this type of product is small in value and since also it averages to zero if there is symmetry about the z axis. Unless the spin quantum number of an individual atom is very large, it is an inadequate approximation to replace $\frac{1}{2}(S_{xj}S_{zj}+S_{zj}S_{xj})$ by $(-M/Ng\beta)S_{xj}$, one's first guess. Instead it is necessary to use the better approximation

$$\tfrac{1}{2}(S_{xj}S_{zj}+S_{zj}S_{xj})=[\langle S_{zj}\rangle_{Av}+\tfrac{1}{2}]S_{xj}=[(-M/Ng\beta)+\tfrac{1}{2}]S_{xj}. \tag{16}$$

The justification of (16) is that if one is close to saturation the important switches in the magnetic quantum number of an atom are those between state $S_z=-S$ of alignment of magnetic moment parallel (i.e. spin angular momentum[8] antiparallel) to the field, and the next most parallel state $S_{zj}=-S+1$. In other words, the effect is more or less[11] neglected of transitions to states having $S_{zj}=-S+2$, $-S+3$, etc. An analogous approximation is surreptitiously made, for instance, in Moller's extension[12] to the case $S>\frac{1}{2}$ of Bloch's spin wave treatment of magnetism at low temperatures. Since it is necessary to suppose that one is close to saturation, the assumptions which we are making in connection with the anisotropic corrections are probably more drastic than those we employed in Section 2 to obtain Kittel's formula for the isotropic case.

When we use (14), (15), and (16) (along with a relation identical with (16) except that x is replaced by y), the expression (13a) becomes

$$\begin{aligned}2[\tfrac{1}{2}S(S+1)-\tfrac{3}{2}\langle S_{zj}^2\rangle_{Av}][(-M/g\beta N)+\tfrac{1}{2}][S_y\textstyle\sum_k K_{jk}(\gamma_{jk}^4-3\beta_{jk}^2\gamma_{jk}^2)\\ +3S_x\textstyle\sum_k K_{jk}(\alpha_{jk}^3\beta_{jk}+\beta_{jk}^3\alpha_{jk})]+2[\tfrac{1}{2}S(S+1)-\tfrac{3}{2}\langle S_{zj}^2\rangle_{Av}]^2\textstyle\sum_k K_{jk}\gamma_{jk}^3\beta_{jk}.\end{aligned} \tag{17a}$$

In writing (17a), we have utilized simplifications afforded by the fact that sums of the form $\sum_k K_{jk}(\alpha_{jk}^2-\beta_{jk}^2)$ or $\sum_k K_{jk}\alpha_{jk}\beta_{jk}$ must vanish for a cubic crystal, since a quadratic dependence on direction cosines is incompatible with cubic symmetry. Also we have assumed the atoms similarly situated, so that the sums over k are independent of j.

The direction cosines α_{jk}, β_{jk}, γ_{jk} which we have used so far are those of $\mathbf{r}_{jk}$ relative to a set of axes x, y, z such that the applied field H is along z and the oscillating field along x. We must now express these direction cosines in terms of those λ_{jk}, μ_{jk}, ν_{jk} of $\mathbf{r}_{jk}$ relative to the principal cubic axes X, Y, Z, together with the direction cosines connecting the x, y, z and X, Y, Z systems. We shall use the notation λ_x, μ_x, ν_x for the direction cosines connecting the x axis with the X, Y, Z ones, with an analogous significance for λ_y, μ_y, ν_y etc. Now because of the equivalence of the principal cubic axes, there are relations of the form

$$\begin{aligned}\textstyle\sum_k K_{jk}(\gamma_{jk}^4-3\beta_{jk}^2\gamma_{jk}^2)&=\tfrac{1}{3}\textstyle\sum_k K_{jk}[\lambda_x^4+\mu_x^4+\nu_x^4-3\lambda_x^2\lambda_y^2-3\mu_y^2\mu_z^2-3\nu_y^2\nu_z^2][1-5(\lambda_{jk}^2\mu_{jk}^2+\mu_{jk}^2\nu_{jk}^2+\nu_{jk}^2\lambda_{jk}^2],\\ \textstyle\sum_k K_{jk}\beta_{jk}\gamma_{jk}^3&=\tfrac{1}{3}\textstyle\sum_k K_{jk}[\lambda_y\lambda_z^3+\mu_y\mu_z^3+\nu_y\nu_z^3][1-5(\lambda_{jk}^2\mu_{jk}^2+\mu_{jk}^2\nu_{jk}^2+\nu_{jk}^2\lambda_{jk}^2)].\end{aligned}$$

If we use these relations and introduce the abbreviations

$$\begin{aligned}f(a,b)&=\lambda_a^4+\mu_a^4+\nu_a^4-3(\lambda_b^2\lambda_a^2+\mu_b^2\mu_a^2+\nu_b^2\nu_a^2),\quad g(a,b)=\lambda_b\lambda_a^3+\mu_b\mu_a^3+\nu_b\nu_a^3,\quad (a,b=x,y,z).\\ Q&=\tfrac{2}{3}\textstyle\sum_k K_{jk}[1-5(\lambda_{jk}^2\mu_{jk}^2+\mu_{jk}^2\nu_{jk}^2+\nu_{jk}^2\lambda_{jk}^2][\tfrac{1}{2}S(S+1)-\tfrac{3}{2}\langle S_{zj}^2\rangle_{Av}][(-M/Ng\beta)+\tfrac{1}{2}],\end{aligned} \tag{18}$$

$$w=[\tfrac{1}{2}S(S+1)-\tfrac{3}{2}\langle S_{zj}^2\rangle_{Av}]/[(-M/g\beta N)+\tfrac{1}{2}], \tag{19}$$

the expression (17a) becomes

$$Qf(z,y)S_y+3Q[g(x,y)+g(y,x)]S_x+Qg(z,y)w. \tag{20a}$$

The corresponding expressions added to the y and z equations of motion are

$$-Qf(z,x)S_x-3Q[g(x,y)+g(y,x)]S_y-Qg(z,x)w,\ Qg(z,x)S_y-Qg(z,y)S_x. \tag{20b, c}$$

When (20a), (20b), (20c) are added to the right sides of Eqs. (10a), (10b), (10c) respectively, it is seen that the

[11] The relation (16) is rigorously correct if the spins are aligned completely antiparallel (see reference 8) to the field, so that the expectation value of S_{zj} is $-S$. If, instead, $\langle S_{zj}\rangle_{Av}-(-S)$ is not identically zero, but small compared with S, use of the familiar relation $(S_{xj}\pm iS_{yj})(M_S;M_S\mp1)=[S(S+1)-M_S(M_S\mp1)]^{\frac{1}{2}}$ shows that the matrix amplitudes connecting a state of given S_{zj} with $S_{zj}+1$ will be considerably larger than those connecting it with $S_{zj}-1$. Hence (16) is a somewhat better approximation for the case of incomplete alignment than might appear at first sight.

[12] C. Moller, Zeits. f. Physik 82, 559 (1933).

equations of motion are of the type form

$$\dot{S}_x = aS_x + bS_y + c_1, \quad \dot{S}_y = cS_x - aS_y + c_2, \quad \dot{S}_z = w^{-1}[-c_1S_x - c_2S_y]. \tag{21a, b, c}$$

The presence of the terms c_1, c_2 in (21a), (21b) is caused by the fact that when one of the principal cubic axes does not coincide with the direction of the applied field, the equilibrium position for the direction of magnetization is not the same as that of the applied field. These c_1, c_2 terms can be effectively eliminated by shifting the location of the z axis. To first powers in c_1, c_2, the direction cosines of the angles which the new z axis makes with the original x and y axes are respectively

$$\frac{(-ac_1 - bc_2)}{(-M/Ng\beta)(a^2+bc)} \quad \text{and} \quad \frac{(-cc_1 + ac_2)}{(-M/Ng\beta)(a^2+bc)}.$$

If second powers of c_1 and c_2 are disregarded, this rotation makes the equations of motion in the new, i.e. slightly rotated coordinate system the same as in the old except that all terms in c_1, c_2 are entirely suppressed.

In virtue of the preceding paragraph we can set $c_1 = c_2 = 0$. The roots of the secular equation are $\pm i(bc+a^2)^{\frac{1}{2}}$. The resonance frequency is therefore

$$\nu = g\beta h^{-1}\{[H + (N_y - N_z)M - Qg^{-1}\beta^{-1}f(z,y)][H + (N_x - N_z)M - Qg^{-1}\beta^{-1}f(z,x)] + 9g^{-2}\beta^{-2}Q^2[g(x,y)+g(y,x)]^2\}^{\frac{1}{2}}. \tag{22}$$

The constant Q involved in (22) is intimately connected with the proportionality factor K_1 appearing in the energy of anisotropy (11). In an earlier paper the writer calculated the amount of magnetic anisotropy to be expected from the present model. This calculation showed that if there is quadrupolar coupling of our type (12), and if Q and w are defined as in (18) and (19), then the relation connecting K_1 and Q is[13]

$$Q = -2K_1/Nw. \tag{23}$$

If the atomic dipoles are nearly all parallel to the applied field, then $\langle S_z^2 \rangle_{Av}$ is very nearly equal to S^2, where S is the spin quantum number of an atom. Also then M is practically the same as $-Ng\beta S$. Under these circumstances (23) reduces to

$$Q = -2K_1 g\beta/M. \tag{24}$$

The formula (22) for the resonance frequency, as it stands, is rather cumbersome, because we have assumed that the constant magnetic field is arbitrarily oriented relative to the principal cubic axes. Our calculation is consequently somewhat more general than Kittel's. He assumed that both the applied and measuring magnetic fields are in the 001 plane, so that in our notation $\lambda_y = \mu_y = \nu_z = \nu_z = 0$. With this specialization (22) becomes

$$\nu = g\beta h^{-1}\{[H + (N_y - N_z)M + 2K_1M^{-1}(\tfrac{3}{4} + \tfrac{1}{4}\cos 4\theta)][H + (N_x - N_z)M + 2K_1M^{-1}\cos 4\theta]\}^{\frac{1}{2}}. \tag{25}$$

where θ is the angle between the constant magnetic field and the 100 axis. Equation (25) agrees exactly with the corresponding formula of Kittel, after correction of the latter for a minor algebraic error[14] which, incidentally, was detected by comparison of his calculation and ours. For the case that the x and z axes are in the 011 plane, Eq. (22) reduces to an expression given by L. R. Bickford.*

4. EFFECT OF DIPOLAR INTERACTION ON THE WIDTH OF THE ABSORPTION LINES

We now turn to the subject of the width of the microwave resonance lines in ferromagnetic media. Four possible mechanisms of line-broadening are (a) interatomic forces of dipolar structure (b) spin-lattice interaction (c) damping caused by the eddy currents involved in the skin effect and (d) dependence of the anisotropy corrections in Eq. (22) on the orientation of the magnetic field relative to the principal cubic axes. We will be concerned primarily with (a). As a matter of fact, (d) is not a true broadening at all, but gives an apparent line-width in powders because the specimen is composed of differently oriented microcrystals whose resonance frequencies consequently do not quite coincide. Thus (d) is inoperative in a single crystal. Also, even in a powder, it is negligible in a substance such as supermalloy whose anisotropy is very small. The importance of (b) is a mooted question. Akhieser[15] actually obtains line-widths due to (b) which are comparable with, or even greater than, the observed widths, but his calculation has been criticized by Polder[4] on the ground that the spin-waves important for resonance are not as short as supposed by Akhieser. Consequently (b) may be less important than Akhieser's results would imply.

If perturbations by eddy currents are neglected, ordinary, i.e., isotropic exchange coupling does not

[13] J. H. Van Vleck, Phys. Rev. **52**, 1195 (1937), especially Eqs. (38), (42), and (43). The quantity B_2 entering in Eq. (42) is the same as $\langle S_{z_i}^2 \rangle_{Av}$ in the present model. The following error is to be noted in Eq. (38); it should contain a factor $\frac{1}{2}$ multiplying Ω_S.

[14] See reference 8 of C. Kittel, Phys. Rev. **76**, 743 (1949).

* L. R. Bickford, Phys. Rev. (to be published).

[15] A. Akhieser, J. Phys. U.S.S.R. **10**, 217 (1946).

broaden the resonance line, since this type of interaction commutes with any component of the total magnetic moment, and so does not spoil the latter's constancy. The simplest kind of non-isotropic potential is that of dipolar structure. Quadrupoles and other higher order poles would be more complicated to treat and would presumably not give any materially different results. It is considerably more difficult to discuss dipolar broadening, even qualitatively, in ferromagnetic than in paramagnetic media. In *loc. cit.*,[6] the writer studied breadths in the latter at some length. Even then, it was not possible to obtain an explicit formula for the line-shape. The best that could be done was to calculate the second and fourth moments of the deviation of the frequency from its mean value, and deduce qualitative conclusions from these computations. In the ferromagnetic case, however, the application of the method of moments strikes a snag if the field is applied in an arbitrary direction. The essential feature of the method which we employed was the use of the invariance of the diagonal sum, but with the exclusion of certain parts of the Hamiltonian, *viz.* the portion non-diagonal in the total magnetic quantum number M, because this portion definitely had the effect of introducing satellite lines[7] rather than of broadening the main line. In ferromagnetic materials, however, the dipolar interaction cannot be regarded as a small perturbation. The gist of our calculation in Section 2 was, in fact, to show how the demagnetization corrections caused by dipolar coupling influence the central resonance frequency. The component of magnetic moment in the direction of the applied field ceases to be a constant of the motion unless two of the demagnetizing factors are equal, and the field is applied along the direction of the third. Unless these conditions are satisfied our previous method cannot be used. We are therefore able to give a formula for the second moment only for the special case of axial symmetry. For this case, the calculation can be made by the same general method as that used in *l.c.*, but with two important changes in detail, as follows:

(a) It is no longer allowable to take

$$\langle S_{xj}^2\rangle_{Av}=\langle S_{xj}^2\rangle_{Av}=\langle S_{yj}^2\rangle_{Av}=\tfrac{1}{3}S(S+1),\quad \langle S_{zj}\rangle_{Av}=0 \qquad (26)$$

since the magnetization cannot be supposed very weak in ferromagnetic bodies.

(b) The coupling of dipolar structure need not be supposed to have a true magnetic origin, or in other words, the coefficient D_{jk} in (2) need not necessarily have the value (3).

The formula for the mean square deviation of the frequency from the Kittel value (1) (with $N_x=N_y$) turns out to be

$$\langle\Delta\nu^2\rangle_{Av}=h^{-2}[\langle S_{zj}^2\rangle_{Av}-\langle S_{zj}\rangle_{Av}^2]\textstyle\sum_k D_{jk}^2. \qquad (27)$$

As is to be expected, this expression reduces to Eq. (10) of reference 6 if one can use (26) and (3), as one can for paramagnetic media with purely dipolar coupling.

The corresponding formula for the mean fourth power deviation would be tedious and unrepaying to calculate. Suffice it to note that $\langle\Delta\nu^4\rangle_{Av}$ would surely contain terms of the order A^2D^2/h^4, which will be very large compared to $3[\langle\Delta\nu^2\rangle_{Av}]^2\sim D^4/h^4$ inasmuch as the exchange coupling coefficient A will be very large in ferromagnetic media. As a result, the lines will have a far smaller half-breadth than one would calculate from (27) under the supposition of a Gaussian shape, for with a given second moment, enhancement of the fourth moment makes the line more sharply peaked. This is the phenomenon of "exchange narrowing" which we explained more fully in *l.c.* Much of the contribution to (27) comes, in fact, from transitions in which the energy change is of the order of magnitude of the exchange integral. Such transitions give rise to absorption lines of vastly higher frequency than the Kittel resonance frequency in which we are interested. The only reason that the expression (27) still remains of the order D^2/h^2 rather than A^2/h^2 is that these transitions are down by a factor of the order A^2/D^2 in intensity as compared with those having nearly the resonance frequency. Lines having frequencies of the order A/h clearly should be regarded as satellites whose contributions to (27) are spurious for our purposes. Exchange narrowing is essentially an expression of the fact that the square root of the expression (27) furnishes a gross overestimate of the effective line-width because these spurious contributions have not been striken out.

Despite the inutility of (27) for quantitative purposes, certain qualitative conclusions can be drawn from (27) as follows:

(I) Exchange narrowing should in general be even more pronounced in ferromagnetic than in paramagnetic media, all other things being equal. The basis for this statement is that the second moment is of roughly the same order of magnitude in both types of media, but ferromagnetic materials will presumably have larger exchange integrals and hence larger fourth moments. There is thus no difficulty in understanding why ferromagnetic substances have much sharper resonance lines than one would calculate from the root mean square deviation of the dipolar field.

(II) Part of the line-breadth may be caused by short-range pseudo-dipolar forces rather than those of true magnetic origin. In another paper[5] the writer stressed the fact that in ferromagnetic materials the coupling coefficients in the potential of dipolar structure usually has a value materially larger than (3). Consequently one must not be surprised if sometimes lines are, despite (a), more diffuse in ferromagnetic than in paramagnetic substances. This situation could arise if the ferromagnetic material has such anomalously large coefficients D_{jk} as to more than offset the tendency towards more narrowing caused by larger exchange integrals. In *l.c.* we did not mention the possibility of anomalous dipolar coefficients in paramagnetic bodies. If the magnetic density is high, such anomalies are

possible, but in general presumably less common than in ferromagnetics. Since effects (I) and (II) work in opposite directions, there is obviously considerable leeway in explaining line-width phenomena.

(III) There should be no discontinuity in the line-width at the Curie point. This is one point on which the theory makes a definite prediction, and is in accord with experiment. Theoretically, as the Curie point is approached from below, the mean values involved in (27) approach the limits (26), and so (27) passes continuously into the corresponding formula of *loc. cit.* for the second moment for the purely paramagnetic case. The same is also true of the higher moments. Experimentally Bloembergen finds that in nickel and supermalloy, the two materials so far studied in this regard, the line-width does not change at the Curie point. This fact, however, does not distinguish between the broadening mechanisms (a), (b), and (c), for all three involve no abrupt changes at the Curie temperature.

(IV) The line-breadth caused by dipolar effects should decrease as the temperature is lowered from the Curie point to the absolute zero, for the expressions $\langle S_{zj}^2\rangle_{Av}$ and $\langle S_{zj}\rangle_{Av}^2$ involved in (27) approach equality as the magnetization approaches its maximum value $Ng\beta S$. The dipolar line-breadth should hence vanish at the absolute zero. Existing experimental data do not extend to very low temperatures, but are of such a character as to make it highly unlikely that the line-width vanishes at $T=0$. In supermalloy, for instance, Bloembergen[16] finds little, if any change in line-width between 300 and 600°K even though the magnetization changes by a factor changes by a factor over 2 in this interval. At 300°, the magnetization is almost as high as at $T=0$, and one would hence expect little further contraction in dipolar broadening to set in below room temperatures. In nickel Bloembergen finds that the line-width actually decreases when the anisotropy increases. These various experimental facts indicate pretty clearly that dipolar coupling between similarly situated atoms, such as is embodied in Eq. (27), is not the main cause of broadening in ferromagnetic materials. Nor can spin-lattice interaction be the chief mechanism of line-broadening at room temperatures and lower, for any broadening of such origin should vary drastically with temperature, and disappear completely at very low temperatures. This difficulty would not arise if the line-width were caused by the interaction of the spins with the eddy currents involved in the skin effect, but unfortunately a calculation by Kittel and Herring[17] shows that this process fails to give the observed width by a factor 10 or so. It is thus at present something of a mystery what is the actual mechanism of line-broadening in ferromagnetic media. It is just possible that theoretically a finite breadth of dipolar origin should persist even at $T=0$ because of crystalline imperfections, or in other words, because the crystal is composed effectively of somewhat disjointedly connected microcrystals, each with slightly different resonance frequencies. It is conceivable that large enough breadths at low temperatures might be obtained if this fashion if there are large short-range pseudo-dipolar forces due to anisotropic exchange.

In this connection one can try generalizing (27) by abandoning the restriction that all atoms are similarly situated, so that $\sum_k D_{jk}$ is no longer independent of j. By a calculation of the same general type as that in *l.c.*, but whose details we omit, it is found that the mean resonance frequency and mean square deviation are then given by

$$\langle \nu\rangle_{Av}=(He/4\pi mc)+\mathfrak{N}^{-1}h^{-1}\textstyle\sum_{j,k} D_{jk}\langle S_{zj}\rangle_{Av} \tag{28}$$

$$\langle \Delta\nu^2\rangle_{Av}=\mathfrak{N}^{-1}h^{-2}\textstyle\sum_{j,k} D_{jk}^2[\langle S_{zj}^2\rangle_{Av}-(\langle S_{zj}\rangle_{Av})^2] +h^{-2}[\mathfrak{N}^{-1}\sum_j(\sum_k D_{jk})^2 -\mathfrak{N}^{-2}(\textstyle\sum_{j,k} D_{jk})^2](\langle S_{zj}\rangle_{Av})^2, \tag{29}$$

where $\mathfrak{N}$ is the total number of atoms in the crystal. This formula is unfortunately rather hard to interpret. If $\sum_k D_{jk}$ is not independent of j, the expression (29) does not vanish at $T=0$, and so gives the impression that the resonance line can remain diffuse even at $T=0$. However, the non-vanishing of (29) at $T=0$ is caused by transitions involving changes in the total spin $\mathfrak{S}$ of the crystal from $\mathfrak{N}S$ to $\mathfrak{N}S-1$. Most of these transitions are associated with energy changes of the order of magnitude of the exchange integral A, and so their contributions to (29) are irrelevant since they represent weak satellites of completely different frequency than the resonance line. Some of these transitions, however, may be more intense than the rest, and involve relatively small changes in exchange energy, so that they should be classed as wings of the central resonance line rather than as satellites. In fact, the lowest Bloch spin waves for $S_z=-(\mathfrak{N}S-1)$ have almost the same exchange energy as that of the sole state $S_z=-\mathfrak{N}S$. It is thus conceivable that with dissimilarly situated atoms, some breadth persists even at $T=0$. When, however, the atoms are similarly situated, the resonance line at $T=0$ will consist of but a single component, as evidenced by the behavior of (27). Physically, this is because it is immaterial energetically which atom has $S_{zj}=-(S-1)$ in a state $S_{zj}=-(\mathfrak{N}S-1)$ when $\sum_k D_{jk}$ is independent of j. Under this condition the dipolar interaction does not break down the selection rule $\Delta\mathfrak{S}=0$ for the matrix elements of S_x connecting $S_z=-\mathfrak{N}S$ with $S_z=-(\mathfrak{N}S-1)$ and the absorption arising from the deepest state $S_z=-\mathfrak{N}S$ consists of but a single line.

5. THE PROBLEM OF THE g-FACTOR IN FERROMAGNETIC RESONANCE

Doubtless we have given the impression that Kittel's formula (1) fits the observed resonance frequencies very well. Actually it does so only if the g-factor be given anomalously large values. For instance, in nickel the values of g yielded by experiments on ferromagnetic

[16] N. Bloembergen, Phys. Rev. (to be published).
[17] C. Kittel and C. Herring, Phys. Rev. **77**, 725 (1950).

resonance range from 2.19 to 2.42. On the other hand, the gyromagnetic ratio found by Barnett for nickel is 1.93. The discrepancies for other materials are set forth in detail in an interesting paper by Kittel.[18]

As Polder,[4,19] Kittel,[18] and the writer[20] have independently pointed out, there is no reason why the g-factors yielded by microwave and magnetomechanical experiments need be the same. Conceptually, they relate to different quantities. The absorption measurements determine the factor g in the formula $E=E_0+Mg\beta H$ for the Zeeman energy states. Kittel aptly calls this kind of g the spectroscopic splitting factor. We shall also follow Kittel in using the letter g' for the anomaly (as compared with the classical orbital value $-e/2mc$) in the ratio of magnetic moment to angular momentum, which is the ratio which enters in gyromagnetic experiments.

Although it is quite possible in principle to understand why g and g' should be different, the theory strikes a snag as soon as one tries to explain quantitatively the discrepancy between g and g'. One can show quite generally that in the first approximation, the deviations of g and g' from 2 should be equal and opposite, so that

$$g-2=2-g'. \tag{30}$$

This relation has been discovered independently by Kittel and the writer. Kittel has already published his derivation.[18] Ours is rather more general, as it is not based on a particular model, and so it is perhaps not superfluous if we give it here.

Proof of (*30*). Let us fictitiously imagine that there are fields H_O and H_S acting solely on the orbital and spin magnetic moments respectively. The actual physical case has, of course, $H_O=H_S$. Let us first consider a one-atom or one-electron system in which the orbital angular momentum is quenched by the crystalline field, i.e., consists solely of non-diagonal elements, and in which spin-orbit coupling is disregarded. It is not necessary to specify anything about the crystalline field. The model can, for instance, be the usual one of a single atom with one or more bound electrons employed in the theory of magnetism by Schlapp, Penney, and others, or it can be the itinerant electron model of conduction band theory, used in magnetic problems by Mott, Brooks,[21] *et al.* If we disregard squares of H_O, the energy levels are of the form

$$E=E_0+2M_S\beta H_S, \tag{31}$$

where M_S is the spin equatorial quantum number. Now introduce as simultaneous perturbations the interaction of the orbital magnetic moment with the field H_O, and the spin-orbit coupling. The portions of the Hamiltonian function corresponding to these two perturbations we denote respectively by V_1 and V_2. Both of these perturbations involve only non-diagonal elements, and so the energy is affected only in the second approximation

$$\Delta E=\sum_l |V_1+V_2|_{jl}^2/h\nu_{jl}.$$

In microwave spectra we are concerned with the linear Zeeman effect, and for this the only relevant part of $|V_1+V_2|^2$ is the cross term $V_1V_2+V_2V_1$. Now V_1 is independent of M_S, and so the only matrix elements of V_2 which can contribute to the cross term are those which connect states j and l having the same values of M_S. These elements arise from the part AL_zS_z of $A\mathbf{L}\cdot\mathbf{S}$ and are proportional to M_S. Therefore

$$\Delta E=\text{const.}+aH_OM_S+O(H_O^2). \tag{32}$$

The constant term we can assume independent of M_S, as we suppose the lowest spin multiplet is not decomposed in the absence of a magnetic field. Because of the Kramers degeneracy, this will always be the case if the spin is $\frac{1}{2}$. For spins of 1 or $\frac{3}{2}$, the multiplet will not be decomposed if there is cubic symmetry. Apart from squares of the magnetic fields, the total energy, which is the sum of (31) and (32), is of the form

$$E=E_0+\beta M_S(2H_S+aH_O). \tag{33}$$

The spectroscopic splitting factor is obtained by setting $H_O=H_S$, and is hence

$$g=2+a. \tag{34}$$

In terms of the partition function $Z=\sum_j \exp(-E_j/kT)$, the anomaly in the gyromagnetic ratio is

$$g'=\frac{[\partial \log Z/\partial H_O+\partial \log Z/\partial H_S]_{H_S=H_O}}{[\partial \log Z/\partial H_O+\tfrac{1}{2}\partial \log Z/\partial H_S]_{H_S=H_O}}$$

inasmuch as the derivatives $-\partial E_j/\partial H_O$ and $-\partial E_j/\partial H_S$ are respectively the orbital and spin magnetic moments of the state of energy E_j. Furthermore we have $a\partial E_j/\partial H_S=2\partial E_j/\partial H_O$, and we may suppose a to be a small quantity, for otherwise the perturbation calculation has no basis. Hence

$$g'=(2+a)/(1+a)=2-a. \tag{35}$$

Equation (30) follows immediately from (34) and (35).

The preceding calculation assumed that the individual atoms or itinerant electrons could be regarded as isolated magnetic units. As long as the Zeeman effect is linear, inclusion of exchange or dipolar coupling between these units does not, however, spoil the validity of (30). Such coupling does not influence the relative

[18] C. Kittel, Phys. Rev. **76**, 743 (1949).
[19] D. Polder, Phys. Rev. **73**, 1116 (1948).
[20] J. H. Van Vleck, Physica **15**, 197 (1949).
[21] H. Brooks, Phys. Rev. **58**, 909 (1940). As Kittel notes, Brooks purports to calculate g', but really computes g. However, because of a counterbalancing error, the numerical result which Brooks gives for g' (g in his notation), is correct, as one suspects since he obtains $g'<2$. The compensating sign change arises because he does not allow for inversion of the spin-orbit parameter for d^9 as compared with d. He implies that use of negative frequency denominators for transitions to unfilled states of lower energy incorporates the effect of this inversion, but actually this is not the case, for the sign behavior of the frequency denominators is the same for d and d^9.

contributions of the orbital and spin moments, and so does not change g'. Exchange interaction commutes with all spatial components of the total magnetic moment, and so does not influence g. The gist of Kittel's calculation, of ours of Section 1, is that the spectroscopic splitting factor is unaltered by dipolar interaction provided one takes for the effective field that given by the radical in Eq. (1).

Inadequacy of (30). Unfortunately, the approximate equality of $g-2$ and $2-g'$ predicted by (30) is not confirmed by experiment. The table in Kittel's paper shows that $g-2$ always exceeds $2-g'$, and is often twice as large. It is improbable that the discrepancies are caused by the fact that (30) includes only the first-order effect of spin-orbit interaction. The higher order perturbations, in the first place, are presumably small. What is more, they act in the wrong direction. If, for instance, one went to the extreme of assuming the crystalline field small compared with the spin-orbit coupling, a model based on the configuration d,[9] the, one most appropriate to nickel, would have $g'=6/5$ a value far too low.

How, then, can one explain the fact that the observed values of g are too high to fit (30)? Kittel reviews a number of suggestions made by various authors, all of which he dismisses as rather unlikely. We should like to add to this list one more remote possibility. In all the derivations of Kittel's fundamental formula, our Eq. (1), the effect of the dipolar and pseudo-dipolar forces on the frequency is included only in the first approximation. This approximation is doubtless adequate if the dipolar coupling is only of true magnetic origin. However, it is just conceivable that higher order corrections might alter the central frequency appreciably if there are large short-range forces of dipolar structure caused by anisotropic exchange. Our calculation shows that in the first approximation, such forces are without influence on the resonance frequency if the atoms are cubically spaced, but there is no assurance that this is true in higher orders. If these pseudo-dipolar effects are large, one would expect that there should be a large anisotropy, since forces of dipolar structure lead to anisotropy in the second approximation,[5] as has been shown by van Peijpe[22] and by the writer. On the other hand, the mean resonance frequency for a powder composed of cubic crystals is influenced by these forces only in the third approximation (apart, of course, from the demagnetization corrections contained in Kittel's formula). The experimental data are not complete enough as yet to reveal whether there is a correlation between the amount of deviation from the formula $g-2=2-g'$ and the amount of anisotropy. Supermalloy is a material with almost no anisotropy. It is unfortunate that no gyromagnetic measurements are available for supermalloy, so as to test whether formula (30) holds much more exactly than usual for this substance. One's guess is that it does not, for such a behavior would be out of line with that for other materials.

It should be pointed out that in Section 3 we derived the expression (25) for the effect of anisotropy on the resonance frequency only for a model in which the anisotropy is caused by the quadrupolar coupling (12). Actually, however, anisotropy can arise from the second-order effect of dipolar interaction, and this is the only mechanism operative if the atomic spin is $\frac{1}{2}$. The reason that we employed the dipolar rather than quadrupolar model in Section 3 is that the latter yields anisotropy in the first rather than second approximation, and so is easier to handle. The great merit of Kittel's macroscopic derivation of (25) is that it does not require any particular model, and so the relation between anisotropy and frequency given in (25) is presumably valid for dipolar as well as quadrupolar coupling. Yet the macroscopic approach by means of effective demagnetization factors is to a certain extent phenomonological. It would be interesting to treat the higher approximations of the dipolar model from the microscopic standpoint, and see whether it gives (25) in the second order, and especially whether it yields a significant shift in the resonance frequency in still higher orders if there are large anisotropic exchange forces. It looks as though we are between Scylla and Charybdis; presumably the higher order corrections yield either effectively isotropic coupling which commutes with the magnetic moment and so does not influence the frequency, or else an anisotropy already included in Kittel's phenomonological approach.

All told, the explanation of the anomalously high spectroscopic g-factors is at present an unsolved problem.

In writing the present paper, the writer has benefited greatly from stimulating discussions with Dr. C. Kittel and Dr. N. Bloembergen.

[22] W. F. van Peijpe, Physica 5, 465 (1937).

Dislocation Models of Crystal Grain Boundaries

W. T. READ AND W. SHOCKLEY
Bell Telephone Laboratories, Murray Hill, New Jersey
(Received January 9, 1950)

The energies and motions of grain boundaries between two crystallites are investigated theoretically using the dislocation model of grain boundaries. Quantitative predictions made for simple boundaries for cases in which the plane of the boundary contains the axis of relative rotation of the grains appear to agree with available experimental data. The quantitative expression for energy per unit area for small angles is approximately $[Ga/4\pi(1-\sigma)]\theta[A-\ln\theta]$ where G is the rigidity modulus, a the lattice constant, σ Poisson's ratio, θ the relative rotation and A approximately 0.23. Grain boundaries of the form considered may permit intercrystalline slip and may act as stress raisers for the generation of dislocations.

1. DISLOCATION MODEL OF THE GRAIN BOUNDARY

DISLOCATION models of crystal grain boundaries have been proposed by Burgers[1] and by Bragg.[2] It has recently been shown that these models have certain quantitative consequences which are directly susceptible to experimental tests, so that theoretical and experimental investigations of grain boundaries may furnish evidence for the presence of particular arrays of dislocations in solids.[3] Of special interest are grain boundaries between crystallites with a small difference in orientation; we shall show that for these the grain boundary energy can be determined as a function of the angle of misfit and the orientation of the boundary.

The energy of a grain boundary between crystal grains will be a function of the relative orientation of the two grains (this involves three degrees of freedom) and the orientation of the boundary surface itself with respect to the two grains (two additional degrees of freedom). Thus a general grain boundary has five degrees of freedom. It is always possible, at least for small orientation differences, to join the two grains with a suitable array of dislocations lying on the prescribed plane of the grain boundary. We shall not prove this general result here, however, but shall deal in detail with grain boundary models for certain specially simple cases, pointing out how the results may be extended so as to apply more generally.

In particular we shall consider a simple cubic lattice in which the relative rotation of the grains takes place about the z axis and the grain boundary contains the z axis; as a consequence, the problem is two-dimensional, since the situation is independent of z. (Although it is not necessary to introduce screw dislocations, which have components of displacement in the z direction, for the simple cubic lattice, they will be required for body-centered and face-centered cubic lattices, and formulas for their energies are given in Appendix D.) The elasticity theory employed is that for an isotropic solid and the quantitative results are only approximate except for small angles of misfit, i.e., large spacing between the dislocations. Some features which will arise for large angles are discussed qualitatively in Section 4.

Figure 1 shows the grain boundary for which quantitative calculations have been made. A plane making an angle φ with respect to the x axis is drawn and the two parts of the crystal are each rotated away from the plane by an angle of $\theta/2$. As is seen, some planes from above and from the right must terminate on the boundary, producing dislocations. The numbers of dislocations of the two types per unit length of grain boundary are readily calculated by thinking of the planes as lines of flow. The flux of "y planes" (i.e.,

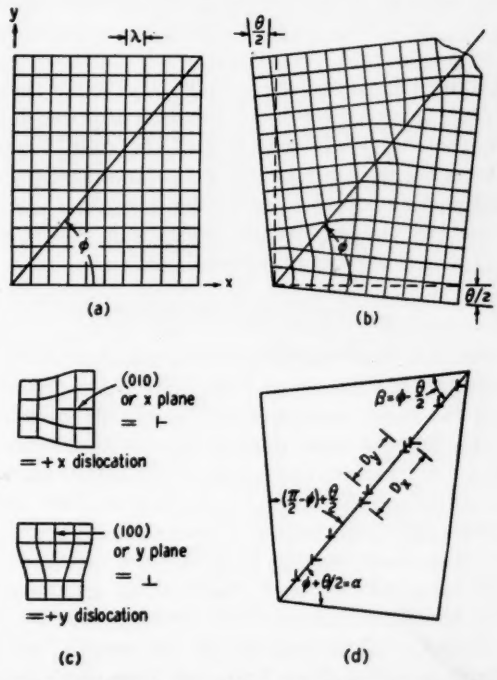

FIG. 1. The dislocation model of a simple grain boundary. (a) Definition of φ, the orientation of the grain boundary. (b) Definition of θ, the angle of misfit. Note that some (100) planes from right ($+x$ planes) and (010) planes from above ($+y$ planes) terminate on the boundary. (c) Symbols for dislocations. (d) Symbolic representation of boundary. *Correction:* The symbol λ should be replaced by a.

[1] J. M. Burgers, Proc. Phys. Soc. **52**, 23 (1940). Proc. Kon. Ned. Akad. V. Wet. Amsterdam **42**, 293 (1939); see also W. G. Burgers, Proc. Kon. Ned. Akad. V. Wet. Amsterdam **50**, 595 (1947).
[2] W. L. Bragg, Proc. Phys. Soc. **52**, 54 (1940).
[3] W. Shockley and W. T. Read, Phys. Rev. **75**, 692 (1949).

x=constant) flowing into the boundary from above is the flux density $(1/a)$ times the cosine of the angle of incidence upon the grain boundary. This leads to a net unbalanced flux per unit length of boundary of

$$\rho_y=\frac{1}{a}(\cos\beta-\cos\alpha)=\frac{2}{a}\sin\varphi\sin\frac{\theta}{2}\doteq\frac{\theta\sin\varphi}{a}, \quad (1)$$

where the approximation holds for small values of θ. This is evidently the number of $+y$ dislocations per unit length of boundary. Similar calculations lead to

$$\rho_x=\frac{1}{a}(\sin\alpha-\sin\beta)=\frac{2}{a}\cos\varphi\sin\frac{\theta}{2}\doteq\frac{\theta\cos\varphi}{a} \quad (2)$$

for the density of $+x$ dislocations. In applying formulas like these, it is advisable to choose the axes so that $0\leq\varphi\leq\pi/2$; otherwise difficulties associated with changes in sign of the dislocation types are encountered.

The spacing between dislocations, D_x and D_y, are given by the formulas

$$D_x=\frac{1}{\rho_x}=\frac{a}{2\cos\varphi\sin\frac{\theta}{2}}\doteq\frac{a}{\theta\cos\varphi}, \quad (3)$$

$$D_y=\frac{1}{\rho_y}=\frac{a}{2\sin\varphi\sin\frac{\theta}{2}}\doteq\frac{a}{\theta\sin\varphi}. \quad (4)$$

At distances from the grain boundary larger than D_x and D_y, the crystal will be substantially unstrained. Hence the energy per unit area of the grain boundary will be concentrated near the boundary itself and will be independent of the size of the crystal. These conclusions are verified by the integration of the stress energy which is given in Appendix B.

2. GRAIN BOUNDARY ENERGY

There are three methods of determining the energy of an array of dislocations: (1) Take the volume integral of the strain energy density over the entire body, (2) integrate the work done in producing the state of strain by the surface forces over the *complete boundary*, which includes the surfaces of discontinuity, that is slip planes, (3) determine the work done in creating the dislocations and bringing them together against forces of mutual attraction and repulsion. It can be shown readily that these three methods give the same energy and that the third reduces to the second, which is mathematically simpler than the first, and involves only integrating the shear stress over the slip planes; since the external boundary, being stress-free, gives no contribution to the work and since the relative displacement of the surfaces adjoining the cut is tangential, the work done on a slip plane is one-half the integral of the tangential, i.e., shearing stress, in the slip direction times the relative displacement, which is constant and equal to one atomic spacing. The factor of one-half comes from the linearity of the stress strain law. The stresses are determined from an infinite sum of Airy stress functions each representing one dislocation.

For a case like that of Fig. 1, it is convenient to evaluate the stress system due to the x dislocations, denoted by $S(x)$, separately from that of the y dislocations $S(y)$. These stress systems individually give a stress field at large distances from the boundary. However, the combination leads to a stress field localized near the boundary, as discussed in connection with Fig. 1.

The energy is calculated by considering one of the y dislocations and calculating the work done on its slip plane by $S(y)$ and $S(x)$. Each of these energies is simply one-half the lattice constant times the integral of the shearing stress over the slip plane. Although $S(y)$ and $S(x)$ individually give divergent terms, these cancel so that a finite result is obtained. It is found also that the interaction of the y dislocation with $S(x)$ is independent of the relative positions on the boundary of the y dislocation and the set of x dislocations; consequently, the work done is the same for the slip plane of each y dislocation. The same result is true for the x dislocations. The energy of the grain boundary per unit length is then simply the energy per slip plane times the number of slip planes per unit length summed over the two types of slip planes. Since the calculations are made for unit length along the z axis, this gives the energy per unit area of grain boundary.

The formula for the energy per unit area of the grain boundary derived in Appendix B is

$$E=E_0\theta[A-\ln\theta], \quad (5)$$

where E_0 depends only on the orientation of the grain boundary and the macroscopic elastic constants:

$$E_0=Ga(\cos\varphi+\sin\varphi)/4\pi(1-\sigma), \quad (6)$$

where G is the rigidity modulus and σ is Poisson's ratio.* The factor $(\cos\varphi+\sin\varphi)$, which is proportional to the total density of dislocations for a fixed value of θ, is valid only for $0<\varphi<\pi/2$; within this range it varies by 30 percent.

The quantity A depends upon φ and upon the energy of the atoms at the dislocation itself, where some atoms do not have the correct number of nearest neighbors and the strain lies well out of the Hooke's law range. This energy may conveniently be expressed by a device used in Appendix B, the procedure being summar-

* For an anisotropic material with cubic symmetry and elastic constants c_{11}, c_{12}, c_{44}, the quantity $G/(1-\sigma)$ in (6) is replaced by

$$\frac{c_{44}}{1-\sigma_{100}}\left(\frac{1}{\alpha}\frac{2(1-\sigma_{100})}{1+\alpha(1-2\sigma_{100})}\right)^{\frac{1}{2}}$$

where $\sigma_{100}=c_{12}/(c_{11}+c_{12})$ is Poisson's ratio referred to the crystal axes and $\alpha=2c_{44}/(c_{11}-c_{12})$ is the anisotropy factor. It is planned to derive this formula in a later paper.

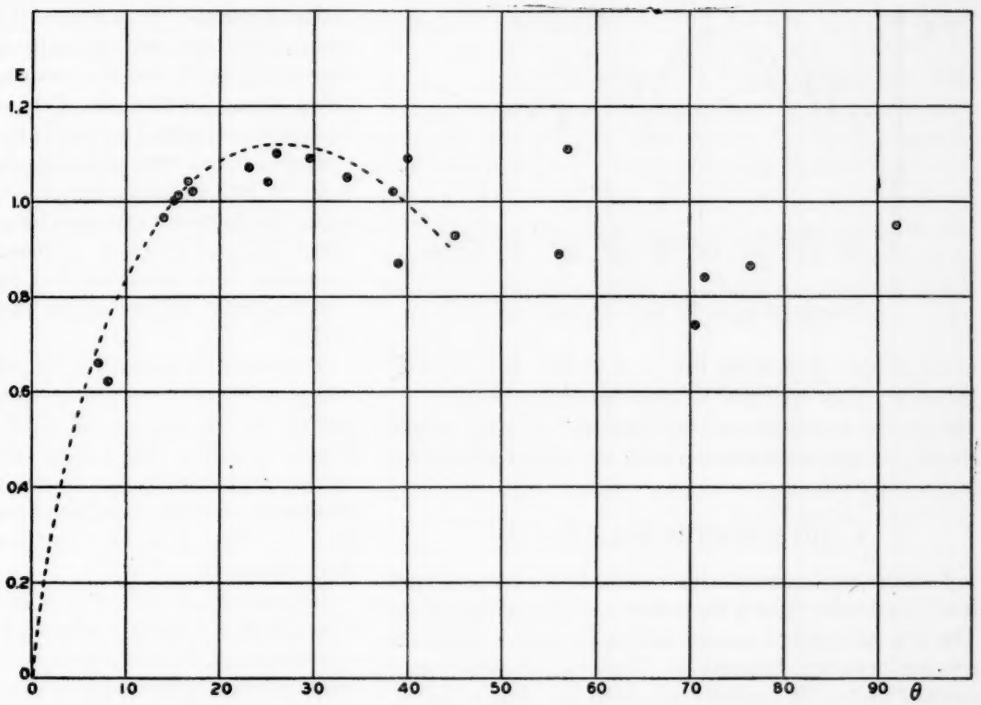

FIG. 2. Energy as a function of θ for grain boundaries. The points show the data of C. G. Dunn for silicon ferrite; see text for orientation. Theoretical curve has $A=0.231$.

ized as follows: The expression for elastic energy density for a single dislocation varies as $(1/r^2)$ from the center of the dislocation and this gives a logarithmic infinity if integrated to $r=0$. Actually it should not be integrated inside of the radius r_l at which the linear Hooke's law breaks down. The energy inside r_l should then be calculated on an atomic basis and added to the elastic energy outside r_l. As is discussed in Appendix B, however, for small angles of misfit precisely the same formula is obtained for the energy if the integration is extended to a radius $r_0<r_l$ such that the elastic energy calculated for the region $r_l>r>r_0$ has the same value as the correct energy inside r_l. In terms of r_0 defined in this way the value of A is

$$A=A_0-\frac{\sin 2\varphi}{2}-\frac{\sin\varphi\cdot\ln(\sin\varphi)+\cos\varphi\cdot\ln(\cos\varphi)}{\sin\varphi+\cos\varphi} \quad (7)$$

with

$$A_0=1+\ln(a/2\pi r_0). \quad (8)$$

The energy of atomic misfit, which enters through A_0, occurs in the energy E with factors, given in (5) and (6), which are directly proportional to the total density $\rho_x+\rho_y$ of dislocations. This is to be expected since this highly localized energy should contribute additively.

From (7) $A-A_0$ as a function of φ is seen to be symmetrical about 45° and to vary between $+0.13$ and -0.15. The maximum A occurs at $\varphi=6.5°$ or 83.5° and the minimum A at 45°. The curve has a cusp at $\varphi=0$ or 90°, where $A=A_0$. The variation in A can be neglected at small angles of misfit, where the $-\ln\theta$—term dominates the energy expression. (But not near the cusps of Section 4.)

Equation (5) will be a good approximation for the energy in a curved boundary if the radius of curvature is large compared to the spacing between dislocations. Letting ds be an element of length of a curved boundary, then the right-hand side of (5) will give dU/ds where U is the energy per unit length in the z direction. Remembering that $|dx|=ds|\cos\varphi|$ and $|dy|=ds|\sin\varphi|$, we then have

$$dU=[Ga/4\pi(1-\sigma)]\theta[A(\varphi)-\ln\theta][|dx|+|dy|].$$

If we can neglect the variation of A with φ, we see that dU is a perfect differential, so that the energy in a segment of boundary connecting two points P and Q will depend only on P and Q, provided that no changes in sign of dx/ds or dy/ds occur along the curve. Thus all boundaries connecting P and Q have the same energy for the same angle of misfit of adjoining grains. Actually there will be a slight preference for a 45° boundary since this gives the minimum A.

The quantity r_0 may be determined by using several approximate but not very accurate methods of estimating the energy in a single dislocation inside the radius r_l. Using Nabarro's[4] result for a pair of dislocations in a simple cubic model, we calculate that $A_0=0.8$. This estimate is not considered very reliable since it depends on the assumption that the interaction between two planes of atoms is based on a sine law of stress and strain.[5] Another estimate of A_0 is obtained from the requirement that the energy vanish when the dislocations are close enough together to produce an angle of

[4] F. R. N. Nabarro, Proc. Phys. Soc. London **LIX**, 256 (1947).
[5] It is shown that a sine law fails except over a narrow range of angles; see W. M. Lormer, Proc. Roy. Soc. **A196**, 135 (1949).

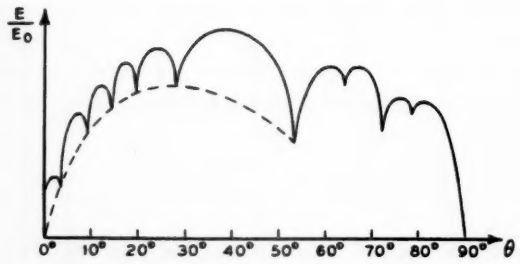

FIG. 3. Energy *versus* θ for $\varphi=0$ grain boundary showing twin boundary cusp at 53° and fine structure.

misfit of 90°. This leads for $\varphi=0$ to $A_0=\ln\pi/2=0.45$. However, this estimate is also unreliable since it involves the extension of the formula to large angles where the approximations used in its derivation are no longer valid.

3. QUANTITATIVE PREDICTIONS

Fortunately, quantitative conclusions can be drawn from the theory which do not involve the value of A_0. The first of these is related to Eq. (3) which gives the spacing between dislocations. These spacings are large enough for small angles θ so as to be within the resolving power of light and electron microscopes. We are not aware of any electron-microscope observations of suitable grain boundaries; however, it is very probable that the spacings predicted from (3) have been observed by P. Lacombe in connection with "veining" in aluminum.[6] Lacombe observes that in a single crystal grain there are faint lines or veins which are revealed as rows of separated etch pits under suitable etching conditions. He has also observed that there are small differences in orientation between the regions separated by the veins. We have proposed that each etch pit originates at a dislocation, where the free energy of the stressed material will be somewhat higher than elsewhere; the pit then grows to large size so that it is observed optically.[3] No attempt has been made to calculate the spacings on the basis of a detailed dislocation model for the actual orientation observed; however, the general order of magnitude for the angles of 10^{-3} radians or less and the spacings of 3×10^{-4} cm or less are in agreement with (3) when a reasonable value for a is used.[7] The behavior of the veins observed by Lacombe is, in other respects, entirely in keeping with the idea that they are widely spaced arrays of dislocations: Under heat treatment they shift to radically different patterns, a result in keeping with the dislocation proposal. In samples 0.2 cm thick, the vein patterns on the two opposite sides are in register to about $\pm2\times10^{-3}$ cm, the mesh size in the vein pattern being about 2×10^{-2} cm. This suggests that the veins represent cylindrical surfaces and are built up of parallel elements which run perpendicularly (within $2\times10^{-3}/2\times10^{-1}=10^{-2}$ radians) through the crystal. Again this is just the behavior expected for an array of dislocations, which must either close on themselves or terminate on a surface. The dislocations in such an array would be under tension and would be perpendicular to the free surface.

The second quantitative conclusion has to do with the energies of grain boundaries and depends only on the energy where strains are small and linear elasticity theory applies. The theory predicts that measured values of grain boundary energy plotted as a function of θ could be fitted by a curve of the form (5), the parameter E_0 being determined without approximations by linear elasticity theory.

Recently C. G. Dunn[8] has measured grain boundary energies on a relative scale as a function of difference in orientation, θ. Dunn's values of φ are not given, it being assumed that orientation of the grain boundary has a small effect. The specimens used were silicon iron (iron with 3.5 weight percent silicon, body centered cubic), with the (110) plane in the plane of the specimen. The

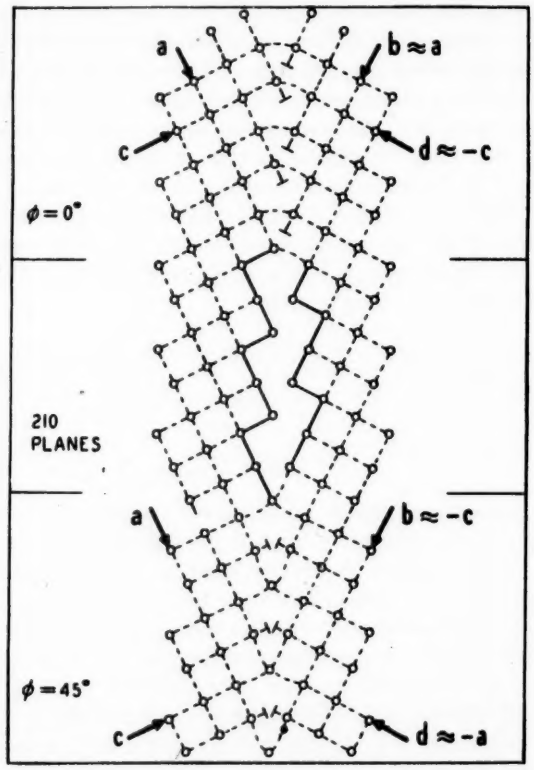

FIG. 4. Grain boundary for twinning on (210) plane showing $\varphi=0$ and $\varphi=45°$ interpretations.

[6] P. Lacombe, Report of Conference on Strength of Solids (The Physical Society of London, 1948). Similar small angle grain boundaries have recently been observed by R. Castaing and A. Guinier in an aluminum-copper alloy. Comptes Rendus 228, 2033 (1949) and La Recherche Aeronatique No. 13, 3 (1950).

[7] We are indebted to Professor Lacombe for confirming, in a personal communication, the conjecture of reference 3 that the data studied there corresponded to a large angle for one specimen and a large spacing for the other. Professor Lacombe indicates that the quantitative aspects of his observations are probably in agreement with (3).

[8] C. G. Dunn and F. Lionetti, Trans. A.I.M.E. 185, 125 (1949).

grain boundary was made as close as possible to perpendicular to the plane of the specimen and the angle of misfit measured between the [001] directions in the two grains. Viewed in the plane of the specimen the atoms are not arranged in a square lattice but in a rectangular lattice, one side being $\sqrt{2}$ times the other. Consequently, $\theta=180°$ is equivalent to $\theta=0°$; $\theta=90°$ constituting a considerable misfit. Dunn's data in relative units are plotted in Fig. 2. The plot has three striking features: a rapid rise of energy with increasing θ in the range 0° to 15°, a maximum and relatively constant energy in the range 20° to 30°, and a dip at about 70°. The first feature is predicted by the theoretical curve, Eq. (5), which has an infinite slope at $\theta=0$. The position of the maximum of the theoretical curve depends on A, the best fit to Dunn's data being given by $A=0.231$, which is the order of magnitude of the estimates. The theoretical curve is shown in Fig. 2 to 45° and is seen to fit the data surprisingly well even at large angles—a result which suggests that compensating errors may cause (5) to be valid over a larger range than is justified by its derivation. We shall return to the dips at 39° and 70° in the next section.

Dislocation models for grain boundaries in the common crystal lattices would involve screw components and possibly half-dislocations and extended dislocations.[9] However, it is not considered worth while to formulate a better theory until energies are measured on an absolute scale for small angle grain boundaries. If such measurements were available, particular dislocation models could be tested by plotting the measured E/θ *vs.* $\log\theta$. Then according to Eq. (5) the experimental points should fall on a straight line[10] of slope E_0. The value of E_0 can be calculated without approximations and depends only on the known constants of the material and the particular dislocation model assumed. An agreement between the calculated and measured values would constitute strong evidence for the dislocation model.

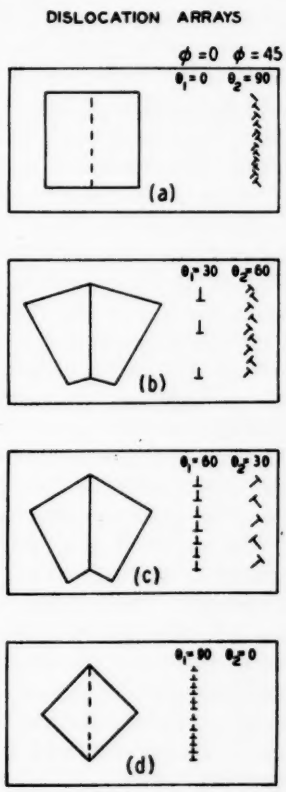

FIG. 5. Comparison of two models for symmetrical grain boundaries.

4. LARGE ANGLE GRAIN BOUNDARY

In this section we shall consider certain general features relating to grain boundaries for large angles θ, the remarks still being restricted to the simple cubic model and to values of φ of 0° and 45° unless otherwise stated.

Equation (5) was derived on the assumption that the spacing of dislocations was uniform for all values of θ. Actually this can only be the case when the spacing determined by relations (3) and (4) is an integral number of lattice constants; that is, dislocations must be separated by an integral number of atomic planes. For instance, if θ corresponds to an average spacing of $3\frac{1}{2}$ planes the actual spacing will be irregular, alternating between 3 and 4. As a result the energy is not a smoothly varying function of angle but instead has a number of sharp minima or cusps. We shall show that these cusps are of the $\theta\ln\theta$ form already discussed for $\theta=0$. A plot of E *vs.* θ showing the more important cusps is given in Fig. 3. The deep cusp in the middle corresponds to a boundary separating twins on the (210) plane. The dashed curve corresponds to (5) and (6). The maxima are treated in Appendix C. There will also be minor cusps between those shown and additional fine cusps for less than 10°.

We shall consider first the reason that cusps are necessary at small values of θ. For $\varphi=90°$ and $\theta=9.4°$, $+y$ dislocations will be required once in every 6 horizontal planes and no x dislocation would be required. For a small increase of $\delta\theta$ in θ from 9.4°, however, dislocations will be required somewhat closer so that occasionally a dislocation will be spaced by 5 planes rather than 6. Where this occurs, it will contribute, at large distances from the grain boundary, the same effect as adding (1/6) of a $+y$ dislocation at each location of a "five" spacing. For small values of $\delta\theta$, these "five" spacings will occur approximately at a spacing of $a/6\delta\theta$. For small values of $\delta\theta$ and large spacings, the energy due to the stress field of these dislocations will come from regions far from the grain boundary and will contribute a term of the order $-(E_0/6)\delta\theta\ln\delta\theta$, since the effective strength of the perturbations is $a/6$.

[9] R. D. Heidenreich and W. Shockley, Report of a Conference on Strength of Solids (The Physical Society of London, 1948), page 57.

[10] It is shown in reference 3 that Dunn's data plotted in this way are well fitted by a straight line—the zero intercept of the line giving A.

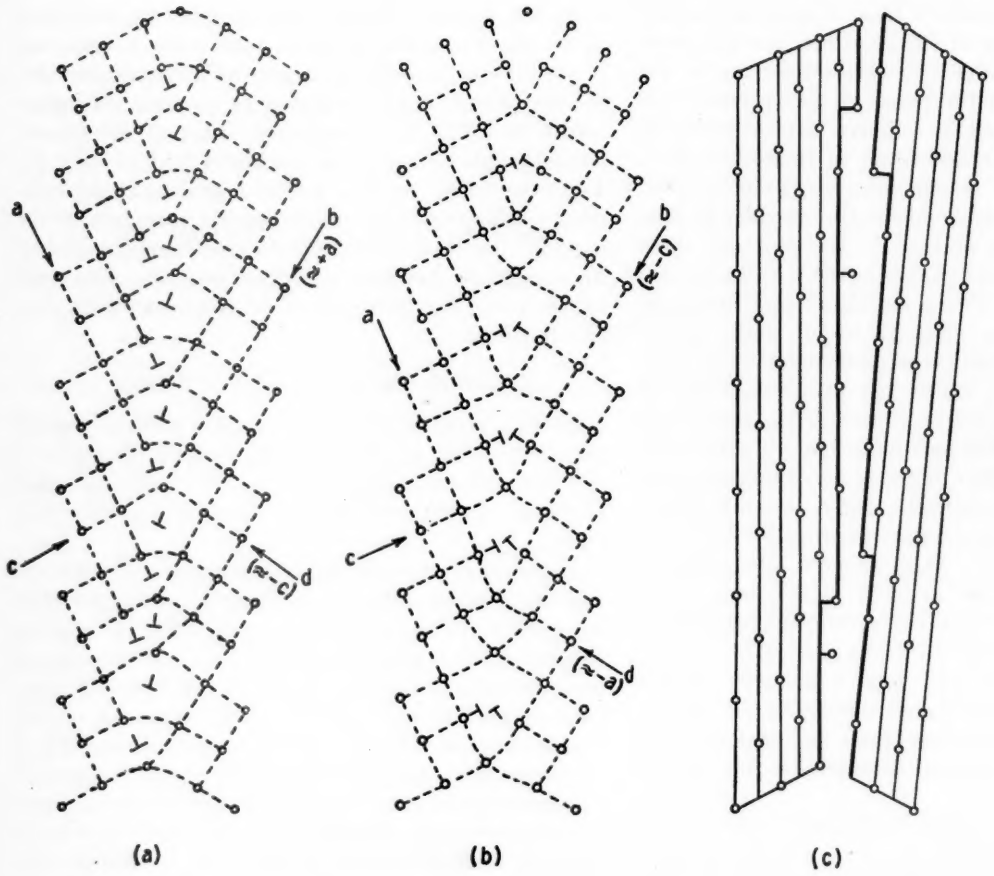

FIG. 6. 60° boundary showing equivalence of $\varphi=0$ and $\varphi=45°$ models and relationship to imperfect (210) surfaces.

A similar $-\delta\theta \ln\delta\theta$ cusp will occur whenever the dislocations are spaced at integral numbers of planes. In addition minor cusps will occur at spacings such as 5.5; because for such a spacing there will be a regular alternation of five and six intervals and a deviation from this, which would require two five spacings to be adjacent, would add a perturbation corresponding to $a/(5+6)=a/11$. This process will obviously continue indefinitely with the conclusion that the E *vs.* θ-curve has cusps at all values of θ which give rational values for the ratio of dislocations to slip planes across the grain boundary.

From a practical viewpoint the extreme fine structure just discussed will be of no interest and will be smoothed out by statistical fluctuations except for the larger cusps. The most important of these occurs at $\theta=53°$, corresponding to twinning across the (210) plane. Figure 4 shows the arrangement of the atoms in this case. The heavy lines represent (210) plane boundaries and the bicrystal may be considered as made up by bringing two grains with these (210) faces into contact.

This twin boundary may be described as made up of arrays of dislocations in either of two ways as shown in Fig. 5. We may start with a model with $\varphi=0$ and increase the angle θ_1 between (010) planes up to 53°, at which point $\tan\theta_1/2=\frac{1}{2}$, corresponding to the twin orientation. If θ_1 is increased to 90°, the grain boundary should disappear as shown in Fig. 5(d). On the other hand, we can start back from 5(d) with $\varphi=45°$ and produce the same series of orientations. Thus for a given orientation of the grains and the grain boundary, two prescriptions can be given for arrays of dislocations which will join the grains. We shall next investigate the difference between these two prescriptions. The conclusion, reached in the following paragraphs, is that the same arrangement of the atoms can be described as either a $\varphi=0$ boundary or a $\varphi=45°$ boundary and, consequently, that two descriptions are really equivalent.

There may, however, be several atomic arrangements which will accomplish the same joining. In Fig. 4, the plane of the grain boundary is a reflection plane between the two grains. A very similar arrangement may be produced by making the grain boundary a glide plane of symmetry. The relative stability of the two structures will depend upon the detailed nature of the interatomic forces. For whatever structure is the most stable, however, the equivalence of the $\varphi=0$ and $\varphi=45°$ models will be true and the dependence of energy upon small deviations of θ and φ from the twin values will be as described below.

In Fig. 4 in the upper part a set of dotted lines and dislocation symbols are shown; these have been constructed in accordance with the $\varphi=0$ model. In terms

of flow lines this interpretation of the atomic arrangement can be described by writing

$$\varphi=0;\quad c\rightleftarrows -d;\quad a\rightleftarrows b,$$

meaning that the c planes running in at the left are thought of as continuing as $-d$ planes to the right and that a and b planes are to be considered as representing the same set in the undistorted crystal. This leads to a density of dislocations of $\rho_a+\rho_b$ where the ρ's are the flux density of plane lines into the boundary. Precisely the same atomic arrangement can be described by the arrangement of dislocations shown in the lower part of Figure 4 according to the scheme

$$\varphi=45°;\quad a\rightleftarrows -d;\quad b\rightleftarrows -c,$$

meaning that the a planes are to be considered as continuations of $-d$ and b as $-c$. The density of dislocations for the $\varphi=45°$ model is seen to be

$$\begin{aligned}&\rho_c-\rho_b \quad \text{for } c\text{-dislocations}\\ &\rho_d-\rho_a \quad \text{for } d\text{-dislocations.}\end{aligned}$$

Combining these leads to a total number of dislocations $(\rho_d+\rho_c)-(\rho_a+\rho_b)=2(\rho_c-\rho_a)$, since by symmetry $\rho_d=\rho_c$ and $\rho_a=\rho_b$. For the angle shown $\rho_c=2\rho_a=2/a(5)^{\frac{1}{2}}$ and both models give a density of dislocations equal to ρ_c.

Now let $\theta_1=90-\theta_2$ deviate slightly from 53°, for example, by increasing to 60°, as shown in Fig. 6a. The density of a and b dislocations will increase for the $\varphi=0$ model so that there will be on the average more than one dislocation per plane of set c striking the boundary. These extra dislocations will give rise to a cusp in the energy curve about the twin angle. We shall next show that for this case also the $\varphi=0$ and $\varphi=45°$ models are equivalent and shall evaluate the effective strength of the added dislocations which produce the cusp. For the $\varphi=45°$ model, the density of dislocations decreases as θ_1 increases from 53° to 60°; consequently there will be less than one dislocation per plane of set c striking the boundary, Fig. 6(b). We shall show algebraically that the number of c-planes having extra dislocations according to the $\varphi=0°$ model just equals the number of c-planes lacking a dislocation according to the $\varphi=45°$ model, and we shall than show geometrically that these two descriptions actually describe the same atomic arrangement.

According to the $\varphi=0°$ model, the density of dislocations is $2\rho_a$ and the excess compared to the density of c-planes is thus $2\rho_a-\rho_c$. According to the $\varphi=45°$ model, the density of dislocations is $2(\rho_c-\rho_a)$ and the excess of c-planes compared to this is $\rho_c-2(\rho_c-\rho_a)=2\rho_a-\rho_c$; this is the algebraic proof. Figure 6(a) shows the 60° boundary with dotted lines joining atoms according to the $\varphi=0°$ dislocation model. In Fig. 6(b) the atoms are joined according to the $\varphi=45°$ model. By observing the difference between the two models of the same atomic arrangement in the vicinity of a perturbation, or region where according to the $\varphi=0°$ model two vertical rows end on the same plane, we see that each pair of $a-b$ dislocations on the same c-plane in the $\varphi=0$ model is equivalent to a missing $c-d$ pair on the same plane in the $\varphi=45°$ model. Although both dislocation models represent the same arrangement of atoms, the model consisting of the fewer dislocations is to be preferred on physical grounds as giving the better method of joining the grains, since the number of atoms per plane having a missing bond is equal to the number of dislocations.

In Fig. 6(c) we show the two surfaces which would be formed if the 60° bicrystal were to be pulled apart. It is seen that these are nearly perfect (210) planes except for steps occurring at the perturbations. These steps correspond to an offset of one (210) plane spacing on each grain or a net normal displacement of two plane spacings. Thus the perturbations are equivalent to dislocations of magnitude $2a/(5)^{\frac{1}{2}}$ with the slip vector perpendicular to the grain boundary. Hence the cusp will have the form of

$$[2/(5)^{\frac{1}{2}}]E_0(\varphi=0)\delta\theta(A_1-\ln\delta\theta)$$

by analogy with the $\varphi=0$ calculation which has a similar dislocation array but with strength a. The value of A_1 will be determined by the atomic misfit on the twin boundary and will be different from A_0.

Probably the most significant feature of the above calculation is that for small angles of deviation the energy of the twin boundary will increase with angle almost as fast [i.e., $2/(5)^{\frac{1}{2}}=0.89$] due to the $-\delta\theta\ln\delta\theta$-term as for a small angle grain boundary.

It is also evident from the general reasoning presented here that similar effects will be produced by varying φ. If the orientation of the two grains is maintained at 53° and the value of φ is changed from 0, the energy will increase as $-\varphi\ln\varphi$ with a coefficient again nearly equal to E_0.

This last prediction of dependence of energy upon φ is in agreement with the observation of Lacombe[11] that when two grains are separated by a boundary consisting in part of a straight twin plane and in part of curved boundary not along the twin plane, the etch used will attack the curved boundary but not the plane boundary, thus showing that large differences in energy are produced by changes in orientation of the grain boundary for the same orientation of the grains.

The dips in Dunn's data of Fig. 2 appear to correspond to expected cusps for the orientation of his crystal. It was seen in Section 3 that, when projected in the plane of the specimen (110), the lattice structure is rectangular with an edge ratio of $1:\sqrt{2}$. The angle θ is measured between [001] directions (short edges). If θ_1 is the angle between the grain boundary and the [001] axis of the first grain, the unit normal to the grain boundary is seen to have components $\cos\theta_1\cos 45°$, $\cos\theta_1\sin 45°$, $\sin\theta_1$. A similar result holds for the second

[11] Report of a Conference on Strength of Solids, University of Bristol (July 1947) published by the Physical Society, 1948.

grain which makes an angle $\theta_2=\theta-\theta_1$ with the boundary. In the symmetrical case $\theta_1=\theta_2=\theta/2$.

Low energy cusps occur when the two crystals are in register on the same atom at regular intervals of a few lattice constants. The condition that the boundary go through lattice points in the first grain is $\tan\theta_1=na_y/ma_x$, where m and n are integers and the atomic spacings a_y and a_x in the plane of the specimen are related by $a_y=\sqrt{2}a_x$. The corresponding condition for the second grain is $\tan\theta_2=\sqrt{2}q/p$, and the two grains will be in register on the same atom at regular intervals along the boundary when the integers m, n, p, q are related by $m^2+2n^2=p^2+2q^2=$ square of distance between common lattice points, the lattice constant a_x in the [001] direction being taken as the unit of length. The grain boundary is the $(m, m, 2n)$ plane in one crystal and the $(p, p, 2q)$ plane in the other.

The most important cusps in energy as a function of angle of misfit and orientation of the grain boundary correspond to the shortest intervals between common lattice points; for example, when $m=n=p=q=1$ the grains are in register on every atom on the boundary and we have a (112) twin, the angle being $\theta=109.4°$. This angle is not in the range of Fig. 2; however, Dunn has recently[12] obtained a value of 0.22 for the energy on the scale of Fig. 2.

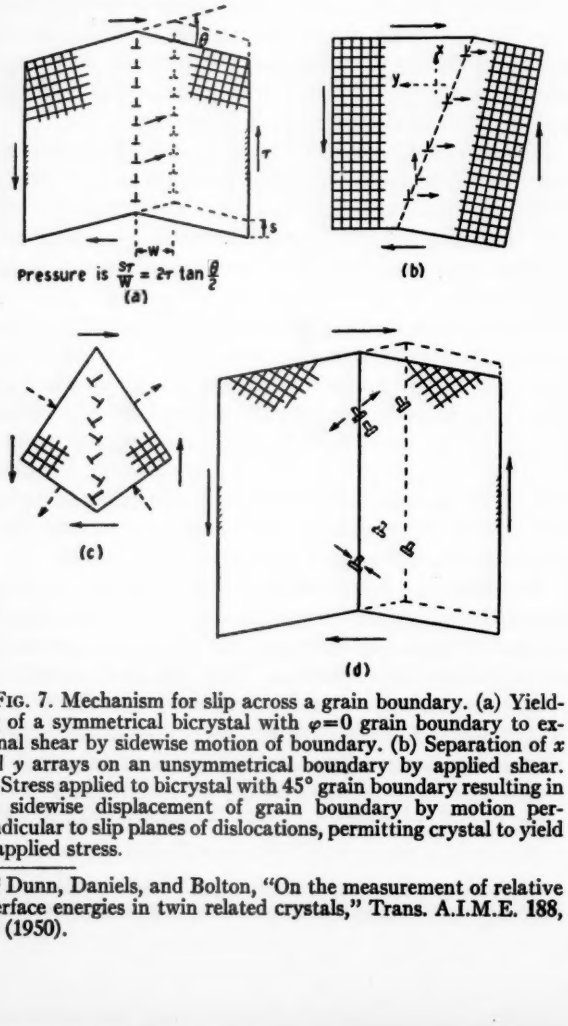

FIG. 7. Mechanism for slip across a grain boundary. (a) Yielding of a symmetrical bicrystal with $\varphi=0$ grain boundary to external shear by sidewise motion of boundary. (b) Separation of x and y arrays on an unsymmetrical boundary by applied shear. (c) Stress applied to bicrystal with 45° grain boundary resulting in (d) sidewise displacement of grain boundary by motion perpendicular to slip planes of dislocations, permitting crystal to yield to applied stress.

[12] Dunn, Daniels, and Bolton, "On the measurement of relative interface energies in twin related crystals," Trans. A.I.M.E. 188, 368 (1950).

The prominent dip in the experimental data near 70° is explained by the fact that the two most important low energy configurations in the range of Fig. 2 both occur at $\theta=70.6°$. One of these configurations is a symmetrical (111) grain boundary with common lattice points spaced at 2.45 lattice constants; the other configuration is unsymmetrical and involves the coincidence of the (110) plane of one grain with the (114) plane of the other, with points of good fit spaced at intervals of three lattice constants. By comparing the arrangement of atoms on the boundary for the (112) and (111) twins it can be seen[13] that the former gives the better fit, in agreement with the lower measured energy.

In the range of Fig. 2 the third and fourth cusps in order of increasing distance between common lattice points would be expected at 50° and 87°, respectively, where no experimental points were taken. The fifth cusp occurs at a symmetrical (221) boundary, where the crystals are in register at intervals of 4.25 lattice constants and the angle is 39°. This explains the low point and scatter in the experimental data at this angle, the scatter at cusp angles being attributed to the variation in grain boundary orientation since the energy at a cusp increases at an infinite rate with deviations in either angle of misfit or boundary orientation.

The 20 percent discrepancy between the points at 56° and 57°, which are not cusp angles, has a different origin. The relative energies were calculated from a minimum energy principle involving the equilibrium of surface tensions at the intersection of three grain boundaries, it being assumed that energy depends principally on angle of misfit and that the effect of grain boundary orientation could be neglected.[8] However, when one boundary is near an energy cusp the derivative of energy with respect to orientation is large and its neglect introduces an error into the calculation of the relative energy of the other two boundaries. The points at 56° and 57° were obtained from the two specimens containing the low energy boundaries with θ near the 70.6° cusp. In Appendix F this point is discussed in detail and the energy *vs.* angle relations are derived for three intersecting grains taking account of the dependence of energy on boundary orientation.

The general behavior of the energy *vs.* angle curve appears to be in qualitative agreement with the extensive system of observations made by C. S. Smith[14] of grain boundary angles. In his study the angles where three grains run together were measured on polished sections of polycrystalline samples and the statistical distribution of observed angles was studied. Even if all grain boundaries had the same energy, so that the three dihedral angles about the common grain edge would each be 120°, the metallographic section would

[13] C. S. Barrett, *Structure of Metals* (McGraw-Hill Book Company, Inc., New York, 1943), p. 315.

[14] C. S. Smith, "Grains, phases and interfaces: An interpretation of microstructure, A.I.M.M.E. Technical Publication No. 2387, Class E, Metals Tech. (June, 1948).

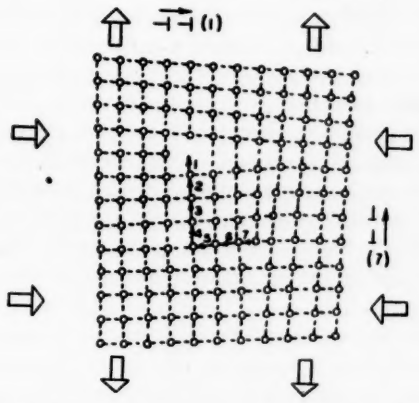

FIG. 8. Motion of dislocations perpendicular to slip planes produced by diffusion of atoms.

introduce a statistical fluctuation in observed angles. Smith found that the statistics of the observed angles were consistent, or at least not strikingly inconsistent, with a single interfacial energy for the boundaries. This at first seems to contradict the predictions made here that the grain boundary energy fluctuates violently and that, as indicated in Fig. 2, energies of less than half the average should occur in about 15 percent of the cases; the impression gained from Fig. 2 is erroneous, however, because it shows the energy as a function of one angle only. If any of the three angles which specify relative orientation of the grains is large, a relatively large grain boundary energy will be obtained. If we assume that the grain boundary energy for a general orientation is the sum of three functions like that of Fig. 2, one for each angle, then we estimate that energies less than 50 percent of the average will be obtained in only about 3 percent of the cases. Consequently, observations of grain boundaries for grains selected at random would show such a small percentage of low energy boundaries that their presence would have only a slight effect on the statistics.

5. DYNAMICS OF THE GRAIN BOUNDARY MODEL

The dislocation model of the grain boundary appears to have the potentiality of giving the "viscous grain boundary" behavior studied extensively by Zener and Kê.[15] Two separate mechanisms are involved in shear across the grain boundary, corresponding to motion of the dislocations in their slip planes and motion perpendicular to the slip planes. (The latter involves diffusion of atoms in a way which we shall shortly illustrate in Fig. 8.)

The two basic processes are shown in Fig. 7. A boundary with $\varphi=0$ is shown and the bicrystal is cut so that the largest faces are parallel to the boundary. If a shear stress τ is applied as shown, the dislocations tend to slide on the slip planes in the direction of the dotted positions. In Appendix A we show that the force acting on a unit length of a dislocation under these conditions is simply τa, so that the pressure on the grain boundary is $\tau a/D_y \doteq \tau\theta$. The same pressure is derived by considering the deformation of the crystal. If we imagine the left grain to be held fixed, then the work done when the boundary moves a distance W is $S\tau$ per unit area, so that the pressure is $S\tau/W=\tau 2\tan\frac{1}{2}\theta=\tau\theta$ for small angles. This type of motion can thus permit relative shear of the two crystals to take place across the grain boundary.

Figure 7(a), however, is a very special case. A more typical situation is shown in (b). Here there are two

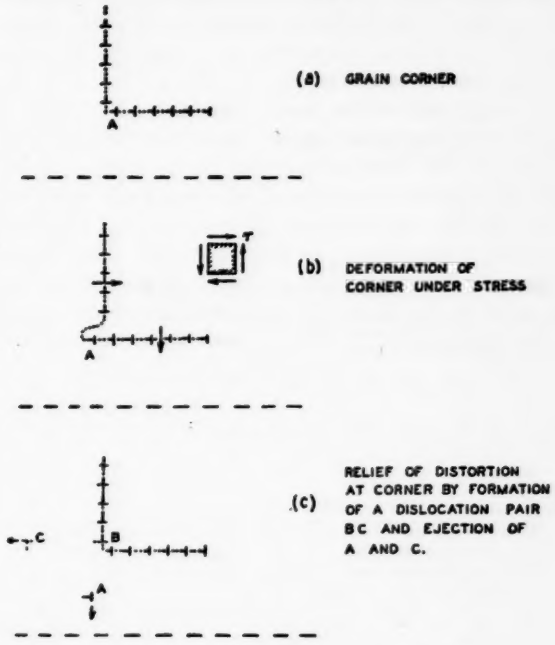

FIG. 9. Formation of a dislocation pair at a grain corner under applied stress.

sets of dislocations and in this case if we move the grain boundary to the right, by sliding the x dislocations to the right and the $-y$ dislocations down, no net shearing motion of the crystal results. The reason for this is that the prescription of dislocations of Eqs. (3) and (4) is just that necessary to permit the two grains to join with a fixed relative orientation; a proof of this statement is given in Appendix E. The difference between (b) and (a) is connected with the limiting behavior as $\varphi\to 0$. As φ becomes very small, the spacing D_y is given by $a/\theta\varphi$. Thus $D_y\to\infty$ as $\varphi\to 0$. As the boundary moves to the right a distance W, however, the $-y$ dislocations move a distance W/φ so that each y plane is cut by $(W/\varphi)/D_y=W\theta/a$ dislocations of y type as it moves. Each of these produces an offset "a" giving a shearing motion of $W\theta$. Inspection shows that the sign of this shear just cancels the $W\theta$ term due to the motion shown in (a). Thus no net shear is produced by motion of the boundary while any $-y$ dislocations are present.

[15] C. Zener, *Elasticity and Anelasticity of Metals* (University of Chicago Press, Chicago, 1948); T. S. Kê, J. App. Phys. **20**, 274 (1949).

If a shearing stress is applied to (b), the dislocations try to slip as shown by the arrows. As a result the x and y sets pull apart until the increasing elastic energy of the material between them balances the applied stress. If the angle φ is small, this will result in curvature of the dense line of dislocations and resultant high stress values. We shall return to the high stresses later in this section in connection with grain boundaries as stress raisers.

The processes which may follow the development of the stressed situation in (b) are illustrated in a simpler form in (c) and (d). Here we show a $\varphi=45°$ boundary with a shearing stress system which develops no shear in the slip planes. The shear stress system is equivalent to a normal stress system shown as dotted arrows. These stresses tend to squeeze out (or pull in) the extra half-planes of atoms. The mechanism whereby this may be accomplished will be discussed below; however, if we assume that the squeezing out actually occurs, then the motion of the dislocations will be as shown in (d). Here we consider two dislocations on a grain boundary which divides the specimen in two; actually there will be many dislocations on the boundary. The normal stresses on the half-planes cause one to shorten and the other to lengthen, moving the dislocations to the dotted positions. The dotted positions, however, correspond to a relative motion of the arrays of the two types of dislocations; and in order to keep the grain boundary in a minimum energy condition, the dislocations will slip in their own planes so as to move to positions in the dotted grain boundary which are at the same height as their original positions. These combined motions produce a net horizontal motion of the grain boundary in which no dislocations cut the (110) planes which are parallel to the top and bottom of the figure. The result is thus a yielding to the shear of amount $S=W2\tan\theta/2$ as for Fig. 7(a).

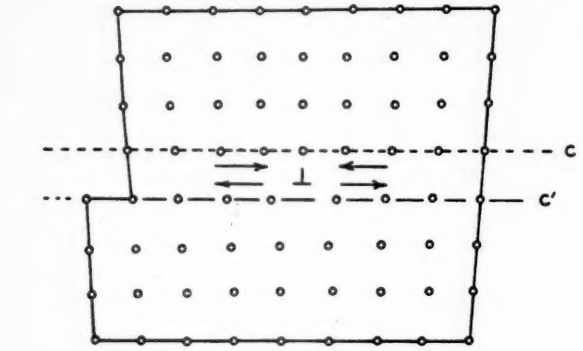

(a)

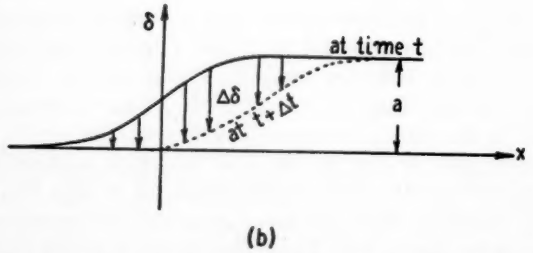

(b)

FIG. 10. The force on a dislocation. (a) Single dislocation in a cubic crystal, showing shearing stresses on planes C and C'. (b) Plot of δ=difference in displacement on C and C' at times t and $t+\Delta t$.

The process which can produce motion perpendicular to the slip plane is shown in Fig. 8, which corresponds to 7(d) turned through 45°. We suppose vacancy diffusion takes place, the process being initiated by jump (1) in the figure which permits the half-plane to grow by one atom, a vacancy being produced next to the advancing edge. This vacancy diffuses until it is filled by jump 7 which shortens the other dislocation by one atom on the leading edge of the half-plane.

The shear produced across a general small angle grain boundary will be a mixture of effects like those considsidered in (a) and (c). For large angle grain boundaries, such as are dealt with in most experiments, the density of dislocations will be so high and the possibilities of alternative descriptions so many that other approaches may be better such as those of Mott[16] and Kê,[17] which consider the boundary to be a mixture of good fit and bad fit. However, the feature discussed in Fig. 8 has one consequence in agreement with experiment: The mechanism involved is that of self-diffusion and, consequently, the activation energy for the process will be the same as that for self-diffusion, in agreement with the findings of Kê for aluminum, α-brass and α-iron.[18]

Even for small angle grain boundaries, however, the theory discussed in connection with Fig. 7 is oversimplified because it neglects the effects of screw components of the dislocations and the possibility of half-dislocations.[19] The screw components are discussed in Appendix D and are seen to exert forces like those of charged wires on each other. These forces will tend to stabilize the dislocation arrays.

The pressure on a grain boundary suggests a mechanism for the creation of dislocation pairs in the interior of polycrystals. As mentioned earlier, an applied shearing stress tends to pull the boundary apart, creating regions of stress concentration. We now show how the distortion of a grain corner under stress could lead to the formation of a dislocation pair at the corner. Consider the right-angle corner illustrated in Fig. 9(a), where the grain in the upper right-hand quadrant is disoriented by a small clockwise rotation relative to the adjoining material. The grain boundary is symmetrical

[16] N. F. Mott, Proc. Phys. Soc. London **60**, 391 (1948).
[17] T. S. Kê, J. App. Phys. **20**, 274 (1949).
[18] T. S. Kê, Phys. Rev. **73**, 267 (1948).
[19] R. D. Heidenreich and W. Shockley, Report of a Conference on Strength of Solids (Physical Society, London, 1948), p. 57.

and runs along the $+y$ and $+x$ axes, which are rows of $+y$ and $-x$ dislocations respectively. When an external shearing stress is applied as shown in (b) the y dislocations are pushed to the right and the $-x$ dislocations are forced downward. The entire pressure on the grain boundary and the forces on the dislocations are held in equilibrium by the corner, which alone prevents the relative displacement of the two segments of the boundary. The corner is thus a region of high strain, the strain energy per unit applied stress being proportional to the area of the boundary and the density of dislocations. As the applied stress is increased, the relative displacement of the two rows of dislocations increases until the distortion of the corner is so severe, as shown in Fig. 9(b), that it is easier energetically to form a dislocation pair BC, Fig. 9(c), where B fills the gap on the grain boundary and A and C are ejected and move under the applied stress to the external surface, thus contributing to the observed slip of the specimen.

In conclusion it may be pointed out that the idea of pressure on a grain boundary due to applied stresses constitutes a prediction from dislocation theory that grain boundaries, and similarly veins like those observed by Lacombe, should displace in a particular way under the influence of applied stress.

The authors would like to express their gratitude for suggestions and encouragement in connection with this research to J. H. Hollomon, C. S. Smith, W. G. Burgers, C. G. Dunn and C. Herring. We are also indebted to Mrs. G. V. Smith and Miss D. T. Angell for computations and other assistance in preparing the manuscript.

APPENDIX A

The Force on a Dislocation

When a dislocation moves under the action of an external stress field, work is done on the boundary by the applied forces. Some of this work goes into increasing the energy of distortion of the crystal and is recoverable, and the remainder is dissipated at the dislocation as heat or acoustical waves. Defining the force on a dislocation as the energy dissipated in moving the dislocation through unit distance on the slip plane, we show, first by an intuitive example and then by a careful analysis of the physical phenomena, that the force per unit length on a line dislocation is the lattice constant times the applied shearing stress in the slip direction.

In the simple example, Fig. 10, let the dislocation move a distance L from one side of a crystal to the other, producing a relative tangential displacement of the upper surface through one lattice constant a. Letting τ be the applied stress on the slip plane the work done is τaL. The elastic energy of distortion in the two parts of the crystal above and below the slip plane is the same before and after slip, so that all of the work has gone into heat. Since an amount of heat τaL has been produced in moving the dislocation through a distance L, it would be reasonable to assume that the force on the dislocation was τa.[20] We shall find by a more thorough analysis that this semi-intuitive result is correct.

If we assume that inertial effects can be neglected, then the energy dissipated is equal to the external work done minus the change in stored energy of distortion. The rate of change of internal energy is equal to the rate at which surface stresses are doing work on the complete boundary of the crystal, which includes not only the external boundary but the internal surfaces of discontinuity, or slip planes. Thus the stored energy is the sum of the external work and the work done on the slip planes—from which it follows that the energy dissipated is the negative of the work done on the slip planes.

Now consider a single dislocation in a cubic lattice, Fig. 10. Let C and C' be the atomic planes adjoining the slip plane. The shearing stresses on C and C' are shown in the figure. Superposed on this anti-symmetrical shear distribution we have the shear stress due to the external field. Figure 10(b) is an approximate plot of the discontinuity in displacement δ across the slip plane, the atoms being in register at the extreme right and offset by one lattice spacing at the left, with a transition region of a few atomic spacings at the dislocation. The dotted curve shows the discontinuity in displacement at a time Δt later, when the dislocation has moved a distance Δx. Clearly the limit $\Delta\delta/\Delta t$ is a symmetrical function of distance x along the slip plane. The rate of doing work on the slip plane is the integral of the shearing stress times the rate of relative displacement $\Delta\delta/\Delta t$ of the planes C and C'. Since the latter is symmetrical, the anti-symmetrical shear distribution due to the dislocation itself gives no contribution, and we have for the rate of energy dissipation

$$\frac{\tau}{\Delta t}\int_c \Delta\delta dx,$$

where τ is the external shear stress, which may be considered constant over the atomic dimension involved, and the integral is the area between the two curves in Fig. 10(b) which is readily seen to be $a\Delta x$. Thus, taking account of signs, the energy dissipated in moving the dislocation a distance Δx is $\tau a\Delta x$ and the force on the dislocation is τa.[21]

In this derivation it has been assumed for simplicity that the slip vector is at right angles to the axis of the dislocation. However, this restriction is readily seen to be unnecessary. In the general case the force on a dislocation is τa where τ is the shearing stress in the slip direction and a is the magnitude of the slip vector or lattice spacing in the slip direction. Thus the result derived applies to dislocations with screw components, which are generally required in an actual face-centered or body-centered cubic lattice.

APPENDIX B

Derivation of the Energy *vs.* Angle Formula

The shear stress τ_{xy} due to a single $+y$ dislocation located at the origin of the coordinate system is[22]

$$\tau_{xy}=\frac{x(x^2-y^2)}{(x^2+y^2)^2}, \tag{B.1}$$

where for convenience lengths are expressed in units of "a" and stresses in units of $G/[2\pi(1-\sigma)]$. The shearing stress due to an infinite row of dislocations, Fig. 1, spaced at a distance D_y along the line inclined at an angle φ to the x axis is

$$\sum_{n=-\infty}^{\infty}\frac{x_n(x_n^2-y_n^2)}{(x_n^2+y_n^2)^2}, \tag{B.2}$$

where

$$x_n=x+nD_y\cos\varphi$$
$$y_n=y+nD_y\sin\varphi.$$

[20] This reasoning is very similar to that of N. F. Mott and F. R. N. Nabarro, Report of a Conference on Strength of Solids (The Physical Society, London, 1948), p. 1.

[21] It may be noted that this differs by a factor of $\pi(1-\sigma)$ from the result computed by J. S. Koehler using linear isotropic two-dimensional elasticity theory (Phys. Rev. **60**, 400 (1941)). This may be attributed to the fact that Koehler does not take account of the work done by the surface forces.

[22] J. S. Koehler, Phys. Rev. **60**, 397 (1941).

From (3) and (4) of Section 1, D_x and D_y are given by

$$D_x = a/(\theta\cos\varphi)$$
$$D_y = a/(\theta\sin\varphi). \tag{B.3}$$

The infinite sum (B.2) is readily transformed to

$$\sum_{n=-\infty}^{\infty} \frac{\partial}{\partial y}\left(\frac{y_n}{2}\right)\left[\frac{1}{x_n+iy_n}+\frac{1}{x_n-iy_n}\right].$$

Using the complex variable $z=x+iy$ and the complex constant $z_1=D_y e^{i\varphi}$ and letting Re mean "real part of," this becomes

$$\mathrm{Re}\sum_{n=-\infty}^{\infty} \frac{\partial}{\partial y}\left(\frac{y+nD_y\sin\varphi}{z+nz_1}\right).$$

Multiplying numerator and denominator by $z-nz_1$ and adding a constant term which vanishes in the differentiation, we have

$$\mathrm{Re}\sum_{n=-\infty}^{n=\infty} \frac{\partial}{\partial y}\left[\frac{(y+nD_y\sin\varphi)(z-nz_1)}{z^2-n^2z_1^2}-\frac{D_y\sin\varphi}{z_1}\right].$$

Since the terms with n odd cancel in pairs, this can be expressed in the form

$$\mathrm{Re}\,\frac{\partial}{\partial y}\left[\frac{z_1 y - zD_y\sin\varphi}{z_1}\right]\sum_{n=-\infty}^{\infty}\frac{z}{z^2-n^2z_1^2}.$$

The sum of the infinite series is known and is equal to

$$(\pi/z_1)\cot(\pi z/z_1).^{23}$$

This gives

$$\mathrm{Re}\left[\frac{\pi}{z_1^2}\frac{\partial}{\partial y}(z_1y-zD_y\sin\varphi)\cot\frac{\pi z}{z_1}\right] \tag{B.4}$$

for the stress caused by the infinite set of $+y$ dislocations. Putting this in the form

$$\mathrm{Re}\left\{\frac{\pi}{z_1^2}\left[D_y\cos\varphi\cot\frac{\pi z}{z_1}-i(z_1y-zD_y\sin\varphi)\frac{\pi}{z_1}\csc^2\frac{\pi z}{z_1}\right]\right\}, \tag{B.5}$$

we see that at an infinite distance from the line of dislocations, where $z=Niz_1$ and $N\to\infty$, the stress approaches $(\pi/D_y)\cos\varphi\sin2\varphi$. A similar analysis for the dislocations with vertical slip planes gives a stress at infinity of $-(\pi/D_x)\sin\varphi\sin2\varphi$. From (B.3) we see that the sum of these is zero, so that the shear stress at infinity vanishes as required.[24]

We shall now calculate the self- and interaction energies of the two sets of dislocations.

The work of interaction on the vertical slip plane of one of the $+x$ dislocations is found by integrating the shear stress (B.4) due to the set of $+y$ dislocations, the integration being taken from x, y to x, $y+R$ where R is very large and x and y are the coordinates of the $+x$ dislocation, with the origin at a $+y$ dislocation. Making use of the fact that the equation of the grain boundary is $y=x\tan\varphi$, the integral of (B.4) with respect to y gives

$$-(\pi R/2D_y)\cos\varphi\sin2\varphi \tag{B.6}$$

for all points on the boundary. Thus the interaction energy is the same for all the $+x$ dislocations. In the same way the work of interaction on the horizontal slip plane of a $+y$ dislocation is found to be

$$-(\pi R/2D_x)\sin\varphi\sin2\varphi \tag{B.7}$$

and is the same for all the $+y$ dislocations.[25]

Since the self-energy per $+y$ dislocation is obviously the same for each dislocation, we consider the dislocation at the origin, where $y=0$, and integrate the shearing stress (B.5) due to the $+y$ dislocations from $x=r_0$ to $x=R$, where r_0 is the radius of a small circle around the dislocation and, as previously explained, is a parameter determined by the local energy of misfit which must be calculated on an atomic basis. This integration gives for the self-energy per $+y$ dislocation

$$\frac{1}{2}\left[\frac{\pi R}{D_y}\sin2\varphi\cos\varphi-\ln\left(\frac{2\pi r_0}{D_y}\right)+\sin^2\varphi\right]. \tag{B.8}$$

It can be seen that varying r_0 changes the energy by a constant amount, independently of the orientation of the adjoining crystals. Thus adjusting r_0 is equivalent to adding the energy of local atomic misfit to the angle dependent energy of the surrounding field. This is a valid procedure provided the angle of misfit is small enough that the local energy of atomic misfit is not dependent on the spacing between dislocations.

The self-energy of the set of $+x$ dislocations is found in the same way to be

$$\frac{1}{2}\left[\frac{\pi R}{D_x}\sin\varphi\sin2\varphi-\ln\left(\frac{2\pi r_0}{D_x}\right)+\cos^2\varphi\right] \tag{B.9}$$

per dislocation.

The work done on a horizontal slip plane is (B.7)+(B.8) equals

$$\frac{\pi}{2}R\sin2\varphi\left[\frac{\cos\varphi}{D_y}-\frac{\sin\varphi}{D_x}\right]-\frac{1}{2}\left[\ln\left(\frac{2\pi r_0}{eD_y}\right)+\cos^2\varphi\right], \tag{B.10}$$

where e is the base of the natural logarithms. The relationships between D_y, D_x, and φ which caused the stress to vanish at ∞ in (B.5) causes the coefficient of R to vanish so that the energy is convergent.

The energy per unit length of boundary is found by dividing the work done on a slip plane by the spacing between slip planes. This gives $[(B.7)+(B.8)]/D_y$ for the $+y$ dislocations, and $[(B.6)+(B.9)]/D_x$ for the $+x$ dislocations. The sum of these is

$$\frac{1}{2}\left[\frac{\cos^2\varphi}{D_y}+\frac{\sin^2\varphi}{D_x}-\frac{1}{D_y}\ln\left(\frac{2\pi r_0}{eD_y}\right)-\frac{1}{D_x}\ln\left(\frac{2\pi r_0}{eD_x}\right)\right] \tag{B.11}$$

or, using (B.3) the energy E per unit area of the boundary is

$$E=E_0\theta[A-\ln\theta] \tag{B.12}$$

where E_0 depends only on φ and the constants of the material and is given in dimensional units by

$$E_0=\frac{Ga}{4\pi(1-\sigma)}(\cos\varphi+\sin\varphi) \tag{B.13}$$

and A depends on r_0 and, therefore, on the energy in the immediate vicinity of the dislocation and is given by

$$A=A_0-\frac{\sin2\varphi}{2}-\frac{\sin\varphi\cdot\ln(\sin\varphi)+\cos\varphi\cdot\ln(\cos\varphi)}{\sin\varphi+\cos\varphi} \tag{B.14}$$

where A_0 is the value of A when the boundary is along a crystal axis and is given by

$$A_0=1+\ln[a/(2\pi r_0)]. \tag{B.15}$$

---

[23] E. P. Adams, *Smithsonian Mathematical Formulae and Tables of Elliptical Functions*, p. 129, No. 6.495, Smithsonian Institute, Washington, D. C. (1922).

[24] From (B.5) it is seen that the stress due to the $+y$ dislocations does not vanish except when $\sin4\varphi=0$ or $z=z_1/2$. Thus in the general case there is a net force on the $+x$ dislocations and the assumed dislocation array is not in equilibrium. However, near the boundary a small change in position corresponds to a relatively large change in stress, so that equilibrium could be satisfied by a slight rearrangement of dislocations involving a deviation of the boundary from a straight line. This would have little effect on the stress energy at distances from the boundary comparable to the spacing between dislocations and therefore would not appreciably affect the calculated energy.

[25] The interaction energies per unit area of the grain boundary are, respectively, $(B.6)/D_x$ and $(B.7)/D_y$, and these in general are not equal. However this does not contradict the conservation of energy because these energies represent the work of interaction on the slip planes only; the total interaction energies should include also the work done on the external surfaces by the stresses at infinity, which do not vanish for each set of dislocations individually.

APPENDIX C

Energies of Irregular Arrays

In this Appendix we consider the case of a symmetrical boundary for angles where the spacing of dislocations is not uniform and the energy is not the same for every dislocation. Angles corresponding to average spacings which are simple ratios like 4/3 or 3/2 can be represented by superposing two or more regular arrays of dislocations with different spacings. For instance, the $\varphi=90°$ model for $\theta=41°$ can be represented as the sum of two arrays as follows

$$XXXOXXXO=XOXOXOXO+OXOOOXOO,$$

where X represents a dislocation and O no dislocation and the spacing between the symbols is one plane. The self-energies of the two arrays are readily obtained from Appendix B, since each set alone corresponds to a single boundary with angle of misfit determined by the spacing. To obtain the interaction energy of two regular arrays we determine a general expression for the energy of interaction between a single dislocation on the y axis and a row of dislocations spaced at regular intervals D along the y axis. Taking the origin at one of the dislocations of the regular array, we let $y<D$ be the coordinate of the single dislocation and find the interaction energy as a function of y.

The shear stress due to the regular array is

$$-\mathrm{Re}\,(\pi x/D)\,\mathrm{csch}^2(\pi/D)(x+iy).$$

Integrating with respect to x from r_0, y to R, y where $R\gg D$ gives

$$-\mathrm{Re}\,[\ln 2\sinh(\pi/D)(r_0+iy)-(\pi r_0/D)\coth(\pi/D)(r_0+iy)]$$

which resuces to the usual formula when $y=0$. When $y\gg r_0$, we have

$$\ln 2\sin(\pi y/D).$$

The energy of interaction is therefore negative for $D/6<y<5D/6$ and positive in the interval $\pm D/6$ about each dislocation of the regular array, the distribution being symmetrical about the minimum energy $-\ln 2$ at $y=D/2$.

For the 41° boundary the interaction energy per unit length for the set spaced at $2a$ is $-\frac{1}{4}\ln 2$. This can be checked by comparing with the interaction energy per unit length for the $2a$ spaced set, which is

$$-\tfrac{1}{4}[\ln 2\sin(\pi/4)+\ln 2\sin(3\pi/4)]=-\tfrac{1}{4}\ln 2,$$

the two interaction energies being equal as required by the reciprocal theorem. Adding the interaction energies to the self-energies gives a total energy of 0.86 as compared with 0.75 given by Eq. (5) on the assumption of a regular spacing of $4a/3$.

For $\theta=37°$ the $\varphi=90°$ model is

$$XXOXXO=XOOXOO+OXOOXO.$$

Here the interaction energy per unit length is $(\frac{1}{3})\ln 2\sin(\pi/3)$ for each regular set giving a total energy of 0.83 as compared with 0.73 for a regular spacing of $3a/2$.

APPENDIX D

Energy of Arrays of Screw Dislocations

The screw components give rise to shear stresses τ_{xz} and τ_{yz} acting in the z direction and on both sets of slip planes. There is no interaction between screw and x and y components but the two types of screws interact with one another, since each set of screws gives rise to shear stresses on the slip planes of the other set. Formulas for the self- and interaction energies will be derived and applied to the special case of symmetrical boundaries for both regular and irregular arrays.

The component of displacement w, in the z direction, for a single screw dislocation is given by

$$w=(b/2\pi)\tan^{-1}(y/x), \qquad (D.1)$$

where b is the z component of the slip vector. This formula shows

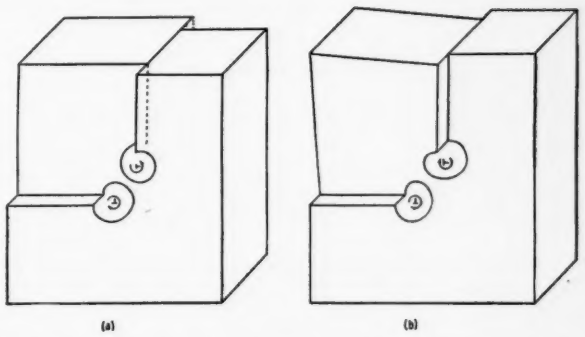

FIG. 11. Interactions between screw dislocations showing that stress fields of unlike dislocations cancel at large distances.

that the elastic behavior of the screw dislocation is the same no matter what slip plane is involved. The stresses due to the dislocation are

$$\tau_{yz}=G\frac{\partial w}{\partial y}=\frac{Gb}{2\pi}\frac{x}{x^2+y^2}$$

$$\tau_{xz}=G\frac{\partial w}{\partial x}=\frac{Gb}{2\pi}\frac{-y}{x^2+y^2}$$

$$\tau_{xy}=0.$$

The calculations of the interaction of screw dislocations is greatly simplified by the fact that one can show a direct correspondence with two-dimensional electrostatic theory. We consider two dislocations with slip vectors b_1 and b_2 and choose two coordinate systems (x_1, y_1) and (x_2, y_2) measured from the dislocations. The energy density in the stress field is then

$$(\tfrac{1}{2}G)(\tau_{xz}^2+\tau_{yz}^2)$$
$$=\frac{1}{8\pi(4\pi/G)}\left[\frac{(2b_1)^2}{r_1^2}+\frac{(2b_2)^2}{r_2^2}+2\frac{2b_1 2b_2}{r_1^2 r_2^2}(x_1x_2+y_1y_2)\right]$$
$$=\frac{1}{8\pi\epsilon}[\mathbf{E}_1+\mathbf{E}_2]^2,$$

where $\mathbf{E}_1$ and $\mathbf{E}_2$ are vectors directed away from the dislocations with magnitudes

$$E_1=2b_1/r_1, \quad E_2=2b_2/r_2$$

and

$$\epsilon=4\pi/G.$$

This shows that the energy density is formally the same as that for two wires with charges per unit length of b_1 and b_2 embedded in a medium with dielectric constant ϵ. We may, therefore, use theorems from electrostatics to calculate the energies of arrays of screw dislocations. (The Taylor type of dislocation cannot be represented in this way, because the u and v displacements are not solutions of Laplace's equation $\nabla^2 u=0$, whereas w is a solution.)

The interaction of two screw dislocations is shown in Fig. 11. It is seen that if the dislocations have opposite signs, their stress fields cancel at distances from them comparable to twice their separations, whereas if they are of the same sign the stress fields add.

The problem of the infinite self-energy of a single dislocation for small distances is again solved by cutting off the integration at such a radius r_0 that the energy inside of the radius at which Hooke's law fails is correctly given. Since the disturbance in a screw dislocation is very different on an atomic scale from that in a Taylor dislocation, the value of r_0 will be different. The same qualitative arguments will apply, however. The use of r_0 corresponds in the electrostatic problem to calculating the energy of charges on the surfaces of hollow cylinders so that the field energy inside the cylinders is negligibly small.

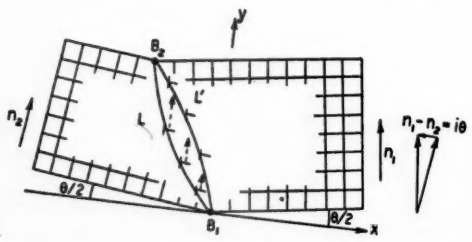

FIG. 12. Displacement of grain boundary by motion of dislocations without relative motion of grains. (y dislocations not shown.)

The potential energy of an array of screw dislocations spaced a distance D apart in a plane will be a minimum when the signs of b alternate corresponding to a grid of alternately changed wires. The potential of such a set of wires must behave as $-(2b/\epsilon)\ln r$ near each plus wire and as $+(2b/\epsilon)\ln r$ near each negative wire. If the wire centers are at $x=0$, D, $2D$, etc., the solution of Laplace's equation which satisfies these requirements and vanishes at large $|y|$ is

$$\text{Real Part of } -(2b/\epsilon)\ln\tan\pi(x+iy)/2D.$$

We shall assume that the dislocations are so far apart that the cylinders of radius r_0 are practically equipotentials; otherwise the approximation that the energies of atomic misfit do not interact is in error. Assuming that, the potential at $x=r_0$, $y=0$ is

$$-(2b/\epsilon)\ln(\pi r_0 2D).$$

The self-energy per dislocation of the array is $(\frac{1}{2})b$ times this potential and the self-energy per unit area, E_s, is $(1/D)$ times this latter:

$$E_s=\frac{1}{D}\frac{b}{2}(2b/\epsilon)\ln 2D/\pi r_0=\frac{Gb^2}{4\pi D}\ln 2D/\pi r_0.$$

In many cases it will not be possible to have the simple alternating scheme of screw components used for calculating E_s. For the $\varphi=0$ and $\varphi=45°$ models, the regularity of the spacing makes it possible and in that case a term of form E_s can be added to E. For small angles both terms are of the form $E\theta(A-\ln\theta)$ and their sum is of the same form, the value of E and A depending on the particular relationship of screw to Taylor components.

If screw dislocations are coupled to the x and y dislocations of the boundary of Fig. 1, the interactions between them will be such as to stabilize the position of the x set in respect to the y set. For example, for the $\varphi=45°$ model, there are equal numbers of x and y dislocations. The most stable arrangement will be that which results in a maximum of cancellation of the screws, Fig. 11, just as if one grid of alternately changed wires were placed next to another so that the changes neutralized. Mathematically, this reduces the screw energy to zero. Physically, it means that the dislocations will draw together until non-linear interactions, which are represented by the r_0 terms, become important.

APPENDIX E

A Theorem on the Displacement of Grain Boundaries for Small θ

Consider two grains whose orientation differs by a small angle θ as shown in Fig. 12. Suppose that at two points B_1 and B_2 on the boundary the two crystals are perfectly in register on the same atom. We wish to show that sliding the set of dislocations which compose the boundary to different places on their slip planes, so as to move the boundary to a new position, does not tend to produce relative shear motion of the two grains. To prove this we consider the number of $+x$ dislocations required for the two positions of the boundary, L and L'. If two unit vectors along the cell edges, as shown, are n_1 and n_2, then the number of $+x$ dislocations will evidently be

$$dS\cdot(n_1-n_2)/a=-dx\cdot\theta/a$$

for small values of θ. Hence, in order to fit the two grains together with the proper number of $+x$ dislocations, the spacing must be θ/a as projected on the x axis. Since sliding the dislocations on their slip planes does not affect this density, slipping the x dislocations from L to L' still leaves the correct density. The same reasoning may be applied to the y dislocations (not shown on Fig. 12). Furthermore, the points B_1 and B_2 are unchanged and are correctly in register for both the distribution of L and L'. Hence the same set of dislocations are the optimum set for both L and L' and, since both L and L' preserve the registration at B_1 and B_2, it is evident that shifting the dislocations from L to L' does not produce relative motion of the two grains.

Any method of moving the boundary connecting B_1 and B_2 to a new position leaves the number of required dislocations of each type unchanged for the entire boundary, but only the sliding of each dislocation on its slip plane preserves the correct number for every segment of the boundary, that is, preserves the correct density.

APPENDIX F

Energy *vs.* Angle Relations for Three Intersecting Boundaries

In this section we obtain the formulas for the energy ratios in a three grain specimen, taking into account the dependence of energy on grain boundary orientation.

Figure 13 shows three grain boundaries intersecting in a line normal to the plane of the drawing at 0. The grain boundary energies are E_1, E_2, and E_3, the angles between boundaries are ψ_1, ψ_2, and ψ_3, and the average orientations of the boundaries with respect to specified crystal axes in the two adjoining grains are φ_1, φ_2, and φ_3.

The energy-angle relations for this case have been derived by C. Herring[26] from the minimum energy principle and in the present notation are given by equations of the form

$$E_1+E_2\cos\psi_3+E_3\cos\psi_2 +\sin\psi_2(\partial E_3/\partial\varphi_3)-\sin\psi_3(\partial E_2/\partial\varphi_2)=0, \quad \text{(F.1)}$$

where the partial derivatives with respect to boundary orientation are measured in the direction of counterclockwise rotation about the intersection.

Equation (F.1) expresses the vanishing of the first-order change of grain boundary energy due to an infinitesimal displacement of the intersection in the plane of the first boundary, it being assumed that the second and third boundaries acquire angles at points separated from 0 by distances which, although still infinitesimal, are large compared to the displacement of 0. Two other equations of which only one is independent are obtained from (F.1) by

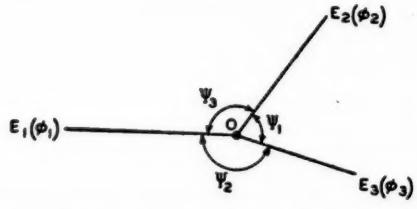

FIG. 13. Three intersecting grain boundaries.

[26] C. Herring, "Surface tension as a motivation for sintering," a paper presented at the Symposium on Physics of Powder Metallurgy, organized by Sylvania Electric Products, Inc., Bayside, Long Island, New York (August 24–26, 1949). Plans have been made to publish the papers of this Symposium in book form.

rotation of subscripts. These equations are satisfied by

$$\frac{E_1}{(1+\epsilon_2\epsilon_3)\sin\psi_1+(\epsilon_3-\epsilon_2)\cos\psi_1}=\frac{E_2}{(1+\epsilon_1\epsilon_3)\sin\psi_2+(\epsilon_1-\epsilon_3)\cos\psi_2}$$
$$=\frac{E_3}{(1+\epsilon_1\epsilon_2)\sin\psi_3+(\epsilon_2-\epsilon_1)\cos\psi_3}, \quad \text{(F.2)}$$

where

$$\epsilon_1=(1/E_1)(\partial E_1/\partial\varphi_1)$$

with similar definitions for ϵ_2 and ϵ_3. When the ϵ's vanish (F.2) reduces to the triangle of forces. When any one of the ϵ's cannot be neglected the triangle of forces gives erroneous values for both of the two independent energy ratios. However if only one boundary, say the first, is near a cusp position so that the other two boundaries have small derivatives with respect to orientation, then (F.1) gives to a good approximation

$$E_1=-E_2\cos\psi_3-E_3\cos\psi_2, \quad \text{(F.3)}$$

where E_2 and E_3 are to be determined from the best fit curve to data obtained from samples where none of the boundaries are near energy cusps. Applying this procedure to Dunn's two specimens each with one boundary near the 70.6° cusp,[27] we obtain 0.77 and 0.78 for the points at 70.5° and 71.5° respectively. As discussed in the text, the triangle of forces gives unreliable values for the energies of the other boundaries in these samples.

For a simple cubic lattice with none of the three boundaries near a cusp position, the ϵ's can be determined by differentiation of (5) of the text, making use of (6) and (7) for the dependence of E_0^* and A on φ. When the variation in A can be neglected, we have

$$\epsilon_1=\frac{\partial}{\partial\varphi_1}\ln E_0(\varphi_1)=\frac{\cos\varphi_1-\sin\varphi_1}{\cos\varphi_1+\sin\varphi_1}=\frac{1-\tan\varphi_1}{1+\tan\varphi_1}$$

with similar expressions for ϵ_2 and ϵ_3. This formula is valid for $0<\varphi<\pi/2$.

[27] C. G. Dunn and F. Lionetti, specimens S10 and S11, reference 8, Table I, p. 128.

Cloud-Chamber Observations of the New Unstable Cosmic-Ray Particles *

A. J. SERIFF, R. B. LEIGHTON, C. HSIAO, E. W. COWAN, AND C. D. ANDERSON
California Institute of Technology, Pasadena, California

(Received March 6, 1950)

Thirty-four "forked tracks" similar to two previously reported by Rochester and Butler have been observed in 11,000 cloud-chamber photographs of cosmic-ray penetrating showers, confirming their conclusion that new unstable neutral and charged particles exist. The lifetime of the neutral particles is found to be about 3×10^{-10} sec., and some information as to the nature of the decay products is given.

1. INTRODUCTION

IN a series of 11,000 cloud-chamber photographs made in a study of penetrating showers, 34 "forked tracks" were observed of the two types previously reported by Rochester and Butler.[1] To interpret these photographs one must come to the same remarkable conclusion as that drawn by Rochester and Butler on the basis of their two photographs; *viz.*, that these two types of events represent, respectively, the spontaneous decay of neutral and charged unstable particles of a new type.

The conclusion that the phenomena actually represent decay processes follows from arguments similar to those previously given by Rochester and Butler. The larger number of events observed in these experiments greatly strengthens these arguments, and thus establishes more firmly the existence of the new unstable particles.

Of our 34 cases, 30 show the decay of a neutral particle resulting in the production of two charged particles, and 4 show the decay of a charged particle resulting in the production of a second charged particle and presumably a neutral particle. We shall refer to these two types of events as decays of the *first* and *second* kinds, respectively. It is possible, of course, that in each type of decay additional neutral particles are also produced.

The cloud chamber used in these experiments was previously employed in measuring the momentum spectrum of the decay particles of μ-mesons.[2] A lead plate 2 cm thick was placed across the horizontal diameter of the chamber, and lead blocks of 20-cm total thickness were placed above the chamber. The chamber, 30 cm in diameter, was in a magnetic field of 6500 gauss, but in the majority of cases track distortions prevent accurate determinations of the momenta of the particles. An arrangement of Geiger counters sensitive to penetrating showers was used to actuate the chamber.

Six decay events (all of the first kind) were observed in 3000 photographs made at Pasadena at 230 meters elevation, and 28 decay events (24 of the first kind and 4 of the second kind) were observed in 8000 photographs made on White Mountain, California, at 3200 meters elevation. Of the Pasadena and White Mountain exposures, about 20 percent and 30 percent, respectively, show showers of penetrating particles; i.e., showers containing two or more roughly collimated, lightly ionizing particles of momentum above 200 Mev/c, of which at least one penetrates the lead plate without evidence of radiative collisions.

Estimates of the specific ionization show that all the charged particles observed in the decay events have a charge equal to that of one electron.

2. DECAY EVENTS OF THE FIRST KIND

A decay of the first kind is characterized by two tracks which form an angle whose vertex is in the gas and whose sides usually extend downward. The angles are distributed between 3.5° and 126°, and are less than 40° in 17 cases. In the great majority of cases the ionization is indistinguishable from the minimum for singly charged particles, and the momenta are above 200 Mev/c. In a few cases, however, especially where the angles are large, the tracks show appreciable curvature and an ionization up to ten times minimum.

Nineteen photographs which show decay events of the first kind also show tracks of additional time-associated particles. In 15 cases, where the orientation of these other tracks determines the position of the nucleon impact in which the particles originated, the orientation of the decay tracks suggests that the unstable neutral particle originated in the same nucleon impact. If the only particles which result from the decay of the unstable neutral particle are the two charged particles which produce the tracks, then the plane defined by these tracks should contain the position of the nucleon impact. In 12 cases this condition is fulfilled within the accuracy of the measurements, but the accuracy is not quite sufficient to rule out the possibility that neutral particles are produced in decays of the first kind.

In one decay of the first kind in which the track of one of the secondary particles was unusually long and of high curvature, the observed ionization and the curvature in the magnetic field place the mass of the particle between 150 m_e (electron masses) and 350 m_e. In five other cases it was similarly found that the mass of one of the particles is less than that of a proton. In

* Supported in part by the joint program of the ONR and the AEC.

[1] G. D. Rochester and C. C. Butler, Nature **160**, 855 (1947).

[2] Leighton, Anderson, and Seriff, Phys. Rev. **75**, 1432 (1949).

no case could limits be placed on the mass of *both* charged secondary particles by this method.

In six decays of the first kind in which secondary particles penetrate the 2-cm lead plate, including three cases in which both secondary particles penetrate the plate, there is no evidence of the production of electron secondaries through radiative collisions. Since the particles all had high momenta, this indicates that neither of the charged decay products is as light as an electron.

The angle of scattering of eight of the secondary particles in the 2-cm lead plate is 10° or less, but in one case an angle of 35° was observed. Since the latter angle can hardly be attributed to Coulomb scattering, a strong nuclear interaction is indicated. The fact that another of the particles is observed to produce a disintegration in the lead plate is additional evidence of a strong nuclear interaction. Two nuclear events in ten traversals of the lead plate correspond to a cross section in lead of about 10^{-24} cm^2. However, there is as yet no evidence that *both* secondary particles have strong nuclear interaction.

The above results do not serve to identify completely the two charged particles which result from the decay of the unstable neutral particles. In terms of known particles, possibilities are (a) two π-mesons, (b) a π- and a μ-meson, or (c) a proton and a meson (π or μ).

The mass of the unstable neutral particles can in principle be calculated on the assumption that only two particles are produced in the decay. Actually, in each case, because of limitations in the determination of momentum, only upper and lower limits could be placed on the mass. Even within these limits it has not been possible so far to find a single value of the mass consistent with all the cases. However, in no case do the data require the mass of the neutral particle to be more than 250 m_e above the sum of the masses of the decay products if these are both mesons, or more than 400 m_e above the sum of the masses if one of the products is a proton. It is possible that the inconsistencies in the mass value may be removed by more complete measurements; of course, the mass calculated in this way cannot be expected to have a single value if neutral secondaries also result from the decay, or if the unstable neutral particles observed have several different masses, such as might be imagined to correspond to different "excited states" of a neutron.

The distribution of the decay points along the lines of flight of the neutral unstable particles was used to estimate the rest lifetime of these particles. Allowance was made for the variation in path length resulting from the geometry of the cylindrical chamber, and the relativistic time dilatation factor was estimated for each case. The mean rest lifetime so obtained is $(3\pm2)\times10^{-10}$ sec.

This lifetime, and the geometry of the apparatus, then permit one to estimate that about 1/10 of the unstable neutral particles produced in the lead blocks, whose lines of flight pass through the chamber, decay inside the chamber. Thus there must have been about 300 such unstable particles produced in the same events which gave rise to the 10,000 ionizing penetrating-shower particles observed in the same series of photographs. That is, the number of unstable neutral particles produced in penetrating showers is about 3 percent of the number of ionizing particles.

3. DECAY EVENTS OF THE SECOND KIND

A decay event of the second kind is characterized by the appearance of a sharp deflection in a track having small curvature, without the appearance of a recoil track. This has been interpreted[1] as showing the decay of a charged particle at the deflection point. In the four cases so far observed, the values of the angular deflection between the two segments of the track are 7°, 15°, 34°, and 40°. In all the decays of the second kind the tracks are short and only a lower limit of 200 Mev/c can be placed on the momenta. In one case, the charged secondary particle penetrates the 2-cm lead plate with no indication of a radiative collision in the plate. This observation and a similar one by Rochester and Butler indicate that the mass of the charged secondary particle is greater than that of an electron.

If the two types of unstable particles had the same mean lifetime, then for each type the number observed to originate in the lead above the chamber and the number observed to originate in the plate inside the chamber should be approximately in the same ratio. Actually, this ratio is quite different for the two types, being 25:5 for decays of the first kind and 1:3 for decays of the second kind. The relative paucity of unstable charged particles observed to originate in the lead blocks indicates that these particles have a shorter mean lifetime than the neutral particles, and are therefore more likely to decay before traversing the distance (about 15 cm) between the lead blocks and the chamber than are the neutral particles. On the other hand, the approximate equality of the number of each kind of particle observed to originate in the lead plate (3 charged *vs.* 5 neutral) suggests that the two kinds of unstable particles are produced in comparable numbers.

It is a pleasure to acknowledge the assistance given by the Naval Ordnance Test Station, China Lake, California in the use of their facilities on White Mountain.

Letters to the Editor

PUBLICATION of brief reports of important discoveries in physics may be secured by addressing them to this department. The closing date for this department is five weeks prior to the date of issue. No proof will be sent to the authors. The Board of Editors does not hold itself responsible for the opinions expressed by the correspondents. Communications should not exceed 600 words in length.

Velocity Dependent Nuclear Interactions*

C. H. BLANCHARD, R. AVERY, AND R. G. SACHS
University of Wisconsin, Madison, Wisconsin
March 21, 1950

RECENT consideration of the relationship between nuclear shell structure and a j–j coupling scheme[1] suggests the investigation of nucleon-nucleon interactions which give spin-orbit coupling directly. Invariance requirements, in non-relativistic theory, limit the possible interactions linear in the nucleon momenta to the forms[2]

$$J(|\mathbf{r}_j-\mathbf{r}_k|)[(\mathbf{r}_j-\mathbf{r}_k)\times(\mathbf{p}_j-\mathbf{p}_k)]\cdot\begin{cases}(\boldsymbol{\sigma}_j+\boldsymbol{\sigma}_k)\begin{cases}\frac{1}{2}(\tau_{j3}+\tau_{k3}) & (1)\\ \frac{1}{2}(1+\tau_{j3}\tau_{k3}) & (2)\\ \frac{1}{4}(3+\boldsymbol{\tau}_j\cdot\boldsymbol{\tau}_k) & (3)\\ \frac{1}{2}(1-\tau_{j3}\tau_{k3}) & (4)\end{cases}\\ (\boldsymbol{\sigma}_j-\boldsymbol{\sigma}_k)\quad \frac{1}{2}(\tau_{j3}-\tau_{k3}) & (5)\\ [\boldsymbol{\sigma}_j\times\boldsymbol{\sigma}_k]\quad \frac{1}{2}[\boldsymbol{\tau}_j\times\boldsymbol{\tau}_k]_3. & (6)\end{cases}$$

Each of these interactions evidently gives spin-orbit coupling directly. The purpose of this letter is to report the results of a brief preliminary investigation of the effects of these forces in the nuclei H^2, H^3, and He^3.

None of the interactions can affect low energy nucleon-nucleon scattering since each transforms like a P function and each conserves relative orbital angular momentum. Hence none of them can couple an incoming S wave either to an S wave or to a wave of higher L. Appreciable effects on high energy scattering are to be expected, however, with possible differences between $N-P$ and $P-P$ scattering resulting from the isotopic spin dependence of the interactions. Because they transform like P functions, none of the interactions can contribute to the binding energy of a nucleus in an S state or in an $S-D$ cross term. Only (4) can contribute to the binding energy of H^2 (and this only in the $D-D$ term), and hence affect the wave function; (1) and (2) cannot because they vanish between unlike nucleons; (3) vanishes in a singlet isotopic spin state; (5) and (6) give no contribution since an antisymmetric spin operator must have a zero average value in a symmetric spin state. Thus the D state contribution of (4) remains as the only possible effect of any of the interactions (1) to (6) on the deuteron. In H^3 and He^3, the first four interactions can contribute to D state binding; (5) and (6) cannot, because of the spin symmetry of a quartet state. Any of the six interactions can introduce P state in H^3 and He^3 through direct coupling with the S state. Kinetic energy considerations, however, suggest that even if these forces are comparable in strength to the central and tensor forces, the wave functions will still be mostly S state.

Owing to their velocity dependence, each of the interactions introduces contributions to nuclear magnetic moments which are additional to the spin and orbital moments of the individual nucleons. These "interaction moments" arise because, on the introduction of an external magnetic field, the operator corresponding to the momentum of the kth nucleon is modified by the substitution $\mathbf{p}_k\rightarrow\mathbf{p}_k-(e/c)\frac{1}{2}(1-\tau_{k3})\mathbf{A}(\mathbf{r}_k)$. Thus the average of the energy of interaction between nucleons contains a term, U, linear in the field, which gives the interaction of an additional moment, $\mathbf{M}_I$, with the field: $U=-(\mathbf{M}_I\cdot\mathbf{H})$.

The H^2 moment is well accounted for by spin and orbital moments, so we assume that no large interaction moment in this nucleus can be tolerated. In H^3 and He^3 there are equal and opposite anomalies[3] of the order of 0.27 n.m. We have estimated the S state interaction moments in these three nuclei for each of the interactions (1) to (6), when introduced with a strength and range comparable to those of the usually assumed forces. The interaction moments of (1), (2), and (3) vanish for the S states of all three nuclei. The interaction moments arising from (5) and (6) can account for the observed anomalies of H^3 and He^3 while giving no contribution to the H^2 moment. The contributions of (4) to the H^3 and He^3 moments, while of the order of the anomalies, are of the *same* sign for the two nuclei and thus incapable of accounting for the anomalies; (4) also gives an appreciable contribution ($\approx$0.25 n.m.) in H^2.

These results may be used to discard interaction (4) as a possibility. As has been shown, the remaining interactions cannot affect the H^2 wave function. The interactions (5) and (6), which can account for the moment anomalies, both vanish between like particles; they differ only in a space exchange factor, since on eliminating the isotopic spin notation they may be written

$$J(|\mathbf{r}_N-\mathbf{r}_P|)[(\mathbf{r}_N-\mathbf{r}_P)\times(\mathbf{p}_N-\mathbf{p}_P)]\cdot(\boldsymbol{\sigma}_N-\boldsymbol{\sigma}_P)\begin{cases}1 & (5')\\ P_{NP^3} & (6')\end{cases}.$$

From these considerations one can conclude that velocity dependent interactions are worthy of serious consideration in phenomeneological studies of nuclear processes. The introduction of one or more of them may aid in understanding: (1) the strong spin-orbit coupling indicated by nuclear shell structure, (2) nuclear magnetic moment anomalies, (3) high energy $N-P$ scattering data,[4] (4) the differences between high energy $N-P$ and $P-P$ scattering.[5]

* This work was supported in part by the AEC.
[1] M. G. Mayer, Phys. Rev. **75**, 1969 (1949); Haxel, Jensen, and Suess, Phys. Rev. **75**, 1766 (1949).
[2] E. P. Wigner, Phys. Rev. **51**, 106 (1937); L. Eisenbud and E. P. Wigner, Proc. Nat. Acad. Sci. **27**, 281 (1941).
[3] R. Avery and R. G. Sachs, Phys. Rev. **74**, 1320 (1948).
[4] R. S. Christian and E. W. Hart, Phys. Rev. **77**, 441 (1950).
[5] H. P. Noyes, Phys. Rev. **77**, 90 (1950).

Deuteron-Proton Scattering at 10 Mev*

K. B. MATHER,† H. J. KARR,‡ AND R. O. BONDELID
Physics Department, Washington University, St. Louis, Missouri
March 16, 1950

THE coincidence scattering chamber referred to in an earlier communication[1] has been applied to the determination of absolute differential cross sections for the elastic scattering of deuterons by protons. Deuterons were accelerated to 10.0±0.2 Mev by the Washington University cyclotron. The scattering media were Nylon and polythylene-terephthalate foils.

In view of the present interest in the d–p interaction, a preliminary report is being made here for angles from 45° to 155° in the center of mass system. Complete publication covering a wider range of angles will be made shortly. Further work, with a photographic scattering chamber in which protons are scattered from deuterium gas is nearing completion.

Table I lists absolute cross sections $\sigma(\theta)$ in the c.m. system as a

TABLE I. Absolute cross sections in c.m. coordinates for deuteron-proton scattering.

θ	$\sigma(\theta)\times10^{25}$ cm² sterad.$^{-1}$
45°	1.78
55	1.55
65	1.32
75	1.10
85	0.89
95	0.71
105	0.59
115	0.57
125	0.68
135	0.97
145	1.46
155	2.09

function of angle θ. These values were derived from a smooth curve drawn through the actual experimental points. As reported here, the data are believed to be correct to within about six percent.

Comparison of our data with the theoretical cross sections of Buckingham and Massey[2] for the energy of our experiment indicates that while agreement is reasonable over a large range of angles considerable departures set in at large angles, the experimental cross sections being much larger than the theoretical beyond about 140°.

* This work was assisted by the joint program of the ONR and the AEC.
† Now associated with the University of Birmingham, Birmingham, England.
‡ Now associated with the Los Alamos Scientific Laboratory, Los Alamos, New Mexico.
[1] Bondelid, Bohlman, and Mather, Phys. Rev. **76**, 865 (1949).
[2] As yet unpublished. This work is an extension of the $n-d$ scattering theory by Buckingham and Massey. We are indebted to Professor Massey for communicating his data to us.

Absorption Bands and Luminescence of LiF Irradiated at Low Temperature

PETER PRINGSHEIM AND PHILIP YUSTER
Argonne National Laboratory, Chicago, Illinois
March 13, 1950

WHEN LiF crystals are exposed at liquid N_2 temperature to x-rays or 1-Mev electron bombardment, in addition to the F-band with peak at 2420A, a band with peak at 3400A is produced in the absorption spectrum. After relatively short exposure to the primary irradiation the peaks of the two bands are of nearly the same height, while the band at 3400A is about twice as wide as the F-band (1.2 ev instead of 0.65 ev at −195°C). With increasing exposure to the primary irradiation, the band at 3400A seems to approach saturation value while the peak of the F-band continues to grow.[1] When the crystal is warmed up from −195° to −135°C and is kept at this temperature, the band at 3400A disappears from the spectrum, while the F-band does not lose more than 50 percent of its initial intensity even when the crystal is warmed to room temperature. By irradiating the crystal at −195°C with light of wave-length 3650A the band at 3400 is almost completely bleached out without change in the F-band (Fig. 1).

The warming up of the samples from −195° to −100°C is accompanied by the emission of a blue luminescence exhibiting in its "glow curve" a single peak at −135°C (Fig. 2) as has been stated also by Ghormley.[2] The end of this luminescence emission coincides with the disappearance of the band at 3400A in the absorption spectrum. If this band is bleached out by irradiation with light of wave-length 3650A before the warming-up process, the shape of the glow curve remains unchanged, but the total light sum is reduced to about 12 percent of its former value. The behavior is not altered if the bleaching light is filtered through a Pyrex glass transmitting the radiation of a high pressure Hg arc down to 3000A. If the filter is replaced, however, by another transmitting some light of wave-lengths down to 2900A the light sum in the glow curve is cut down to about 1 or 2 percent (curves 2 and 3 in Fig. 1), while the peak of the F-band is only slightly affected. Thus it is proved that the energy for the "thermoluminescence" in the temperature range from −190 to −100°C is not provided in the main by the disappearance of F-centers, but is intimately related to the disappearance of the hitherto unknown band at 3400A. There is good reason, however, to believe that the absorption with peak at 3400A is not due to a single band but to the superposition of at least two bands.

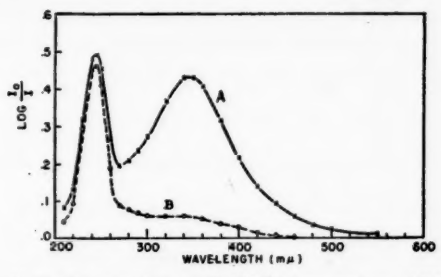

FIG. 1. Absorption spectrum at liquid N_2 temperature of LiF-crystals exposed to x-rays for 15 min. at liquid N_2 temperature. Curve A: without further treatment. Curve B: after bleaching 1 hour at liquid N_2 temperature with 3650A light.

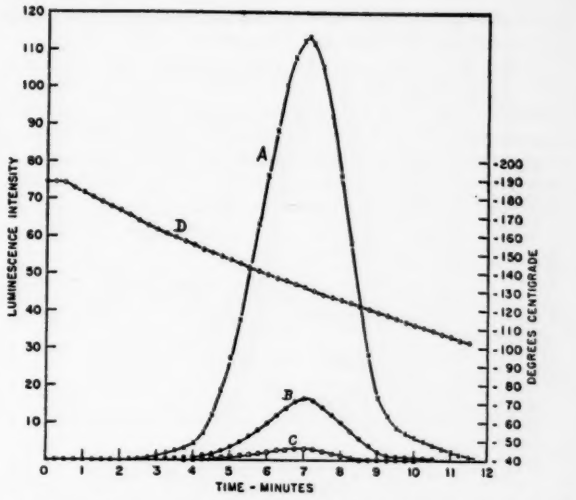

FIG. 2. Glow curves of LiF crystals exposed to x-rays for 15 min. at liquid N_2 temperature. Curve A: without further treatment. Curve B: bleached 1 hour with 3650A light from AN-6 Hg-arc. Curve C: bleached 20 min. with light from AN-6 Hg-arc transmitted through 2.6-mm Pyrex glass. Curve D: temperature *versus* time.

When, after warming up to room temperature, the band at 3400A of a heavily bombarded crystal has completely disappeared, the crystal slowly acquires a deep blue color due to the formation of a new band with peak at 6200A which is quite stable at −195°C. At room temperature, however, this band gives way to a narrow band with peak at 4450A so that the color of the crystal changes from blue through green to yellow. When this stage is reached no further changes occur in the optical properties of the crystal even when it is kept in full daylight at room temperature for several weeks.[3]

[1] Casler, Pringsheim, and Yuster, Argonne National Laboratory, 3rd Quarterly Report (1949), ANL-4380 (pertinent material unclassified).
[2] J. A. Ghormley, Oak Ridge National Laboratory, 3rd Quarterly Report (1949), ORNL-499.
[3] R. Casler and P. Pringsheim, Argonne National Laboratory, 1st Quarterly Report (1948), ANL-4204 (pertinent material unclassified).

Microwave Absorption Spectra of POF_3*,†

SAMUEL J. SENATORE
K-25 Laboratories, Carbide and Carbon Chemicals Division, Union Carbide and Carbon Corporation, Oak Ridge, Tennessee
March 13, 1950

THE lowest rotational transition of the POF_3 rotational spectrum ($J=0\rightarrow1$, $K=0$, $v=0$) has been observed in Stark fields as high as 9.26 e.s.u. With these high fields, the line is shifted 330 Mc/sec. No departure from the expected quadratic Stark law has been observed with these high fields. The line frequency may be given by the expression

$$\nu=9186.99(\pm0.04)+3.507E^2(\text{Mc/sec.}),$$

where the applied electric field is given in e.s.u. This yields a B_0 value of 4593.50±0.02 Mc/sec. and a dipole moment of 1.735 Debye units. The uncertainty in the Stark electrode spacing contributes the overwhelming portion of the probable error in the

evaluation of the dipole moment although this uncertainty should not exceed two percent.

If the PF_3 group in the POF_3 molecule is assumed to have the same dimensional configuration as was assumed for the PF_3 molecule[1] itself, the PO distance computed on the basis of the observed moment of inertia is 1.85A. This abnormally large value suggests that either the configuration of the PF_3 group in these two molecules differs, or that the FPF angle of $104\pm3°$ assumed by Gilliam, Edwards, and Gordy is too large.

While the $J=2\rightarrow3$ transition has been observed, measurements on this line have not been completed.

* This paper is part of a thesis submitted to the University of Tennessee in partial fulfillment of the requirements for a master of science degree in physics. The writer is indebted to Dr. D. F. Smith for his valuable assistance and guidance.

† This document is based on work performed for the Atomic Energy Commission by Carbide and Carbon Chemicals Division, Union Carbide and Carbon Corporation, at Oak Ridge, Tennessee.

[1] Gilliam, Edwards, and Gordy, Phys. Rev. **75**, 1014 (1949).

β-Decay and the Nuclear Shell Model

L. W. NORDHEIM
Duke University, Durham, North Carolina
February 27, 1950

THE application of the nuclear shell model[1–4] leads to an almost complete understanding of the allowed or forbidden character of β-decays. The results find their simplest expression in the spin-orbit coupling scheme.[3,4]

For *odd-A* nuclei the following rules can be formulated:[5]

(1) The straggling of ft values is much reduced when the transitions are sorted out according to type.

(2) The mirror nuclei for a very distinct super-allowed group.

(3) Normal allowed transitions are those in which the assigned orbital momentum is unchanged, irrespective whether $\Delta I=0$ or 1 (i.e., Gamow-Teller selection rules). The values of $\log(ft)$ range mostly from 4.8 to 5.5.

(4) Transitions with $\Delta L=2$, $\Delta I=1$ (allowed according to G.T. rules) have definitely higher ft values, comparable to the first forbidden group.

(5) Transitions with $\Delta L=1$ (i.e., change in parity) and $\Delta I=0, 1$ are first forbidden with $\log(ft)$ mostly in the range 6.5 to 7.5, but with some stragglers.

(6) Transitions with $\Delta L=1$; $\Delta I=2$ have definitely higher $\log(ft)$ values, mostly between 8 and 9 (compare Shull and Feenberg, reference 5).

(7) Higher forbidden transitions have $\log(ft)$ values >9.

(8) There is no discernible trend towards higher ft values with increasing mass number.

There are some ambiguities in the interpretations, but no direct contradictions in over 100 cases where sufficient information is available.

The *even-A* nuclei present a somewhat more complex situation. The even-even nuclei have, to all our knowledge, zero spin, while in odd-odd nuclei there is a coupling of neutron and proton groups each with spins.

In the cases where the transition goes to the ground state, the, say, odd neutron is transformed into a proton which has to pair up with the already present odd proton to give zero spin. The orbital assignments can then be taken from the data on odd-A nuclei. If this is done, the ft values fall into exactly the same classification as given. This demands that in this class of transitions the spins of the neutron and proton groups must have antiparallel orientations, giving minimum resultant spin.

There is another class of nuclei in which one must assume the resultant spin to be high (compare Na^{22}, Lu^{176}). They are characterized by decay schemes with series γ-rays sometimes of great complexity. The following empirical rule distinguishes the nuclei which belong to the two classes.

(9) If the odd proton and neutron groups have different relative orientation of intrinsic spin and orbital momentum (that is, $I_1=L_1+1/2$; $I_2=L_2-1/2$) then the total spin is $|I_1-I_2|$. If they have the same relative orientation (that is, both $I=L+1/2$ or both $I=L-1/2$), then they combine to a high resultant spin.

This rule can also be expressed by saying that the intrinsic spins of the odd proton and neutron line up parallel as in the deuteron under maintenance of the j–j coupling. It cannot yet be decided, however, whether the neutron and proton spins in the high class are actually parallel.

The rule is confirmed in about 60 clear cases. The two exceptions are Li^6, which should have spin 3 like B^{10}, and K^{40} whose $D_{3/2}F_{7/2}$ configuration should give spin 2, while 4 is observed and required to explain its lifetime.

The existence of rule 9 shows that the neutron and proton configurations in odd-odd nuclei are largely independent of each other. The same conclusion is indicated by the persistence of the isomeric rule[1,2] for odd-odd nuclei, which suggests strongly that most isomeric states are due to competition of orbits within one group (protons or neutrons) while isomerism produced by a large resultant spin of neutrons and protons seems to be comparatively rare.

An extensive paper showing the complete material on β-decay is in preparation.

[1] E. Feenberg and K. C. Hammack, Phys. Rev. **75**, 1877 (1949).
[2] L. W. Nordheim, Phys. Rev. **75**, 1894 (1949).
[3] M. G. Mayer, Phys. Rev. **75**, 1969 (1949); (material to be published).
[4] Haxel, Jensen and Suess, Phys. Rev. **75**, 1766 (1949).
[5] Based on independent surveys with substantially the same results by M. G. Mayer and S. Moszkowski, and the author. The latter's work covers also even-A nuclei. The findings of Feenberg and Hammack, reference 1, and F. B. Shull and E. Feenberg, Phys. Rev. **75**, 1768 (1949), are also in complete agreement with the rules given here.

Theories of High Values of Alpha for Collector Contacts on Germanium

W. SHOCKLEY
Bell Telephone Laboratories, Murray Hill, New Jersey
March 17, 1950

THE collector point contact of a type-A transistor shows current multiplication in the sense that a hole arriving at the collector may lead to the emission of (α_i-1) extra electrons where α_i is the intrinsic α of the collector. Experimental evidence indicates that values of α_i at least as large as 10 occur.

Bardeen and Brattain have proposed that the space charge of holes passing through the barrier layer produces an increase in electron current through an enhanced field emission effect.[1] While this theory explains values of α frequently observed, it is limited to values of (α_i-1) not much larger than b, where b is the ratio of electron mobility to hole mobility moving through the barrier. This limit is set by the condition that for this value of (α_i-1), the added electron charge density would cancel the hole charge density leaving no net charge to enhance the field emission.[2] This leads to a maximum value of 3 for α_i using J. R. Haynes' value of 1700 and 3600 cm²/volt-sec. for the drift mobilities. Patch effects may raise this value somewhat, but not up to the larger experimental values.

Generation of secondary electrons by energetic holes has been proposed. This can be rejected because of the low collector voltages observed by W. G. Pfann[3] required to produce high α values and the stability, rather than exponential increase, of α with increasing collector voltage.

Two theories are presented below, both based on mechanisms using the charge of the holes.

Trap theory. If the barrier region contains a density of traps capable of holding holes, then in effect the value of b will be increased in this region and the hole space charge enhanced.

p–n hook theory. We shall describe this theory in connection with its possible application in p–n–p transistors.[4] Suppose that there is a thin layer M (for "multiplying") of p-type material

separating the collector region C, taken to be n-type from the base B. This base-collector structure resembles an n–p–n transistor, similar to a p–n–p transistor. Holes arriving at M will be held by a "hook" in the potential energy curve and will bias the p–n junction M–C forward and provoke an electron flow from C into M. If M is thin, the electrons will diffuse through it and fall through the potential drop across B–M; B–M is an n–p junction biased in reverse by the collector voltage. The theory of p–n–p transistors can be applied to this process and it can be seen that very high values of α can arise in this way.

I am indebted to many of my colleagues for discussions of theories and experiments related to high values of α.

[1] J. Bardeen and W. H. Brattain, Phys. Rev. **75**, 1208 (1949).
[2] This reasoning is very similar to that of L. P. Hunter, Phys. Rev. **77**, 558 (1950).
[3] W. G. Pfann, personal communication.
[4] W. Shockley, Bell Sys. Tech. J. **28**, 435 (1949).

Internal Conversion Coefficients for Co^{60}

M. A. Waggoner, M. L. Moon, and A. Roberts
Department of Physics, State University of Iowa, Iowa City, Iowa
March 9, 1950

RECENTLY several papers[1,2] have appeared in which the results of elaborate calculations of internal conversion coefficients are given. These are believed to be accurate to a few percent. It was our purpose in undertaking this investigation to attain sufficient accuracy in the experimental determinations to provide a significant test of the theory. For this reason we selected for our first experiments Co^{60} for which the gamma-rays are known to be quadrupole from angular correlation experiments.[3]

The measurements were made by means of a double-coil, thin-lens spectrometer in which considerable care had been taken to reduce the background due to scattering. For the setting used in these experiments the transmission was 2.40 percent and the half-width about 3.0 percent. Since it was necessary for us to use sources of slightly different diameters (ranging from 4.45 to 5.50 mm) we calibrated half-width against source diameter and found a slight increase with source diameter. Accurate knowledge of the half-width is essential to the integration of the β-spectrum. In measuring the transmission of the spectrometer we used the β-spectrum of several Co^{60} sources which had been calibrated by coincidence measurements. Because of window effects our data were not good below about 120 kev and we reconstructed the momentum plot by extrapolating to zero the straight Fermi plot (allowed) observed at higher energies. The end point for the β-spectrum was found to be 318.7 ± 4.0 kev. The Co^{60} used was high specific activity material obtained from the Oak Ridge National Laboratory and was mounted on a 3-ply laminated backing (zapon-Formvar-zapon) and then covered with a single zapon film. Each of these films was less than 30 $\mu g/cm^2$. The three strongest sources were less than 0.20 mg/cm^2; the other three used, less than 0.016 mg/cm^2. Effects due to source charging were eliminated. The spectrometer was calibrated against the crystal spectrograph values[4] for the Co^{60} gamma-ray lines.

The values we obtain for the coefficients of conversion in the K, L, M shells together (unresolved) for the two gamma-rays from Co^{60} and the theoretical values[1] of the conversion coefficients for electric quadrupole radiation in the K shell are shown in Table I.

For all other types of radiation the conversion coefficients differ from those for EQ by a factor of at least two. Supposing the $L+M$ conversion and screening effects to contribute about 10 percent, our results classify both gamma-rays as electric quadrupole. Comparison with angular correlation measurements[3] then fixes the spins and parities of the three nuclear levels involved as: 0, 2, 4; same (even).

Although agreement between theory and experiment seems quite good, more exact comparison cannot be made until the theoretical values for the effects of $L+M$ conversion and screening have been calculated. The present results are in agreement with those published by Deutsch and Siegbahn[5] within the relatively large error of the latter; however, the classification of both gamma-rays now seems unambiguous.

TABLE I. Internal conversion in excited states of Ni^{60}.

E (Mev)	$\alpha_{exp}\times10^4$	Theoretical value: $\alpha_K^{(2)}\times10^4$
1.1715	1.733 ± 0.061	1.545
1.3316	1.286 ± 0.035	1.175

[1] Rose, Goertzel, Spinrad, Harr, and Strong, Phys. Rev. **76**, 184 (1949).
[2] J. R. Reitz, Phys. Rev. **77**, 10 (1950).
[3] E. L. Brady and M. Deutsch, Phys. Rev. **74**, 1541 (1948).
[4] Lind, Brown, and Du Mond, Phys. Rev. **76**, 591 (1949).
[5] M. Deutsch and K. Siegbahn, Phys. Rev. **77**, 680 (1950).

Comment on Mobility Anomalies in Germanium

G. L. Pearson, J. R. Haynes, and W. Shockley
Bell Telephone Laboratories, Murray Hill, New Jersey
March 17, 1950

IT appears probable that the simple theory of spherical energy surfaces in the Brillouin zone for both holes and electrons in germanium may have to be modified in view of experimental results on mobility and magneto-resistance.

In this letter we shall quote the results of three methods of determining mobility:

Drift mobility. The technique of obtaining the mobility of injected current carriers in germanium by the direct measurement of their transit times over known distances and under the influence of known electric fields has been improved so that measurements with an error of less than 5 percent are obtained. This improvement over earlier equipment[1,2] consists largely in the substitution of pulse techniques for d.c. measurements leading to an unambiguous determination of transit time. The measurements include data on samples of both n- and p-type single crystals as well as on crystals grown by different techniques.

Hall mobility. Only under certain simplifying assumptions is $(8/3\pi)R\sigma$ theoretically equal to the mobility. We shall refer to the experimentally determined value of $R\sigma$ as the *Hall mobility*. Hall mobilities were obtained using the identical samples described above, excepting that the electron mobility values were obtained on n-type material and hole mobility on p-type, the reverse of the drift experiment. The most probable values for $(8/3\pi)$ times the Hall mobility are 1700 cm^2/volt-sec. for holes and 2600 cm^2/volt-sec. for electrons[3] although the experimental accuracy of this method is equal to that of the drift method, the spread in mobility values from sample to sample is much larger, being 1600 to 2200 cm^2/volt-sec. for holes and 2400 to 2900 cm^2/volt-sec. for electrons. (We do not find the large spreads or very high values reported by Dunlap.[4])

Conductivity mobility. Samples of germanium with radioactively determined concentrations of added antimony were found to have a conductivity which was linear in the added antimony and corresponded[5] to the mobility given in Table I. The experimental uncertainty in this work was quite large, due in part to grain boundary effects for which corrections were attempted. Agreement between drift and conductivity mobility is to be expected unless electron-hole collisions are important or appreciable trapping is involved, neither of which is probable for germanium.

TABLE I. Mobilities in cm^2/volt-sec. in germanium.

	$(8/3\pi)\times$Hall mobility	Drift mobility	Conductivity mobility
Electrons	2600 ± 300	3600 ± 180	3350 ± 400
Holes	$1700+500-100$	1700 ± 90	——

An interpretation, planned for later publication, of the Hall coefficient formula[6a] shows that the Hall mobility may be much

less than the drift mobility for re-entrant energy surfaces like those possible for degenerate energy bands[6] and, in fact, may even change sign.

Further evidence that the energy bands are not spherical is furnished by the large and anisotropic magneto resistance effects in germanium single crystals.[7]

We are indebted to Drs. J. Bardeen and F. Seitz for helpful discussions of the theory.

[1] J. R. Haynes and W. Shockley, Phys. Rev. **75**, 691 (1949).
[2] Shockley, Pearson and Haynes, Bell Sys. Tech. J. **28**, 344 (1949).
[3] G. L. Pearson, Phys. Rev. **76**, 179 (1949).
[4] W. C. Dunlap, Jr., Phys. Rev. **77**, 759 (1950).
[5] Pearson, Struthers and Theuerer, Phys. Rev. **75**, 344 (1949); **77**, 809 (1950).
[5a] A. H. Wilson, *The Theory of Metals* (Cambridge University Press, London, 1936), Eq. (362).
[6] W. Shockley, Phys. Rev. **78**, 173 (1950).
[7] G. L. Pearson and H. Suhl, to be reported at Oak Ridge meeting.

l-Type Doubling in OCS and HCN

H. H. NIELSEN
Mendenhall Laboratory of Physics, Ohio State University, Columbus, Ohio
March 20, 1950

THE two components of the rotation-vibration states of a linear molecule in an excited perpendicular vibration level are separated by *l*-type doubling, l being the quantum number of angular momentum so that $l=V, V-2, \cdots 0$ or 1). The doubling is predicted by theory[1] to be $\Delta\nu=qJ(J+1)$ where $q=q_0(V_s+1)=(B_e^2/\omega_s)[1+4\sum_{s'}\xi_{ss'}^2\lambda_s/(\lambda_{s'}-\lambda_s)](V_s+1)$ when $|l|=1$, ω_s being the degenerate vibration frequency and $\xi_{ss'}$ the Coriolis coupling factors. Recent measurements by Shulman and Townes[2] have shown that q is, indeed, proportional to (V_s+1), thereby verifying one phase of the theory of *l*-type doubling. Calculations on the quantities q_0 for comparison with experimental values have been impeded largely because of the complicated nature of $\xi_{ss'}$. We shall report in this letter on the evaluation of q_0 for two molecules, namely OCS and HCN.

The quantities $\xi_{ss'}$ have been determined by A. H. Nielsen[3] for the linear XYZ molecule. He gives the following values

$$\xi_{21}=-[M_1M_3/\sigma I^{(e)}]^{\frac{1}{2}}(Z_1^0-Z_3^0)\cos\gamma-[M_2\Sigma/\sigma I^{(e)}]^{\frac{1}{2}}Z_2^0\sin\gamma$$

and

$$\xi_{23}=[M_1M_3/\sigma I^{(e)}]^{\frac{1}{2}}(Z_1^0-Z_3^0)\sin\gamma-[M_2\Sigma/\sigma I^{(e)}]^{\frac{1}{2}}Z_2^0\cos\gamma,$$

where M_2 is the central atom, $\sigma=M_1+M_3$, $\Sigma=M_1+M_2+M_3$, Z_i^0, the equilibrium values of the coordinates and

$$\left.\begin{matrix}\sin\gamma\\ \cos\gamma\end{matrix}\right\}=\pm 2^{-\frac{1}{2}}\{1\pm[(k_1-k_3)^2(4k_4^2-(k_1-k_3)^2)]^{\frac{1}{2}}\}.$$

The constants k_i are defined as follows: $k_1=\mathfrak{K}_1/\mu_1^{\frac{1}{2}}$, $k_3=\mathfrak{K}_3/\mu_3^{\frac{1}{2}}$, $k_4=\mathfrak{K}_4/(\mu_1\mu_3)^{\frac{1}{2}}$ with $\mu_1=M_1M_3/(M_1+M_3)$ and $\mu_3=M_2\sigma/\Sigma$ and $\mathfrak{K}_1=\{K_1(M_3/\sigma)^2+K_2(M_1/\sigma)^2\}$, $\mathfrak{K}_3=K_1+K_2$, $\mathfrak{K}_4=\{-K_1(M_3/\sigma)+K_2(M_1/\sigma)\}$, where K_i are the valence force constants of $2V=K_1\delta Q_1^2+K_2\delta Q_2^2$ in which $\delta Q_1=Z_2-Z_1$, and $\delta Q_2=Z_3-Z_2$. One may, moreover, quickly show that $\sum_{s'}\xi_{ss'}^2=1$.

The force constants K_1 and K_2 used in this calculation have been taken from the tables of Herzberg[4] and are the following: $K_1=8\times10^5$ dynes/cm, $K_2=14.2\times10^5$ dynes/cm for OCS and $K_1=5.8\times10^5$ dynes/cm, $K_2=17.9\times10^5$ dynes/cm for HCN. Computation of the quantities $\xi_{ss'}$ for these molecules is now a simple matter. These in turn lead to values of $q_0=3.17$ Mc/sec. for OCS which is in complete agreement with the measured value[1] and $q_0=113.6$ Mc/sec. for HCN which is about 2 percent in excess of the measured value 111.8 Mc/sec. given by Shulman and Townes. When one considers that the K_1 and K_2 were determined from the band centers and not from the harmonic frequencies this agreement must be regarded as satisfactory.

Shulman and Townes have, moreover, reported a higher order effect in the *l*-type doubling of HCN. This manifests itself in a deviation of the quantity $q/J(J+1)$ which is proportional to J and of the order of magnitude $q(B_e/\omega_s)$. We have attempted to calculate this effect which involves a fourth-order perturbation calculation. We find a correction to the $(l/l\pm2)$ components of the energy matrix of a little more than $2B_e(B_e/\omega_s)^3(V_s+1)J^2(J+1)^2$. The following argument which is of a symmetry nature, may be used to support this. The correction required must be a correction to the (l/l) or the $(l/l\pm2)$ elements, and since for linear molecules $l=K$, also to the (K/K) and $(K/K\pm2)$ elements of the energy matrix. The matrix components must contain terms proportional to J^3 if the deviation to $q/J(J+1)$ is to be proportional to J. Such terms can arise only from terms in the Hamiltonian of the molecule proportional to P_x and P_y to some odd power. Such terms have only $(K/K\pm1)$, $(K/K\pm3)\cdots$elements and, therefore, only $(l/l\pm1)$, $(l/l\pm3)\cdots$elements.

The differences between the deviations in the states $J=8$ and $J=10$, and $J=10$ and $J=12$ have been calculated by our method. One obtains 0.13 Mc/sec. and 0.16 Mc/sec. respectively compared to 0.18 Mc/sec. measured for both of these instances. While the data of Shulman and Townes certainly fit a linear relation better than the one derived here, it is suggested that the next approximation may bring the two into agreement and that to this approximation our expression is substantially correct.

[1] H. H. Nielsen, Phys. Rev. **77**, 130 (1950).
[2] R. G. Shulman and C. H. Townes, Phys. Rev. **77**, 421 (1950).
[3] A. H. Nielsen, J. Chem. Phys. **11**, 160 (1943).
[4] G. Herzberg, *Infrared and Raman Spectra* (D. Van Nostrand Company, Inc., New York, 1945), p. 174.

Proton Groups from the Alpha-Particles Bombardment of Beryllium*

WILLIAM O. MCMINN, M. B. SAMPSON, AND M. LOREN BULLOCK
Department of Physics, Indiana University, Bloomington, Indiana
March 20, 1950

BOMBARDMENT of a 0.23 mg/cm² surface density metallic beryllium target with 21.94 Mev alpha-particles from the cyclotron has produced four proton groups. We have calculated Q-values for the reaction $Be^9(\alpha,p)B^{12}$ and three energy levels of B^{12} and have obtained a value for the mass of B^{12}.

Protons emerging from the target at 90° from the incident beam were counted by means of a dual proportional counter in a coincidence and discriminator circuit as described by Brolley, Sampson, and Mitchell.[1] The pulse discriminator was adjusted so that only pulses were counted which corresponded to the peak of the Bragg curve. Proton energies were calculated from aluminum absorption using unit absorber foils of 1.06 mg/cm² surface density. The alpha-particle beam energy was measured by aluminum absorption after scattering from a gold foil of 0.17 mg/cm² surface density. The residual range of the counter and the surface density of the beryllium target were measured with the aid of thorium C′ alpha-particles. The beryllium target was prepared by vacuum evaporation from a tungsten filament. Smith's calculations[2] were used in determining proton energies from aluminum absorption.

Proton groups, relative intensities and calculated Q-values and excitations are given in Table I.

The −7.02 Mev Q-value of our end group gives a calculated atomic mass of 12.01839 for B^{12} which may be compared with the value 12.01827±0.00009 calculated by Hornyak and Lauritsen.[3]

A low intensity proton group of 2.98 Mev energy was observed with variable intensity with different beryllium targets and is

TABLE I. Proton groups from $Be^9(\alpha,p)B^{12}$.

Proton energy Mev	Relative intensity	Q-value (Mev)	B^{12} energy level (Mev)
7.02	1	−7.02	0
6.06	2	−8.06	1.04
5.26	25	−8.93	1.91
3.25	40	−11.11	4.09

thought to be due to oxygen or carbon contamination. Work on the alpha-particle bombardment of these elements is being done in this laboratory.

We wish to thank Mr. Robert G. Cochran who has constructed the beam integrator used in this work. Mr. William Stefanich has devoted much time and skill in the operation of the cyclotron for which we are grateful.

* This work was assisted by a joint program of the ONR and AEC.
[1] Brooley, Sampson, and Mitchell, Phys. Rev. **76**, 624 (1949).
[2] J. H. Smith, Phys. Rev. **71**, 32 (1947).
[3] W. F. Hornyak and T. Lauritsen, Phys. Rev. **77**, 160 (1950).

Operation of a 300-Mev Betatron*

D. W. KERST, G. D. ADAMS, H. W. KOCH,† AND C. S. ROBINSON
Physics Department, University of Illinois, Urbana, Illinois
March 20, 1950

GEIGER counter yield trials of our new betatron were successful on the first attempt. After a few minutes of operation, the yield was read on an ionization chamber. The present yield which can be held at 315 Mev is about 1000 r/min. at one meter behind $\frac{1}{8}$-in. Pb at 6 PPS and 80-kv injection. Injecting with a rising voltage wave form has increased the output by a factor of about 5 over that using a flat-topped pulse. The field at the 122-cm orbit radius rises sinusoidally from -50 to $+9200$ gauss with a 60 c.p.s. wave form. The flux-forced central core changes from -14 to $+16$ kilogauss simultaneously. Compensation for the 9 percent orbital radiation loss is achieved by supplying a shaped flux pulse in a separate package of iron which links the orbit but not the flux-forcing circuit. This peaked flux pulse is also used to expand the electron beam out to the x-ray target.

The ease with which good yield was obtained is attributed largely to freedom from disturbing magnetic and electrostatic bumps at injection time. Contributing design features[1] are:

(1) Each of the six field magnets is constructed of identical $\frac{1}{2}$-in. bundles of laminations. This insures that each bundle is carried through the same magnetic cycle, resulting in azimuthal uniformity of residual magnetic field and of field lag due to eddy currents.

(2) The circular pole faces are continuous except for $\frac{1}{8}$-in. spacers between field magnets. This minimizes field lag at these joints.

(3) Large eddy-currents were prevented by 0.005-in. Kraft paper every $\frac{1}{4}$ in. in the stacking of the flux core and of the field magnets.

(4) The interior of the porcelain vacuum tube was coated with liquid bright palladium except at the bottoms of grooves $\frac{1}{16}$ in. wide and $\frac{1}{8}$ in. deep which serve as accelerating gaps. The coating resistance was quite uniform and about 20 ohms between ends of each 60° section.

The test for bumps in the magnetic field was a measurement of the time of zero field at all azimuths. An electron gun with a three-slit collimator 2 in. long was used in this test. This detector could be moved around in the gap while the pulse at zero field was observed on an oscillograph. The azimuthal variation of field at injection is less than ± 0.13 gauss except at the six-field magnet junctions where lags 5° in azimuth and as much as 0.5 gauss exist and except at a small region near the coil terminals where the field is 0.2 gauss early. The radial magnetic field at the orbit must be kept small. This was observed by taking the time difference between zero field with the detector against the bottom pole and zero field with the detector against the top pole. The radial field is less than ± 0.13 gauss except at field magnet junctions where bumps as high as 0.4 gauss exist. The residual magnetic field between 300-Mev pulses is 4.5 gauss. It is azimuthally uniform within ± 0.15 gauss. The radial variation of this residual field is similar to the pulsed field distribution.

The doughnut-shaped porcelain vacuum tube has an approximately elliptical cross section with minimum inside diameters about $4\frac{7}{8}$ in. and $9\frac{1}{8}$ in. It was fabricated in 20° sections which were rigidly joined in groups of three by a soldering technique. These 60° groups could be manipulated into place in the pole gap where the final seals were made by the atmospheric compression of Neoprene gaskets. The injector filament is a 1-in. long coil of 0.020-in. tungsten wire; other electrode sizes are proportionally enlarged from earlier types. The peak current injected is about one ampere.

The magnets[2] are all stacked with high quality transformer laminations. The flux magnet contains 275 tons and the six-field magnets contain 11 tons each. The field magnets are excited by two coils outside the pole rim and a coil in the gap, connected in series opposing so as not to excite the flux core. The energy stored in the capacitor bank is about 170,000 joules, of which about 85 percent is used to energize the field magnet gap and 15 percent is used to energize the flux magnet. Unidirectional pulsing is used and a synchronous mechanical switch is employed to reverse the connections to the capacitor bank.

The flux core has a bias winding of 2600 ampere-turns empirically distributed to minimize leakage flux. The choke coil in the bias circuit is also designed for particle analysis.

Meson tracks have been observed in photographic emulsions.

* Assisted in part by the joint program of ONR and AEC.
† Present address: Betatron Section, National Buruea of Standards, Washington, D. C.
[1] Kerst, Adams, Koch, and Robinson, Phys. Rev., **75**, 330 (1949). See also "An 80-Mev model of a 300-Mev betatron," Rev. Sci. Inst. (to be published).
[2] *Life*, March 20, 1950, pp. 129–132.

Quantum Electrodynamics—Second-Order Corrections to the Current Operator

THOMAS A. GREEN
Institute of Physics, University of Geneva, Switzerland
March 20, 1950

WE have calculated the second-order corrections to the current operator for electrons interacting with non-charged, vector mesons, obtaining results for electrodynamics in the limit of vanishingly small meson mass. This procedure was adopted to avoid the difficulties encountered in the quantization of the Maxwell field and to obtain determinate expressions in the infra-red terms.

The S-matrix was developed from the integral theory based on causality, invariance, and unitarity, proposed by Stueckelberg and Rivier.[1] This S-matrix has the same form as that obtained from a differential theory. However, the potential function $D^c(x-y)$ appearing in the space time integrals is not defined at the origin. We have,[2]

$$D^c(x-y) \sim D^s(x-y) + \tfrac{1}{2}iD^1(x-y), \quad x \neq y.$$

As a starting point in the calculation, we use the customary integral representations for D^s and D^1 which lead to the well-known indeterminate (infinite) charge and mass "renormalizations." Then, using the method discussed by Stueckelberg and Rivier,[2] we redefine the products of the potential functions in each matrix element in such a way that they are everywhere finite, but arbitrary at the origin. This method gives the same finite part obtained by Schwinger through an integration by parts,[4] but gives a finite arbitrary constant in lieu of a divergent integral. Thus we obtain matrix elements which are finite but which contain arbitrary constants.

We determine these arbitrary constants in such a way that (1) there are no charge or mass renormalizations, and (2) the passage to vanishing meson mass introduces no divergence except that associated with the infra-red catastrophe.[5] These conditions suffice to determine all the arbitrary constants in the matrix elements, and we obtain a completely determined expression for the second-order correction to the current operator. In the limit in which the ratio of the mass of the meson to that of the electron becomes very small, our results agree with those of Schwinger,

except for the fact that in the calculation of the infra-red terms, his expression[6]

$$(\pi/\lambda^2)[\ln(\lambda/2k_{\min})+1]$$

is replaced by

$$(\pi/\lambda^2)\ln(\lambda/|\mu|),$$

in which μ is the meson mass.

[1] E. C. G. Steuckelberg and D. Rivier, Helv. Phys. Acta, **23**, 215 (1949).
[2] For an electron $D^a(x)$ corresponds to $\bar{S}(x)$, and $D^1(x)$ corresponds to $S^{(1)}(x)$ in Schwinger's notation.
[3] E. C. G. Steuckelberg and D. Rivier, Helv. Phys. Acta, **23**, 236 (1949).
[4] J. Schwinger, Phys. Rev., **76**, 790 (1949), Eqs. (A32) and (A65).
[5] Terms inversely proportional to the square of the meson mass appear in the matrix elements.
[6] J. Schwinger, reference 4, Eq. (1.107).

A Variational Principle for the Computation of Reflection Coefficients

G. Toraldo di Francia
Institute of Physics of the University, Florence, Italy
February 24, 1950

In recent years several writers have dealt with variational principles for the computation of phase shifts[1] and transmission cross sections.[2] It seems worth noticing that the same approach is useful for calculating the reflection coefficient of a potential barrier.

Let u satisfy the one-dimensional wave equation

$$d^2u/dx^2+k^2(x)u=0, \tag{1}$$

where $k(x)$ is a given continuous function, which has the constant real values k_0 for $x<0$ and k_1 for $x>d$ respectively, being unrestricted (possibly complex) inside the barrier $0<x<d$. We write u in the form

$$u=f(x)\exp(ik_0x)+g(x)\exp(-ik_0x), \tag{2}$$

$f(x)$, $g(x)$ being everywhere continuous, together with their first derivatives, and subject to the conditions

$$\begin{aligned} &f(x)=1, \quad g(x)=\rho \quad \text{for} \quad x\leqslant 0, \\ &f(x)=\tau\exp[i(k_2-k_0)x], \quad g(x)=0 \quad \text{for} \quad x\geqslant d. \end{aligned} \tag{3}$$

Let us define

$$I=\int_0^d u(d^2u/dx^2+k^2u)dx.$$

By means of (1), (2), (3) it is easily seen that

$$\delta I=2ik_0\delta\rho. \tag{4}$$

This is a variational principle for the reflection coefficient ρ. We can either choose the trial functions $f_t(x)$, $g_t(x)$ containing n coefficients $c_1\cdots c_n$ and then determine these coefficients from the equations $\partial I_t/\partial c_i=0$, $\partial I_t/\partial\rho=2ik_0$, as made by Huang,[3] or simply, following the approach of Kohn,[4] derive from (4) the formula

$$\rho=\rho_t-I_t/2ik_0. \tag{5}$$

The soundness of Eq. (5) may be tested by means of the two following examples. Let us take for u inside the barrier the WKB approximation $u=(k_0/k)^{\frac{1}{2}}\exp(i\int_0^x k(\xi)d\xi)$. This trial function is a rather rough one, because it corresponds to $\rho_t=0$. Nevertheless, inserting it in (5), we readily find

$$\rho=\frac{i}{8}\int_0^d dx(3k^{-5}k'^2-2k^{-3}k'')\exp\left(2i\int_0^x k(\xi)d\xi\right)$$

in agreement with a first approximation[5] derived by other methods, which is valid when the variation of k is very small inside a wave-length, and $k\neq 0$.

As a second example, suppose we have inside the barrier $k(x)=k_0+\gamma(x)$, where γ represents a periodic function, whose average value inside a period is zero. Moreover one must have everywhere $|\gamma(x)|\ll k_0$. In this case we see that the WKB approximation can be written without appreciable error as $u=\exp(ik_0x)$. Inserting this function in (5), with $k^2=k_0^2+2k_0\gamma$, one finds

$$\rho=i\int_0^d \gamma(x)\exp(2ik_0x)dx. \tag{6}$$

If the barrier contains many times the period a of γ, the preceding integral gives a non-negligible value of ρ only when $2k_0=n2\pi/a$, i.e., when a is an integral multiple of the half-wave-length. This is a well-known result (Bragg reflection, Lippmann plates[6]). Equation (6) is also quantitatively in agreement with an elementary theory.

[1] L. Hulthén, K. Fysiogr. Sällsk. Lund Förhandl. **14**, No. 21 (1944); Arkiv f. Mat. Astr. o. Fys. **35A**, No. 25 (1948). J. Schwinger, Phys. Rev. **72**, 742A (1947). I. E. Tamm, J. Exp. Theor. Phys. USSR **18**, 337 (1948). J. M. Blatt and J. D. Jackson, Phys. Rev. **76**, 18 (1949). S. S. Huang Phys. Rev. **76**, 477 (1949).
[2] H. Levine and J. Schwinger, Phys. Rev. **74**, 958 (1948); **75**, 1423 (1949). J. W. Miles, Phys. Rev. **75**, 695 (1949).
[3] S. S. Huang, Phys. Rev. **76**, 1878 (1949).
[4] W. Kohn, Phys. Rev. **74**, 1763 (1948).
[5] O. E. H. Rydbeck, Trans. Chalmers Univ. Technol. Gothenburg, No. 74 (1948).
[6] K. Försterling, Physik. Zeits. **14**, 265 (1913).

Element 98*

S. G. Thompson, K. Street, Jr., A. Ghiorso, and G. T. Seaborg
Radiation Laboratory and Department of Chemistry, University of California, Berkeley, California
March 15, 1950

Definite identification has been made of an isotope of the element with atomic number 98 through the irradiation of Cm^{242} with 35-Mev helium ions in the Berkeley Crocker Laboratory 60-inch cyclotron. The isotope which has been identified has an observed half-life of about 45 minutes and probably has the mass number 244. The observed mode of decay of the 98^{244} is through the emission of alpha-particles, with energy about 7.1 Mev, which agrees with predictions, and other considerations involving the systematic of radioactivity in this region indicate that it should also be unstable toward decay by electron-capture.

The chemical separation and identification of the new element was accomplished through the use of ion exchange adsorption methods employing the resin Dowex-50. The element 98 isotope appears in the eka-dysprosium position on elution curves containing 4.6-hour Bk^{243} (formed by a d,n reaction from deuteron impurity in the same bombardment) and the bombarded Cm^{242} as reference points; that is, it precedes berkelium and curium off the column just as dysprosium precedes terbium and gadolinium. The experiments so far have revealed only the tripositive oxidation state of eka-dysprosium character but practically no attempts at oxidation to possible IV and V states have been made as yet.

The successful identification of so small an amount of an isotope of element 98 was possible only as a result of the accurate predictions of the chemical[1] and radioactive[2] properties.

It is suggested that element 98 be given the name californium (symbol Cf) after the university and state where the work was done. This name, chosen for the reason given, does not reflect the observed chemical homology of element 98 to dysprosium (No. 66) as the names americium (No. 95), curium (No. 96), and berkelium (No. 97) signify that these elements are the chemical homologs of europium (No. 63), gadolinium (No. 64), and terbium (No. 65), respectively; the best we can do is point out, in recognition of the fact that dysprosium is named on the basis of a Greek word meaning "difficult to get at," that the searchers for another element a century ago found it difficult to get to California.

It is a pleasure to acknowledge the special help in the bombardment of the curium samples of Professor J. G. Hamilton, G. B. Rossi, T. M. Putnam, Jr., M. T. Webb, and the operating crew of the 60-inch cyclotron in the Crocker Laboratory. The successful handling in a safe manner of the radioactivity involved was made possible through the use of the excellent protective equipment provided by Nelson Garden, the members of his Health Chemistry Group, and Mr. C. M. Gordon. We wish also to thank E. K.

Hulet and G. H. Higgins for their assistance in the experiments. We are happy to acknowledge the continued support and interest of Professor E. O. Lawrence in this work.

* This work was performed under the auspices of the U.S. AEC.
[1] G. T. Seaborg, Nucleonics **5**, No. 5, 16 (1949).
[2] Perlman, Ghiorso, and Seaborg, Phys. Rev. **77**, 26 (1950).

Radioactivity in Hafnium*

J. M. Cork, A. E. Stoddard, W. C. Rutledge, C. E. Branyan, and J. LeBlanc
Department of Physics, University of Michigan, Ann Arbor, Michigan
March 20, 1950

A LONG-LIVED radioactivity in Hf^{181} activated by slow neutrons was first observed[1] by Hevesy and Levi and reported as having a half-life of 55 days. Subsequent spectrometric studies of similar specimens irradiated in the Oak Ridge pile showed[2] the presence of four internally converted gamma-rays. A level scheme utilizing these gamma-rays, but with divergent energy values, was proposed[3] by Wiedenbeck and Chu.

Continued investigation of other specimens now allows a more accurate evaluation of previously reported energies and reveals many electron lines not observed previously. These electron energies as obtained by internal conversion and by photo-emission from lead are presented in two groups. In Table I are those electron lines whose identification seems to be established beyond question. In Table II the remaining 13 electron lines are listed. These latter lines are so numerous and so closely spaced as to energy that their interpretation at the present time is not unique.

Table I. Electron energies identified.

Electron energy	Identification	Energy sum
25.7 kev	K(Lu)	89.1 kev
65.2	K^1	132.4
68.5	K^2	135.7
77.8	L(Lu)	88.1
85.5	M(Lu)	87.9
121.7	$L_{1,2}^1$	132.8
123.0	L_3^1	132.9
124.5	L^2	135.6
130.3	M^1	133.0
132.1	N^1	132.7
133.5	M^2	136.2
277.3	K^3	344.5
278.9	K(Lu)	342.3
331.4	L(Lu)	341.7
340.0	M(Lu)	342.4
414.0	K^4	481.2
469.5	L^4	480.6
478.0	M^4	480.7
543.8	K^5	612.0

A short-lived activity (10.2 hr.) previously unreported, appeared to exist in the pure specimen. The half-life associated with the beta-decay of Hf^{181} is here followed through five octaves and found to be 45 days. The associated gamma-rays following beta-emission would be in tantalum ($Z=73$). The K–L–M differences observed for most of the strong electron lines are characteristic of tantalum as shown in Table I, yielding five gamma-rays whose energies are 132.7, 135.7, 344.5, 481.0, and 612 kev and assigned arbitrary numbers in the order of increasing energy. These energies fit almost perfectly on the amended level scheme of Wiedenbeck and Chu as shown in Fig. 1. By the use of a coincidence magnetic beta-spectrometer (to be described elsewhere) Dr. R. G. Shreffler has shown conclusively that the 132.7 kev and the 135.7 kev lines are in sequence with the 344.5 kev line but the coincidence rate is greater for the latter two than for the first and last lines. The 481 kev line is found to be in coincidence with the 132.7 kev line but not with the 344.5 kev line. This behavior is exactly as would be expected in the branching scheme of Fig. 1. The K/L conversion ratios are about one for γ_1 and only about one-fifth for γ_2.

Table II. Electron energies not positively identified.

Electron energy	
127.0 kev	146.0 kev
135.0	148.7
137.0	193.8
139.0	197.5
141.0	199.7
142.5	203.2
144.5	

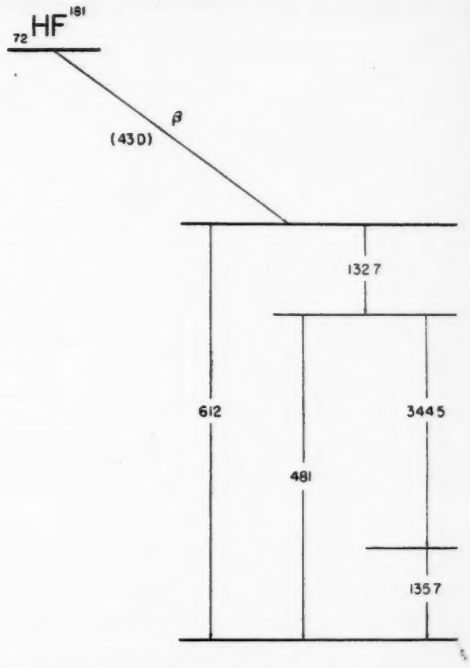

Fig. 1. Energy levels in Ta^{181}, following beta-emission from Hf^{181}.

Hf^{176} could be produced in the pile by neutron capture in Hf^{174} (0.18 percent) or by the $(n,2n)$ reaction of Hf^{176} (5.3 percent). This isotope would decay by K-capture to Lu^{175} ($Z=71$) and has been reported[4] to have a half-life of 70 days, and to emit a gamma-ray whose energy by absorption in lead was 350 kev. Two groups of the electron lines shown in Table I have K–L–M differences characteristic of lutecium and yield gamma-energies of 88.7 and 342.1 kev. Many of the electron lines in Table II can equally well be interpreted as due to gamma-rays in lutecium. There is no evidence however, of a 70 day half-life component in the specimens here studied. On aging beyond the 45-day activity a remaining relatively strong activity persists whose half-life appears to be greater than one year. This problem can ultimately best be resolved by the use of enriched stable isotopes.

* This investigation was made possible by the joint support of the AEC and ONR.
[1] G. Hevesy and H. Levi, Kgl. Dansk. Mat. Fys. **15**, 11 (1938); S. Benedetti and F. McGowan, Phys. Rev. **70**, 569 (1946).
[2] Cork, Shreffler, and Fowler, Phys. Rev. **72**, 1209 (1947).
[3] M. Wiedenbeck and K. Chu, Phys. Rev. **75**, 226 (1949); Mandeville, Scherb, and Keighton, Phys. Rev. **75**, 221 (1949).
[4] G. Wilkinson and H. Hicks, Phys. Rev. **75**, 696 (1949).

Excitation Curve for Protons in the Reaction $F^{19}(d,p)F^{20}$ *

S. C. Snowdon
Bartol Research Foundation of The Franklin Institute, Swarthmore, Pennsylvania
March 6, 1950

THE total cross section for the production of protons in the reaction

$$F^{19}+H^2 \rightarrow F^{20}+H^1 \qquad (1)$$

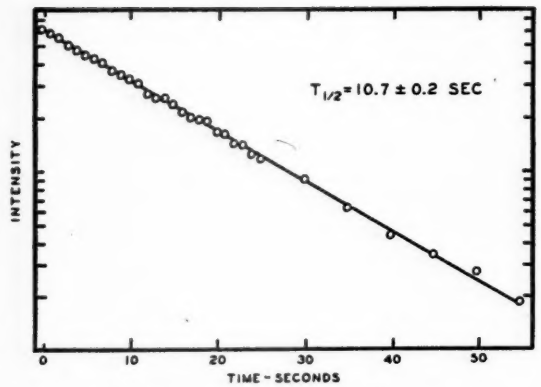

FIG. 1. Decay curve of F^{20}(10.7 ±0.2 sec.).

has been investigated in the deuteron energy range 0.7 Mev to 1.8 Mev. In this reaction the residual nucleus decays according to

$$F^{20} \rightarrow Ne^{20} + \beta^-, \tag{2}$$

where the β-rays are emitted isotropically. Hence a measurement of the yield of the β-rays provides a convenient means of measuring the total cross section of reaction (1).

The production of F^{20} takes place according to the equation,

$$dN/dt + \lambda N = \sigma n d I/e, \tag{3}$$

where N is the total number of F^{20} atoms present at time t, λ is the disintegration constant, σ is the total cross section, n is the number of bombarded nuclei per cubic centimeter, d is the target thickness, e is the charge on the electron, and I is the deuteron beam current. Because of the relatively long half-life, radioactive equilibrium is not established in a negligible time. Therefore, the presence of the term dN/t does not allow the use of the usual current integrator to normalize the yield of the reaction when the current fluctuations are unknown. In order to annul the effects of any current fluctuations, a "leaky" integrator was constructed using an electronic electrometer to measure the voltage across a parallel combination of a resistor R and a polystyrene condenser C. The deuteron beam charges up the condenser whose voltage is determined by the equation,

$$dV/dt + V/RC = I/C. \tag{4}$$

If the time constant RC is set equal to $1/\lambda$, the mean lifetime of the radioactivity, and if both the integrator and the activity are started from zero, then

$$N = \sigma n d C V/e. \tag{5}$$

This proves to be a convenient relation for the measurement of the cross section even if the bombarding beam is not steady.

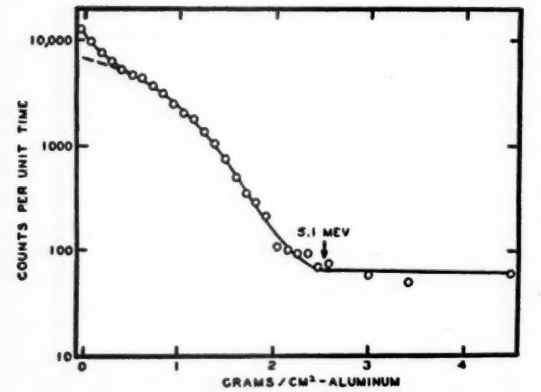

FIG. 2. Absorption in aluminum of the beta-rays from F^{20}. Near zero absorber the positrons from N^{13} are present.

In order to take the data, the deuteron beam is turned on until the voltage on the integrator is somewhat above a previously chosen normalizing value. The beam then is turned off completely and the condenser is allowed to decay until the normalizing voltage is reached, at which time the counters are turned on for one minute. Coincidence counting was used to reduce the γ-ray background, the first counter of this pair being placed two inches from the target. An aluminum absorber of $\frac{1}{16}$-in. thickness was placed in front of the coincidence arrangement in order to stop the positrons produced by the deuteron bombardment of the carbon contamination on the target. The target consisted of a thin CaF_2 layer (25 μg/cm²) evaporated onto a 0.001-in. molybdenum foil.

When a value of 12.4 sec., as given by Bowers and Burcham,[1] was used for the half-life of F^{20}, the yield data were quite inconsistent. By adjusting the time constant of the integrator to about 15.5 sec. (or a half-value time of 10.7 sec.) it was possible to get the same yield for short and long bombardment runs. To check this new value of the half-life a decay curve was taken by introducing, after each successive normalized bombardment, a one-second additional delay before turning on the counters. Figure 1

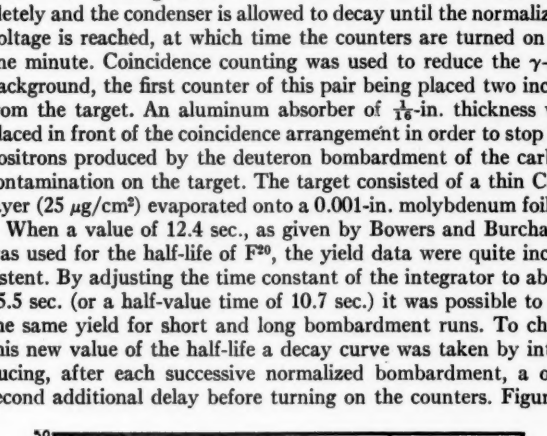

FIG. 3. Total cross section for the reaction $F^{19}(d,p)F^{20}$. The points on the yield curve were normalized by using a "leaky" integrator whose time constant corresponded to the F^{20} half-life of 10.7 sec.

shows the results of this measurement, the value of the half-life being 10.7±0.2 sec.

An absorption curve of the β-rays, shown in Fig. 2, was taken in order to estimate the zero absorber yield of the β-rays, 100 mg/cm² being used as the contribution of the counters and the target backing to the absorber thickness. The sharp rise near zero-absorber thickness is due to the positron activity from deuterons on carbon. It may be noted that by using Feather's equation the end point of the β-ray absorption curve is consistent with 5.1 Mev as given by Bowers and Burcham.[1] The background is probably due to a combination of annihilation radiation and γ-rays given out in the decay of the excited states in Ne^{20} associated with the F^{20} decay.

The cross section was calculated by using the extrapolated zero-absorber yield, the solid angle as determined from the coincidence counter geometry, and a target thickness that was determined by taking the ratio of the area under a thin target yield curve of the 873.5 kev resonance in the $F(p,\gamma)$ reaction to the height of the step in the thick target yield curve of the same substance.

Figure 3 shows the cross section as a function of the deuteron bombarding energy. The estimated uncertainty in the relative values of the cross section is about 2 percent; whereas, in the absolute cross sections the uncertainty may be as much as 30 percent because of difficulty in measuring the target thickness.

The author wishes to thank Mr. C. P. Swann for his generous assistance throughout the experiment and Dr. C. E. Mandeville for informative discussions regarding coincidence counting technique.

* Assisted by the joint program of the ONR and the AEC.

[1] Bowers and Burcham, Proc. Roy. Soc. 173, 379 (1939).

Investigation of Color Centers by a Single-Photon Counting Method

A. J. DEKKER AND A. H. MORRISH
*Department of Physics, University of British Columbia, Vancouver, Canada**
March 20, 1950

THE detection of nuclear particles by means of scintillation counters has received much attention in the last few years. The energy of the incident particles is partly converted into a large number of visible photons by using a suitable phosphor. A photo-multiplier tube, coupled to the crystal then produces voltage pulses.

It is evident that when a "photon-emitter" is placed in front of a photo-multiplier, single photons may be counted. Such a photon-emitter may be obtained by irradiating alkali-halide crystals with x-rays. The x-ray energy absorbed by the crystal is partly stored in the form of excited electrons trapped by lattice defects. The excited electrons recombine with the holes with the emission of photons. These photons were observed with the use of an R.C.A. 5819 photo-multiplier coupled to the irradiated crystal. The irradiation with x-rays and the mounting of the crystal on the photo-multiplier window were carried out in the dark to prevent unnecessary bleaching of the colored crystals.

The electronic circuits, consisting of a preamplifier and linear amplifier and linear amplifier of gain 60X, and a scale of 640, were conventional. About 1300 volts from a highly stabilized, low ripple power supply was applied to the tube. The distribution of pulses obtained from the crystal was roughly similar to the distribution of noise pulses from the photo-multiplier with approximately the same maximum pulse height, but were much greater in number, suggesting that single photons were being counted.

Some preliminary results obtained at room temperature are shown in Fig. 1. Curves *I* and *II* correspond respectively to single crystals of NaCl and KBr. Both crystals had been irradiated with 55 kv 3ma x-rays at a distance of 9 cm from the source for 15 minutes. Curves *III* and *IV* both refer to the KBr crystal just mentioned, but irradiated at a distance of 5 cm from the source for 15 minutes. The noise pulses constituted less than 0.07 counts per minute in the scale of 640 which is so small that they cannot be shown conveniently on the graph. That curves *III* and *IV* do not coincide is perhaps due to the fact that the high voltage in the tube was slightly different for the two cases and the pulse size distribution is very critical to a change in this voltage. We should note that curve *I* for NaCl gives only part of the observations and appreciable counting rates were observed even after a day.

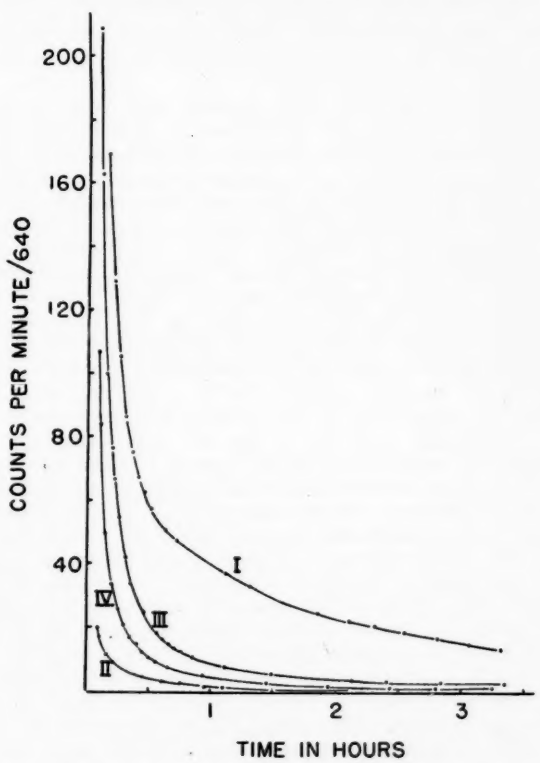

FIG. 1. Counting rate as a function of time after irradiation with x-rays. Curve *I* corresponds to NaCl and curves *II*, *III*, and *IV* to KBr crystals.

Preliminary experiments have also been carried out keeping the crystals at the temperature of dry ice. For the same discriminator setting and the same time after irradiation the counting rate for NaCl and KBr was only about 0.05 percent of that at room temperature. Also, the time interval over which the counting rate falls to half its initial value is less by a factor of 4 at dry ice temperature compared with room temperature.

The strong temperature dependence of the counting rate shows that direct recombination of a trapped electron with a hole in the upper filled band is very unlikely. Apparently recombination can only take place after the electrons are excited into the conduction band.

The investigations are being continued in the hope that quantiative measurements may lead to a better understanding of the decay processes involved.

* This research was partially supported by the Defence Research Board of Canada, Ottawa.

Photovoltaic Effect of $P-N$ Junctions in Germanium*

M. BECKER AND H. Y. FAN
Purdue University, Lafayette, Indiana
February 23, 1950

A PIECE of germanium, one part of which is a p-type semiconductor and the other part is N-type, forms at the junction a barrier of high resistance and photosensitivity. Light which is effective photoelectrically is practically entirely absorbed within a very small thickness ($<10^{-3}$ cm). In samples having a thickness of a fraction of a millimeter and more only a part of the junction area is activated and generates an emf V_p. This emf is in series with r, the resistance of the activated part of the barrier. In parallel with this combination are the resistance R of the unactivated part of the barrier and the capacitance C of the barrier. The barrier is in series with the bulk resistance of the sample, which is comparatively negligible, and the input resistance R_e of the amplifier. To obtain maximum voltage R_e should be large compared with R. Figure 1 shows curves of measured voltage *versus* R_e for two temperatures. The experiments reported below were made with sufficiently large R_e so that its effect can be neglected.

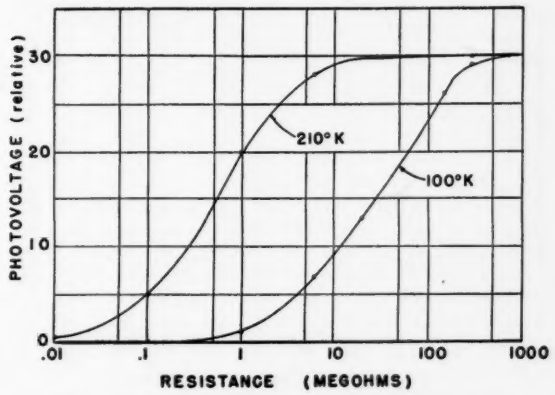

FIG. 1. Effect of external load resistance on photo-voltage.

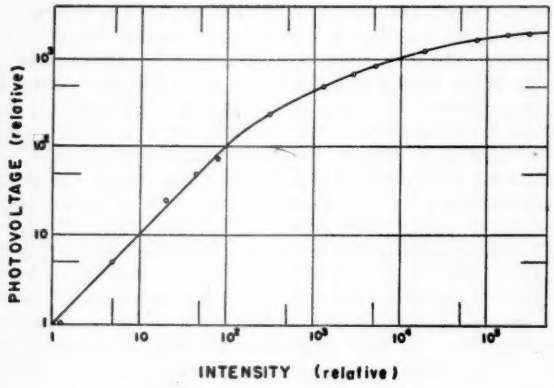

FIG. 2. Photo-voltage as function of light intensity.

It has been shown[1] that the photo-emf developed across a $P-N$ barrier is given by

$$V_p=\frac{kT}{e}\left(\log\frac{n_p}{n_N}-\log\frac{n_{po}}{nN_o}\right)\approx\frac{kT}{e}\log\frac{n_p}{n_{po}}=\frac{kT}{e}\log\left(1+\frac{\Delta n_p}{n_{po}}\right),$$

where n is the concentration of conduction electrons and subscript o refers to the state of thermal equilibrium without illumination. The value of Δn_p is determined by the balance between the rate of excitation, which is proportional to light intensity, and the rate of relaxation. It follows from this equation that V_p increases approximately linearly with the light intensity only for $\Delta n_p<n_{po}$; it increases more slowly at higher intensities. Figure 2 shows the measured photo-voltage as a function of the light intensity.[2]

The relaxation of excited electrons is due to: (1) current flow through R, (2) volume recombination and (3) diffusion and recombination at the surfaces.[3] Since R increases, and the recombination rate decreases, with decreasing temperature, the sensitivity should increase. The experimental result is shown in Fig. 3. The light intensities used were kept sufficiently low to insure linearity of response. At 100°K the sensitivity is about 10,000 times higher than at room temperature; with the sample in a metal Dewar background light scattered into the window was sufficient to produce a photovoltage already in the non-linear region. With R_s equal to the room temperature value of R the photo-voltage was still several times higher than at room temperature, indicating that the increase of R alone does not account for all of the increase in sensitivity. The drop of response toward long wave-length is due to the decrease in excitation rate. The absorption of germanium drops very sharply beyond 1.7μ corresponding to the forbidden-energy gap.[4]

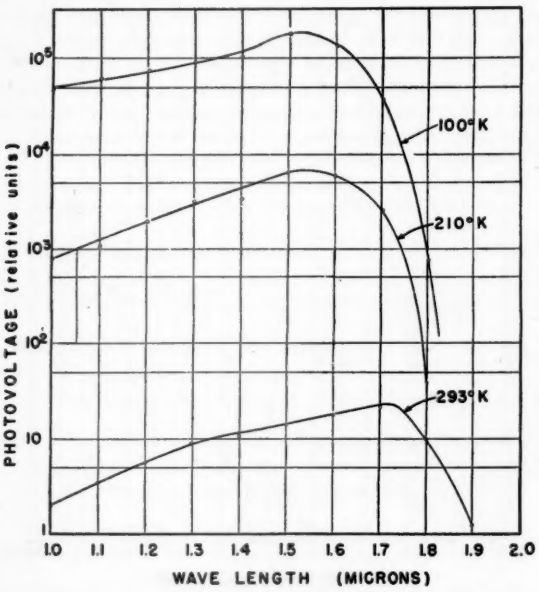

FIG. 3. Temperature dependence of spectral response.

Observations were made of the building up and the decay of the photovoltage under pulsed irradiation. These processes are approximately exponential. The values of the time constant measured for a certain sample are 1500 μsec. at 100°K, 130 μsec. at 210°K, and less than 12 μsec. at room temperature. For sufficiently large R_s (see Fig. 2) these values are independent of R_s. It must be pointed out that the speeds of these processes depend not only on the rate of change of V_p but are affected also by the values of C and R. If V_p changes very fast then the building up and decay will have simply a time constant CR. However, observations made with different values of R_s and external capacitance across the sample indicate that this is not the case. The experiments are being continued.

* Work assisted by a Signal Corps Contract.

[1] H. Y. Fan, Phys. Rev. **75**, 1631 (1949).

[2] Results obtained using white light were reported earlier, M. Becker and H. Y. Fan, Phys. Rev. **75**, 1631 (1949).

[3] H. Suhl and W. Shockley, Phys. Rev. **75**, 1617 (1949).

[4] M. Becker and H. Y. Fan, Phys. Rev. **76**, 1530 (1949).

Neutron Groups from $Be^9(\alpha,n)C^{12}$

C. E. BRADFORD AND W. E. BENNETT
Illinois Institute of Technology, Chicago, Illinois
March 13, 1950

THE radium-beryllium mixture is commonly used as a source of neutrons. It gives a continuous distribution of neutron energies up to 13 Mev. The neutrons are produced by a wide distribution of α-particle energies and are emitted at all angles to the α-particles. Several earlier efforts[1] have been made to infer excited states of the residual C^{12} nucleus from the neutron spectrum.

We have bombarded a thick beryllium target with 1.4 Mev α-particles produced in the Illinois Institute of Technology electrostatic generator. Ilford C2 plates 100 microns thick were exposed at 90° to the beam. Two thousand tracks of recoil protons within 12° of the neutron direction were measured. The number of tracks within 0.1 Mev energy intervals was plotted, using a range-energy curve for the plates.[2] The number of neutrons was obtained from the number of measured tracks of recoil protons by applying a suitable geometrical correction[3] and a correction for cross section for neutron-proton scattering. The energies were increased by 2.7 percent, the average amount by which the neutron energies exceed the energies of the recoil protons. The final energy spectrum of the neutrons is shown in Fig. 1. The thickness of the target did not contribute greatly to the breadth of the groups. A thick target yield curve showed that half of the neutrons were produced by α-particles of energies between 1.27 and 1.40 Mev.

The Q-values corresponding to the two groups were computed in two different ways. Using a mean energy for each group and a mean effective bombrading energy, Q was found to be 5.65 and 1.19 Mev for the high and low energy groups, respectively. This gives the energy of the excited state of C^{12} as 4.46 Mev. The second computation used the procedure outlined by Livingston and Bethe[4] and assumed that the range straggling in the plates would not be much greater than in air. It led to Q-values of 5.78 and 1.34 Mev and an energy of the excited state of C^{12} of 4.44 Mev. The difference between the two sets of results is caused by some unexplained breadth of the groups. The Q-value calculated from masses is 5.72±0.08 Mev. The agreement in either case is satisfactory, since the range-energy relation for the plates may be in error by 2 percent.

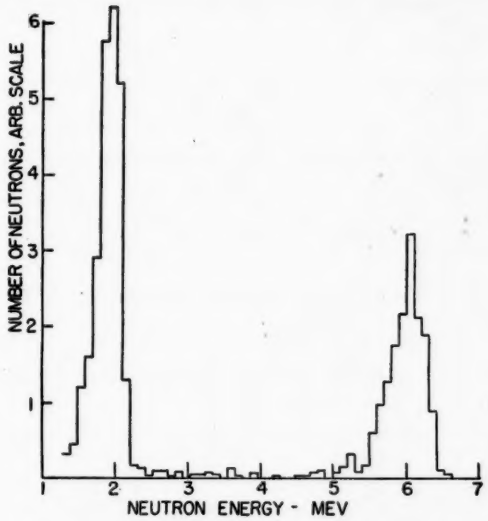

FIG. 1. Energy spectrum of neutrons from $Be^9(\alpha,n)C^{12}$.

Another excited state of C^{12} at about 3 Mev has sometimes been reported. There is no evidence of such a neutron group at this bombarding energy. We exposed another plate in the forward direction and 90 tracks were measured on it. It gave the same two groups of neutrons but in a different ratio of intensities. The low energy group was 0.4 times the intensity of the high energy group. The data shown in Fig. 1 gives 1.6 for this ratio. A further study of the angular distribution of the neutrons has been started in this laboratory.

[1] W. F. Hornyak and T. L. Lauritsen, Rev. Mod. Phys. **20**, 191 (1948).
[2] Lattes, Fowler, and Cuer, Nature **159**, 301 (1947).
[3] H. T. Richards, Phys. Rev. **59**, 796 (1941).
[4] M. S. Livingston and H. A. Bethe, Rev. Mod. Phys. **9**, 281 (1937).

The Natural Activity of Lanthanum

R. W. PRINGLE, S. STANDIL, AND K. I. ROULSTON
Physics Department, University of Manitoba, Canada
February 27, 1950

THE general criteria for beta-decay[1] indicate that of two nuclei Z^A and $(Z-1)^A$, the one with the greater atomic mass is unstable against beta-decay to the other. Thus the existence in nature of stable pairs of isobaric nuclei of neighboring atomic number is unlikely, and the occurrence of the exceptional pairs Z^A, $(Z-1)^A$ is accounted for as due to a very long half-life for beta-decay of the unstable member of the pair, because of nuclear spin and parity changes. The known beta-activities of K^{40} (1.4×10^9 years),[2] Re^{187} (4×10^{12} years),[3] Lu^{176} (2.4×10^{10} years),[4] and Rb^{87} (6.3×10^{10} years),[5] support this view, but there exist also the pairs (Sb^{122}, Te^{123}), (In^{115}, Sn^{115}), and (Cd^{113}, In^{113}), and the double anomalies[6] (Ba^{138}, La^{138}, Ce^{138}) and[7,8] (T^{50}, V^{50}, Cr^{50}) for which no activities have yet been observed due to extremely long lifetimes, the very low energy of the disintegration, or the difficulty of detecting K-capture processes when the specific activity is low. It is of interest to point out also that La^{138} and V^{50} are the only apparently stable odd-odd nuclei above N^{14}.

The recent development of a scintillation gamma-ray spectrometer of extreme sensitivity[9,10] means that a method is now available by which gamma-radiation due to a possible activity might be detected from a large mass of the isotope to be examined, and its energy analyzed to indicate whether the radiation could be due to minute traces of impurities (Th, U, K). Initial tests were made with materials of ordinary purity and feeble activities were observed which might be attributed to thorium contamination. However, these usually disappeared when extremely pure materials were used, as in the case of cerous oxalate from which impurities were removed by several hydrolysis.[11] We wish, nevertheless, to report an activity obtained with lanthanum which could not be removed in this way even after treatment in an ion exchange column to remove traces of rare earth metals, and which could not be identified as being due to any likely contaminant. The material was used in the form of 39 g of lanthanum trioxide, in an arrangement similar to the one with which we recently investigated the gamma-ray activity of potassium.[10] Figure 1

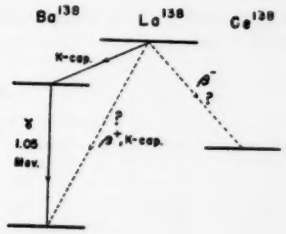

FIG. 2. Suggested disintegration scheme for La^{138} (half-life $\leqslant 1.2\times10^{11}$ years).

gives the differential pulse height distribution, corrected for background, of the secondary electrons produced by the gamma-radiation in the crystal, and the background curve for reference. The distribution has been compared with similar curves for K^{40} and Co^{60}, and from the approach to the axis[10] it would appear that the main component is a gamma-ray of energy (1.05 ± 0.05) Mev. The rise in the distribution curve at low energies is due to degenerate radiation and the loss of electrons from the surfaces of the crystal. However, it is not impossible that a low energy component is also present.

We have estimated the number of gamma-quanta of energy 1.05 Mev to be (0.7 ± 0.1) quanta/sec.-g of ordinary lanthanum, and have used data obtained with potassium to check the result. If we use the known abundance of La^{138} (0.086 percent) in lanthanum,[6] we obtain a half-life of 1.2×10^{11} years for the disintegration of La^{138}, assuming that one gamma-ray accompanies each disintegration. This period therefore represents an upper limit to the half-life. A search has been made with a thin window beta-counter (1 mg/cm²) for negative electrons or positrons from a source of lanthanum trioxide 100 mg/cm² thick. Any particles present of energy 100 kev or more must be in amount less than 0.4 per sec. per gram of lanthanum. It seems likely therefore that the 1.05 Mev gamma-ray is associated with a K-capture process to Ba^{138} (Fig. 2). It is worth while pointing out that no information is yet available on the spins of the nuclei involved. No attempt has yet been made to detect this K-capture directly. The examination of the other anomalous groups for possible activities is being continued.

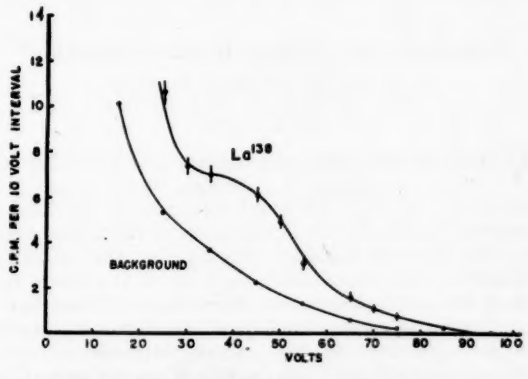

FIG. 1. Scintillation spectrometer study of the gamma-ray activity of lanthanum.

Our thanks are due the National Research Council of Canada for financial support of some of this work.

[1] L. Rosenfeld, *Nuclear Forces* (Interscience Publishers, Inc., New York), Chapter 3.
[2] See for example, E. Gleditsch and T. Graf, Phys. Rev. **72**, 640 (1947).
[3] S. N. Naldrett and W. F. Libby, Phys. Rev. **73**, 487 (1948).
[4] A. Flammersfeld, Zeits. f. Naturforschung **2**, 86 (1947).
[5] S. Eklund, Arkiv 33A, No. 14 (1945).
[6] Inghram, Hayden, and Hess, Phys. Rev. **72**, 967 (1947).
[7] D. C. Hess and M. C. Ingrham, Phys. Rev. **76**, 1717 (1949).
[8] W. T. Leland, Phys. Rev. **76**, 1722 (1949).
[9] Pringle, Roulston, and Taylor, Rev. Sci. Inst. (April, 1950).
[10] Pringle, Standil, and Roulston, Phys. Rev. **77**, 841 (1950).
[11] We are extremely grateful to Dr. D. S. Russell and Dr. Fitch of the Chemistry Division, N.R.C., Ottawa, for their cooperation in this work.

Gamma-Rays from Terbium 160*

J. M. Cork, C. E. Branyan, W. C. Rutledge, A. E. Stoddard, and J. M. LeBlanc
Department of Physics, University of Michigan, Ann Arbor, Michigan
March 20, 1950

THE radioactivity of terbium 160, produced by neutron capture, was first reported[1] by Bothe as having a half-life of 73.5 days. Subsequently a specimen irradiated in the Oak Ridge pile was shown[2] to emit many electrons by the internal conversion of gamma-rays. Further spectrometric studies on a highly purified sample kindly made available by Dr. G. E. Boyd of the Oak Ridge National Laboratory, show all the lines previously observed and many additional electron lines. Photographic spectra have been obtained both by internal conversion and by photo-emission in lead and uranium.

A summary of the energies of the conversion electrons and the photo-electrons from lead is presented in Table I, together with their interpretation and the energy sums. The gamma-energies are shown collectively in Table II.

TABLE I. Electron energies from terbium 160.

Electron energy	Interpretation	Energy sum	Electron energy	Interpretation	Energy sum
32.9 kev	K^1	86.3 kev	194.7 kev	M^4	196.6 kev
36.9	Auger L	44.9	205.3	L^8	214.4
39.5	K^2	93.0	209.6	Ph–K^7	297.5
42.3	Auger M	44.4	228.0	K^6	281.7
71.0	Ph–$L_{1,2}^1$	86.2	243.4	K^7	297.6
73.4	Ph–L_3^1	86.4	273.0	L^6	282.1
76.3	Ph–L_1^2	92.1	282.4	Ph–L^7	297.6
78.0	$L_{1,2}^1$	86.6	289.0	L^7	298.1
79.0	L_3^1	86.8	293.5	Ph–M^7	297.4
82.5	Ph–M^1	86.4	296.0	M^7	298.0
84.7	M^1	86.6	303.0	Ph–K^9	390.9
86.1	N^1	86.5	321.6	K^8	375.2
108.4	Ph–K^4	196.3	356.6	K^{10}	410.3
122.5	K^3	176.2	788.4	Ph–K^{11}	876.3
127.3	Ph–K^5	215.2	823.0	K^{11}	876.0
143.0	K^4	196.6	866.0	L^{11}	875.0
161.4	K^5	215.1	873.7	Ph–K^{12}	961.6
168.0	L^3	176.6	908.0	K^{12}	961.7
180.8	Ph–L^4	196.6	953.0	L^{12}	962.0
187.0	L^4	196.2			

The 12 gamma-rays may be arranged on a rather simple level scheme as shown in Fig. 1. The observed and expected energies

TABLE II. Summary of the gamma-rays in dysprosium 160.

Arbitrary number	Energy kev	Arbitrary number	Energy kev
γ^1	86.5	γ^7	297.8
γ^2	92.6	γ^8	375.2
γ^3	176.2	γ^9	391.0
γ^4	196.4	γ^{10}	410.3
γ^5	214.7	γ^{11}	876
γ^6	282.0	γ^{12}	962

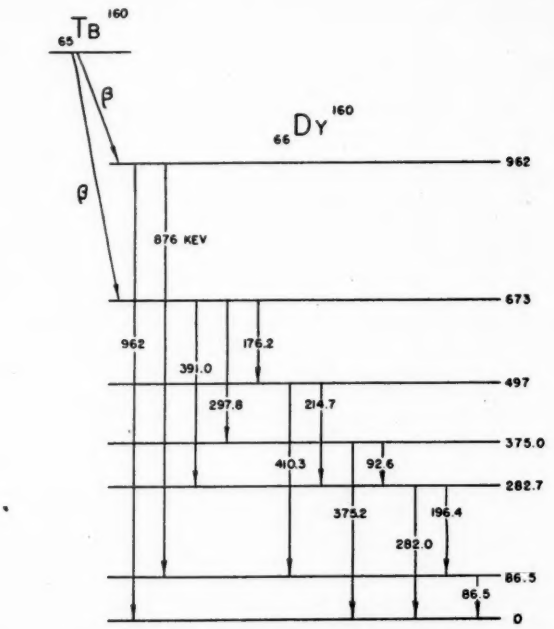

FIG. 1. Energy levels in dysprosium 160, following beta-emission from terbium 160.

for the possible transitions agree well within the experimental limits of accuracy. It is believed that the beta-spectrum consists of at least two electron groups whose maximum energies were reported first[2] as 882 and 546 kev and later[3] as 860, 521, and 396 kev, indicating a possible third group. The level scheme in Fig. 1 would be compatible with two beta-energies whose difference is slightly less than either of the reported sets of values as indicated. The beta-energy of lowest value would probably be accompanied by a gamma-ray of very high energy only slightly converted and hence not observable with the sample intensity available.

The half-life of the highly purified specimen followed through three octaves is found to be 76.0 days, confirming our previous report.

* This investigation was made possible by the joint support of the AEC and the ONR.
[1] W. Bothe, Naturwiss. **31**, 551 (1943); Zeits. f. Naturforschung **1**, 173 (1946); Krisberg, Pool, and Hibdon, Phys. Rev. **74**, 44 (1948).
[2] Cork, Shreffler, and Fowler, Phys. Rev. **74**, 240 (1948).
[3] Burson, Blair, and Saxon, Phys. Rev. **77**, 403 (1950).

Thermoelectric Voltage in Lead Telluride*

Ralph Wyrick and Henry Levinstein
Syracuse University, Syracuse, New York
March 6, 1950

WHEN an evaporated lead telluride film containing excess tellurium is baked in a vacuum, the resistance is first found to rise and after continued baking begins to drop. The thermoelectric power for the same film rises at first, then drops to zero at the resistance maximum, then reverses. The behavior of a particular lead telluride film is shown in Fig. 1. It is similar to the effect in lead sulfide observed by Hintenburger.[1] When lead telluride contains an excess of telliurium, conduction is by positive holes as is indicated by the positive thermoelectric voltage. Baking removes tellurium from the film. When stochiometric proportions are reached the thermal voltage reduces to zero and the

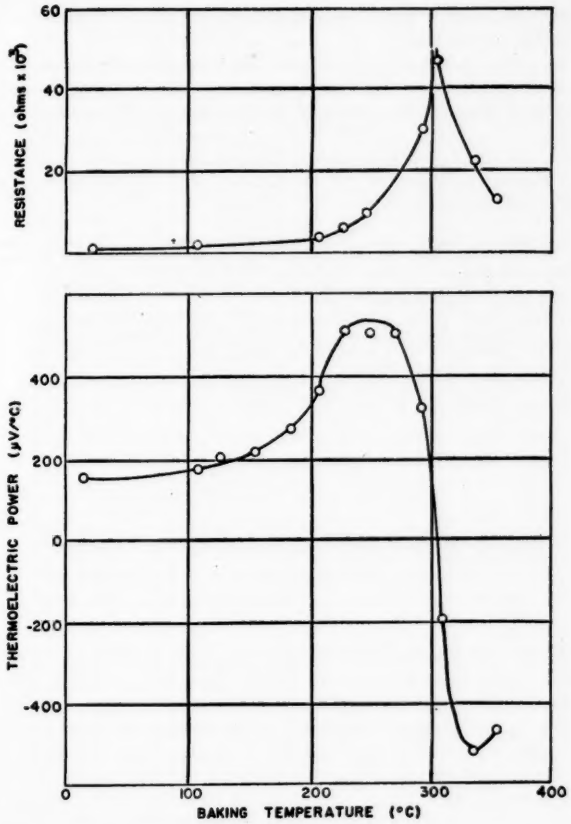

FIG. 1. Thermoelectric power and resistance of a lead telluride film as a function of film composition.

resistance reaches a maximum. Additional baking produces an excess lead film, as is indicated by the negative thermal voltage (electronic conductivity). The process has also been reversed. If one begins with an excess lead film and admits air into the vacuum system, the film resistance rises at first, then drops as the pressure in the vacuum system approaches atmospheric pressure. The thermal voltage is negative at first, becomes zero at the resistance maximum, then becomes positive. The diffusion of oxygen into the lattice thus changes the film from an electronic to a hole conductor. Additional experiments are now in progress to compare the results obtained with a hole conductor containing excess tellurium with those obtained when an excess lead film is made a hole conductor by the addition of oxygen.

* This work has been supported by the Air Materiel Command.

[1] H. Hintenburger, Zeits. f. Physik 119, 1 (1942).

The Temperature Dependence of Organic Scintillation Counters

S. H. LIEBSON AND J. W. KELLER, JR.
Electricity Division, Naval Research Laboratory, Washington, D. C.
March 17, 1950

THE temperature dependence of the light output of organic phosphors when subjected to gamma-radiation was measured for several different crystals and mixtures. Previous measurements by Graves and Koch[1] indicate irregularities in the light output of crystals as a function of temperature which they attributed to properties of the lattice. Their experimental arrangement was such that both photo-multiplier and crystal were varied in temperature during the course of the measurement. Measurements by Kelley and Goodrich[2] were made on anthracene radiated with β-particles. The present investigation differs in that the photo-multiplier was kept at liquid nitrogen temperatures while the crystal temperature could be varied in a separate insulated chamber. The light output was guided to the photo-multiplier by means of a Lucite rod or hollow aluminum tube depending on the type of crystal to be used and the extent of the contributions of the Lucite scintillations to those of the crystal under investigation. Measurements were made on the pulse distributions and total light output under gamma-ray excitation from a radium source. For pulse height distributions, the discriminator of the amplifier-scaler was so set as to reject Lucite scintillations. These measurements were consistent with measurements made on the total light output of the crystals, subject to the same excitation, the results of which are shown in Fig. 1. If we assume with Franck and Livingston[3] that the energy transfer process is one of sensitized fluorescence, the data suggest two possible explanations for the different characteristics of the same percentage of anthracene and stilbene in naphthalene; either the quenching occurs at the trapping molecule, or the quenching occurs during the exciton travel in the lattice. This quenching being greater for naphthalene-stilbene mixtures leads us to believe that it is due to the greater possibility of energy reflection from the stilbene molecule, subjecting excited naphthalene molecules to thermal perturbations for longer periods of time. This is further borne out by the lower quantum efficiencies for naphthalene-stilbene mixtures as compared to naphthalene-anthracene mixtures. No differences were found between temperature measurements on single crystals or their powders.

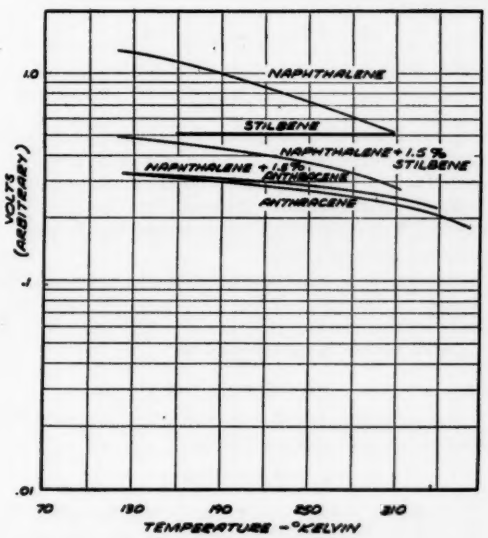

FIG. 1. Temperature variation of integrated light output.

The naphthalene and anthracene single crystals were obtained from the Harshaw Chemical Company. The anthracene used in mixtures with naphthalene was obtained from Eastman Kodak Company. The stilbene crystal was grown by Dr. S. Zerfoss and Mr. L. R. Johnson of this Laboratory, and the other samples were made by solidifying from the melt in a metallographic specimen press.

[1] J. D. Graves and G. E. Koch, Interim Report ADP-84, Radiological Def. Lab.
[2] G. G. Kelley and M. Goodrich, Phys. Rev. 77, 138 (1950).
[3] J. Franck and R. Livingston, Rev. Mod. Phys. 21, 505 (1949).

A Variational Method for Non-Conservative Collisions

MELVIN LAX
Physics Department, Syracuse University, Syracuse, New York
March 20, 1950

ENERGY is conserved in all collisions, providing one describes a closed physical system. Often, however, the collision process can be described phenomenologically without a complete knowledge of the final form of the absorbed energy. A description of the latter may be avoided by dealing with an open physical system. Apparent energy (or particle) losses then require the introduction of non-hermitian volume or surface operators. For example, conversion of sound energy to heat may be accounted for by adding a viscous term to the wave equation. Capture of neutrons by a nucleus is most conveniently described by a non-hermitian surface boundary condition.[1]

Fortunately, one of the most powerful methods of dealing with conservative collisions, the variational method, can be applied with little change to the non-conservative case.

The Schrödinger equation can be written as

$$(E-H)\Psi_a=V\Psi_a, \tag{1}$$

where V is the (possibly) non-hermitian perturbation. If Φ_a is an incident wave in direction a associated with the unperturbed Hamiltonian H, the total wave Ψ_a is a sum of incident and scattered waves

$$\Psi_a=\Phi_a+(E-H)^{-1}V\Psi_a, \tag{2}$$

where $(E-H)^{-1}$ is the reciprocal associated with outgoing waves:[2]

$$(E-H)^{-1}=P(E-H)^{-1}-i\pi\delta(E-H). \tag{3}$$

(Here P implies that the Cauchy principal value is to be used in integrations.)

Introducing the transition operator

$$T\Phi_a=V\Psi_a, \quad T_{ba}=(\Phi_b, V\Psi_a), \tag{4}$$

the scattered wave can be written in the form

$$(E-H)^{-1}T\Phi_a. \tag{5}$$

Dirac has shown that the coefficient of the "outgoing" reciprocal in the momentum representation is the scattering amplitude. In other words T_{ba} is an exact expression for the scattering (or transition) amplitude[3] that is usually represented in the Born approximation by V_{ba}. A direct proof of this statement can be given in the time-dependent representation.

Our problem then is to obtain a variational expression for T_{ba} with the help of the integral Eq. (2). Since the form of (2) is altered in problems with surface boundary conditions, we consider instead a more general integral equation,

$$\Psi_a=\Phi_a+LV\Psi_a, \tag{6}$$

where L is an arbitrary, possibly non-hermitian operator. We also introduce an associated adjoint equation

$$\Psi_b'=\Phi_b+L\dagger V\dagger\Psi_b', \tag{7}$$

where Ψ_b' is closely related to the time-reversed solution $\Psi_b(-t)$. With the help of the auxiliary solution we can construct three equivalent expressions for the transition amplitude T_{ba}:

$$T_{ba}=(\Phi_b, V\Psi_a)=(\Psi_b', [V-VLV]\Psi_a)=(\Psi_b', V\Phi_a). \tag{8}$$

Furthermore we can construct an expression

$$T_{ba}=\frac{(\Psi_b', V\Phi_a)(\Phi_b, V\Psi_a)}{(\Psi_b', V\Psi_a)-(\Psi_b', VLV\Psi_a)} \tag{9}$$

that is stationary with respect to independent variations in Ψ_b' and Ψ_a. This expression is essentially the same as those used by Schwinger.[4] However, neither V nor L need be a hermitian operator.

If L and V are *symmetric* operators, the correct solutions are related by

$$\Psi_b'=\Psi_{-b}^*, \tag{10}$$

where $\Psi_{(-b)}$ is a state associated with an incident wave in a direction opposite to b.

In order to test the accuracy of the variational expression (9) in a dissipative case the following problem was considered: scattering of sound from a strip of absorbing material. Accuracy of 2 percent or better over the whole frequency range was obtained with the simplest trial function. This success is partly explained by the independence of (9) to changes of normalization of the unknown functions.[5]

[1] Feshbach, Peaslee, and Weisskopf, Phys. Rev. 71, 145 (1947). See H. Bethe, Phys. Rev. 57, 1125 (1940) for a treatment of same problem with a non-hermitian volume operator.
[2] P. A. M. Dirac, *Quantum Mechanics* (Oxford University Press, New York, 1947), Third Edition, p. 193.
[3] Reference 3, p. 199, Eq. (38). See also M. Lax, following letter, Eq. (4).
[4] J. Schwinger and H. Levine, Phys. Rev. 74, 958 (1948). See J. M. Blatt and J. D. Jackson, Phys. Rev. 76, 18 (1949), Eq. (2.11) for application of (4) to phase shift calculations.
[5] A. Levitas and M. Lax, "Scattering and absorption from an acoustic strip," J. Acous. Soc. Am. (to be published).

On a Well-Known Cross-Section Theorem

MELVIN LAX
Physics Department, Syracuse University, Syrcause, New York
March 20, 1950

ANY collision process that removes particles from an incident beam must be accompanied by forward scattering whose function is to interfere with the main beam and produce a shadow. This is the physical basis for the proportionality between the imaginary part of the forward scattered amplitude and the total collision cross section. This theorem has been proved for a variety of special cases.[1] It may be of interest to indicate a simple proof general enough to include the following possibilities: (1) inelastic as well as elastic scattering, (2) creation and destruction of particles, (3) forces of any type—including spin dependent and non-central forces, (4) non-conservative forces; i.e., non-hermitian operators. (The significance of such forces are discussed in the preceding letter[2] hereafter referred to as A.)

Eliminating Φ_a from the forward scattered amplitude

$$T_{aa}=(\Phi_a, V\Psi_a)$$

with the help of (A2) we obtain:

$$(\Phi_a, V\Psi_a)=(\Psi_a, V\Psi_a) -(\Psi_a, V\dagger[P(E-H)^{-1}-i\pi\delta(E-H)]V\Psi_a). \tag{1}$$

Simplify the last term with the help of (A4) and take the imaginary part:

$$ImT_{aa}=Im(\Psi_a, V\Psi_a)-\pi(\Phi_a, T\dagger\delta(E-H)T\Phi_a). \tag{2}$$

This may be rewritten in more familiar units as:

$$-2/\hbar ImT_{aa}=w+w', \tag{3}$$

$$w=2\pi/\hbar\,\Sigma_b|T_{ba}|^2\delta(E_a-E_b), \tag{4}$$

$$w'=-2/\hbar\,Im(\Psi_a, V\Psi_a). \tag{5}$$

Here w represents the transition probability to all observed final states b and w' the transition probability associated with "true" absorption processes. Dividing by the incident flux we obtain the theorem that the forward scattered amplitude is proportional to the sum of scattering plus absorption cross sections.

In an elastic scattering problem whose asymptotic solution has the form $\exp(ikz)+f(r)^{-1}\exp(ikr)$, where f is the angular dependent scattering amplitude the cross-section theorem would be written:

$$(4\pi/k)Imf(a\leftarrow a)=\int|f|^2d\Omega-(2m/\hbar^2k)Im(\Psi_a, V\Psi_a), \tag{6}$$

where k is the propagation constant and $v=\hbar k/m$ is the incident flux. The two terms on the right are the scattering and capture cross sections respectively.

The significance of the cross-section theorem is best understood from the viewpoint of a multiple scattering problem. A distribution of scatterers can be replaced by a medium with a modified index of refraction and an attenuation. For a random distribution of scatterers the equation of the coherent wave $\langle\psi\rangle$ in the medium is:[3]

$$(E-H-\bar{T})\langle\psi\rangle=0, \quad \bar{T}_{ba}=nT_{aa}\delta_{ba}, \tag{7}$$

where $\bar{T}$ has only diagonal matrix elements and n is the density of scatterers. Thus the phase velocity is determined primarily by the real part of T_{aa} and the attenuation by the imaginary part.

It is also possible to interpret (9) in the language of a decay problem. Since T_{aa} represents the energy shift of state a, $|\Psi_a|^2$ has the time dependence $\exp[-2ImT_{aa}/\hbar]$. Thus (9) states that the rate of decay of state a is equal to the total transition probability from state a to all other states *including* a.

In a true decay problem, the right-hand side of (4) would include transitions only to states $b\neq a$. To prove the theorem appropriate to decay problems, we note that there is no incident wave. Thus the Schrödinger equation takes the integral form

$$\Psi_a=(E-H)^{-1}V\Psi_a. \tag{8}$$

Introducing the projection operator P_a associated with state Φ_a and $Q_a=1-P_a$, the corresponding annihilation operator we can separate the term associated with state Φ_a by multiplying (8) by (P_a+Q_a). Since

$$(E-H)^{-1}P_aV\Psi_a=(E-H)^{-1}P_aT\Phi_a=(E_a-E_a^0)T_{aa}\Phi_a$$

and T_{aa} represents the energy shift we obtain:

$$\Psi_a=\Phi_a+(E-H)^{-1}Q_aV\Psi_a. \tag{9}$$

This differs from the collision case (A2) by the factor Q_a which suppresses state a. Equation (2) becomes:

$$ImT_{aa}=Im(\Psi_a, V\Psi_a)-\pi(\Phi_aT\dagger Q_a\delta(E-H)T\Phi_a) \tag{10}$$

and the sum in (4) is over $b\neq a$.

[1] G. C. Wick, Phys. Rev. **75**, 1459(A) (1949). W. Pauli, *Meson Theory of Nuclear Forces* (Interscience Publishers, Inc., New York, 1946), p. 46 ff. H. C. Van de Hulst, Physica **15**, 740 (1949). E. Feenberg, Phys Rev. **40**, 40 (1932).
[2] M. Lax, Phys. Rev. **78**, 306 (1950).
[3] M. Lax, Phys. Rev. **77**, 756(A) (1950).

Comparison of the Isotopic Constitution of Terrestrial and Meteoritic Sulfur

J. MACNAMARA AND H. G. THODE
Department of Chemistry, McMaster University, Hamilton, Ontario, Canada
March 14, 1950

THE isotopic content of elements in meteorites and a comparison of the meteoritic and terrestrial values are of considerable interest. Recently results have been reported for gallium,[1] copper,[2] iron,[3] and sulfur.[4] Although in most cases only 1 or 2 samples of each were investigated, the results show no variation in isotopic ratios. In the case of carbon where variations in the isotopic ratios up to 5 percent occur in terrestrial sources, Murphey and Nier[5] have reported variations up to 2.5 percent between samples of meteoritic carbon. Recent results of Trafimov[4] indicated little or no variation in the isotopic content of terrestrial and meteoritic sulfur with the exception of sea water sulfate, which was found to be slightly enriched in S^{34}.

However, in view of the marked variation in the S^{32}/S^{34} ratio found by Thode, Macnamara, and Collins[6] for different terrestrial compounds of sulfur, it seemed important to study the isotopic composition of meteoritic sulfur and to establish the relation between the isotopic composition of terrestrial and meteoritic sulfur. Ten samples of troilite from four siderite and two stony meteorites have been analyzed with a 180-degree direction focusing mass spectrometer of the Nier type.[7] The S^{32}/S^{34} ratios obtained for these samples are given in Table I. All the samples were compared with the same standard used in our previous work, and the relative ratios are probably good to 0.1 percent or better. It is seen that the S^{32}/S^{34} ratios for meteoritic samples are constant within the probable limits of error and that the value coincides approximately with the average value found for terrestrial sulfur[6] (see Fig. 1).

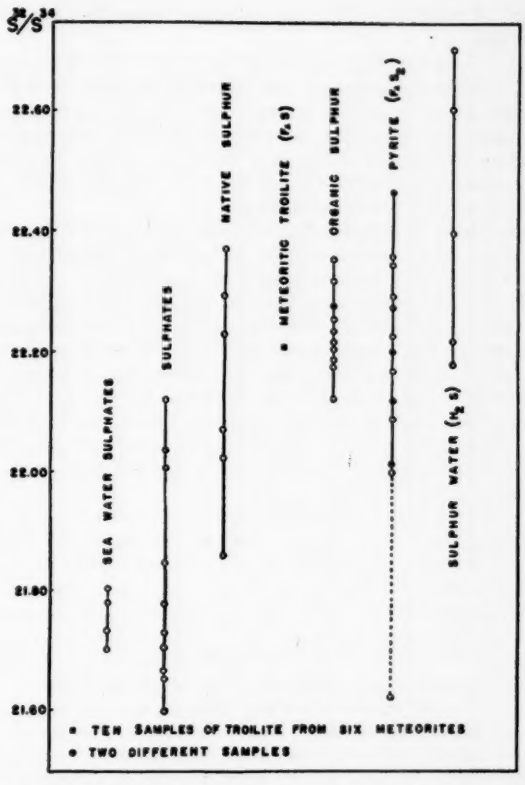

FIG. 1. Isotopic distribution of S^{34} in terrestrial and meteoritic sulfur.

TABLE I. Isotopic distribution of S^{34} in meteoritic sulfur.

Type of meteorite	Name and location	S^{32}/S^{34} ratio
Siderite	Canyon Diablo, Arizona	22.21±0.01
Siderite	Canyon Diablo, Arizona	22.22±0.01
Siderite	Canyon Diablo, Arizona	22.21±0.01
Siderite	Canyon Diablo, Arizona	22.21±0.01
Siderite	Waterville	22.20±0.01
Siderite	Duchesne, Duchesne Co., Utah	22.23±0.01
Siderite	Duchesne, Duchesne Co., Utah	22.24±0.01
Siderite	El Toba, Argentine	22.22±0.01
Aerolite	"Beenham," Union Co., New Mexico	22.20±0.01
Siderolite	Brenham, Kiowa Co., Kansas	22.23±0.01

Since the abundance of the sulfur isotopes vary markedly in samples of terrestrial sulfur, it is important that the source of sulfur be stated where absolute abundances are involved. In this regard, it would be well to quote absolute abundances on the basis of meteoritic sulfur in view of the remarkably constant values found in these samples. The absolute abundances of the sulfur isotopes found in this laboratory for a representative sample of meteoritic sulfur are given in Table II. The chemical atomic

TABLE II. Absolute isotopic abundances of meteoritic sulfur.

Mass	Percentage
32	95.018
33	0.750
34	4.215
36	0.017

weight of meteoritic sulfur was calculated from these results to be 32.064.

It is most interesting that the isotopic content of sulfur samples from a single meteorite and from different meteorites should be constant to better than 0.1 percent. This is in striking contrast to the fairly large variations (2.5 percent) found by Murphey and Nier[5] for the isotopes of carbon in meteorite samples. Relatively large variations in isotopic ratios occur for both the carbon and sulfur isotopes in terrestrial sources.

It is clear from theoretical and experimental evidence that these variations in terrestrial samples are due to fractionation that occurs in biological and geological processes because of differences in the chemical properties of isotopic molecules. A comparison of the isotopic ratios obtained for meteoritic and terrestrial sulfur illustrated in Fig. 1 suggests that at the time the earth was formed the isotopic content of sulfur was the same as that now found for meteoritic sulfur, but that fractionation has occurred since, thereby spreading out the ratios above and below the base value. The remarkably constant isotopic ratios found for meteorites, however, indicate that meteoritic sulfur has not been subjected to the same fractionation processes.

There is a great deal of evidence to show that meteorites originated from within the solar system. Work on the isotopic content of various elements in meteorites, including our results for sulfur, bears this out. If we accept the view that meteorites resulted from the disintegration of a planet by some celestial catastrophe then we might expect sulfur from stony meteorites, which probably originated from the crust of the ancestral planet to show variations in isotopic content as do sulfur samples from the earth's crust. The stony meteorites examined to date, however, show no variation in the isotopic content of sulfur, which was found to be the same in all meteorites.

We wish to thank Drs. V. B. Meen, H. H. Nininger, and E. P. Henderson for the samples of meteoritic troilite, and Dr. R. P. Graham for helpful discussions. The financial assistance of the National Research Council is gratefully acknowledged.

[1] Inghram, Hess, Brown and Goldberg, Phys. Rev. **74**, 343 (1948).
[2] H. Brown and M. G. Inghram, Phys. Rev. **72**, 347 (1947).
[3] G. E. Valley and H. H. Anderson, Phys. Rev. **59**, 113 (1941).
[4] A. Trafimov, Doklady Akad. Nauk. U.S.S.R. **66**, 181 (1949).
[5] B. F. Murphey and A. O. Nier, Phys. Rev. **59**, 771 (1941).
[6] Thode, Macnamara, and Collins, Can. J. Research **B27**, 361 (1949).
[7] Thode, Graham, and Zeigler, Can. J. Research **B23**, 40 (1945).

Thermoelectromotive Force of Superconducting *versus* Normal Junctions of the Same Metal

M. C. Steele
Naval Research Laboratory, Washington, D. C.
March 15, 1950

MEASUREMENTS of temperature variation of the thermoelectromotive force of superconducting *versus* normal junctions of the same metal have been made for tin and lead. The experimental technique differs from that of Keesom and Matthijs[1] in that they employed magnetic shielding and several circuits of the metal in series, whereas the present work required no magnetic shielding and only one circuit. A wire of the metal to be studied was connected to a d.c. voltage amplifier (breaker type) by copper leads. The temperature of the two points of contact with the leads was adjusted to have one portion of the specimen superconducting and the remainder normal. By applying appropriate magnetic field strengths over the entire length of the wire the temperature of the superconducting-normal junction can then be varied. If the two points of contact are maintained at constant temperature throughout the course of the experiment, the voltage differences observed can be attributed to the temperature variation of the thermoelectromotive force of the superconducting-normal junction. If the contact temperatures do change during the experiment, the observed voltages have to be corrected from data obtained by calibrating the circuit with varying contact temperatures (usually only one contact need be made variable) in the absence of magnetic fields. Taking the voltage of the superconducting-normal junction as zero at T_c (where T_c is the superconducting transition temperature for zero magnetic field) the observed voltage differences can be summed to give the desired absolute voltage for temperatures below T_c. Using this procedure data were obtained from 2.30°K to 3.72°K for tin and from 4.22°K to 7.26°K for lead.

Figure 1 shows a log-log plot of E/E_0 *versus* $1-(T/T_c)^2$ for the data obtained with tin and lead. E is the thermoelectromotive force of the superconducting-normal junction; E_0 is the value of E at 0°K (obtained by extrapolation); T is the temperature ($T \leqq T_c$). It is seen that the data for both these elements can be represented by the reduced equation

$$E/E_0 = 1-(T/T_c)^2, \tag{1}$$

where $T_c = 3.72$°K, $E_0 = 5.5\times10^{-8}$ volts for tin, and $T_c = 7.26$°K, $E_0 = 59\times10^{-8}$ volts for lead. The parabolic relation given by Eq. (1) can be derived from the Fermi gas model[2] if it is assumed that the Thomson coefficient, σ, of a superconductor is zero. This assumption is supported in the case of lead, by the experiments of Daunt and Mendelssohn.[3]

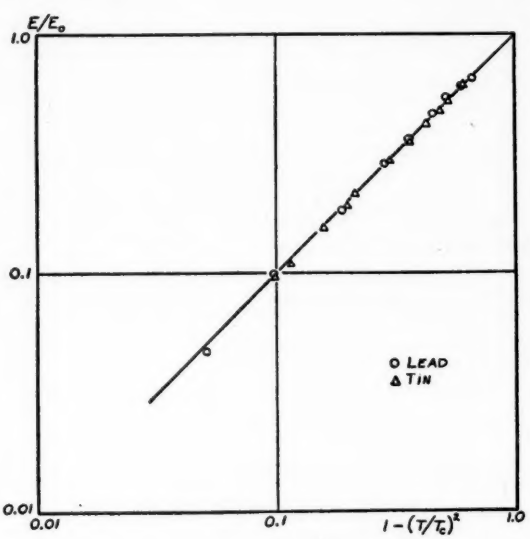

FIG. 1. Logarithmic plot of E/E_0 as a function of $1-(T/T_c)^2$.

These results can be used to calculate the value of γ, where γT is the electron contribution to the specific heat, by combining Eq. (1) with the free electron theory expression for the Thomson coefficient. The relation found is

$$\gamma = 3eE_0/T_c^2, \tag{2}$$

where e is the electronic charge and γ is expressed per atom of material. Using the values of E_0 and T_c given above, and converting to a mole basis, it is found that γ is 2.7×10^{-4} and 7.7×10^{-4} cal. per mole per (deg. K)^2 for tin and lead respectively.

Preliminary experiments with lead having small amounts of impurity (total impurity ~1.5 percent) have shown that not only does E decrease by as much as a factor of 5, but also Eq. (1) no longer represents the data adequately.

A detailed account of the work reported above, as well as the results of experiments in progress at this date, will be given in the near future. The author wishes to thank Dr. R. T. Webber for having suggested the subject of this investigation.

[1] W. H. Keesom and C. J. Matthijs, Physica **5**, 437 (1938).
[2] G. C. Pimentel and R. K. Sheline, J. Chem. Phys. **17**, 644 (1949). J. G. Daunt and K. Mendelssohn, Proc. Roy. Soc. **A185**, 225 (1946).

The Effect of Magnetic Fields on the Response of Gamma-Scintillation Counters

J. D. GRAVES
Naval Radiological Defense Laboratory, San Francisco, California
March 13, 1950

A MARKED change in the response of scintillation detectors has been observed with their use in magnetic fields. The extent of this effect has been determined for several conditions.

A 1P21 photo-multiplier tube and a phosphor were mounted in a light-tight brass cylinder and the cylinder was placed in a long, stationary solenoid. Variable direct current through the solenoid windings was used to produce axial magnetic fields, and a constant voltage was applied to the photo-multiplier. Radium was used as the source of gamma-radiation. Two phosphors, a $CaWO_4$ crystal, $\frac{1}{4}$ inch in diameter and 1 inch long, and a NaI(Tl) aggregate approximately $\frac{3}{8}$ inch$\times\frac{1}{2}$ inch were used.[1] Magnetic fields of the magnitude used here had no apparent effect upon the light output of the phosphors.

In Fig. 1, curves I and III show a maximum counting rate at a magnetic field strength of about 12 gauss directed from the base through the photo-multiplier. Curves II and IV for fields directed toward the base, show a diminishing counting rate with increasing magnetic field.

Figure 2 shows integral bias curves taken for the two phosphors without the applied magnetic field, and with 11.7 gauss applied axially and directed from the base. With both phosphors the percentage change in counting rate between the two field strengths decreased with decreasing discrimination level. It appears that for a given phosphor, extrapolation of these curves will result in a common ordinate intercept for both field strengths. The effect of the magnetic field appears as a simple change in amplification of the photo-multiplier, as evidenced by the constant percentage change in the discrimination level at the two field strengths for any one counting rate.

Figure 3 shows that the maximum total anode current occurs at approximately 12 gauss directed from the base. The current is seen to drop rapidly with increasing fields directed toward the base. Curves similar to those in Figs. 1–3, with the exception of a shifting of the field strength for maximum response, were obtained for several photo-multiplier tubes. A variation in shape and position of the curves with applied voltage was observed.

Nearly exponential integral bias curves of the form

$$N_1 = N_0 \exp(-s_1 v)$$

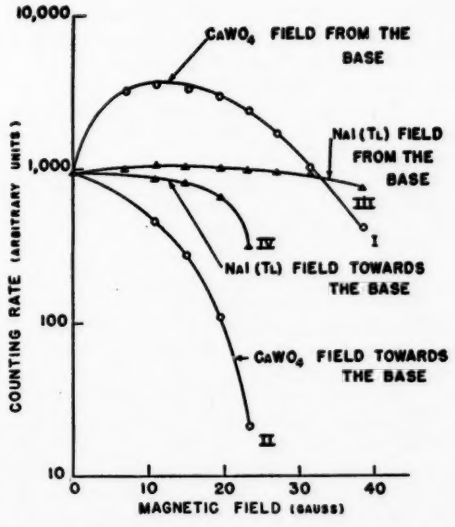

FIG. 1. Fixed discrimination level counting rate from scintillation counters as a function of axial magnetic field strength. Radium gamma-field adjusted to give equal counting rates at zero applied field for the two materials.

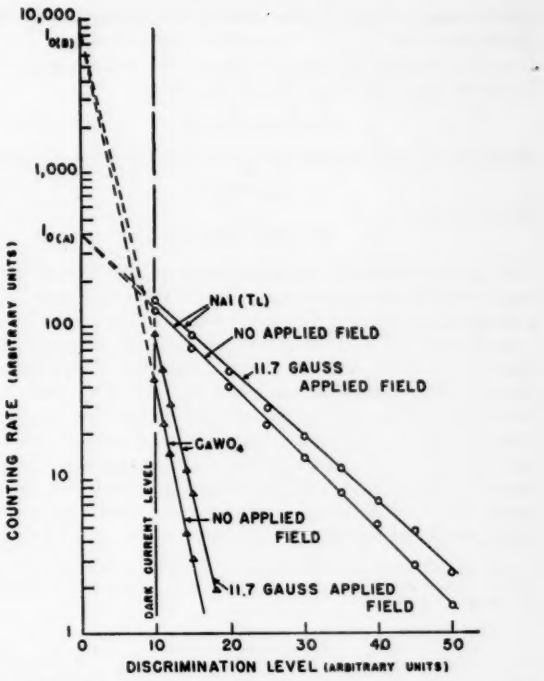

FIG. 2. Integral bias curves for the sintillation counters at zero applied field and 11.7 gauss directed axially from the base.

were observed, where N_1 is the counting rate, N_0 the total number of scintillations occurring, $-s_1$ the slope, and v the discrimination level. This distribution was due in part to the energy distribution of the Compton and photo-electrons, statistical variations within the tube, and edge effects and optical transmission properties of the phosphor.

In any distribution, if N_0 is independent of the tube amplification, the ratio of counting rates at any two amplifications is dependent only upon some function of the discrimination level. In this case the ratio is exponential with v, or

$$R = N_1/N_2 = \exp[(s_2 - s_1)v].$$

Since the slope of the integral bias curve is a function of the efficiency of the crystal as well as of the tube amplification, the

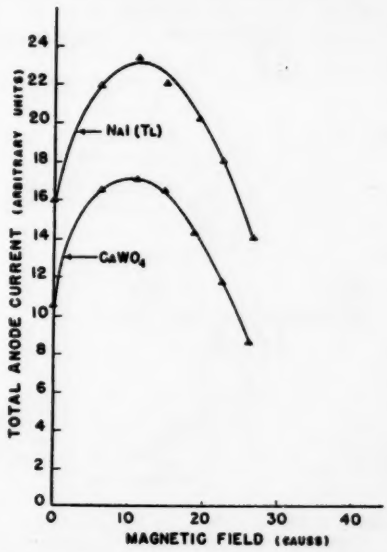

FIG. 3. Total current output for the scintillation counters as a function of axial magnetic field strength directed from the base.

relative effect of tube amplification on R for phosphors of different efficiencies is of interest. The relation between slopes $(-s_1)$ and $(-s_2)$ at two amplifications for phosphor A and slopes $(-s_3)$ and $(-s_4)$ for phosphor B can be shown to be

$$s_1/s_3=s_2/s_4=n.$$

Hence the relation between the counting rate ratios R_A and R_B is

$$R_A=R_B^n.$$

From Fig. 2,

$$R_{CaWO_4}=R^5_{NaI(Tl)}. \quad (1)$$

If the time constants of the pulse are independent of the pulse amplitude, the percentage change in anode current resulting from a change in magnetic field would be constant for both phosphors.

In the case of $CaWO_4$ a 40 percent change in counting rate was observed when the field was changed from 0 to 1.5 gauss through the tube. Discrimination took place just above the dark current level. This corresponds roughly to the change that would result from positioning the tube axially with and against the earth's field. The 3 percent change predicted from expression (1) for this same field change with NaI(Tl) was not detectable with the experimental accuracy observed. The change in total current for the 1.5 gauss change was about 9 percent.

[1] The NaI(Tl) sample was obtained through the courtesy of R. Hofstadter, Princeton University, and the $CaWO_4$ sample was obtained from the Linde Air Products.

Radioactive Decay of the Neutron*

ARTHUR H. SNELL, FRANCES PLEASONTON, AND R. V. MCCORD
Oak Ridge National Laboratories, Oak Ridge, Tennessee
March 6, 1950.

EXPERIMENTAL evidence concerning the instability of the neutron[1] has been obtained with the apparatus shown in Fig. 1. A beam of neutrons from the Oak Ridge uranium-graphite reactor passed longitudinally (perpendicular to paper) through an evacuated tank shown in section. An electric field was applied between an open-sided cylindrical electrode (+) and a plane electrode (−) such that positive particles appearing in this region of the beam would be accelerated upward through 8 kv and would be focused upon the enlarged first plate of a secondary electron multiplier situated behind an aperture in the negative electrode. The aperture and the multiplier plates were 7.3 cm long in the direction parallel with the beam. The two-celled beta-proportional counter placed below the beam had an effective length of about 11 cm.

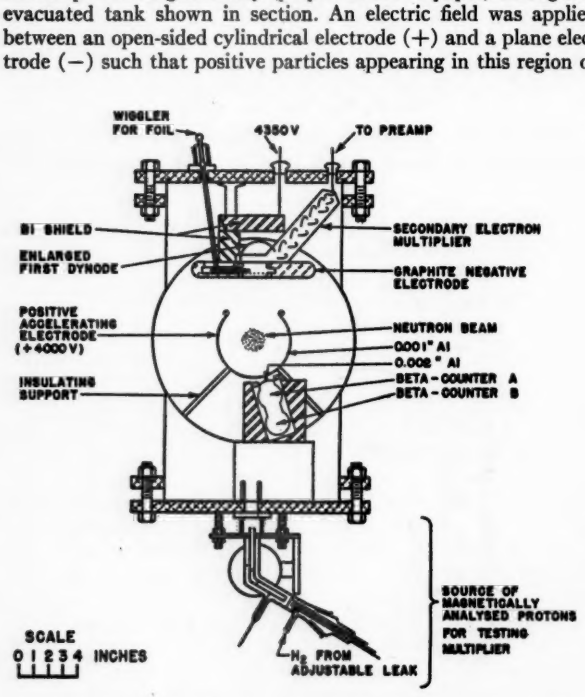

FIG. 1. Apparatus used for seeking beta-proton coincidences arising from neutron decay. The neutron beam is indicated in section at the center. A vertical electric field accelerates the protons upward and focuses them upon the secondary electron multiplier; the beta-particles register in the double beta-proportional counter below.

TABLE I. Coincidences with 0.25 μsec. delay.

Conditions	Transverse electric field	Genuine coincidence rate cpm	Field-sensitive genuine coincidence rate cpm	Remarks
Normal	on off	0.74 ±0.05 0.08 ±0.04	0.66 ±0.07	Conditions would allow neutron decay coincidences to appear.
Boron interrupting slow neutron beam	on off	0.13 ±0.03 0.03 ±0.03	0.10 ±0.04	B^{10} shutter known to leak about 10% of the slow neutrons through thin spots.
Cadmium in beam, eliminating slow neutrons and substituting strong source of capture gammas	on off	0.18 ±0.08 0.17 ±0.10	0.01 ±0.13	Pile power reduced until individual counting rates about equal to those in other tests. (Factor 1/7.)
3 sq. ft. Cd wrapped around vacuum tank	on off	0.73 ±0.08 0.19 ±0.07	0.54 ±0.11	Neutrons again present in beam. Local captures increased many fold.
0.0002 in. Al foil covering multiplier aperture	on off	0.05 ±0.04 0.05 ±0.04	0.00 ±0.06	Reassuring check; contributes little new.
H_2 gas in vacuum tank to 5 times base pressure	on off	0.73 ±0.05 0.06 ±0.04	0.67 ±0.07	No more field-sensitive coincidences than in 1, 4 or 8.
0.051 in. Al over AB counter window	on off	0.11 ±0.04 0.12 ±0.03	−0.01 ±0.05	Sufficient Al to stop betas of expected energy (0.8 Mev).
Repeat 1	on off	0.75 ±0.04 0.08 ±0.03	0.67 ±0.05	

Triple coincidences were sought; namely, coincidences between discharges of counter A and counter B resulting from beta-particles emitted from neutrons in the beam, and pulses in the multiplier caused by the focused product protons.

Because of stray radiation the single counting rates were high (~75,000 per minute in A and B, and 1500 per minute in the multiplier). With an effective resolution time of 1.3 μsec., the random coincidence rate was almost equal to the expected genuine rate. Genuine coincidences were nevertheless observed. They could be divided into two classes:

(1) Coincidences which appeared when no special delays were were introduced in the circuits. These coincidences did not depend upon the presence of the electric field. They were probably caused by fast secondary electrons in the background radiation, which traversed the three detectors. They do not concern us further.

(2) Coincidences which appeared when 0.25 μsec. delay was inserted in the AB counter channel. These coincidences depended upon the presence of the electric field across the beam. A field plot had shown that 0.25 μsec. was approximately the minimum time required for a recoiling proton to be collected upon the multiplier.

Table I gives some observations made with the 0.25 μsec. delay in the AB channels. Random coincidence rates which have been subtracted were about 0.9 counts per minute throughout. A field-sensitive effect was present (column 5) which was the same under conditions 1, 4, 6, and 8, but which essentially vanished under conditions 2, 3, 5, and 7. Tests were also made with the reactor off, using a pure gamma-source (Co^{60}) to actuate the detectors to approximately the same individual rates as prevailed when the

reactor was on; no significant field-sensitive effects appeared either in the coincidences or in the single counting rate of the multiplier alone.

Taken together, these observations indicate the existence of coincident events involving on the one hand the appearance of positive particles with low energy and of roughly protonic mass, and on the other hand the discharge of counters by something which could penetrate 0.003 inch of aluminum but failed to penetrate 0.054 inch of aluminum. In addition, the events depended upon the presence of slow neutrons in a manner unconnected with their capture gamma-rays, and they did not involve ionization processes in the residual gas.

The observations would be explained completely and without internal contradiction if neutrons in free flight transform spontaneously into protons with the emission of beta-particles having a maximum energy of less than about 0.9 Mev.

We are not yet in a position to give an accurate value for the half-life of the neutron because of difficulties in evaluating the collecting geometry, in which beta-proton directional correlations are involved. A half-life in the range 10–30 minutes would, however, be consistent with all of our observations.

E. F. Shrader, D. Saxon, and L. C. Miller have collaborated actively in the experiment in the past. We are indebted to W. H. Jordan for generous help in the electronics.

* This document is based on work performed under Contract No. W-7405, eng. 26 for the Atomic Energy Project at Oak Ridge.

[1] J. Chadwick and M. Goldhaber, Proc. Roy. Soc. **A151**, 479 (1935).

Radioactive Decay of the Neutron

J. M. Robson
Atomic Energy Project, National Research Council of Canada, Chalk River, Ontario, Canada
March 13, 1950

BY using a thin magnetic lens spectrometer in conjunction with an electrostatic field, the positive particle from the radioactive decay of the neutron has been identified as a proton. The source of neutrons was a beam from the Chalk River pile from which the pile gamma-rays had been filtered by a 5-in. bismuth plug at the reacting core end of the collimator. Figure 1 shows a plan view of the apparatus mounted outside of the pile shield with the beam entering the aluminum vacuum tank through a 0.005-in. aluminum window and emerging through a 0.018-in. window into the beam catcher.

The high voltage electrode in the form of a hollow half-cylinder of 0.005-in. aluminum was held at a positive potential to ground

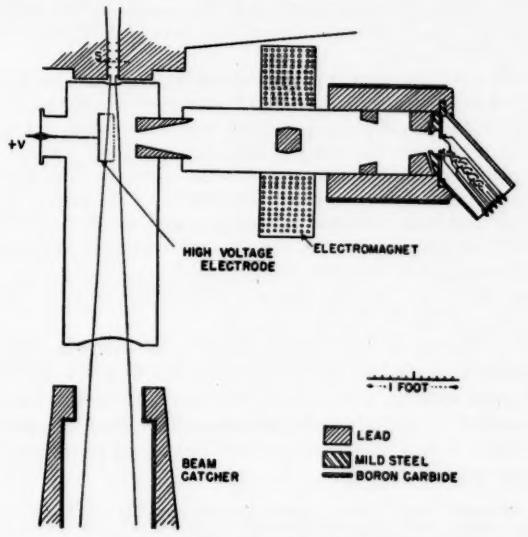

FIG. 1. Plan view of the apparatus.

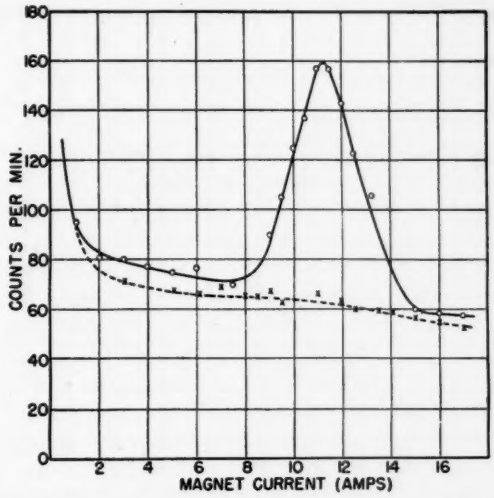

FIG. 2. Electron multiplier counting rate as a function of magnetic field for a potential of 15 kv on the high voltage electrode. The solid curve corresponds to the boron shutter "out" and the dotted curve to the boron shutter "in."

so that low energy positively charged particles such as protons resulting from the neutron decay were deflected through the entrance aperture into the thin magnetic lens spectrometer. The counter at the end of the spectrometer was an electron multiplier shielded from the magnetic field by mild steel shaped to deflect the field away from the beryllium-copper electrodes. A thin shutter of boron carbide power held between two 0.005-in. aluminum windows could be inserted in the beam at S in the pile shield to shut off the thermal neutrons without appreciably scattering the other components of the beam.

The procedure in the experiment was to set a definite voltage on the electrode and record the counting rate of the electron multiplier as the magnet current was varied. Figure 2 shows the results obtained with 15 kv on the electrode, and consists of two curves one with the boron shutter "out" and the other with the shutter "in." The peak on the "out" curve occurs at the correct magnetic field to focus protons of the energy received from the electrostatic field. With the boron shutter "in", the general features of the counting rate curve are similar except that the peak disappears. The difference in the counting rates observed between 2 and 7 amp. and above 15 amp. is probably due to gamma-rays from the capture of thermal neutrons scattered by the vacuum chamber windows and by the air between the vacuum chamber and beam catcher.

At accelerating potentials under 10 kv it would have been possible with the magnetic field available to observe the peak corresponding to singly ionized molecular hydrogen. No significant peaks other than that corresponding to protons were observed at any potential. The pressure in the vacuum tank was varied to see if any of the protons arose from spurious effects in the residual gas. No significant effect was observed with air or oil vapor between pressures of 7×10^{-7} mm and 5×10^{-6} mm of mercury, measured with an ionization gauge. Above the latter pressure the electrostatic field tended to break down under the stray magnetic field near the high voltage electrode. A gamma-ray source placed near the vacuum tank increased the background but did not affect the proton peak. It thus appears probable that the proton peak corresponds to the decay of neutrons, and is not due to other pile radiation or to any effect of the residual gas in the vacuum tank.

An estimate of the half-life of the neutron can be obtained from the number of protons striking the first surface of the electron multiplier, the efficiency of the collecting and focusing system and the density of neutrons in the beam.

To obtain the number of protons striking the first surface of the electron multiplier a set of curves similar to Fig. 2 was obtained at

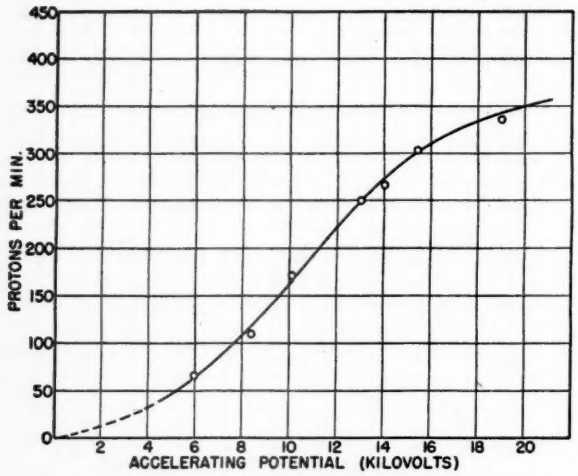

FIG. 3. Variation of number of focused protons with the potential on the high voltage electrode.

different bias settings using a set of discriminators and scalars simultaneously fed from the pulse amplifier. The height of the proton peak was estimated from each curve and a bias curve was then plotted. An extrapolation to zero bias gave an estimate of the number of protons striking the first multiplier electrode on the assumption that at zero bias the multiplier was 100 percent efficient for protons of these energies.[1] Figure 3 shows the variation of the number of protons with the accelerating potential.

A mechanical model[2] was used to investigate the efficiency of the electrostatic collection system at different proton recoil energies and the shape of the high voltage electrode was chosen to minimize the effect of the recoil energy on the resulting efficiency. The acceptance of the magnetic spectrometer was calculated from its geometrical constants. From these estimates the collection and focusing efficiency should reach a saturation value at about 22 kv; it appears from Fig. 3 that the number of detected protons did begin to reach saturation at approximately this potential. The density of slow neutrons in the beam was measured by the activity produced in calibrated manganese foils with and without cadmium. From the values thus obtained the limits for the half-life of the neutron are a minimum of 9 minutes and a maximum of about 25 minutes.

[1] J. M. Robson, Rev. Sci. Inst. 19, 865 (1948).
[2] V. K. Zworykin and J. A. Rajchman, Proc. I.R.E. 27, 558 (1939).

The Half-Life of Po^{208} *

D. H. TEMPLETON
Radiation Laboratory and Department of Chemistry, University of California, Berkeley, California
March 21, 1950

THE properties of Po^{208} have been described in a previous paper[1] in which the half-life was reported as "about 3 years," based on decay during 10 months of a mixture of Po^{208} and Po^{210} (and a small amount of Po^{209} which was not then recognized). By that time the silver plates on which the polonium was deposited had tarnished so badly that two new samples of the same polonium were mounted on platinum for more careful decay measurements. These samples have now been observed for three years. In the mean time Kelley and Segrè[2] have reported the half-life of Po^{208} as 3.0 ± 0.2 years and have described Po^{209}.

Several alpha-counters of the ionization chamber type were used in the course of the measurements. Each time they were used they were standardized by means of a sample of Th^{230}. Cognizance was taken of the growth of daughters in the Th^{230} sample, but this amounts to only 0.05 percent in three years. Statistically significant differences were observed in the counting efficiencies of

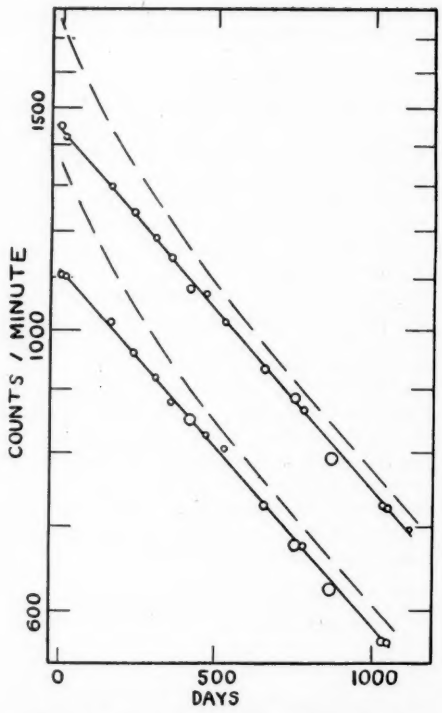

FIG. 1. The dashed curves represent the total activity of each sample; the points and solid lines represent the activity due to Po^{208}. The radius of each circle approximates twice the probable statistical error.

the various counters only on a few occasions when very discordant results revealed external disturbances or defective equipment. The activity due to Po^{210} in each sample was calculated from the pulse-analysis data obtained earlier when the activities due to Po^{208} and Po^{210} were about equal, combined with the value 138.3 days[3] for the half-life of Po^{210}. The contribution of Po^{209} to each sample was derived from pulse analyses made at the end of the experiment, when it amounted to about 4 percent of the activity. Neglect of the decay of Po^{209} during the 3-yr. period causes no significant error if its half-life (estimated as 200 years[2]) is 100 years or more.

The logarithm of the derived counting rate of Po^{208} in each sample is plotted as a function of time in Fig. 1. The best straight lines through these points, derived by the method of least squares with the points weighted inversely as the squares of their probable errors, had slopes corresponding to half-lives of 2.887 ± 0.015 and 2.921 ± 0.015 years.

Pulse analyses taken at the end of the experiment showed broad peaks typical of a moderately thick sample. Since the peaks observed when the samples were fresh were sharp, this was interpreted as evidence that the polonium had diffused somewhat into the platinum. Such diffusion lowers the counting rates because some particles must emerge nearly parallel to the surface of the sample, and must therefore penetrate a large amount of matter, even if the depth is small. A careful consideration of the data led to the conclusion that the average depth of the polonium was about 200A and that the decrease in counting rate due to this cause was of the order of 0.7 percent.

If a correction of 0.03 years is made for the diffusion error, the final result for the half-life of Po^{208} is 2.93 ± 0.03 years. The probable error includes estimates of the reliability of the counting rates and of the corrections for diffusion and for the other polonium activities. It has been assumed that loss of polonium from the sample has not occurred.

* This work was carried out under the auspices of the AEC.
[1] Templeton, Howland, and Perlman, Phys. Rev. 72, 758 (1947).
[2] E. L. Kelley and E. Segrè, Phys. Rev. 75, 999 (1949).
[3] W. H. Beamer and W. E. Easton, J. Chem. Phys. 17, 1298 (1949).

Proceedings of the American Physical Society

MINUTES OF THE MEETING AT NEW YORK, FEBRUARY 2–4, 1950

THE 297th meeting of the American Physical Society, being the 1950 Annual Meeting, was held in New York City on February 2, 3, and 4, 1950. (Last year's Annual Meeting was designated as the 1948 Annual Meeting, for the sake of continuity with the times when the Annual Meetings were held just before New Year's day; we now break that continuity.) Measured by registration, this was the largest meeting in the history of the Society; we had never had so many as 2000 registrants before, this time we had 2070. Measured by number of papers it was slightly smaller than the corresponding meeting of the previous year (231 ten-minute papers). The congestion also seemed to have slackened, and it is possible that we had a lesser attendance but a still lesser proportion of non-registrants. Anyway, it was a very big meeting! Five simultaneous sessions were the order of each day.

The Local Committee at Columbia University performed its huge task with its customary extraordinary competence (the two adjectives seem to contradict one another, but both are right). The Secretary would like to exhibit to the entire Society the eleven-page compendium of instructions drawn up by this Committee, with assignments of room supervisors, slide operators, and lights' operators to every one of the twenty-nine sessions, plus other assignments to lobby, registration desk, and placement register. All of this immeasurably complicated business was under the direction of W. W. Havens, Jr., and among his principal assistants were A. M. Sachs and Irving Resnick. The American Institute of Physics provided the staff at the registration desk. Services were also rendered, by persons unknown to this office, to the Division of Electron Physics at its meeting at Washington Square College of New York University, and to the Division of High-Polymer Physics at its meetings at the Polytechnic Institute of Brooklyn.

Eight invited papers—among which I include the Retiring Presidential Address of F. W. Loomis and the after-dinner speech of F. Seitz—appeared on the general programme: their titles are listed hereinafter. It is understood that the speeches of Loomis and Seitz are to be published in the *Bulletin of the Atomic Scientists*. In addition, nuclear physics benefited by a Symposium on Nuclear Shell Structure, the authors and the titles being listed on a following page.

Each of our four Divisions presented a half-day Symposium; half a day to each Division is the maximum time now allowed for Divisional sessions of invited papers at Columbia University, for a reason which needs no statement. The givers and the titles of the papers in these Symposia are listed hereinafter. In addition, the Division of Electron Physics held a two-day meeting (on January 31 and February 1) at Washington Square College of New York University; and the Division of High-Polymer Physics held sessions at the Polytechnic Institute of Brooklyn on February 2 and 4. By recent action of the Council, these "separate" meetings of the Divisions—"separate" meaning here that they do not encroach on the space placed at the disposal of the Society by Columbia University—are liberated from certain of the constraints imposed by necessity on the general meetings of the Society. At separate meetings, the Divisions may allow more than ten minutes for the presentation of a "contributed paper," without forfeiting the right to have the abstracts of such papers printed in *The Physical Review*. The abstracts of the papers presented at Washington Square and at Brooklyn are therefore printed at the end of these Minutes, following upon the abstracts of the ten-minute papers offered at the general meeting.

The banquet of the American Physical Society and of the American Association of Physics Teachers was held on Friday evening February 3, those present numbering 328. The after-dinner speech, already mentioned in these pages, was given by F. Seitz: its title was "Physicists in the Cold War."

At the Business Meeting of the Society, held on the Friday morning with the customary slim attendance, the Tellers of Election reported (by letter) that I. I. Rabi had been elected President of the Society for 1950; C. C. Lauritsen had been elected Vice-President; K. K. Darrow, G. B. Pegram and J. T. Tate had been re-elected Secretary, Treasurer, and Managing Editor, respectively; Harvey Brooks, R. F. Christy, and Bruno Rossi had been elected to the Board of Editors; H. A. Bethe had been elected to the Council. It was necessary to hold a run-off election to fill the second vacancy of the Council: this resulted in the election of J. W. Beams. The Secretary reported that the membership of the Society was 9000: this obviously rounded figure represents the best estimate that can be made, in view of such facts as the failure of certain recently elected members to qualify thus far and the presence in our files of the names of numerous members who have not responded to notices sent to their latest known addresses. This

figure also includes our 113 Japanese members, from most of whom no word has been received since before the war.

The Council met on February first. It elected to Membership 217 candidates and to Fellowship 102 candidates, whose names are printed hereinafter. The remarkably great number of elections to Fellowship results from a systematic effort, undertaken by several special committees and finally by the Council as a whole, to comb the Membership List for cases of members worthy of Fellowship whose friends had overlooked the duty of sponsoring them. This job is not yet completed.

Authorization was granted by the Council for the establishment of a Division of Chemical Physics in the American Physical Society: an organizing committee headed by R. S. Mulliken is preparing the plans.

Elected to Fellowship: Raymond V. Adams, Julius Ashkin, Yardley Beers, Persa Raymond Bell, Jr., G. Bernardini, Garrett Birkhoff, John Blatt, Marietta Blau, David Bohm, Hugh Bradner, Helmut L. Bradt, R. Robert Brattain, R. G. Breckenridge, Giuseppe Cocconi, Marcello Conversi, Robert Cornog, Dale R. Corson, Ernest D. Courant, Dean B. Cowie, Eugene C. Crittenden, Jr., Baldwin R. Curtis, G. C. Danielson, Leo P. Delsasso, Howard D. Doolittle, Harold E. Edgerton, N. E. Edlefsen, Leonard Eisenbud, W. C. Elmore, C. T. Elvey, Richard M. Emberson, Peter P. Ewald, Carl F. Eyring, Leslie L. Foldy, Stanley P. Frankel, William B. Fretter, David H. Frisch, Erwin R. Gaerttner, Serge Golian, G. K. Green, Earle C. Gregg, Jr., Kenneth Greisen, Benno Gutenberg, Harvey Hall, David Halliday, Bernard Hamermesh, Wayne E. Hazen, A. Carl Helmholz, Arthur Hemmendinger, Frank L. Hereford, Jr., W. A. Higinbotham, Robert Hofstadter, Leopold Infeld, J. M. Jauch, Joseph Kaplan, Thomas J. Killian, Arthur F. Kip, J. B. Horner Kuper, Robert V. Langmuir, Willard F. Libby, E. J. Lofgren, Emmeth A. Luebke, C. E. Mandeville, Marvin M. Mann, Joseph E. Mayer, Ralph L. McCreary, Ralph E. Meagher, Donald H. Menzel, David Middleton, Philip Morrison, Seth H. Neddermeyer, Leonard O. Olsen, Frank Oppenheimer, A. Pais, Wolfgang K. H. Panofsky, R. Pepinsky, Bernard Peters, Oreste Piccioni, John R. Platt, E. H. Plesset, Bruno Pontecorvo, R. V. Pound, Wilson M. Powell, D. A. Quarles, Simon Ramo, William Rarita, Victor H. Regener, Robert Curtis Retherford, Howard L. Schultz, Erwin F. Schrader, Charles S. Smith, Jr., Hartland S. Snyder, Arthur K. Solomon, H. Guyford Stever, James A. Van Allen, Arthur H. Warner, Wallace Waterfall, Albert Wattenberg, P. R. Weiss, Gregor Wentzel, G. C. Wick, Volney C. Wilson, and Harold A. Zahl.

Elected to Membership: Louis K. Acheson, Jr., John E. Ainsworth, Jr., Alfred H. Aitken, William Parker Alford, Simonne Allard, Raymond A. Allen, Robert C. Allen, Hugo Atterling, Theodore Auerbach, William Thomas August, Robert Palmer Auty, Robert A. Bailey, Donald H. Baird, Roger E. Batzel, Walter C. Beckham, John K. Beling, Warren Lee Bendel, John A. Berberet, Conrad Heinrich Biber, Brebis Bleaney, Hans Boemmel, Aage Niels Bohr, Harry M. Bowman, James N. Bradford, Stanley Breen, *James J. Brophy, Albert R. Brosi, Russell B. Bryan, Frank P. Buff, Mario Bunge, Geoffrey R. Burbidge, Edward Burke, Richard L. Burling, Sidney M. Cadwell, Robert Calfee, Ray N. Cauble, Zenobius V. Chraplyvy, Feng Kan Chuang, Herbert Mottram Clark, Joseph D. Clement, Hans O. Cohn, James A. Coleman, John Convey, Robert L. Cooper, Malcolm Correll, Robert Cortell, Franklyn G. Creese, Robert W. Crews, Marshall F. Crouch, Harold Ormand Curtis, Melvin Cutler, Rob Roy Cyr, Paul M. Dandurand, Philip N. Daykin, George Dean, Robert J. Debs, Owen P. Dickson, Mary I. Donnelly, Cecil Eugene Duncan, Brian B. Dunne, Jr., James Durlacher, William Eiselstein, Tilden Euster, Henriette Faraggi, Giuseppe Romolo Fidecaro, Manus R. Foster, Francis L. Friedman, Robert M. Fristrom, Solomon Frost, Jack N. Gadel, Avery M. Gage, Aaron I. Galonsky, Gerald R. Garrison, Richard Lawrence Garwin, Robert K. Golden, Jacobo M. Goldschvartz, Martin Goldstein, Bernard Gregory, Carl Greifinger, Maurice Griffel, Peter H. Haas, Uri Haber-Schaim, Kenneth George Halvorsen, John N. Harris, Melvin A. Harrison, Roger Hayward, Bertram Heil, Edward J. Hennelly, Gerhart R. Hennig, John M. Hood, Jr., Henry John Hrostowski, Ming-kuei Hu, Craig C. Hudson, James N. P. Hume, Charles Harve Humphrey, Vincent Jaccarino, Ralph A. Jack, Moses Gamzen Jacobson, Joseph Jaffe, Frank E. Jaumot, Jr., James Farris Jenkins, Jr., Horace R. Johnson, John C. Johnson, Rosalie Joseph, Hellmut J. Juretschke, George T. Kallman, Stanley L. Kameny, Lien-Pei Kao, Glenn Keister, William E. Keller, Paul R. Kintzinger, Terje Kjeldaas, Jr., Alfred Kleider, Melvin Klerer, A. Morris Koblenz, Boris V. Korvin-Kroukovsky, Valdemar Kowalowski, Bernard A. Kulp, Walter C. Lamphier, Henry L. Laquer, Eugene J. Lauer, James M. LeBlanc, Irwin L. Lebow, Theodore E. LeLoup, Andrew Lenard, David Lichtman, Robert Loyd Lillestrand, John Linsley, William H. Louisell, David Lupfer, William Van Rensselaer Malkus, Lawrence James Marks, Charles Martin, H. C. Martin, Daniel L. Massignon, Joseph W. Mather, Jacob Mazur, Aubrey L. McLellen, Jr., Gordon McClure, Robert L. McCormack, John L. McLucas, Robert Charles Miller, R. Douglas Moffat, Harold J. Morowitz, Giacomo Morpurgo, Paul L. Morrison, Jr., John H. Muller, William W. Mullins, John P. Neissel, E. A. Nesbitt, George Nestor, James Blakey Newman, Velmo Lee Norris, G. P. S. Occhialini, Jay Orear, Lorne A. Page, Carolyn Parker, Sidney Passman, Jane Shera Pease, Willis B. Person, William Peters, Arthur V. Phelps, Lucy W. Pickett, George R. Pitnam, Jr., Spencer L. Plehaty, David Polur, S. James Press, *Giampietro Puppi, Martin G. Redlich, Richard S. Rettie, Shepard Roberts, Thomas E. Roberts, Jr., Charles Rubinstein, Wyman C. Rutledge, Harold Salwen, Harold Samelson, Albert J. Saur, Abraham Savitzky, Milton Schach, Robert A. Schluter, Lawrence A. Schmid, Harry J. Schulte, Jr., Dr. Paul Schulz, Merrill B. Scott, Ganapathy Shrikantia, Paul H. Sidles, Albert Silverman, Richard C. Sirrine, Edward Cutrer Smith, Michel Soutif, Wallace P. Spaulding, Fred N. Spiess, Ralph Henry Stahl, Jorge P. Staricco, Alonzo E. Stoddard, Jr., Don R. Swanson, John C. Swartz, Theos Jardin Thompson, Sam B. Treiman, Lucio Vallese, Juanita Hubbard Wagner, Nathan S. Wall, Peter P. Wegener, David B. Wehmeyer, Jose F. Westerkamp, John A. Wethington, Jr., George W. Wheeler, Alan Whittaker, Armin T. Wiebke, Anthony J. Wilk, Arthur H. Williams, Joel Q. Williams, Allan N. Wilson, Shi-Shu Wu, Kenneth Yass, Frink Mansfield Young, and Robert Gaines Young.

*One sponsor only.

KARL K. DARROW, *Secretary*
American Physical Society
Columbia University
New York 27, New York

Invited Papers on the General Programme

Neutron evaporations produced by cosmic rays. G. BERNARDINI, *Columbia University.*

Physical viewpoints in quantum electrodynamics. R. P. FEYNMAN, *Cornell University.*

Neutron mirrors. D. J. HUGHES, *Brookhaven National Laboratory.*

Can physics serve two masters? F. W. LOOMIS, *University of Illinois.*

Recent developments in quantized field theories. W. PAULI, JR., *Eidgenossische Technische Hochschule and Institute for Advanced Study.*

Physicists in the cold war. F. SEITZ, *University of Illinois.*

Turbulence and the evolution of spiral nebulae. C. F. VON WEISZAECKER, *University of Chicago.*

Recent investigations on the shapes of beta-ray spectra. C. S. WU, *Columbia University.*

Symposium on Nuclear Shell Structure

W. D. HARKINS, *University of Chicago.*
V. F. WEISSKOPF, *M. I. T.*
MARIA GOEPPERT-MAYER, *Argonne National Laboratory.*
L. W. NORDHEIM, *Duke University.*
EUGENE FEENBERG, *Washington University.*

Symposium of the Division of Electron Physics

Imprisonment of resonance ratiation in mercury vapor. A. O. MCCOUBREY, D. ALPERT, AND T. HOLSTEIN, *Westinghouse.*

Recent work on the ratio of the magnetic moments of electron and proton, and related atomic constants. E. M. PURCELL, *Harvard University.*

Scintillation counters and photo-multipliers. G. A. MORTON, *RCA Laboratories.*

Photo-conductivity and optical absorption in BaO crystals. WINFIELD W. TYLER, *Cornell University.*

Symposium of the Division of Solid-State Physics

Behavior and properties of grain boundaries. R. SMOLUCHOWSKI, *Carnegie Institute of Technology.*

Energy bands and electron mobilities in non-polar crystals. J. BARDEEN, *Bell Telephone Laboratories.*

The shape of absorption lines in dielectrics. H. FROEHLICH, *University of Liverpool.*

Symposium of the Division of High-Polymer Physics

Mechanism of plastic flow in single crystals. F. SEITZ, *University of Illinois.*

Structure and physical properties of crystalline polymers. H. LEADERMAN, *National Bureau of Standards.*

Rheological properties of glass. W. A. WEYL, *Pennsylvania State College.*

Internal friction in solids. C. ZENER, *University of Chicago.*

Static and dynamic viscosities of amorphous polymers. A. V. TOBOLSKY, *Princeton University.*

Discussion. Led by M. L. HUGGINS, *Eastman Kodak Company.*

Symposium of the Division of Fluid Dynamics

Stability theory of viscous flows. C. C. LIN, *M. I. T.*

Transonic flow. W. R. SEARS, *Cornell University.*

Development of supersonic airfoil theory. J. C. EVVARD, *Lewis Flight Propulsion Laboratory.*

Symposium on Dielectrics of the American Institute of Electrical Engineers

Dielectrics in Electrical Engineering. A. VON HIPPEL, *M. I. T.*

Structure and Polarization of Atoms and Molecules. J. C. SLATER, *M. I. T.*

Relaxation Phenomena in Liquids and Solids. C. P. SMYTH, *Princeton University.*

Modern Plastics. H. MARK AND T. ALFREY, *Polytechnic Institute of Brooklyn.*

Conduction Phenomena in Gases. J. P. MOLNAR, *Bell Telephone Laboratories.*

Conduction in Liquids and Plastics. R. M. FUOSS, *Yale University.*

Fluorescence and Phosphorescence. P. PRINGSHEIM, *Argonne National Laboratory.*

Crystals

A1. The Status of the Measurement of the Properties of Some Piezoelectric Crystals.* KARL S. VAN DYKE, *Wesleyan University.*—Comparison is made of static and resonator methods for determining piezoelectric constants and of the values of the constants of KDA (potassium dihydrogen arsentae, tetragonal) and of EDT (ethylene diamine *d*-tartrate, monoclinic) by the two methods. Measurements by Niemiec and by Officer** on KDA are cited, and measurements by Niemiec on EDT compared with values given by Jaffe, by Mason, and by Bechmann and Lynch. The latter authors appear not to have been aware of an unpublished revision of his values by Mason to which attention was called by Jaffe, and of the limited circulation of these values in A Handbook of Piezoelectric Data† in which the revised values were used through Mason's courtesy. Niemiec's measurements now in progress confirm the values for EDT used in the Handbook as fairly representative. Success of the resonator method, even for the piezoelectric constants of thickness-shear plates, is demonstrated when adequate attention is given to the distribution of strain in a given mode of vibration.

* Work supported by U. S. Army Signal Corps.
** C. B. Officer, Thesis, "Piezoelectric Properties of Potassium Dihydrogen Arsenate," Wesleyan University, June, 1948. Not published.
† K. S. Van Dyke, Parts II of Fifth and of Sixth Semi-Annual Reports to Signal Corps (January 21, 1948 and July 28, 1948) under the above mentioned contract.

A2. Anelastic Effects in Ionic Crystals. R. G. BRECKENRIDGE AND A. L. WARD, *National Bureau of Standards.*—The internal friction in single crystals of NaCl, LiF, and K Br has been studied by observations of the decay of free torsional oscillation of a composite piezoelectric resonator consisting of a *Y*-cut quartz bar with the crystal cemented to one end. The *Q* of the resonator is calculated from the logarithmic decrement of the decay curves. Plots of *Q* as a function of temperature for the composite resonator show three minima not found for the quartz alone. These increases in the loss are attributed to relaxation processes in the ionic crystal. The activation energies for the processes have been determined. A tentative identification of the loss mechanisms may be made for the two processes of lower energy because of the good agreement found with previously reported values for the activation energy for self diffusion in NaCl[1] and for reorienting pairs of vacancies through cation migration[2] in all three cases. It is suggested that the process of highest energy may be the reorientation of pairs through anion migration.

[1] D. Mapother and R. J. Maurer, Phys. Rev. 73, 1260 (1948).
[2] R. G. Breckenridge, J. Chem. Phys. 16, 959 (1948).

A3. Anelasticity of Quartz Crystals. RICHARD K. COOK AND ROBERT G. BRECKENRIDGE, *National Bureau of Standards.*—By means of the piezoelectric effect, measurements have been made of the variation with temperature of (1) the *Q* of a bar executing free torsional oscillations, and (2) the equivalent series resistance of bars driven at their fundamental longitudinal frequencies. For each of the three bars studied, it was

found that the internal dissipation had a maximum value at a temperature between room temperature and the inversion temperature of 573°C. Measurements of the equivalent series resistance as a function of frequency were made in order to decide whether or not the dissipation had an Arrhenius-type variation with temperature. The origin of the dissipation is uncertain. For two of the bars, the maximum dissipation increased after the bars were heated to temperatures a little below inversion. In these cases, the dissipation is probably due to twinning. For another bar, however, the dissipation was not significantly changed by heating to temperatures near inversion, and hence it is surmised that the bar had some sort of a lattice imperfection.

A4. Vibrations of a Circular Crystalline Plate.* SHEPARD BARTNOFF, CHARLES R. MINGINS, AND JOSEPH F. CLAYTON, *Tufts College.*—In an effort to obtain expressions which fit the situation more satisfactorily than existing relations, the problem of a vibrating crystal has been attacked by tensor methods. Cylindrical coordinates are set up appropriate for the analysis of the vibrations of a circular Y'-cut quartz plate. The matrices transforming from rectangular coordinates to the new coordinates are evaluated and tensor methods, using these matrices, are applied to express the piezoelectric equations, the piezoelectric constants, and the elastic constants in the new system. For a given applied electric field, the strains, expressed in terms of contravariant displacements, are used in the piezoelectric equations to describe the stresses in terms of these displacements. The resulting stress expressions are substituted into the equations relating the stresses to the contravariant force components. There then result three equations involving the three contravariant displacements and their derivatives. The general motion of any point of the crystal is given by that solution of these three equations which satisfies boundary conditions. The boundary conditions are evaluated for a circular crystal clamped at its circumference.

* This work is sponsored by the Frequency Control Branch of the Signal Corps.

A5. Intense Multiple Reflection of Electrons. L. G. SCHULZ, *University of Chicago.*—When thin films of alkali halides are formed by evaporation on mica substrates the atoms in a (111) plane of the crystals in the deposit tend to match the hexagonal atomic network in the cleavage surface of the substrate. Electron diffraction patterns taken by reflection from films containing crystals in twinned relationship were found to contain strong "extra spots." These spots are attributed to intense multiple reflection involving successive diffraction by crystals of both orientations. Extra spots can be used to give information on the structure of the sample, such as crystal size and perfection of orientation. In addition, multiple reflection can be employed in the study of very thin films which fail to give good diffraction patterns by direct methods. For convenience, a systematic procedure was developed for predicting the position and approximate intensity of extra spots. A consequence of multiple reflection is a shifting of the relative intensities of all diffraction spots which enhances the weak reflections at the expense of stronger ones. This could account for some of the reported anomalies in intensity given by electron diffraction.

A6. Oriented Overgrowth of Alkali Halides on Ag, Bi, Sb, and Fe. GERALD W. JOHNSON, *Brookhaven National Laboratory.**—Royer[1] gave as one condition for the occurrence of oriented overgrowth that the substances have the same type of binding. While the orientation of evaporated metallic films by cleaved ionic crystals is well known, there have been few reports of epitaxy of ionic crystals crystallized from solution on metals. Recently here several cases of this type of epitaxy have been found. Sodium chloride was completely oriented on silver films having {100} and {111} planes exposed. NaCl, KCl, and RbCl all were oriented on the {111} plane of Bi, while only NaCl was oriented by the {111} of Sb. On polycrystalline Ag, Bi, and Sb sodium chloride crystals were oriented by almost every grain. On polycrystalline Fe only CsCl was oriented and only for particular orientations of the Fe grains. From the number of cases of epitaxy noted here for polycrystalline aggregates clearly closeness of fit of lattice cannot be a strict criterion for oriented growth. The requirement that the type of binding of the two structures be the same must be relaxed. On polycrystalline substrates growth across boundaries often occurred without modification which suggested that the orientations are determined in the nucleation stage.

* Work performed under the auspices of the AEC.
[1] L. Royer, Bull. Soc. Franc. Mineral. 51, 7 (1928).

A7. Studies of Gas Adsorption on the (100) Face of a Copper Crystal by Low Speed Electron Diffraction.* ROBERT E. SCHLIER AND H. E. FARNSWORTH, *Brown University.*—The diffraction tube permits a wide variation of temperature of the crystal during observations. For a well-outgassed crystal part of the surface is covered with a monolayer of a double-spaced face-centered structure, the gas atoms being located directly above the copper atoms. A small part of the surface is covered with a single-spaced simple-cubic structure. When the pressure in the tube is increased for ten-minute intervals at room temperature, no adsorption of air, nitrogen, or CO_2 takes place until a critical pressure is reached. At this pressure adsorption occurs in a single-spaced simple-cubic structure and the double-spaced face-centered structure is no longer observed. The critical pressures are: 0.5μ for air, 10μ for N_2, and 1μ for CO_2. At the temperature of dry ice there is no critical pressure but adsorption is observed at a pressure as low as 0.001μ for all three gases. For air and nitrogen the adsorption occurs gradually in the same structure as is observed at room temperature. However, at the lower temperature, CO_2 does not adsorb in the single-spaced simple-cubic structure or any other structure which has been found.

* Assisted by ONR and Research Corporation of New York.

A8. The Photoelectric Work Function of a Silver Film on the (100) Face of a Silver Crystal.* EDWARD KELLY, H. E. FARNSWORTH, AND EDWARD N. CLARKE,** *Brown University.*—Doubly distilled silver is deposited by evaporation onto the (100) face of a silver crystal which has been outgassing in a high vacuum. The work function after deposition of the film is approximately 0.1 ev less than that of the crystal before deposit. Subsequent low temperature heating of the crystal and film at a temperature of 35° to 40°C causes the work function to increase to approximately its original value. These results are consistent with the view that the work function of a microcrystalline film is less than that of the bulk metal support and is a function of the type of support. Measurements are in progress with a low speed electron diffraction arrangement in the phototube to follow any changes in structure which occur.

* Assisted by ONR and Research Corporation of New York.
** Socony Vacuum predoctoral fellow.

A9. An Explanation for "Extra Levels" in Rare Earth Crystal Spectra. HARVEY WINSTON, *University of California, Berkeley.*—A consideration of just the unit cell has been shown sufficient to give vibrational selection rules in crystals; this turns out to be true also for electronic spectra in many cases. Bethe's classification of electronic levels in the site is a first step in obtaining the unit cell classification. It is shown that the number of crystalline levels arising from a free ion level J is not limited to $2J+1$. The results of Freed and Weissman on the visible spectrum of EuF_3 led them to assign J values of 0,

2, and 3 to the upper levels; the present treatment indicates that 0, 1, and 2 are possible, in accord with other work. These ideas also make plausible the observed doubling of lines in many rare earth salts, the "hyperfine structure" of Hellwege. The method is general; the ultraviolet spectrum of crystalline benzene can be explained by it. Experiments in progress are designed to compare the predicted and observed polarization properties.

A10. Structure and Growth Mechanism of Photolytic Silver in Silver Bromide. CHESTER R. BERRY AND ROBERT L. GRIFFITH, *Eastman Kodak Company.*—An investigation has been made by x-ray and electron diffraction of single crystals of pure silver bromide during the process of photolytic decomposition induced by irradiating the crystals with light from a mercury vapor lamp. The orientation of the silver determined from the x-ray diffraction patterns is quite different from the orientations determined from the electron diffraction patterns. It has been found that these differences are not due to any production of silver by the x-ray or electron beams, but correspond to differences in the silver orientations in the body and near the surface of the silver bromide crystals. Two different mechanisms of silver separation in the two regions of the crystals appear to account for the observed silver orientations. In the interior, the silver separation seems to depend on the existence of dislocations and the motion of cations, but near the surface it depends on the production of *F*-centers during the escape of bromine and on the subsequent aggregation of these *F*-centers, as described by Mitchell.[1]

[1] J. W. Mitchell, Phil. Mag. 40, 249 (1949).

A11. Crystal Strain Energy in Solid Solutions. ROBERT L. SCOTT, *University of California, Los Angeles.*—Non-zero heats of formation of solid solutions result partially (for ionic crystals, almost entirely) from strain energy arising when particles of different sizes are built into a single lattice. A more general treatment than those of previous authors expresses the lattice energy as a sum of pair potentials $\epsilon(r-r_0)$ expanded about r_0, the interatomic distance corresponding to minimum energy. The leading term in each of these series (aside from ϵ_0) is $B(r-r_0)^2$; B can be deduced theoretically or calculated from compressibilities. By neglecting all but nearest neighbor interactions (except for coulomb terms) and by minimizing the energy with respect to the single parameter r, expressions for the strain energy and for the deviation from Vegard's law are obtained, the leading terms of which depend solely upon the B's, the concentrations, and the square of the difference of the lattice parameters. This strain energy is critical in determining solubilities and in depressing melting points of solid solutions. At room temperature a difference in lattice parameters of more than 4 percent for ionic crystals, 8 percent for molecular crystals, and 14 percent for metals precludes complete miscibility. Calculations indicate that inaccuracies resulting from the approximations of a single interatomic distance are significant.

A12. A Neutron Diffraction Study of Vitreous Silica. I. W. RUDERMAN, *Columbia University.*—The neutron transmission of a 9.59 g/cm² disk of transparent vitreous silica was obtained with the Columbia neutron velocity spectrometer at neutron wave-lengths up to 6.3A. Well-defined diffraction peaks were found at wave-lengths corresponding to interplanar spacings of 0.7, 1.1, 1.7, 1.9, 2.2, and 2.7A. Other peaks, which were not as well resolved, were also found. The peak at 1.1A is the most prominent. Previous careful x-ray studies by Warren[1] on vitreous silica have shown only a broad peak at 4.2A and three weak and poorly resolved peaks corresponding to shorter spacings. Front and back reflection x-ray photographs of samples cut from the specimen used for the neutron study showed only the well-known diffuse pattern. The relation of these results to the current theories of the amorphous state will be discussed.

[1] Warren, Krutter, and Morningstar, J. Am. Ceram. Soc., 19, 202 (1936).

A13. Lattice Constants of Zinc Oxide. J. MCGANNON, R. HELLER, AND A. H. WEBER, *Saint Louis University.*—Since ZnO is a useful material for calibration of electron wavelengths in electron diffraction studies, a precision determination of the crystallographic cell edge a and the axial ratio c/a of powdered ZnO (Analytic Reagent), hexagonal structure, has been made by x-ray diffraction employing the Debye-Scherrer powder technique. A cylindrical (diam., 0.025 in.; length, 0.5 in.) specimen was used in a cylindrical camera of radius 57.296 mm and exposed to CuK radiation from a Picker x-ray unit for three hours. The resulting data was analyzed by the Cohen analytical method[1] which corrects for errors usually present. Values of Cu wave-lengths were taken as $\lambda K\alpha_1 = 1.54050$A and $\lambda K\alpha_2 = 1.54434$A.[2] Radii of Debye-Scherrer rings were measured to five significant figures and $\sin\theta$ was interpolated accurately from eight-place trigonometric tables.[3] Data from at least 25 films each containing 14 measurable lines in the back-reflection region will be presented. The precision and consistency of the results will be discussed.

[1] M. Cohen, Rev. Sci. Inst. 6, 68 (1935).
[2] E. A. Wood, Phys. Rev. 72, 430 (1947).
[3] *Tables of Sines and Cosines for Radian Arguments*, Fed. Works Proj. Ad., New York City (1940).

Beta-Emitters from Neutron to Neodymium

C1. Radioactive Decay of the Neutron. A. H. SNELL, F. PLEASONTON, AND R. V. MCCORD, *Oak Ridge National Laboratory.*—Coincidences have been observed between discharges in a beta-proportional counter placed near a neutron beam from the Oak Ridge Reactor and pulses from an electron multiplier placed approximately opposite the counter. A transverse electric field accelerates positive particles appearing in this region of the beam through 8 kv and focuses them upon the first plate of the multiplier. The coincidences depend upon the presence of this field. They do not appear when (1) the beam is interrupted by a boron or a cadmium shutter, and (2) the reactor is off and the detectors are actuated by Co^{60} gamma-rays. The coincidence rate is not increased (1) if H_2 gas is introduced into the tank; or (2) the apparatus is surrounded by Cd (thereby increasing the local neutron captures by a large factor). Thus the coincidences are associated with positive particles and slow neutrons, and not with gamma-rays. A slight delay in the counter channel is necessary to reveal them, time-of-flight considerations accordingly show that the particles are of roughly protonic mass. These observations are interpreted as showing that the events are beta-proton coincidences associated with neutron decay. The derived half-life lies in the range 10 to 30 minutes as previously reported.

C2. The Beta-Spectrum of He^6. VICTOR PEREZ-MENDEZ AND HAROLD BROWN, *Columbia University.*—The β-spectrum of He^6 has been observed in a semi-circular focusing spectrometer modified so as to permit study of a gaseous source. The He^6 is produced by the (n, α) reaction on finely divided beryllium powder in an internal cyclotron probe, using the fast neutrons produced by bombarding a beryllium plate with the deuterons from the 36″ Columbia cyclotron. The He^6 was pumped to the spectrometer using He^4 as a carrier gas. The equivalent thickness of the source was 0.1 mg/cm², and the thickness of the window separating it from the spectrometer was 1.8 mg/cm². The radius of curvature of the spectrometer was 13.6 cm, and the resolution employed about 5 percent. The spectrum obtained shows the allowed shape down to about 200 kev. Its end-point is established as (3.21 ± 0.015) Mev, which gives He^6 an $ft_{\frac{1}{2}}$ value of about 570.

C3. Beta-Spectrum of Be^{10}. L. FELDMAN AND C. S. WU, *Columbia University.*—In a Letter to the Editor,[1] we concluded that the β-ray spectrum of Be^{10} may well be a D_2 spectrum as predicted theoretically by Marshak.[2] Subsequent investigations in various laboratories[3] have substantiated this conclusion. Recently we received an electro-magnetically enriched Be^{10} source[4] through the Isotope Division of the Atomic Energy Commission. The average BeO source thickness used in this investigation was around 0.3–0.4 mg/cm², deposited on a thin formvar-polystyrene film (0.1 mg/cm²). The high transmission solenoid spectrometer (~8 percent transmission and 8 percent resolution) was used with thin Nylon window counter (0.6 mg/cm²) requiring no window correction on the measured data above 100 kev. Preliminary investigations of the β-spectrum of the enriched Be^{10} thus obtained follows a D_2 forbidden spectrum closely for three quarters of the whole spectrum. The upper energy limit is again 555±5 kev. The good agreement between the experimentally observed and the theoretically predicted Be^{10} spectrum is a good test of the present theory of β-decay.

[1] C. S. Wu and L. Feldman, Phys. Rev. **76**, 698 (1949).
[2] R. E. Marshak, Phys. Rev. **75**, 513 (1949).
[3] Fulbright and Milton, Phys. Rev. **76**, 1271 (1949); R. P. Bell group, private communication; D. J. Hughes group, private communication.
[4] Produced by Carbide and Carbon Chemical Corp., Y-12 Research Lab., Oak Ridge, Tennessee.

C4. The β-Spectrum of Be^{10}. D. E. ALBURGER, *Brookhaven National Laboratory,** AND D. J. HUGHES** AND C. EGGLER, *Argonne National Laboratory.*—The beta-ray spectrum of Be^{10} has been measured using a lens spectrometer. The source was formed by neutron irradiation of Be in the Hanford pile followed by careful chemical purification. 1200-fold electromagnetic enrichment to 0.3 percent Be^{10} was then performed at Oak Ridge under the direction of C. P. Keim. Enriched BeO was finally deposited in suspension over an area 1.5 cm in diameter on a 0.08 mg/cm² Nylon backing. Effects of the 0.4 mg/cm² source thickness and 17 percent resolution used because of the low Be^{10} activity were investigated by separate experiments on the Na^{22} positron spectrum which has about the same end point. Thin sources of Na^{22} run under the same conditions and corrected for resolution and 0.5 mg/cm² counter window thickness showed accurate linearity of the Kurie plot down to 100 kev. Sources ~0.4 mg/cm² of Na^{22} mixed in inert BeO gave linear Kurie plots down to 170 kev. The Kurie plot of Be^{10} with additional correction by Marshak's D_2 factor is linear from the 560±5 kev end point down to about 180 kev and has deviations below that point similar to the thick Na^{22} source results. This indicates that the Be^{10} beta-ray distribution follows the theoretical D_2 shape at least down to 100 kev.

* Research carried out under contract with the AEC.
** Now at Brookhaven National Laboratory.

C5. Beta-Spectrum of Na^{22}. P. A. MACKLIN, L. J. LIDOFSKY, AND C. S. WU, *Columbia University.*—Na^{22} is a positron emitter with a fairly long half-life. From its ft value, it is classified as twice forbidden. Its β-spectrum was investigated by the M.I.T. group[1] and appeared to be allowed from upper energy limit down to 220 kev. Below 220 kev there were no published results on its distribution. Recently the Na^{22} spectrum was reinvestigated in our solenoidal spectrometer (8 percent transmission and 4 percent resolution). The source, whose average thickness was less than 50 μg/cm², was mounted on a 10 μg/cm² backing. The Fermi plot appeared linear from the upper energy limit of 542±5 kev down to around 25 kev. The deviation below 25 kev could be very well accounted for by the source thickness and local variations in the source thickness. The upper energy limit was consistent for several runs with different resolution widths, but is considerably lower than the previously reported value of 575 kev.[1] Compton electrons from the annihilation radiation and from the 1.3 Mev γ-rays were also investigated.

[1] Good, Peaslee, and Deutsch, Phys. Rev. **69**, 313 (1946).

C6. Beta-Spectrum of S^{35}. LEONARD GROSS*, ** AND DONALD R. HAMILTON, *Princeton University.****—A new type of electrostatic beta-ray spectrograph has been constructed for the measurement of low energy spectra. This electrostatic spectrograph is in the form of a hemisphere in which electrons move radially outward in the direction of a retarding electric field. The prime advantage of this apparatus lies in the high resolving power obtainable, accompanying sufficient intensity to permit the replacement of conventional GM counter detection in favor of d.c. current detection. The beta-spectrum of S^{35} in the region below 30 kilovolts has been investigated. The S^{35} spectrum shape was found to be in agreement with the predictions of the Fermi theory even in this extremely low energy region. With a source less than 0.5 microgram/cm² thick (chiefly calcium sulfate) on a 3.1 microgram/cm² collodion backing, the Fermi plot was a straight line down to 6 kev. The deviation below 6 kev is attributed to backscattering and absorption in the source and backing.

* This work was performed under the tenure of an AEC predoctora fellowship.
** Presently at Hughes Aircraft Co., Culver City, California.
*** Supported in part by the ONR.

C7. Disintegration of Zinc 65 by Positron Emission.* RUTH A. COHN AND J. D. KURBATOV, *The Ohio State University.*—Previously it has been reported that 2.2 percent of zinc 65 decays by emission of 320 kev positrons to the ground state of copper 65.[1] In the present study of Zn^{65}, evidence was obtained for the existence of converted photons of ~210 kev in coincidence with 320 kev positrons. The coincidences were obtained: (1) for positrons and gamma-rays of ~210 kev, (2) for positrons and electrons of ~200 kev, (3) for ~210 kev gamma-rays and annihilation radiation. The conversion ratio N_e/N_γ was estimated from coincidence measurements to be ~0.1. Independently, the presence of electrons of ~200 kev was verified by observations in a cloud chamber. It is concluded that Zn^{65} decays by positron emission to an excited state of Cu^{65} which is about 210 kev above the ground state.

* Assisted by a grant of The Graduate School of The Ohio State University.
[1] W. M. Good and W. C. Peacock, Phys. Rev. **69**, 680 (1946).

C8. Bromine 80 and Its Isomers. I. J. LIDOFSKY, P. A. MACKLIN, AND C. S. WU, *Columbia University.*—Br^{80}, a classic case in the history of isomerism,[1] emits two soft gamma-rays of energies 49 and 37 kev. The 49 kev is probably completely internally converted[2] and is assigned as magnetic octupole radiation because of the half-life and the ratio of K to L internal conversion coefficients as determined by the absorption method.[3] We have recently investigated the internal conversion electron lines and the continuous spectra of Br^{80} and Br^{82} in the Columbia solenoidal spectrometer. The energy found for the two gamma-rays is 36.3 kev and 48.1 kev. From the conversion coefficients obtained, we substantiate the assignment of the 48.1 kev gamma-ray as magnetic octupole but strongly suggest that the 36.3 kev gamma-ray is electric dipole. The upper energy limit of the Br^{80} spectrum is 1.99 ±0.01 Mev while exhibiting the allowed shape.

[1] Segrè and Helmholz, Rev. Mod. Phys. **21**, 291 (1949).
[2] Grindberg and Roussinow, Phys. Rev. **58**, 181 (1940).
[3] Berthelot, Ann. de physique **19**, 219 (1944).

C9. Radioactive Y^{87} and Sr^{87}. B. E. ROBERTSON, W. E. SCOTT, AND M. L. POOL, *The Ohio State University.*—The activities of the Y^{87} isomer have been investigated by cyclotron bombardments of strontium targets electromagnetically enriched in the various strontium isotopes. The 14-hour and 3.3-day activities previously ascribed to Y^{87} have been produced by alpha-bombardment of an enriched Sr^{84} sample, confirming this mass assignment as the result of the reaction $Sr^{84}(\alpha, p)Y^{87}$.

In agreement with previous reports that the 3.3-day activity decays by K-capture to 2.7-hour Sr^{87}, a Sr $K\alpha$ x-ray line has been obtained on a curved-crystal spectrograph film exposed to samples of the 3.3-day yttrium. In addition to the well-known 0.37 Mev gamma-ray of the 2.7-hour strontium, a higher energy gamma-ray of 0.5 Mev energy has been found to be associated with this activity as shown by a β-ray spectrogram of its conversion electrons and lead absorption measurements. The characteristic radiations of the 14-hour yttrium activity are observed to be 1.1 Mev positrons associated with K-capture decay to 2.7-hour Sr^{87}. A small amount of 0.7 Mev positron activity is found associated with the 3.3-day activity. It is concluded that the 14-hour and 3.3-day activities of Y^{87} decay independently to 2.7-hour Sr^{87} and that the 14-hour activity has the higher energy level of this isomeric pair.

C10. Disintegration of Cesium 131 and Metastable State of Xenon 131.* LIN-SHENG CHENG AND J. D. KURBATOV, *The Ohio State University.*—The metastable state of Xe^{131} has been observed by several authors[1,2] in disintegration studies of I^{131}. In the present work, this excited state of Xe^{131} was identified as a product of disintegration of Cs^{131}, the latter being produced by radioactive Ba^{131}. Cs^{131} of very high specific activity was separated from Ba^{131} without carrier. It was established that Cs^{131} decays mainly by orbital electron capture to the ground state of Xe^{131} and by a small fraction to the excited state of Xe^{131}. The metastable state of Xe^{131} was identified by converted 163 kev photons and by $T_{\frac{1}{2}}$ equal to $11\frac{1}{2}$ days. The conversion ratio N_K/N_L was found experimentally to be 4.5. Independently, conversion coefficients of the 163 kev photon of Xe^{131*} were calculated for different changes in angular momentum of electric and magnetic 2^l-pole radiations. The closest agreement between experimental data and the calculations was obtained for a magnetic radiation with a change in angular momentum equal to four and $N\beta_K{}^l+N\beta_L{}^l/N_\gamma = 19.5$. $T_{\frac{1}{2}}$ of Xe^{131*} was measured using separated Xe gas.

* Assisted by a grant of the Alumni Development Fund of The Ohio State University.
[1] Brosi, DeWitt, and Zeldes, Phys. Rev. 75, 1615 (1949).
[2] J. M. Cork, Phys. Rev. 75, 1621 (1949).

C11. Radiations from the 33-Hour Cerium (143).* E. SHAPIRO AND C. E. MANDEVILLE, *Bartol Research Foundation.*—The 33-hour activity was induced in CeO_2 irradiated by slow neutrons in the Oak Ridge pile. In order to study Ce^{143} free of its 13-day praseodymium daughter element, chemical separations were carried out repeatedly during the course of the investigation. The beta-rays were found to have a maximum energy of about 1.1 Mev. Three gamma-ray components were found in lead absorption curves having energies of 0.87 Mev, 0.20 Mev, and 40 kev. All of these gamma-rays were observed to decay with the 33-hour period. A coincidence absorption curve gave 0.89 Mev as the maximum gamma-ray energy. The beta-gamma coincidence rate seemed also to decay with the 33-hour period and was within relatively poor statistical accuracy, independent of the beta-ray energy. The magnitude of the beta-gamma coincidence rate showed that on the average, each beta-ray is accompanied by 0.18 Mev of gamma-ray energy. Very few beta-rays are coupled with the hard gamma-ray of energy 0.89 Mev.

* Assisted by the Joint Program of the ONR and the AEC.

C12. Some Characteristics of the 11-Day Neodymium.* C. E. MANDEVILLE, *Bartol Research Foundation.*—The 11-day activity of Nd^{147} was induced in pure Nd_2O_3 irradiated by slow neutrons in the Oak Ridge pile. Two beta-ray groups, having end points at 0.17 Mev and 0.78 Mev and an intensity ratio of 1:2, were resolved by aluminum absorption, and a lead absorption curve of the quantum radiations showed that two gamma-rays are present, having energies of 35 kev and 0.58 Mev. The softer gamma-ray is about fourttieen mes more intense than the harder one at 0.58 Mev. The beta-gamma-coincidence rate of Nd^{147} was observed to decrease from an extrapolated value of 0.21×10^{-3} coincidence per beta-ray at zero absorber thickness to 0.13×10^{-3} coincidence per beta-ray at an aluminum absorber thickness of 25 mg/cm², remaining constant thereafter. These data show that both beta-ray groups are coupled with gamma-radiation. No beta-beta-coincidences were observed in the decay of Nd^{147}.

* Assisted by the Joint Program of the ONR and the AEC

Mesons, Cosmic-Ray Stars, and Bursts

D1. The Detection of Photo-Mesons and the Relative Cross Section of Carbon and Hydrogen for their Production. J. STEINBERGER AND A. S. BISHOP, *University of California, Berkeley.*—The positive mesons produced in the photon beam of the synchrotron are detected in scintillation counters by means of the delayed coincidence technique. A meson is counted if it stops in the last crystal of a telescope and if its decay electron is detected in the same crystal at a time coincident with one of several delayed gates started by the original meson pulse. The relative counting rates in the delay channels measure the half-life of the μ-meson, providing a test on the reliability of the method. The $\pi^+\rightarrow\mu^+$ decay, which precedes the $\mu^+\rightarrow e^+$ decay, is not resolved in this apparatus. In a first application of this method we have measured the relative cross section for the production of photomesons in carbon and in hydrogen at 90° in the laboratory system as a function of the meson range. The hydrogen results are obtained from a carbon-paraffin difference. The photons have a bremsstrahlung energy spectrum with a maximum of about 300 Mev. About 4000 counts were obtained with a $\mu\rightarrow e$ lifetime of 2.1 ± 0.1 μsec. The total cross section at 90° *per proton* is greater for hydrogen than for carbon.

D2. Magnetic Deflection of Cosmic-Ray Mesons Using Nuclear Plates.* IAN BARBOUR,** *University of Chicago.*—A method has been described[1] in which the mass and charge sign of mesons are investigated by exposing two nuclear plates with an air gap separating their parallel emulsion surfaces in a perpendicular magnetic field; the radius of magnetic curvature of the trajectory in the air gap can be computed from the orientation of the tracks left by a given particle in the two emulsions. Preliminary results reported[2] have been extended by a flight for 6 hours at 90,000 ft., using our 65-lb. permanent magnet, field strength 12,800 gauss. Analysis of tracks has been completed, the charge signs determined, and values for the mass computed for each case. Probable errors will be discussed, and the best mass value for each type of meson determined by a least-squares fit of curves of constant mass on a range-curvature plot.

* Assisted by the Joint Program of the ONR and the AEC.
** Now at Kalamazoo College, Kalamazoo, Michigan.
[1] C. F. Powell, Nature 161, 473 (1948); I. Barbour, Phys. Rev. 74, 507 (1948).
[2] I. Barbour, Phys. Rev. 76, 320 (1949).

D3. Semi-Automatic Device for Analyzing Events in Nuclear Emulsions. ROBERT RUDIN, MARIETTA BLAU, AND SEYMOUR LINDENBAUM, *Columbia University.*—The apparatus is built around a microscope with a motor-driven stage, moved by selsynmotors either in the X or Y direction, or by a steering device in any desired direction, at variable speed. The track is observed through an eyepiece and simultaneously projected onto a small slot before a photo-multiplier, the output of which is recorded on a chart moving with a speed equal to 2000 times the stage speed. On the same chart, the vertical component of motion (the magnified manual focusing movement of the observer) and the angular direction of stage travel are recorded. If only the geometric properties of the track are

wanted (scattering or angular relationship of tracks in stars), the X-Y-steering is used and 3 coordinates of a series of points are recorded simultaneously and used for calculations. In cases where the accumulation of grains is too heavy to be analyzed (heavy tracks, dense shower cores), direct photometric comparison of track against background is used. Technical details and measuring results are given.

D4. Investigation of Cosmic-Ray Stars and Slow Protons with a Silver Chloride Crystal. FREDERICK C. BROWN AND J. C. STREET,* *Harvard University.*—A disk of silver chloride six cm in diameter and one cm thick was cut from a crystal grown from the melt. It was operated as an ionization detector well below saturation where it has been shown that the height of conduction pulses is very nearly proportional to the energy released over a wide range of energy. Pulse distributions at elevation 11,200 feet and at sea level were recorded for two types of events: (1) a simple recording of pulses from the crystal above a discriminator setting of 900μ volts ~30 Mev, (2) a similar recording but a counter telescope required the presence of a single ionizing particle above the crystal of energy sufficient to penetrate one cm of lead. Additional counters indicated that in about ten percent of the events of type (2) a single particle is present below ten cm of lead under the crystal. Analysis shows that protons stopping in and just below the crystal, as well as stars, contribute to the rates up to ~60 Mev, whereas larger pulses are due mainly to stars. With certain assumptions it is possible to calculate the relative production of stars by protons and neutrons. The variation of rates with altitude will be discussed.

* Assisted by the Joint Program of the ONR and the AEC.

D5. Disintegration of Nuclei by π^- Mesons.* W. CHESTON AND L. GOLDFARB, *University of Rochester.*—Kodak nuclear emulsions were exposed to the π-meson beam of the 130-in. Rochester cyclotron by S. W. Barnes. The energy spectrum of protons emitted in the disintegration of the nuclei which absorbed the π^- mesons was obtained by determining the specific energy loss and/or residual range of these protons. The former was obtained by measuring the grain densities of meson and proton tracks of known residual range. 10 ± 2 percent of the mesons give rise to protons with energies $\geqslant 30$ Mev.[1] One of the emitted protons was found to have an energy greater than 100 Mev. 35 percent of the mesons stop without producing stars; 45 percent of these give rise to recoil of the absorbing nucleus. The proton energy spectrum, star size distribution, and nuclear recoils will be discussed; comparisons will be made with the results of other observers[2] and with theory.[3] To date, 429 meson events have been investigated; this work is being extended.

* This work was assisted by the Joint Program of the ONR and the AEC.
[1] This is four times the number observed by Adelman (Abstract for Stanford Meeting of the Am. Phys. Soc.).
[2] D. H. Perkins, Phil. Mag. No. 305, June, 1949.
[3] S. Tamor, Phys. Rev. 77, 42 (1950).

D6. Cosmic-Ray Phenomena in Extremely Thick Emulsions.[1] PIERRE DEMERS, *Université de Montréal.*—Baseless sheets 150μ thick of author's emulsion No. 2 modified,[2] have been prepared, stacked together forming a continuously sensitive homogeneous mass. Sheets are separated for processing and examination. Such stacks 4 to 12 mm thick (*6.4 to 19.2* m *air*), were irradiated 2 hours at 25–35-km altitude on 14 VII 49. Some advantages follow: homogeneous medium; identity, energy and history of all tracks single or in stars. The complete tracks for 10–14 branched stars have been followed in 4–6 sheets, sometimes a second star is formed in another sheet at the end of a long branch. δ-rays along α-tracks 15 mv and more are visible thanks to sensitivity, and very small size of the grains, which also reveals the existence of two branched stars made of a long track (α, p, μ) and a very short recoil, making up 10–20 percent of all stars; these stars may be expected to be more abundant at lower levels. A grant from NRC is gratefully acknowledged.

[1] Ann. Acfas (19) (to be published).
[2] Science 110, 380 (1949).

D7. The Dependance of High Altitude Star and Meson Production Rates on Absorbers. MARIETTA BLAU, JOHN NAFE, AND HERBERT BRAMSON, *Columbia University.*—Photographic emulsions (mainly Ilford C_2 emulsions, 200 microns) shielded with lead and copper have been exposed for 3 hours at an altitude of 93,000 feet in Minnesota ($\lambda = 55°$N) in order to investigate the effect of absorbing material upon the rate of star and meson production. The plates were placed horizontally in cut out sections of truncated pyramids of copper and lead so that the absorber thicknesses were 11.3, 22.6 g/cm^2 in the case of copper and 11.3, 22.6, and 33.9 g/cm^2 in the case of lead. Furthermore one set of horizontal plates were placed in about 4 cm distance of the copper pyramid resting on a vertically placed box of plates. Comparing star and meson production in the different sets, distinct transition effects have been observed. The result will be discussed and compared with those of other authors.

D8. Statistical Considerations Concerning the Mass of the μ-Meson. O. HALPERN AND H. HALL, *University of Southern California.*—Recent cloud-chamber observations[1] of 75μ-meson decay processes gave a wide energy distribution of the decay-electrons; the authors[1] inferred from their data a value of 217 ± 4 electron masses for the mass of the μ-meson assuming the other decay products to be neutrinos. In this determination the mass of the μ-meson was taken to be twice the maximum observed electron-energy. A more accurate evaluation assuming various distribution functions[2] for the energy spectrum of the decay electron leads to an increase in the value for the mass of the μ-meson of about 2½ percent. If the electron-spectrum should approach its maximum value with zero slope, an assumption which is made unlikely by the data published, then the statistical correction would become very much larger.

[1] Leighton, Anderson, and Seriff, Phys. Rev. 75, 1432 (1949).
[2] Cf., e.g., J. Tiomno, Phys. Rev. 76, 856 (1949).

D9. On the Nuclear Collision Path Length for π-Mesons. W. E. HAZEN, *University of Michigan.*—If the nuclear collision cross section for high-energy π-mesons is about the geometrical cross section, we should expect a difference between the μ-meson and the π-meson spectra above 10^{11} ev. Greisen[1] has suggested that the underground depth-intensity data are most readily explained in terms of competition between $\pi-\mu$-decay and π-nuclear collisions. Another consequence of the proposed decay-collision competition is a variation in the μ-meson spectrum with zenith angle and a consequent dependence of underground intensity (below some critical depth) not only on earth absorber thickness but also on zenith angle. The earth absorber thickness at which a zenith-angle dependence first appears determines the energy where nuclear collisions compete with decay in the upper atmosphere. Thence, we could proceed to calculate unambiguously the collision path length. Existing data show that the underground intensity depends only on the thickness of earth absorber to thicknesses of 1100-m w.e. Therefore, nuclear collisions do not compete with decay for π-meson energies $<3.5\times10^{11}$ ev and the nuclear-collision path length for high energy π-mesons is greater than 150 g/cm^2 of air.

[1] K. Greisen, Phys. Rev. 73, 521 (1948).

D10. Properties of Cosmic Rays under 1100 Ft. of Earth. C. A. RANDALL, *University of Michigan.*—In a salt mine at 707-m water equivalent the angular distributions and absolute

vertical intensities of the hard component and of combined soft and hard have been determined from G-M counter measurements. Absorption curves in Pb and C were obtained. The ratio of soft to hard component was measured; its dependence upon angular distribution and upon the least energy which can penetrate the counters and absorber was taken into account. A range-energy relation for mesons of energy up to 5×10^3 Bev was calculated; this was done by using average meson energy loss due to ionization calculated by Halpern and Hall, calculating average meson energy loss due to radiative collisions from the Christy and Kasaka bremsstrahlung cross sections, and normalizing to Smith's calculations at 100 Mev. By means of this range-energy relation the meson energy spectrum in the mine was deduced. The spectrum was used to calculate soft-to-hard ratio and to estimate a tentative extension of the meson spectrum at sea-level to 5×10^3 Bev. Results are consistent with the assumptions: that only μ-mesons carry cosmic-ray energy to 707-m w.e., and that the soft component consists of electron and photon secondaries, existing in their familiar cascade symbiotic relation, and arising from knock-on and bremsstrahlung processes.

D11. A Fluctuation of the Nuclear Disintegration Rate in Photographic Emulsions Exposed in the Stratosphere Following a Solar Flare.* J. J. LORD AND MARCEL SCHEIN, *University of Chicago.*—Photographic plates exposed at 95,000 ft. in the stratosphere by free balloons approximately 22 hours following the large solar flare of May 10, 1949,[1] showed an increase of approximately 50 percent in the rate of production of stars having less than 10 prongs. The frequency of occurrence of heavy nuclei during the balloon flight on May 10th and during a flight on the night of November 30th will be discussed.

* Assisted by the Joint Program of the ONR and the AEC.
[1] A. H. Shapley and R. M. Davis, Jr., Science 110, 159 (1949).

D12. Large Cosmic-Ray Bursts under Thick Absorbers at 11,500 Feet Elevation.* THOMAS G. STINCHCOMB, *University of Chicago.*—Using a Carnegie model C meter, experiments on bursts of more than 200 particles under a minimum spherical absorber of 122 g/cm² lead have been carried out at Climax, Colorado. Counters to detect air showers energetic enough to penetrate this minimum absorber indicate that only 3 percent of these bursts are in coincidence with such air showers. For bursts of more than 2000 particles the percentage is 13 percent. Subtracting these bursts due to air showers, one finds a power law for the integral frequency *versus* size distribution with an exponent 1.99 ± 0.09 having no variation with burst size detectable within error indicated. Additional large spherical absorbers of 181 g/cm² lead and 135 g/cm² iron indicate that the mean free paths of this burst producing radiation are 440 ± 65 g/cm² lead and 220 ± 25 g/cm² iron. Varying the area covered by an additional plane absorber of 129 g/cm² iron above the minimum spherical lead absorber indicates that within experimental error of 6 percent no radiation enters at zenith angles larger than 35 degrees. If this radiation were nucleonic in origin with a mean free path in air of 140 g/cm², one would expect 24 percent of the radiation at zenith angles more than 35 degrees.

* Assisted by the Joint Program of the ONR and the AEC.

D13. Cosmic-Ray Bursts at High Altitudes.* G. N. WHYTE, *Princeton University.*—A series of thin-walled, spherical ionization chambers of the type developed by Coor[1] have been flown to altitudes exceeding 90,000 ft. at geomagnetic latitudes 0°, 29°, and 35°. The frequency of cosmic-ray bursts due to the formation of more than 10^5 ion pairs in the chamber has been recorded as a function of altitude at these latitudes. Preliminary considerations indicate that the effects of primary and secondary rays in producing bursts can be separated. The interpretation of the altitude dependence of the burst rate will be discussed in terms of the primary flux of heavy nuclei and protons and the multiplication of the proton and neutron components by nuclear disruptions.

* Assisted by the Joint Program of the ONR and the AEC.
[1] Thomas Coor, Princeton University thesis (1948).

Theoretical Physics, I

E1. "Bremsstrahlung" in High Energy Nucleon-Nucleon Collisions. ALBERT SIMON, *University of Rochester.*—The "bremsstrahlung" accompanying high energy nucleon-nucleon collisions has been calculated by Ashkin and Marshak[1] in analogy with coulombic bremsstrahlung. This approach, using an empirically determined nuclear potential, necessarily omits the "exchange" terms which arise in the appropriate third-order field-theoretic calculation. The phenomenological treatment also predicts a photon spectrum of the form $(E_0-k)^{\frac{1}{2}}(dk/k)$, where E_0 and k are the energies of the nucleon and photon, respectively, in the cm system. We have calculated nucleonic bremsstrahlung in a field-theoretic way using scalar theory with scalar coupling and pseudoscalar theory with pseudoscalar coupling. The results for the spectra, making the same approximation as in (1), are: $\sigma_s(k)dk\sim(E_0-k)^{\frac{1}{2}}(dk/k)$; $\sigma_p(k)dk\sim(E_0-k)^{\frac{1}{2}}kdk$. It also turns out that the "exchange" terms are larger than the "ordinary" terms. In particular, for $E_0=125$ Mev, the "exchange" terms contribute 1–2 times as much as the "ordinary" terms (over the range $k=E_0/2$ to E_0) for both scalar and pseudoscalar theories. The bearing of these results on the Berkeley experiments[2] will be discussed. This work was assisted by the Joint Program of ONR and AEC.

[1] J. Ashkin and R. E. Marshak, Phys. Rev. 76, 58 (1949).
[2] Bjorklund, Moyer, and York, Phys. Rev. (in press).

E2. Deuteron Photo-Effect at High Energies. L. I. SCHIFF, *Stanford University.*—The results described at the Stanford meeting of the American Physical Society (December, 1949, Abstract B8) are being applied to the computation of the cross section for photoelectric disintegration of the deuteron by high energy gamma-rays. The object of the calculation is to provide a basis for distinguishing between the two forms of neutron-proton interaction (Yukawa and exponential) that appear to be most successful in explaining the high energy neutron-proton scattering.[1] These interactions are closely simulated by potentials for which the ground-state deuteron wave function can be found in a convenient analytic form. Electric quadrupole as well as electric dipole transitions are considered, as are the effects of nucleon interaction on the final states.

[1] R. S. Christian and E. W. Hart (private communication).

E3. Multiple Scattering in an Infinite Medium. H. W. LEWIS, *University of California, Berkeley.*—The integro-differential diffusion equation which describes the multiple scattering of a particle in an infinite medium is studied without the usual small angle approximation. The angular distribution irrespective of position is found exactly as a series of Legendre polynomials, and as a function of track length, taking into account energy loss. This series converges slowly when small angle scattering is important, in which case the solution recently obtained by Snyder and Scott is applicable, but converges rapidly otherwise. Exact closed expressions are also derived for the moments of the longitudinal and radial distributions, and for various correlation functions of position and direction of the scattered particle.

E4. Phase Shifts in *p-d* Scattering and Exchange Forces. J. L. GAMMEL, *Cornell University.*—Verde[1] gives rigorous integral formulas for the phase shifts (δ's) in *n-d* scattering. In this paper his method is extended to *p-d* scattering. Tensor forces are neglected, which is satisfactory below 10 Mev with the

usual tensor forces.[3] It is found that the Coulomb barrier decreases the p-d δ's compared to the n-d δ's by a factor which is about 0.8, but which depends on L and the energy. The integral formulas are used to formulate a Born approximation for the P and D δ's. Calculation with a nuclear potential $(W+BP_\sigma+HP_\tau-MP_x)U(r)$ where P_σ, P_τ, and P_x are spin, charge, and space exchange operators, respectively, taken with the experimental[3] δ's shows that B and H must be small, in agreement with the high energy scattering data. The results are remarkably independent of W and M, however. An interpretation of the observed P and D phases is given.

[1] Mario Verde, Helv. Phys. Acta 22, 339 (1949).
[2] Roy Thomas, Phys. Rev. 76, 1002 (1949).
[3] Sherr, Blair, Kratz, Bailey, and Taschek, Phys. Rev. 72, 662 (1947); C. L. Critchfield, Phys. Rev. 73, 1 (1948).

E5. Some Calculations Concerning Neutron-Proton Scattering with Tensor Forces.* L. BIEDENHARN AND J. M. BLATT, *M. I. T.*—The Schwinger variational method gives an expansion of $k\cot\delta$ in terms of the energy,[1,2] which is general enough to include the presence of tensor forces. Previous analysis of the available scattering data[3] has been made on the assumption that tensor force effects are negligible. We have obtained values of the first three terms of the above expansion for the square well and Yukawa well shapes, for relevant ranges and depths, consistent with a binding energy of 2.237 Mev, a quadrupole moment of 2.73×10^{-27} cm^2 and a "percentage D-state" of 2–6 percent. The tensor force is found to cause no significant change in the results given in reference (2).

* This work has been supported in part by the ONR and the AEC.
[1] J. M. Blatt, Phys. Rev. 74, 92 (1948).
[2] J. M. Blatt and J. D. Jackson, Phys. Rev. 76, 18 (1949).

E6. The Range of Tensor Forces and the Theory of H^3.* ROBERT L. PEASE AND HERMAN FESHBACH, *M. I. T.*—The theoretical evaluation of the binding of H^3 is very sensitive to the range of tensor forces. We have calculated this binding energy for the potential

$$V(r_{12})=-[(1-g/2+(g/2)\sigma_1\cdot\sigma_2)V_cf(r_{12}/r_c)+S_{12}V_Tf(r_{12}/r_t)].$$

For f we have employed the Yukawa well: the range of central forces r_c was chosen to equal that obtained from proton-proton scattering; the range of tensor forces r_t was varied. The other constants were determined from two-body data. A variational method was employed in which the S state and the three possible D states were included. It was found that all of the D states made important contributions. The ratio of the tensor to central range is close to 1.4. The corresponding equivalent triplet range for n-p scattering is 1.74×10^{-13} cm, in excellent agreement with the most recent determinations.[1]

* Supported in part by the ONR and the AEC.
[1] Hughes, Ringo, and Burgy (in press).

E7. On the Phenomenological Theory of Exchange Moments. R. K. OSBORN AND L. L. FOLDY, *Case Institute of Technology.*—As first pointed out by Siegert, the existence of exchange forces in nuclei implies the existence of accompanying exchange currents. Sachs has calculated an expression for these, by making the Hamiltonian containing exchange potentials gauge invariant, and applied it to the calculations of exchange magnetic moments in H^3 and He^3. The Hamiltonian obtained by Sachs is not the most general admissible one. More generally the exchange current density is found to depend on a vector function whose irrotational part is completely determined by gauge invariance but whose solenoidal part is arbitrary except for the requirements (following from conditions of translational invariance and symmetry in all nucleons on the Hamiltonian) that it be translationally invariant and antisymmetric under the exchange of the spin and space coordinates of each pair of nucleons. In the resultant exchange moments, the irrotational part leads to the same expression as obtained by Sachs, while the solenoidal term contribution contains the spin operators of the nucleons in particular combinations together with arbitrary functions of the nucleon separation. Villars' exchange moment expression, as obtained from meson theory, is included as a special case and hence the exchange contributions to the moments of H^3 and He^3 are explicable on a phenomenological basis, contrary to the results obtained in Sach's special case. This work has been supported by the AEC.

E8. The Cross Section of $(n, 2n)$ Reactions Near the Threshold.* GEORGE SNOW, *Brookhaven National Laboratory.*—The energy dependence of the cross section of $(n, 2n)$ reactions near the threshold is derived using the nuclear dispersion theory formalism.[1] Configuration space is divided into three regions: An internal region, corresponding to the compound nucleus, an intermediate region, in which one neutron and the remaining nucleus are sufficiently far apart so that their nuclear interaction vanishes, and an external region, in which two neutrons do not interact with the residual nucleus. Boundary conditions are derived for the stationary wave function in the external region. An approximation to these boundary conditions allows the determination of the external region wave function, whose asymptotic form yields the result $\sigma(n, 2n)\cong(E-E_t)^2$, where E is the incident neutron energy in the center of mass system, and E_t is the $(n, 2n)$ threshold energy. The neutron-neutron interaction in the external region does not alter the energy dependence of $\sigma(n, 2n)$ near the threshold. This derivation is valid for an energy range too small to allow comparison between theory and experiment. A crude perturbation theory argument yields the same result for $\sigma(n, 2n)$.

* Research carried out at Brookhaven National Laboratory, under the auspices of the AEC.
[1] E. P. Wigner and L. Eisenbud, Phys. Rev. 72, 29 (1947).

E9. Variational Methods and Cross-Section Theorem for Non-Conservative Collisions. MELVIN LAX, *Syracuse University.*—Recent applications of variational methods to transition problems have been generalized to include the possibility of absorption (capture). Let ϕ_a and ψ_a be the unperturbed and perturbed states and V be the interaction potential inducing transitions. The exact transition probability from state ϕ_a to state ϕ_b may be obtained by replacing the Born approximation matrix element $(\phi_b, V\phi_a)$ by $T_{ba}=(\phi_b, V\psi_a)$. A variational expression is found for the transition amplitude, T_{ba}, in terms of ψ_b, ψ_a and corresponding solutions of a suitable adjoint equation. The latter must be introduced because of the non-hermitian nature of the operators involved in an absorption problem. Collisions induced by hermitian operators obey the known theorem that the total cross section is proportional to the imaginary part of T_{aa}, the scattering amplitude in the forward direction. This theorem, equivalent to the unitary nature of the Heisenberg S matrix, expresses the conservation of probability. (If only one form of particle is involved, the conservation of particles.) For non-conservative collisions we show that the cross-section theorem remains valid providing the total cross section is now interpreted to include the capture cross section. A check on the accuracy of the variational method is given in an adjoining abstract by A. Levitas.

E10. Statistical Theory and the Angular Distribution of Nuclear Reactions. L. WOLFENSTEIN, *Carnegie Institute of Technology.*—Nuclear reactions involving high energy particles are commonly treated on the assumption that a compound nucleus is formed in which the original projectile loses its identity. It should not be expected, however, that the resultant angular distribution is isotropic. Conservation principles require that the angular momentum of the compound nucleus be polarized, because of the polarization of the incident

orbital angular momentum. This polarization displays itself partly in the polarization of the outgoing nuclei at certain angles and partly as an anisotropy in their angular distribution. As a simple example, a single outgoing neutron group from a collision of two spin zero particles is considered. It is assumed that many compound nuclear states are involved and that the transition probabilities to the final states can be determined from statistical concepts. If orbital angular momenta up to $4\hbar$ are effective and if the residual nucleus has a spin $\frac{1}{2}$ the forward intensity is calculated to be five times that at 90°. The angular distribution is characteristically symmetrical about 90°. For larger residual nuclear spins the distribution is more isotropic. Applications to (α, n) and (d, n) reactions will be discussed.

Cosmic Rays

G1. On the Extraordinary Increase of Cosmic-Ray Intensity on November 19, 1949. SCOTT E. FORBUSH, *Carnegie Institution of Washington*, AND THOMAS B. STINCHCOMB AND MARCEL SCHEIN, *University of Chicago.*—Beginning about $10^h\,45^m$ GMT on November 19, 1949, there occurred the largest increase in cosmic-ray intensity yet observed. By 11^h GMT the ionization at sea level under 12 cm Pb was 43 percent above normal at Cheltenham (geomagnetic latitude $\Phi = 50°$N) and at Godhaven ($\Phi = 80°$N). At Huancayo ($\Phi = 0°$, elevation 11,000 ft.) no increase was detected. At Climax (elevation 11,500 ft.) the ionization under similar shielding increased to about 180 percent above normal in 15 min. and remained at least 100 percent above normal for about an hour, decreasing exponential-wise to near normal in about seven hours. The absolute magnitude of the increase at Climax was about ten times greater than at Cheltenham. This large increase with altitude appears to rule out mesons or soft component, leaving relatively low energy protons, or neutrons, or possibly some unknown radiation, to account for the effect.

G2. On a Difference-Equation Method for Solving Diffusion Equations in Cosmic-Ray Shower Theory and Similar Problems. W. T. SCOTT, *Smith College.*—The equations dealt with may be written $\partial F/\partial t - \beta \partial F/\partial E = L_E F(E, t)$, where L_E is a linear, integral operator involving cross sections for elementary physical processes, and β is a constant. The method requires that these cross sections be homogeneous functions of the energy, as in the case of high energy cascades. Hence, a combined Laplace-Mellin transform can be usefully employed: $g(p, s) = \int_0^\infty e^{-st} dt \int_0^\infty (E/\beta)^p F(E, t) dE$. Applying these transforms to the original equation, we obtain a difference equation for g: $pg(p-1, s) + V_s(p) g(p) = \varphi(p)$, where $\varphi(p)$ is the Mellin transform of the initial condition. Using the behavior of g as $p \to \infty$, the difference equation may be solved by iteration. The resulting infinite series may be written as a contour integral through the use of an infinite product representation of the nth term, that can be generalized for non-integral values of n.[1] The final result is an exact solution of the original equation, satisfying the boundary conditions exactly, in the form of a triple complex integral. Suitable evaluations by use of the calculus of residues, combined with the saddle-point method, lead to numerical results.[2]

[1] First obtained by H. S. Snyder, Phys. Rev. **75**, 906 (1949).
[2] H. S. Snyder, Phys. Rev. **76**, 1563 (1949).

G3. A Hodoscope Study of Local Cosmic-Ray Showers. K. SITTE, *Syracuse University.*—The collision mean free path of charged particles which produce penetrating showers in lead has been measured with a more rigid selection of the penetrating events than that used in similar experiments of other authors. The results prove a dependence of the collision cross section on the total shower energy: The mean free path is (162 ± 10) g/cm² for showers of 200 g/cm² minimum penetration, and (196 ± 13) g/cm² for showers of 100 g/cm² minimum penetration. The vertical intensity of the charged shower-producing radiation at 3260 m altitude is $(1.6 \pm 0.3) \times 10^{-3}$ cm^{-2} sec.$^{-1}$ sterad.$^{-1}$. This is only one-tenth of the intensity one would expect from the observed primary proton flux and the absorption coefficient of fast nucleons in air, and indicates the predominance of "soft" nuclear collisions for low energy primaries.—Local soft showers originated by ordinary μ-mesons in lead were observed, and the electronic nature of the shower particles established. They occur in about one of 10^8 traversals of a μ-meson.

G4. Cosmic-Ray Showers Observed in a Cloud Chamber Triggered by Neutron Coincidences.* E. C. FOWLER AND J. C. STREET, *Harvard University* AND W. B. FOWLER AND R. D. SARD, *Washington University.*—The 565 accepted sets of photographs[1] have been examined for cosmic-ray showers. As expected from the results of V. Cocconi-Tongiorgi,[2] there are many photographs showing air showers and penetrating showers. There are 124 expansions showing nuclear interactions or electromagnetic cascade showers or mixed showers, as defined below. Of these, 62 are nuclear interactions, defined as events with at least three tracks having a point in common, and with at least one dense track or alternatively three penetrating tracks. Of these, five appear to be nuclear cascades, i.e., there are two nuclear interactions in the chamber. In some of the 62 cases, an outgoing particle can be identified as a slow meson. There are 47 electronic showers, defined as events with five or more bundles of three or more rays each between the two bottom Pb plates and containing no detectable heavily ionizing or penetrating particles. Some of these appear to be of very high energy. There are 15 mixed showers, containing recognizable electrons and heavily ionizing or penetrating particles. Examples illustrating these events will be discussed.

* This work was supported by the Joint Program of the ONR and the AEC.
[1] See the abstract G5, "Stopped cosmic-ray particles observed in a cloud chamber triggered by neutron coincidences," by Fowler, Fowler, Sard, and Street.
[2] V. Cocconi-Tongiorgi, Phys. Rev. **73**, 923 (1948); Cocconi, Cocconi-Tongiorgi, and Greisen, Phys. Rev. **74**, 1867 (1948).

G5. Stopped Cosmic-Ray Particles Observed in a Cloud Chamber Triggered by Neutron Coincidences.* W. B. FOWLER AND R. D. SARD, *Washington University*, AND E. C. FOWLER AND J. C. STREET, *Harvard University.*—To examine further the coincidences between neutrons and charged particles,[1] we have used them to trigger the cloud chamber[2] containing three Pb plates (approximately 10 g cm^{-2} each), seven Al foils and one graphite plate (2.0 g cm^{-2}). The chamber was beneath fourfold G-M tube telescopes[3] (no Pb) and above an anti-coincidence tray on a paraffin block containing BF_3 counters. A telescope-neutron coincidence triggered the chamber, anti-coincidences being indicated. Locale: Climax (3400 m). The 565 accepted sets of photographs have been examined for stoppings of particles entering the chamber with minimum ionization. There are, respectively, seven and 14 cases of stoppings in the two bottom Pb plates; of the 14 at least three show the increased ionization expected for a meson stopped in the upper part of the plate. In addition, we note seven cases of increased ionization on leaving the bottom plate, which could be mesons stopped immediately below. Two possible interpretations of the stoppings—negative μ-mesons stopped by ionization loss, and minimum ionization protons producing stars of which only one particle, heavily ionizing, emerges,—will be discussed.

* Work supported by the Joint Program of the ONR and AEC.
[1] Sard, Ittner, Conforto, and Crouch, Phys. Rev. **74**, 97 (1948); Sard, Conforto, and Crouch, Phys. Rev. **76**, 1134 (1949).
[2] Cool, Fowler, Street, Fowler, and Sard, Phys. Rev. **75**, 1275 (1949); Cool, thesis, Harvard University (1949); E. C. Fowler, thesis, Harvard University (1949).

G6. Relativistic Showers in Nuclear Emulsions (I).* L. S. OSBORNE, B. T. FELD, AND I. L. LEBOW, *M. I. T.*—We have examined NTB3 nuclear emulsions, exposed in balloon flights to about 90,000 ft. at various latitudes, and analyzed 15 high energy stars characterized by the emission of collimated groups of minimum ionizing particles (average, ten per event). These events also show a less collimated component of near-relativistic particles (energies between 0.1 and 0.5 mc^2) as well as heavy tracks (below 0.1 mc^2). Eight stars have a minimum track opposite the shower, presumably a relativistic proton. The angular distribution of all tracks was measured with respect to the "shower axis," defined as the geometric axis of the shower of minimum ionization tracks. The heavy particle distribution is spherically symmetric. Comparing the minimum charge carried by these "boiled off" particles, the stars separate into two groups: five with minimum charge between two and five and ten between 15 and 40. The groups are interpreted as disintegrations of light (C, N, O) and heavy (Ag, Br) nuclei, respectively. Coulomb scattering measurements on eight near-minimum tracks identified one meson and seven protons. The angular dispersion and the average multiplicity of both minimum and near-minimum tracks are less for events involving light nuclei than for the heavy.

* Assisted by the Joint Program of the ONR and AEC. Plates courtesy of Brookhaven National Laboratory.

G7. Relativistic Showers in Nuclear Emulsions (II).* B. T. FELD, I. L. LEBOW, AND L. S. OSBORNE, *M. I. T.*—Using the data from the previous abstract, identification of the near-minimum tracks as protons and the excess of tracks over nuclear charge in the stars imply that the minimum ionization tracks are predominantly mesons. Plotting the average angular dispersion, $\bar{\psi}$, *vs.* the multiplicity, N, of these tracks, for each event, the light nucleus collisions lie significantly below those for the heavy nuclei; $\bar{\psi}$ decreases with N in both cases. We have calculated $\bar{\psi}$ for a single, meson producing nucleon-nucleon collision assuming various energy spectra, angular distributions, and multiplicities of mesons in the center-of-mass system. Comparison with the experimental points shows possible agreement for the light nuclei but definite disagreement for the heavy nuclei under any reasonable assumptions. The above, plus the multiplicity of near-relativistic protons, strongly suggests that meson production in a nucleus is by a cascade process, with relatively low multiplicity in each nucleon-nucleon encounter. The decrease of the ratio of minimum (meson) to near-minimum (proton) tracks from light to heavy nuclei suggests that sharing of the incident energy is sufficiently rapid to decrease the meson production efficiency when the thickness of nuclear material traversed is doubled from light to heavy nuclei.

* Assisted by the Joint Program of the ONR and AEC.

G8. Directional and Latitude Survey of Cosmic Rays at 95,000 Feet. I. Experimental Procedure.* T. STIX, K. DWIGHT, R. SABIN, AND J. R. WINCKLER, *Princeton University.*—A total of 17 Skyhook balloon flights were made at geomagnetic latitudes 0°, 20°, 30°, and 40° to determine the directional distribution of cosmic-ray intensity at 95,000 feet. The principal measuring instrument was a Geiger tube telescope of three trays, each 10×10 in., with 50-in. separation between top and bottom tray. A 3-cm Pb filter was placed just above the bottom tray for most flights. An electric motor drove the telescope in azimuth and periodically varied the zenith position. The counting rate and orientation of the telescope and the atmospheric pressure were radio-telemetered continuously to the ship. A description of the apparatus and the methods of standardization, as well as the advantages and limitations of the experiment, will be presented. The work took place during July and August of 1949 aboard the USS Norton Sound on a cruise from Port Hueneme, California, to Jarvis Island and return.

* Assisted by the Joint Program of the ONR and AEC.

G9. Directional and Latitude Survey of Cosmic Rays at 95,000 Feet. II. Interpretation of Vertical Flux Data. K. DWIGHT, R. SABIN, T. STIX, AND J. R. WINCKLER, *Princeton University.*—The vertical flux of ionizing particles was measured at 15 g/cm² atmospheric depth at 0°, 20°, 30°, and 40° geomagnetic latitude and previously at 52° and 56°. These data are in satisfactory agreement with rocket experiments and other balloon measurements, and are interpreted using the vertical cut-off energy at each latitude. Assuming a *number* spectrum of the type $N(E)=CE^{-\gamma}$ for the primary radiation, preliminary fitting shows that γ varies with energy but has an average value of about 1.8. N is the number of particles of the energy E contained in unit energy interval. This gives for the *energy* spectrum, $N(E)E$ an exponent $\gamma-1=0.8$ instead of the value 1.8 which is often assumed for this spectrum. The vertical flux of ionizing particles at 0° latitude at 15 g/cm² atmospheric depth is considerably higher than the primary flux estimated from the atmospheric depth-ionization measurements.

* Assisted by the Joint Program of the ONR and AEC.

G10. Directional and Latitude Survey of Cosmic Rays at 95,000 Feet. III. Interpretation of Azimuthal and Zenithal Data.* J. R. WINCKLER,** K. DWIGHT, R. SABIN, AND T. STIX, *Princeton University.*—The azimuthal distribution was measured at zentih angles of 20°, 40°, and 60° at geomagnetic latitudes of 0°, 20°, and 40°N at atmospheric depths of about 20 g/cm². The E-W asymmetry was also studied as a function of depth between 20 and 200 g/cm² with and without a 3-cm Pb shield. These measurements show that the E-W difference is roughly constant far into the atmosphere, but the percent asymmetry decreases with increasing depth. A large E-W effect is observed even in the total radiation between 20 and 200 g/cm², at the peak of the total intensity curve. The percent asymmetry to be expected for all positive primaries may be predicted from the latitude variation of the vertical flux. The observed E-W asymmetries are all smaller than predicted. This difference will be discussed in terms of negative primaries, direct atmospheric effects, and secondary particles moving outside the atmosphere.

* Assisted by the Joint Program of the ONR and AEC.
** Now at University of Minnesota.

G11. Matters Pertaining to the Magnetic Deviation of Cosmic-Ray Particles in the Atmosphere.* W. F. G. SWANN, *Bartol Research Foundation.*—The possibility of a telescope recording from below requires consideration in the case of low energy rays at high altitudes. Any ray traveling vertically upward and coming originally from above must have passed through a condition in which it was horizontal. Taking into account absorption, it is possible to show that any proton entering a telescope vertically from below at 100,000 ft. would have its horizontal portion more than 3.8×10^6 cm below the telescope. For alpha-particles, the distance is greater, so that, both for protons and α-particles, there would be no room between the earth's surface and the telescope to describe the orbit. For mesotrons, the distance would be less than 100,000 ft. However, mean life considerations demand that, regardless of the nature of energy loss, the fraction of any group of mesotrons which could survive long enough to turn through a right angle is $e^{-12.4}$. The numerical integrations involved in the problem have been carried out by Mr. Stephen S. Forbes under the writer's direction.

* Assisted by the Joint Program of the ONR and AEC.

G12. The Increase in the Primary Cosmic-Ray Intensity at High Latitudes, and the Non-Existence of a Detectable Permanent Solar Magnetic Field.* MARTIN A. POMERANTZ, *Bartol Research Foundation.*—The primary cosmic-ray intensity at Churchill, Man. ($\lambda = 69°$N) has been compared directly with that at Swarthmore, Pa. ($\lambda = 52°$N). The measurements, obtained with identical vertical quadruple-coincidence counter trains, have revealed an increase at the more northern station caused by the presence in the primary radiation of particles having energies below that which would have been permitted had the sun's magnetic field been effective to the extent previously assumed. The ratio of intensities is $I_T(0,69°)/I_T(0,52°) = 1.46$. *Intensity vs. altitude* curves were obtained with several different thicknesses of absorber interposed in the counter trains. There is no indication of any diurnal variation which could be in conformity with the existence of a permanent dipole-moment at the sun. The differential energy distribution at the low energy end of the primary cosmic-ray spectrum cannot be evaluated exactly because of absorption considerations, but it is doubtful that the exponent in an inverse power-law representation is as large as has usually been assumed. It is concluded that the sun possesses no detectable permanent magnetic field and, on the basis of the present experiments, an upper limit of 0.6×10^{33} gauss-cm^3, as compared with the previously quoted value of 10^{34} gauss-cm^3, may be assigned as a maximum possible value of the dipole-moment.

* Assisted by the Joint Program of the ONR and AEC. Field expedition sponsored by National Geographic Society.

G13. Measurement of the Cosmic-Ray Intensity as a Function of Altitude at a Geomagnetic Latitude of 28 Degrees.* M. L. VIDALE AND MARCEL SCHEIN, *University of Chicago.*—Through the courtesy of the ONR a counter experiment was carried out at 28° geomagnetic latitude with balloons launched from the aircraft carrier, Palau. Measurements were made on the soft and hard component using a fourfold coincidence arrangement with 0 and 12 cm Pb. The hard component showed a maximum at 6 cm Hg pressure. The maximum in the soft component occurred at a pressure of 10 cm Hg. The latitude effect of the hard component was observed to be 300 percent at 92,000 ft. elevation above sea level. This value is in agreement with measurements made on the latitude effect of large nuclear disintegrations initiated by primaries. The frequency of multiple coincidences detected under 12 cm Pb did not show any increase from 10 cm Hg to 1.2 cm Hg, in contrast to similar measurements at a geomagnetic latitude of 51° were an increase by a factor of two has been found.[1] Possible explanations of this effect will be discussed.

* Assisted by the Joint Program of the ONR and AEC.
[1] Schein, Yngve, and Bowen (unpublished results).

G14. Measurements on the Latitude Effect of the Neutron Component of Cosmic Radiation at High Altitudes.* LUKE C. L. YUAN,** *Princeton University.*—Measurements on the intensity distribution of slow neutrons in the free atmosphere using balloon-borne equipment similar to those used in previous experiments[1] were made at the equator and at 27°N geomagnetic latitude. Two proportional counters filled with enriched boron trifluoride (96 percent B^{10}) at a pressure of 50 cm Hg were employed. One counter was shielded with 0.030-in. cadmium and the other counter was shielded in tin of the same thickness for the compensation of possible effects caused by stars produced in the cadmium shield. The high voltage system for the counters were pressurized to prevent any effect caused by corona discharge at the high voltage terminals which might appear as neutron counts.

The balloon-borne equipment ascended to an altitude of 92,000 ft. at the equator. The results obtained show a maximum in the intensity distribution as a function of altitude in a manner similar to that[1] obtained at Princeton, New Jersey (geomagnetic latitude 51° 46'N). An absorption depth $\lambda = 225$ g/cm^2 was obtained in agreement with our previous measurements[2] made on a B-29 airplane at lower altitudes.

* Assisted by the Joint Program of the AEC and ONR.
** Now at Brookhaven National Laboratory, Upton, Long Island, New York.
[1] Luke C. L. Yuan, Phys. Rev. **74**, 504 (1948); Luke C. L. Yuan (to be published shortly).
[2] Luke C. L. Yuan, Phys. Rev. **76**, 1267 (1949); Luke C. L. Yuan, Phys. Rev. **76**, 1268 (1949).

Beta-Emitters; Nuclear Scattering

H1. Radiation from Au^{197*}(7×10^{-9} sec.).** F. K. MCGOWAN, *Oak Ridge National Laboratory.*—Using a delayed coincidence scintillation spectrometer both the radiation announcing the formation of the isomeric state in Au^{197*}(7 ± 1) $\times10^{-9}$ sec.[1] and the radiation resulting from its decay have been measured. Huber *et al.*[2] have observed that four percent of the disintegrations of Hg^{197}(23 hr) lead to a 7.5-sec. isomeric state in Au^{197} and 96 percent of the disintegrations are followed by γ-ray transitions corresponding to 135 and 165 kev which are strongly converted. With the delayed coincidence scintillation spectrometer K and L conversion electrons of the 135 kev transition appeared in the spectrum of the delayed radiation. The ratio N_K/N_L is $\lesssim 1$. The K and L conversion electrons corresponding to the 165 kev transition, which announces the formation of the short-lived isomeric state, were observed. In this case $N_K/N_L \sim 0.1$.

** This document is based on work performed for the AEC at Oak Ridge National Laboratory.
[1] F. K. McGowan, Phys. Rev. **77**, 138 (1950).
[2] Huber, Steffen, and Humbel, Helv. Phys. Acta **21**, 192 (1948).

H2. A Delayed Coincidence Measurement of $Hg^{203,205}$. DANIEL BINDER, *Yale University.*—An attempt has been made to measure the half-life of the γ-ray level in the beta-gamma cascade emission from $Hg^{203,205}$ by a delayed coincidence measurement. A proportional counter is used as the beta-ray detector and a 931A photo-multiplier with an anthracene crystal as the gamma-detector. A symmetrical resolution curve with a half-width of 7×10^{-8} sec. was obtained by sending beta-rays from P^{32} through the proportional counter into the photo-multiplier. The coincidence *versus* delay curve obtained with $Hg^{203,205}$ placed between the detectors is also symmetrical. An upper limit for the half-life may be determined by using theoretical expressions for the curves and finding what value of the half-life produces a distinct asymmetry. By this method an upper limit of 2×10^{-8} sec. was obtained. Further investigations of γ-ray levels are in progress.

* Assisted by the Joint Program of the ONR and the AEC.

H3. Low Energy Photons from Radioactive Nuclei.* GERTRUDE SCHARFF-GOLDHABER,** E. DER MATEOSIAN, M. MCKEOWN AND A. W. SUNYAR, *Brookhaven National Laboratory.*—Low energy photons have been observed for a number of radioactive nuclei with the help of an argon filled proportional counter. Results have been obtained as shown in Table I. The 24-kev electrons reported by Teillac[1] for Pa^{231} and interpreted as L-electrons of a 44-kev transition are reinterpreted as M-electrons of the 27-kev transition. Although no unconverted γ-rays could be detected from U^{234}, comparison with other α-emitters indicates that the L-radiation is caused by a

TABLE I.

	Sm^{151} (a)	Tb^{161}(?) (b)	Pa^{231} (c)	U^{234} (d)
Energy of γ-rays in kev.	21	26	27	—
X-rays observed	L	K, L	L	L

(a) Separated from fission products by Glendenin and Marinsky.
(b) Produced by slow neutron bombardment of Gd in Oak Ridge.
(c) Prepared by M. Studier, Argonne National Laboratory.
(d) Isotopically enriched at Y-12, Oak Ridge.

highly converted nuclear transition following at least one quarter of the α-transitions, rather than by excitation of the electronic shell by the α-rays as suggested by Macklin and Knight.[2]

* Research carried out at Brookhaven National Laboratory under the auspices of the AEC.
** On leave from the University of Illinois.
[1] J. Teillac, C. R. 229, 650 (1949).
[2] R. L. Macklin and G. B. Knight, Phys. Rev. 72, 435 (1947).

H4. Isomerism in Pb^{204} and Radiations of Bi^{204} and Bi^{206}. A. W. SUNYAR, D. E. ALBURGER, G. FRIEDLANDER, M. GOLDHABER,* AND G. SCHARFF-GOLDHABER,* *Brookhaven National Laboratory.***—The even-even isomer Pb^{204} (68 min.) is found to decay in two steps. A 905-kev γ-ray ($\sim$10 percent internally converted, K/L ratio $\sim$1.5) is followed by a 374-kev γ-ray ($\sim$5 percent internally converted, K/L ratio $\sim$2) with a half-life of 3×10^{-7} sec. The results can be interpreted by assuming that a transition of multipole order 6 is followed by one of multipole order 3. This requires a spin between 7 and 9 units for the upper metastable state of remarkably high excitation energy (1279 kev). The Pb^{204} was separated from its parent, Bi^{204} (12 hours), which was produced by deuteron bombardment of lead in the MIT cyclotron. The internal conversion electrons were studied in a lens spectrograph. Bi^{204} studied in equilibrium with its daughter, showed additional lines corresponding to a 217-kev transition. Weaker lines might have been masked because of the presence of Bi^{206} (6.4 days) which shows an extraordinary number of lines corresponding to the following γ-ray energies: 182, 234, 260, 341, 396, 470, 505, 536, 590, 803, 880, 889, 1020, 1097, 1720 kev.

* On leave from the University of Illinois.
** Under the auspices of the AEC.

H5. Photo-Neutron Production.* E. DER MATEOSIAN AND M. GOLDHABER,** *Brookhaven National Laboratory.*—Because of the incomplete state of our knowledge of gamma-rays of sufficient energy to disintegrate Be or D we have recently begun a systematic search for such gamma-ray emitters. The photo-neutrons are slowed down in paraffin and detected by $B^{10}F_3$ counters. The sensitivity of the arrangement is such that one microcurie Ra inside Be produces 35 counts per minute, above a background of 10 counts per minute. With this sensitivity the difficulty lies not in the detection of weak gamma-ray branches (of the order of 10^{-6} or less) but rather in the exclusion of photo-neutron producing impurities. Two new cases were established: Ag^{110} (225 days) and Bi^{206} (6.4 days) which produce photo-neutrons in Be but not in D_2O. For approximately equal γ-intensities measured by an air ion chamber shielded with $\frac{1}{4}$-inch lead, the neutron counting rate was 1/2000 for Ag^{110}, and $\frac{1}{3}$ for Bi^{206} in comparison with $Ra-\gamma-Be$. The energy of the gamma-rays responsible is not yet known for Ag^{110}, but from Bi^{206} a 1.72 gamma-ray has been observed in a lens spectrometer to which the photo-neutrons can be ascribed (see preceding abstract).

* Research carried out under the auspices of the AEC.
** On leave from the University of Illinois.

H6. Proton-Proton Scattering at 340 Mev. C. WIEGAND AND O. CHAMBERLAIN, *University of California.*—We have measured proton-proton scattering at 340 Mev using the externally deflected beam of the 184-inch Berkeley cyclotron. Two coincidence counter methods are employed to detect the scattered protons from a polyethylene target: (a) a telescope of three proportional counters in line and very similar to that used for neutron-proton scattering,[1] (b) a telescope of two small proportional counters to count one scattered proton and a larger proportional counter at approximately 90° to count the other scattered proton. The larger counter is moved close enough to the target to count every proton whose counterpart reaches the small counter telescope. At the present time method (b) gives cross sections about 15 percent lower than method (a). Backgrounds are taken by substituting equivalent carbon targets for the polyethylene. The proton beam current is measured by an ionization chamber which has been calibrated against a Faraday cup. The average results are: $d\sigma/d\Omega$ in 10^{-27} cm^2 sterad^{-1} at 90°, 5.5±0.6; 62°, 5.4±0.6; 41°, 5.6±0.8; where angles and cross sections are in the center of mass system. These cross sections are about twice the theoretical maximum for pure s-scattering.

[1] Hadley, Kelly, Leith, Segrè, Wiegand, and York, Phys. Rev. 75, 351 (1949). Fig. 2.

H7. Magnetic Deflection Method for Observing Proton-Proton Scattering at 250 Mev.* O. A. TOWLER, JR. AND C. L. OXLEY, *University of Rochester.*—The magnetic field of the University of Rochester 130-in. synchro-cyclotron has been used to deflect the protons scattered by polyethylene and carbon targets. The scattered protons strike photographic plates which are placed along a nearly radial probe. The probe, lying just above the lower pole, is shielded from particles traveling in the general direction of the circulating beam by 2 to 4 inches of copper. At a given position along the probe the protons from p-p scattering arrive in a nearly collimated group which corresponds to a well-defined angle of p-p scattering. With the present apparatus such groups of proton tracks have been observed corresponding to scattering angles ranging from 50° to 80° (laboratory). If the number of protons counted in the plates is plotted against the entrance angle, a much lower and broader peak is observed from a carbon target than is observed from the hydrogen in the polyethylene target. From the measurement of the C^{11} beta-activity of the target it is expected that cross sections can be obtained relative to the $C^{12}(p, pn)C^{11}$ cross section.

* Assisted by the Joint Program of the AEC and ONR.

H8. Scattering of 4.5 and 5.5 Mev Neutrons by Deuterons.* E. WANTUCH, *Brookhaven National Laboratory.*—Atmospheric pressure deuterium gas was bombarded with neutrons from the $D(d, n)He^3$ reaction. Incident deuterons were accelerated in the Van de Graaff Generator at the Department of Terrestrial Magnetism. Recoil deuterons (but not disintegration protons) were measured with thin window twofold coincidence proportional counters of 1 microsecond resolving time. Table I shows preliminary results. Background was at most $\frac{1}{3}$ of total counts. The counting errors are ±10 percent, due mostly to uncertainties in monitoring. On the basis of Hunter and Richards' yield values[1] for the D-D reaction, the differential scattering cross section at 0° (in the center-of-mass system) was determined to be 0.25±0.10 barn per steradian. The results are compared with the theory of Buckingham and Massey.[2]

TABLE I.

Scattering angles in lab. system / Neutron energy, Mev	0°	10°	20°	30°
	Net number of coincidences			
5.5±0.1	2300	2400	1200	400
4.5±0.2	2300	2000	1200	—

* Research carried out under the auspices of the AEC.
[1] G. T. Hunter and H. T. Richards, Phys. Rev. 76, 1445 (1949).
[2] R. Buckingham and H. Massey, Proc. Roy. Soc. A179, 123 (1941).

H9. High Energy Electron-Proton Scattering. M. N. ROSENBLUTH AND L. I. SCHIFF, *Stanford.*—In connection with the pending completion of the Stanford linear electron accelerator it has been thought worth while to estimate as accurately as possible the results to be expected from high energy

electron-proton scattering. As corrections to the usual Mott scattering formula we have considered: (a) recoil and magnetic moment of the proton treating it as a Dirac particle of finite mass and having an anomalous Pauli magnetic moment; (b) Spreading of charge and magnetic moment due to the virtual meson cloud; (c) Radiative corrections to scattering as calculated by Schwinger. Calculation (a) has been carried out in a relativistically invariant way; (b) has been done by assuming that the proton charge and magnetic moment are spread over a meson Compton wave-length part of the time. At relatively low energies (100 Mev) and small angles the important contributions are from radiative corrections and proton recoil. At high energies and large angles the other effects are of comparable importance. The meson cloud also has been treated in a relativistically invariant way. Numerical values of these corrections will be presented.

Miscellany in Electrical Physics

HA1. Efficiency of the Thermoelectric Process. G. PRESTON BURNS, *Mary Washington College of the University of Virginia.*—Formulas for the efficiency of the thermoelectric process have been derived for the following cases: (1) External load is different from the internal resistance of the couple. (2) Couple delivers maximum power. (3) Efficiency of the couple is maximum. The maximum efficiency of the process is given by

$$\text{efficiency}=\frac{e^2(T_h-T_c)}{e^2T_h+8\rho k+4(\rho k)^{\frac{1}{2}}(e^2T_h+4\rho k)^{\frac{1}{2}}},$$

where e is the thermoelectric power of the couple, T_h the temperature of the hot junction, T_c the temperature of the cold junction, ρ the specific electrical resistance and k the specific heat conductivity of the elements. If both elements of the couple are made to satisfy the Wiedemann-Franz-Lorenz relation and the temperatures of the junctions are 27°C and 427°C, respectively, then for maximum efficiency the external load is 3.91 times the internal resistance of the couple. For $e=1000$ microvolts per degree centigrade this yields an efficiency of 33.9 percent.

HA2. Effective Reduction of Scattering of Electron Beams in Tissue by Means of a Magnetic Field. W. H. BOSTICK, *Tufts College.*—The root-mean-square scattering for 20-Mev and 50-Mev electrons incident on tissue has been calculated, layer by layer, with the use of the expression for the mean-square scattering angle $\bar{\theta}_i^2=(K/E_i)^2l_i$, where E_i is the average energy in Mev of the electron in the layer, $K=21$ Mev, l_i is the thickness of layer number i in radiation units, and where the angle $(\bar{\theta}_i^2)^{\frac{1}{2}}$ is required to be small. The total mean-square scattering angle for n layers is then

$$\bar{\theta}^2=(\bar{\theta}_1^2+\bar{\theta}_2^2+\cdots\bar{\theta}_n^2).$$

The calculated root-mean-square trajectories in tissue show that electrons are, on the average, scattered far away from their original target. The results of approximate calculations on the effect of a magnetic field parallel to the electron beam indicate that this departure from the intended target can be markedly reduced with a magnetic field of 10,000 oersteds.

HA3. Multiple Scattering Effects in the Measurement of Maximum Electron Ranges. FRANK L. HEREFORD, *University of Virginia.*—Recent data concerning the practical maximum range of monoenergetic electrons ($3\text{ Mev}<E<12$ Mev) in aluminum[1] yield values which fall below a computed curve[2] normalized to agree with previous data in the region of lower energy ($E<3$ Mev). It is normally assumed that the practical maximum range, R_p, as well as the absolute maximum range,[3] R_0, is determined by a small number of the incident electrons which do not experience appreciable scattering in the absorber. Hence, the thickness of the absorber is assumed equivalent to the actual trajectories. While this is valid for those electrons determining R_0, it cannot be absolutely valid for those determining R_p which are stopped within a smaller thickness as a result of multiple scattering in the absorber. Such a scattering effect can be accounted for by means of a semi-empirical correction to the computed lengths of trajectory to give corresponding absorber thicknesses, R_p. The values so computed agree well with the experimental values in both aluminum[1] and copper (data to be published).

[1] F. L. Hereford and C. P. Swann, Phys. Rev. **76**, 570 (1949).
[2] W. A. Fowler, C. C. Lauritsen, and T. Lauritsen, Rev. Mod. Phys. **20**, 237 (1948).
[3] As defined by E. Bleuler and W. Zunti, Helv. Phys. Acta. **19**, 376 (1946).

HA4. Percent Beta-Ray Transmission through Thin Windows. EDWARD STURCKEN, ROBERT HELLER, AND ALFRED H. WEBER, *St. Louis University.*—The percent transmission (I/I_0) of monoenergetic electrons in the range 16–32 kilovolts was measured for thin Nylon films (0.02 mg/cm² to 0.1 mg/cm²). The monoenergetic beam was obtained from an electron diffraction camera. The beam was incident on a Scheelite crystal counter employing a 1P21 photomultiplier tube. Thin windows were inserted in front of the crystal counter by means of an "O" ring sealed probe. Ten second counting periods were used. The average value of I_0 was controlled to give a probable error in counting of less than 0.2 percent. Thin Nylon films (0.05 mg/cm²) gave percent transmissions varying from 10 percent at 16 kilovolts to 70 percent at 32 kilovolts. Slides will be presented showing the percent transmission as a function of electron energy (16–32 kv) for thin films of Formvar, mica and Nylon.

HA5. Radiation Characteristics of a Turnstile Antenna in a Cylindrical Shield.* DAVID S. SAXON,** ALFREDO BAÑOS, JR.,** *University of California, Los Angeles,* AND LOUIS L. BAILIN, *National Bureau of Standards.*—Radiation characteristics have been established for a turnstile antenna in a cylindrical shield. This antenna consists of perpendicularly crossed wires driven by a sinusoidal current distribution, harmonic in time, and differing in phase by 90° between members of the cross. The shield is assumed to be a perfectly conducting cylindrical can open at one end and its diameter is taken to be of the order of a fraction of the driving wavelength. The axis of the shield is perpendicular to the plane of the antenna, passing through its center. The excitation of an infinitely long circular wave-guide by the above current distribution is considered first and conditions under which only the dominant (TE_{11}) mode is important are determined. The essential radiation problem can then be regarded as one in which a semi-infinite circular guide, excited by a TE_{11} mode, radiates into free space. This problem has been formally solved by Levine and Schwinger[1] and using their results, values of the reflection coefficient and gain function have been computed by the National Bureau of Standards, Institute for Numerical Analysis, University of California, Los Angeles. The results of this theory are compared with experiment and with the Kirchhoff method.

* Supported in part by the ONR.
** Consultant for the National Bureau of Standards.
[1] To be published soon. The authors express their appreciation for the private communication of these results.

HA6. On the Radiation Patterns of Dielectric Rods of Circular Cross-Section.* C. W. HORTON, F. C. KARAL, AND C. M. MCKINNEY, *University of Texas.*—A systematic study is being made of the radiation patterns of untapered dielectric rods of circular cross section for different modes of excitation, diameters, and lengths. Theoretical patterns are calculated from equivalent electric and magnetic currents.[1] These surface currents are evaluated by assuming, as a first approximation, that the fields in the dielectric radiator are the same as those in an infinitely long dielectric guide. The resulting theoretical pattern has three parameters; the length, diameter, and the

wave-length of the guided wave. In a careful study of the $TM_{0,1}$ mode in a sequence of five rods of diameter 0.87λ and lengths 2λ to 10λ, it is found that excellent agreement between theory and experiment is obtained if one uses 65 percent of the diameter of the rod for the diameter of the radiating surface. Thus in this series one can correct for the effect of the termination of the rod by using an equivalent rod of the same length but of smaller diameter but whose dielectric constant is such that the wave-length of the guided wave is unchanged.

* The work described in this paper was done at the Defense Research Laboratory under the sponsorship of the Bureau of Ordnance, Navy Department.

[1] See R. B. Watson and C. W. Horton, J. App. Phys. 19, 661–70 (1948).

HA7. The Analog Solution of Simultaneous Partial Differential Equations by Means of Passive and Active Electrical Networks. JAMES H. GREEN, JR., AND VICTOR B. COREY, *Fredric Flader, Inc.*—A general method of obtaining the analog solution of simultaneous partial differential equations by means of iterative electrical networks is developed. The basic theory depends upon developing a formal analogy between the finite difference form of the equations to be solved and the equations describing the distribution of potential in an electrical network. Application of the theory results in the solution of certain simultaneous groups by the use of passive networks containing such circuit elements as resistors, capacitors and inductors, and of more complex groups by means of active networks containing amplifiers. Illustrations are provided in which the general method is applied to the design of practical simulators, and equations are derived which relate specific values of circuit components to the coefficients contained in the equations to be solved. The theory is extended to cover groups of "n" simultaneous partial differential equations. Experimental results obtained on a one-dimensional simulator are found to compare, within expected experimental error, with the exact solutions of the simulated equations for certain cases where the analytical solutions may be obtained.

Theoretical Physics, II

J1. Dependence of Fermi $|M|^2f$ on Z for Certain Isotopic Numbers. D. N. KUNDU AND M. L. POOL, *The Ohio State University.*—The logarithm of the half-life t of radioactive odd A nuclei is approximately a linear function of Z for a constant value of $A-2Z=I$. Both odd and even Z $(0<Z\leqslant 60)$ have been examined for $I=-1$ to 21 for nuclei on the positron-emitting side of the valley of stability. Abrupt departure from linear dependence sets in as t approaches infinity. Within the range of validity of this linear relationship $\log t=-\alpha Z+\delta$, it follows that $|M|^2f=Ae^{0.434\alpha Z}$, where $|M|=|\int\cdots|$ is the nuclear matrix and f the usual integral Fermi function.[1] The constant α has approximately the same value 0.35 for all values of I except for $I=-1$ when $\alpha=0.13$. A may be estimated from the straight lines plotted. Though in general both $|M|$ and f may individually be complicated functions of Z, the product $|M|^2f$ has a simple exponential dependence. The curves also help predict the half-lives of probable isotopes for given Z and I. The change in the value of α may be related to the fact that one group has neutron excess and the other, neutron deficiency. The case of decay by K-capture with its different form for f is evidenced by a change in the value of δ.

[1] E. J. Konopinski, Rev. Mod. Phys. 15, 209 (1943).

J2. On the Nuclear Quadrupole Moment of Li^7. R. D. PRESENT, *University of Tennessee* AND E. FEENBERG, *Washington University.*—Recent measurements unexpectedly determine the sign of the moment as positive.[1] The estimated magnitude is uncertain because of lack of resolution in the experimental line and the uncertain value of the electric field gradient. Assuming the ground state to be $1s^22p^3\,{}^2P_{3/2}$ the calculated moment is -6 in units of $\langle r^2\rangle_{2p}/25$. Configuration interaction modifies this result if the ground state eigenfunction contains an admixture of P state functions belonging to low odd-parity configurations.[2] In the "equal-forces" approximation, which we use throughout, all components of the ground state function are characterized by a definite symmetry[3] corresponding to the partition [3] or supermultiplet $(\frac{1}{2},\frac{1}{2},-\frac{1}{2})$. A variational calculation of the moment has been made taking into account the symmetrized P state functions arising from $1s^22p^23p$ (two) and $1s^22p^24f$ (one). Oscillator eigenfunctions were used to obtain ratios of $\langle r^2\rangle$. The maximum value of the moment is 2.32 in the above units. Calculations with P states from the remaining low configurations $1s^22s2p^3$ and $1s^22p^33d$ are incomplete; however these can only increase the maximum above 2.32. We conclude that a positive quadrupole moment is not inconsistent with a pure P ground state for Li^7.

[1] P. Kusch, Phys. Rev. 76, 138 (1949).
[2] The magnetic moment is unaffected by an admixture of P states.
[3] The configuration $1s^22p^3$ gives no D states of this symmetry.

J3. Space Exchange Magnetic Moments in Light Nuclei.* L. SPRUCH, *M. I. T.*—The calculations were based on Sachs'[1] phenomenological theory and on the independent particle model. Spin exchange moments were not included. Uncertainties in the form, strength, and range of the neutron-proton interaction, in the fractional part of the interaction which is of an exchange nature, and in the shell dimensions, cause the calculated values to be uncertain by a factor of about 5. For L-S coupling, the values found for Li^7, Be^9, B^{11}, C^{13}, N^{15}, and in the $3d$ shell for ^2D states, for Ne^{21}, Na^{23}, Cl^{37}, and K^{39} were -0.04, -0.01, 0.1, 0.05, 0.1, -0.4, -0.1, 0.4, and 0.4 nuclear Bohr magnetons, respectively. For $j-j$ coupling, the values for B^{11} $(^2p_{3/2})^{-1}$ and $C^{13}(^2p_{1/2})$ were 0.2 and -0.09; N^{15} and K^{39} had the same values as above. Since spin exchange moments were not included, no agreement with experiment was expected; the values are nevertheless large enough for some nuclei to be quite significant. Heavier nuclei will probably tend to have larger space exchange moments.

* AEC postdoctoral fellow.
[1] R. G. Sachs, Phys. Rev. 74, 433 (1948).

J4. The Monte-Carlo Method in Quantum Mechanics. GILBERT W. KING, *Arthur D. Little, Inc., and M. I. T.*—If one averages over a time of appropriate length the lowest stationary state $\psi_0(\xi)$ can be found by repeated applications of the Hamiltonian on an arbitrary state. This may be done by the transformation $t=iht$ on the time-dependent Schroedinger equation, to get Ulam's form $\partial u/\partial t=\Delta^2u-Vu$, where $u=\psi(\xi)e^{-\lambda t}$ in time reaches the configuration $\psi_0(\xi)$, the amplitudes decaying with a logarithmic decrement equal to the lowest energy. A solution of this "diffusion" equation can be found by a stochastic process, the points in ξ, t space moving $\Delta\xi$ in time Δt by a random process, and increasing in weight at each step by $e^{-V\Delta t}$. If all possible random walks were to be taken, the final distribution would be precisely that obtained by iterative methods of solving the corresponding difference equation. If the step function, $x_n=n\Delta x$ be replaced by orthogonal functions, the diffusion process occurs in a Hilbert space, and if all random walks were to be taken the process becomes that of iterating the Heisenberg matrix on an arbitrary vector. Excited states can be obtained by imposing nodes where "particles" become annihilated. The method will be illustrated by the harmonic oscillator and particle in a box.

J5. On the Probability Distribution of Recurrence Times. A. J. F. SIEGERT, *Northwestern University.*—Recurrence time probabilities are mentioned in various fields of physics and it seemed of interest to find a simple case for which an exact solution for the recurrence time probability could be found.

Markoffian random functions are known to be unsuitable, but we could solve the problem for the stationary Markoffian random-process with continuous time.† Let $p_{ik}(t-t_0)$ be the conditional probability that a system which was in state i at time t_0 is in state k at t, $\rho_i(t)dt$ the probability that a system returns to i for the first time at a time between t and $t+dt$ after leaving, and τ_i the mean persistence time, and $\rho_i^*(\lambda)$ and $p_{ik}^*(\lambda)$ the Laplace transforms of these functions, then $\rho_i^*(\lambda)=1-\lambda\tau_i\{[\lambda p_{ii}^*(\lambda)]^{-1}-1\}$. The obvious relation between mean persistence time, mean recurrence time, and probability of state i can be verified by expansion to first order in λ.

† For discrete Markoffian Processes cf. M. Kac, Am. Math. Monthly **54**, 369 (1947).

J6. Relativistic Kepler Problem. M. H. JOHNSON AND B. A. LIPPMANN, *Naval Research Laboratory.*—Besides the usual integrals of motion, **M** and j (in Dirac's notation) the relativistic equations for a charge in a Coulomb field admit

$$A=\boldsymbol{\sigma}\cdot\mathbf{r}r^{-1}-i(\hbar c/e^2)(mc^2)^{-1}j\rho_1(H-mc^2\rho_3)$$

as another integral of motion. Since A and j anticommute, the pairs of states with the same $|j|$ are degenerate. Thus the existence of A establishes the "accidental" degeneracy in the relativistic Kepler problem just as the existence of the axial vector establishes the degeneracy with respect to l in the corresponding non-relativistic problem.

J7. Accelerated and Rotating Coordinate Systems. H. C. CORBEN, *Carnegie Institute of Technology.**—The use of conformal transformations to relate mutually accelerated coordinate systems possesses the disadvantage that rotating systems, and hence the Thomas precession effect, cannot be easily included in the scheme. However, rotating and accelerated observers may be discussed simultaneously by considering the transformation $x^*=Sx$. Here x denotes the $(\mathbf{r}, ict)$ coordinates relative to an inertial observer O of an event on the space-time path of a particle P^*; $x^*(\equiv\mathbf{r}^*, ict^*)$ denotes the coordinates of the event relative to another observer O^*, and S is an orthogonal operator which is a function of the interval s along the path of P^* in system O. If $\Omega=S'\dot{S}$ ($'$ = transpose, $\cdot=d/ds$) then Ω is antisymmetrical, and writing $c\Omega_{jk}=\epsilon_{jkl}\omega_l$, $c^2\Omega_{j4}=if_j$ ($j, k, l=1, 2, 3$) then, when P^* is fixed relative to O^*, f_j and ω_j may be regarded as the relativistic acceleration and angular velocity of P^* relative to O. The velocity of light is invariant for these transformations. This offers a relatively simple method of describing kinematical composition laws for acceleration and angular velocity in relativity theory.

* Supported in part by ONR contract.

J8. The Hamiltonian of Einstein's Theory of Gravitation with Electromagnetic Field.* PETER G. BERGMANN, ROBERT PENFIELD, RALPH SCHILLER, AND HENRY ZATZKIS, *Syracuse University.*—After the development of the general canonical formalism of covariant field theories,[1] we have constructed the Hamiltonian density corresponding to the general theory of relativity with electromagnetic terms. It turns out that the simplest possible Hamiltonian is quadratic in the momentum densities canonically conjugate to the gravitational and electromagnetic potentials and linear in the momentum densities conjugate to the coordinates, which represent energy and linear momentum densities. In their canonical form, the field equations are first-order differential equations, solved with respect to the (time) derivatives. To test the power of the new formalism, we have examined the motions of field singularities. While our results agree with those of the Einstein-Infeld-Hoffmann theory, we can develop rigorous expressions for the particle accelerations in any given situation; integration of the equations of motion would, of course, also require expansions.

* Supported by ONR.

[1] Bergmann and Brunings, Rev. Mod. Phys. **21**, 480 (1940).

J9. Covariant Spinor Theory.* JACK HELLER, *Polytechnic Institute of Brooklyn,* AND PETER G. BERGMANN, *Syracuse University.*—The laws of nature appear to possess both general covariance and spin properties. We have therefore developed further the formalism proposed by Schrödinger, Schouten, and others, in which the spin transformations are independent of the coordinate transformations. The basic (Dirac) spin matrices are determined by equations involving only Kronecker symbols on the right, and by the requirement that they are self-adjoint with respect to an invariant indefinite Hermitian form. The ordinary metric tensor is then formed from the Dirac matrices algebraically. The spinor connections are determined only partly by the condition that the covariant derivatives of the Dirac matrices vanish. There results a "spin curvature tensor" and a corresponding scalar, but the latter turns out to equal Riemann's curvature scalar. Thus, the most obvious variational principle not involving electromagnetic cross terms merely yields Einstein's equations of gravitation. We are now examining the effects of quantization.

* Supported in part by ONR.

J10. On the Quantization of Einstein's Gravitational Field Equations. A. SCHILD AND F. A. E. PIRANI, *Carnegie Institute of Technology.*—The following points illustrate the method: (1) By splitting off a divergence term, the usual Lagrangian $(-g)^{\frac{1}{2}}R$ of gravitational theory is replaced by a first order differential expression. (2) Weiss'[1] method of quantization of field theories characterized by first order Lagrangians, can be carried out in a non-metrical "amorphous" space. The gravitational equations may be regarded as differential equations for the field variables $g_{\mu\nu}$ in an amorphous space and the quantization procedure can be applied to them. (3) The gravitational field equations are written in Hamiltonian form, the Hamiltonian being a function of coordinates, momenta and velocities. Point (2) above was first stated by Bergmann and Brunings.[2] The Hamiltonian (3) is obtained, using a method developed by Dirac[3] for Lorentz invariant theories.

[1] Proc. Roy. Soc. **A169**, 102 (1938).
[2] Rev. Mod. Phys. **21**, 480 (1949).
[3] Mimeographed lecture notes, Second Seminar, Canadian Mathematical Congress, August 1949.

J11. Approximate Solutions of the Field Equations in Einstein's Generalized Theory of Gravitation. HANS FREISTADT, *University of North Carolina.*—Quasi-static solutions of the field equations of Einstein's "Generalized Theory of Gravitation,"[1] in which matter is represented by singularities are investigated by means of an expansion in powers of small parameters. The difficulty of expressing the Γ in terms of the g is overcome by an expansion in which the Γ at each order of the approximation are expressed in terms of the Γ of lower order and the g. In lieu of the anti-symmetric field Eqs. (15) of reference 1, the more stringent equations $R_{ik}=0$ are used, which were privately communicated to the author by Professor Einstein. The Lienard-Wiechert fields satisfy these equations (uniquely if one excludes magnetic poles) up to the order investigated so far, which is the second.

[1] Rev. Mod. Phys. **20**, 35 (1948).

Miscellany in Nuclear Physics

L1. High Intensity Ion Source for Cyclotrons. R. S. LIVINGSTON, R. J. JONES, AND R. E. WRIGHT, *Carbide and Carbon Chemicals Corporation.*—The characteristics of a hot-cathode arc-type ion source have been determined with d.c. applied potentials. More than one half of the atoms in the hydrogen gas fed into the source are converted to ions. The ratios of H^+, H_2^+, and H_3^+ have been measured mass spectrographically. Protons account for 85 percent of all ions formed when the source is adjusted to optimize this quantity. Ion current is

an increasing function of applied potential, as expected, with currents above 10^5 μa observed at 10 kv. The performance of this source has also been studied in a small cyclotron, in which protons were accelerated up to 2 Mev with applied *rf* potentials of 10–20 kv peak. The attenuation of circulating ion current with radius, was measured by means of a movable probe. The dimensions of the arc chamber have been chosen to avoid interception of ions on their first revolution. The source may be of particular interest for machines where only small dee voltages are available. This is based on work performed under contract with the AEC.

L2. Asymmetry of Nuclear Fission. DAVID L. HILL, *Vanderbilt University.*—The asymmetry of nuclear fission is related to the dynamics of the liquid drop model in terms of a treatment developed in collaboration with Professor John A. Wheeler. Certain conjectures are discussed along with their testing by means of extensive numerical calculations executed, as an endowed problem, on the IBM SSEC. Successive computed nuclear shapes are shown to illustrate how the irreducible zero-point asymmetric surface oscillations persist in the elongating form to cause an unequal mass division. Results are given both for uranium and for that element of high atomic number for which the conventional dumbbell shape of unstable equilibrium degenerates into a sphere.

L3. Range of α-Particles in Water and Ice. H. G. DE CARVALHO,* *National Institutes of Health.*—The range of α-particles in water is an important constant for evaluating the biological effects of densely ionizing radiations on tissue. The early measurements on the range of 5 to 8 Mev α-particles in water made with the aid of scintillation screens are about 30 percent low when compared with ranges computed from stopping power laws. To determine the nature of the discrepancy the range of α-particles in water and ice have been measured by means of nuclear emulsions sensitive to residual alpha-energies of about 0.2 Mev. Specially prepared radiocolloid aggregates of polonium and radium sulfate served as micropoint sources, suspended in either water or ice in direct contact with the emulsion. Preliminary measurements show a range in water of 39 microns for RaF, 67 for RaC′, and ranges of 42 and 73 microns respectively in ice. These values are in closer agreement with the Bragg law than the scintillation measurements, and exhibit only a 1 to 4 percent departure from ranges computed by modern stopping power theory. This method of range measurement is of general applicability to liquids that do not destroy emulsion sensitivity and to highly active alpha-emitters capable of radiocolloid aggregation.

* Public Health Service Research Fellow of the Experimental Biology and Medicine Institute on leave of absence from Laboratorio da Producao Mineral, Brasil.

L4. Ratio of N^{15}/N^{14} in Gases Occluded in Radioactive Minerals. HERMAN YAGODA AND WILLIAM C. WHITE, *National Institutes of Health.*—In a study of the occluded gases in radioactive minerals by means of the mass-spectrometer, the isotopic ratio of N^{15} to N^{14} was found to be invariably higher than in samples of atmospheric air or in nitrogen isolated from nitrogenous compounds. For primary uranium and thorium minerals studied the N^{15} content varied between 0.532 to 0.614 atom percent, as compared with the normal abundance of 0.376. The abundance of N^{15} increases progressively with the geological age of the specimen over a range of (50 to 1000)10^6 years. Different specimens of pitchblende of the same Pb/U age exhibit closely agreeing N^{15}/N^{14} ratios, suggesting a new age indicator. The nitrogen ratio is independent of the chemical composition and the uranium content of the host mineral. Thus samarskite (11.3 percent U_3O_8) and uraninite (91 percent U_3O_8) both from the same region, 250×10^6 years old, show a N^{15} abundance of 0.549 ± 0.015 and 0.546 ± 0.009, respectively. Attempts at measuring the N^{15}/N^{14} ratio in old non-radioactive minerals have failed owing to insufficient occluded gas for analysis. The available data suggests that the nitrogen may have been a component of the minerals at the time of their formation, and that the N^{15}/N^{14} ratio increased as a result of the more rapid diffusion of the lighter isotope. Alternative hypothesis based on nuclear reactions will be discussed.

L5. Packing Fractions of Fe^{56}, Ni^{58}, and Ni^{60}.* HENRY E. DUCKWORTH AND HOWARD A. JOHNSON, *Wesleyan University.*—A large Dempster-type double-focusing mass spectrograph has been used to photograph the doublets Si^{28}-$Fe^{56}/2$, Si^{29}-$Ni^{58}/2$, and Si^{30}-$Ni^{60}/2$. The ions were obtained from a high frequency discharge between a silicon electrode and one of stainless steel, containing about 10 percent nickel. Exposure times of 30–40 seconds were adequate for the first doublet while exposure of 3–5 minutes were needed for the other two. The separations Si^{28}-Si^{29} and Si^{29}-Si^{30}, assumed to be integral, provided suitable mass scales. The following packing fraction differences were found: Si^{28}-Fe^{56}, $\Delta f=(3.32\pm0.02)\times10^{-4}$ from five photographs; Si^{29}-Ni^{58}, $\Delta f=(3.07\pm0.03)\times10^{-4}$ from five photographs; Si^{30}-Ni^{60}, $\Delta f=(2.90\pm0.01)\times10^{-4}$ from eight photographs. The probable errors are based on the internal consistency of the data. No experiments were done to determine the effect of pressure on the doublet spacing, but all exposures were taken with the pressure less than 5×10^{-6} mm in the analyzing region. Assuming the packing fractions $Si^{28}=-(4.8\pm0.07)\times10^{-4}$, $Si^{29}=-(4.6\pm0.07)\times10^{-4}$ and $Si^{30}=-(5.6\pm0.10)\times10^{-4}$, as given by H. A. Bethe and R. F. Christy, one can calculate $Fe^{56}=-(8.1\pm0.08)\times10^{-4}$, $Ni^{58}=-(7.9\pm0.08)\times10^{-4}$ and $Ni^{60}=-(8.7\pm0.10)\times10^{-4}$. Typical doublets will be shown and the agreement between these values and other recently reported ones will be discussed.

* This work was supported by the AEC.

L6. Co-60 γ-Ray Penetration through Large Masses of Water. GLADYS R. WHITE,* *National Bureau of Standards* (Introduced by U. Fano).—An experiment was conducted in a 60-foot water tank at the Naval Gun Factory in effectively spherical geometry. Two Co-60 sources of 0.34 and 4.9 curies were used. Dosage was measured at distances from 30 to 180 cm (corresponding to a maximum attenuation of the primary radiation by a factor of $e^{-11.4}=1.1\times10^{-5}$) using sealed Kelley-Koett ionization chambers of the pen type. At short distances the results matched those obtained at M.I.T.[1] The dosage decreases with distance less rapidly than according to an $\exp(-\mu r)/r^2$ law owing to the building up of secondary radiation. The "build-up factor" increases a little faster than linearly. Its largest observed value was approximately 23. The experimental data will be compared with current theoretical predictions.[2]

* Supported by the ONR.
[1] Levin, Weil, and Goodman, M. I. T. Tech Rep. 22, June 15, 1949.
[2] Fano, Hurwitz, and Spencer, Phys. Rev. Feb. 1, 1950.

L7. Integral Relationships between Atomic and Nuclear Quantities. ENOS E. WITMER, *University of Pennsylvania.*—In 1946 the writer[1] stated that hc/e^2 is very probably *exactly* 861. The most recent values of α are consistent with this idea. Integer 861 is $\frac{1}{2}\times42\times41$. This suggests that 42 is an important number, possibly related to the fact that space is three-dimensional. We now note that the binding energy of the deuteron is $4M_p/41^2$ or 2232 kev in excellent agreement with the recent measurements. M_p is the proton mass. The recent accurate determinations of e/m indicate that M_p/m is close to 1836, and we believe it is *exactly* 1836. Using the values of R_∞, N, and c given by Birge in 1945 and these two integral relationships involving 861 and 1836, we can calculate the fundamental atomic constants very accurately. Also it seems probable that the nuclear magnetic moments are in accord

with these ideas about the importance of integers; see Abstract No. SP1 and note the remarkable agreement of the calculated value of the magnetic moment of the proton in Bohr units with the experimental values. Our value of e is $(4.80290\pm0.00020)\times10^{-10}$ e.s.u., and of e/m is $(1.758972\pm0.000073)\times10^{7}$ e.m.u. g^{-1}.

[1] Proc. Nat. Acad. Sci. 32, 283, 1946.

Discharge in Gases; Mass Spectrometry

M1. A "High Vacuum" Cold Cathode Gaseous Discharge. I. R. SENITZKY, *Signal Corps Engineering Laboratories and Columbia University.*—By suitably combining low d.c. and low r-f voltage, and a magnetic field perpendicular to both electric fields, a cold cathode gaseous discharge is produced at extremely low pressures. In a specially built magnetron, with pressure less than 10^{-7} mm and with a cold uncoated Nickel cathode, a typical situation is the following: 40 volts on anode, 10 microwatts of 3.4 cm r-f power flowing into magnetron, and a magnetic field near 3100 gauss, produce 1.5×10^{-8} ampere direct anode current. Dependence of anode current on magnetic field, r-f power, d.c. voltage, and pressure, is shown. Anode current flows only if magnetic field is within a critical range near cyclotron value, and exhibits one or more maxima within this range. Lower limits exist for d.c. voltage (around 18 volts) and r-f power, below which there is no self-sustained discharge. Anode current increases with r-f power if d.c. voltage is below about 400 volts. Above this voltage, r-f power loses control, and discharge characteristics change. A simple theory is presented, showing that, if electrons leave cathode with zero velocity, a combination of d.c. and non-uniform tangential r-f fields at the cathode is necessary for self-sustained discharge.

M2. Holes and Retrograde Arc Spot Motion in a Magnetic Field. JEROME ROTHSTEIN, *Signal Corps Engineering Laboratories.*—If cathode spot current density is 10^5 amp./cm^2 with a sixth ionic, 10^{23} ions arrive per cm^2 per sec. With spot surface atomic density 10^{16}/cm^2, the area occupied by a surface atom emits five electrons and collects one ion every 10^{-7} second on the average. Ions transport both vacant energy levels to the electronic configuration and energy to maintain spot excitation (high electron "temperature"). A fraction of the current in the spot must thus consist of holes which increases with hole lifetime. It is proposed that as in the anomalous Hall effect the holes are deflected in the "wrong" (retrograde) direction, nascent electron emission following the effectively positive holes, whence ions later formed by collision outside the spot return bringing holes and excitation to a region shifted in the retrograde direction. At high pressure photons could contribute substantially to spot excitation without hole generation whence reversal of motion as observed. Increased magnetic field gives larger hole deflection and so greater retrograde velocity and higher reversing pressure as observed. Very large increases slow down and then reverse the motion possibly because the pre-annihilation trajectory doubles back on itself, hole effects thereby progressively cancelling out.

M3. Role of Cathode Temperature in a Glow Discharge. HAROLD JACOBS AND JACK MARTIN, *Evans Signal Laboratory.*—Experiments were conducted to study the properties of a glow discharge tube* utilizing an oxide coated cathode and argon gas. The sparking potential was found to decrease with increasing cathode temperature (300°K–750°K). However, the regulation voltage showed a slight rise, as the temperature of the cathode was increased in this range. The current density decreased in the same interval. The effect is attributed to metastable states of the gas.

* Acknowledgment should be made to Mr. K. M. McLaughlin, of RCA, Harrison, New Jersey, for suggestions in the design of the experimental tubes.

M4. Further Measurements of Formative Time Lags of Spark Breakdown in Air.* L. H. FISHER AND B. BEDERSON, *New York University.*—Previously[1] reported measurements of the formative time lags of spark breakdown in a plane parallel gap in air have been extended with an improved power supply. With the new circuit, the delays can be measured extremely close to the threshold voltage for breakdown. The new measurements have been carried out as a function of pressure, plate distance, and over-voltage. The formative time lags very close to threshold have been found to be of the order of 100 microseconds and longer. These lags are at least ten times as long as those we have previously reported. Varying the approach voltage by as much as 4 kv does not affect the results appreciably. The number of initiating electrons at the cathode has been varied by a factor of ten and this again does not materially alter the results.

* Supported by the ONR and the Research Corporation.
[1] L. H. Fisher and B. Bederson, Phys. Rev. 75, 1615 (1949).

M5. Interpretation of Formative Time Lags of Spark Breakdown in Air at Low Overvoltages.* B. BEDERSON AND L. H. FISHER, *New York University.*—An attempt has been made to account for the long formative time lags observed in the passage of an electric spark in air in a plane parallel gap by (1) secondary emission by positive ions at the cathode, and (2) by the enhancement of field intensified ionization due to field distortion.[1] For mechanism (1) an equation for electron and positive ion charge densities as a function of position, time, and overvoltage is developed (no field distortion), and it is assumed that the time for a spark to form is the time for the positive ion density to reach a critical value at the anode. It is then assumed breakdown could proceed by the streamer mechanism. It is shown that mechanism (1) is not in accordance with the experimental data as regards the variation of the time lags with pressure, plate distance, and overvoltage. For mechanism (2), the positive ions created by the primary electron avalanches produce a locally strengthened field upon approaching the cathode, thus magnifying Townsend's first coefficient in that region. Thus an effective secondary mechanism is produced. The transient equation for the growth of the current by mechanism (2) is more in accordance with the experimental facts. The role of photo-ionization in mechanism (2) will be discussed qualitatively.

* Supported by the ONR and the Research Corporation.
[1] See, for example, Varney, White, Loeb, and Posin, Phys. Rev. 48, 818 (1935).

M6. Electron Density and Spectroscopic Measurements in Metal Vapor Afterglows. P. DANDURAND AND R. B. HOLT, *Harvard University.*—Measurements have been made of the rate of electron density decay following the removal of the excitation for pulsed microwave (3000 mc/sec.) discharges through cesium and mercury vapor. Following S. C. Brown's technique, the shift of the resonant frequency of a microwave cavity due to the presence of the electrons was observed as a function of time. Simultaneous observations of the emission spectrum of the discharge plasma were made by means (1) of a high speed mechanical shutter (resolving time 2 microseconds) plus a high intensity spectrograph and (2) of a pulsed photo-multiplier equipped with various optical filters. As might be expected, electron density and light intensity measurements indicated an exponential decay at low pressures (below 0.2 mm) in both cases. The data allow the calculation of ambipolar diffusion coefficients according to the usual theory. Interpretation of electron density data in metal vapors at high pressures is complicated by the fact that the expected collision frequency is of the same order of magnitude as the frequency of the search signal. This effect has been investigated theoretically and experimentally. The light intensity measurements, since they are independent of electrical

properties, give a check on the electron density measurements in this range.

M7. Temperature Variation of Mass Spectra of Hydrocarbons. ROBERT M. REESE, VERNON H. DIBELER, AND FRED L. MOHLER, *National Bureau of Standards.*—Intensity distribution in mass spectra of hydrocarbons is known to depend markedly on the temperature of the ionization chamber.[1] We have observed ion current per unit pressure and relative intensity in the temperature range 50° to 300°C for selected mass peaks in the spectra of paraffins, olefins, acetylenes, and cyclics. Data were obtained with a Consolidated mass spectrometer equipped for temperature control of the ionization chamber by taking measurements as the temperature increased from room temperature to 300°C. The pattern coefficient (ratio of a mass peak to the maximum peak in the spectrum) for the molecule ion in general decreases rapidly with increasing temperature and the change for most other peaks is small or zero. The pattern coefficient for the molecule ion of *n*-butane decreases from 20 percent at 100°C to 10 percent at 300°C, for *n*-hexane it changes from 32 percent to 13 percent, for 2,3-dimethylbutane it changes from 10 percent to 2.9 percent and for 2,5-dimethylhexane it changes from 15 percent to 2.4 percent. The change is less for unsaturated hydrocarbons and cyclics. Results will be presented in tables of percent change per degree at 250°C.

[1] C. E. Berry, J. Chem. Phys. 17, 1164 (1949).

M8. The Non-Magnetic Radio Frequency Mass Spectrometer. WILLARD H. BENNETT, *National Bureau of Standards.*—The non-magnetic radio frequency mass spectrometer has been developed and refined considerably beyond the form described previously.[1] A three-stage form of this instrument has been developed which eliminates all harmonics, and by so doing attains much greater sensitivity. The instrument has advantages in ordinary gas analysis because of its simplicity. It has advantages in studies of solids because it uses no slits and all the ions coming from a solid surface are used in the analysis. The instrument can be used in the analysis of the ions present in gaseous discharges because no strong magnetic field is needed for the operation of the instrument. The results of some measurements will be presented which demonstrate the great flexibility and sensitivity using both positive and negative ions, for determining the ions arising either at a solid surface or in the vapor phase, and in distinguishing between the points of origin of each mass component.

[1] Willard H. Bennett, Phys. Rev. 74, 1222A (1948).

M9. The Omegatron. J. A. HIPPLE, H. SOMMER, AND H. A. THOMAS, *National Bureau of Standards.*—The recently reported[1] method of measuring the mass-to-charge ratio of ions by measuring their cyclotron resonance frequency in a magnetic field will be discussed. With the first model a resolution of 1 part in 5000 has been attained for N_2^+ and 1 part in 10,000 for H^+—these figures being based on the width of the peak at the base. A field of approximately 5000 gauss was used and the ions at resonance are accelerated until they attain an orbit radius of 0.9 cm before striking the ion collector. The effect on resolution and intensity of adjustment of the various parameters will be described. A revised model which will be located in a more uniform magnetic field is nearing completion and the initial performance characteristics of this model will be presented.

[1] Hipple, Sommer, and Thomas, Phys. Rev. 76, 1877 (1949).

M10. Total Ionization of Hydrocarbons from Mass Spectral Data. FRED L. MOHLER AND STAFF OF MASS SPECTROMETRY SECTION, *National Bureau of Standards.*—Mass spectral data[1] are commonly presented in terms of the intensity of each peak relative to the maximum peak and the sensitivity (current per unit pressure in the gas reservoir) for the maximum peak. The sensitivity for mass 43 of *n*-butane is also given and the ratio of the sum of the mass peaks times sensitivity for the compound to the corresponding product for *n*-butane gives the total ionization relative to *n*-butane. A diaphragm type of micromanometer in which small displacements are measured electrically has for the first time made it possible to measure sensitivity of the heavier hydrocarbons with reliability. It is found that the total ionization of isomers is nearly equal or at least falls in a narrow range. Thus, for the 35 nonames the mean value of total ionization is 1.94 ± 0.13 relative to *n*-butane; for 18 octanes, 1.79 ± 0.06; for 17 C_8H_{16} cyclics, 1.57 ± 0.06; for 9 heptanes, 1.69 ± 0.05, for 5 hexanes, 1.54 ± 0.06; for 14 hexenes, 1.46 ± 0.05; 6 pentenes and 11 C_8H_8 isomers both give 1.03 ± 0.04.

[1] Catalog of Mass Spectral Data API Research Project 44.

M11. Ionization Potentials of some Molecules Commonly Used in Counters. RAYMOND KAUFMAN, *New York University.*—Ionization potentials of some molecules were determined experimentally by the electron bombardment method. Electrons were accelerated between a cathode and grid and retarded between the grid and a plate. The electron current stream was measured with a high sensitivity galvanometer in conjunction with a d.c. amplifier. By plotting curves of grid potential *versus* plate current when the gas was present in the tube, it was possible to determine by the drop in current when ionization took place. In order to calibrate the equipment, some gases whose ionization potentials are known were measured along with the unknowns. The following ionization potentials were observed: Neon 20.8 volts; methane 15.2; ethyl acetate 9.5; ammonia 10.1; argon 15.4; boron trifluoride 10.25. Butane showed a curve with a break at 10.4 and propane at 11.0 but the interpretation of this is probably complicated by dissociation phenomena.

Acoustics; Atmospheric Physics; Astrophysics

N1. Analysis of Multiple Echo Effect Arising from the Release of a Stored Wave Train. LOUIS GOLD, *University of Colorado.*—A generalized theoretical treatment is presented of a problem which has direct application to the phenomenon of multiple echo patterns as employed for propagational studies of high frequency sound waves in various media. An analysis is made of the functional dependence of the number of observable echoes in terms of a prescribed threshold sensitivity db^* of a detecting device, and the storage medium parameters, which are the effective absorption coefficient α and the boundary reflection coefficient R. The equation derived is

$$N=\left(\frac{db^*}{10}+\log\frac{R}{1-R}\right)\Big/\left(\log R-\frac{2\alpha d}{2.303}\right),$$

where d is the length of the storage system. This relation has values $Ropt$ for which N is a maximum, and it is shown that $N_{max}=1/1-Ropt$. The solutions for N_{max} are actually difficult to express explicitly since $Ropt$ must be evaluated from the condition for a maximum

$$\frac{Ropt}{1-Ropt}\log Ropt+\log(1-Ropt)-\frac{\alpha d\log e}{1-Ropt}=db^*/10.$$

N2. On the Non-Specular Reflection of Sound. VICTOR TWERSKY, *New York University.*—The non-specular reflection of plane waves of sound by various rigid, non-absorbant, nonporous surfaces composed of either semicylindrical or hemispherical bosses (protuberances) on an infinite plane has been analyzed. Exact solutions for the problem of the single

boss and a plane wave at arbitrary angle of incidence have been derived through consideration of a cylinder or sphere and two simultaneously incident "image waves." Finite patterned distributions of such bosses were then treated and the far-field solutions obtained subject to the restriction that the secondary excitations be neglected. (The equivalent problems for cylinders and spheres were also considered as well as the second-order solution which takes into account interactions of nearest neighbors.) These solutions were found to contain the characteristic Fraunhofer terms for a grating or lattice. The asymptotic solutions for the single bosses ($Kr \gg 1$, $Ka < 1$) were then extended to consider finite and infinite uniform random distributions. The solutions for the finite distributions were found to contain the characteristic Fraunhofer terms for similarly shaped apertures. The solutions for the infinite distributions were found to be remarkably similar when expressed in terms of the volumetric departure from the plane per cm² of distribution.

N3. Analysis of Acoustic Scattering by Variational Methods. ALFRED LEVITAS, *Syracuse University.*—The variational methods discussed in a previous abstract by Melvin Lax have been applied to the scattering and absorption of sound by a strip of absorbing material placed on a hard wall. These results have been compared with an exact calculation by Pellam[1] and the results are accurate to within 1.5 percent. This problem differs from most scattering problems in that the perturbation exists solely on the surface. An integral equation is obtained for the surface pressure. This integral equation is used to construct a variational principle for the scattering amplitude. The scattering cross section is obtained by integrating the absolute square of the scattering amplitude over all directions. The total cross section is proportional to the scattering amplitude in the forward direction and therefore available variationally. Because the scattering surface is infinite, the forward direction is the direction of specular reflection. Maximum absorption per unit panel width is shown to occur when the panel-width is zero. Maximum scattering per unit panel width is shown to occur when the ratio of panel width to wave-length is approximately two to three.

[1] J. R. Pellam, J. Acous. Soc. Am. 11, 396 (1940).

N4. The Pressure at Which a Rarefaction Wave Initiates Cavitation in Sea Water.* A. B. ARONS, *Woods Hole Oceanographic Institution and Stevens Institute of Technology.*—Measurements at various ranges of the amplitude of the surface reflection of the shock wave produced by an underwater explosion provide evidence to support the view that the rarefaction wave causes bulk cavitation in sea water at positive absolute pressures of about 8 lb./in.². This would imply that, under these circumstances, the cavitation bubbles are formed by the evolution of dissolved gases rather than by the tensile "fracture" of the liquid, and that the pressure within the cavitation bubbles is therefore considerably higher than the vapor pressure of water at the temperature of the experiment.

* Work supported by the Navy Department, Bureau of Ordnance.

N5. Refraction Effect in Interferometry of Boundary Layer of Supersonic Flow along Flat Plate.* G. P. WACHTELL, *Princeton University.*—Large density gradients, as in the boundary layer of the supersonic flow along a flat plate, cause curving of the light rays used in interferometry. This curving produces an error in interferometric evaluation of the gas density. Taking into account the optical system between boundary layer and photographic plate,** it is found that the error depends on h, the distance of the focal plane from the channel exit window, and vanishes, in first approximation, when h is one-third of the distance, D, between channel windows. The thickness, t, of the exit window and higher order terms depending on higher powers of D and higher derivatives of density may produce an appreciable error even when $h = D/3$. In the Palmer Laboratory wind-tunnel, however, where $D = 3$ in., $t = 1$ in., the error for density gradient $< 3 \times 10^{-3}$ g cm^{-4}, and second derivative $< 2 \times 10^{-1}$ g cm^{-5}, is negligible when $h = D/3$.

* Performed under a contract with the ONR.
** D. Bershader and G. P. Wachtell, Phys. Rev. 76, 880 (1949).

N6. Abnormally Low Molecular Rotation and Upper Atmosphere Temperatures. LEWIS M. BRANSCOMB, *Harvard University.*—Rotational profiles of night sky band spectra have been interpreted as indicating consistently lower upper atmosphere temperatures than are obtained from almost every other source of information. This apparent inconsistency may be removed if we assume the night sky bands are excited by electron impact, for all the conditions will then be fulfilled for the occurrence of abnormally low rotation in the excited molecules, as predicted by Oldenberg.[1] An experiment is described which verifies this prediction. For gas temperatures from 400 to 670°K rotational temperatures from the second negative bands of O_2^+ were found by two methods of analysis to be in qualitative agreement with the predicted relation $T_{rot} = T_{trans}\, B'/B''$, where B'/B'' is the ratio of the inertias in the initial and final states of the excitation process. The upper atmosphere temperature problem is discussed in the light of these results, with special reference to temperature measurements from night sky and auroral spectra. The effect of this change in inertia on the excitation of the Schumann-Runge bands of O_2 and the identification of these bands in the night sky is also discussed.

[1] O. Oldenberg, Phys. Rev. 46, 210 (1934).

N7. The Distribution of Atomic and Molecular Oxygen in the Upper Atmosphere. H. E. MOSES* AND TA-YOU WU,** *Columbia University.*—Theoretical calculations are carried out to determine the distribution of atomic and molecular oxygen and the temperature in the region of 100–125 km. It is assumed that solar radiation is responsible for photodissociation of molecular oxygen and (as justified from theoretical considerations) that the recombination of the atoms by twobody radiative processes is much more probable than by threebody collisions. From the conditions for a steady state, which are that for any given volume (a) the number of dissociations equals the number of recombinations and (b) in these processes the energy of radiation which is absorbed equals that of the radiation which is emitted, together with an appropriate form of the barometric equation, one can calculate the number density of molecular oxygen, the number density of atomic oxygen, and the temperature, all as functions of height, provided that the temperature and temperature gradient are known at one height. The results of the calculations indicate that dissociation is not complete until around 200 km and that the maximum number density of atomic oxygen (which occurs at about 100 km) is about 10^{11}/cm³ and is thus considerably less than that estimated by previous workers.

* Present address: Institute for Applied Math. and Mech., New York University.
** Present address: National Research Council of Canada, Ottawa.

N8. High Dispersion Studies of the Solar Spectrum.* ROBERT M. CHAPMAN, JOHN H. SHAW, AND DUDLEY WILLIAMS, *The Ohio State University.*—A high dispersion, Pfund-type prism-grating spectrograph has been used to re-examine the solar spectrum in the region between the visible and 6μ. Several thousand absorption lines, some of solar and some of terrestrial origin have been observed. Curves showing telluric absorption bands due to O_2, CO_2, CO, N_2O, and HDO will be exhibited. The CO absorption has been observed on

numerous occasions and hence CO must be regarded as a "permanent" constituent of the atmosphere in this locality. The bands due to N_2O and HDO are well resolved into rotational lines. The possibility of the existence of other atmospheric constituents will be discussed.

* This work was done under Contract between The Ohio State University Research Foundation and Watson Laboratories of the Air Materiel Command, Red Bank, New Jersey.

N9. Radiation Equilibrium in the Stratosphere.* GILBERT N. PLASS AND JOHN STRONG, *The Johns Hopkins University.*—The outward radiation emitted from the stratosphere by the 15μ CO_2 and O_3 bands is less than 260 microcalories/cm^2 sec. The radiation absorbed in the stratosphere by the O_3 band at 9.6μ from the blackbody radiation from the earth's surface, minus the O_3 emission, is about 120 microcalories/cm^2 sec. The ozone in the stratosphere also absorbs ultraviolet radiation from the sun. These three effects together with the losses from 50μ H_2O band give the main contribution to the heat balance in the stratosphere. The heat loss from the 15μ CO_2 band has been calculated assuming that the line width is given by the Lorentz pressure broadening formula and is directly proportional to the pressure. The calculation and results will be described. It is found that the radiation from a given optical thickness of emitting gas is *independent* of its height, giving a strong differential cooling of the lower layers. An equilibrium characterized by constant temperature at all heights is possible by balancing the radition lost by the 15μ bands against that absorbed by the ozone. The above ideas help to understand the discontinuity in temperature lapse rate at the tropopause and the discrepancy between experimental and theoretical lapse rate in the tropopause.

* This work was supported in part by the ONR.

N10. On the History of the Noble Gases. P. MORRISON, *Cornell University.*—Recent work on cosmic isotope abundance gives fairly reliable fractionation factors f for the noble gases, where f is the ratio of the observed terrestrial abundance to the interpolated cosmic abundance for a given gas. The course of the f curve as a function of atomic weight shows a very steep dependence of f on A for the light gases, but not for the heavy ones. If diffusion of positive-energy molecules out of an attracting gravitational field is the main mechanism for noble-gas loss, this implies two main stages of assembly for the planetary material. All gases were lost in the first stage at a rather low temperature from a very diffuse mass; in the second stage temperature and gravitational acceleration both increase markedly. Limits can be given for the temperature and density variations in time. The implications of such data for the present theories of planetary formation are examined. Some extension is made to compound-forming elements and to other planetary bodies. The large terrestrial excess of A^{40} is supplied by the K-capture of potassium. The conditions imposed by this process upon the early history of the earth's crust are considered for a range of values of the not-very-well-known branching ratio.

N11. The Temperature in an Accreting Planet. A. E. BENFIELD, *Harvard University.*—The temperature of a planet growing by accretion rises as a result of the gravitational field in and near it. At first, when the gravitational field is small, the temperature is low. Later, the temperature at the *surface* of the planet becomes high, due to the kinetic energy of the incoming accreting material, as has already been shown.[1–3] During its growth a temperature increase in the *interior*, however, also takes place, due to its compression by the accumulating overyling material. A calculation based on thermodynamics, using the computations of astrophysicists and information about the properties of matter at high pressures, indicates a temperature not exceeding 2000°C at the center of a planet, having the size of the earth, due to the effect of compression alone.[3] This does not seem high enough to ensure melting, but other factors will contribute toward raising the temperature. A considerable uncertainty exists in these calculations due to our ignorance of the behavior of materials at pressures as high as 3×10^6 atmospheres.

[1] D. ter Haar and H. Wergeland, Kgl. Norske Vid. Sels. Forhandlinger Bd. 20, No. 14, 52 (1948).
[2] F. Hoyle, M.N.R.A.S. 106, No. 5, 406 (1946).
[3] A. E. Benfield (in press).

Semi-Conductors

OA1. Nucleon-Bombarded Silicon. K. LARK-HOROVITZ, M. BECKER, R. E. DAVIS, AND H. Y. FAN, *Purdue University.*—The resistivity of P and N type silicon increases under nucleon bombardment.[1] Low resistivity silicon (~.03 ohm-cm) was investigated before and after intensive neutron irradiation in the Oak Ridge reactor.** The resistivity increased to over 10,000 ohm-cm. Heat treatment cycles of irradiated silicon show a resistivity *vs.* temperature curve with a slope indicating deep-lying impurity levels in the forbidden band (>0.7 to 0.8 ev). The transmissivity increases at $\lambda>2\mu$ after irradiation. There is a strong absorption band around 1.6μ (0.7 ev), barely detectable in unbombarded material. This confirms the interpretation of the electrical measurements and is confirmed also by a greater absorption of the bombarded material near the band edge, due to the production of a greatly increased number of absorbing centers effective at $\lambda<2\mu$.

* Supported in part by a Signal Corps contract.
** We are indebted to J. C. Pigg (O.R.N.L.) for these exposures in the reactor.
[1] K. Lark-Horovitz *et al.*, Phys. Rev. **73**, 1256 (1948); **76**, 442 (1949).

OA2. Impedance Characteristics of Grain Boundaries in High Resistivity *N* Type Germanium.* N. H. ODELL AND H. Y. FAN, *Purdue University.*—The d.c. electrical properties of these barriers are discussed in the accompanying paper by Taylor and Fan. Impedance characteristics have been measured** as functions of frequency and temperature. The voltage applied to the barrier was kept small compared with kT. Measurements were made between 400 kilocycles and 4 megacycles. It was observed that barrier capacity computed from impedance measurements is independent of frequency at temperatures below 0° centigrade. At higher temperatures, the capacity is observed to decrease as signal frequency increases. For small applied voltages, the barrier impedance should be independent of frequency if the current across the barrier is carried by electrons, the sample being N type. This agrees with measurements below 0° centigrade. With increasing temperature, the share of the current at the barrier carried by holes increases. It can be shown that barrier impedance of hole current should show frequency dependence. For the sample used, this seems to be the case above 0° centigrade. It was also observed that barrier capacity decreases with decreasing temperature.

* This work was assisted by Signal Corps contract.
** We wish to thank Professor R. P. Siskind, E. E. Department, for discussions and experimental facilities.

OA3. Efficiency of γ-Counters. R. J. HART, K. RUSSELL, AND R. M. STEFFEN, *Purdue University.**—The local efficiency of cylindrical γ-counters with Bi-cathode was measured with a well-collimated γ-beam of different energy. The intensity of the γ-beam was calibrated with an anthracene scintillation counter. The amount of radiation absorbed in the anthracene was detected with an efficiency of (96±6) percent. It has been

shown that the local efficiency $\epsilon(x, y)$ of the Bi counter (x=distance of the incident beam from counter-axis, y=distance from middle section of the counter) varies considerably; $\epsilon(0, y)$ being much smaller than $\epsilon(r, y)$ (r=inside radius of counter). The γ-efficiency for cylindrical counters $\epsilon(x, 0)$ can be calculated approximately as $\epsilon(x, 0)=\mu[\{(r+d)^2-x^2\}^{\frac{1}{2}}-[(r^2-x^2)]^{\frac{1}{2}}\}$; μ, coefficient of γ-absorption in Bi, d, the effective thickness of the Bi-cathode. The agreement with the measured values of $\epsilon(x, 0)$, corrected for the finite width of the γ-beam is good. The calculated average efficiency $\bar{\epsilon}=(2/rL)\int_0^r\int_0^{L/2}\epsilon(x, y)\,dx\,dy$ (L: length of counter), also agrees well with $\bar{\epsilon}$ obtained by coincidence measurements.

* Supported by contract with ONR.

OA4. Temperature Dependence of Photovoltaic Effects on *P-N* Barriers in Germanium.* H. Y. FAN AND M. BECKER, *Purdue University.*—Photo-voltaic effects on germanium *P-N* barriers produced by deuteron bombardment are investigated from room temperature to −190°C. Monochromatic light of different wave-lengths is used. For all wave-lengths used, from 0.9μ to 1.9μ, the photo-voltage increased greatly with decreasing temperature: about 5 times from 20°C to 0°C and about 80 times from 0°C to −70°C. With light pulses rising to full intensity in 15μ sec. and taking the same time to fall off, no time lag in the rise and fall of photo-voltage can be observed both at 20°C and at 0°C. At −70°C delays in build up and falling off is observed, with a time constant ~130 μsec. The shape of photo-voltage pulses seems to be independent of the wave-length of the light, although at the short wave-lengths used the light is absorbed in a very thin layer, whereas light of 1.8μ produces excitation throughout the thickness of the sample.[1]

* Work assisted by Signal Corps contract.
[1] M. Becker and H. Y. Fan, Phys. Rev. **76**, 1530 (1949).

OA5. D.C. Characteristics of High Resistance Barriers at Crystal Boundaries in Germanium.* W. E. TAYLOR AND H. Y. FAN, *Purdue University.*—Grain boundaries in high resistivity *N* type germanium are often found to have a high resistance to the passage of current in either direction. The current-voltage characteristic in both directions resembles the back characteristic of the germanium rectifier. Similar results were observed by Benzer[1] with a mechanical germanium-germanium point contact. The high resistance of grain boundaries can be removed by nucleon bombardment to *P* type; by converting the material back to *N* type by heat treatment the original condition can be restored.[2] Pearson also has reported the removal of such high resistance regions by heat treatment methods. The high resistance can be explained by natural barriers on both sides of the grain boundary resulting from localized energy states within the energy gap. For applied voltages smaller than kT the current is given by $i=ATe-e\varphi/kT$ Vap, where $e\varphi$ is the energy difference between the top of the barrier and the Fermi level. Measured values of $lu(kT)$ in the range from 20°C to −50°C give a straight line with a slope corresponding to about 0.5 ev for the value of φ.

* Assisted by a Signal Corps contract.
[1] S. Benzer, "Ge-ge contacts," Progress Report, Department of Physics, Purdue University, November, 1946.
[2] Lark-Horovitz and Davis, "Bombardment of semiconductors by nucleons," Progress Report, Department of Physics, Purdue University, January, 1948.

OA6. Resistivity of Semiconductors Containing both Acceptor and Donator Impurity Levels.* C. S. HUNG AND V. A. JOHNSON, *Purdue University.*—The Hall coefficient and resistivity have been measured as functions of temperature down to about 10°K for a number of germanium samples. For samples of intermediate purity, the mobility behavior indicates that the resistivity below 100°K is almost entirely due to scattering of carriers by impurity ions. As the temperature decreases to very low values, the resistivity becomes increasingly greater than the value calculated from the Conwell-Weisskopf formula[1] on the assumption that all impurity ions have the same sign and thus that their number is given directly by the Hall coefficient. However, the formula predicts the observed resistivity satisfactorily on the assumption that both acceptor and donator impurity atoms are present in the material. For example, in *N*-type material, N_p acceptor impurity atoms would take up an equal number of electrons from donator atoms, thus producing N_p negative impurity ions and N_p positive ions in addition to the n positive ions corresponding to n conduction electrons. The scattering of carriers is due to the $n+2N_p$ impurity ions rather than to the n ions whose presence is indicated by the Hall coefficient.

* Work assisted by Signal Corps contract.
[1] E. Conwell and V. F. Weisskopf, Phys. Rev. **69**, 258 (1946).

Biophysics and High-Polymer Physics

OB1. A Large Water-Prism Monochromator. R. B. SETLOW AND D. J. FLUKE,* *Yale University.***—The determination of the action spectrum of protein molecules, viruses, and bacteria quite often requires the use of high intensity ultraviolet light. The investigation of possible fine-structure in the action spectrum also demands that the monochromator used to isolate a given wave-length interval be capable of passing a 30A band when using slits of the order of one millimeter wide. The limitation on the slit width is set by the use of capillary-arc light sources of about this width.[1] A monochromator satisfying these conditions will be described in detail. The focussing elements are spherical aluminized-mirrors of 25 cm diameter and 50 cm focal length. The dispersing element is a 60° water prism with quartz side-faces. The use of water as the prism material gives adequate dispersion and negligible absorption down to 2000A. Wave-length variation is obtained by rotation of the prism about a vertical axis. The monochromator is comparatively inexpensive.

* U. S. Public Health Fellow.
** Assisted by AEC.
[1] R. M. Hoffmann and F. Daniels, J. Am. Chem. Soc. **54**, 4226 (1932).

OB2. An Apparatus for Ultraviolet Irradiation of Viruses at the Temperature of Liquid Hydrogen. DONALD J. FLUKE,* *Yale University.***—A technique for monochromatic ultraviolet irradiation of viruses at liquid air and liquid hydrogen temperatures has been worked out. The viruses are deposited in small areas of dried film on aluminum foil covering a cylindrical brass flask containing the refrigerant. The upper section of the flask is a stainless steel tube of considerably smaller diameter, working through a Wilson seal in the top plate of an outer vacuum envelope. A quartz window in one side of the outer envelope permits the ultraviolet beam from a monochromator to be directed upon the several areas on the inner flask, the Wilson seal affording change of specimens. A radiation shield cooled by liquid air effectively surrounds the inner flask. The top plate joins the rest of the outer envelope by a gasket seal, so that the inner flask and its shield can be withdrawn for deposition and recovery of the specimens.

* U. S. Public Health Research Fellow.
** Assisted by the AEC.

OB3. Cyclotron Bombardment of Enzymes and Viruses. ERNEST POLLARD AND F. FORRO, JR.,* *Yale University.***—A technique for deuteron and alpha-particle bombardment of dry enzymes and viruses has been developed. The basic requirement is a beam which is somewhat defocussed so that it is uniform across an area of about ¾ inch. This is achieved by a deflecting magnet and a long evacuated tube so that irradiation takes place two meters from the magnet. The dry specimens are introduced on coverslips placed on a copper disk which prevents undue temperature rise. Exposure is by

means of an electrically operated shutter. The beam is measured both on the entire bombardment chamber and also by a Faraday cup. The ionization density of the beam can be varied by means of foils placed over the exit port for the beam. The inactivation cross section so obtained correlates with molecular dimensions and offers promise as a method of measuring the internal structure of viruses.

* Public Health Research Fellow.
** Assisted by the AEC.

OB4. Double Crystal and Slit Methods in Small Angle X-Ray Scattering.* PAUL KAESBERG, W. W. BEEMAN, AND H. N. RITLAND, *University of Wisconsin.*—An angular resolution of about 10 seconds of arc is obtainable in small angle scattering experiments using a calcite double crystal spectrometer in the parallel position and Cu K_α radiation. However, the rather large wing background at large angles makes the detection of radiation from weakly scattering materials difficult. Of the order of 10^6 counts per second are detected with a stationary, water cooled copper target and parallel crystals. Wing backgrounds do not fall much below 10^2 counts per second. Wing heights may be considerably reduced by the addition of a third calcite crystal placed parallel to the second crystal and rotated with it. With this modification the double crystal spectrometer is a useful instrument for most scattering experiments in which extremely high resolution is desired. However, it is inferior to a slit system and Geiger counter arrangement when lesser resolution but high sensitivity are required. A slit instrument with an angular resolution of 4 or 5 minutes of arc provides an effective incident flux of more than 10^6 counts per second while wing intensities may be as low as 1 count per second.

* Supported by the ONR and the Wisconsin Alumni Research Foundation.

OB5. The Shapes and Hydrations of Several Protein Molecules in Solution.* W. W. BEEMAN, PAUL KAESBERG, AND H. N. RITLAND, *University of Wisconsin.*—Using the slit collimator and Geiger counter described in the previous abstract, the radii of gyration of several protein molecules in dilute aqueous solution have been determined from the angular distribution of the small angle x-ray scattering. Asymmetry factors can be calculated with the help of the known molecular volumes. Hydrations may also be estimated from the asymmetries and the frictional ratios. The molecules to be discussed are lysozyme, $R=16.0$A; β-lactoglobulin, $R=24.6$A; ovalbumin, $R=24.0$A; bovine hemoglobin, $R=23.9$A; bovine serum albumin, $R=26.6$A; and human γ_2-globulin, $R=37.0$A. Some possibilities and limitations of the method will be pointed out.

* Supported by the ONR and the Wisconsin Alumni Research Foundation.

OB6. Statistical Theory of Volume Effect in a Long Chain Molecule. CHAN-MOU TCHEN, *National Bureau of Standards.*—The purpose of this paper is to find the non-Gaussian distribution function of the distance between the endpoints of a material flexible chain, by eliminating certain configurations containing overlaps of volume. To this aim, first a continuous Markoff's probability function is calculated in order to study the interaction between an arbitrary pair of points on the chain, for a given distance r between the endpoints. Second, we consider the cross-interaction acting upon a given pair of points by the presence of other close points. Such cross-interactions are manifested in the entanglements of the loop or loops which have to be formed in order to have a close approach between the given pair of points. The *mechanism of entanglements of loops* is studied by investigating a new probability function called "*cross-interaction probability*" which is a more general one than the Markoff's probability function. It is found that a loop containing a large number of links will have a large number of configurations, and hence will have more chances to escape any entanglement than shorter loops. The ratio of the non-Gaussian distribution for the chain with volume effect to the Gaussian distribution for the chain without volume effect is found to be constant $\exp(-v^*)$, where: $v^*=C_2(n)^{\frac{1}{2}}\exp(-z^2)$, $z^2=(3/2)(r^2/nb^2)$ with $n=$number of links, $C_2=(b_1/b)^3$, $b=$length of one link, and $b_1=$a critical distance of interaction. From the above non-Gaussian distribution function, the most probable values of the square distance between the endpoints has been calculated: the ratio of this value in a chain with volume effect to the same value in an ideal chain without volume effect is found equal to $1+C_2(n)^{\frac{1}{2}}e^{-1}$ for small values of the parameter $C_2(n)^{\frac{1}{2}}$, and equal to $\ln[C_2(n)^{\frac{1}{2}}]$ for large values of the parameter.

OB7. Plasticity and Elasticity: Some Fundamental Concepts. M. L. HUGGINS, *Eastman Kodak Company.*—Viscosity in simple liquids and plastic flow and elasticity in metals and in high polymers are discussed with the aid of energy diagrams for simplified models. The essential requirement for long-range elasticity is the possibility of reversible shifts of parts of the molecules, relative to neighboring molecules. For high elasticity without plastic flow, some part of every molecule must be permanently prevented from moving, relative to some part of an adjacent molecule, either by forces too strong to be broken in the time available by the temperature motions, aided by the applied stress, or by the cooperative action of several (or many) weak forces. Under certain conditions, several small energy humps are equivalent to a single large one. Oriented and crystalline regions can thus act effectively as cross-links. Plastic flow occurs if some molecules are not locked at any point with adjacent ones.

OB8. Infra-Red Spectra of Some Fibrous Protein in Polarized Radiation. MARTIN GOLDSTEIN AND RALPH S. HALFORD, *Columbia University.*—Infra-red spectra in polarized radiation have been obtained for representative members of the three classes of fibrous proteins. The region from 3 to 6 microns was studied with a CaF_2 prism, that from 6 to 14 microns with a rocksalt prism. A silver chloride polarizer was used throughout. The observations could be made with the electric vector of the incident radiation either perpendicular to the fiber axis, or parallel to it. Both β-keratins, such as fibroin and feather keratin, and collagens, from a number of mammalian sources, show differences between spectra taken in these two ways that are consistent with an extended or nearly extended polypeptide chain structure. α-keratins including myosin and porcupine quill show only small effects of a different sort. The effects in α-keratins do not lend themselves readily to interpretation, but some deductions as to the orientation of certain chemical bonds in the structure can be made.

Reactions of Transmutation

P1. Angular Distribution of the Alpha-Particles from the $Li^7(p, \alpha)\alpha$ Reaction.* F. L. TALBOTT AND A. BUSALA, *Catholic University of America.*—The angular distribution of alpha-particles from the reaction Li^7 (p, α) α has been investigated from 0.5 to 1.4 Mev in steps of 0.1 Mev. A photographic emulsion technique was used which permits counts to be made at many angles. As many as 15 angles were counted in some instances. Most calculations are based on the counting of over 20,000 alpha-tracks. Several sets of such calculations have been averaged at each energy. The curves show clearly the presence of a $\cos^4\theta$ term as indicated by Heydenburg *et al.*[1] and the coefficients of $\cos^2\theta$ and $\cos^4\theta$ are in good agreement with their values where the two experiments overlap in the region above 1.0 Mev.

* This work was supported in part by the ONR.
[1] Heydenburg, Hudson, Inglis, and Whitehead, Phys. Rev. 73, 241 (1948).

P2. Neutrons from the Disintegration of Beryllium by Deuterons.* W. D. WHITEHEAD AND C. E. MANDEVILLE, *Bartol Research Foundation.*—Ilford C_2 emulsions, making an angle of zero degrees with the incident beam, were irradiated by neutrons from the reaction $Be^9(D, n)B^{10}$ when a beryllium target of thickness 100 Kev was bombarded by deuterons of energy 1.62 Mev supplied by the Bartol Van de Graaff generator. Groups of recoil protons were observed corresponding to Q-values of (-0.74), 0.73, 2.19, 3.70, and 4.39 Mev, indicating excitation levels in B^{10} at 0.69, 2.20, 3.66, and 5.13 Mev with a probable error of 0.10 Mev or less. The group of negative Q-value did not appear for a bombarding energy of 1.20 Mev, because the low energy neutrons did not record against the general background of the plates. In a separate experiment at 1.62 Mev, the recoil protons of $C^{13}(D, n)N^{13}$ were shown to have a range twice as great as that of the negative Q group. The group of negative Q constitutes 20 percent of the total thin target yield at 1.62 Mev deuteron energy, agreeing in energy and intensity with the analysis of counter data given by the Rice group.[1]

* Assisted by the Joint Program of the ONR and the AEC.
[1] Evans, Malich, and Risser, Phys. Rev. 75, 1161 (1949).

P3. Proton Groups from the Deuteron Bombardment of Boron. W. O. BATESON, *Yale University.**—A preliminary investigation of the proton groups emitted at 90° when separated B^{10} [1] is bombarded by 3.8 Mev deuterons from the Yale cyclotron has been made. Groups with 147.2, 105.0, 67.0, 58.5, 35.1, 26.3 and 19.2 cm of air equivalent range were found, corresponding to Q values of 9.18 ± 0.06, 7.03 ± 0.06, 4.70 ± 0.06, 4.15 ± 0.10, 2.26 ± 0.06, 1.36 ± 0.10 and 0.70 ± 0.10 Mev. The fourth, sixth, and seventh of these are new, the other four values being in reasonable agreement with previous work.[2] Bombardment of ordinary boron has revealed no additional groups due to $B^{11}(d, p)B^{12}$, but these may be masked by the very prolific groups at 19 and 26 cms from $B^{10}(d, p)B^{11}$.

* Assisted by the ONR and the AEC.
[1] 96 percent B^{10} was obtained from Oak Ridge.
[2] J. D. Cockcroft and W. B. Lewis, Proc. Roy. Soc. 154, 246 (1936). Pollard, Davidson, and Schultz, Phys. Rev. 57, 1117 (1940).

P4. Deuteron Bombardment of C^{14}.* EMMETT L. HUDSPETH AND CHARLES P. SWANN, *Bartol Research Foundation.*—A target of 400 $\mu g/cm^2$ of $BaCO_3$ (containing approximately 40 percent C^{14} and obtained from Oak Ridge) has been bombarded by deuterons. Neutrons were recorded on photographic plates while bombarding at 1.26 Mev. Groups of proton recoils consistent with the formation of N^{15} in its known[1] excited states were observed. The most intense groups correspond to Q-values of 8.0 and 2.6 Mev. The cross section for this reaction is somewhat greater than for the $C^{13}(d, n)$reaction at the same bombarding voltage. Deuteron bombardment of C^{14} yields high energy beta-rays, which we ascribe to the decay of B^{12}. An absorption curve in aluminum is apparently identical with that obtained from B^{12} as formed in $B^{11}(d, p)$. The $C^{14}(d, \alpha)B^{12}$ reaction is a strong source of beta-rays at 750 Kev; the yield increases rapidly with bombarding voltage. Limits on bombarding voltage prevent formation of C^{15}. Coincidence absorption of the Compton recoils produced by gamma-rays emitted during bombardment indicates a strong gamma-ray of energy about 5 Mev (in addition to others of lower intensity), consistent with the nature of the neutron spectrum.

* Assisted by the Joint Program of the ONR and the AEC.
[1] W. F. Hornyak and T. Lauritsen, Rev. Mod. Phys. 20, 217 (1948) have summarized the relevant data.

P5. Evidence for the Reactions $N^{14}(\gamma, \alpha)B^{10}$ and $O^{16}(\gamma, \alpha)C^{12}$. A. G. W. CAMERON AND C. H. MILLAR, *Chalk River Laboratory.*—An Ilford type E1, 100 micron, nuclear research emulsion was exposed under paraffin and cadmium to 200 r of γ-radiation from the 24 Mev betatron at the University of Saskatchewan. A modified Van der Grinten grain gradation development[1] of the plate minimized γ-ray fogging and suppressed proton tracks. Many 3- and some 4-pronged α-particle stars were found due to the photo-disintegration of C^{12} and O^{16} respectively; and among many single α-particle tracks, due presumably to photo-alpha reactions in Ag and Br, were several each associated with a short heavy recoil track at the origin. These last were interpreted as photo-alpha reactions in light nuclei. With the range-energy relation in functional form and the average effective charge of the recoiling nucleus assumed as approximately 60 percent of the nuclear charge, these examples can be unambiguously allocated to one or the other of the reactions $N^{14}(\gamma, \alpha)B^{10}$ and $O^{16}(\gamma, \alpha)C^{12}$. In addition, range-energy curves for B^{10} and C^{12} in type E1 emulsion have been obtained for the region 1–5 Mev. Agreement with measurements[2] of C^{12} in gases is satisfactory.

[1] H. Yagoda, *Radioactive Measurements with Nuclear Emulsions* (John Wiley and Sons, Inc., New York, 1949), p. 62.
[2] G. A. Wrenshall, Phys. Rev. 57, 1095 (1940).

P6. Energy Levels in N^{15}.* R. MALM AND W. W. BUECHNER, *M. I. T.*—The proton groups from N^{14} targets bombarded with 1.5-Mev deuterons have been studied using semicircular magnetic analysis. Preliminary Q-values found for the observed groups are 8.61, 3.32, and 3.29 Mev. With lesser resolution, the latter two groups appear as a single peak and probably correspond to the group previously reported as having a Q-value of 3.18 Mev. The present work indicates the existence of energy levels in N^{15} at 5.29 and 5.32 Mev.

* This work has been assisted by the Joint Program of the ONR and the AEC.

P7. Energy Levels of the F^{20} Nucleus from the $F^{19}(d, p)F^{20}$ Reaction. R. C. ALLEN AND WALDO RALL, *Yale University.**—Lead fluoride, evaporated on a gold foil, was bombarded by 3.9-Mev cyclotron deuterons. Protons were detected at 90° with respect to the deuteron beam by means of a highly biased proportional counter. Aluminum absorption techniques gave proton groups of extrapolated range 68.2, 58.5, 53.8, 49.4, 41.3, 34.0, 30.2, 24.3, and 19.0 equivalent air (cm). These ranges correspond to energy levels of 0.0 ($Q_0=4.29$ Mev), 0.64, 0.98, 1.31, 1.95, 2.57, 2.90, 3.49, and 4.07 Mev, respectively. Probable errors on all but the highest level are within 0.08 Mev, that of the last level being 0.20 Mev. The levels are in good agreement with the 0.7-, 1.0-, 1.35-, and 1.9-Mev levels found earlier by Bower and Burcham[1] using lower beam energies. The levels appear to be integral multiples of a unit energy of 320 Kev. In terms of this unit the levels exist at 2, 3, 4, 6, 8, 9, 11, and 13, all agreeing well within the probable errors.

* Assisted by the ONR and the AEC.
[1] Bower and Burcham, Proc. Roy. Soc. 173, 379 (1939).

P8. Excitation Curve for Protons in the Reaction $F^{19}(d, p)F^{20}$.* S. C. SNOWDON, *Bartol Research Foundation.*—The excitation curve for the total yield of the reaction $F^{19}+H^2\rightarrow F^{20}+H^1$ has been studied by measuring the β-ray yield from the reaction $F^{20}\rightarrow Ne^{20}+\beta-$. In order to annul the effect of fluctuations in the beam current, $I(\tau)$, it was necessary to construct a special integrator which measures $\int_0^t I(\tau)e^{-\lambda(t-\tau)}\,d\tau$, where λ is the disintegration constant for the β-decay. Preliminary results indicate a smooth rise in the yield curve from 0.7 Mev to 1.8 Mev.

* Assisted by the Joint Program of the ONR and the AEC.

P9. Alpha-Particles from $F^{19}(p, \alpha)O^{16}$.* E. N. STRAIT, D. M. VAN PATTER, AND W. W. BUECHNER, *Massachusetts Institute of Technology.*—The alpha-particle groups from thin

targets containing fluorine bombarded by protons have been analyzed at 90 degrees using a 180-degree focusing annular magnet. The proton incident energy is measured by analyzing the elastically scattered protons from a thin Formvar target. All energy measurements are determined using polonium alpha-particles as standard. The Q-values for the alpha-particles going to O^{16} in the ground state and first excited state for gamma-radiation have been measured as $Q_0=8.068$ and $Q_1=1.969$ Mev. These values are in good agreement with the recent measurements of Chao, Tollestrup, Fowler, and Lauritsen[1] who find $Q_0=8.101\pm0.030$ and $Q_1=1.977\pm0.008$ Mev. The relative intensities of the alpha-groups corresponding to the formation of O^{16} in the pair level and the ground state are being investigated at proton energies between 1.1 and 1.4 Mev at reported pair resonances.[2]

* This work has been assisted by the Joint Program of the ONR and the AEC.
[1] Chao, Tollestrup, Fowler, and Lauritsen (private communication).
[2] Bennett, Bonner, Mandeville, and Watt, Phys. Rev. 70, 882 (1946).

P10. d-p Reactions with Separated Neon Isotopes.* A. ZUCKER AND W. W. WATSON, *Yale University.*—With neon gas enriched 93 percent Ne^{22} or to 99 percent Ne^{20} we confirm the observations of Elder, Motz, and Davison,[1] who used less well-separated isotopes, on the $Ne^{20}(d, p)Ne^{21}$ and $Ne^{22}(d, p)Ne^{23}$ reactions. Aided by the enrichment factor of 3 for Ne^{21} in the "heavy" neon, we find a new long-range proton group assigned to $Ne^{21}(d, p)Ne^{22}$ with a Q of 7.00 ± 0.10 Mev for the reaction. Consideration of these and other reactions involving the neon isotopes and neighboring elements shows that the mass of Ne^{21} is 21.00062 ± 0.00010, and that the new proton group indicates an excited state at 1.37 Mev in the Ne^{22} nucleus. The mass of Ne^{23} obtained by us agrees just within the limits of error with that obtained from the reaction $Ne^{23}(\beta^-)Na^{23}$. The latter gives the mass of Ne^{23} as 23.00160 ± 0.00040.

* Assisted by the AEC.
[1] Elder, Motz, and Davison, Phys. Rev. 71, 917L (1947).

P11. Neutrons from Deuterons on Magnesium (25).* C. P. SWANN, C. E. MANDEVILLE, AND W. D. WHITEHEAD, *Bartol Research Foundation.*—Isotopic Mg^{25}, obtained from the Y-12 plant, Carbide and Carbon Chemicals Corporation, Oak Ridge, was irradiated by deuterons of energy 1.47 Mev, supplied by the Bartol Van de Graaff generator. Recoil protons, knocked on in the forward direction by the emitted neutrons, were observed in Ilford C_2 emulsions located 10 cm from the target at angles of zero and ninety degrees with the incident beam. At both angles, four groups of neutrons were noted having Q-values of 0.45, 1.95, 3.58, and 5.58 Mev, indicating nuclear energy levels in Al^{26} at 2.00, 3.63, and 5.13 Mev. The probable error in the location of the levels is estimated as 0.10 Mev. The mass of Al^{26} is calculated to be $(25.9935\pm9.0\times10^{-4})$ mu. Measurements concerning neutron spectra resulting from the reactions $Mg^{24}(D, n)Al^{25}$ and $Mg^{26}(D, n)Al^{27}$ are in progress.

* Assisted by the Joint Program of the ONR and the AEC.

P12. Proton Groups from the Deuteron Bombardment of Aluminum, Sodium, and Manganese. W. D. WHITEHEAD* AND N. P. HEYDENBURG, *University of Virginia and Carnegie Institution of Washington.*—Thin targets of sodium, aluminum, and manganese were bombarded with deuterons from the large statitron at the Department of Terrestrial Magnetism, and the protons were observed at 90° to the beam with an argon filled proportional counter. The counter was biased to count protons at the end of their range and the ranges of the groups were measured in air and aluminum. Proton groups due to oxygen and carbon were found with all targets.

Element	Bombarding energy	Average Q
Na	2.0, 2.5, 3.0	4.77, 4.23, 3.45, 2.94, 2.22, 1.33, .96, .78, .50, .12
Al	3.0	5.72, 4.71, 4.35, 4.07, 3.49, 3.05, 2.69, 2.39, 2.08, 1.59, .94, .70, .46, .04
Mn	3.0	5.01, 3.47, 3.13, 2.85, .48, .13, −.19

* AEC Predoctoral Fellow, now at Bartol Research Foundation.

P13. Proton-Gamma-Ray Coincidence Study of the Energy Level Scheme of Si30. H. H. LANDON, *Yale University.**—The energy level scheme of Si30 was studied by means of a proton-gamma-ray coincidence technique using the $Al^{27}(\alpha, p)$ reaction. The protons were observed at 90° with respect to the incident alpha particle beam. Preliminary Q values estimations were made by examining the proton group structure and the following results obtained. $Q_1=2.4$, $Q_2=0.0$, $Q_3=-1.3$, $Q_4=-2.6\pm0.2$ Mev. The gamma-rays giving coincidences with protons from the first and second excited states were studied by measuring the absorption coefficients in copper. Preliminary estimates strongly suggest that a hard and soft component exist indicating that the gamma-ray from the second excited state comes from a transition directly to the ground state.

* Assisted by the ONR.

P14. Excitation Function of $Ta^{181}(d, p)Ta^{182}$.* KUAN-HAN SUN, F. A. PECJAK, R. A. CHARPIE, J. F. NECHAJ, *Westinghouse Research Laboratories and the University of Pittsburgh.*—The excitation function of $Ta^{181}(d, p)Ta^{182}$ up to 15.0 Mev deuteron energy was measured by the stack foil (10 mg/cm²) technique. The half-life (115 days) and the energy of the two β-groups (0.52 and 1.1 Mev) observed were in agreement with the literature data. The reaction $Al^{27}(d, p\alpha)Na^{24}$, previously studied by Clarke,[1] was used for monitoring the deuteron beam by placing an Al-foil (2 mg/cm²) in front of the Ta-stack. The relative yields are 1.00, 1.08, 0.96, 0.54, 0.18, 0.01, and 0.00 for deuteron energies of 15.0, 13.5, 12.0, 10.5, 9.0, 7.5 and 6.0 Mev, respectively. The ratio of the cross section at 15 Mev for the Ta- and Al-reactions was found to be 35. This yields an absolute cross section of 0.89 barn for the Ta-reaction using the corresponding cross section of the Al.[1] A thick target yield curve was also obtained. At 15.0 Mev the yield was 0.97 rd/μah of the deuterons.

* Assisted by the Joint Program of the AEC and the ONR.
[1] E. T. Clarke, Phys. Rev. 71, 187 (1947).

P15. Spectrum of Neutrons from Ta(dn). R. A. PECK, JR., *Brown University.**—Neutron energies from this reaction have been studied using recoil proton tracks in Eastman NTB emulsions. 14 Mev deuterons from the Massachusetts Institute of Technology cyclotron were used to bombard a 1 mil tantalum foil. The exposed plates were processed and examined, following a conventional microphotographic procedure.[1] The spectrum (2 Mev and above) shows a strong preference for the lowest neutron energies. The expected maximum energy is approximately 16 Mev, but to date none greater than 14.5 Mev has been observed. Some evidence of group structure appears in most of the spectrum (below 12 Mev), but the yield is so far insufficient to show structure at higher energies (lower excitation of the product W^{183} nucleus). When the data are plotted in the form $\log(N/E)$ *vs.* E breaks appear in the slope. The nuclear temperature[2] obtained from the slopes of this line is approximately 0.7 Mev,

changing to 1.3 Mev above 4.7 Mev and to 3.6 Mev above 7.1 Mev.

* Exposures were made at the Massachusetts Institute of Technology, with the support of the ONR.
[1] R. A. Peck, Jr., Phys. Rev. **76**, 1279 (1949).
[2] V. F. Weisskopf, Phys. Rev. **52**, 295 (1937).

Nuclear Magnetic Resonance; Molecular Hyperfine Structure

Q1. The Absolute Value of the Gyromagnetic Ratio of the Proton. R. L. DRISCOLL, H. A. THOMAS, AND J. A. HIPPLE, *National Bureau of Standards.*—Since our previous report on this work,[1] a careful study of the sources of error has continued. The measurements have been repeated with symmetrical shims instead of the unsymmetrical ones previously used. The magnetic field distribution was checked immediately before and after each run. The main contributing error had been caused by the asymmetry of the copper wire employed in the construction of the precision rectangular coil for measuring the magnetic field. The uncertainty due to this cause has been greatly reduced by measuring this wire after dismantling the rectangular coil. These studies and others which will be described indicate that the accuracy will be much higher than previously reported. Consequently, there will be less uncertainty in the values of e/m of the electron and of the Faraday.

[1] H. A. Thomas, R. L. Driscoll, and J. A. Hipple, Phys. Rev. **75**, 902 (1949).

Q2. The Internal Diamagnetic Field Correction in Precision Measurements of the Proton Magnetic Moment. NORMAN F. RAMSEY, *Harvard University.*—In recent high precision experiments involving the proton magnetic moment, the internal diamagnetic field correction to the measurement has become an important limitation to the precision of the result. This correction arises from the fact that the protons being measured are contained in a molecule, such as H_2, whose electrons to some extent magnetically shield the nucleus. An exact theoretical evaluation of this correction for molecules has been impossible because one important term in the correction is extremely difficult to evaluate. In the present paper it is pointed out that this difficult term is directly related to the spin-rotational interaction constant of the molecule, which has been experimentally measured in certain cases, notably H_2. With the notation characteristic of the subject the diamagnetic correction is

$$\frac{H'(0)}{H}=-\frac{e^2}{3mc^2}\int\frac{|\Psi|^2}{r}d\tau+\frac{1}{6}\alpha^2\frac{a_0a^2}{(\mu_0m/M)}\left\{\frac{2Z(\mu_0m/M)}{a^3}-\frac{\mu}{M}H_p\right\}.$$

The first term has been evaluated from Nordsieck wave functions by Anderson to be -3.24×10^{-5}, and the second can be determined from the experiments of Kellogg, Rabi, Ramsey, and Zacharias with the result that $[H'(0)]/H=[-3.2_4+0.53]\times10^{-5}=2.7_1\times10^{-5}$.

Q3. Regulation of Large Electromagnets Using Proton Resonance. H. A. THOMAS, *National Bureau of Standards.*—Our experience in regulating electromagnets by means of nuclear resonance, first suggested by Bloch,[1] has shown that field stability of the order of a few parts per million may be obtained. The resonance absorption signal from a proton sample may be fed into a power amplifier which may be used to regulate the field directly by means of auxiliary coils on the magnet or by driving the field of the exciter for the main generator. Large magnets having time constants of the order of 5 seconds or larger introduce more difficult problems in hunting that require special attention. The two systems of regulation mentioned above and the necessary anti-hunt methods will be discussed and performance data given for a 1-ton magnet and a 36-ton magnet.

[1] F. Bloch, Phys. Rev. **70**, 460 (1946).

Q4. Nuclear Spin Relaxation in KH_2PO_4, KH_2AsO_4, $NH_4H_2PO_4$, and $NH_4H_2AsO_4$. ROGER NEWMAN AND EDWARD M. PURCELL, *Harvard University.*—Studies have been made of the proton magnetic resonance absorption at 30 Mc in KH_2PO_4, KH_2AsO_4, $NH_4H_2PO_4$ and $NH_4H_2AsO_4$ from liquid air temperature to room temperature. Both line shapes and relaxation times have been measured. The potassium salts, which undergo ferroelectric transitions,[1] show closely similar magnetic resonance properties. Their relaxation times show relatively small variation in the temperature interval studied. The characteristic times derived therefrom do not obey any simple exponential law in the reciprocal temperoture. In the ammonium salts, which have para-electric properties,[1] there are two minima in the relaxation time *vs.* temperature curves, one minimum corresponding to a temperature where the acid hydrogens are the most effective relaxation agent and the other to a temperature where the ammonium hydrogens are most effective. The line shape is also of a composite character. This is most clearly shown below 100°K where the absorption lines appear to be superpositions of the broad NH_4 line for which NH_4Cl is typical, and the narrow line found in KH_2PO_4 or KH_2AsO_4.

[1] G. Busch, Helv. Physica Acta **11**, 269 (1938).

Q5. Factors Influencing the Positions of Nuclear Magnetic Resonances.* W. C. DICKINSON, *M. I. T.*—It has been found that the shift of a nuclear magnetic resonance on addition of paramagnetic ions is a function of the resonating nucleus and the chemical compound in which it is contained. Shifts can be either positive or negative, both for a spherical and transverse cylindrical sample shape. The magnitude of this paramagnetic shift is sometimes sufficient to affect the results of a high precision measurement when paramagnetic ions are added to shorten the thermal relaxation time. In the course of this investigation it was discovered that the position of the fluorine resonance is dependent on the chemical compound containing the fluorine atom. Such shifts never have been observed or predicted previously for liquids. The largest separation between resonances observed to date is (1.05 ± 0.03) gauss in a field ≈7000 gauss for the fluorine resonances in BeF_2 and $C_2F_3Cl_3$, the latter one coming at the lower applied field. Nuclear resonance shifts in metals,[1] interpreted as being due to the conduction electrons, are larger by about an order of magnitude.

* This work has been supported in part by the Signal Corps, the Air Materiel Command, and the ONR.
[1] W. D. Knight, Phys. Rev. **76**, 1259 (1949).

Q6. Nuclear Magnetic Moment of S^{33}.* C. K. JEN, *Harvard University.*—An attempt has been made to determine the nuclear magnetic moment of S^{33} from the Zeeman effect of an OCS^{33} ($J=1\rightarrow2$) rotational line in the microwave range.[1] The OCS^{33} molecule was present in the carbonyl-sulfide sample in its natural isotopic abundance of about 0.7 percent. The nuclear magnetic moment is calculated from the observed Zeeman data on the basis of an IJ coupling between the nuclear spin and molecular rotation, using the known spin value $I(S^{33})=3/2$.[1] The molecular g-factor for OCS^{33} (0.026 in nuclear units), used in the calculations, is deduced from the data on the Zeeman splitting of the $J=1\rightarrow2$ rotational lines of OCS^{32} and OCS^{34}. The present estimate of the nuclear moment is considered rather crude, chiefly due to low line intensities and insufficient resolution. A provisional estimate gives $|\mu(S^{33})|=0.9$ n.m. The sign of the moment, while seemingly positive, has not been established. This result is within

the Schmidt limits and is in general agreement with the "one-particle" picture for the nuclear shell structure.[2,3]

* Supported by Navy, Signal Corps and Air Force under ONR contract.
[1] C. H. Townes and S. Geschwind, Phys. Rev. **74**, 626 (1948).
[2] E. Feenberg and K. C. Hammack, Phys. Rev. **75**, 1877 (1949).
[3] L. W. Nordheim, Phys. Rev. **75**, 1894 (1949).

Q7. Radio Frequency Spectrum of $TlCl^{35}$. C. A. Lee, R. O. Carlson, B. P. Fabricand, and I. I. Rabi, *Columbia University.*—The radiofrequency spectrum of $TlCl^{35}$ has been investigated by the molecular beam electrical resonance method.[1,2] The quadrupole interaction constant, due to the Cl^{35} nucleus for the first rotational state and zeroth vibrational state, has the value $eqQ=-15.79$ mc/sec. (± 0.04 mc). There is an increase of about $\frac{1}{2}$ percent of this interaction for the first vibrational state. In the above notation $q=(\partial^2 V)/(\partial Z^2)$.[3] This coupling constant is approximately fifty times that of chlorine in KCl and 1/7 that for atomic chlorine. Further details of this spectrum will be discussed.

[1] H. K. Hughes, Phys. Rev. **72**, 614 (1947).
[2] J. W. Trischka, Phys. Rev. **74**, 718 (1948).
[3] J. Bardeen and C. H. Townes, Phys. Rev. **73**, 97 (1948).

Q8. Molecular Beam Spectrum of $TlCl^{35}$ and $TlCl^{37}$ at Zero Fields. H. Zeiger, D. Bolef, and I. I. Rabi, *Columbia University.*—The zero-field spectrum of $TlCl^{35}$ and $TlCl^{37}$ has been observed using the molecular beam magnetic resonance method.[1] Two of the observed lines can be attributed to the quadrupole interactions of Cl^{35} and Cl^{37}. Each of these lines is in turn split by an $\bar{I}\cdot\bar{J}$ interaction due to chlorine. The quadrupole interactions are $eqQ_{35}=15.84\pm 0.10$ mc and $eqQ_{37}=12.48\pm 0.10$ mc, where $q=(d^2V)/(dz^2)$.[2] The ratio $Q_{35}/Q_{37}=1.27$, which agrees with the value of 1.28 obtained by atomic beam methods.[3] The splitting due to the $\bar{I}\cdot\bar{J}$ interaction can be expressed as that due to an equivalent magnetic field at the chlorine nucleus. The magnetic field per rotational quantum number, H', has the value $H'=3.4$ gauss for Cl^{35} and $H'=3.2$ gauss for Cl^{37}. The line shape is due to the $\bar{I}\cdot\bar{J}$ interaction and the variation of eqQ with rotational and vibrational state.

[1] W. A. Nierenberg and N. F. Ramsey, Phys. Rev. **72**, 1075 (1947).
[2] J. Bardeen and C. H. Townes, Phys. Rev. **73**, 97 (1948).
[3] Davis, Jr., Feld, Zabel, and Zacharias, Phys. Rev. **76**, 1076 (1949).

Q9. Resonant Modulation, A New Technique in Radio Spectroscopy.* S. H. Autler and C. H. Townes, *Columbia University.*—Splitting of a microwave absorption line has been observed upon application of a weak oscillating electric field whose frequency is such that it induces transitions between either the initial or final energy level of the line and some other level of the molecule. Consider three levels a, b, and c of a molecule. Suppose ν_{ac} ($\nu_{ac}=(E_c-E_a)/h$) lies in the microwave region while ν_{ab} is much smaller, say 40 megacycles. Assume $a\rightarrow c$ and $a\rightarrow b$ are allowed transitions. If an r-f field is applied across the wave guide in which the microwave absorption line, ν_{ac}, is being observed, the line splits into two components when the r-f field is made resonant with ν_{ab}. The amount of splitting depends upon the intensity of the r-f field; and the relative intensity of the two components into which the line splits depends sensitively on the deviation from the resonant frequency. This effect has been observed on the l-type doublet of OCS and the hyperfine structure of AsF_3. A theory has been developed which agrees closely with the observations although there are small unexplained discrepancies. It is hoped that use of resonant modulation will allow somethat improved accuracy in measuring fine and hyperfine structure.

* Work supported jointly by the Signal Corps and the ONR.

Q10. Magnetic Electron Spin—Nuclear Spin Interaction In the Rotational Spectrum of NO_2.* K. B. McAfee, Jr., *Harvard University.*—The microwave spectrum of NO_2—a slightly symmetric top molecule whose ground state is a doublet with spin momentum 1/2—has been studied by means of a Stark-effect spectrograph. The observed spectrum consists of six absorption lines of average and equal intensity extending over a range of approximately 85 mc at 26,600 mc and several other very weak lines. Identification of the rotational transition as $J=6_{06;-6}\leftrightarrow 5_{15;-4}$ was made possible by means of Zeeman-effect measurements. The observed hyperfine structure is ascribed to the magnetic spin-spin interaction of the resultant electron spin with the nitrogen nucleus, and the interaction of the electron spin with molecular rotation. The spin-spin interaction energy for symmetric top molecules given by Van Vleck is:

$$W_{I_s}=-\frac{1}{5}g_I\beta_I\beta\frac{\bar{I}}{r^3}\left[1-\frac{3K^2}{J(J+1)}\right]\left[\frac{F(F+1)-J(J+1)-3/4}{2}\right]\times\left[\frac{G(G+1)-F(F+1)-I(I+1)}{2F(F+1)}\right],$$

where r is the radius of the free spin and $S=1/2$; $G=F+I, \cdots [F-I]$. Application of the above to NO_2 yields agreement to ± 2 mc, while the magnetic coupling constant represented by the multiplicative factor is determined to be 206 ± 10 mc.

* This work supported in part by the ONR.

Q11. Microwave Magnetic Resonance Spectra of NO. Robert Beringer and J. G. Castle, Jr., *Yale University.**—The magnetic resonance absorption of gaseous nitric oxide occurs as a symmetric nine-line spectrum arranged in three triplets. The separation of the triplets arises from perturbations of nearby molecular levels. The separation of 30 Mc/sec. within each triplet arises from the magnetic interaction of the nuclear magnetic moment of N^{14} and the molecular magnetic moment. This interpretation is supported by the line intensities and the absolute value of the triplet spacings which have been calculated by H. Margenau and A. F. Henry. The absolute intensity of the spectrum has been measured and compared with theory. A method for obtaining the line widths from the dependence of the observed shapes on the modulation amplitude will be discussed. The line widths are closely the same for the nine lines and are proportional to the gas pressure near 1 mm Hg.

* Assisted by the ONR.

Ferroelectricity, Ferromagnetism, Cryogenics

R1. Preliminary Results with Macrocrystals of Ferroelectric Barium Titanate. A. deBretteville, Jr. and G. Katz, *Signal Corps Engineering Laboratories.*—Crystal rods of barium titanate 17.5 mm in diameter by 23 mm in length have been grown by Mr. Harold D. Williams of the Harshaw Chemical Company. X-ray reflections using monochromatic radiation were made of the 100 plane on a 3 mm thick wafer cut at an orientation of 45° to the long axis of the rod. This orientation was initially obtained by cleavage. Evidence of twinning was shown by the two clearly separated spacings of the c and a axes ($c-a$ approximately 0.04A) in the fourth order. Gold electrodes were sputtered on the wafer and a field of 16,800 volts/cm was applied for less than one second. Re-examination with the x-ray spectrometer showed almost complete orientation along the polar c axis. A permanent piezoelectric effect as well as a permanent charge was observed with a vacuum tube voltmeter. From knowledge of the orientation of the crystal in the rod, a 110 cut was made and subsequently verified by x-ray reflection. This sample was made from material supplied by the Titanium Division, National Lead Company. In general, the crystals are not homogeneous in orientation throughout but large enough

areas are available to enable physical measurements to be made.

R2. The Behavior of $BaTiO_3$ Crystals under Hydrostatic Pressure.* W. J. MERZ, *M. I. T.*—The effect of hydrostatic pressures (up to 5000 atmos.) on the Curie point and on the transition near 0°C was determined by measuring the dielectric constant as a function of temperature and pressure. It was found that the Curie point shifts to lower temperatures with increasing pressures. The shift is linear at least up to about 2500 atmos., with a gradient of ca. $dT/dp = -5.8\times10^{-3}$ °C/atmos. With the help of Ehrenfest's formula for second-order transitions one can calculate the change of the specific heat and of the compressibility at the Curie point. The specific heat change is in good agreement with direct measurements. With the knowledge of the compressibility and of the expansion coefficient, it is possible to calculate the Curie temperature as a function of the lattice constant. These results are in a good agreement with the relation between Curie point and lattice constant obtained from mixed crystals of $BaTiO_3$ and $SrTiO_3$. The characteristic of dielectric constant *vs.* temperature retains its general shape except for a slight increase in the peak value. For the transition point near 0°C we find a similar shift to lower temperatures, but at about 1500 atmos. the trend reverses and the transition temperature increases with increasing pressure.

* Sponsored by the ONR, the Army Signal Corps, and the Air Force.

R3. The Electro-Mechanical Coupling of $BaTiO_3$ Single-Domain Crystals.* M. E. CASPARI, *M. I. T.*—The d_{31} piezoelectric coefficient of $BaTiO_3$ single-domain crystals was investigated from room temperature to above the Curie point by measuring the strain component along the *a*-axis developed by d.c. electric fields applied along the *c*-axis. Hysteresis effects were observed, compelling one to distinguish between true piezo effects and effects produced by the orientation of domains. Prepolarization tends to minimize such domain effects and makes the remaining hysteresis curves reproducible. Thus good estimates of the d_{31} coefficient can be made. The domain effects can be saturated at very high field strengths, but thermal expansion due to the finite resistivity of the crystal makes measurements at such high field strengths inaccurate. At room temperature the coefficient is about twice as large as the d_{36} coefficient of KH_2PO_4 at the same temperature. Near the Curie point the effect was found to be many times larger. Although the crystal structure above the Curie point has a center of symmetry and is thus not piezoelectric, this large effect was found to persist above the Curie point at high fields, but decreased steadily. This is assumed to be due to the fact that a tetragonal crystal structure is induced by large fields above the Curie point.

* Sponsored by the ONR, the Army Signal Corps, and the Air Force.

R4. A Simple Model for Ferroelectricity. P. W. ANDERSON, *Bell Telephone Laboratories.*—A simple theoretical model for substances showing ferroelectric behavior is being investigated. An assembly of slightly anharmonic oscillators, with potential for each oscillator of the type $V=[(sx^2)/2]+[(px^4)/2]$ $p \ll s^2$ is assumed to interact according to the Lorentz force. Curves of polarization *vs.* local field F are derived and combined with the Lorentz local field to give curves for saturation polarization, dielectric constant ϵ, etc. The slope of the $1/\epsilon$ *vs.* T curve about the Curie point for $BaTiO_3$, and of the saturation polarization *vs.* T for relatively low temperatures (20–100°C) are not inconsistent with reasonable values for p; however, the transition at the Curie point appears to be much more rapid than can be accounted for by this theory, and to have unexplained accompanying effects. It is suggested that this is due to fluctuations, and some ideas on fluctuations are outlined.

R5. On the Triangular Ising Net. G. H. WANNIER, *Bell Telephone Laboratories.*—Kaufman[1] introduced a systematic method for evaluating the partition function of certain cooperative assemblies. When we apply it to the triangular Ising net we get essentially new results if the coupling is antiferromagnetic. Results on the triangular net have been published,[2] but they apply only to ferromagnetism. The calculations cover both types of coupling and show (a) that the antiferromagnetic binding energy is only 1/3 of the corresponding ferromagnetic one; (b) that the system has a finite entropy at absolute zero which equals 0.3383R; (c) that the system is disordered at all temperatures and has no Curie point. The calculation throws some light on the behavior of actual antiferromagnets which often have elementary magnets in a face centered cubic arrangement. In making such comparisons one must keep in mind (a) the sharp distinction for antiferromagnets between an Ising interaction and exchange coupling,[3] (b) the possibility of next nearest neighbor interaction through superexchange.[4]

[1] Bruria Kaufman, Phys. Rev. **76**, 1232 (1949).
[2] G. H. Wannier, Rev. Mod. Phys. **17**, 50 (1945).
[3] Lamek Hulthen, Arkiv. f. Math., Astr. o. Fys. **26A** (1938).
[4] P. W. Anderson (to be published).

R6. Interaction between Paramagnetic Ions in Crystals.* NORMAN ELLIOTT, *Brookhaven.*—The magnetic susceptibilities of manganous fluoride and solid solutions of manganous and zinc fluorides obey the Weiss-Curie law over a wide temperature range. The paramagnetic Curie temperature is found to be linearly dependent on the manganous ion concentration. The results will be discussed in relation to the Heisenberg exchange interaction.

* Work done under the auspices of the AEC.

R7. Memory in Simple Ferromagnetic Domain Crystal. H. J. WILLIAMS AND W. SHOCKLEY, *Bell Telephone Laboratories.*—Studies of hysteresis loops have been made for a simple "picture frame" crystal of silicon iron.* The force 2×(Saturation Magnetization)×(Applied Field)×(Wall Area), required to move the domain wall is found to be a function not only of the wall position but of the previous wall motion, the wall remembering its past positions up to nearly 0.1 cm of motion. The proposed explanation is that secondary domains," "Néel Spikes," form around crystal inclusions or cavities and tend to cling to the wall as it moves past. These exert a force on the wall as they are stretched (actually observed) up to their breaking point and furnish a force varying up to ~0.02 oersted. A local force without memory of 0.003 oersted is also found. This probably corresponds to local strain and smaller inclusions that do not form secondary domains but otherwise impede the motion of the wall. Integrated expressions for the theoretical hysteresis loop, obtained for a simplified form of the force of a single secondary domain, are generally consistent with experiment.

* Williams, Bozorth, and Shockley, Phys. Rev. **75**, 155, 178 (1949).

R8. Dynamic Experiments with a Simple Domain Boundary in a Ferromagnetic Crystal. W. SHOCKLEY, H. J. WILLIAMS, AND C. KITTEL, *Bell Telephone Laboratories.*—Studies have been made of the Bloch wall velocities under applied magnetic fields in the ferromagnetic single crystal discussed in the preceding abstract. The wall velocity appears to be a linear function of the applied field and of the resistivity, as determined by varying the temperature. The behavior is accounted for in a quantitative way by the eddy currents induced in the crystal by the motion of the wall. The wall appears to move so that the energy input from magnetization reversal is equal to the eddy current losses. It appears that in large magnetic fields the domain wall becomes distorted and perhaps may tend to close on itself. For the case of self-closure in

large fields the radial wall velocity at radius r is given by $v=[H\rho c^2/32\pi^2 M_s r \ln(R/r)]$, where ρ is the resistivity in e.s.u., and R is the equivalent radius of the crystal cross section. For our crystal the wall velocity is roughly of the order of 3 cm/sec./oersted.

R9. Magnetic Resonance Absorption in Magnetite at Low Temperatures.* L. R. BICKFORD, JR., *M. I. T.*—The microwave resonance absorption technique, at both 1.25- and 3.3-cm wave-lengths was used to study the ferromagnetic crystalline anisotropy characteristics of magnetite, Fe_3O_4, in the vicinity of its low-temperature transition. The experiments were performed on synthetic single crystals at temperatures down to −195°C. The transition in magnetite, which occurs at ca. −160°C, is characterized by anomalous effects in specific heat, magnetization, and electrical conductivity. At temperatures above the transition, the crystalline and magnetic symmetry is cubic. The behavior of magnetite in the resonance experiments below the transition seems to indicate that the magnetic symmetry is uniaxial in this temperature region. This conclusion is consistent with the findings of other investigators. Below the transition the magnetic axis is the [100] direction most nearly parallel to a strong magnetic field which was applied to the crystal as it cooled through the transition. At temperatures not far below the transition it is possible to change the magnetic axis from one [100] direction to another by means of a strong magnetic field.

*Sponsored by the ONR, the Army Signal Corps, and the Air Force.

R10. Specific Heat Determination on Non-Metallic Ferrites.* T. R. MCGUIRE AND LOUIS N. HOWARD,** *Naval Ordnance Laboratory.*—Following a method developed by Sykes[1] the specific heat (C_H) of Ferroxcube III was determined in the temperature range from room temperature through the Curie temperature (ca 150°C) to 300°C. C_H remained constant at approximately 0.20±0.01 calories/°C g. The expected change in specific heat at the Curie temperature is 0.05 calorie/°C g based upon the reported composition of this material.[2] The sensitivity of the apparatus was such that changes of 0.02 calorie/°C g could have been detected. Specific heat data are correlated with measurements taken of the temperature variation of the intensity of magnetization and the magnetic susceptibility.

* This work was supported in part by the ONR.
** Now at Swarthmore College, Swarthmore, Pennsylvania.
[1] C. Sykes, Proc. Roy. Soc. 148A, 422 (1935).
[2] J. L. Snoek, *New Developments in Ferromagnetic Materials* (Elsevier Publishing Company, Inc., 1947), p. 91.

R11. The "Heterocharge" of Carnauba Wax Electrets. A. D. FRANKLIN, *Franklin Institute* (Introduced by C. T. Chase).—By insulating the electret material from the electrodes with sulfur disks during polarization of the electret, it has been possible to produce the "heterocharge" without the "homocharge." The decay characteristics of the "heterocharge" so produced have been studied as a function of time and temperature of polarization.

R12. Thermal Conductivity of Copper and Tin at Liquid Helium Temperatures. F. A. ANDREWS, D. A. SPOHR, AND R. T. WEBBER, *Naval Research Laboratory.*—The thermal conductivity of rods of highly pure copper (polycrystalline) and tin (single crystal) has been measured at temperatures available with liquid helium. The temperature gradient along the rods was determined by means of helium gas thermometers employed differentially. The thermal conductivity of the copper was found to increase linearly with the temperature over most of the range measured, reaching a value of 2.32 watt/cm °K at 4.0°K. This is in excellent agreement with the results of Allen and Mendoza,[1] and in accord with the theory of Makinson.[2] The temperature dependence of thermal conductivity of the tin crystal was similar to the results found by Hulum[3] for polycrystalline tin.

[1] J. F. Allen and E. Mendoza, Proc. Camb. Phil. Soc. 44(2), 280 (1948).
[2] R. E. B. Makinson, Proc. Camb. Phil. Soc. 34, 474 (1938).
[3] J. K. Hulm, Nature 163, 368 (1949).

R13. The Theory of Superconductivity.* L. TISZA, *M. I. T.*—The standard electronic theory of metals operates with a definite sequence of steps in building up the crystal. First a single electron is coupled with a periodic field, then the inter-electronic coupling is taken into account only by Fermi statistics. The addition of further coupling terms has failed to account for superconductivity. The theory to be presented uses from the outset many-electron wave functions corresponding to bond structures extending over the entire crystal. The condition of superconductivity is essentially the occurrence of quantum resonance of at least three bond structures equivalent under the translation group of the crystal. The formalism leads in a reasonable approximation to the London relation. On the basis of an empirical classification one distinguishes between hard and soft superconductors. It is noteworthy that these are located in regions of the periodic table in which the importance of covalent binding has been postulated by Hume-Rothery[1] and Pauling[2] on the basis of empirical evidence other than superconductivity.

* This work has been supported in part by the Signal Corps, the Air Materiel Command and the ONR.
[1] W. Hume-Rothery, *The Structure of Metals and Alloys* (London, 1936), p. 21ff.
[2] L. Pauling, Phys. Rev. 54, 899 (1938).

R14. Magnetic Field Penetration in Superconducting Lead. M. C. STEELE, *Naval Research Laboratory.*—The magnetic susceptibility of small superconducting lead spheres (radius $\sim 10^{-3}$ cm) has been determined by a self-inductance method. Using relations derived from the London[1] theory for reducing the data, the penetration depth, λ, is calculated for three different lead samples at 4.22°K. Results indicate that λ is $1.3\pm0.3\times10^{-5}$ cm at this temperature. It is also found that within experimental error λ is not a function of the size of the sphere. The importance of using smaller sized particles and accounting for interaction effects is emphasized if future colloid investigations are to give reliable results for testing the London theory.

[1] F. London, Physica 3, 450 (1936).

R15. Lambda-Points of Solutions of He^3 in He^4 below 1°K. J. G. DAUNT AND C. V. HEER, *Ohio State University.*—Measurements have been made of the transition (lambda) temperatures at which solutions of He^3 in He^4 first show superfluidity by observation of the thermal isolation of a vessel which contained the solutions and which was cooled to low temperature by a paramagnetic salt. The incidence of superfluidity was accompanied by a high heat influx to the solution produced by a convection of film flow to the high temperature together with return flow in the vapor phase. The solution with the highest concentration, namely 89 percent He^3, had a lambda-temperature of 0.38°K; solutions with smaller He^3 content (concentrations down to 40 percent He^3 were investigated) show higher lambda-temperatures ranging up to 1.1°K. It was concluded that pure He^3 could not be superfluid above 0.25°K and most probably is not superfluid down to 0°K. The He^3 mixture was kindly supplied by the Isotopes Division of the AEC.

R16. Superconducting Temperature of Lead. D. B. Cook, H. A. Boorse, and M. W. Zemansky, *Columbia University.**—The superconducting temperature of lead in the absence of an applied magnetic field has been observed in many laboratories by measurements of electrical resistance. In the present experiments the transition temperature was measured by an a.c. induction method which reflects changes in the permeability of a cylindrical specimen of lead used as the core of a secondary coil surrounded by a primary coil carrying an alternating current of 1000 c.p.s. Specimens were cooled from 10.3°K to their transition temperature in a cryostat utilizing desorption of helium gas from charcoal. A helium gas thermometer with large room temperature volume was used to measure temperatures to an accuracy estimated as 0.04 deg. with a sensitivity of 0.01 deg. Using lead of maximum purity obtainable the transition temperature was found to be 7.22 ± 0.04°K in good agreement with the average of the results obtained by resistance measurements. The variation of transition temperature with the intensity of an applied longitudinal magnetic field was observed and found to be in agreement with the values of Daunt.[1]

* Research sponsored by ONR.
[1] J. G. Daunt, Phil. Mag. 28, 24 (1939).

Atomic Spectra; General Optics

S1. Isotope Shift in the Lines of Pb I.* W. W. Watson and C. E. Anderson, *Yale University.*—We have extended the investigation begun by Manning[1] on the isotope shifts in the lead spectrum, using material enriched in the 204 isotope. Nine of the strongest Pb I lines in the violet and ultraviolet showing isotope structure and Pb 207 h.f.s. have been measured. For all lines with measurable structure the 204–206 interval is less than the 206–208 interval. The resonance line $\lambda 2833\ [6p^3(\frac{1}{2}\frac{1}{2})_0-6p7s(\frac{1}{2}\frac{1}{2})_1]$ and $\lambda 3639\ [6p^3(\frac{1}{2}\frac{1}{2})_1-6p7s(\frac{1}{2}\frac{1}{2})_1]$ both yield measurements unaffected by superposed 207 h.f.s. For these the ratio of the 204–206 and 206–208 intervals is 0.89 and 0.82, and the ratio of the 206–207 to the 207–208 interval is 0.69 and 0.60, respectively. Most of this splitting is attributable to the interaction with the $7S$ electron in the upper state. Splittings in the $6p6d$ levels ($\sim$0.050 cm^{-1}) indicate perturbations by $6p7s$ and $6p8s$. These Pb isotope shifts give further evidence of increasing nuclear stability in the progression 204 to 208. Some inconsistencies in the classification of certain Pb I lines also will be discussed.

* Assisted by the AEC.
[1] T. E. Manning, Phys. Rev. 76, 464(A) (1949).

S2. The Oscillator Strength for the $4s-4p$ Transition in Ca II.* L. C. Green and N. E. Weber, *Haverford College.*—A number of computations have been made of the oscillator strength or f-value for the $4s-4p$ transition in Ca II. Three fields were used to obtain the necessary wave functions: a self-consistent field, both with and without exchange, and a field of the Kramer's type. With each field, the radial integrals for the dipole moment, for two forms of the dipole momentum, and for the dipole acceleration were evaluated. Each of these radial integrals was then used to calculate two values of the oscillator strength. One value was obtained using the observed energy difference, and a second using the difference of the eigenvalues of the particular wave functions employed in computing the radial integrals. Values from the same field and values from different fields were found to be in closer agreement when the calculated, rather than the observed, energies were employed. Comparison of the various results suggests that the true value of the oscillator strength for this transition probably lies within ±0.10 of the value 1.08.

* The major part of this work was supported by the ONR, Contract No. N8 onr-570, Project No. NR 010-016.

S3. Configuration Interactions in the Pb III Spectrum. J. N. P. Hume and M. F. Crawford, *University of Toronto.*—Although the theory of configuration interactions is formulated in Condon and Shortley's *Theory of Atomic Spectra*, little has been done in the way of definite and detailed calculations of these effects. The Slater parameters were evaluated for the perturbed configurations of the two-electron spectrum, Pb III and the wave functions of 32 levels were calculated in terms of the L-S functions. The wave functions for many of these levels were found to be linear combinations of the L-S functions of two or more configurations, and precise configuration assignments were made for these levels. Using these functions excellent agreement was obtained between the calculated and observed g-values, hyperfine structure interval factors and isotope shifts. The isotope shift and the hyperfine structure interval factor for the $6S$ electron were determined as 0.50 cm^{-1} and 2.60 cm^{-1}, respectively. The isotope shifts can be accounted for on the basis of the field theory alone. The calculations indicate that the wave functions for two of the levels are slightly in error, but confirm the correctness of all the others. It is thus established that the theory is capable of an internally consistent explanation of all the spectroscopic properties.

S4. The First Spark Spectrum of Manganese. C. W. Curtis, *Lehigh University.*—The classification of approximately 700 lines of the Mn II spectrum has previously been reported.[1] These classifications include only quintet-quintet, septet-septet, and a few intersystem transitions. Recently the analysis has been extended[2] to include over 450 additional lines, most of which arise from terms of the triplet system. This system has been placed relative to the normal state, $3d^5(^6S)4s\ ^7S_3$, by numerous combinations between triplet and quintet levels. The lowest lying terms of this spectrum should arise from the $3d^6$ and $3d^54s$ configurations, and in the case of the latter be based on sextet and quartet limit structures. Of 18 septet, quinet, and triplet terms, which could result from these structures, all but the three highest have been located.

[1] Curtis, Phys. Rev. 53, 474 (1938).
[2] We are indebted to Professor M. Catalan, Ciudad Universitaria, Madrid, Spain, for furnishing unpublished data on the Zeeman patterns of certain lines critical to the analysis.

S5. Electronic Excitation of L_{III} States.* George L. Rogosa and Guenter Schwarz, *Florida State University.*—The electronic excitation of the L_{III} state of $5d$ transition elements has been measured as a function of the energy of the bombarding monoenergetic electrons. Data were taken for an energy region extending from about 30 ev below the excitation potential to 30 ev above. A double-crystal x-ray spectrometer was used as a monochromator, set to pass the peak of the $L\alpha_1$ line into a Geiger counter. The highly stabilized x-ray tube voltage was changed in steps of 2 v, and the intensity, recorded in the Geiger counter, measured at a function of the voltage. This intensity is a measure of the electronic excitation of the L_{III} state. The resulting curves show a very pronounced structure. For tantalum, for example, the intensity-energy curve shows a plateau of about 10 ev width, starting at a position of 6 ev above the excitation potential.

* This work was begun by one of us (G. S.) in 1941; interrupted by the war; and additional data obtained later at the Johns Hopkins University by G. L. R.

S6. Improved Wadsworth Mounting for a Concave Grating Spectrometer.* W. J. Taylor, G. P. Koch, and H. L. Johnston, *Ohio State University.*—A concave grating spectrometer (21 ft. radius, 15,000 lines per in.) of the Wadsworth type suitable for both photographic and photoelectric recording has been constructed. The grating which is illuminated with parallel light, is mounted on a moving beam, directly over the

main bearing about which the beam pivots. The plate, or exit slit (for photoelectric recording), is mounted on the other end of the beam, and is maintained in focus by a cam and reciprocating mechanism as the beam moves. The main component of the wave-length drive is a 10-ft. lathe bed and screw. As the screw rotates it advances a plate mounted on the lathe parallel to the incident beam of light. The plate in turn engages a roller fixed to the beam, and thus drives the latter. This mechanism produces an accurately linear wave-length scale such that one revolution of the screw represents (approx.) 23A (11.5A in the second order) over the entire range of 1800–12,000A; 1/500 revolution is significant. This design makes possible an improved method of photoelectric scanning, in which the exit slit is maintained on the normal to the grating as the beam is driven (as opposed to the use of several fixed settings of the beam).

* This work was supported in part by the ONR under contract with The Ohio State University Research Foundation.

S7. Variable Thickness Low Temperature Infra-Red Absorption Cell.* R. B. HOLDEN, W. J. TAYLOR, AND H. L. JOHNSTON, *Ohio State University.*—An infra-red absorption cell of unique design has been constructed and has proved very convenient for the study of the spectra of liquids and solids at low temperatures. The metal members on which the windows are mounted are joined by a short metal bellows, so that the separation of the windows, and therefore the sample thickness, can be varied continuously within certain limits. This motion is controlled by three micrometer screws spaced at 120° intervals around the bellows, and turned in unison by an annular gear. The windows are of AgCl, 11.5 mm thick, with a deep recess cut in the rim to allow a gasket seal and at the same time permit the flat inner faces of the windows to be brought into contact. An excellent vacuum-tight seal is obtained with Teflon gaskets and spring loading. Gases or volatile liquids are condensed into the cell through a fine metal tube soldered to the cell, and may then be frozen. The cell is suspended in an evacuated cryostat in the optical path of a Perkin-Elmer spectrometer. The sample thickness may be varied without removing the cell from the cryostate by means of a shaft which emerges through a Wilson seal.

* This work was supported in part by the ONR under contract with The Ohio State University Research Foundation.

S8. Optical Alignment of a Recording Near Infra-Red Spectrophotometer. JAMES L. LAUER, *Sun Oil Company.*—Refractive indices of an EDF-3 glass prism suitable for a Littrow-type instrument covering the region from 0.6 to 2.0μ were obtained and a cam designed for continuous scanning at a rate constant with respect to wavenumber. With mirrors and slits aligned and the prism oriented for a visible Hg emission line at which its refractive index was known, the Littrow mirror was turned through angles determined by an optical lever and the relative intensities and corresponding mirror positions of the infra-red Hg lines were found by observing the current of a PbS photo-conductive cell placed behind the exit slit. The lines were identified by comparison with benzene absorption bands. The angle of incidence on the prism was measured as the angle between a transit's telescope aligned above the prism for sighting the entrance slit through the collimating mirror and a telescope provided with a Gaussian eyepiece, rigidly mounted parallel to and below the former, lined up with the normal to a prism face. Data thus obtained yielded all the required information.

S9. A Ratio-Recording Double Beam Infra-Red Spectrophotometer Using Phase Discrimination and a Single Detector. ABRAHAM SAVITZKY AND RALPH S. HALFORD, *Columbia University.*—A simple modification will be described for converting a Perkin-Elmer infra-red spectrophotometer to double beam operation for direct recording of percent transmission *versus* wave-length. A phase discrimination system is used, requiring no changes in the optical system, and no sacrifice of versatility or ease of prism interchange. A complete spectrum over the rocksalt region may be obtained in 25 min. with good resolution, and with no attention from an operator. Samples as small as 1×6 mm can be studied. The system is readily adaptable to other spectrophotometers, including those in the visual and ultraviolet range, the only limitation being sufficiently rapid response by the detector. A Golay pneumatic detector was employed in the present application.

S10. The Diffraction Pattern in the Plane of a Circular Aperture. C. L. ANDREWS, *General Electric Research Laboratory.*—The diffraction patterns in the planes of circular apertures from one to eight wave-lengths in diameter have been measured when a plane-polarized electromagnetic wave was incident normally on the aperture. A circuital integral based on Thomas Young's theory of diffraction yields the distribution of intensity over the aperture quantitatively. A demonstration of diffraction by an aperture four wave-lengths in diameter will be given employing microwaves of 2500 Mc.

S11. Combination Two-Circle Goniometer and X-Ray Spectrometer. M. L. BARON AND A. DEBRETTEVILLE, JR., *Signal Corps Engineering Laboratories.*—A combination instrument consisting of a two-circle goniometer and x-ray spectrometer suitable for the study of crystals was designed and fabricated in Squier Signal Laboratory. A crystal can be oriented optically by using the instrument as a goniometer. X-ray techniques can then be used to study the crystal by replacing the collimator and telescope with a monochromatic x-ray beam and a Geiger counter. Absolute intensity measurements can be made by fixing the Geiger counter at twice the Bragg angle and rotating the crystal at 8° per hour from $\theta_{\text{Bragg}}-\Delta\theta$ to $\theta_{\text{Bragg}}+\Delta\theta$. Back-reflection angles of up to 160° are obtainable. The result of a test on synthetic halite (400) reflection, gave a structure factor of 12.7 compared with Max Renniger's value of 12.67.

Reactions of Transmutation; Theories of Elementary Particles

U1. Studies of Disintegrations by 14-Mev Deuterons.* M. S. LIVINGSTON, K. BOYER, H. E. GOVE, J. A. HARVEY, AND M. DEUTSCH, *M. I. T.*—The following three papers describe experimental results obtained by bombarding thin targets of many elements with 14-Mev deuterons produced in the M.I.T. cyclotron. A magnet focuses the emergent beam on a target in an observation chamber behind a 4-ft. concrete wall. Detection instruments mounted on two movable arms are used to observe angular distributions and coincidences between nuclear radiations. A triple-coincidence proportional ionization chamber with variable aluminum absorber gives differential number-range curves for charged particle products. Protons and alphas are identified uniquely and with zero background even for ranges shorter than scattered deuterons. Group structure is observed for all targets. Amplifiers, coincidence circuits, and recording instruments are arranged to record the data rapidly and automatically. Crystal counters for gamma-rays and chambers to detect recoil nuclei are used in coincidence with the proton counter. Studies are in progress of nuclear excitation levels indicated by the proton and alpha-groups, of the variation in angular distribution of individual groups, of coincidences between proton groups and gamma-rays and on the protons of low energy which have anomalously high intensities.

* Assisted by the Joint Program of the AEC and ONR.

U2. The Energy Spectrum of Protons from (d, p) Reactions.* KEITH BOYER, *M. I. T.*—The proton energy spectra resulting from 14-Mev deuteron bombardment of thin targets have been determined for many elements randing from Be^{9} to Be^{209}. Considerable group structure is evident for most of the elements studied in energy regions corresponding to both bound and virtual levels. In the heavier elements the energy resolution is not sufficient to determine whether most of the groups are due to one or two individual levels, or to fluctuations in level density. However, where checks could be made against levels known from γ-ray transitions induced by slow neutron capture, the higher energy proton groups were found to correspond to no more than three levels. In the lighter elements the groups were well resolved and could be identified with individual levels. Eight levels were found in $Be^{9}(d, p)Be^{10}$ having an average separation of about 1.2 Mev. The two lowest levels had excitation thresholds of about 7 Mev explaining why they have not been found previously. A level at 1 Mev was definitely established in $C^{12}(d, p)C^{13}$. An unexpectedly large number of low energy protons was found especially in the heavy elements. For elements in the region of gold the distribution had a broad maximum at about 5 Mev when viewed at 90°.

* Assisted by the Joint Program of the AEC and ONR.

U3. Angular Distributions of Protons Emitted in Reactions Induced by 14-Mev Deuterons.* HARRY E. GOVE, *M. I. T.*—Protons are found to be concentrated in the forward direction in all elements studied. The ratio of intensity at 20° to that at 135° varies from 10 to 50. This is interpreted as being associated with the stripping process. In addition for light elements such as C, Al, and Ni in which individual groups can be resolved, the number of protons in a given group, in some cases, shows maxima at various angles. It is assumed that these sharp angular maxima are associated with the unique nuclear energy state in which the neutron was left initially. Present theory of the stripping process is inadequate to explain such maxima. In heavier elements in which the proton spectrum is continuous, the angular variation of segments of the spectra was measured. It is observed in general that the distribution is more strongly forward for higher energy protons. The reaction $Au^{197}(d, p)$ shows the number of protons rising from 30° to a rather broad peak about 60° and dropping off toward back angles independent of proton energy.

* Assisted by the Joint Program of the ONR and AEC.

U4. Neutron Binding Energies from (d, p) Reactions.* J. A. HARVEY, *M. I. T.*—Q-values have been determined for the maximum energy proton group from (d, p) reactions in many elements. The targets in general were 0.5 mil thick. The energy loss for deuterons was obtained by inserting the target in the deuteron beam; the target thickness for protons by the range reduction of a known high energy proton group. Accepting the aluminum ground state group Q-value as 5.50 Mev, tentative Q-values (in Mev) for a few target elements where the highest energy proton group is well resolved are: Pb^{206}(4.48), Pb^{207}(5.14), Pb^{208}(1.70), Bi^{209}(1.95), Fe_{s}^{4}(7.1), Fe^{56}(5.4), Ni^{58}(6.8), Zr^{90}(5.0), Zr^{91}(6.5). In order to identify the highest energy group observed with the ground state of the residual nucleus, coincidence studies were made between protons and γ-rays for the lighter elements. Also the bismuth and lead Q-values correspond to ground state groups, since their sum agrees with the value (13.6 Mev) calculated from radioactive decay energies. Neutron binding energies computed from the Q-values are compared to previous experimental results and theoretical predictions.

* Assisted by the Joint Program of the AEC and ONR.

U5. On the Self-Stress of the Electron. S. BOROWITZ, W. KOHN, AND J. SCHWINGER, *Harvard University.*—It is known that the vanishing divergence of the stress tensor of an electron interacting with the vacuum electromagnetic field implies formally a vanishing self-stress. Nevertheless, previous calculations[1] have led to a finite value for this quantity. This result arises as a consequence of the ambiguities which accompany the divergences of quantum electrodynamics. It has been possible to resolve the difficulty in the following way: The divergence of the second-order correction of the stress-tensor can be written as the difference of two similar non-convergent momentum integrals, which are related by a translation in the momentum variable. To retain a divergenceless stress tensor it is necessary to impose the rule that such integrals shall be invariant under a momentum translation. This rule is simply an expression of gauge invariance. On calculating the self-stress one encounters the integral of a gradient in momentum space. This may be regarded as the difference of two integrals, of the same nature as those above and differing by an infinitesimal translation. According to our rule, therefore, the self-stress vanishes. It may be noted that any theory compatible with gauge invariance which makes the integrals convergent will automatically lead to a null result for the self-stress.

[1] A. Pais and S. T. Epstein, Rev. Mod. Phys. 21, 445 (1949).

U6. On the Dirac Theory of Spin ½ Particles and Its Non-Relativistic Limit. L. L. FOLDY, *Case Institute of Technology,* AND S. A. WOUTHUYSEN,* *University of Rochester.*—By a canonical transformation a representation of the free-particle Dirac theory is obtained in which positive and negative energy states are separately described by two-component wave functions. Playing an important role in this representation are new operators for position and spin of the particle. The components of the time derivative of the new position operator all commute and have for eigenvalues all values between c and $-c$. The new spin operator is a constant of the motion unlike the conventional spin operator. By a comparison of the new Hamiltonian with the non-relativistic Pauli Hamiltonian for spin ½ particles, one finds that the new rather than the conventional operators pass over into the position and spin operators in the Pauli theory in the non-relativistic limit. The transformation to the new representation is also made in the case of interaction with an external electromagnetic field, and yields essentially the Pauli Hamiltonian in the non-relativistic limit. An examination of the relationship between the new and conventional position operator casts some light on the question of why a Dirac electron shows electromagnetic properties characteristic of a particle of finite extension. This work was supported at Case by the AEC and at the University of Rochester by the Joint Program of ONR and AEC.

* Now at University of Amsterdam, Amsterdam, Netherlands.

U7. Relativistic Model of a Finite-Sized Electron. G. J. YEVICK, *Stevens Institute of Technology.*—The Lagrangian formulation of quantum mechanics developed by Feynman[1] not only furnishes a basis for the Feynman prescription for calculating electron-photon processes but also constitutes one possible framework from which future theories may arise. This framework is more general than the Hamiltonian formalism. As an illustration we have considered a new model of a finite-sized electron suggested to us by some recent work of Yukawa's (unpublished) on non-local fields. (We have been unable as yet to obtain a connection between Feynman's methods as applied to this model and Yukawa's theories.) For our model, the basic idea is that the classical charge-current density of the electron exists only along its velocity four-vector. Unlike the Feynman and Mc Manus model, the charge-current density is localized in a small region of space-time. It also differs from the model recently proposed by

Bohm and his collaborators[2] in that there are no internal degrees of freedom. This makes it much simpler to handle. Quantization is achieved by formally using the Lagrangian method of Feynman.

[1] See Ann Arbor Summer Symposia Notes (1949).
[2] Bohm, Weinstein, and Kouts, Phys. Rev. 76, 867 (1949).

U8. Interaction between Elementary Particles. ALFRED LANDÉ, *Ohio State University.*—A finite self-field for classical particles was obtained[1] from $c^2t^2-r^2=a^2$ as the basic communication law through which the point center surrounds itself by a Maxwell or meson potential. The same communication law leads to equations of motion for a system of particles, derivable from a least action principle which is a generalization of that described by Feynman.[2] However, instead of a more or less arbitrary smoothed out δ-function representing the "structure" of the particle, the variation principle involves an exact δ-function with shift of origin. The vacuum Maxwell or meson field equations are thereby secured everywhere without exception, and the result is a consistent *unitary theory* of interaction at a distance between particles including finite self-reaction; the field plays the role of an auxiliary scheme only. Translation into quantum theory involves a ψ-function dependent on the individual time coordinates of the various particles as well as on their space and spin coordinates.

[1] A. Landé, Phys. Rev. 76, 1176 (1949).
[2] R. P. Feynman, Phys. Rev. 74, 939 (1948).

U9. The Self-Energies of Electrons and Photons. HARTLAND S. SNYDER,* *Brookhaven National Laboratory.*—It has generally been supposed that the self-energy of an electron as determined by the application of perturbation theory to the interaction of the electron-positron field with the electromagnetic field is necessarily infinite. However, by the use of appropriate limiting procedures one can make both the electron and photon self-energies vanish in order α. The procedure used is relativistically invariant. A paper concerning these matters is being prepared for publication.

* Work performed at Brookhaven National Laboratory under the auspices of the AEC.

U10. Covariant Description of Extended Charges. D. BOHM, M. WEINSTEIN, AND H. KOUTS, *Princeton University.*—A simple relativistic description of an extended charged particle can be obtained by specifying the charge-current distribution in the rest system as a function of the proper time. If one requires the distribution to be spherically symmetric in the rest system, charge-current is not conserved. To obtain conservation one must add a spinlike term which takes into account the Lorentz transformation which the rest system undergoes when the particle is accelerated.* The equations of motion have been investigated and it was found that self-acceleration does not take place provided that the non-electromagnetic mass is greater than $\frac{1}{3}$ the electromagnetic mass. In the linear approximation one finds the same self-oscillations that occur in the non-relativistic theory.** The theory is not causal in the most restricted sense, but all features of causality required to provide a consistent description of the relation between past and future are retained if the acceleration in the rest system is limited to be less than C^2 divided by the radius of the particle.

* Bohm, Weinstein, and Kouts. Phys. Rev. 76, 867 (1949).
** D. Bohm and M. Weinstein, Phys. Rev. 74, 1789 (1948).

U11. Isobaric State of Nucleon. R. E. MARSHAK, *University of Rochester.*—Recent evidence for highly multiple meson and gamma-production in a large star[1] (R-star) favors the pseudoscalar field for the π-meson. When this evidence is coupled with the low cross section found for the scattering of π-mesons by nucleons,[2] one is tempted to return to the strong coupling formulation as an explanation of both phenomena.[3] Using symmetric pseudoscalar strong coupling theory,[4] one obtains a unique nucleonic scource size $a\sim 0.3\ \hbar/Mc$ (M is the nucleon mass) from the scattering data. Using the same theory for the multiplicity of meson production,[5] one obtains $g^2/\hbar c\sim 0.1$ from the data on the R-star.[1] These numbers lead to an excitation energy of $2\mu c^2$ (μ is the π-meson mass) for the lowest isobaric state of the nucleon. The isobaric excitation energy is very sensitive to the multiplicity N ($\sim N^{-3}$) but even a value greater than μc^2 need not exclude observation of an isobaric state.[6]

[1] Kaplon, Peters, and Bradt, Phys. Rev. 76, 1735 (1949); Marshak, Phys. Rev. 76, 1736 (1949).
[2] Fretter, Phys. Rev. 76, 511 (1949).
[3] Oppenheimer and Schwinger, Phys. Rev. 60, 150 (1941).
[4] Pauli and Dancoff, Phys. Rev. 62, 85 (1942).
[5] Lewis, Oppenheimer, and Wouthuysen, Phys. Rev. 73, 127 (1948).
[6] Tomonaga, Prog. Theor. Phys. 1, 109 (1946).

U12. On the Electromagnetic Interaction of Mesons of Zero Spin. F. ROHRLICH, *Cornell University.*—The convergence of the interaction of a scalar (pseudoscalar) meson field with the electromagnetic field has been investigated. A sufficient condition for the convergence of the nth order term in the scattering matrix is: $E\geq 5$ (if $n\geq E$) or $2E-n\geq 5$ (if $n\leq E$). E and n are the number of external lines and corners of the corresponding Feynman diagram. It follows that there are at most seven primitive divergent diagrams. One of them, the scattering of light by an external field to third order, vanishes identically due to an obvious extension of Furry's theorem to bosons. The remaining six diagrams are: the meson self-energy, vacuum polarization, the Lamb-shift, Compton-effect and Møller-interaction both to fourth order, and the scattering of light by light. The last process is found to be finite due to cancellations. The other processes can be shown to be finite when mass and charge are properly renormalized, *except for the fourth order Møller-interaction which remains logarithmically divergent.* Similar to the scattering of mesons by mesons via virtual nucleons this divergence can only be removed if a fourth order direct interaction is added to the Hamiltonian.

U13. Quantization of Wheeler-Feynman's Electrodynamics. F. J. BELINFANTE AND J. S. LOMONT, *Purdue University.*—Even if W.-F.'s electrodynamics does not directly describe photons, one might perhaps hope to describe nature by mere quantization of the *electronic* field in it, treating for instance a Compton effect as an initial transition of an excited atom to its ground state, subsequent acceleration of a free electron and final exciting of an "absorber" atom. A quantized W.-F. electrodynamics does not seem possible simultaneously in Heisenberg *and* in interaction representation. One might formulate a variational principle equivalent to W.-F.'s assumptions, for a quantized field $\psi(x, y, z, t)$, in *Heisenberg* representation, using anticommutativity and arrangement of factors for excluding self-interactions. This leads to a Dirac equation for ψ with interaction terms instead of a potential four-vector in it. However, it probably cannot be consistent with the canonical anticommutation relations in more than one Lorentz frame, so that we drop this theory for lack of relativistic covariance. As positon theory requires use of $\psi=\psi^{(+)}+\psi^{(-)}$, while this splitting of ψ is invariant in interaction representation only, one might perhaps hope better results in interaction representation. The generalized Schrödinger equation for $\Psi[\sigma]$ describing such quantized W.-F. theory, however, cannot be expected to be integrable.

Molecular Spectroscopy, Microwave and Infra-Red

V1. Nuclear Quadrupole Coupling and Ionic Character of Molecules.* C. H. TOWNES AND B. P. DAILEY, *Columbia University.*—The nuclear quadrupole coupling of Cl^{35} in a

TABLE I.

Molecule	Electronegativity difference Cl−X	Cl^{35} Quadrupole coupling constant (megacycles)	Percent ionic character
ICl	0.6	−82.5	9
FCl	−1.0	−146.0	25
TlCl	1.7	−15.79	82
NaCl	2.1	0±1	≥97

molecule can be shown to be rather directly related to its coupling in the atomic state and to the nature of its molecular bond. If the Cl is negatively ionic, the quadrupole coupling is small because the charge around the Cl nucleus is essentially spherical; if the Cl is positively ionic, the coupling is large because two electrons rather than only one are missing from a complete shell. Quadrupole coupling constants for the four diatomic molecules in Table I allow determination of the importance of ionic structures and hence a fairly complete curve of ionic character *versus* electronegativity difference for this type of molecule. Values of ionic character are consistently higher than those usually derived from dipole moments. Since quadrupole coupling is more simply related to ionic character than are dipole moments, these values are probably more reliable.

* Work supported jointly by the Signal Corps and ONR.

V2. Determination of Double-Bond Character from the Microwave Spectrum of Planar Asymmetric Top Molecules with a Quadrupolar Nucleus. J. H. GOLDSTEIN, *Emory University*, AND J. K. BRAGG, *Cornell University*.—Under certain simplifying assumptions there may be derived, from the pure rotational spectrum of an asymmetric top molecule containing a nuclear electric quadrupole, the quantity $\Delta = eQ(\partial^2 V/\partial\xi^2 - \partial^2 V/\partial\eta^2)$, where ξ and η are axes perpendicular to the bond to the quadrupolar nucleus and V is the electrostatic potential at this nucleus. If the molecule is planar and ξ lies in the plane, deviations of Δ from zero give a quantitative measure of the double-bond character of the bond to the nucleus, as formulated in atomic orbital theory. This measure is independent of other properties of the bond. For the two molecules for which Δ has so far been obtained, CH_2CHCl[1] and CH_2CFCl[2], the results are 4 and 5 percent double-bond character, respectively.

[1] J. H. Goldstein and J. K. Bragg, Phys. Rev. **75**, 1453 (1949).
[2] Bragg, Madison, and Sharbaugh (to be published).

V3. Centrifugal Distortion in the Formaldehyde Molecule.* RICHARD B. LAWRANCE, *M. I. T.*—The theory of rotation-vibration interaction and centrifugal distortion in non-rigid molecules[1] has been in existence for nearly 14 years but has not heretofore been successfully subjected to experimental verification. The pure rotation spectrum of formaldehyde H_2CO contains within the easily accessible microwave region a large number of lines (30) and participating J-values (zero through 30). We have looked for and observed 17 of these transitions, as well as six lines in the $H_2C^{13}O$ spectrum. We have developed a simple distortion-correction formula for the special case of $\Delta J=0$, $\Delta K=0$ transitions in molecules of small asymmetry parameter δ, and obtain a very good fit. Our distortion corrections and rotational constants thus constitute an independent experimental determination which can be critically compared with the values obtained from the Wilson-Howard theory using infra-red force constants. The agreement is quite satisfactory.

* This work has been supported in part by the Signal Corps, the Air Materiel Command and ONR.
[1] E. B. Wilson, Jr. and J. B. Howard, J. Chem. Phys. **4**, 260 (1936).

V4. The Rotational Spectrum and Molecular Structure of PCl_3.* P. KISLIUK AND C. H. TOWNES, *Columbia University*.—The $J=4\rightarrow5$ transition has been observed in PCl_3 for all four of the isotopic combinations of chlorine. Theory shows that each line is split into several hundred hyperfine components by the chlorine quadrupole coupling.[1] Complete solution of the resulting pattern would be very time consuming, but the observed structure of three broad lines in PCl_3^{35} can nevertheless be qualitatively understood. The center of the patterns for PCl_3^{35} and PCl_3^{37} are at 26,171 and 24,875 megacycles respectively. Even without solving the hyperfine structure the molecular parameters can be calculated with reasonable accuracy. For the P–Cl distance one obtains 2.044±0.01 A and for the Cl–P–Cl angle 99° 56′±1°.

* Work supported jointly by the Signal Corps and the ONR.
[1] R. Bersohn, Thesis, Harvard University, 1949.

V5. The Microwave Spectrum of CH_3SiF_3. H. T. MINDEN, J. M. MAYS,* AND B. P. DAILEY, *Columbia University*.—H. S. Booth and R. W. Morrow have kindly prepared for us a sample of CH_3SiF_3, the microwave spectrum of which we have investigated. The $J=2-3$ and the $J=3-4$ pure rotational transitions of this symmetric top molecule have been observed at 22,295 mc and at 29,727 mc, respectively. The spectrum is very similar to that of CH_3CF_3.[1] In the $J=2\rightarrow3$ transition three lines about 10 mc apart are detectable, a fourth very weak line was observed about 20 mc higher than the strongest line. Five lines about 20 mc apart were observed for the $J=3\rightarrow4$ transition. All lines showed the typical Stark effect for a $\Delta J=1$, $\Delta K=0$ symmetric rotor transition. The most intense lines in each group is assigned to the ground state of torsional vibration. The succeeding lines decreasing regularly in intensity and frequency are assigned to excited torsional levels. The intensity ratios for the various lines give the energy separations through the relationship $I_1/I_2=\exp(h\nu/kT)$. The increase in the degenerate moment of inertia in the excited torsional states is tentatively explained by the repulsion of the C−H and Si−F bonds as the molecule twists away from the torsional equilibrium position.

* Eastman Kodak Fellow.
[1] Dailey, Shulman, and Minden, Phys. Rev. **75**, 1319 (1949).

V6. Microwave Transitions between *l*-Type Doublets of HCN.* R. G. SHULMAN** AND C. H. TOWNES, *Columbia University*.—A new type of transition involving *l*-type doubling has been observed in the linear molecule HCN. A search of the HCN spectrum was made in an attempt to find the rotational spectrum of the dimer $(HCN)_2$. No lines caused by the dimer appeared, but five lines were found between 9000 and 36,000 Mc. The frequencies, Stark effects and intensities are those to be expected from transitions between the split *l*-type doublet levels of quantum numbers $v_2=1$, $J=6$, 8, 10, 11 and 12 and $\Delta J=0$. Frequencies are given by $\nu=q(1+\epsilon J)J(J+1)$ where the ordinary *l*-type doubling constant $q=223.549$ Mc and ϵ, which is of the order B/ω_2, represents a small deviation from the form hitherto assumed for *l*-type doubling. The HCN dipole moment for this vibrational state, $v_2=1$, was found to be 2.957±0.025 Debye units from the Stark splitting.

* Work sponsored jointly by the Signal Corps and ONR.
** Present address: Chemistry Dept., California Institute of Technology.

V7. Pressure Shift and Broadening in Micro-Wave Spectra. A. G. ROUSE, A. V. BUSHKOVITCH, L. C. JONES, C. A. POTTER, AND W. F. SULLIVAN, *Saint Louis University*.—The microwave spectrograph employed has two absorption cells, and the absorption line for each cell is displayed alternately on an oscilloscope by means of an electronic switch. The pressure in one cell is maintained at a low constant value, the pressure in the other cell is varied or a foreign gas added. Half widths and shifts were measured by superimposing pips on the trace corresponding to a known frequency difference. Effects of polar and non-polar foreign gases have been studied.

V8. Absorption of Millimeter Waves in ND_3.* J. H. N. LOUBSER** AND J. A. KLEIN, *Columbia University.*—The inversion spectrum of ND_3 has been examined at pressures near one atmosphere in the frequency range 24,000–145,000 mc. The first excited vibrational state ($v_2=1$) produces a resonance at 117,000 mc compared with the infra-red value of 102,000 mc and a theoretically calculated value of 83,000 mc. Measurements of the shape of the absorption curve caused by inversion in the excited state show that the fine structure is considerably more widely spaced than in the case of the NH_3 ground state inversion. At 24,000 mc almost the entire absorption of 3.4×10^{-3} cm^{-1} at atmospheric pressure is due to the tail of the ND_3 ground state inversion which (theoretically) occurs near 4000 mc. The ratio of the line breadth parameter of ND_3 to that of NH_3 is 0.88 which is close to the expected ratio of collision frequencies assuming identical cross sections. The millimeter waves were obtained from magnetron harmonics and measurements made essentially as previously described,[1] except that silicon crystals were found to give satisfactory detection down to wavelengths as short as 1.6 mm and were used to some extent.

* Work supported jointly by the Signal Corps and the ONR.
** Carbide and Carbon Post-Doctoral fellow in physics.
[1] J. H. N. Loubser and C. H. Townes, Phys. Rev. 76, 178 (1949).

V9. The Infra-Red Spectra of Crystalline Ammonia and Deutero-Ammonia. D. F. HORNIG AND F. P. REDING, *Brown University.*—The infra-red spectra of thin sublimed films of crystalline NH_3 and ND_3 were studied at −190°C. Sharp bands for NH_3 were observed at 528 (medium), 1059 (strong), 1642 (m) 3223 (m) and 3380 (s) cm^{-1}. The regions 1360–1670; 3100–3360 cm^{-1} contain broad superimposed bands with maxima at 1410, 1500, 1590, and 3297 cm^{-1}. Further broad bands were found at 1840, 2120 and 3536 cm^{-1}. Sharp bands for ND_3 were observed at 819 (s), 1196 (m), 2318 (m), and 2502 (s) cm^{-1}. Since the films of ND_3 were very thin, there was only slight evidence of broad bands. In crystals fundamentals are sharp while combinations and overtones may be broad; if the sharp lines in both spectra are assigned in the previous order to ν_5 (the torsional oscillation perpendicular to the figure axis), ν_2, ν_4, ν_1, and ν_3, the fundamental frequencies are close to those of the gas and the frequency ratios between NH_3 and ND_3 are reasonable. The more diffuse bands require detailed consideration of crystalline interaction, but it seems likely that the spectrum is consistent with a crystal composed of simple molecules, contrary to suggested interpretations of the Raman spectrum.[1]

[1] G. B. B. M. Sutherland, Proc. Roy. Soc. (London) 141A, 546 (1933).

V10. Infra-Red Spectra for Single Crystals of Ammonium Nitrate and Thallous Nitrate in Polarized Radiation. RALPH S. HALFORD AND ROGER NEWMAN, *Columbia University.*—Infra-red spectra have been obtained for thin sections from single crystals of NH_4NO_3(IV), NH_4NO_3(III) and $TlNO_3(\gamma)$ in radiation polarized successively along different crystal axes. Spectra for the first two crystals show (1) that absorptions attributable to molecular modes of nitrate ion are strongly polarized in directions predicted by the general theory[1] of crystal spectra; (2) that envelope structure resulting from combinations between lattice modes and molecular modes is present but not uniquely polarized, again in agreement with general theory;[1] (3) that absorptions attributable to ammonium ions appear to be unpolarized, indicating that these ions are disordered from rotation or other causes. Spectra for the third substance can be used to complete the determination of its crystal structure. One band for this substance has a remarkable envelope structure consisting of a strongly polarized central branch and, at room temperature, three pairs of symmetrically distributed, virtually unpolarized satellites. At −160°C there are no less than seven distinct satellites on the high frequency side with damped out counterparts on the low frequency side.

[1] H. Winston and R. S. Halford, J. Chem. Phys. 17, 607 (1949).

V11. Intermolecular Forces in Benzene, VERNON MYERS, *Pennsylvania State College.*—The long range attractive forces between benzene molecules are computed from optical dispersion data, and the short range repulsive forces are estimated from the known deviations from the perfect gas law.[1] If the repulsive forces are approximated by a hard sphere model with a molecular diameter of 4.52A, the difference between the experimental and calculated second virial coefficient is approximately −3 percent at 318°K and 3 percent at 358°K. When the repulsive forces are represented by $C\exp(-R/0.28A)$ with the potential minimum at 4.45A, the discrepancy is reduced to about −2 percent at 318°K and 0.5 percent at 358°K. The depth of the potential minimum for the hard sphere assumption is −0.11 ev while the depth for the exponential repulsion is −0.078 ev.

[1] Lambert, Roberts, Rowlinson, and Wilkinson, Proc. Roy. Soc. 196A, 113 (1949).

Semi-Conductors; Phosphors; Miscellany in Solid-State Physics

W1. Recovery of Selenium Rectifiers after Passing of Short Current Pulses. K. LEHOVEC, *Signal Corps Engineering Laboratories.*—The impedance of a selenium rectifier is changed after a current pulse in the blocking direction has passed through it. The pulses discussed in this paper were kept so small that the change in impedance was fully reversible. The dependence of this change on recovery time was studied for pulses of various lengths (0.05–300 sec.) and of various heights (0.05–0.5 mA/cm^2) at different temperatures. It was found that the change in impedance was nearly independent of pulse length for a given pulse height if a certain threshold length was exceeded. The product, threshold length times pulse height is found to correspond to 3×10^{14} electrons per cm^2. The recovery time decreases rapidly with increased temperature. Possible alternate explanations of the discussed observations are mentioned based on trapping of carriers in the barrier layer, and on the migration of ions.

W2. Microwave Conductivity of Semiconductors.* RICHARD F. GREENE** AND SOL E. HARRISON, *University of Pennsylvania.*—A method has been devised for measurement of the dielectric constant and conductivity, ($10^{-4}<\sigma<10$ ohm^{-1} cm^{-1}, at 3 cm wave-length), of semiconductors. A thin cylinder of semiconducting material is inserted into the center of a rectangular wave guide parallel the electric field of the TE_{10} mode, and the input impedance of the guide is measured. The measurement is made by a balanced bridge method using magic tees, and the calculation of impedance involves only measurements of plunger displacements. Using a method of Schwinger's the relation between the input impedance and the dielectric constant and conductivity has been calculated for the above geometry. In semiconductors at this frequency the displacement current may be comparable to the conduction current, rendering conventional treatments of the problem inapplicable. It was also necessary to examine critically the bearing of relaxation time, surface conductivity, sample thickness, and skin effect.

* Supported in part by the Bureau of Ships.
** John F. Frazer Fellow.

W3. Conductivity and Hall Coefficient of Zinc Oxide Semiconductor.* E. E. HAHN** AND P. H. MILLER, JR., *University of Pennsylvania.*—The dark electrical conductivity, σ, and Hall coefficient, R, of sintered spectroscopically pure zinc

oxide powder samples are measured over a temperature range from 83°K to 625°K using both the usual d.c. potentiometer probe method and an a.c. (4000 c.p.s.) set; the circuit and advantages of the a.c. set are described. In this reproducible range, $\ln \sigma$ is not linear with $1/T$ but exhibits a maximum occurring at higher T and σ-values the higher the sintering temperature. R is negative and the Hall data can be fitted by $R=(1/\rho)\exp(E/kT)$ where ρ and E increase with sintering temperature. Analysis of the electronic carrier concentration, calculated from Hall data, indicates non-degenerate extrinsic conduction due to thermal excitation of donators lying about 0.04 ev below the conduction band. The donators are believed to be interstitial zinc atoms formed during the sintering process and whose concentration increases with higher sintering temperatures; the lattice spacing increases after sintering.

* Work supported by Bureau of Ships.
** Now at RCA Laboratories, Princeton, New Jersey.

W4. Some Electrical Properties of Zinc Oxide Semiconductor.* P. H. MILLER, JR. AND E. E. HAHN,** *University of Pennsylvania.*—Impedance measurements of sintered zinc oxide samples as a function of frequency show that the conductivity is frequency dependent ($\nu \sim 10^7$ c.p.s.); it is shown that the conductivity is determined by grain boundary layers while the Hall coefficient is determined by the grains,[1] leading to spurious low conductivity and carrier mobility values when measured and calculated by the usual methods. Conductivity measurements are made from room temperature to 1040°K using the a.c. voltmeter-ammeter method. Above 650°K the logarithm of conductivity *versus* inverse temperature is linear and is similar to the results of previous workers; the frequency effect in this range is considered negligible since the conductivity is believed to be intrinsic, arising from thermal excitation of electrons from the filled to the conduction band. This thermal gap is about 2 ev and corresponds to the ultraviolet optical absorption edge at 3.2 ev; the yellow coloring of worked or good conducting samples is attributed to a shift, caused by strains, of this absorption edge into the visible.

* Work supported by Bureau of Ships.
** Now at RCA Laboratories, Princeton, New Jersey.
[1] Hahn, Russell, and Miller, Phys. Rev. 75, 1631 (1949).

W5. Low Temperature Instability of Germanium. G. T. JACOBI AND W. C. DUNLAP, JR., *General Electric Company.*—Certain samples of germanium, when heated from 0°C to 200°C and then quenched to 0°C, do not revert to their original conductivity, but assume a higher value, followed by exponential decay to the original value. Hall effect measurements indicate a thermal excitation of electronic carriers at the higher temperatures. These carriers return to the normal state only after a period of time. The "excess" conductivity is in some cases two or three times the equilibrium conductivity at 0°C. Time constants for six samples showing this effect ranged from 44 to 93 hr. at 0°C. One finds that the density of active carriers is roughly $n_a = A\exp(-\Delta E/kT)$, where $A \sim 10^{21}$/cm³, $\Delta E \sim 0.5$ ev. The time constant τ for the relaxation process was found to obey a similar relation $\tau = \tau_0 \exp(+\Delta F/kT)$ with $\tau_0 \sim 10^{-8}$ sec., $\Delta F \sim 0.5$ ev. The effect apparently can be produced by cooling N-type ingots from the melting point to room temperature in about an hour. A discussion is given of the source of these effects, especially the hypothesis that there are adjacent states of impurity atoms that are easily convertible into each other. One of these states may be active, the other inactive, or one may lead to donor, the other to acceptor action.

W6. The Optical Band Width of *F* Centers at Liquid Helium Temperatures. E. BURSTEIN AND J. J. OBERLY, *Naval Research Laboratory.*—Theory[1] suggests that the width of the absorption bands of F centers, electrons trapped in negative ion vacancies, should be proportional to the square root of the absolute temperature. Previous measurements by Mollwo[2] down to liquid hydrogen temperatures indicated, however, a finite residual band width at low temperatures. Measurements have now been repeated and extended to liquid helium temperatures confirming Mollwo's observations. For example, a band width of 0.17 ev is observed in both annealed and unannealed KCl at liquid helium temperatures. It is suggested that the finite width of the F center bands at low temperatures is due to the existence of a distribution of frequencies which results from variations in the configuration about the F center brought about by the random distribution of vacancies, aggregates of vacancies and impurities in the crystal.

[1] N. F. Mott and R. W. Gurney, *Electron Processes in Ionic Crystals* (Oxford, 1940), p. 116.
[2] E. Mollwo, Zeit. f. Physik 85, 56 (1933).

W7. Trapping in Zinc-Sulfide-Type Phosphors.* RICHARD H. BUBE, *Radio Corporation of America and Princeton University.*—The phenomena of luminescence have been used to investigate the nature of trapping in ZnS-type phosphors. Measurements of thermostimulated emission (glow curves) and of the decay of phosphorescence emission were obtained for temperatures between −196° and 200°C for samples of cubic and hexagonal ZnS:Cu(0.0–0.3), [NaCl(2)], specially prepared from pure ZnS with no spectroscopically detectable impurities, and for other samples of ZnS-type phosphors. Traps of 16 different depths from 0.20 to 0.75 ev were identified from the glow peaks found for temperatures above −160°C. Comparison of the glow curves shows that if traps of a given depth are present, they are present with the *same* depth in *all* ZnS-type phosphors, regardless of activator, presence or absence of NaCl in the preparation, or the crystal form. It is concluded that traps are located at substitutional sites, principally omission defects, in ZnS-type phosphors, because a study of the nature of crystal defects in ZnS-type phosphors shows that only substitutional sites have the required invariance to account for the experimental results. An hypothesis concerning the correlation between trap depth and type of omission defect is advanced. Other effects of trapping, including retrapping of electrons, have been studied.

* Work done on Contract between ONR and RCA.

W8. Determination of Stresses in Evaporated Metal Films.* R. W. HOFFMAN AND E. C. CRITTENDEN, JR., *Case Institute of Technology.*—The internal macrostress in evaporated metal films has been measured directly by observing the change in curvature of a thin substrate strip. The "beam constants" of the substrate strip were determined by loading with a known force. Deposition at elevated surface temperature introduces a stress, in addition to the intrinsic film stress, through differential expansion of the film and the substrate. These two stress types were separated by observation of the substrate deflection as a function of temperature for small temperature changes. Stress relief due to curvature of the substrate and effects of cross curvature have been evaluated. Fe, Co, and Ni films have been prepared using soft glass approximately 0.002 in. thick as a substrate material. Film thicknesses were determined from the saturation magnetization of the specimens. The intrinsic stress observed for cobalt deposited at 200°C at a rate of 0.01 mg/cm²/min. is 3×10^9 dynes/cm² tension and is independent of thickness in the range studied (1000–4000A). The differential expansion stress is 1.5×10^9 dynes/cm² tension. The stresses for iron and nickel under these conditions are the same order of magnitude.

* This work supported by the ONR.

W9. The Relation of Stress and Rupture in Evaporated Metal Films to Distortion Decay.* E. C. CRITTENDEN, JR. AND R. W. HOFFMAN, *Case Institute of Technology.*—The

intrinsic tensile stress in evaporated films of Fe, Co, and Ni, determined by the method of the preceding abstract, is found to undergo irreversible increase by as much as 100 percent when films deposited in the range of 80°C to 200°C are aged at temperatures above their deposition temperatures. The electrical conductivity also increases irreversibly during such an aging. This indicates that distortions of the type described by Vand[1] decay with a decrease in volume for these metals. The density of distortions indicated by stress and electrical resistance increases both with decreased surface temperature during deposition and with increased rate of deposition. This is consistent with a temperature sensitive surface mobility of arriving metal atoms. Application of these principles makes it possible to control the film tension within certain limits. Rupture has been observed during aging at elevated temperatures of films deposited below 100°C. Long delayed rupture has been observed for similar films aged at room temperature. It seems likely that the commonly observed limiting thickness for rupture results from the tensile force generated by this mechanism.

* This work supported by the ONR.

[1] V. Vand, Proc. Phys. Soc. 55, 222 (1943).

W10. Quantitative Prediction of Grain Boundary Energies by Anisotropic Dislocation Theory. W. T. Read (*Introduced by W. Shockley*), *Bell Telephone Laboratories.*—Dislocation models of grain boundaries between crystallites having a small angle of misfit, θ, have been proposed and the grain boundary energy calculated from two-dimensional isotropic elasticity.[1] This paper illustrates methods of joining two cubic crystals by appropriate dislocation arrays and presents the results of calculations based on anisotropic elasticity. The energy is $E_0\theta[1-\ln\theta/\theta_m]$ where the angle, θ_m, of maximum energy depends on the inelastic energy near the dislocation and must be determined from experimental data and E_0 is uniquely determined by the dislocation model in terms of the three elastic constants c_{11}, c_{12}, c_{44}. For a symmetrical boundary with relative rotation of the adjoining grains about the [100] axis E_0 is $[(c_{11}+c_{12})a/4\pi][(c_{11}-c_{12})c_{44}/(c_{11}+c_{12}+2c_{44})c_{11}]^{\frac{1}{2}}$ where a is the slip vector. Assuming E *vs.* θ has Dunn's shape,[2] $\theta_m \doteq 25°$; and for copper the relatively constant, large θ, energy is 400–600 ergs/cm^2. Models for grain boundaries and energy formulas have been obtained also for body centered cubic crystals, for relative rotation about the normal to the boundary, and for various orientations of the boundary.

[1] W. Shockley and W. T. Read, Phys. Rev. 75, 692 (1949).
[2] C. G. Dunn and F. Lionetti, Metals Trans., February, 1949, p. 132.

W11. Interfacial Energies *vs.* Tensions in Polycrystalline Matter. John P. Nielsen, *New York University.*—In fluid films tension and energy are interchangeable in reference to the driving force toward equilibrium configuration, while for grain boundaries the interchangeability is not permissible because for crystals interface tension is undoubtedly anisotropic. A definitive experiment may be used to determine which postulate is the correct one for grain boundaries. Consider three hexagonal grains (e.g. zinc), after extended anneal, in a triangular prism, with sides A, B, and C, and A and $B\alpha°$ to each other, such that the (010) planes of the three grains are all parallel to the bisecting plane of α. Two grains meet at a plane parallel to the prism base and have random [001] direction, while the third grain has this direction perpendicular to the prism base. The three grains meet so that the junction line s connects A and B. Corresponding interfacial energies at s on A and B will be equal. Equivalent sets of angles at s on A and B excludes the tension postulate, while non-equivalency excludes the energy postulate.

W12. Field Electron Emission from Dielectrics. R. T. K. Murray and Alexander Mackenzie, *Long Island University.*—The emission of field electrons from sulphur has been investigated employing a counter. The cathode consisting of a 2-mm polished layer of sulphur on a steel sphere was placed over an aluminum window and the gap distance varied with a micrometer head working through a metallic bellows. Potentials up to 30 kv were applied to the cathode. The behavior of the observed currents was similar to that for a metallic cathode namely an initial erratic emission at low fields with a gradual stabilization at higher fields to give currents of the order of 10 electrons per second at fields of 150 kv/cm. The electron emission results from the superposition of two fields that arising from the surface polarization charges and that arising from the field in the dielectric their ratio being given by $K-1$. From a conditioned cathode the currents increase exponentially with the field according to the Fowler-Nordheim relation and to give no evidence of a gradual accumulation of a positive surface charge. It appears that the similarity in behavior of dielectric and metallic cathodes is to be explained by the electronic conductivity of the dielectric at the emitting points resulting from the high local fields.

W13. Measurement of Thermal Conductivity of Metals at High Temperature.* C. L. Hogan and R. B. Sawyer, *Lehigh University.*—The Forbes bar method has been used in determining the thermal conductivity of steel alloys, nickel, and inconel in the temperature range 0°–900°C. The method has been modified so that it is no longer necessary to know the specific heat as a function of temperature of the sample under test. Further improvements in technique include the measurement of rate of heat loss under steady state conditions thus eliminating a graphical analysis from cooling curve. An analysis of the heat flow problem is included to show that the mutually incompatible assumptions of plane isotherms in the sample and simultaneous radial heat loss leads to an error much less than the usual experimental error of the determination and can thus be neglected. Electrical conductivities have been simultaneously measured in order to check the range of validity of the Wiedemann-Franz-Lorentz law.

* Sponsored by Bell Aircraft Corporation.

W14. Experimental and Theoretical Transient Heat Propagation in a One-Dimensional Composite Material. Herbert A. Elion, *M. W. Kellogg Company.*—The importance of the effect of thermal conductivity was noted while conducting experiments involving molten lead near its solidification point, and solid carbon steel. A theoretical treatment gave the transient temperatures to be expected in either material. The case treated was for two semi-infinite flat plates of finite thickness. The hot plate is held at a constant temperature at one boundary and the cold plate insulated.* Transient temperatures were measured experimentally. The experimental results indicate the importance of the conductivity effect over the smaller natural convection effect for the case treated. The primary errors introduced in the empirical results are those of estimating physical properties (thermal conductivity, specific heat, and density), and equipment accuracy. (Heat perturbations introduced by the temperature sensing device in the steel were kept to a minimum by a special physical construction.)

* Theoretical analysis and curves by M. Yachter and H. A. Elion.

Chemical Physics

Y1. An Interionic Attraction Theory for Regions of Solutions near High Potential Surfaces. Arthur L. Loeb, *M. I. T.*—Langmuir[1] discussed the forces between lyophobic colloid particles on the assumption that ions of charge opposite to that on the colloid particle move only in the field of the colloid charge, without interacting with each other. With the colloid particles highly charged, the concentration of gegenions is sufficiently high to warrant analysis of interionic forces, but

the Debye-Hückel theory is insufficient here because it assumes low potentials and spherical symmetry. An extended interionic attraction theory was developed to avoid these two limitations, and checked in special cases against known results. First the Debye-Hückel equation was solved for regions of solutions near phase boundaries, and secondly a differential equation was developed for the Langmuir case of two parallel, highly charged planes. A correction was then made for Langmuir's expression of the average potential between the walls, the osmotic pressure was calculated including interionic forces, and a new interpretation given to the average potential as distinct from the potential used in the Boltzmann distribution law in determining concentration distribution between the walls.

[1] Langmuir, J. Chem. Phys. 6, 873 (1938).

Y2. On the Specific Heat of Liquid-Vapor Mixtures. LOUIS GOLDSTEIN, *Los Alamos Scientific Laboratory.*—The experimental verification of general thermodynamical relations connected with phase changes is of interest inasmuch as it may yield information both on the macroscopic and, indirectly, elementary properties of such transformations. The general formulas derived by Ehrenfest for phase changes of higher order are of particular importance in this respect. In view of current experimental work on liquid-vapor mixtures it seemed appropriate to call attention to the following result. One group of these general formulas determines also the discontinuities of the constant volume specific heat, as well as of those of other thermodynamical quantities, of liquid-vapor mixtures at the crossing of the saturation line of the fluid in its pressure-volume diagram. Using the abundant data available for water, we have verified the important relations connecting the discontinuities of the constant volume specific heat with those of $(\partial p/\partial v)_T$ and $(\partial p/\partial T)_v$. One may thus look upon the transformations of such mixtures into pure phases as apparent higher order phase changes accompanied by discontinuous variations of the derivatives of several thermodynamical variables.

Y3. Measurements of Gas Adsorption on Metals Using a Radioactive Tracer Method.* ALBERT D. CROWELL** AND H. E. FARNSWORTH, *Brown University.*—Copper and nickel sheets with total surface areas of one to two square centimeters have been exposed to CO_2 containing C^{14} at pressures of less than 1 mm Hg and temperatures below 500°C. Activated adsorption is measured with a counter method after removing the specimen from the gas chamber. The metal is outgassed at high temperatures in a high vacuum before exposure to the gas. Measurements as a function of temperature and pressure are being obtained for polycrystalline samples before extending the observations to a study of metal single crystal surfaces.

* Assisted by ONR and Research Corporation of New York.
** AEC predoctoral fellow.

Y4. Application of A Mass Spectrometer to the Study of Surface Reactions at Low Pressures.* STANLEY A. LANDEEN, H. E. FARNSWORTH, AND RUSSELL K. SHERBURNE, *Brown University.*—A Nier-type mass spectrometer has been used for the investigation of a surface catalytic reaction, the hydrogenation of ethylene over nickel. First attempts at observing the reaction with constant gas flow past the catalyst showed that the percentage yield of ethane by this method was too small to be observed. A change was then made to a static system, first using nickel prepared from Ni $(NO_3)_2$, and finally using a piece of nickel sheet 8 cm² in total surface area, electrolytically polished until it was found to appear smooth under 400× magnification. Preceding each set of observations the nickel surface was cleaned by alternate oxidation and reduction at 400°C. The measurements were made by sampling the gas at regular intervals as the reaction proceeded. Easily measurable catalytic activity was obtained at 140°C for gas pressures as low as 1 mm Hg and the variation of reaction rate with pressure was obtained in the pressure range of 1 to 12 mm Hg. It is planned to use the instrument to investigate the variation of catalytic activity for the different faces of metal single crystals.

* Assisted by ONR and Research Corporation of New York.

Y5. Pressures in Hydrogen-Oxygen Detonations.* W. E. GORDON, *University of Missouri.*—Previous measurements[1] of the pressures in $2H_2-O_2$ with tourmaline piezoelectric gauges, have given values in essential agreement with the Chapman-Jouget theory. With greater refinement in the calibration of the gauges, and somewhat different experimental conditions, the pressures are found often to be much lower than theoretical, even though the velocities are very close to the theoretical value. Also, although the velocities indicate a steady-state, the pressures vary widely at different points in the tube. A re-examination of the von Neumann-Chapman-Jouget theory[2] is indicated. The gauges were calibrated with shock waves in air, produced in a tube by a hydrogen-oxygen detonation behind a cellophane diaphragm, the pressures being obtained from the measured velocities through the Hugoniot relation. The decay of such shock waves was found to follow a very simple law, and it was possible to obtain quite precise calibrations with shock waves of comparable shape and amplitude to detonation waves.

* This work supported by ONR.
[1] W. E. Gordon, Third Symposium on Combustion, Flame and Explosion Phenomena (Williams and Wilkins, 1949), p. 579.
[2] J. v. Neumann—OSRD Report No. 1140.

Y6. Zero-Point Equation of State at Extreme Pressures. W. M. ELSASSER, *University of Pennsylvania.*—Bridgman[1] has measured densities of many metals and alkalihalides up to 1.10^5 atmos. The results of Jensen[2] indicate that a Thomas-Fermi model (with exchange correction) gives a good approximation for the density of simple substances from about 10^7 atm. on up. It is possible to introduce thermodynamical and structural criteria which, although not rigorous, help in interpolating densities through the remaining gap. We endeavor to show that in many instances densities of relatively simple substances can be predicted for the gap region with fair reliability without going through elaborate Hartree calculations. The results have significant applications to the interpretation of seismic data from deep layers and to the analysis of the constitution of these layers.

[1] Proc. Am. Acad. 76, No. 1 (1945), No. 3 (1948).
[2] Zeits. f. Physik 111, 373 (1938).

Y7. Entropy of Non-Equilibrium Systems. RICHARD C. RAYMOND, *The Pennsylvania State College.*—In some cases the entropy of a non-equilibrium system may be defined as the thermodynamic entropy which the system components would have at equilibrium minus the information entropy required to construct the actual system from its equilibrium components. The generalized entropy so defined is consistent with the second law of thermodynamics in all the cases so far investigated, and together with a strict interpretation of thermodynamic equilibrium it helps to reconcile some of the discrepancies between the thermodynamic definition of entropy and that derived from statistical mechanics.

SUPPLEMENTARY PROGRAMME

SP1. Integral Expressions for Nuclear Magnetic Moments. ENOS E. WITMER, *University of Pennsylvania.**—The magnetic moment of the proton is $[1876/(1836\times671)](1-1/861)$ Bohr magnetons, yielding 1.521013×10^{-3} B.m. in remarkable agreement with experiment. Believing that M_p/m is exactly 1836, this is formula (1): $[k/671](1-1/861)\mu_N$ with $k=1876$. The known magnetic moments of other nuclei are apparently represented by formula (1) with k usually an integer, and in one case at least a simple rational number. For n^1, H^1, H^2, H^3, Be^9, and B^{11} the experimental values of k are very close to integers. For He^3 k is $35^2\times7/6$. For C^{13} and F^{19} the k, though less accurately known, appear to be integral. Note that (1) has the factor $(1-1/861)$, whereas the magnetic moment of the electron is $(1+1/861)$ Bohr magnetons.

* To be given after Session L if the Chairman rules that time permits.

MEETING OF THE DIVISION OF ELECTRON PHYSICS AT WASHINGTON SQUARE COLLEGE OF NEW YORK UNIVERSITY, JANUARY 31 AND FEBRUARY 1, 1950

(Joint Meeting with the Panel on Electron Tubes of the Research and Development Board)

Invited Papers

Thoria as a cathode emitter. W. E. DANFORTH, *Bartol Research Foundation.*

Government support and thermionics. E. R. PIORE, *ONR.*

Experimental techniques involved in thermionic studies of clean metals. W. B. NOTTINGHAM, *M. I. T.*

Effect of impurities on thermionic emission from platinum. A. ERTEL, *Westinghouse.*

Oxide-cathode research at the University of Missouri. A. EISENSTEIN, *University of Missouri.*

Photoelectric techniques in the study of ionic semiconductors. LEROY APKER, *G. E.*

Principal processes in thermionic emission and electrical conductivity of BaO. L. P. SMITH, *Cornell University.*

Review of some facts on temperature variation of activation energies. CONYERS HERRING, *Bell Telephone Laboratories.*

Contributed Papers

EP1. Notes on Thoria and Other Refractory Materials. LEO J. CRONING, *Ratheon Manufacturing Company.*—The occurrence and purification of thoria is discussed to provide a better understanding of experimental results obtained by various investigators. The chemistry of thorium compounds is complex and closely connected with that of the rare earths. "Thoria" may contain over three percent impurities; its specific surface may vary from lot to lot by an enormous amount; the supplier may be any one of a dozen commercial sources or private laboratories each of whom may have several grades. A simple experiment was devised to obtain comparative data on the reaction of thoria with metals. The design and construction of a special secondary emission tube is described. The ratio of secondary to primary emission of a directly heated thoria cathode was found to be 1.4 at room temperature and increased to 1.9 at 900°C. A study was conducted on evaporation of refractory materials including Al_2O_3, B, BN, B_4C, Cb, CeO_2, Cr, CrC, Cr_2O_3, Ir, Mo, MoC, Os, Pt, Rh, Ru, SiC, Ta, TaC, Th, ThO_2, Ti, TiC, TiN, VC, W, WC, ZrC, and ZrO_2. Equipment, procedure and results are described. The experiments illustrate the adverse effects of poor vacuum on tube deposits in addition to eliminating substances with unsuitable vapor pressure.

EP2. Rate of Disappearance of Thoria from Coated Filaments. E. SHAPIRO, *Bartol Research Foundation* (Introduced by W. E. Danforth).—Studies were made of the rates of disappearance of thoria from thoria-coated tungsten and molybdenum filaments as functions of temperature and emission. It was found that, in the temperature range 2050° to 2250°K, the drawing of current from the coated filament did not affect the rate of disappearance of thoria. In this temperature range, the rate of evaporation of thoria is given by the equation: $\log r$ (g cm^{-2} sec.$^{-1}$) $=-3.71\times(10^4/T)+9.84$, and the calculated vapor pressure of thoria is $\log P$ (mm Hg) $=-3.71\times(10^4/T)+11.53$. The heat of vaporization is 171,000 cal./mole.

EP3. Thermal Emissivity Changes of Thoria-Coated Tungsten Filaments. O. A. WEINREICH, *Bartol Research Foundation.*—The total and spectral emissivities of thoria-

coated W filaments are being investigated with particular reference to effects of thermal processing and other activation procedures. The filament temperature is measured by its resistance using potential leads. Reversible and irreversible changes of emissivity are observed. These occur as a result of heat treatment and passing current through the coating. In some cases the change of the emissivity can be correlated with changes of thermionic emission. Fresh coatings heated to 1300°C showed initial emissivity values as low as 0.2 for $\lambda = 0.655$. After flashing to 2600°C the emissivity increased to 0.65 at 1300°C but prolonged heating at this temperature dropped the emissivity to 0.4. The increase is believed to be brought about by a reaction between thoria and tungsten. The total emissivity of the fresh cathode was about 0.2 at 1400°C and after flashing to 2600°C, it increased to about 0.4. Reverse electron bombardment causes increases in emissivity, comparable to those caused by flashing to 2600°C. At present, only the total and spectral emissivities at 0.655μ have been investigated. Measurements of the energy distribution between 0.6 and 12μ for different states of the thoria-coated W filaments are under way.

EP4. Experimental Use of Thoria Cathodes in High Voltage Rectifier Tubes. S. T. YANAGISAWA AND T. H. ROGERS, *Machlett Laboratories, Incorporated* (Introduced by H. D. Doolittle).—Thoria has been used as an emitting material in magnetron cathodes and in cathodes for medium voltage transmitting tubes. However, the use of thoria cathodes with extremely high inverse voltages has not been previously investigated, even though earlier experiments have indicated high emission efficiencies and ability to withstand the effects of ion-bombardment. The purpose of this investigation was to determine the feasibility and desirability of the use of thoria cathodes in high voltage rectifier tubes for x-ray service, as this application constitutes a most suitable medium for evaluating their performance under maximum voltage conditions. Cathode life, emission efficiency, and the effect of thoria evaporation upon high voltage performance were examined in particular. The existing methods of fabricating thoria cathodes were surveyed and tried. The emission and high voltage characteristics of the various types of thoria cathodes were empirically investigated by incorporating them into standard high voltage x-ray valve tube designs. Pure thoria ceramic cathodes were used with good stability up to 130 PKV inverse. Catephoretically coated tantalum wire had the best emission characteristics and was used successfully in tubes up to 110 PKV inverse. Tentative conclusions were that thoria cathodes are feasible for tubes rated up to 110 PKV.

EP5. Base-Metal Effects in Thoria-Coated Filaments. HERBERT NELSON, *Radio Corporation of America.*—Adherence of the thoria to the metal base, ease of thermionic activation, and level of thermionic emission reached have been studied as a function of base material. The base metals used in the investigation were tungsten, molybdenum, tantalum, and platinum. Thoria adherence was found best with platinum and tantalum, and poorest with tungsten. Thermionic activation was easily achieved in all cases except with platinum. The final level of thermionic emission reached at 1900° K.B.T. was the same, about 5 amp./cm², for molybdenum, tungsten, and tantalum. At lower temperatures, however, higher values were invariably obtained with molybdenum than with tantalum.

EP6. Electrical Conductivity of Sintered Thoria. W. E. DANFORTH AND F. H. MORGAN, *Bartol Research Foundation.*—The conductivity of sintered thorium oxide in good vacuum is being studied, the temperature range of the present experiment extending to 1800°C. Specimens are subjected to currents up to several amperes per square centimeter and the resistance determined between potential leads. Resistance is essentially ohmic over this range and contact phenomena with the molybdenum endpieces are not prominent. The state of activation is variable, dependent upon heat treatment and passage of current. In the highest activation yet reached, resistance values as low as 1 ohm-cm at 1200°C were obtained by prolonged passage of 10 Amp./cm². Exposure to atmospheric pressure produces deactivation. Relatively unactivated material showed two activation energies 3.4 and 0.8 ev, the former possibly corresponding to thermionic emission through interstices following Loosjes and Vink. Activation by drawing current gives a single component of about 1.8 ev effective. An attempt was made to account for activation by current as electrolytic generation of (thorium) impurity centers. Reasonable assumptions regarding mobility and percent ionic conduction fail to account for the rapidity of this activation.

EP7. Investigation of Contaminants in Vacuum Tubes. PAUL D. WILLIAMS, *Eitel-McCullough, Inc.*—In an ONR sponsored program, vacuum tube materials are being studied on the mass spectrometer as a means of identifying the volatile components released under temperature and in vacuum. Of four glasses so far studied, Nonex glass yields carbon monoxide and water at temperatures below previous bake-out temperatures. "705–2" glass contributed only oxygen after bake-out. Ceramic "Ai-200" is considerably freer of volatiles below 1000°C. Above this temperature carbon monoxide is evolved. Ceramic "Ai-200" and quartz heated to their softening points, have not contaminated carburized thoriated tungsten emission in zirconium-gettered tubes.

EP8. Certain Refractory Compounds as Thermionic Emitters. D. L. GOLDWATER, AND R. E. HADDAD, *Bartol Research Foundation* (Introduced by W. E. Danforth).—Several refractories of the nitride, boride and carbide families are investigated as sources of thermionic electrons. An activation pattern qualitatively common to several of the compounds is observed. Emission data for the final state of activation is presented. Data concurrently obtained for thoria are also given for comparison. True temperature used in the Richardson equation is obtained by correction from brightness temperature. Temperature correction curves have been obtained by two methods. These curves can be satisfactorily represented in the region of thermionic emission by one value of spectral emissivity, which values are listed, for the materials studied.

EP9. Refractory Thermocouples and Emissivity Determinations. F. H. MORGAN, *Bartol Research Foundation.* (Introduced by W. E. Danforth).—The thermoelectric power of several refractory thermocouples was investigated. W-Ta for temperature measurements up to 3000°C, W-Mo up to 2600°C, Ta-Mo up to 2600°C and W-W/Mo (alloy 50 percent Mo/50 percent W) up to 2900°C. The resulting curve for W-Ta was quite different from that found in existing literature. The validity of the curve was checked by taking the difference between the W-Mo and the Mo-Ta curves. Basic calibration was carried out using several melting points and the results interpolated by means of an optical pyrometer. Employing these thermocouples, the spectral emissivity of thoria and other cathode materials was easily obtained. For thoria $e = 0.4$ up to 1800°C, further increase in temperature increases the spectral emissivity, e being 0.55 at 2000°.

EP10. Effect of Impurities on Thermionic Emission from Platinum. A. ERTEL, *Westinghouse Electric Corporation* (Introduced by J. W. McNall).—Previous investigators

reported high values of the thermionic work function ϕ and emission constant A for platinum before rigorous heat treatment resulted in more dependable results. This paper describes emission measurements on #1 grade and C.P. platinum (Baker) both of which had low values of ϕ and A before continued heat treatment at high temperatures. Experiments with #1 platinum indicated the presence of an electropositive impurity. Emission-temperature curves show a "clean-up" temperature between 1850° and 1930°K and a gradual decrease in emission to that of pure platinum. Electron projection studies showed the "eruption" of the impurity from the wire surface. Richardson data taken at higher temperatures for the semi-clean wire yielded $\phi = 5.27$ ev and $A = 64$ amp./cm^2 deg.^{2} Although the C.P. material showed a similar impurity, another impurity was indicated by the violent bursts of emission occurring for decreasing temperatures in the range from 900° to 1100°K. Electron projection study showe eruptions in this temperature range. The thermionic constants for relatively clean wires were found to be $\phi = 5.32$ to 5.47 ev and $A = 100$ to 160 amp./cm^2 deg.^{2} Results of spectroscopic and x-ray diffraction analyses are presented.

EP11. Thermionic and Secondary Emission Properties of Magnetron Cathodes and Their Influence on Magnetron Operation.* ROBERT L. JEPSEN, *Columbia University.*—The use of various pure metals as cathodes, with and without an auxiliary "priming" cathode, has made it possible to separate, to a considerable extent, the roles of thermionic and secondary emission. It is found that an important operating characteristic of a magnetron employing a secondary emission cathode is the existence of a maximum current boundary on the V-I performance chart. This boundary is directly correlated with the secondary emission properties of the cathode. It is also found that in the low current region percentage back bombarding power increases rapidly as anode current is decreased. It is further indicated that back bombarding electrons strike the cathode within a preferred angle range, thus increasing the effective secondary emission ratio over what it would be for normal incidence. A simple picture has been proposed for understanding, qualitatively, the maximum current boundary. In this picture it is necessary to consider only stable thermionic and secondary emission properties of pure metals. The chief unsolved problem remaining seems to be an electron dynamical one. It relates to some type of interaction in which the electrons participate, and which results in the observed dependence of percentage back bombarding power on anode current.

* Work supported jointly by the Signal Corps and the ONR.

EP12. Noise Spectra from Vacuum Tubes at Ultra Low Frequencies.* R. W. BOGLE,† *University of Michigan.*—Spectral measurements of vacuum tube emission noise have been made for the frequency range from 10,000 c.p.s. to 1/100 c.p.s. This work was undertaken to test the Johnson "flicker effect" theory[1] which relates the frequency dependent characteristic encountered at low frequencies with cathode hot spots of finite lifetime. Attention was particularly directed toward the inverse proportionality dependence of r.m.s. noise voltage on frequency required by this theory, and also the point of frequency below which the noise spectrum should become flat. The experiments showed no sure evidence of flattening. Further, a marked deviation from simple inverse frequency proportionality was found. The frequency-determining elements used in the experimental equipment were Twin-T feed-back amplifiers. At the lowest frequencies, a Brown recording d.c. galvanometer was used as an output voltmeter. Spectral measurements were made on a variety of tubes, including commercial types as well as some specially constructed. Tubes with all of the common emitting materials were tested.

* Supported by Navy contract.
† Now at Applied Physics Laboratory, The Johns Hopkins University.
[1] J. B. Johnson, Phys. Rev. 26, 71 (1925).

EP13. A Preliminary Study of the Work Function of Contaminated Metal Surfaces. P. H. MILLER, JR. AND B. J. ROTHLEIN,* *University of Pennsylvania.*—A beam of electrons is passed between a reference plate and a metal surface to be studied and these plates are electrically connected with each other. A change in work function causes a change in the field between the two plates, which in turn produces a deflection of the electron beam. The apparatus in its present form is capable of measuring a change in work function of 0.05 volt. Observations have been made on the changes of work function in partially outgassed tantalum, zirconium, and tungsten, as these surfaces are allowed to cool from temperatures between 1000° to 2000°C. There is evidence for two types of layers which can influence the contact potential difference by as much as several volts.

* Now with Sylvania Electric Products.

EP14. Thermionic Emission, Conductivity, and Contact Potential Difference Measurements.* WILLIAM J. PRICE,† *Battelle Memorial Institute.*—A special vacuum tube was built for the study of cathode materials. By means of this tube, measurements of the thermionic emission and conductivity were made on the same cathode; also, the contact potential difference between the cathode and a tungsten foil was obtained. The tube consisted of a stationary cathode and two movable anodes arranged so that they could be alternately moved into position. The cathode was a molybdenum cylinder with the emitting material coated on the closed end. Conductivity measurements were made by observing the voltage required to produce a given cathode current as the distance between one movable anode and the cathode was decreased to zero. Thermionic emission data were obtained by observing the saturation current drawn to the same electrode. The other movable anode, consisting of a tungsten foil, was used for measuring the contact potential difference between the cathode and tungsten; the Kelvin method was employed. Cathodes, with thoria coatings, were studied in this tube. The conductivity was found to be proportional to the thermionic emission over a considerable temperature range and for widely differing conditions of activation. The change in the work function following thermal activation of the cathodes was obtained by thermionic emission measurements and by contact potential difference measurements. This change was found to be essentially the same by the two methods.

* Supported by Wright-Patterson Air Force Base and Evans Signal Laboratory.
† Now at USAF Institute of Technology, Wright-Patterson Air Force Base.

EP15. The Use of Radioactive Sr in Some Thermionic Experiments on Thin Films. H. W. ALLISON AND GEORGE E. MOORE, *Bell Telephone Laboratories.*—Radioactive strontium isotopes are being used as tracers to measure the minute quantities of Sr and SrO involved in thermionic emission experiments on thin film (1–10 monomolecular layers) cathode systems. These thin film systems consist of an evaporated deposit of Sr or SrO on tungsten ribbons. Electron emission measurements at low temperatures on these definable systems indicate a thermionic activity comparable to that of the more complex commercial BaO–SrO cathode. The sensitivity of the tracer method permits measurement of the following properties of these films: 1. The amount of SrO (or Sr) required to

produce any observed activation. 2. The rate of loss of Sr (or SrO) on heating the films at any practical operating temperature. 3. Whether the deposited Sr (or SrO) migrates to the reverse side of the receiver ribbon at specific test temperatures. Sr was chosen rather than Ba because of the more convenient properties of its radioactive isotopes. The technique will be described and quantitative results given.

EP16. Electrical Conductivity of Oxide Cathode Coatings. D. A. WRIGHT, *G. E. C. Research Laboratories, Wembley, England* (Introduced by Geo. E. Moore).—Conductivity measurements on activated coatings give results in agreement with the Vink-Loosjes theory, which it is shown implies Ba concentration of the order 10^{20} atoms/cm³. Hall effect measurements indicate 10^{14} electrons/cm,³ at 1100°K, and free path 2.10^{-5} cm. This result may not in fact be inconsistent with the Vink-Loosjes theory. *P*-type conductivity is not encountered in well activated coatings, and is a feature developing while drawing emission under non-activating conditions. It is due to oxidizable impurities in the coatings. Rapid poisoning or activating effects at low temperatures emphasize the importance of phenomena at surfaces, and it is suggested that these are associated with electron or hole movement rather than ion movement.

EP17. On the Interpretation of Conduction and Thermionic Emission of (Ba−Sr)O Cathodes. F. K. DU PRÉ, R. A. HUTNER, AND E. S. RITTNER, *Philips Laboratories, Inc.*—A semiconductor model for (Ba−Sr)O cathodes is proposed comprising a full band and a conduction band separated by a gap ~1.7 ev, donor levels ~0.3 ev and acceptor levels ~1 ev below the conduction band, and an electron affinity ~1 ev. It is assumed, for simplicity, that there is a fixed concentration of acceptors. ($\sim 1.5\times10^{17}$/cm³) in a given cathode, and the process of activation is interpreted as a gradual increase in the concentration of the donors (up to $\sim 3\times10^{17}$/cm³). The combination of this model with Vink's[1] concept of conduction by an electron gas in the pores of the oxide coating explains the following facts (exclusive of those already enumerated by Vink): the variation in conductivity slope and Richardson work function with increasing activation, the existence of *p*-type conductivity changing to *n*-type with increasing temperature, the magnitude of the emission current density (i), the difference between the Richardson work function (ϕ_{Rich}) and that determined from contact p.d. measurements, the linear relationships between log$o$ and log$i$ and also between logA_{Rich} and ϕ_{Rich} for different stages of activation.

[1] H. J. Vink, thesis, Leiden (1948). See also R. Loosjes and H. J. Vink, J. App. Phys. 20, 884 (1949), and Philips Research Reports 4, 449 (1949).

EP18. An Investigation of Magnesium as an Additive to the Nickel Base of an Oxide Cathode. RALPH FORMAN AND GLENN F. ROUSE, *National Bureau of Standards.*—The degree to which small amounts of magnesium added to the nickel base of an oxide cathode may affect the thermionic properties of the cathode is being investigated. Techniques for adding magnesium to an electrolytic nickel base have been worked out and the rate of diffusion of magnesium through nickel at elevated temperatures is being studied. A double diode of planar type has been chosen as the means for comparing the thermionic properties of two cathodes. Direct current and pulsed emission tests are made, the pulse voltages being of 250 and 500 microseconds duration. The performance of a cathode on an electrolytic nickel base has been checked by making a tube in which all metal parts, other than the tungsten heater, were of electrolytic nickel. It has been found that under certain conditions an oxide cathode on an electrolytic nickel base activates more rapidly than does one on a Mg−Ni base. Current decay effects which are often observed in pulsed emission are believed to be due in part, or perhaps wholly, to processes occurring at the anode.

EP19. Diode Studies of Oxide-Coated Cathodes. H. E. KERN AND R. T. LYNCH, *Bell Telephone Laboratories* (Introduced by J. A. Burton).—A description of the Bell Laboratories planar-type test diode will be given, together with a brief summary of the diode standard processing procedure. This will include a description of a precision method for the application of cathode coatings. The method of determining cathode emission, the conditions of aging and lifeing of the diode, and the criteria for tube failure will be discussed. The quality control chart method for analyzing emission and life data will be described. This will be illustrated by a chart showing the reproducibility of the standard diode. Finally, some typical results obtained from the diode program will be reported.

EP20. Thermionic Properties of Dense Oxide Cathodes. J. A. BURTON, H. E. KERN, AND R. T. LYNCH, *Bell Telephone Laboratories.*—The thermionic properties of the smooth, dense alkaline earth oxide coatings described by Kern and Lynch in the preceding paper have been investigated as a function of cathode temperature and pulse duration. The voltage-current characteristics of these diodes have been measured using pulses varying in duration from one microsecond up to one thousand seconds. The decay of cathode emission with time under these conditions will be discussed briefly. A comparison will be made between the observed current-voltage characteristics and those expected for an ideal diode of similar geometry in the retarding field region, the space charge limited region, and also for accelerating fields up to 50,000 volts per centimeter. At normal operating temperatures and for pulses sufficiently short so decay effects are negligible, the observed slopes of Schottky plots agree closely with those theoretically expected for a patch free surface.

EP21. A Study of Cathode Behavior in Fluorescent Lamps. E. F. LOWRY, E. L. MAGER, AND H. H. HOMER, *Sylvania Electric Products, Inc.*—In the mercury vapor atmosphere of fluorescent lamps, oxide-coated cathodes exhibit phenomena requiring consideration in any theory of emission from oxide-coated metal surfaces. Visible manifestations on the tube wall of these phenomena are: (1) *Spots*—occurring during electrode operation as anode (alternating half-cycles on a.c.), chiefly alkaline earth metal. (2) *Bands*—rings of discoloration, chiefly mercury oxides. The cathode coating, responsible for discolorations, is continuously disintegrating during operation. End of life occurs when the coating is completely stripped from the core metal. Addition of about five percent zirconium dioxide to such cathode coating nearly tripled the life of the fluorescent lamp, allowing life rating to be increased from 2500 to 7500 hours. Simultaneously, discolorations have been practically eliminated for the first 5000 hours. The formation of *spots* and *bands* is explainable in absence of zirconium dioxide by reactions occurring at the interface between the core metal and the alkaline earth oxides. The action of zirconium dioxide in suppressing discoloration and disintegration is less readily explainable, being complicated by the fact that when ZrO_2 is added in proper amounts both spots and bands are absent, but excess ZrO_2 will produce greater blackening than if none at all were used.

EP22. The Decay and Recovery of the Pulsed Emission of Oxide-Coated Cathodes. R. M. MATHESON AND L. S. NERGAARD, *Radio Corporation of America.*—The decay and recovery of the pulsed emission of cathodes consisting of BaO on nickel is studied. The emission of the cathodes is measured in diodes of cylindrical geometry having water-cooled copper

anodes spaced 0.019 inch from the cathode. Most of the diodes show a decay of anode current when first put in pulse operation. Decays of 2–50 percent are observed during 150 μsec. pulses. The decay tends to disappear when the tubes are aged under pulse conditions. The peak current is a linearly decreasing function of the logarithm of the duty cycle, even when there is no perceptible decay during the pulses. The rate of decrease is independent of the pulse repetition rate and decreases with cathode temperature. Current-voltage characteristics during the pulse and recovery periods are obtained by short sampling pulses. A comparison of these characteristics with computed ideal characteristics does not discriminate unambiguously between a variation of emission and a variation of internal cathode impedance as a source of current decay. Studies to separate the contributions of these effects are in progress.

EP23. Life Tests of Oxide-Coated Cathodes—An Engineering Report. J. O. McNALLY, *Bell Telephone Laboratories.*—The continued use for many years of the oxide-coated cathode in thermionic vacuum tubes for communication purposes has led to the development of types of tubes having in general satisfactorily long thermionic lives. This paper describes a number of the factors involved in obtaining these lives. The mortality curve is shown and discussed for a number of tube types. It is shown that the cathode temperature at which the tube is operated is important in establishing the life. The effects of operating the cathodes at various current densities are discussed.

EP24. Convenient Methods for Thermionic Emission Calculations. H. F. IVEY AND C. L. SHACKELFORD, *Westinghouse Electric Corporation.*—Calculation of the temperature at which a given thermionic emission will be obtained from a certain material (assuming the thermionic constants are known) is complicated by the presence of the T^2 term in Richardson's equation. The desired temperature can, of course, be found by trial and error and interpolation. It is the purpose of this paper, however, to present four simple methods of calculating the temperature. These methods may, of course, be used to calculate any one of the quantities ϕ, A, T, and J if the other three are known. The first of these methods is algebraic and involves reducing Richardson's equation to a simple form involving the temperature only in the exponential term. Two graphical means of determination will also be described. The fourth method presents the results in the form of a nomograph. The accuracy to be expected from each method is discussed.

EP25. A "Figure of Merit" and a "Quality Ratio" for D.C. Emission from Oxide-Coated Cathodes. C. D. RICHARD, JR., *Superior Tube Company* (Introduced by A. Lederman).—A graph of d.c. emission as a function of cathode temperature is often used in test work with oxide-coated cathodes, particularly with diode tubes where other characteristics are not feasible. Previously E_f-I_s curves were judged by visual comparison only. The portion of this emission curve of greatest value in rating performance of tubes is the "knee" of the curve. This knee, which varies widely in curvature, is a transition point between the "space-charge limited" and "temperature-limited" emission regions of the E_f-I_s curve. A "figure of merit" (the slope of a tangent to the knee from an arbitrary origin) makes it possible to specify this point with a number. When the figure of merit for a test material is divided by the figure of merit for the control lot, a "quality ratio" is obtained. Use of this method correlates well with visual judgments of the curves and also with actual radio tube performance of the cathode materials. It works with lots of close similarity as well as those of wide differences. Previously proposed methods lack this range of application.

EP26. Determination of Oxide Cathode Performance in Diode Tubes through Figures of Merit. THOMAS H. BRIGGS, *Superior Tube Company* (Introduced by A. Lederman).—Richard's paper described a method for calulating a "figure of merit" and "quality ratio" for standard diode tubes. Particular use of them has been made in evaluation of certain cathode performance characteristics. *Rate of cathode activation* and *life performance* are clearly indicated by this method. Migrations of the knee of the E_f-I_s curve are concisely shown. This is the best measure of d.c. emission quality found so far. Through the figure of merit, changes in cathode activity with time can be traced. The quality ratio allows comparison at any period with the control standard. *Chemical composition* of cathode base metals is important to d.c. emission performance. Correlation of the effects of various alloy additives is made more simple and reliable through use of FM and QR figures. A linear relationship has been found between the arbitrarily determined figure of merit for d.c. emission and quality ratings of the log of low field and log of pulsed emission ratings proposed by Cardell and others. This is the first time such a correlation has been shown, and it should be of value in development of the theory of thermionic emission.

EP27. Ceramic Heaters and Cathodes for Electron Tubes. T. R. PALUMBO, *Ceramic Heater Cathode Resistor Company* (Introduced by A. Bramley).—A specially prepared conductive ceramic rod has been applied as a tube heater and filamentary cathode. The conductive material is prepared by subjecting a preformed pure ceramic material, such as Al_2O_3, to a hydrocarbon atmosphere, e.g., methane, at a temperature ranging from 700°C–900°C. The coefficient of conductivity of the resultant product varies with the carbon content of the gas or gas mixtures, the furnace temperature and the time of exposure, i.e., the speed at which the rods are fed through the furnace. We have shown, however, that conductivity is not induced by a cracking of the hydrocarbon followed by a deposition of free carbon on the ceramic, but by the formation of a chemical compound involving the ceramic material and the carbon. X-ray studies have been made. The material so obtained has a negative coefficient of resistance and high current carrying characteristics. An unusual property of this ceramic is that when it is used as a base with a standard cathode coating such as (Ba, Sr, Ca) carbonates or azides, it will support the same thermionic emission as the customary coated nickel sleeve under the same conditions of operation.

EP28. Effects of Controlled Impurities in Nickel Core Metal on Thermionic Emission from Oxide-Coated Cathodes.* HAROLD JACOBS,† GEORGE HEES,‡ AND WALTER CROSSLEY,‖ *Sylvania Electric Products, Inc.*—Emission measurements were made over a 500-hour life period on oxide-coated cathodes having 18 different binary nickel-alloy core metals. The samples of nickel and of the additive (both of highest purity) were vacuum melted together in order to provide a rigid control on the composition of each alloy. All tubes were processed under the same controlled conditions. An empirical emission equation $I=A'\exp(-e\Psi/BT)$ was used. The parameters Ψ and A' were found to vary in such a manner that, over life, the following relationship existed: $\log A'=K\Psi+B$ where K and B are constants. Some alloys which appear to be especially suitable as base metals for oxide-coated cathodes are aluminum-nickel, chromium-nickel, molybdenum-nickel, and thorium-nickel. Alloys which resulted in poorest emission were boron-nickel, beryllium-nickel, and iron-nickel.

* This work was undertaken in cooperation with the United States Army Signal Corps Engineering Laboratories, Evans Signal Laboratory, Belmar, New Jersey.

† Now at Evans Signal Laboratory, Thermionics Branch, Belmar, New Jersey.

‡ Sylvania Product Development Laboratories, Kew Gardens, New York.

‖ Now at Polytechnic Institute of Brooklyn, Brooklyn, New York.

MEETING OF THE DIVISION OF HIGH-POLYMER PHYSICS AT THE POLYTECHNIC INSTITUTE OF BROOKLYN, FEBRUARY 1 AND 3, 1950

HPP1. Incubation of Plastic Shocks in Certain Polymeric Films. JOHN KAUFFMAN AND WALLER GEORGE, *Naval Research Laboratory.*—The existance of a time delay between the rapid application of a load and the appearance of plastic flowing has been demonstrated in mild steel by Clark and Wood. Recently, the authors have discussed a similar time delay for the appearance of a form of localized plastic flowing in commercial polyamide films. The localization involves a through-the-thickness reduction of the specimen (a type of local necking) which can be made to propagate along the specimen. It has been tentatively interpreted in terms of von Kármán's plastic wave theory as a "plastic shock." Under suitable dead weight loading the "shock" is observed to propagate after the elapse of the delay time. Plastic flowing events occur within this delay time which lead to the abrupt formation of the shock. The collection of these events preceeding the final localization of flowing is termed its "incubation." This paper will describe the incubation processes with the aid of motion pictures and polarized light for selected polyamide and polyethylene films. The description will include the initiation and growth of "bands" of distortion in regions of maximum average shear stress and their collapse into the fully formed shock.

HPP2. Fracture Markings in Plastics. J. A. KIES AND A. M. SULLIVAN, *Naval Research Laboratory.*—Many of the gross features of fracturing in solids can be modeled and chosen features can be emphasized on fractures in selected polymeric solids. Discontinuous fracture and backward propagation of isolated elements simultaneous with the advance of crack head are demonstrated. The origins of chevrons and other geometrical markings, such as ellipses, hyperbolas and river systems on the fracture surface are explained in terms of multiple initiations and relative propagation speeds of fracturing. The sequence of events by which rod-shaped shards are thrown out during conchoidal fracturing is described. Shatter markings provide a mechanistic explanation of brittle behavior under high overloads. Variations of fracture appearance with over-all speed of propagation in cellulose acetate and Lucite plates are discussed. A few examples of the applicability of these studies to the interpretation of some large scale fractures in various materials are cited.

HPP3. Crystallization and Second-Order Transitions in Silicon Rubbers.* C. E. WEIR, W. H. LESER, AND L. A. WOOD.—In the course of an investigation to determine which rubbers might be suitable for use at low temperatures, interferometric measurements of the length-temperature relationships of silicone rubbers have been made. Crystallization was found between −60° and −67°C in Dow-Corning Silastic X-6160 and in General Electric 9979G silicone rubber, the latter of which contains no filler. Crystallization between −75° and −85°C was found in Silastic 250. Melting occurred over a range of temperature above the temperature of crystallization. The volume change on crystallization varied from 2.0 to 7.8 percent. No crystallization or melting phenomena were observed in Silastic X-6073 between −180° and +100°C. All types of silicone rubber exhibited a second-order transition at about −123°C, the lowest temperature at which such a transition has been observed in a polymer. The coefficient of linear thermal expansion of silicone rubbers containing no filler was found to be about 40×10^{-5}/°C between −35° and 0°C.

* The work reported here was supported by the ONR and the Office of The Quartermaster General.

HPP4. Random Noise in Dielectric Materials. R. F. BOYER, *The Dow Chemical Company.*

HPP5. Equivalent Effects of Time and Temperature in the Shear Creep and Recovery of Elastomers. F. S. CONANT, G. L. HALL, AND W. JAMES LYONS, *Firestone Tire & Rubber Company.*—An explicit relationship is set forth for the time-temperature dependence of the *viscoelastic* phenomena in the superelastic polymers. An empirical equation that was found to represent adequately the above-mentioned relationship over the entire multiple-temperature curve is of the form: $\log t=[C_\alpha/(T-b)]+C_\beta$. Experimental verification is given for the equivalent influence of time and temperature on the creep and recovery of compounds based on Hevea, GR-S, Neoprene GN, butaprene and butyl rubber. A comparison of the empirical equation with that of a theoretical reaction-rate equation of Tobolsky and Eyring indicates a temperature dependence of the energy of activation.

HPP6. Elastoviscous Properties of Polyisobutylene III. Relaxation of Stress in Whole and Fractionated Polymers; Effect of Carbon Black. R. D. ANDREWS, F. H. HOLMES, AND A. V. TOBOLSKY, *Princeton University.*

HPP7. A Non-Destructive Mechanical Test for Wool Fibers and Some Preliminary Results. HARRIS M. BURTE, *Textile Research Institute.*—The slope of the force extension curve in the linear region before the yield point can, for wool fibers, be non-destructively measured at five- to ten-minute intervals. The change of this slope with time is used to follow the course of the heterogeneous reaction between wool and some reagent. Woods[1] determined the dependence of Young's modulus on relative humidity, but did not investigate any rate phenomena. Data are presented on the interaction between concentrated aqueous solutions of neutral salts and wool fibers. Two processes occur: (a) relatively rapid hydration or dehydration of the fiber until equilibrium with the partial pressure of water over the salt solution is attained; (b) relatively slow absorption of salt ions by the fiber. Very concentrated salt solutions dehydrate the fiber so completely that absorption of salt ions is not possible. Swelling experiments, and experiments involving other mechanical properties, confirm this view. The interaction between wool fibers and aqueous solutions of large organic molecules follows a similar pattern. The effect of fiber size and type on the rate of absorption has been studied. The absorption of ions is probably diffusion rate controlling.

[1] Woods, Proc. Leeds Phil. Lit. Soc. (Sci.) **3**, 577 (1940).

HPP8. Some Theoretical Considerations of Dynamic-Property Data on Textile Specimens. W. JAMES LYONS, *The Firestone Tire & Rubber Company.*—Early stretch-vibrometer data, of quite extensive character, on the frequency dependence of the interval friction μ of a Nylon monofil, has been found to conform to the relation $\mu=[\mu_2/(1+\omega^2\tau_2^2)]+\mu_3$ which was deduced independently by Tobolsky and Eyring from considerations of molecular structure. Among other constants evaluated was the relaxation time for the secondary-bond network τ_2, which was found to have the value 9.3 sec. By more sensitive graphing methods than had been used heretofore, it was confirmed for the Nylon data that the hyperbolic relationship between resonant frequency ω_0 and internal friction μ holds equally as well as the foregoing

equation. The two relationships are shown to be nearly equivalent in the experimental range. On evaluation of graphical parameters, the equation $\mu\omega_0=2.47\times10^9$ ergs/cm³ was obtained. Using the same graphical method with a set of data on 11/4/2 cotton cord the relation $(\mu+0.9)\omega_0=7.05\times10^9$ ergs/cm³ was established.

HPP9. Fundamental Studies of Plasticization of PVC. M. L. DANNIS, *B. F. Goodrich Research Center.*—The softening of a hard resin, polyvinyl chloride, by a liquid, dioctyl phthalate occurs through a set of processes in sequence. Imbibition of the liquid is accompanied by volume reduction in the system. Dilatometer methods evaluate the amount and rate of volume decrease. The rate is temperature dependent, activation energy about 80 kcal. Solution of liquid into the resin follows with no further volume, but large dielectric change. Dielectric changes are measured on material in a cylindrical condenser, using a Schering bridge, and are rate dependent, activation energy about 110 kcal. Data are best described, assuming that segments of the polymer molecule "react" independently of one another. At fixed temperatures, "reaction" rates are directly proportional to vapor pressure of the liquid. The dielectric change may be treated similarly to a chemical reaction between a solid and a vapor, and free energy of activation, ΔF^{**}, evaluated. ΔF^{**} is constant for various liquids with one resin. $\Delta E^{**}=\Delta H^{**}+L$ in this system, where ΔE^{**} is Arrhenius activation energy, ΔH^{**} energy barrier, L latent heat of vaporization of the liquid.

HPP10. Load-Induced X-Ray Line Broadening in Nylon Filaments. WALLER GEORGE AND JOHN KAUFFMAN, *Naval Research Laboratory.*—The load-induced microscopic structural changes in highly oriented Nylon filaments were followed by changes in the x-ray fiber diffraction pattern as a function of the resulting strain. Observations made include (1) changes in the dimensions of the fiber spots, and (2) a decrease in ratio of the intensity of amorphous to crystalline x-ray scattering. These new results for Type 200 du Pont Nylon indicate a change in the microdeformation mechanism at a strain corresponding to the inflection of the load-strain diagram (14 percent elongation). The mechanism for smaller plastic strains appears to involve a rotation of the crystallized domains toward alignment with the fiber axis, accompanied by a small over-all additional crystallization. For strains larger than the inflectional strain, the mechanism seems to involve a progressive reduction in the domain size, and a reduction in alignment with the fiber axis. Both effects appear to saturate in the vicinity of the rupture strain. These results are discussed in terms of load-induced effects found in metal single and polycrystals. It is suggested that the qualitative features observed may be representative of a wide class of load or strain induced microdeformation reactions in the solid state.

HPP11. Emulsion Polymerization with Ultrasonic Vibration. A. S. OSTROSKI AND R. B. STAMBAUGH, *The Goodyear Tire and Rubber Company.*—Emulsion-type polymerization reactions have been accelerated by irradiation with ultrasonic energy. A magnetostriction oscillator at 15 kc gave essentially the same results as a piezoelectric oscillator at 500 kc. The rate of formation of polystyrene was doubled and higher final yields obtained using about 0.03 watt of vibrational power per cc of latex. Experiments were made to separate local heating effects from the pure vibration energy. A thermostatted stainless steel cell was developed for irradiating butadiene emulsions under pressures up to 60 p.s.i. About ½ watt of vibrational power per cc of latex doubled the rate of reaction for GR-S, Redox and Redsol formulas. The ultrasonic intensity apparently must exceed a critical value before any appreciable accelerative effect is observed. The time to reach a given yield of polymer is approximately inversely proportional to the power used.

HPP12. A Rotating Specimen Mount for Use with X-Ray Spectrometer in Measuring Crystallite Orientation of Cellulosic and Other Textile Fibers. LEON SEGAL, JOSEPH J. CREELY, AND CARL M. CONRAD, *Southern Regional Research Laboratory.*—The quantitative evaluation of crystallite orientation in textile fibers by x-ray methods is discussed. It is found that photographic recording and photometering of the resulting films can be replaced by automatic recording on a strip chart with the aid of an x-ray spectrometer with Geiger-Müller counter. The design and details are given for a specimen holder capable of properly positioning and rotating a bundle of fibers in the x-ray beam so that the 002 or other selected diffraction arc passes before the window of the counter. A tentative procedure is outlined for evaluating with the aid of this apparatus, the crystallite orientation of a bundle of cellulose fibers. Some typical recordings of the intensity curves of the 002 arcs from ramie, cotton and high tenacity rayon are presented.

HPP13. On Crazing of Linear High Polymers. C. C. HSIAO AND J. A. SAUER, *The Pennsylvania State College.*—The effect of various variables, such as type of stress, stress magnitude, duration of stressing, and environment on the initiation and development of crazing in linear polymers is discussed. The basic nature of crazing is investigated in some detail for polystyrene specimens by means of the light microscope, the electron microscope and the x-ray spectrometer. The results of these observations and their bearing on the fundamental group structure of the polystyrene molecules is presented. The relationship between crazing and orientation is discussed, as well as the effect of both of these factors on the mechanical properties. The experimental results are compared, wherever possible, with the previously reported data of other investigators. A short discussion is then given of a theory of crazing from the point of view of the molecular structure of the material.

HPP14. Equation of State for High Polymers. R. S. SPENCER AND G. D. GILMORE, *The Dow Chemical Company.*—In a former paper,* the authors suggested the following equation of state, $(P+\pi)(V-\omega)=RT$, where π is the internal pressure (or cohesive energy density) and ω is the volume at absolute zero. It was found that this equation was in good agreement with data on the thermal expansivity and isothermal compressibility of polystyrene. The present paper reports isothermal compression measurements on polymethyl methacrylate, polyethylene, cellulose acetate, and ethyl cellulose, within the fabrication range of temperature. The above equation of state is shown to apply equally as well to these thermoplastics as to polystyrene and values are given for the constants π and ω. The usefulness of this relationship is illustrated in a brief discussion of some phases of the injection molding process.

* R. S. Spencer and G. D. Gilmore, J. App. Phys. **20**, 502 (1949).

HPP15. Behavior of Granulated Polymers under Pressure. R. S. SPENCER, G. D. GILMORE, AND R. M. WILEY, *The Dow Chemical Company.*—In such fabricating processes as extrusion and injection molding it is frequently necessary to force a granulated polymer through a channel. Frictional forces between polymer and channel walls lead to a drop in pressure through the granular material. Simultaneously, the applied pressure causes a compaction of the granules. Assuming that the granular mass has certain fluid-like properties, a simple theoretical expression for pressure transmission

is derived. Comparison with data on Saran powders and granular polystyrenes shows good agreement between theory and experiment. The effect of lubrication is shown also. The compaction of granular polystyrene follows the same pattern as that observed in the earth's crust. The porosity decreases exponentially with increasing pressure. The "compressibility coefficient" for the porosity of granular polystyrene is comparable with that given for clays and shales.

HPP16. Mechanical Properties of Oriented Polystyrene Films. LAWRENCE E. NIELSEN AND ROLF BUCHDAHL.—Cast films of polystyrene were oriented by stretching at temperatures above the softening temperature of the material and then cooled. A factorially designed experiment was carried out in which the amount of stretching, temperature of stretching, time held in the stretched state before cooling, and effect of several cycles of stretching before cooling were investigated as they affect the birefringence, the stress-strain properties, dynamic modulus and damping, and the softening temperature of polystyrene. In general, the value of the stress-strain properties (modulus, elongation to break, and ultimate strength) in the direction of stretch, the dynamic modulus, and the birefringence all increase with an increase in the amount of stretching, a decrease in temperature, an increase in rate of cooling after stretching, and a decrease in the number of times the film was stretched before finally cooling. The values of many of the mechanical properties are more closely related to the birefringence than to the amount of hot stretching. The softening temperature is decreased in direct proportion to the birefringence. Annealed films give higher softening temperatures than films which have been stretched and then allowed to shrink before cooling.

HPP17. The Transition Phenomenon of Polymeric Substances. R. BUCHDAHL, L. E. NIELSEN, AND R. E. POLLARD, *Monsanto Chemical Company.*—The mechanical properties of high polymers are determined by the location of the transition range on the temperature scale; the transition region is defined as the temperature range where the mechanical loss factor goes through a maximum and where the dynamic elastic modulus changes by several decades. Below the transition temperature the polymer is a rigid brittle solid and above this temperature the polymer is a rubber-like material. The addition of low molecular weight plasticizer to the polymer lowers the transition temperature and changes the width of the transition. Quantitative changes of the transition temperature will be explained in terms of plasticizer concentration, compatibility of the plasticizer-polymer system and in terms of a transition in the plasticizer. For copolymers the transition range can be predicted from the volume of the two components and their respective transition temperatures. The behavior of polymer blends in terms of the transition phenomenon is discussed briefly and a possible interpretation of the general transition phenomenon will be given.

HPP18. Dispersion of Dynamic Rigidity and Viscosity in Concentrated Polyvinyl Acetate Solutions. JOHN D. FERRY, W. M. SAWYER, GEORGE V. BROWNING, AND ARTHUR H. GROTH, JR., *University of Wisconsin.*—Data for the dynamic mechanical properties of solutions of polyvinyl acetate in 1,2,3-trichloropropane, obtained from both transducer and wave propagation measurements, superposed for all concentrations from 5 to 40 percent and all temperatures from −3° to 41°C when the reduced dynamic rigidity, $G'T_0/Tc$, and the reduced dynamic viscosity, η'/η, are plotted against the reduced frequency, $\omega\eta T_0/Tc$; G'=real part of complex dynamic rigidity, η'=real part of complex dynamic viscosity, η=steady flow viscosity, c=concentration in g/cc, T=absolute temperature, T_0=298°K. This behavior can be predicted by postulating that each elastic mechanism has a rigidity proportional to T and to c and that the relaxation times of all mechanisms have the same dependence on c and T. The two universal dispersion curves are characteristic of a given polymer sample, representing the mechanical properties in a hypothetical standard state of unit density and unit viscosity at 298°K. From either dispersion curve, the distribution of relaxation times may be obtained over about 5 cycles of logarithmic time. The distribution indicates a relatively sharp cut-off at the upper end which may be attributed to the finite molecular length of the linear polymer.

HPP19. The Effect of Excluded Volume on the Configurations of Long Chain Molecules. GILBERT W. KING, *Arthur D. Little, Inc., and M. I. T.*

HPP20. Concentration Dependence of Viscosity of Solutions of Macromolecules. JACOB RISEMAN AND ROBERT ULLMAN, *Polytechnic Institute of Brooklyn.*—The method of Kirkwood and Riseman, used to account for hydrodynamic interaction between elements of the same chain are extended to include interactions between elements of different chains, responsible for the hydrodynamic effects leading to the concentration dependence of viscosity. The dumbbell and rod-shaped molecule will be treated. Smoluchowski's result for pair interaction appears as a first-order approximation. The viscosity calculation is carried out by considering the average shearing stress across a plane and yields for the viscosity a generalized binomial form, $\eta=\eta_0/1-f(c)$. $f(c)$ depends on the distribution function of elements on the same and different chains. At low concentrations, a uniform distribution has been assumed, leading to a $k'[\eta]^2$ as the coefficient of the C^2 term. A method of iteration would give $f(c)$ as an infinite power series in the concentration, and the corresponding viscosity as a doubly infinite power series. The generalized binomial form thus obtained therefore bears some resemblance to empirically proposed equations for the viscosity.

HPP21. The Stress-Strain Behavior of Thermally Shortened Collagen Tendons. NORMAN M. WIEDERHORN AND GERALD V. REARDON, *United Shoe Machinery Company.*—In order to gain information concerning the structure of collagen, the stress-strain behavior of thermally contracted (denatured) kangaroo tail tendon was studied. It has been determined that when this material is highly swollen with appropriate swelling agents it obeys the kinetic theory of rubber elasticity for relatively large deformations. The material is apparently cross-linked by covalent linkages and the average molecular weight of the chain between points of crosslinking has been determined to be 54,000±7000. This corresponds to approximately 600 amino acid residues, so that the concentration of amino acids involved in cross-links is of the order of 0.2 percent.

HPP22. Molecular Weights from Flow Birefringence and Intrinsic Viscosities. M. D. SCHOENBERG AND F. R. EIRICH, *Polytechnic Institute of Brooklyn.*—An empirical relationship is proposed relating the quotient $(n_s-n_0)/q\eta_0C$ to the molecular weight and intrinsic viscosity. The constant obtained for a single fraction in a given solvent from experimental flow birefringence and intrinsic viscosity data, when applied to flow birefringence and intrinsic viscosity measurements on other fractions of the same polymer in the same solvent, gives molecular weights that are in agreement with those obtained by other measurements. The molecular parameters b and ζ are obtained by calculating the rotatory diffusion constant of Riseman-Kirkwood. At large gradients the above relationship no longer is applicable, which effect is attributed in part to a "stretching" phenomenon.

Author Index to Papers Presented at the New York Meetings

Alburger, D. E., D. J. Hughes, and C. Eggler—No. C4
Allen, R. C. and Waldo Rall—No. P7
Allison, H. W. and George E. Moore—No. EP15
Anderson, P. W.—No. R4
Andrews, C. L.—No. S10
Andrews, F. A., D. A. Spohr, and R. T. Webber—No. R12
Andrews, R. D., F. H. Holmes, and A. V. Tobolsky—No. HPP6
Arons, A. B.—No. N4
Autler, S. H. and C. H. Townes—No. Q9

Barbour, Ian—No. D2
Bardeen, J.—No. F2
Baron, M. L. and A. deBretteville, Jr.—No. S11
Bartnoff, Shepard, Charles R. Mingins, and Joseph F. Clayton—No. A4
Bateson, W. O.—No. P3
Bederson, B. and L. H. Fisher—No. M5
Beeman, W. W., Paul Kaesberg, and H. N. Ritland—No. OB5
Belinfante, F. J. and J. S. Lomont—No. U13
Benfield, A. E.—No. N11
Bennett, Willard H.—No. M8
Bergmann, Peter G., Robert Penfield, Ralph Schiller, and Henry Zatzkis—No. J8
Beringer, Robert and J. G. Castle, Jr.—No. Q11
Bernardini, G.—No. I3
Berry, Chester R. and Robert L. Griffith—No. A10
Biedenharn, L. and J. M. Blatt—No. E5
Bickford, L. R., Jr.—No. R9
Binder, Daniel—No. H2
Blau, Marietta, John Nafe, and Herbert Bramson—No. D7
Bogle, R. W.—No. EP12
Bohm, D., M. Weinstein, and H. Kouts—No. U10
Borowitz, S., W. Kohn, and J. Schwinger—No. U5
Boyer, Keith—No. U2
Boyer, R. F.—No. HPP4
Bostick, W. H.—No. HA2
Branscomb, Lewis M.—No. N6
Breckenridge, R. G. and A. L. Ward—No. A2
Briggs, Thomas H.—No. EP26
Brown, Frederick C. and J. C. Street—No. D4
Bube, Richard H.—No. W7
Buchdahl, R., L. E. Nielson, and R. E. Pollard—No. HPP17
Burns, G. Preston—No. HA1
Burstein, E. and J. J. Oberly—No. W6
Burte, Harris M.—No. HPP7
Burton, J. A., H. E. Kern, and R. T. Lynch—No. EP20

Cameron, A. G. W. and C. H. Millar—No. P5
Caspari, E.—No. R3
Chapman, Robert M., John H. Shaw, and Dudley Williams—No. N8
Cheng, Lin-Sheng and J. D. Kurbatov—No. C10
Cheston, W. and L. Goldfarb—No. D5
Cohn, Ruth A. and J. D. Kurbatov—No. C7
Conant, F. S., G. L. Hall, and W. James Lyons—No. HPP5
Cook, D. B., H. A. Boorse, and M. W. Zemansky—No. R16
Cook, Richard K. and Robert G. Breckenridge—No. A3
Corben, H. C.—No. J7
Crittenden, E. C., Jr. and R. W. Hoffman—No. W9
Croning, Leo J.—No. EP1
Crowell, Albert and H. E. Farnsworth—No. Y3
Curtis, C. W.—No. S4

Dandurand, P. and R. B. Holt—No. M6
Danforth, W. E. and F. H. Morgan—No. EP6
Dannis, M. L.—No. HPP9
Daunt, J. G. and C. V. Heer—No. R15
deBretteville, A., Jr. and G. Katz—No. R1
de Carvalho, H. G.—No. L3
der Mateosian, E. and M. Goldhaber—No. H5
Demers, Pierre—No. D6
Dickinson, W. C.—No. Q5
Driscoll, R. L., H. A. Thomas, and J. A. Hipple—No. Q1
Duckworth, Henry E. and Howard A. Johnson—No. L5
du Pré, F. K., R. A. Hutner, and E. S. Rittner—No. EP17
Dwight, K., R. Sabin, T. Stix, and J. R. Winckler—No. G9

Elion, Herbert A.—No. W14
Elliott, Norman—No. R6
Eisasser, W. M.—No. Y6
Ertel, A.—No. EP10
Evvard, J. C.—No. T3

Fan, H. Y. and M. Becker—No. OA4
Feenberg, E.—No. X5
Feld, B. T., I. L. Lebow, and L. S. Osborne—No. G7
Feldman, Larry and C. S. Wu—No. C3
Ferry, John D., W. M. Sawyer, George V. Browning, and Arthur H. Groth, Jr.—No. HPP18
Feynman, R. P.—No. K2
Fisher, L. H. and B. Bederson—No. M4
Fluke, Donald J.—No. OB2
Foldy, L. L. and S. A. Wouthuysen—No. U6
Forbush, Scott E., Thomas B. Stinchcomb, and Marcel Schein—No. G1
Forman, Ralph and Glenn F. Rouse—No. EP18
Fowler, E. C., J. C. Street, W. B. Fowler, and R. D. Sard—No. G4
Fowler, W. B., R. D. Sard, E. C. Fowler, and J. C. Street—No. G5
Franklin, A. D.—No. R11
Freistadt, Hans—No. J11
Froehlich, H.—No. F3

Gammel, J. L.—No. E4
George, Waller and John Kauffman—No. HPP10
Goeppert-Mayer, M.—No. X3
Gold, Louis—No. N1
Goldstein, J. H. and J. K. Bragg—No. V2
Goldstein, Louis—No. Y2
Goldstein, Martin, and Ralph S. Halford—No. OB8
Goldwater, D. L. and R. E. Haddad—No. EP8
Gordon, W. E.—No. Y5
Gove, Harry E.—No. U3
Green, James H., Jr. and Victor B. Corey—No. HA7
Green, L. C. and N. E. Weber—No. S2
Greene, Richard F. and Sol E. Harrison—No. W2
Gross, Leonard, and Donald R. Hamilton—No. C6

Hahn, E. E. and P. H. Miller, Jr.—No. W3
Halford, Ralph S. and Roger Newman—No. V10
Halpern, O. and H. Hall—No. D8
Harkins, W. D.—No. X1
Hart, R. J., K. Russell, and R. M. Steffen—No. OA3
Harvey, J. A.—No. U4
Hazen, W. E.—No. D9
Heller, Jack and Peter G. Bergmann—No. J9
Hereford, Frank L.—No. HA3
Hill David L.—No. L2
Hipple, J. A., H. Sommer, and H. A. Thomas—No. M9
Hoffman, R. W. and E. C. Crittenden, Jr.—No. W8
Hogan, C. L. and R. B. Sawyer—No. W13
Holden, R. B., W. J. Taylor, and H. L. Johnston—No. S7
Hornig, D. F. and F. P. Reding—No. V9
Hsiao, C. C. and J. A. Sauer—No. HPP13
Horton, C. W., F. C. Karal, and C. M. McKinney—No. HA6
Hudspeth, Emmett L. and Charles P. Swann—No. P4
Huggins, M. L.—No. OB7, Z16
Hughes, D. J.—No. I2
Hume, J. N. P. and M. F. Crawford—No. S3
Hung, C. S. and V. A. Johnson—No. OA6

Ivey, H. F. and C. L. Shackelford—No. EP24

Jacobi, G. T. and W. C. Dunlop, Jr.—No. W5
Jacobs, Harold, George Hees, and Walter Crossley—No. EP28
Jacobs, Harold and Jack Martin—No. M3
Jen, C. K.—No. Q6
Jepsen, Robert L.—No. EP11
Johnson, Gerald W.—No. A6
Johnson, M. H. and B. A. Lippmann—No. J6

Kaesberg, Paul, W. W. Beeman, and H. N. Ritland—No. OB4
Kaufman, Raymond—No. M11
Kauffman, John and Waller George—No. HPP1
Kelly, Edward, H. E. Farnsworth, and Edward N. Clarke—No. A8
Kern, H. E. and K. T. Lynch—No. EP19
Kies, J. A. and A. M. Sullivan—No HPP2
King, Gilbert W.—No. J4. HPP19
Kisliuk, P. and C. H. Townes—No. V4
Kundu, D. N. and M. L. Pool—No. J1

Landé, Alfred—No. U8
Landeen, Stanley A., H. E. Farnsworth, and Russell K. Sherburne—No. Y4
Landon, H. H.—No. P13
Lark-Horovitz, K., M. Becker, R. E. Davis, and H. Y. Fan—No. OA1
Lauer, James L.—No. S8
Lawrance, Richard B.—No. V3
Lax, Melvin—No. E9
Leaderman, Herbert—No. Z12
Lee, C. A., R. O. Carlson, B. P. Fabricand, and I. I. Rabi—No. Q7
Lehovac, K.—No. W1
Levitas, Alfred—No. N3
Lewis, H. W.—No. E3
Lidofsky, Leon, Philip Macklin, and C. S. Wu—No. C8
Lin, C. C.—No. T1
Livingston, M. S., K. Boyer, H. E. Gove, J. A. Harvey, and M. Deutsch—No. U1
Livingston, R. S., R. J. Jones, and R. E. Wright—No. L1
Loeb, Arthur L.—No. Y1
Loomis, F. W.—No. O1
Lord, J. J. and Marcel Schein—No. D11
Loubser, J. H. N. and J. A. Klein—No. V8
Lowry, E. F., E. L. Mager, and H. H. Homer—No. EP21
Lyons, W. James—No. HPP8

Macklin, Philip, Leon Lidofsky, and C. S. Wu—No. C5
Malm, R. and W. W. Buechner—No. P6
Mandeville, C. E.—No. C12
Marshak, R. E.—No. U11
Matheson, R. M. and L. S. Nergaard—No. EP22
McAfee, K. B., Jr.—No. Q10
McCoubrey, A. O., D. Alpert, and T. Holstein—No. B1
McGannon, J., R. Heller, and A. H. Weber—No. A13
McGowan, F. K.—No. H1
McGuire, T. R. and Louis N. Howard—No. R10
McNally, J. O.—No. EP23
Merz, W. J.—No. R2
Miller P. H., Jr. and E. E. Hahn—No. W4
Miller, P. H., Jr. and B. J. Rothlein—No. EP13
Minden, H. T., J. M. Mays, and B. P. Dailey—No. V5
Mohler, Fred L.—No. M10
Morgan, F. H.—No. EP9
Morrison, P.—No. N10
Morton, G. A.—No. B3
Moses, H. E. and Ta-You Wu—No. N7
Murray, R. T. K. and Alexander Mackenzie—No. W12
Myers, Vernon—No. V11

Newman, Roger and Edward M. Purcell—No. Q4
Nelson, Herbert—No. EP5
Nielsen, John P.—No. W11
Nielsen, Lawrence E. and Rolf Buchdahl—No. HPP16
Nordheim, L. W.—No. X4

Odell, N. H. and H. Y. Fan—No. OA2
Osborn, R. K. and L. L. Foldy—No. E7
Osborne, L. S., B. T. Feld, and I. L. Lebow—No G6
Ostroski, A. S. and R. B. Stambaugh—No. HPP11

Palumbo, T. R.—No. EP27
Pauli, W., Jr.—No. K3
Pease, Robert L. and Herman Feshbach—No. E6
Peck, R. A., Jr.—No. P15
Perez-Mendez, Victor and Harold Brown—No. C2
Plass, Gilbert and John Strong—No. N9
Pollard, Ernest and F. Forro, Jr.—No. OB3
Pomerantz, Martin A.—No. G12
Present, R. D. and E. Feenberg—No. J2
Price, William J.—No. EP14
Purcell, E. M.—No. B2

Ramsey, Norman F.—No. Q2
Randall, C. A.—No. D10
Raymond, Richard C.—No. Y7
Read, W. T.—No. W10
Reese, Robert M., Vernon H. Dibeler, and Fred L. Mohler—No. M7
Richard, C. D., Jr.—No. EP25
Riseman, Jacob and Robert Ullman—No. HPP20
Robertson, B. E., W. E. Scott, and M. L. Pool—No. C9
Rogosa, George L. and Guenter Schwarz—No. S5
Rohrlich, F.—No. U12
Rosenbluth, M. N. and L. I. Schiff—No. H9
Rothstein, Jerome—No. M2
Rouse, A. G., A. V. Bushkovitch, L. C. Jones, C. A. Potter, and W. F. Sullivan—No. V7
Ruderman, I. W.—No. A12
Rudin, Robert, Marietta Blau, and Seymour Lindenbaum—No. D3

Savitzky, Abraham and Ralph S. Halford—No. S9
Saxon, David S., Alfredo Baños, Jr., and Louis L. Bailin—No. HA5
Scharff-Goldhaber, Gertrude, E. der Mateosian, M. McKeown, and A. W. Sunyar—No. H3
Schiff, L. I.—No. E2
Schild, A. and F. A. E. Pirani—No. J10
Schlier, Robert E. and H. E. Farnsworth—No. A7
Schoenberg, M. D. and P. R. Eirich—No. HPP22
Schulz, L. G.—No. A5
Scott, Robert L.—No. A11
Scott, W. T.—No. G2
Sears, W. R.—No. T2
Segel, Leon, Joseph J. Creely, and Carl M. Conrad—No. HPP12
Seitz, Frederick—No. Z11
Senitzky, I. R.—No. M1
Setlow, R. B. and D. J. Fluke—No. OB1
Shapiro, E.—No. EP2
Shapiro, E. and C. E. Mandeville—No. C11
Shockley, W., H. J. Williams, and C. Kittel—No. R8
Shulman, R. G. and C. H. Townes—No. V6
Siegert, A. J. F.—No. J5
Simon, Albert—No. E1
Sitte, K.—No. G3
Smoluchowski, R.—No. F1
Smith, O. H.—No. O2
Snell, A. H., F. Pleasonton, and R. V. McCord—No. C1
Snow, George—No. E8
Snowdon, S. C.—No. P8
Snyder, Hartland S.—No. U9
Spencer, R. S. and G. D. Gilmore—No. HPP14
Spencer, P. S., G. D. Gilmore, and R. M. Wiley—No. HPP15
Spruch, L.—No. J3
Steele, M. C.—No. R14
Steinberger, J. and A. S. Bishop—No. D1
Stinchcomb, Thomas G.—No. D12
Stix, T., K. Dwight, R. Sabin, and J. R. Winckler—No. G8
Strait, E. N., D. M. Van Patter, and W. W. Buechner—No. P9
Strucken, Edward, Robert Heller, and Alfred H. Webber—No. HA4
Sun, Kuan-Han, F. A. Pecjak, R. A. Charpie, and J. F. Nechaj—No. P14
Sunyar, A. W., D. E. Alburger, G. Friedlander, M. Goldhaber, and G. Scharff-Goldhaber—No. H4
Swann, C. P., C. E. Mandeville, and W. D. Whitehead—No. P11
Swann, W. F. G.—No. G11

Talbott, F. L. and A. Busala—No. P1
Taylor, W. E. and H. Y. Fan—No. OA5
Taylor, W. J., G. P. Koch, and H. L. Johnston—No. S6
Tchen, Chan-Mou—No. OB6
Thomas, H. A.—No. Q3
Tisza, L.—No. R13
Tobolsky, A. V.—No. Z15

Towler, O. A., Jr. and C. L. Oxley—No. H7
Townes, C. H. and B. P. Dailey—No. V1
Twersky, Victor—No. N2
Tyler, Winfield W.—No. B4

Van Dyke, Karl S.—No. A1
Van Vleck, J. H.—No. O3
Vidale, M. L. and Marcel Schein—No. G13
Von Weiszaecker, C. F.—No. K1

Wachtell, G. P.—No. N5
Wannier, G. H.—No. R5
Wantuch, E.—No. H8
Watson, W. W. and C. E. Anderson—No. S1
Weinreich, O. A.—No. EP3
Weir, C. E., W. H. Leser, and L. A. Wood—No. HPP3
Weisskopf, V. F.—No. X2
Weyl, W. A.—No. Z13
White, Gladys R.—No. L6
Whitehead, W. D. and N. P. Heydenburg—No. P12
Whitehead, W. D. and C. E. Mandeville—No. P2
Whyte, G. N.—No. D13
Wiederhorn, N. M. and G. V. Reardon—No. HPP21
Wiegand, C. and O. Chamberlain—No. H6
Williams, Paul D.—No. EP7
Williams, H. J. and W. Shockley—No. R7
Winckler, J. R., K. Dwight, R. Sabin, and T. Stix.—No. G10
Winston, Harvey—No. A9
Witmer, Enos E.—No. L7, No. SP1
Wolfenstein, L.—No. E10
Wright, D. A.—No. EP16
Wu, C. S.—No. I1

Yagoda, Herman and William C. White—No. L4
Yanagisawa, S. T. and T. H. Rogers—No. EP4
Yevick, G. J.—No. U7
Yuan, Luke C. L.—No. G14

Zeiger, H., D. Bolef, and I. I. Rabi—No. Q8
Zener, Clarence—No. Z14
Zucker, A. and W. W. Watson—No. P10